HOLOCENE GEOMAGNETIC SECULAR VARIATION IN THE WESTERN UNITED STATES: IMPLICATIONS FOR THE GLOBAL GEOMAGNETIC FIELD

Thesis by

Duane Edwin Champion

In Partial Fulfillment of the Requirements

for the Degree of

Doctor of Philosophy

California Institute of Technology

Pasadena, California

1980

ACKNOWLEDGEMENTS

The initial phases of this investigation were conducted while the author was an Energy Related Graduate Trainee. Field expenses were defrayed by a grant from the McCarthy Foundation and the NSF-RANN division contract AER76-00634. Some field support and all laboratory support was provided by the United States Geological Survey at Menlo Park, California and Flagstaff, Arizona. Able field assistance was provided by Moses Ma, David Blum, Carolyn and Linda Shoemaker, and Janet and John Ferrari. For their help on hot, sweaty, freezing, rainy and snowy days I am very thankful. A large number of geologists have generously shared information and personal knowledge of the geology of the volcanic rocks that were studied. Conversations with Robert Coe, John Hillhouse, Abdulwahab Khodair and Edward Mankinen were helpful and important during the course of the laboratory work.

Primary acknowledgement goes to two individuals without whom the project would not have been successful. Eugene Shoemaker suggested the problem and encouraged me to do it, helped me secure the support, sweated with me on the outcrop and provided thoughts and insight critical to the study. When I left Caltech to go to the U.S. Geological Survey, I had had one seminar in paleomagnetism. What I know now about secular variation, paleointensity, instrumentation and plain common sense, I owe mostly to Sherman Grommé.

ABSTRACT

A record of Holocene geomagnetic secular variation in the western United States has been measured from volcanic rocks dated by ^{14}C. Analysis of errors associated with the paleomagnetic techniques used suggests that all laboratory measurement errors are smaller than those introduced by deformation of the volcanic units and the errors of orientation of cores in the field. The dispersion in the calculated virtual geomagnetic poles introduced by the geographic spread of sample localities around the western United States is less than the average uncertainty from an individual locality, about 2 deg.

The history of secular variation of field direction in the western United States has been reconstructed where sufficient time control exists. This history can be approximately reconstructed for the past 3000 years; in this time period, inclination varied from 44 to 72 deg and declination varied from 344 to 22 deg. These variations of the local field direction have periods between 500 and 1500 years. Prior to 3000 years B.P., the available observations allow reconstruction of the secular variation history only for short time intervals. The mean VGP obtained from paleofield directions measured from 77 volcanic units of Holocene and late Pleistocene age in the western United States does not coincide with the geographic pole of the Earth, but is displaced 2.5 deg from the geographic pole in a direction away from the sampled region. This displacement is just at the limit of significance at 95 percent confidence.

Using a 10^{-5} torr vacuum furnace, paleointensities have been obtained by the Thelliers' method from both high-temperature oxidized and unoxidized basic volcanic rocks. Specimens which have undergone incomplete high-temperature oxidation in nature commonly fail the Thellier experiment; the relationship between NRM lost and TRM gained in a known magnetic field is not linear. Despite the vacuum, oxidation can still occur above 300°C in the furnace ovens. The best determinations of paleointensity come from specimens in which the remanence resides primarily in single phase titanomagnetite or in intergrowths of Ti-poor magnetite in ilmenite which have been formed by natural high-temperature oxidation. Paleointensity determined from these specimens varies from 0.364×10^{-4} T to 0.865×10^{-4} T (1.0×10^{-4} T = 1 Oe); the period of oscillation of paleointensity is about 500 to 1000 years. Close agreement has been found between the paleointensity measurements from this study and those from archeomagnetic studies in the southwestern United States. The similarity of the periods of intensity variation to those of field direction changes may indicate that variations of the nondipole components of the geomagnetic field dominate both.

By combining paleomagnetic and archeomagnetic data from globally distributed localities, the magnetic dipole can be shown to have wobbled with a period as short as 2000 years. Local variation of the field can be described as the consequence of fluctuation of the dipole moment, wobble of the dipole, and longitudinal drift of a nondipole field similar to that of the present. During the Holocene, the dipole moment of the Earth has fluctuated with a period of

approximately 8000 years, though when viewed from a single region, the fluctuation of the dipole moment is obscured by variation of nondipole components of the field.

TABLE OF CONTENTS

Page

APPENDICES

LIST OF FIGURES

LIST OF TABLES

Chapter 1

INTRODUCTION

Changes in the geomagnetic field at any one place on the Earth on a year-to-year time basis are termed secular variations. These variations in field direction and intensity constitute the normal behavior of the geomagnetic field and are driven by fluid motions in the outer core of the Earth. Secular variation is a regional phenomenon, that is changes can occur over local areas and be little manifested in adjacent areas. Observations of secular variation at widely separated localities in the world are our best information regarding the dynamic processes within the core. Only when we understand the fundamental aspects of secular variation can the large-amplitude prehistoric geomagnetic effects such as excursions and reversals be understood well at all.

The present study is concerned with the secular variation of the geomagnetic field in the western United States during the Holocene. It was thought that by collecting a detailed record of secular variation from the western United States, a substantive contribution to the knowledge of the behavior of the geomagnetic field could be made. Direct observations of the geomagnetic field in the western United States have been made since the middle of the 19th century. In Europe, direct observations have been made as early as the 16th century. Archeomagnetic measurements of the history of secular variation in the southwestern United States have extended back to

A.D. 500 using ceramic materials and hearths from the Pueblo cultures.

The remanent magnetization of dated Holocene lava, agglomerate, and welded tuff is used in this study to extend the secular variation record. Volcanic rocks have a strong, stable remanent magnetization and are known to record accurately the geomagnetic field at the time of their extrusion. A volcanic rock has the disadvantage of possessing only an instantaneous record of the geomagnetic field, whereas secular variation can produce large changes in periods of time as short as a few centuries. Thus unless many dated volcanic rocks are available, preferably in a stratigraphic sequence, only a skeletal outline of secular variation can be reconstructed. Lake sediments can preserve continuous records of secular variation through a detrital remanent magnetization taken on by the sediments as they are deposited. Unfortunately, lack of within-sediment time control and integration of the geomagnetic record for lakes with slow sedimentation rates can diminish the utility of these records. Combinations of instantaneous geomagnetic records from dated volcanic rocks and continuous geomagnetic records from lakes with high sedimentation rates will eventually provide the most complete record of secular variation.

Volcanic rocks of Holocene and late Pleistocene age occur in nine conterminous states in the western United States. Of these, 31 lava flows, three deposits of volcanic agglomerate, and two ash-flow tuffs were found which both provided accurate information on paleodirections or paleointensities of the geomagnetic field and are sufficiently well dated to be useful in determining the history of

the geomagnetic field. Localities of the dated volcanic units studied are shown in Figure 1. Most of the dated volcanic units sampled are located in the Cascade Province, and the rest are on the Snake River Plain or are scattered in the Basin and Range Province. In addition to the dated units, approximately 50 other volcanic units of Holocene or very late Pleistocene age were sampled and measured. These volcanic units are distributed in the same regions as the dated units, but with a greater proportion from the Snake River Plain. The approximate age assignments of these latter units are based on their appearance, stratigraphic relationships and vegetative cover. Although not useable for constructing the history of the geomagnetic field, the directions of magnetization of these poorly dated volcanic units provide a more complete statistical picture of paleomagnetic field directions than can be obtained from the more accurately dated units alone.

The volcanic units were dated, in most cases, by ^{14}C analysis of carbonized plant material overridden or engulfed by lava flows. Most of the carbonaceous material was obtained either from tree molds penetrating a lava flow or from excavations under the margins of thin lava flows. The material itself was typically hard massive charcoal from carbonized roots or tree trunks or more finely divided if from smaller bushes or shrubs. A few of the dates are from black, carbonized A horizons in soil overlain by young lava flows. The volcanic units in the vicinity of Sunset Crater in Arizona were dated on the basis of stratigraphy and by comparing their recorded field directions with the dendrochronologically dated archeomagnetic

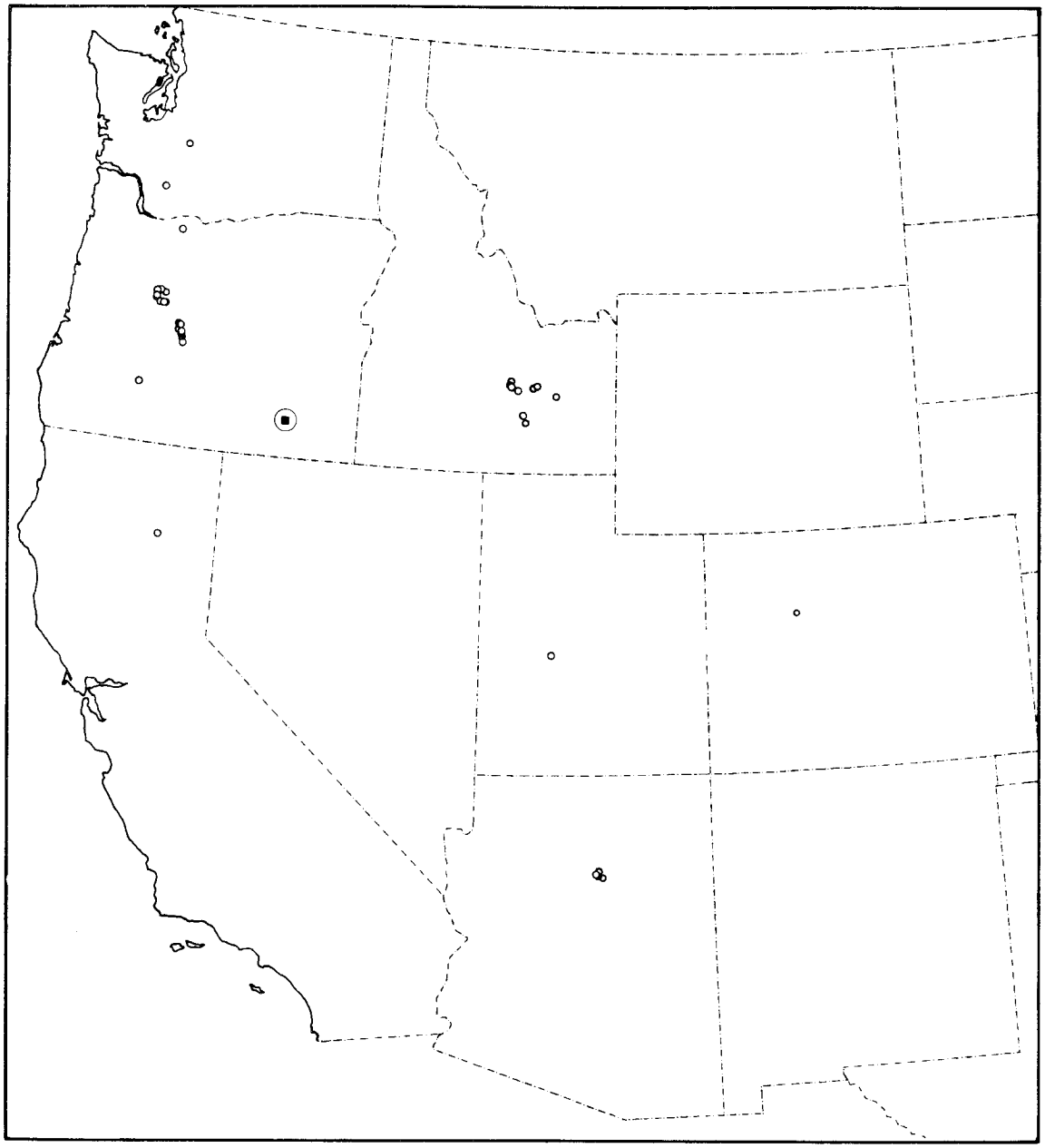

Fig. 1--Map of western United States showing localities of dated Holocene volcanic units sampled in this investigation. The solid square with circle around it is the mean position of the sample localities.

record of Dubois (1974). Through the efforts of this study, four new ^{14}C dates were acquired, one each for the Sugar Pine Butte Flow, Lava Butte and North Summit Flow, all on the Northwest Rift of Newberry Crater, Oregon; the fourth is for the Wapi Lava Field on the Snake River Plain, Idaho. A large number of volcanic units exist, principally in the Cascade Province, that probably could be dated by ^{14}C methods, and many of these have been sampled for the present study but a significant amount of geologic work would need to be done to acquire this additional time control.

Measurement of both geomagnetic paleodirection and paleointensity was attempted for all dated volcanic units sampled. The paleointensity method used was that of the Thelliers with certain modifications. Results of these measurements are described in chapters 3 and 4. Chapter 5 describes the global geomagnetic field behavior implied by the available records of secular variation. By combining the paleodirection and paleointensity measurements from this study with similar data, mostly archeomagnetic measurements, an improved understanding of global secular variation over the last 10,000 years has been reached. In particular the character of regional nondipole secular variation, relative proportion of the secular variation due to dipole versus nondipole sources and the nature of regional versus global geomagnetic intensity variations are discussed in detail.

Chapter 2

FIELD METHODS

While paleomagnetic sampling in the field is generally a routine procedure, the outcrop character of the units sampled during this study required some techniques that are worth a short description. Holocene lava flows present a special problem for paleomagnetic sampling because they are very rarely dissected by erosion. Hence, the interior parts of the flows generally are inaccessible except where the flows are structurally disturbed. Samples for this study in most cases were taken from the original surfaces of the flows. Samples were taken from parts of these flows where the surfaces were structurally coherent and where there appeared to be little evidence of deformation or rotation of the surface of the flow after cooling.

Most lava flows sampled have pahoehoe surfaces, indicative of a fluid behavior of the lava until it cooled and congealed. Sampling sites were chosen on broad nearly level surfaces on pressure plateaus of pahoehoe flows. Small domical upbowings of the surface coined "turtlebacks" are a ubiquitous feature on these plateau surfaces. Analysis of the directions of remanent magnetization from samples from these turtlebacks revealed small rotations around horizontal axes of the preserved direction of magnetization. By sampling the crests of these dome structures it was possible to avoid these small rotations.

Lava gutters were found to be structurally stable localities for sampling aa flows which otherwise have extremely rough incoherent surfaces. The rough surfaces of aa flows frequently gave tight groupings of field directions, indicating the physical deformation of the surface occurred above the Curie temperature of the magnetic minerals of that flow, that is, before the remanent magnetization was acquired. Occasionally, small coherent flow surfaces could be found scattered around the generally rough surface, probably the result of upward injections of fluid lava through the clinker cover. At several localities road outcrops, which had been cut through the rough surfaces to the massive interiors of the flows, provided good outcrops for sampling. On some aa block flows, the only structurally stable parts of the surfaces were constructional features such as spatter cones or ramparts. Though specimens of spatter are rather friable and difficult to handle, their remanent magnetizations are very stable, and have high coercivities.

On two occasions, volcanic bombs on the rims of cinder cones were sampled in the absence of a better site. At the cinder cone of Sunset Crater, Arizona, samples were taken from small volcanic bombs embedded in lightly welded cinders on the rim of the cone. The close alignment of the directions of magnetization of these bombs showed that they acquired their stable magnetization after their deposition on the cone.

As a check on the structural stability of the sample sites, at least two separate sites on each volcanic unit were sampled. A minimum of six independent cores was taken from each site. A

diagram of the sampling terminology is given in Figure 2. If the cone of 95 percent confidence of the mean direction of magnetization (alpha 95) of one site did not overlap the mean and alpha 95 of the second site, then additional sites were sampled until a consensus among sites was reached. Clearly anomalous sites were rejected. If each of three or four sites gave distinct mean directions at the 95 percent confidence level, they were all averaged for the final mean direction. Of the dated and undated localities sampled, only four were rejected; three localities occurred on extremely rough surfaces and at the fourth, the structural discordance had been obscured by a discontinuous overlying deposit of pumice.

In situ measurements of the present direction of the geomagnetic field were made at each site to determine whether significant local anomalies existed that might have affected the measured paleodirections. Inclination measurements were made at each site with a magnetic dipping needle to a precision of 0.5 deg. The measurements were made with the instrument at eye height, approximately 5 ft. The declination for each site was obtained by averaging the difference between magnetic azimuth and sun compass azimuth for each core at the site. Declination measurements were by nature more dispersed than inclination measurements because the magnetic azimuths for each core were made by placing the magnetic compass against the back edge of the sun compass. At this 4- to 6-in. proximity to the lava's surface, relief of the surface of the lava, itself magnetic, introduced significant dispersion into the magnetic azimuth measurement. Comparison was then made between the field measurements of declination and inclination and

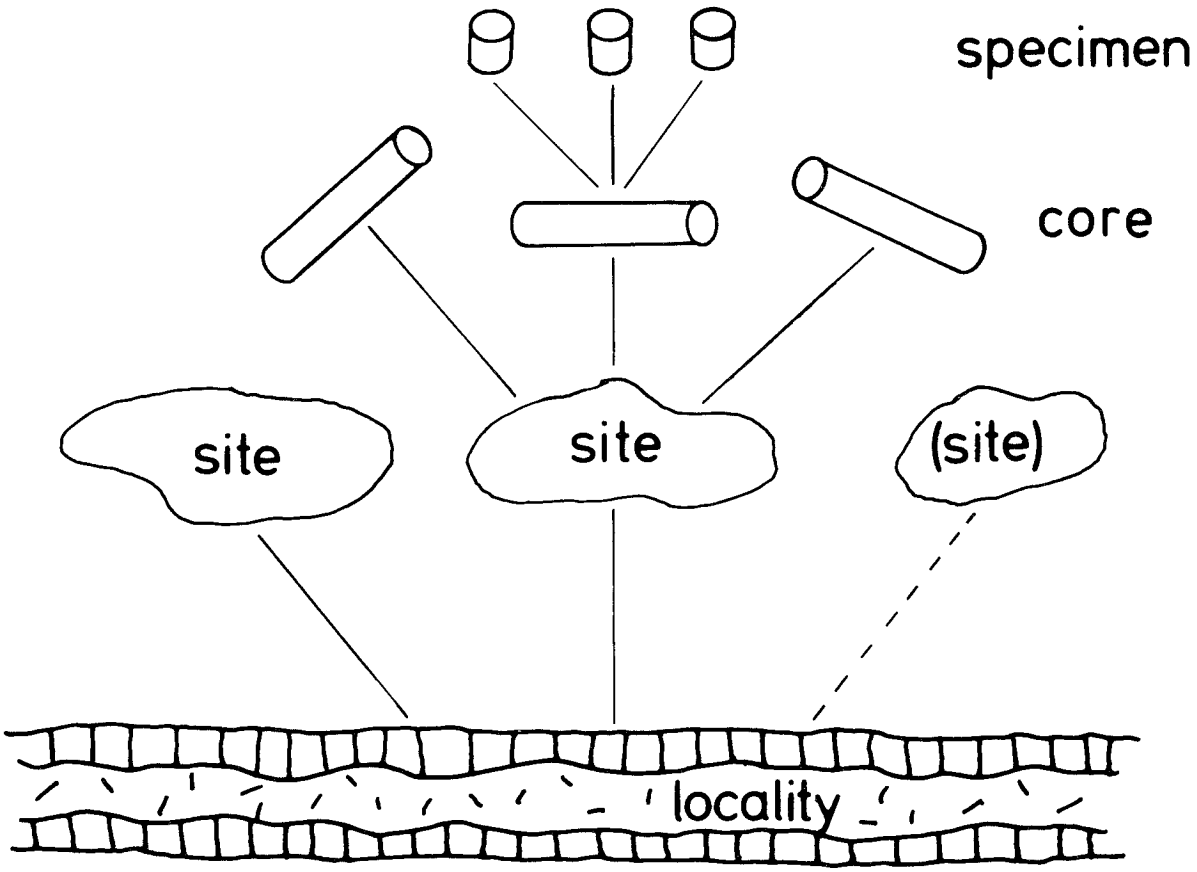

Fig. 2--Sample tree of terminology used in this study.

the regional values of declination and inclination given by the 1975.0 epoch isogonic and isoclinic maps for the United States. In few instances were the locally measured field directions, that is the combination of the inclination and declination measurements, found to deviate more than 1 or 2 deg from the regional field direction for a locality. Where the deviations were greater, the magnetic edge effect due to a local step in the topography could be shown to be the cause of the magnetic deviation. While these measurements are strictly of the present field, they show that local pre-existing magnetic anomalies cannot have significantly affected the paleo-directions recorded by the volcanic units studied.

Considerable care was exercised in the field in the identification of the lava flows to which reported ^{14}C ages properly apply. In most instances, other workers were the source of the ^{14}C age information and their published reports and maps were the only information available concerning the location of ^{14}C dated samples. Where feasible, paleomagnetic samples were chosen as close as possible to the ^{14}C sample location to ensure that the magnetic measurements pertained to the dated unit. If the ^{14}C sample location could be identified, the paleomagnetic site was located directly on the dated flow unit to remove all ambiguity with regard to what was sampled. An effort was made to understand the field relations of every unit that was sampled, to ascertain if the relationships cited in the published reports between the ^{14}C samples analyzed and the volcanic units were correct. For each flow sampled, observations were made on the stratigraphic relationships to other flows and to sediments,

on the development or absence of soil profiles and on the extent and type of vegetation growing on the flow. These latter observations were also used to make field estimates of the approximate ages of undated flows. Despite this care, at least one error was made, but later corrected. The wrong lava flow was sampled on the basis of an incorrect geologic report. In a number of cases, substantial field work was necessary to verify or establish the field relationships of the volcanic units sampled.

The direct field sampling procedures used in this study are relatively standard methods used by many laboratories and involve little in the way of new methods. The samples for paleomagnetic measurement were obtained with a portable gasoline powered drill as 1-in. diameter cores, 3 to 4 in. long. Orientations of the cores were measured by standard methods to a precision of about 1 deg by means of a spirit level and sun compass, prior to removal from the outcrop. The sun compass plate is mounted on a hinged orienting tube with a clinometer at one side which can be read accurately to 0.5 deg. The plate has a 360 deg circle inscribed on its surface in a clockwise sense with marks every 2 deg. The 0 deg mark is to the orienter's right as he faces the core. The gnomon used are thin and a variety of lengths as required by the various angular heights of the sun in the sky during the day. The right ascension angle can be read off the sun compass plate to an accuracy of 0.5 deg. The exact precision of the orientation process is somewhat complex and will be discussed in greater detail below.

Chapter 3

SECULAR VARIATION OF DIRECTION OF THE GEOMAGNETIC FIELD IN WESTERN UNITED STATES

The directions of the geomagnetic field have changed with time in the western United States. They will be treated as a separate topic in this chapter, both because of the familiarity of paleo-directional analysis procedures for many workers and the ease of measurement. Measurement of the direction of remanent magnetization of a specimen remains the most reliable of paleomagnetic techniques.

Quite apart from the geophysical information that it provides, the record of directional secular variation can be used for important geological purposes. It will have great utility as a correlation and dating tool for any geologic problem involving rock units which may have recorded it. The correlation use will be conceptually identical to the use presently put to the polarity reversal record of the geomagnetic field. But instead of time resolution of 100,000s or millions of years, the time resolution will be on the order of centuries. At certain times of rapid field direction change, the routine precision of measurement will allow time resolution to fractions of a century. The possible geologic uses of such time resolution within a geologic unit can easily be imagined.

Other attempts to measure the record of secular variation have been made in the western United States. They augment a very short record of historic measurement of the directions of the geomagnetic

field. Comparison with three of the best records will be made in this chapter.

In this chapter the laboratory methods used to measure the magnetic moment of samples will be described and the errors associated with these measurements will be analyzed. An analysis of the present regional variation of the geomagnetic field will be used to ascertain the angular size of the area over which observations from different localities may be combined without introducing serious error. The paleodirections themselves are then presented and the secular variation of the geomagnetic field during parts of the Holocene is described for western United States. Comparisons of the paleodirections obtained in this study are then made with two records of secular variation from lake sediments.

Laboratory Methods

All measurements in this study were performed in the paleomagnetic laboratory of the United States Geological Survey at Menlo Park, California. Cores taken in the field were cut in the laboratory into 1-in. long specimens. The natural remanent magnetization of these specimens (NRM) was measured with a spinner magnetometer of a type described by Doell and Cox (1965).

The azimuth of plunge of the axis of each core was calculated from sun compass field measurement with a digital computer, using an algorithm written by T. C. Van Flandern of the U.S. Naval Observatory. The field orientation data and magnetometer measurements were reduced with the aid of the computer algorithm of Doell and Cox (1967), to obtain the direction and intensity of magnetization for each specimen. A mean direction of magnetization for each site was then computed by standard statistical methods (Fisher, 1953).

One specimen from each site was chosen for stepwise alternating field demagnetization up to a peak field of 100 mT. The choice of specimen was based on the disparity of its NRM direction to those of the rest of the site. This was done to determine whether isothermal remanent magnetization (IRM) or viscous remanent magnetization (VRM) were present in the specimen and if so to determine what demagnetization fields would be required to remove them. Standard demagnetizing steps of 2.5, 5, 10, 20, 30, 40, 60, 80, and 100 mT were used. If both of the pilot specimens from the two sites in a lava flow showed no change in direction of magnetization, beyond normal error of measurement, the remaining specimens from that locality

were judged to be free of determinable secondary magnetization and the NRM measurements were used to estimate the paleodirection of the geomagnetic field. If the remanent magnetization of either of the pilot specimens changed significantly during demagnetization then all specimens in that locality were cleaned at a peak alternating field at which the direction of the pilot specimen became stable. The grouping of remanent magnetization directions for each site was then examined to see whether secondary components of magnetization appeared to have been removed from all specimens. If dispersion of directions suggested that secondary magnetization was still present in some specimens, then all specimens were cleaned at the next highest alternating field and judged again. Removal of IRM or VRM was not required for 75 percent of the dated sites.

The magnetization remaining after secondary magnetization was removed is interpreted as a thermoremanent magnetization (TRM) acquired by the rock when it originally cooled. The mean TRM direction of the samples taken from a given lava flow is used as an estimate of the direction of the local geomagnetic field at the time the lava cooled. Precisely how good this estimate is has seldom been field tested. Doell and Cox (1963) tested the directions of remanent magnetization of modern Hawaiian lavas against the field which coexisted in Honolulu about 400 km away. The disagreement was insignificant at the 95 percent confidence level, but the local field had not been measured on Hawaii and small differences in the field may have existed between there and Honolulu. Laboratory studies by Robertson (1963) showed that the mean direction of artificial

thermoremanent magnetization from a group of 28 specimens from 28 sites in the Mt. Dromedary intrusive complex were parallel with a 95 percent cone of confidence of 2 deg, to the known laboratory field.

During the course of this study several examples of very close agreement in magnetic field direction of two widely separated localities in a given volcanic unit were discovered. These occurrences were in volcanic units characterized by very low dispersion of magnetization directions. As such these occurrences can be taken as limiting cases of how well the TRM within a volcanic unit will parallel the ancient paleofield direction. The two localities, 30 km apart, in the Hell's Half Acre Field gave field directions which differed by only 0.26 deg of arc. Two localities on the Wapi Lava Field separated by 12 km gave field directions 0.65 deg of arc apart. Two outcrops in the welded pumice deposit associated with the 6640 years B.P. eruption about 9 km apart on the flanks of Mt. Mazama gave field directions only 0.11 deg of arc apart. Together, these examples demonstrate that the TRM acquired by a volcanic unit can very closely parallel the apparent direction of the geomagnetic field at the time the volcanic unit cooled. If there is a misalignment of TRM and the ambient field, the bias in orientation must apply to widely separated parts of the flow. Such a bias is associated with rocks with a very strong magnetization in excess of 10^{-2} emu/cc; a magnetization strength not seen in this study.

Analysis of Errors

Sources of error in estimating paleodirections of the geomagnetic field from measurements of the specimens taken include: (1) the physical and structural character of the volcanic units sampled, (2) sample orientation in the field, (3) local magnetic anomalies existent at the time of cooling of the volcanic unit, (4) error of measurement of the magnetic moment of specimens in the laboratory, both in accuracy and precision, and (5) the magnetic character of the volcanic unit itself which, due to secondary magnetizations or inhomogeneities, may affect the ultimate precision with which the overall magnetization of that unit may be measured. Not all sources of error can be evaluated independently from the field and laboratory data obtained. Hence some errors will be roughly estimated by comparison of the sum of variance of independently determined errors with the observed variance of directions of magnetization of sites.

Error of laboratory measurement of the magnetic moment of individual specimens will be described first as it is the easiest to evaluate, and observations are fairly abundant. Bias of the instrument is a very minor source of error; all magnetometers in the Menlo Park laboratory are occasionally calibrated against a known standard specimen. Extremely high accuracy of the angular measurement from the spinner magnetometer is not required, as the measurement procedure involves a forward and reverse spin sequence by means of which any small angular bias is averaged out. Imprecision comes from three sources: (1) magnetometer noise, (2) operator reading and recording errors, and (3) error of placement of a specimen in

the cubical holder of the magnetometer. Electronic noise in the magnetometer is sufficiently low that repeat measurements of a given spin were always within a few tenths of a percent of total signal for the highly magnetized rocks measured in this investigation. The Doell and Cox algorithm for the fast spinner magnetometers evaluates angular errors and magnitude errors separately, with the directions calculated only from the phase angles for which the precision is much higher than the magnitudes. Normal operator errors of large magnitude can be identified by means of the redundancy in the measurement procedure and corrected, in part, because they are flagged by the computer program. Placing the specimen in the holder probably is a major component of the error of measurement. The brass scribe line put on the cores in the field is 2 or 3 deg wide. In the laboratory, this scribe line is re-marked with a diamond scribe line 1 deg wide. This is done manually and certainly is not an extremely precise process, though it is done with great care. This diamond scribe line is then aligned with the line on the cubical specimen holder for the magnetometer during the measuring process.

Measurements obtained during the course of the laboratory work for this study provide the basis for determination of the precision of laboratory measurement. Two measurements of the NRM of each specimen used in alternating field demagnetization tests were made. These measurements, as far as operation of the magnetometer is concerned, were strictly independent from each other. The angles between the directions obtained by replicate measurements calculated for each of 162 specimens are plotted as a histogram in Figure 3. The mean

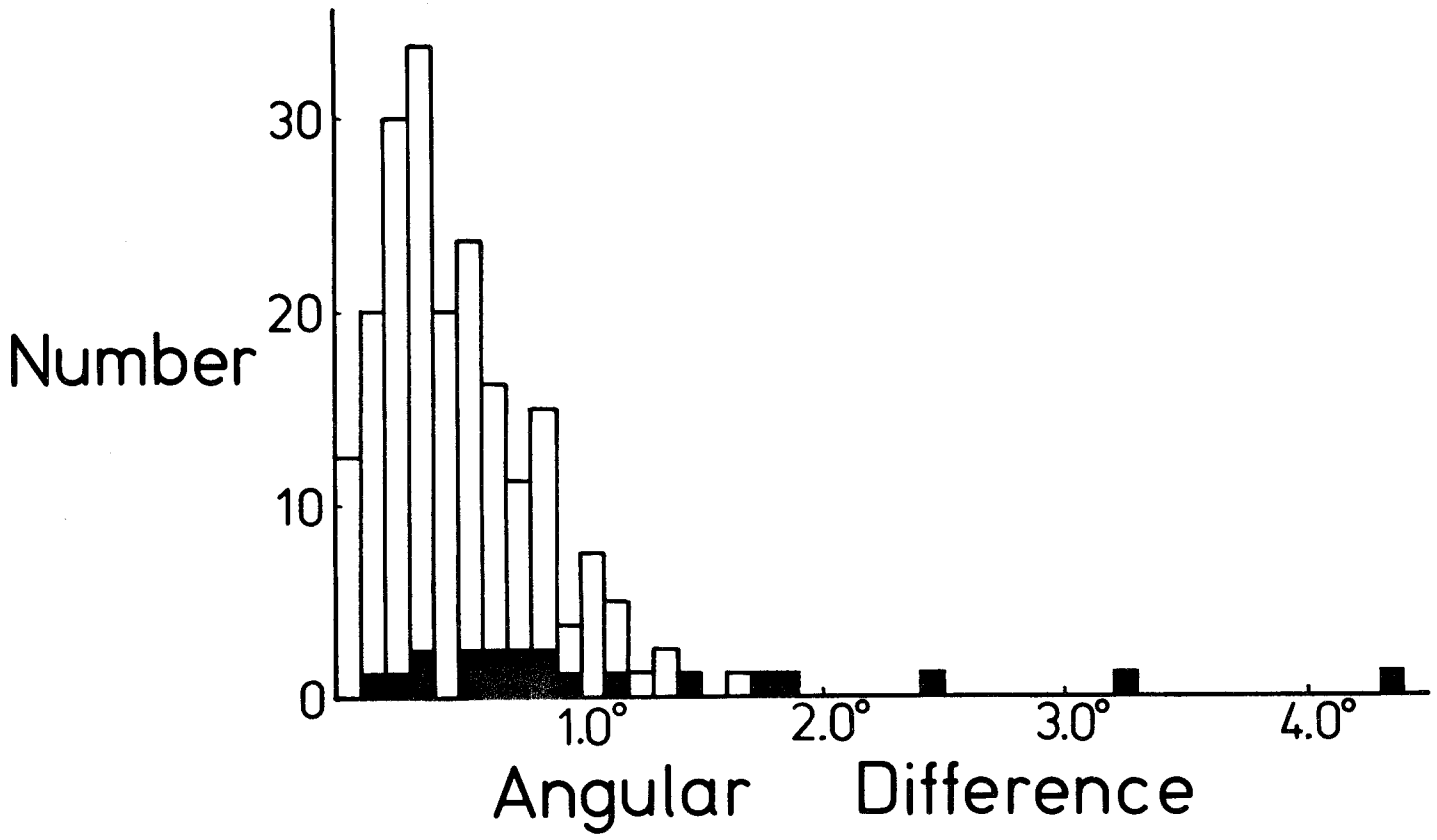

Fig. 3--Histogram of the angular difference between replicate measurements of NRM for 162 specimens selected for AF demagnetization tests. Solid columns are for specimens bounded by three orthogonal cylindrical surfaces. All other specimens are simple right circular cylinders.

angular difference is 0.57 deg, the standard deviation of the difference is 0.53 deg and the mode is between 0.3 and 0.4 deg. The distribution of angular difference is approximately Poisson, as would be expected. The median angular deviation from the mean direction is given approximately by $0.57°/\sqrt{2} = 0.40°$. Results from specimens that were initially "overcored" so that they were bounded by three orthogonal cylindrical surfaces for measurement in a different magnetometer are shown in black on Figure 3. It is clear from the histogram that remeasurement of these latter specimens yields more widely scattered results. This is due to the shape of these specimens which is inappropriate for the specimen holder used with the magnetometer in the laboratory in Menlo Park. About 12 percent of the dated specimens studied had been "overcored" in this manner.

Errors of field orientation measurement of the cores to be taken for paleomagnetic measurement are a significant component of the total error. Doell and Cox (1963) assumed, from mechanical considerations, that the precision of magnetic compass orientation was about 2 deg. This number does not include the dispersion caused by magnetic edge effects of the surface being sampled, which can be 2 to 3 deg or more if the compass is close to a rough lava surface. Because of this latter error a sun compass was used for orientation of all cores measured in this investigation.

Position of the shadow of the sun compass gnomon and position of the inclinometer on the orienting device were read in the field to the nearest 0.5 deg. A special study was performed to ascertain the inherent precision of setting and reading the inclinometer and

of reading the sundial for a single core axis during the course of a day. The standard deviation of 15 inclinometer measurements was 0.3 deg, and the standard deviation of reduced azimuths obtained from 15 sundial readings was 0.3 deg as well. The reading of accurate time necessary to obtain sun compass orientations was a negligible source of error, as the sun moves approximately 1 deg in azimuth in 4 min of time. Generally, the times for reading of the sun compass were known to within 5 to 10 sec. The principal sources of orientation error are due to scribing the orientation marks on the cores and to the irregularity of shape of the cores, which arises from imperfect drilling technique. A close assessment of the magnitude of these errors is difficult. The brass scribe line put on a core in the field is on the order of 2 to 3 deg in width. In the laboratory, a finer line is scribed by diamond along the center of the original brass line. Determination of the center of the brass line may have an error of 1 to 2 deg.

The total dispersion of magnetic directions observed at an individual site is due to a combination of measurement errors, orientation errors and structural incoherence and other sources of error. As will be shown, structural incoherence probably is the dominant source of error at most sites. At the sites with the lowest angular dispersion, which probably have the highest structural coherence, the observed dispersion provides an estimate of the other sources of error. Orientation error probably is the dominant component of this error. The lowest dispersion sites have 1 to 1.5 deg of angular standard deviation. This is consistent with the

rough estimate of orientation errors due to scribing and irregular shape of cores. On this basis, the total orientation angular standard deviation is on the order of 1.5 deg.

Errors due to structural rotation of individual parts of lava flows or pyroclastic deposits apparently constitute the major source of dispersion of paleomagnetic directions observed at most localities. In block flows or slab pahoehoe flows, easily recognized physical rotations of the components of the surface are nearly ubiquitous. The magnitudes of these rotations are generally several tens of degrees or more, and such surfaces were never sampled in this study. More troublesome are rotations of the order of 5 deg or less on the much more coherent surfaces that were sampled. These small rotations are more difficult to detect. The structural rotation may occur at different scales: (1) rotations of small structural blocks over distances of meters and (2) tilts of larger structural units which are detectable only by differences in magnetic direction between sites in the same lava flow.

While the error due to rotation of small structural blocks at a given site can only be estimated by subtracting other known sources of dispersion, the dispersion due to tilting can be derived by comparison of sites. The difference between the mean angular dispersion within sites and the mean angular dispersion within localities is an estimate of the mean angular dispersion due to real deviation in remanent magnetic direction between sites. This deviation is due to a combination of structural tilt and the difference in ambient field direction at the time of acquisition of TRM. A check of the difference in

measured present magnetic inclination between sites at each locality reveals a mean difference of 0.39 deg. Most of this difference is due to error of measurement, as the mean difference between repeated measurements at a site is 0.57 deg. From this we infer that the mean difference in ambient field between sites at the time the rocks were magnetized was also small, probably less than 0.4 deg, and possibly less than 0.1 deg. The difference between mean angular variance of sites and mean angular variance of localities is 0.27 deg^2. Almost all of this variance must be due to structural tilt, the mean of which is about 0.5 deg.

Local magnetic anomalies, that is, departures of the local geomagnetic field from the regional field represented by the U.S.A. polynomials used to generate the magnetic field charts, may contribute to error in interpretation of the history of regional secular variation. In the terrains where most of the sampling for this study was done, strongly magnetized volcanic rocks at or near the surface produce local magnetic anomalies as a consequence of the geometry of the eruptive products. Edges of lava flows, cinder cones and spatter ramparts all affect the local magnetic field. In order to reduce these anomalies, sample sites on lava flows were deliberately chosen away from flow margins. However, magnetized bodies in the subsurface also contribute to the observed magnetic field. In order to evaluate the magnitude of the local anomalies, measurements of the present local declination and inclination at most sample sites were taken as described earlier. The differences between these measurements and the values of declination and inclination from the magnetic field

charts constitute an estimate of the local magnetic anomaly. The mean inclination anomaly is 1.1 deg and the mean declination anomaly is 1.3 deg. These means are probably representative of the magnitudes of the anomalies at the times that the volcanic units sampled were magnetized. In calculating these means, only observed values of both inclination and declination free of surface edge effects and the influence of lightning strikes were used. These effects were detected by large dispersion of the measurements at a site. For inclination, one-half the observations were used, and for declination only one-fourth. Because the measurement of declination comes from observations taken so close to the lava surfaces the majority are significantly contaminated by surface edge effects.

Secondary magnetizations, IRM or VRM, undoubtedly contribute to the dispersion of measured magnetic directions of each site. Despite the steps taken to remove these secondary magnetizations, it is not possible to remove them completely in all cases. IRM probably is the largest source of this error. In rare cases, a specimen had to be discarded because of incomplete removal of secondary magnetization even at fields higher than a 400 mT peak alternating field. A study of the amount of dispersion due to unremoved secondary magnetization was performed using the best mean angular standard deviations. Localities were divided into two groups; (1) those that required no alternating field cleaning and (2) those that did. Localities with large dispersions due to physical rotations of the rocks were eliminated from this study. Only those outcrops in pahoehoe flows and massive outcrops in aa flows were used, a total of 94 localities.

The mean angular standard deviation for localities that required alternating field cleaning was insignificantly different at the 95 percent confidence level from those localities that did not. The dispersion due to secondary magnetization is thus effectively negligible compared to other sources.

The magnetization of most rocks probably is heterogeneous at the scale of the specimens measured. These heterogeneities can be a result of flow banding, vesiculation, differences in rate of cooling as a function of depth, for specimens collected at the original surface of a flow, or phase changes which have occurred in the rock at either high or low temperatures. As a test of the error due to heterogeneity, the NRM of two specimens from each of 25 cores was measured. Difference between each pair of measurements of the directions embodies the sample measurement error, core irregularity error and heterogeneity of magnetization over 1 in. distances. The cores for this study were picked for the uniformity of their shape; thus core irregularity error should be minimum. The mean angular difference between two specimens from each of 25 cores was found to be 1.60 deg, corresponding to an approximate median angular standard deviation of 1.13 deg. Removing the dispersion due to measurement from this figure leaves 1.06 deg of angular standard deviation due to heterogeneity of magnetization and core irregularity error combined.

Review of the known sources of error suggests that rotation of relatively small structural blocks at each sampling site is the principal cause of observed dispersion of measured direction of magnetization at most localities. Figure 4 is a histogram of the

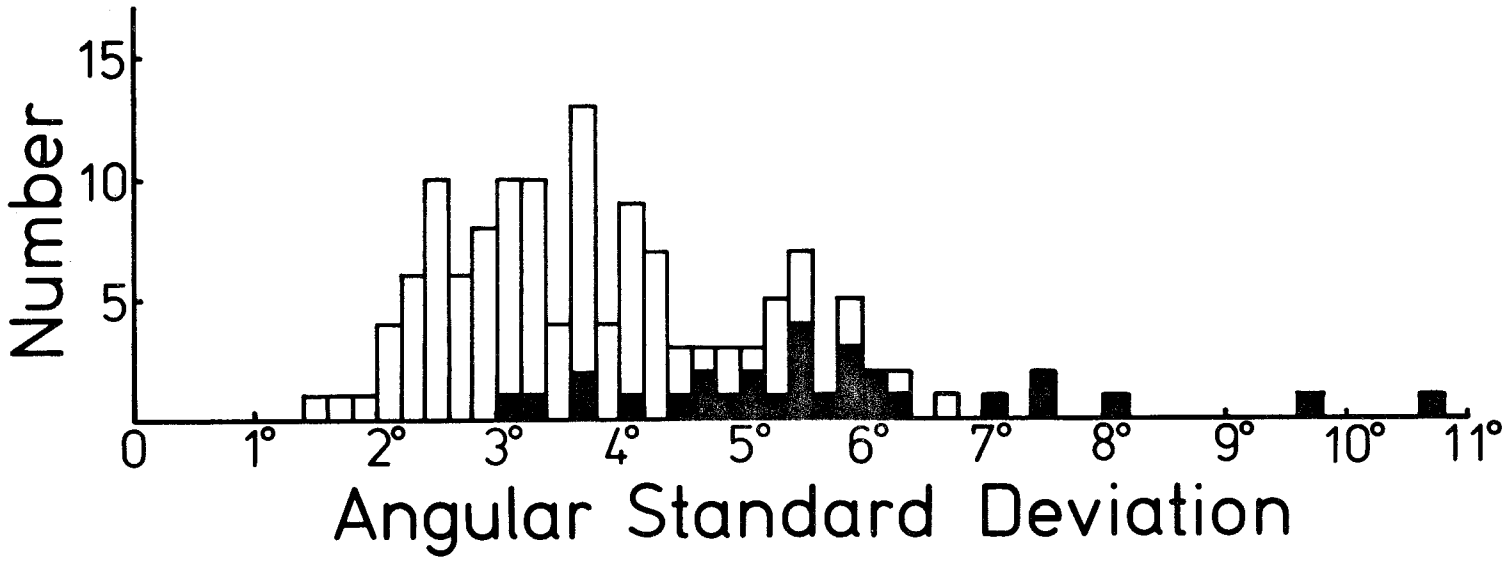

Fig. 4--Histogram of angular standard deviation in degrees for 135 localities sampled. Solid columns are for localities which from field relationships were expected to show more dispersion of directions because of possible structural rotation of small structural blocks.

distribution of angular standard deviation for 135 localities sampled in this study. The angular standard deviation for localities ranges from 1.47 deg to 10.79 deg, and the mean is 3.99 deg. The total angular variance of direction at a locality is the sum of the variances associated with each source of error. Squares of estimated mean angular standard deviation for each source of error other than rotation of small structural blocks are as follows: error of field orientation, 2.25 deg^2; error of laboratory measurement, 0.16 deg^2; magnetic inhomogeneity of rocks, 1.12 deg^2; unremoved components of secondary magnetization, 0 deg^2; large-scale structural tilt, 0.27 deg^2; and differences of magnetic anomaly between sites, 0.01 deg^2. The figure for angular variance due to error of field orientation contains variances due to errors of laboratory measurement and magnetic heterogeneity of the rocks as well, and it has been estimated to be between the combined variances from those sources and the lowest variances from sites from this study. Subtracting the sum of identifiable variances from the mean variance for localities of 15.92 deg^2 yields an unexplained variance of 13.39 deg^2 or an angular standard deviation of 3.66 deg. Most of the unexplained variance is probably attributable to rotations of small blocks.

Choice of sampling sites is the most critical factor in achieving high precision in estimation of paleodirections from Holocene volcanic rocks. On Figure 4, the black columns on the histogram are for localities on aa and block flows where the surface appears less coherent than at most other localities. The localities judged in the

field to have less coherence have a substantially higher mean angular standard deviation.

Present Regional Variation of the Geomagnetic Field

The broad geographic distribution of the localities studied requires that appropriate methods be used for comparison of the geomagnetic field at different localities. To do this the present geomagnetic field will be used to ascertain what these methods are and what limitations regarding comparisons exist. This tacitly assumes that the relative magnitudes of dipole and nondipole parts of the present geomagnetic field are representative of the past, and that the nondipole portion has always varied at a greater rate than the dipole part. The present declination at the ^{14}C dated localities ranges from 14 to 21.5 deg, and the inclination ranges from 62.5 to 70.5 deg. Virtual Geomagnetic Poles (VGPs) calculated for these localities, using the present field directions generated from the 1965.0 IGRF, deviate by as much as 1.4 deg from the mean and have a standard deviation of 0.7 deg. As calculation of a VGP embodies the explicit assumption that the observed field direction results from a geocentric dipolar field, the observed dispersion of VGPs arises from the nondipole components of the real geomagnetic field. The technique of calculating VGPs appears to be the best method of comparison for different localities despite the observed dispersion. It is desirable to evaluate the probable dispersion of the VGP in the past, as this past dispersion affects the precision of reconstruction of the secular variation history of the region under study.

Shuey and others (1970) investigated alternate methods for comparing or normalizing geomagnetic field directions from scattered localities. They showed that the VGP method is clearly superior to

the "axial dipole" method, in which correction is made only for differences in latitude between sites. In their study of the VGP method, a set of predicted declinations and inclinations for a given site were found which corresponded to the VGPs determined from observed declinations and inclinations at other sites lying short angular distances away. The distribution of predicted declinations and inclinations was then compared with the observed declination and inclination at the site. The analysis was performed at 132 given sites, on a grid between 50° N. and 50° S., using the 1965.0 International Geomagnetic Reference Field (IGRF) spherical harmonic coefficients. For a given angular separation between surrounding sites and grid sites, the angular standard deviation for the predicted directions of the field was found to be largest for separations from grid sites along north-south lines and smallest for separations along east-west lines. For separation along a given geographic azimuth, the angular errors of predicted declination and inclination were found to be linearly proportional to the angular separation between surrounding sites and grid sites. The average angular standard deviation of predicted field direction for north-south separation is 0.34 deg per degree of separation and for east-west separation is 0.23 deg per degree of separation. Dispersions of predicted declination and inclination were found to be higher in the southern hemisphere than in the northern hemisphere.

In order to examine the dispersion of VGPs and also to study regional gradients of intensity of the nondipole field, three broad regions in the northern hemisphere have been selected in this paper

for further analysis. Each region is 60 deg by 60 deg and is centered on the Fortieth Parallel. Centers for the three regions were chosen at 230° E. longitude (a point in the Pacific), where the VGP position varies slowly as a function of site longitude (Fig. 5), at 90° E. longitude (a point in Asia), where the VGP varies at an intermediate rate, and at 345° E. longitude (a point in the Atlantic), where the VGP varies rapidly with site longitude. These regions overlap slightly at some of their northern corners.

The angular difference between the total field and the dipole component of the geomagnetic field was calculated from the IGRF at 5 deg intervals of latitude and longitude for each region selected. Intensity of the nondipole component of the geomagnetic field was also calculated for the same positions. In most of the Pacific region the angular difference between the total field and the dipole component does not exceed 3 deg (Fig. 6a); intensity of the nondipole component generally lies between 1000 μT and 6000 μT (Fig. 6b) and, in most cases, is less than 10 percent of the total field. Variation of VGP position with site longitude is small in this region primarily because the nondipole component of the geomagnetic field is small. Where the nondipole component of the geomagnetic field is larger, as in the Asian region (Fig. 6d) and the Atlantic region (Fig. 6f), VGPs are more widely dispersed causing larger angular differences between local field directions and those calculated from VGPs at the center of these regions (Fig. 7). In these latter regions the intensity of the nondipole component generally lies between 7000 μT and 15,000 μT. The angular difference between the total

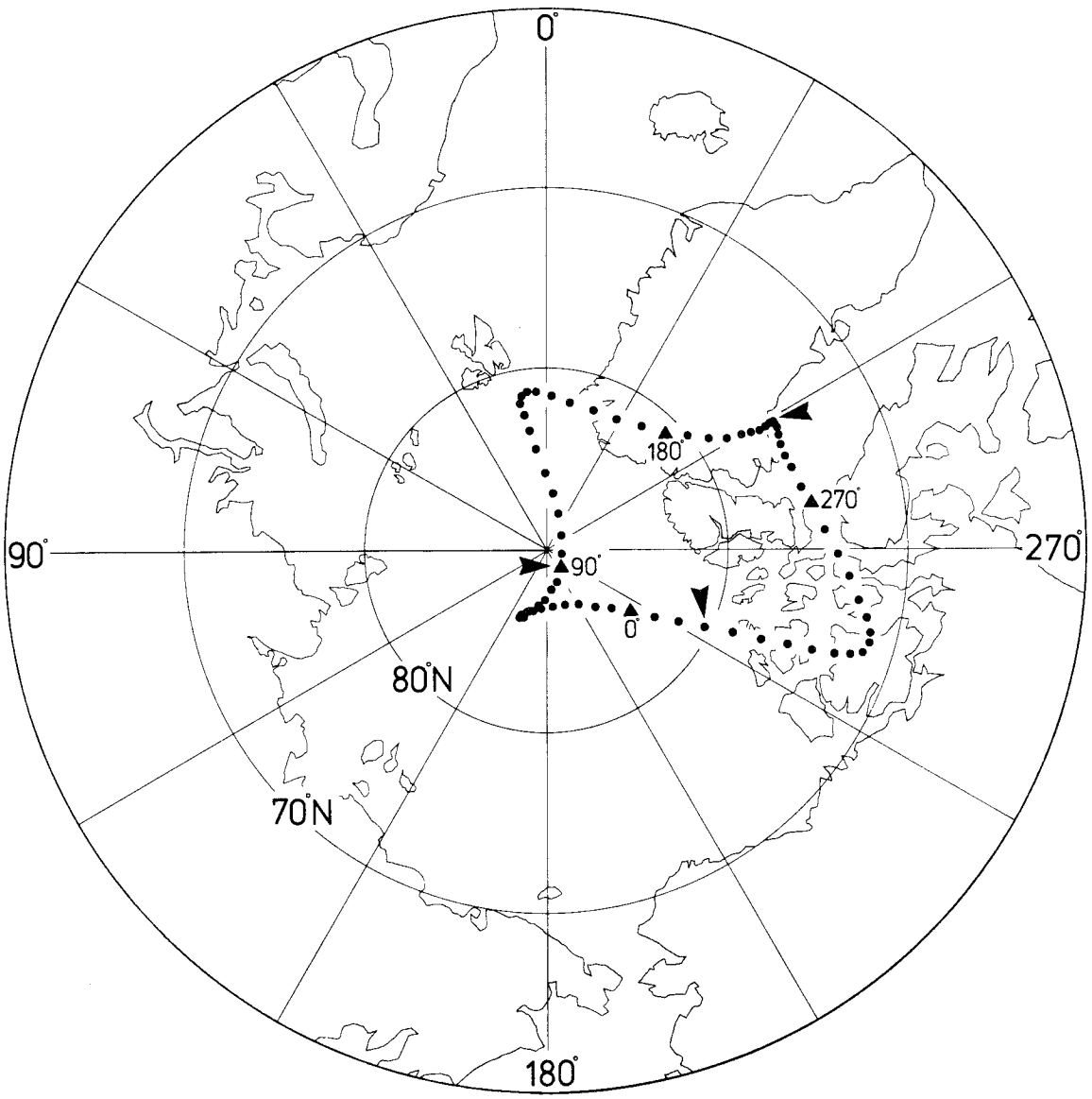

Fig. 5--Equal area projection of north polar area showing Virtual Geomagnetic Poles (VGPs) calculated from the 1965.0 IGRF at sites on the Fortieth Parallel at intervals of 5 deg longitude. VGPs for positions at 0°, 90°, 180°, and 270° E. longitude are shown with solid triangles. VGPs at centers of regions studied are marked by arrows.

Fig. 6--Maps of three broad regions in the northern hemisphere showing angular difference between total field and the dipole component of the geomagnetic field (a, c, and e), and the intensity of the nondipole component of the geomagnetic field (b, d, and f). These maps are based on the 1965.0 International Geomagnetic Reference Field. Maps a and b are equal-area projections from the Pacific region at 40° N., 230° E.; c and d are from the Asian region at 40° N., 90° E.; and e and f are from the Atlantic region at 40° N., 345° E.

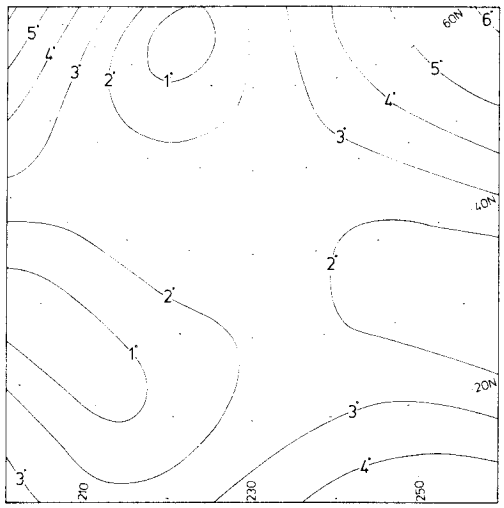

6a

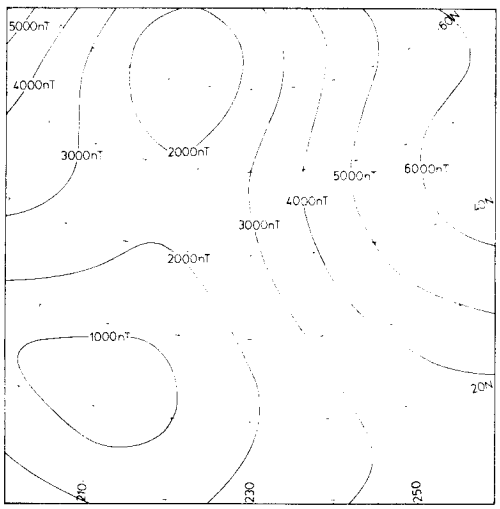

6b

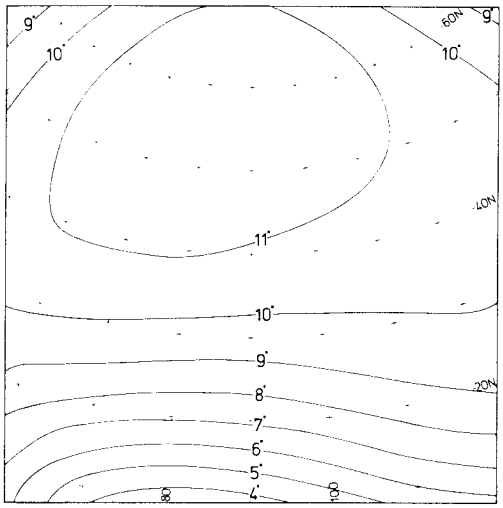

6c

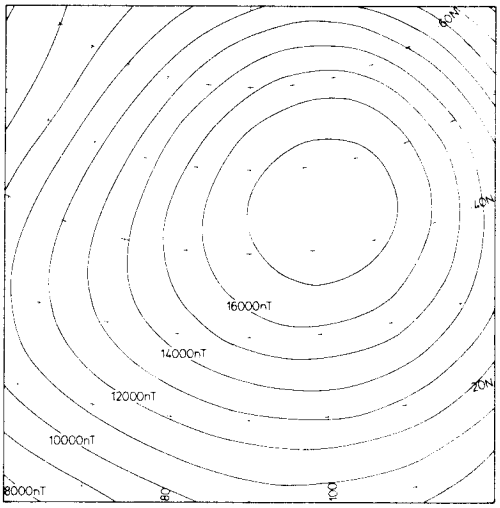

6d

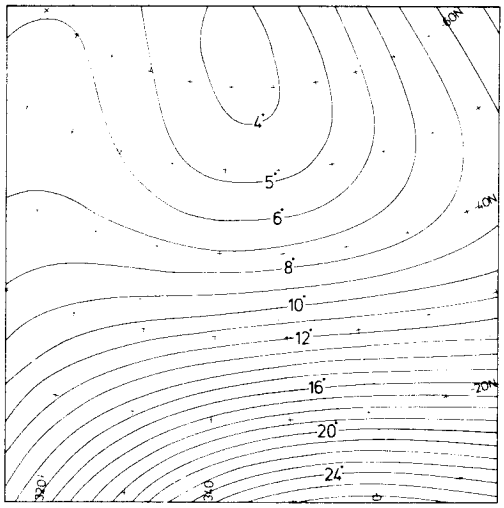

6e

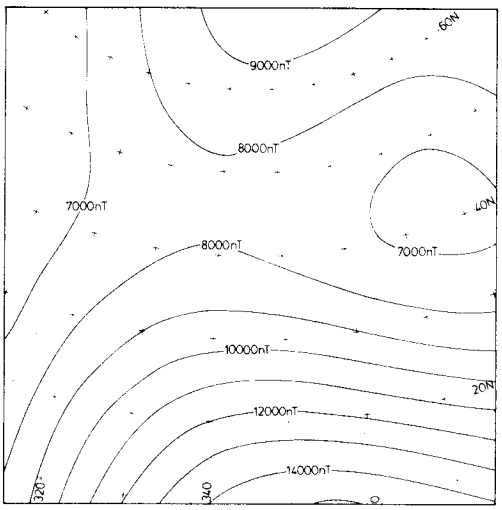

6f

Fig. 7--Maps of three broad regions in the northern hemisphere showing angular difference between local field directions from the 1965.0 IGRF and the field directions calculated from the VGP corresponding to the field direction at the center of each region (a, c, and e) and the vector magnitude difference between the total field vector at each point and the total field vector calculated from the VGP at the center of each region (b, d, and f). Maps a and b are equal-area projections from the Pacific region at 40° N., 230° E.; c and d are from the Asian region at 40° N., 90° E.; and e and f are from the Atlantic region at 40° N., 345° E.

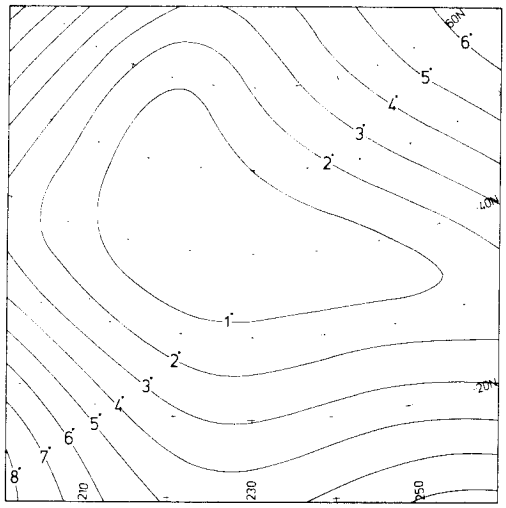

7a

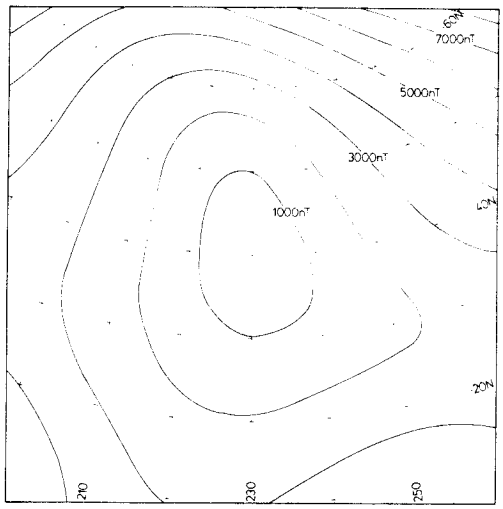

7b

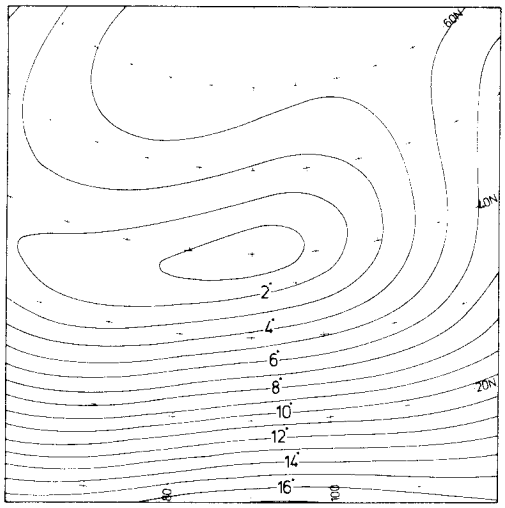

7c

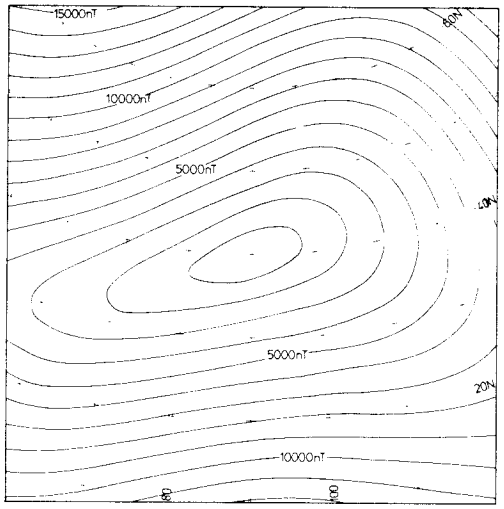

7d

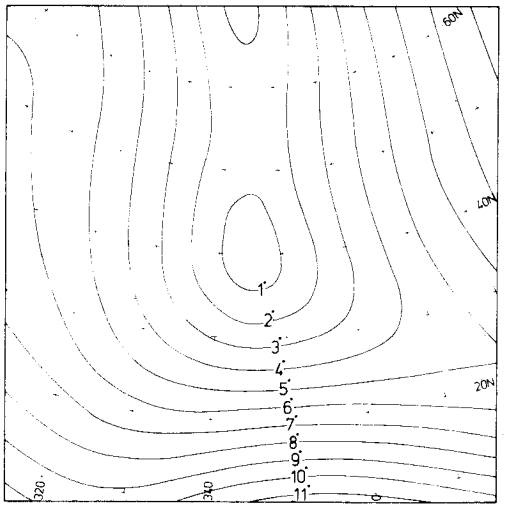

7e

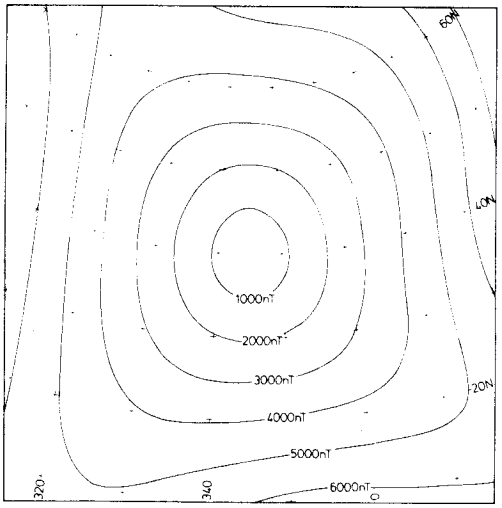

7f

field and the dipole component is 4 to 11 deg in the Asian region (Fig. 6c) and 4 to 26 deg in the Atlantic region (Fig. 6e). The large angular differences observed in the Asian and Atlantic regions reflect the fact that major foci of the nondipole field lie within or close to these regions.

In this paper field directions from different localities will be compared directly. It is desirable to know, therefore, the limiting distance at which dispersion of field directions resulting from the nondipole component of the field, would be expected to exceed the average confidence limits of the paleomagnetic field directions for individual localities. For each of the three regions studied, the angular difference between the actual field direction and the direction derived from the VGP corresponding to the field direction at the center of the region was found at each interval of 2 deg of latitude and longitude. In the Pacific region, with low average nondipole component, the angular difference of observed field directions from that calculated from the VGP for the center of the region is less than 1 deg over an irregular area extending 50 deg in longitude and 20 deg in latitude (Fig. 7a). In the Asian region the angular difference of observed field directions from that calculated from the VGP for the center is less than 1 deg over an elliptical area of 20 deg of longitude by 5 deg of latitude and less than 2 deg over an area extending 50 deg in longitude and about 10 deg in latitude (Fig. 7c). In the Atlantic region the angular difference of field directions is less than 1 deg over an area of about 10 deg of longitude by 10 deg of latitude and is less than 2 deg over an

area extending 20 deg in longitude and more than 30 deg in latitude (Fig. 7e). The Asian and Atlantic regions represent worst cases for positions near 40 deg latitude in the northern hemisphere.

The gradient of the field direction deviation from that at the center of each region was determined by averaging the deviation computed at 2 deg latitude-longitude grid points falling in successive rings around the center. The innermost area averaged extends to a 5 deg distance from the center; beyond 5 deg each ring has a width of 2.5 deg. At the boundaries of each region the last complete ring extends to 30 deg. Each ring was divided into four segments of 90 deg arc length; the arcs are bounded by lines extending northeast-southwest and northwest-southeast from the center of the region. Mean field direction deviation was found for each ring segment and the gradient of mean field direction deviation in the north, east, south and west directions out to 30 deg was obtained for the Pacific, Asian, and Atlantic regions (Fig. 8).

The angular difference between field directions calculated through the VGP formula from a centrally located reference field and those actually observed tends to be linear out to angular distances of 30 deg from the reference site. Separations between localities in north-south directions lead to larger angular differences than those in east-west directions. Using the standard deviation angular distance of localities from the mean locality of this study, 4.8 deg, one could project typical errors introduced. At this angular distance, 0.5 to 1.5 deg of error would be introduced by using a VGP model to predict field directions from an adjacent dated control locality.

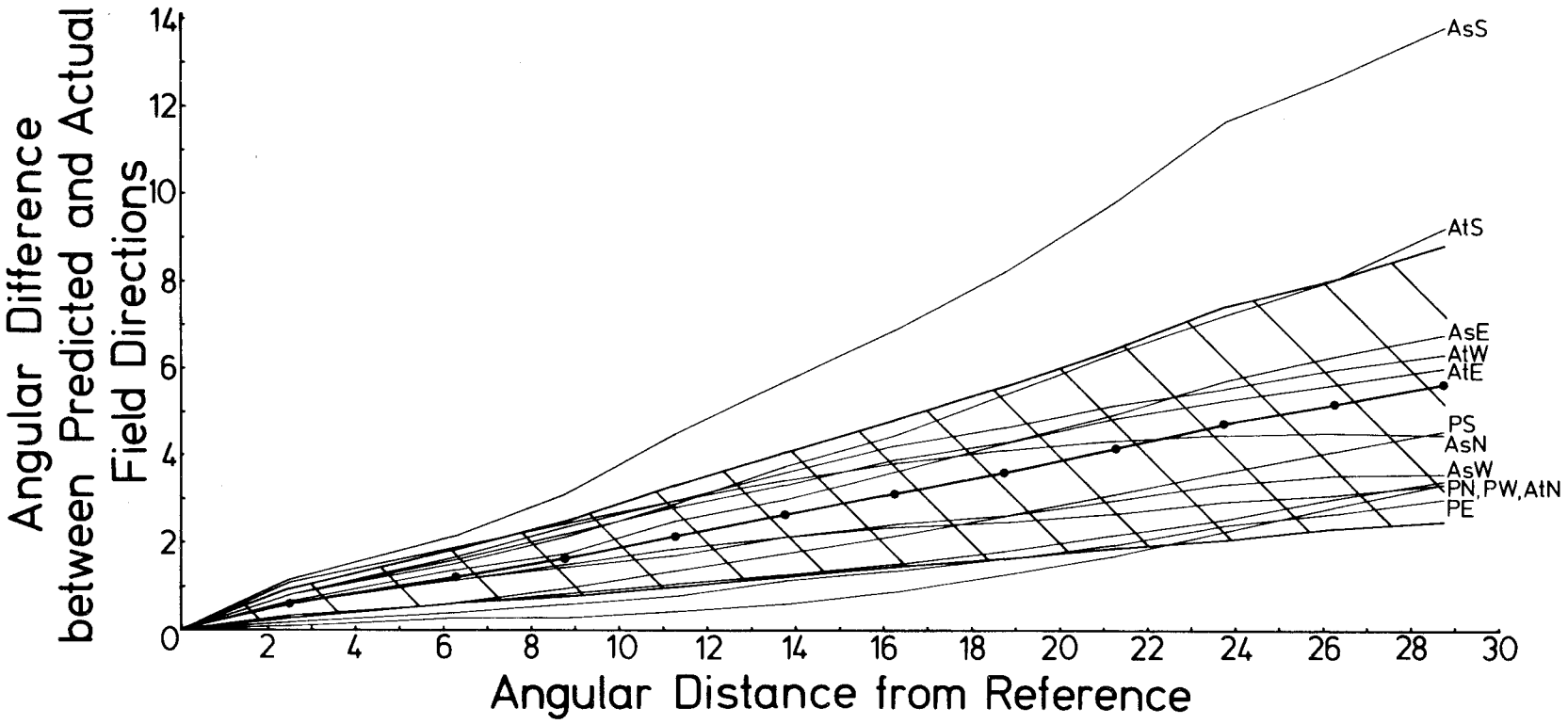

Fig. 8--Deviation of field directions as a function of angular distance for three test points in the northern hemisphere. Test points are on the Fortieth Parallel at 90°, 230°, and 345° E. longitude (Asian, Pacific and Atlantic regions). Deviation of field directions as a function of distance is shown for the four cardinal directions for each test point. AsN, AsE, AsS, and AsW, are deviations of field directions to the north, east, south, and west of the Asian test point; PN, PE, PS, and PW are for corresponding directions from the Pacific test point; and AtN, AtE, AtS, and AtW are for the Atlantic test point. Average deviation of field directions for all four directions from all three of the test points is shown as the heavy line with dots. Limits of cross-hatched area are at one standard deviation from the mean.

This error is smaller than the alpha 95s routinely produced in this study and would not affect the accuracy of secular variation age determinations. For maximum angular separations, between the mean locality and the localities in northern Arizona, 8.5 deg, the error in predicted field directions could be as much as 3 deg for the very worst cases. This would affect interpretation of a secular variation path using VGPs from widely separated localities. Considering the limited number of dated flows available, the localities in Arizona need to be included. If one desired an extremely detailed and accurate record of secular variation however, the above study of field direction errors implies that the Pacific Northwest should be compiled separately from the Southwest.

In this study, field intensities will be compared to compile a record of secular variation of intensity for the western United States. Because of this it is desirable to know the limiting distance at which gradients in the nondipole field introduce significant errors in a compilation of intensity determinations at individual localities. For each of the three regions studied, the magnitude of the difference between the field vector calculated from the Virtual Dipole Moment (VDM) at the center of the region and the field vector at each interval of 2 deg of latitude and longitude was calculated. In the Pacific region the magnitude of the vector difference is less than 1000 μT out to angular distances of 10 deg and less than 2000 μT out to distances of 15 deg or more (Fig. 7b). In the Asian region, the magnitude of the vector difference is less than 1000 μT over an elliptical area of 3 deg of latitude by 7 deg of longitude and less

than 2000 μT over an area of 6 deg of latitude by 14 deg of longitude (Fig. 7d). In the Atlantic region the magnitude of the vector difference is less than 1000 μT over a circular area extending 6 deg of longitude and 5 deg of latitude and less than 2000 μT over an area 12 deg of longitude by 11 deg of latitude (Fig. 7f). Once again the Atlantic, and in particular the Asian, regions represent worst cases for positions near 40° N.

In a manner identical to the analysis of the field directions, gradients have been computed from the center of each test region in north, south, east and west directions and are shown in Figure 9. Gradients of the magnitude of vector difference are linear to 20 deg distances and mostly linear to 30 deg distances. The Asian test region produces the four steepest gradients, which is not surprising considering the fact that the center of the test region is near the great Siberian nondipole focus. The mean magnitude of vector difference at a 4.8 deg angular distance from the center of each region is 1050 μT with one standard deviation of that value from 600 μT to 1450 μT. For the large angular distances between the mean locality and the localities in Arizona, the error in the magnitude of the field vector would be as much as 2400 μT when nondipole gradients were steepest. This error is only about 5 percent of the intensity of the present field near the Fortieth Parallel, or as will be shown, of the ancient intensities described in chapter 4. As this error is a vector quantity expressed as a difference between the reference and observed intensity vectors, the actual error in paleointensity determination, a simple difference in the vector magnitudes, would

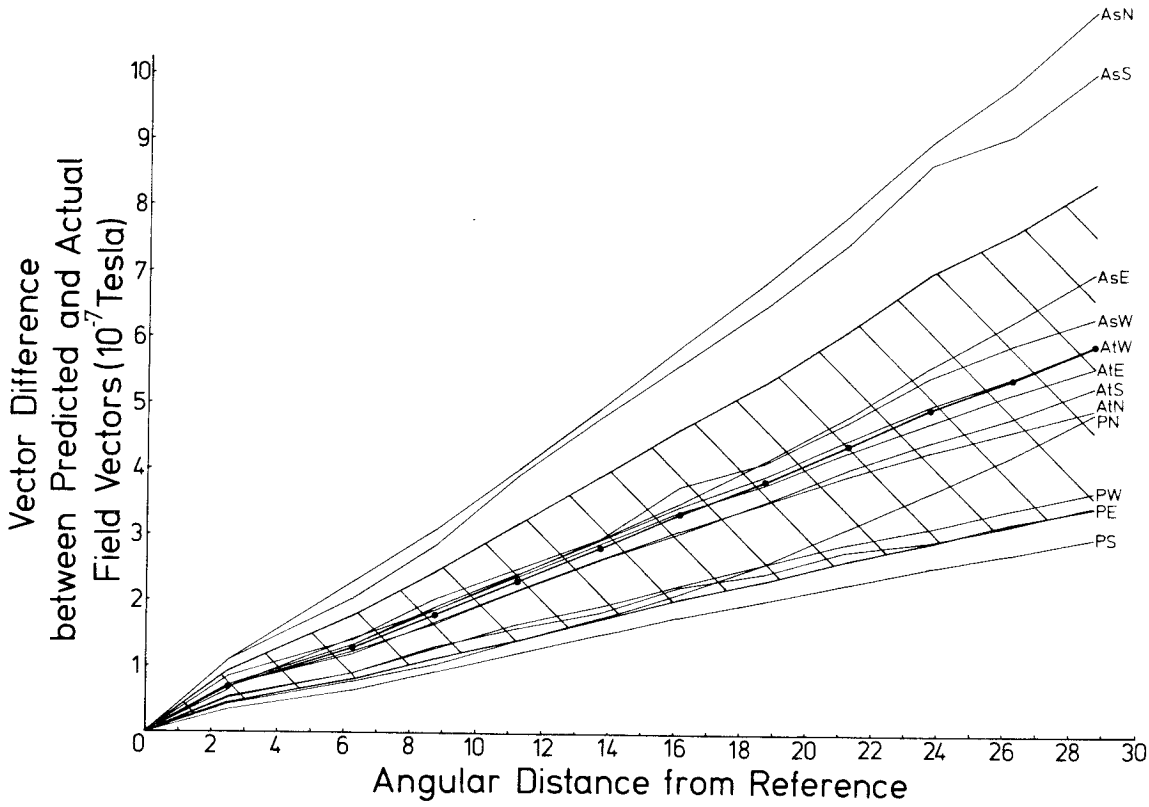

Fig. 9--Vector magnitude difference as a function of angular distance for three test points in the northern hemisphere. Location of test points is identical to those illustrated in Figure 8. The vector magnitude difference as a function of distance is shown for the four cardinal directions for each test point. Notation for test point and direction are identical to Figure 8. Average vector magnitude difference for all four directions from all three of the test points is shown as the heavy line with dots. Limits of cross-hatched area are at one standard deviation from the mean.

always be less than or equal to the error suggested from this study.

The overall impression from the above studies on field direction and intensity is that the errors introduced in the use of VGP and VDM models for localities that are scattered over short angular distances, is not great, providing angular distances of 10 deg between localities are not exceeded. Even at distances shorter than this, errors, particularly in field directions, can exceed typical alpha 95 values. Given the small number of dated localities used in this study, all must be considered together. In the future when more data are available the secular variation records of areas as close as the Pacific Northwest and the Southwest should probably be compiled separately to minimize these possible errors.

Observed Secular Variation of Field Direction from Holocene Volcanic Rocks

Directions of magnetization of the dated Holocene volcanic rocks in the western United States provide a framework for reconstructing the secular variation history of the past 7000 years. Table 1 lists all the basic data for each of the dated lava flows and pyroclastic deposits. Conversion of the ^{14}C dates to absolute ages in Table 1 was made through the use of published correction tables based on ^{14}C measurements of segments of dendrochronologically dated wood (Damon, Long, and Wallick, 1972). These tables represent one of several possible conversions available, but are thought to be the best (S.W. Robinson, pers. commun.). Details on the geologic setting and references which provide the basic age data for each locality are given in Appendix 1. The magnetic directional data range from fair to excellent. For the majority of localities, alpha 95 is less than 2 deg. This high precision has been achieved largely because of the young age of the volcanic rocks and the care invested in the field and laboratory work.

To compare the localities listed in Table 1, projections of the north polar area have been prepared, dividing the data set into several time intervals for clarity of presentation. Figure 10 shows all VGP data for units younger than 1500 years B.P. (0 B.P. is A.D. 1950). Each VGP is surrounded by its oval of 95 percent confidence. The present pole position has been calculated from the present declination and inclination at the position of the mean locality for this study. Data from two other studies have been included in this

Table 1. Paleodirectional data for dated Holocene lava flows and volcanic deposits for which reliable directions of magnetization have been obtained.

	LLA, deg	LLO, deg	H, mT	n	D, deg	I, deg	k	α95 deg	PLA, deg	PLO, deg	Age Carbon 14	Absolute Age
1. Ice Spring Field, Black Rock Desert, Utah	38.93	247.49	30	17	352.13	63.69	390	1.81	81.38	207.57	660±170	1290AD
2. Sunset Crater, San Francisco Volcanic Field, Arizona	35.36	248.50	40	22	350.06	58.71	398	1.55	81.12	188.81	---	1250AD
3. Bonito Flow, San Francisco Volcanic Field, Arizona	35.38	248.48	--	29	346.37	58.11	499	1.20	78.61	179.97	---	1230AD
4. Gyp Crater, San Francisco Volcanic Field, Arizona	35.35	248.54	--	21	345.01	61.42	407	1.58	76.33	194.82	---	1190AD
5. Vent 512, San Francisco Volcanic Field, Arizona	35.33	248.58	--	22	347.45	62.19	221	2.09	77.37	202.43	---	1190AD
6. Kana-a Flow, San Francisco Volcanic Field, Arizona	35.39	248.57	--	19	353.68	65.05	406	1.67	77.40	228.45	---	1150AD
7. West Belknap Flow, McKenzie Pass, Oregon	44.32	238.01	--	20	359.77	52.11	349	1.75	78.40	58.96	1400±100 1590±160	476AD
8. South Belknap Cone Flow, McKenzie Pass, Oregon	44.24	238.14	--	19	0.22	44.74	392	1.70	72.12	57.51	1775±400	173AD
9. Cave Basalt Flow, Mt. Saint Helens, Washington	46.11	237.79	--	12	344.37	60.58	462	2.02	77.87	131.40	1860±250* 1925±95	2AD
10. Craters of the Moon Flow, near Rattlesnake Butte, Idaho	43.30	246.68	--	24	351.64	63.92	409	1.47	83.61	180.75	2110±90 2050±80	176BC
11. Watchman Flow, Craters of the Moon, Idaho	43.39	246.51	--	13	350.93	64.40	489	1.88	82.97	183.43	2140±60	249BC
12. Trenchmortar Flat Flow, Craters of the Moon, Idaho	43.41	246.47	--	12	357.14	64.92	352	2.32	85.98	217.34	2235±80*	363BC
13. Wapi Field, Snake River Plain, Idaho	42.85	246.83	--	25	13.18	62.77	991	0.92	80.36	324.42	2270±50	404BC
14. Kings Bowl Field, Snake River Plain, Idaho	42.96	246.78	--	24	13.17	61.92	906	0.98	80.38	331.19	2130±130* 2090±470 2360±150	373BC
15. South Puyallup Block and Bomb Flow, Mt. Rainier, Wash.	46.81	238.10	--	12	22.42	51.29	223	2.92	67.33	1.04	2350±250	499BC
16. Four in One Flow, McKenzie Pass, Oregon	44.21	238.19	--	11	10.36	72.48	118	4.23*	75.04	260.02	2550±165	750BC
17. Yapoah Flow, McKenzie Pass Oregon	44.26	238.20	--	19	14.01	61.41	506	1.49	79.68	332.97	2550±165 to 2883±175	---
18. Little Belknap Flow, McKenzie Pass, Oregon	44.26	238.18	--	24	7.06	44.16	422	1.44	70.77	38.56	2883±175	1169BC
19. Clear Lake Flow, Sand Mountain, Oregon	44.36	238.01	10	24	6.26	49.47	194	2.13	75.11	36.53	2705±200 2990±300 3200±220	1279BC
20. Blue Lake Crater, Santiam Pass, Oregon	44.41	238.23	--	15	356.46	68.12	461	1.79	82.79	220.29	3440±250	1881BC
21. Hackleman Creek Flow, Sand Mountain, Oregon	44.40	238.00	--	12	2.56	50.25	1323	1.19	76.46	48.60	3850±215	2409BC
22. Hell's Half Acre Field, Snake River Plain, Idaho	43.40	247.55	--	24	2.11	65.16	579	1.23	85.91	268.07	4100±200*	2728BC
23. Dotsero Flow, Dotsero, Colorado	39.64	252.95	20	12	352.65	59.38	464	2.02	84.34	170.87	4150±300	2792BC
24. Lava Cascade Flow, NW Rift, Newberry Crater, Oregon	43.79	238.71	--	24	352.57	55.28	69	3.60	80.20	96.75	5800±100	4680BC

Table 1. Continued

	LLA, deg	LLO, deg	H, mT	n	D, deg	I, deg	k	α95 deg	PLA, deg	PLO, deg	Age Carbon 14	Absolute Age
25. Sugar Pine Butte Flow, NW Rift, Newberry Crater, Oregon	43.83	238.64	30	12	353.71	58.21	98	4.41	83.17	104.49	5870±60	4751BC
26. Forest Road Flow, NW Rift, Newberry Crater, Oregon	43.82	238.71	--	20	353.93	51.80	574	1.36	77.66	83.40	5960±100	4840BC
27. Surveyor Flow, Newberry Crater, Oregon	43.64	238.75	--	24	354.09	53.28	169	2.28	79.18	85.82	6080±100	4958BC
28. North Summit Flow, NW Rift, Newberry Crater, Oregon	43.75	238.76	--	13	355.30	54.93	119	3.81	80.96	83.89	6090±60	4968BC
29. Gasline Flow, NW Rift, Newberry Crater, Oregon	43.91	238.65	--	12	343.10	57.10	367	2.27	76.11	130.54	6150±65*	5026BC
30. Lava Butte Flow, NW Rift, Newberry Crater, Oregon	43.92	238.62	--	22	351.49	58.35	245	1.98	81.98	114.11	6160±65	5036BC
31. Lava Cast Forest Flow, NW Rift, Newberry Crater, Oregon	43.82	238.71	--	21	352.88	52.46	188	2.32	77.88	88.37	6150±210 6380±130	5137BC
32. Crater Lake Ash Flow Deposit, Crater Lake, Oregon	42.88	237.91	--	41	354.73	73.01	575	0.93	73.97	227.93	6640±250*	--
33. Parkdale Flow, Mt. Hood, Oregon	45.49	238.37	10	23	23.47	61.23	269	1.85	72.86	330.63	6890±130	--
34. Cerro Grande Lava Field, Snake River Plain, Idaho	43.35	247.20	10	22	355.88	57.01	663	1.21	83.45	97.18	10780±300*	--
35. Northeast Sunset Flow, Craters of the Moon, Idaho	43.53	246.50	20	18	21.08	59.69	1012	1.09	74.10	340.07	11120±300*	--
36. North Robbers Flow, Snake River Plain, Idaho	43.38	247.02	30	17	339.39	47.14	237	2.32	67.62	121.51	11940±300*	--

LLA and LLO are north latitude and east longitude of sampling localities. H is peak alternating demagnetizing field. n is number of oriented samples. D and I are declination eastward and inclination downward of mean remanent magnetization. Parameters k and α95 are precision parameter and radius of 95% confidence cone. PLA and PLO are north latitude and east longitude of virtual geomagnetic pole. Carbon 14 age is that of standard 5568 year half-life with analytical standard deviation. Absolute age was determined from the conversion tables of Damon et al.(1972), using midpoint of carbon 14 age. Asterisks (*) denote information explained in full in Appendix 1.

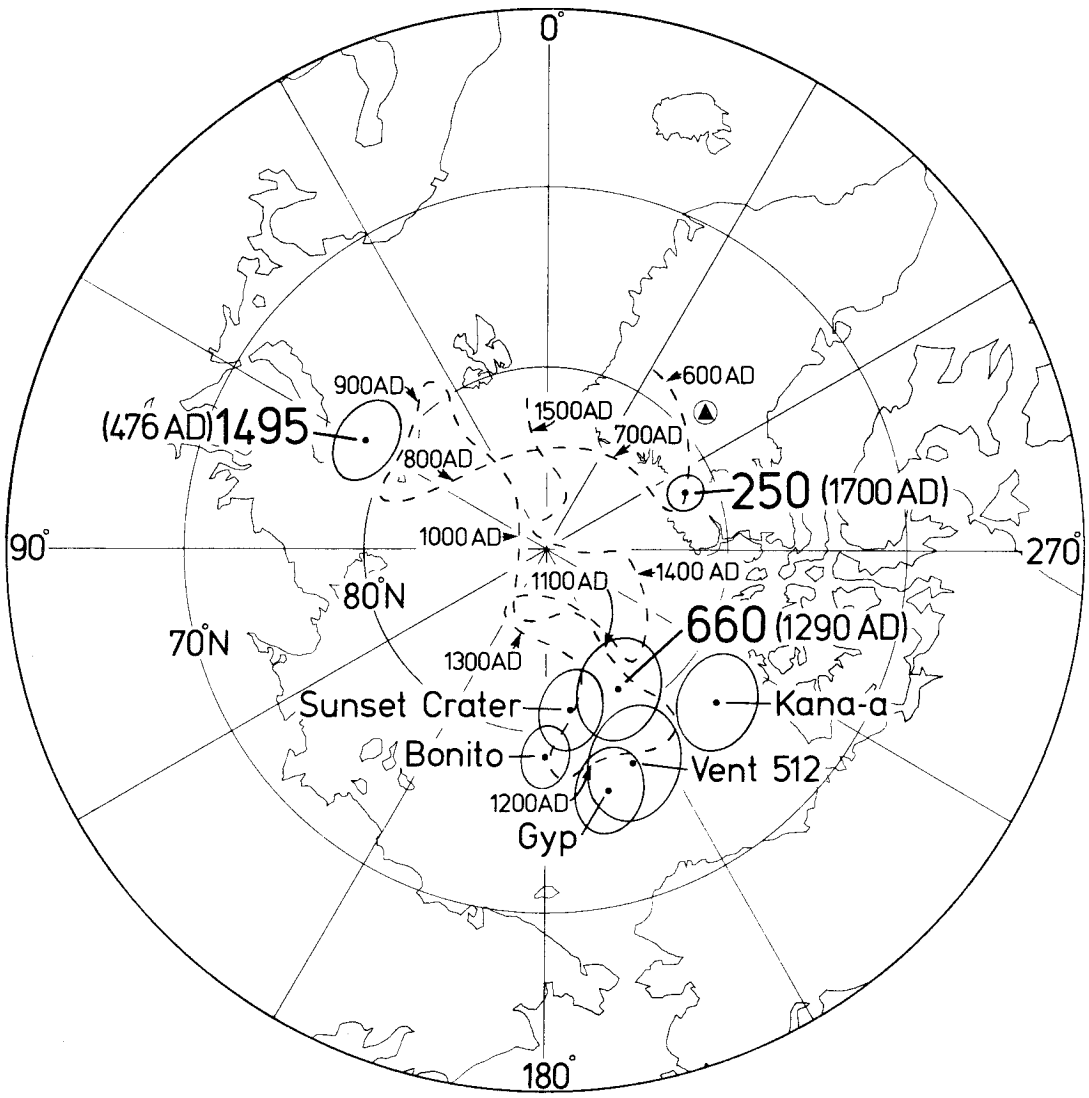

Fig. 10--Equal-area projection of north polar area showing virtual geomagnetic poles and ovals of 95 percent confidence for all dated volcanic units younger than 1500 years B.P. Large dark numbers indicate ages in years B.P. Names denote volcanic units in San Francisco Volcanic Field, Arizona. Present geomagnetic pole position for mean site location is shown by dark triangle within a circle. The dashed line with absolute age tick marks is the VGP path from DuBois (1974). The 250 years B.P. (A.D. 1700) point is from the Aiyansh Flow in British Columbia reported by Symons (1975).

figure. The VGP for the Aiyansh lava flow of British Columbia, dated at 250 ± 130 years B.P. (Symons, 1975), has been shown to illustrate the general VGP path for the western United States near the end of this period. It is reasonable to expect the mean VGP for the western United States at 250 years B.P. to be within 3 to 4 deg of the Aiyansh VGP, which was obtained from a locality at 55 deg latitude. The dashed line with tick marks indicating absolute ages is from the work of DuBois (1974) on dendrochronologically dated hearths in the southwestern United States and shows the VGP path from A.D. 600 to A.D. 1500. The data supporting this VGP path have not been published, but for reasons to be discussed, it is believed that DuBois' path is reliable. Sternberg and others (1978), in a partial replication of DuBois' work, have found no discrepancies between the data sets. In particular, the age control available through dendrochronology and ceramic artifact correlation is excellent. DuBois' data span a period during which the Pueblo cultures of southwestern United States flourished. The overall character of DuBois' record is very similar to the longest observatory records available.

The data from the San Francisco Volcanic Field, Arizona, require some explanation. An extensive blanket of ash was produced by the eruption of the Sunset Crater cinder cone during the period of occupation of the region by the prehistoric Sinagua Indians (Colton, 1932, 1937, 1945). From dendrochronological dating of pit houses buried by the ash and from the first appearance of Sunset Red pottery, which contains the ash as temper, Colton (1945) dated the first major eruption between A.D. 1046 and A.D. 1069. Smiley (1958) inferred

that a major eruption occurred between the growing seasons of 1064 and 1065 from the time of beginning of a long series of compressed rings in pine beams recovered from the Wupatki pueblo constructed after the main ash eruption. Another eruption postdates the growing season of A.D. 1067 (Breternitz, 1967). Other eruptions may have followed for a period of several decades as suggested by tree ring growth anomalies from beams at Wupatki and other ruins. The Kana-a lava flow was next erupted; it flowed over the earlier extensive ash blankets and was partly buried beneath a younger more restricted ash deposit. Still younger oxidized deposits of cinders and bombs were then laid down around Gyp Crater and Vent 512. The Bonito lava flow erupted from the base of Sunset Crater after most of the pyroclastic activity. The youngest unit in the eruptive sequence is a deposit of lightly welded cinders and bombs that form the rim of the Sunset Crater cone.

Different units within the Sunset eruptive sequence have different directions of magnetization. As may be seen from Figure 10, the VGPs from these units fall on or adjacent to DuBois' path for the period between A.D. 1100 and A.D. 1300. No direction has been obtained for the major ash blanket, but a lava flow from Vent 512, which underlies the extensive ash from Sunset Crater, might have formed close to A.D. 1064. The thick cover of later ash deposits has prevented location of a suitable outcrop for paleomagnetic sampling of this flow. Ages have been assigned in Table 1 to the various units sampled in the Sunset Crater eruptive sequence on the basis of

the fit of their VGPs to the DuBois curve. An eruptive history lasting about 200 years appears to be indicated for Sunset Crater.

Figure 11 shows VGPs for the interval of time 3000 to 1500 years B.P. For this time interval all VGP data are from the Pacific Northwest, so error due to geographic dispersion of localities should be small. Between the separate VGPs, arrows have been added which show the generalized time sequence between known positions. The overall motion of the VGP with time follows a clockwise loop, with more erratic motion at approximately 2500 years B.P. Given the complexity of motion of the VGP indicated by DuBois' record in the most recent 1500-year time period, much more VGP movement could have occurred in the time interval of Figure 11 that is not represented by the directions measured in the dated lavas. As drawn in Figure 11, the VGP for the South Puyallup Block and Bomb Flow, dated at 2350 years B.P., suggests a secular variation date of approximately 2750 years. If the 2350 B.P. age for the South Puyallup Block and Bomb Flow is correct, rapid VGP motion is required between 2550 and 2245 B.P. Another interpretation would put the position of the VGP for 2350 years B.P. between the positions of VGPs for the Four-in-One Flow at 2550 years B.P. and the King's Bowl Flow at 2245 years B.P. in time. This would be in better agreement with the ^{14}C age information, but require rapid steepening and shallowing of field directions. The former interpretation was chosen to simplify the VGP path, but to resolve the ambiguity of choice, more information is critically needed. The remainder of the VGP path is fairly easy to interpret without invoking rapid changes in rate and direction of motion.

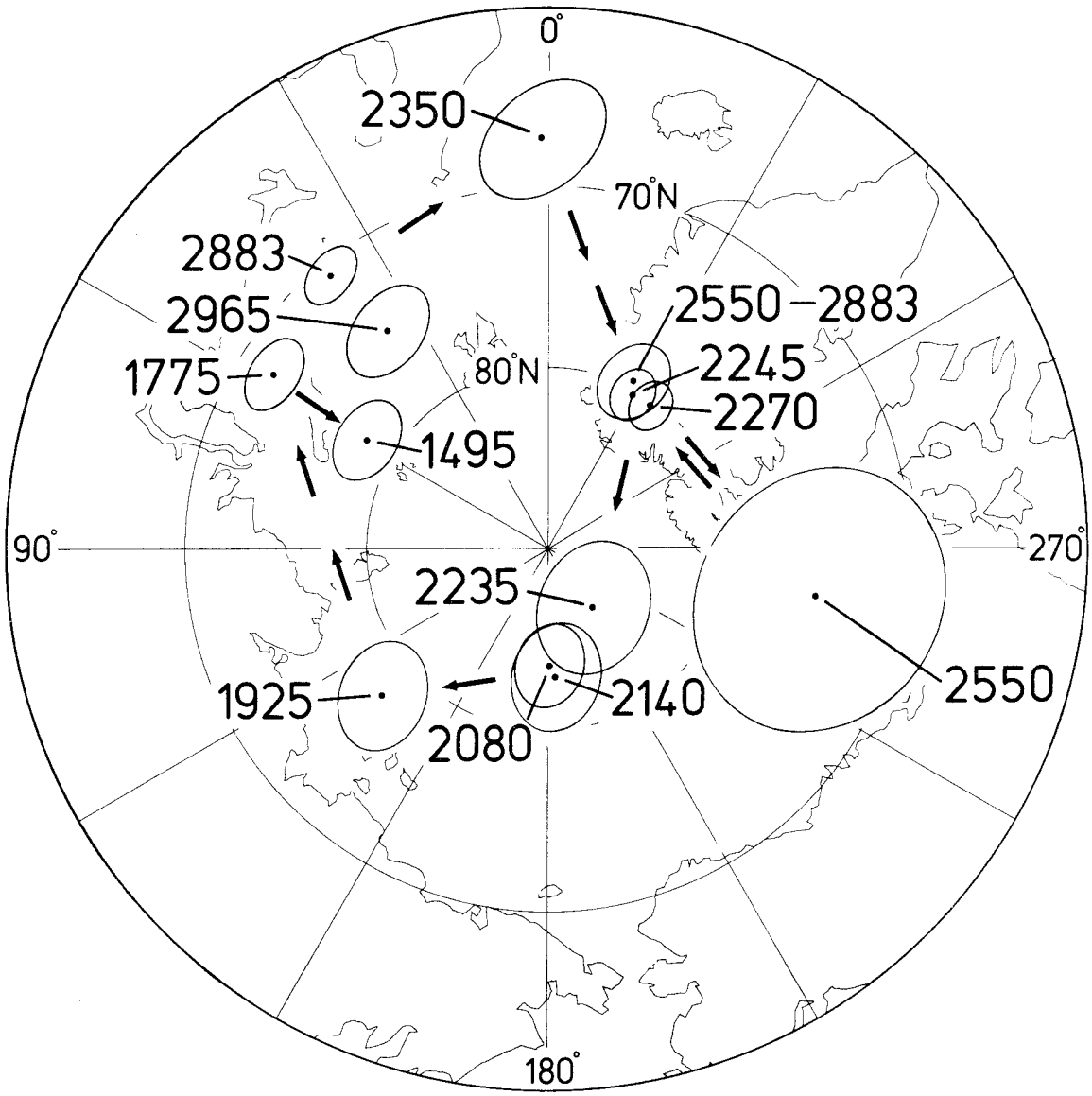

Fig. 11--Equal-area projection of north polar area showing VGPs and oval of 95 percent confidence for all dated volcanic units between 3000 and 1500 years B.P. Large dark numbers indicate ages in years B.P. Arrows indicate generalized time sequence between VGP positions.

VGPs for the interval of time 4150 to 2900 years B.P. are shown in Figure 12. Here the small number of pole positions make interpretation of the VGP path with time uncertain. The reconstruction presented has a back and forth motion, but time gaps of 450, 410 and 250 years at different points, allow the possibility of far more complicated motions than those shown.

VGPs for the time interval 6900 to 5800 years B.P. are shown in Figure 13. Again time gaps of 250 and approximately 500 years allow more complicated VGP motions than can presently be shown. The grouping of VGP data for the Newberry Crater area presents a problem in interpretation of the VGP path using the ^{14}C control alone. The ^{14}C ages indicate that the flows span an interval of 350 to 580 years. Yet the grouping of the VGPs suggests, by analogy to DuBois' curve, that the total span of time may be less, approximately 100 to 200 years.

Part of this age discrepancy at Newberry Crater can be explained by errors in applying the ^{14}C dates to the lava flows, resulting from the large diameter of the pine trees around which tree molds were formed and preserved. To allow retrieval of the charcoal for dating, tree molds must be of sufficient diameter to allow access for a person, usually 2 ft or more. A Ponderosa pine tree that large can be 200 years in age or older. Charcoal from the interior of a tree will yield a date for its youth rather than its death. The necessity of collecting charcoal from the bottom of a tree mold makes it impossible to know whether the charcoal came from the interior or exterior of the tree trunk. Hence, some of the dates from the Newberry Crater area are probably "old," relative to the actual

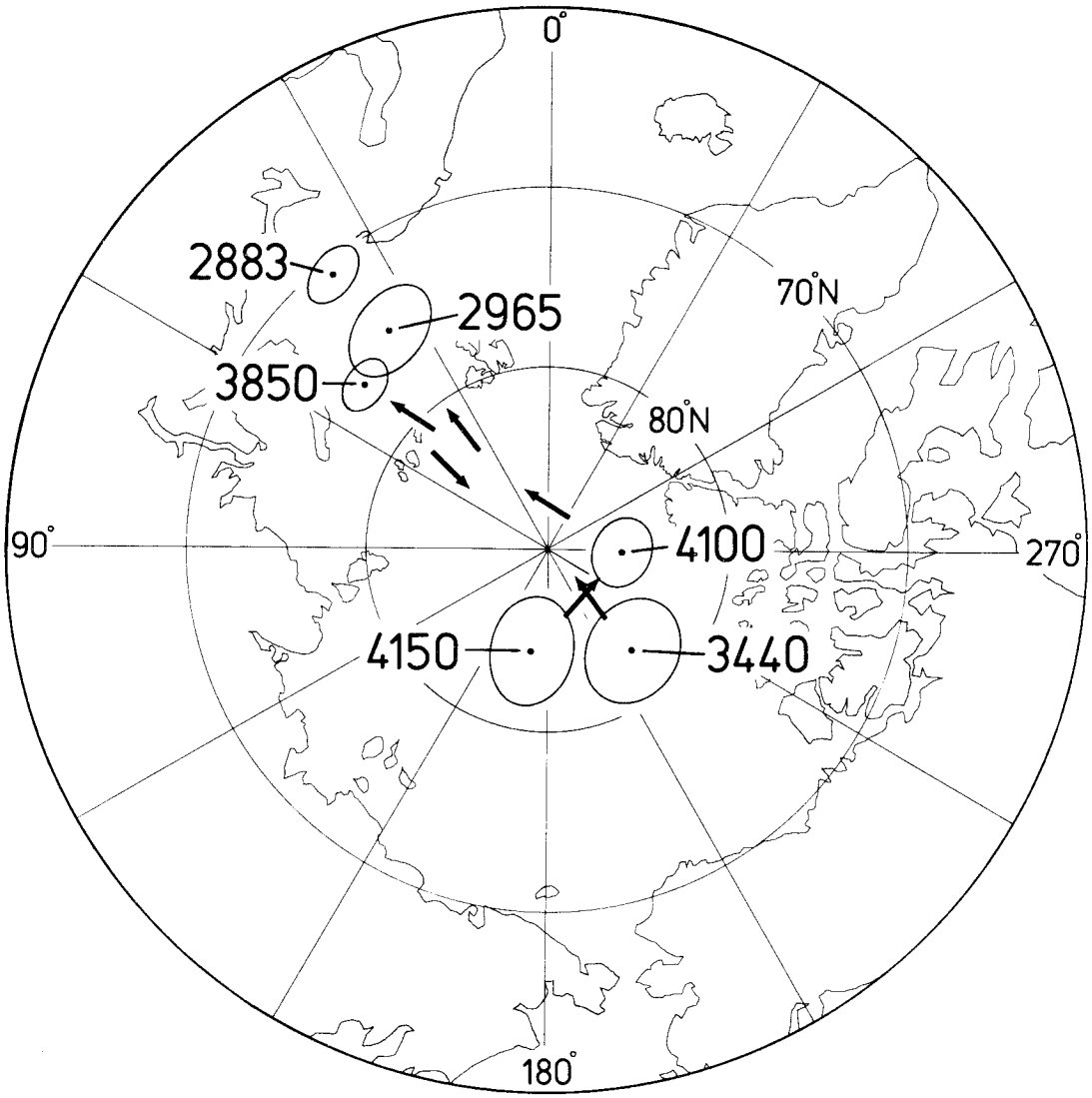

Fig. 12--Equal-area projection of north polar area showing VGPs and ovals of 95 percent confidence for all dated volcanic units between 4150 and approximately 2900 years B.P. Large dark numbers indicate ages in years B.P. Arrows indicate generalized time sequence between VGP positions.

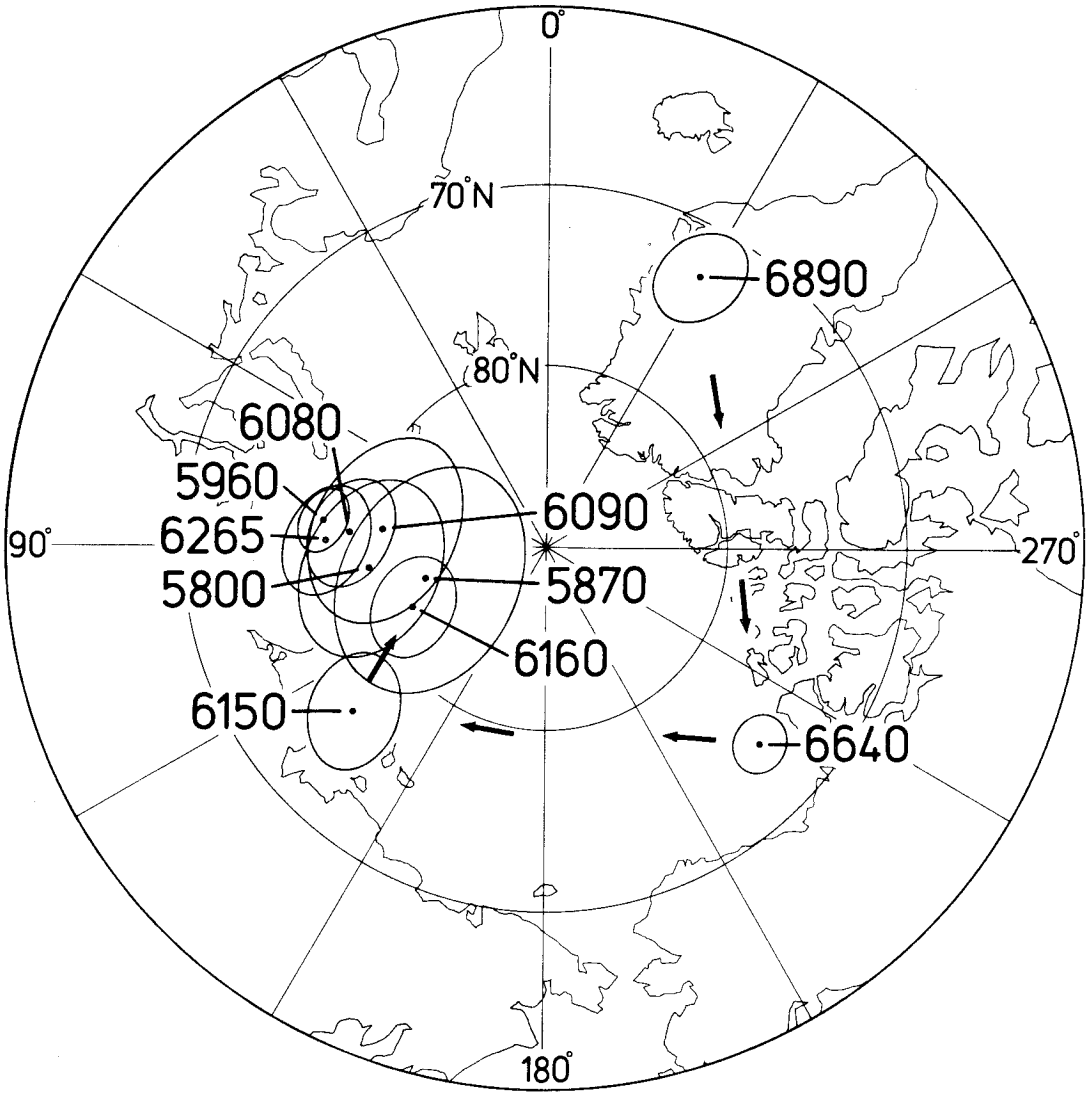

Fig. 13--Equal-area projection of north polar area showing VGPs and ovals of 95 percent confidence for all dated volcanic units between 6890 and 5800 years B.P. Large dark numbers indicate ages in years B.P. Arrows indicate generalized time sequence between VGP positions.

charring of the tree trunk by the lava flow. This source of error, when added to the normal range of analytical errors and the fact that the dates were done in several laboratories may explain part of the spread of ages of the lava flows in the Newberry Crater area.

Stratigraphic overlap is rare for dated flows in the Newberry Crater area, but two occurrences are known: (1) cinders from the Lava Butte eruption overlie the Gasline Flow, and (2) the Lava Cascade Flow overlies the flows in the Lava Cast Forest. Unfortunately, the VGP for the Lava Cascade Flow is so poorly determined that it includes the Lava Cast Forest VGP at the 95 percent confidence level. The overlap of Lava Butte Flows at 6160 years B.P. on Gasline Flows at 6150 years B.P. suggests the reconstruction as shown in Figure 13, which is opposite in sense to the small difference in the ^{14}C ages.

No VGP diagram will be presented for the oldest three flows from this study, Cerro Grande, Northeast Sunset and North Robbers Flows, as the time separations between them are too large for adequate reconstruction of a VGP path.

Comparison of Direction of Magnetization of Volcanic Rocks and of Holocene Lake Sediments

Scattered age control and the general lack of stratigraphic superposition of the control points from this study make comparisons with more continuous records of Holocene secular variation quite valuable. The value of comparison lies both in the identification of anomalous control points due to errors in age control or magnetic orientation and in the possibility of using the continuous records, stretched between the control points from this study, to make a complete reconstruction of directional secular variation for the western United States. Few records of Holocene secular variation have been obtained from lake sediments. In the western United States, Lake Tahoe and Yellowstone and Jackson Lakes in Wyoming have been sampled and their records of secular variation have been measured for at least part of the time period covered by this study. Farther to the east, in the vicinity of the Great Lakes, many records of Holocene secular variation have been obtained from lake sediments. Most of these records have little or no absolute time control within the sampled cores, a common characteristic requiring the assumption of linear sedimentation rates within the cores. A secular variation record from Lake St. Croix in Minnesota is the best midwestern record currently available.

Information regarding the secular variation record from Lake Tahoe sediments has been published in abstract form twice (Dodson and others, 1977; Henyey and others, 1977) and recently as a journal article (Palmer and others, 1979). The useful secular variation

record as obtained from the lower parts of sediment cores has stronger NRM intensities, while the younger parts show lower NRM intensities and more directional instability. In particular, the inclination rarely equals or exceeds the mean axial inclination expected for Lake Tahoe, suggesting a faulty paleomagnetic record. The total span of time covered is thought to be 20,000 to 30,000 years based on the interpretation of ash layers within the core, and correlations between the Lake Tahoe core and sediments near Mono Lake.

The paleomagnetic inclination record from Yellowstone and Jackson Lakes in Wyoming published by Shuey and others (1977) is shown in Figure 14. Declination was uncontrolled in the coring process and could not be convincingly reconstructed. The solid line represents the composite inclination record from all cores sampled. No independent time control was obtained by Shuey and his coworkers; the inclination record was normalized to absolute time by comparison with DuBois' (1974) inclination record from the southwestern United States. The VGP path specified from DuBois' work was used to predict inclination values for southwestern Wyoming for the period A.D. 600 to A.D. 1500. The secular variation record earlier than that controlled by DuBois' data was reconstructed on the assumption that the sedimentation rate remained constant. DuBois' (1974) normalized record of inclination is shown on Figure 14 with a dotted line. The solid data points with error boxes are from the present study or, in the instance of the point at A.D. 1700, are from the Aiyansh Flow reported by Symons (1975). Both the data from the present study

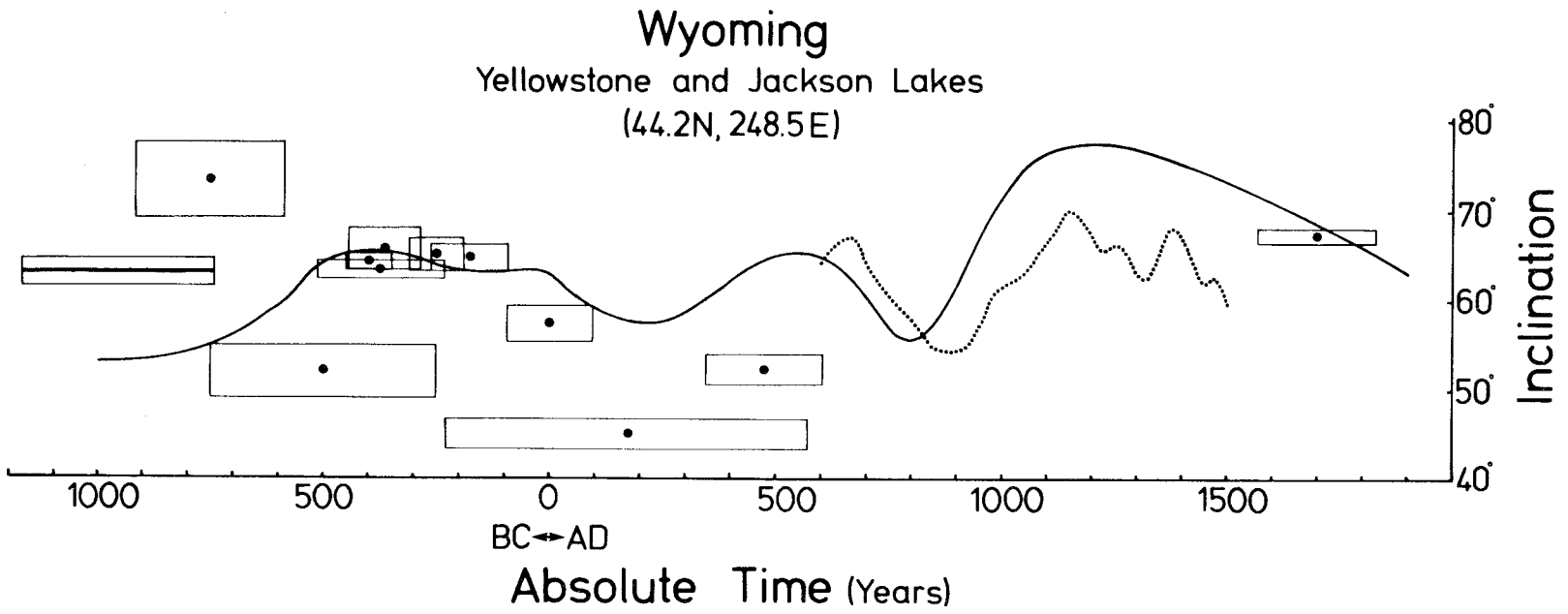

Fig. 14--Comparison of inclination records from Jackson and Yellowstone Lakes (Shuey and others, 1977) with those of DuBois (1974), Symons (1975), and the present study transformed through VGPs to southwestern Wyoming. Solid line is lake sediment data, dotted line from DuBois (1974) and data points with error boxes from Symons (1975) and the present study.

and that of Symons have been transformed through the VGP formula to the location of Yellowstone and Jackson Lakes. The control points from Sunset Crater and the Ice Spring Field have been left off Figure 14, as they add no additional time control for this comparison.

The composite record of inclination from the Wyoming lakes does not appear to fit the record from lavas and archeological sites very well. A disagreement of as much as 12 deg of inclination between the lake record and DuBois' curve and the lack of comparable high frequency variation in the lake record is troubling. The lack of detail in the Wyoming record is possibly a function of the process of averaging several records, but it is more likely that a delay time in the acquisition of the detrital remanent magnetization (DRM) has averaged the higher frequencies of secular variation. While some of the inclinations from lavas coincide with the inclinations observed in the Wyoming lake sediments, for example in the time range from 400 to 100 B.C. and at A.D. 1700, there are also large discrepancies. Again, the observed differences may be due chiefly to the averaging process by which the Wyoming record was constructed, which has smoothed out significant portions of the high frequency inclination variation. For instance, consider the inclination low at A.D. 200. It is conceivable that the averaging process has reduced the amplitude of this fluctuation in the composite lake record. Another error could lie in changes in sedimentation rate so that the time normalization of the upper portion of the core is inappropriate for the bottom.

A record of Holocene secular variation from Lake St. Croix, Minnesota, has been briefly reported by Lund and others (1976). The details of this record have not yet been published, but the senior author has kindly provided a copy of the declination and inclination data which are shown in Figure 15. Lake St. Croix data are shown as solid points and data from this study as open squares. The data from the volcanic rocks have been transformed through the VGP equation to the location of Lake St. Croix. Data of this study from the southwestern United States and also the record of DuBois have not been included on Figure 15 because of the large angular separation between Lake St. Croix, particularly in latitude. The angular separation between Lake St. Croix and the mean locality in the Pacific Northwest is 17.3 deg. At this angular separation one should expect an average of 3.4 deg of angular error from transformation through a VGP (Shuey and coworkers (1970) would predict 4 deg for this east-west separation), with a range of errors from 1.6 to 5.3 deg. Worst cases could have as much as 7.5 deg of error. Considering the angular size of nondipole features of the geomagnetic field, these potential errors should not obscure major agreement between the volcanic rocks and the lake sediments if it exists. The Lake St. Croix record has internal time control from nine ^{14}C dates, indicated on Figure 15 as arrows along the time axis. In addition, the density of sampling seems tight enough, at least for the past 4500 years, to specify all the important direction changes the lake sediment may have recorded.

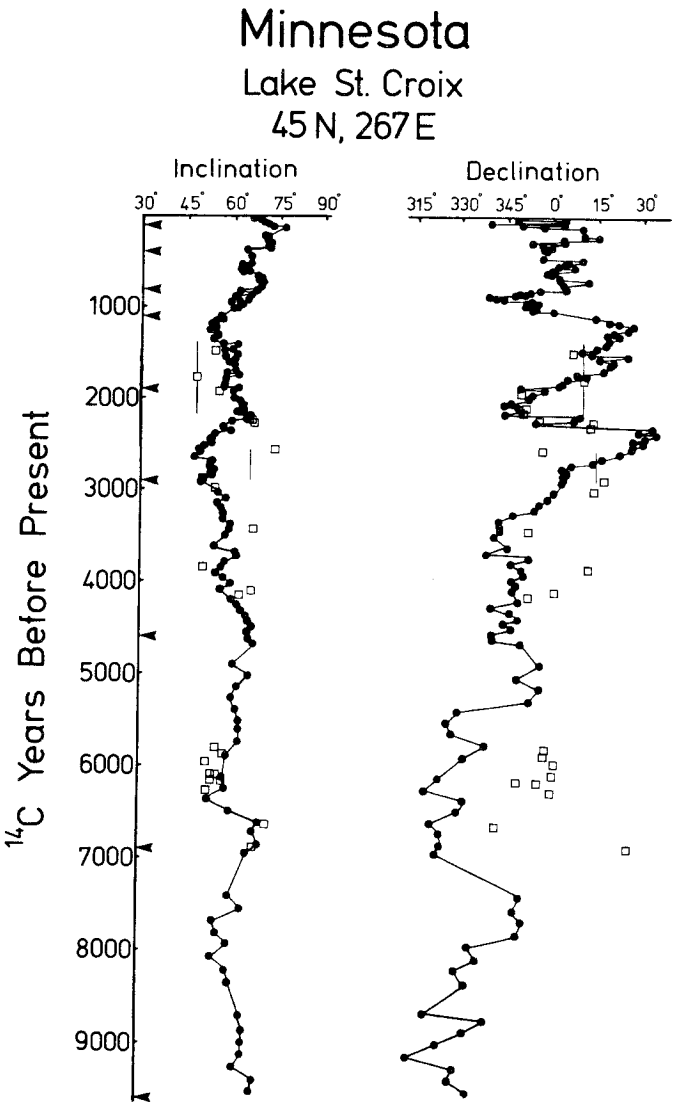

Fig. 15--Comparison of declination and inclination records from Lake St. Croix, Minnesota, taken by Lund and Banerjee, with directions predicted for this location by VGPs calculated from dated volcanic deposits from western United States. Solid dots represent lake sediment data; open squares are directions transformed through VGPs from the present study. Vertical bars in time dimension show possible age span for two units which have poor ^{14}C age dates. Arrows at time axis show position of ^{14}C dates controlling lake sediment age.

The agreement in inclination between the volcanic rocks and the lake sediments is remarkably good. An example is shown in the record between 6000 to 7000 years B.P., where a change of 20 deg in about 400 years has been recorded by both the volcanic rocks and the lake sediments. Large discrepancies between the two records occur at 1775 years B.P., likely due to a large error in the ^{14}C date of the volcanic rock, and between 2900 to 2550 years B.P., where a high inclination event recorded by volcanic rocks has little similarity to the lake sediment secular variation record. Recalling the discussion of the VGP path during this period of time from a previous section in this chapter, one or more control points in this period may have erroneous age or direction of magnetization data. Other discrepancies in inclination are smaller and may be due either to larger errors in the VGP transformation than have been assumed or to a poor recording of higher frequency variations by the lake sediments.

The azimuthal orientation of the lake sediment cores was not controlled during the coring process, but a process was developed by Lund and Banerjee to recover this information later. Coring of these sediments was done in two holes with overlapping sampling depths staggered at 0.5 m intervals. By comparing the values of declination at the bottom of a meter-long core with those of the middle of the core from the adjacent hole, a continuous declination record could be obtained. The top of the entire assembled declination record was then normalized to the present declination at Lake St. Croix. While the later portions of the declination record from the lake

sediments seems to be in reasonable agreement with the results from the volcanic rocks, prior to 3000 years B.P. the two records diverge. In addition, the Lake St. Croix declination record clearly deviates from an average value of 0 deg below this point. While this reconstruction of declination has worked well at the top of the core, Lund and Banerjee admit that a systematic westward twist may have been imparted to the lower portions of the core. Twisting of the core probably is the cause of the strong discrepancy in declination prior to 3000 years B.P.

Ultimately, the most accurate and complete record of Holocene secular variation will be constructed using control points from volcanic deposits and continuous records from alluvial deposits and lake sediments which have some internal time control. Records of this kind do not at present exist for the western United States. The volcanic data presented in this study are an important first effort, but the existence of long time gaps means that the effort is preliminary. The lack of a long record of secular variation from a lake located in the western United States with internal time control within the sediment is the greatest limitation on the compilation of a complete record of secular variation. Lake St. Croix is located too far east to fill this need and the Wyoming lake core is too short and apparently inaccurately records the geomagnetic field. Optimistically, one can only hope that a complete lake sediment record of secular variation will soon be forthcoming.

Chapter 4

SECULAR VARIATION OF INTENSITY OF THE GEOMAGNETIC FIELD IN WESTERN UNITED STATES

This chapter discusses the results of geomagnetic paleointensity measurements made by the Thelliers' double heating method on the same collection of Holocene volcanic rocks upon which the directional studies were performed. The method for this analysis is described, the general rock properties affecting the intensity determination are discussed, examples of the intensity determination process are presented and the observed variation is outlined for the Holocene, where time control exists. In addition, a combination of the results from this study and that of Sternberg and Butler (1978) allows a rather detailed evaluation of the last 3000 years of intensity variation for the western United States.

Objectives of these paleointensity experiments were multiple. As part of an expanding program of paleointensity research at the U.S.G.S. at Menlo Park, work was devoted to young volcanic rocks to show that the Thelliers' method can routinely produce reliable paleointensity information. The record of variation itself is valuable as a geophysical property of the Earth as manifested in the western United States and can be compared to similar records from other parts of the world. And lastly, the intensity variation can be used for purposes of geologic correlation in a manner similar to that of the directional changes in the western United States.

Succeeding sections within this chapter and the next will document successful completions of each of these objectives.

Method of Paleointensity Determination

The basic method used in this study for the analysis of paleointensities is that originally developed by the Thelliers over a 20-year span of time (Thellier, 1938; Thellier and Thellier, 1959). While other methods of paleointensity determination have been suggested (Wilson, 1961; Van Zijl and others, 1962; Shaw, 1974; Banerjee and Mellema, 1974), only the Thelliers' method enjoys universal acceptance for reliability. The assumptions underlying the Thelliers' method and various causes of non-ideal behavior of rocks to which the method has been applied are discussed by Coe (1967a, b), and Smith (1967). Refinements of the method have been described by Coe and Grommé (1973).

Recently, a program of paleointensity investigations of young volcanic rocks has been performed in the paleomagnetic laboratory of the U.S. Geological Survey at Menlo Park, California (Khodair and Coe, 1975; Coe, Grommé, and Mankinen, 1978; Abokhodair, 1977). In these studies, the stepwise heatings of the Thelliers' analysis were carried out in a vacuum of 10^{-5} torr. The partial vacuum stops or slows oxidation of the principal magnetic phases in volcanic rocks, a common cause of failure of the Thelliers' method. Through the kindness of Dr. Sherman Grommé, the equipment in his laboratory was made available for this investigation.

The procedure used for the Thelliers' experiment in this study is as follows. Three specimens were selected from each locality after completion of measurements of NRM and af demagnetization, where required. Those specimens were chosen which were free of VRM and IRM or appeared to carry the least VRM or IRM. If alternating field

demagnetization was required on all specimens from a locality, a second set of specimens was cut from the most suitable cores for the Thellier experiment. The Thellier experiment was not performed on any specimen which had been previously demagnetized by alternating field. As shown by Coe and Grommé (1973), prior af demagnetization causes a nonlinear behavior of the specimen in the Thellier experiment.

Small diameter cores were taken from each specimen chosen or from adjacent specimens in the same core for measurement of saturation magnetization as a function of temperature with a thermomagnetic balance (Doell and Cox, 1967). These measurements give bulk Curie temperature determinations and provide maximum estimates of the blocking temperature spectrum of each specimen. The measurements were carried out in 10^{-4} torr vacuum to ascertain the reversibility of strong-field induced magnetization with heating in an environment similar to that in which the Thellier experiment would be performed. Substitutions were made for any specimen which showed highly irreversible thermomagnetic curves.

The apparatus in which the Thellier experiments are performed has six independently controllable nonmagnetic ovens, each holding five specimens. Heating is controlled by 24 thermocouples connected to a chart recorder, to within 2° to 3°C of a desired temperature. The ovens are enclosed in a Rubens coil 8 ft in diameter, capable of maintaining a magnetic field less than 50 nT within the volume occupied by the ovens. Auxiliary windings on the Rubens coil array are controlled through a negative feedback loop by an orthogonal fluxgate array in the center of the oven system, in order to cancel

time variations in the ambient magnetic field. Each oven is enclosed in a long solenoid, so that an axial magnetic field up to 100 μT can be applied to the specimens in any one oven without affecting the others. The applied magnetic field can be controlled routinely to within 0.2 percent of the 50 μT value used in this study.

Groups of five specimens were chosen for simultaneous Thellier experiments in individual ovens. The specimens were grouped on the basis of similarity of thermomagnetic curves, but the multiple specimens from each given flow were run in separate ovens. This choice was made to protect against systematic bias in interpretation and against experimental error ruining all specimens from a given flow. First, NRM measurements are made for all the specimens, as this measurement is the basis for normalization of all calculations and for the Arai NRM-TRM plots (Arai, 1963). From the thermomagnetic curves, a temperature was chosen for each of the six ovens, intended to remove 5 to 10 percent of the NRM, and the samples were heated in zero field. After cooling to 20°C the remaining magnetic moments of each of the specimens were measured. Changes of direction and intensity at each heating step were scrutinized for possible removal of VRM or IRM components and to be sure that the blocking temperature distribution for each specimen was similar to that expected from the thermomagnetic measurements. The specimens were then reheated to the same temperature, but this time in a magnetic field of 50 μT produced by the axial solenoids surrounding each oven. The field is applied from the beginning of the heating to the end of cooling, as it has been shown that turning the field on for only the cooling

cycle stimulates spontaneous decay of the NRM (Levi, 1975). After heating in the applied field, the direction and intensity of magnetization are measured in each specimen. This double heating and measuring procedure is then repeated at successively higher temperatures until the NRM of the specimen has been totally removed, or until the magnetization of the specimen changes in an irregular manner. The entire procedure requires about 2 to 3 months to complete. Some specimens were heated as many as 65 times.

During the course of each Thellier experiment, graphs of NRM remaining versus temperature are kept as well as Arai NRM-TRM diagrams. Assuming the independence of the partial thermoremanent magnetization (PTRM) acquired between two temperatures, each pair of heatings to a given temperature can be plotted on the Arai diagram. The NRM remaining at each heating step should plot as a linear function of the TRM gained; the product of the slope of this function with the applied field is taken as the estimate of the ancient field intensity. Deviation from linearity shows that the sample has failed the Thellier experiment.

Thermomagnetic Properties of Paleointensity Specimens

The Thellier double heating procedure used in this study places strict requirements on the magnetic mineralogy of the specimens. The magnetic phases must be relatively inert to oxidation or reduction during repeated heating and cooling at 10^{-5} torr vacuum; significant alteration of the magnetic phases invalidates the experiment. Abokhodair (1977) has outlined magnetic changes that occurred in specimens from historically dated lava flows on Hawaii whose NRM was acquired in a known geomagnetic field, when heated in the ovens used in this investigation. In general, Abokhodair believes specimens containing titanomagnetite are partly oxidized by repeated heating in 10^{-5} torr vacuum, while samples containing the products of high-temperature oxidation in nature, that is intergrowths of magnetite and ilmenite, may be partly reduced.

It is the premise of this study that partial or complete natural high-temperature oxidation of original titanomagnetite appears to be the dominant factor that determines the success of the paleointensity determinations in this study. Many of the specimens used in this study typically have been oxidized at high temperature naturally to at least some degree and commonly to a great degree. If complete high-temperature oxidation of a specimen has already occurred naturally the specimen normally yields an excellent paleointensity determination. If natural high-temperature oxidation has been relatively incomplete, that is, an assemblage of titanomagnetite, magnetite and ilmenite is present so that two Curie temperatures are observed in the thermomagnetic curves, then the specimen typically yields poor determinations

of paleointensity owing to continued oxidation during the course of the experiment. If high-temperature oxidation has barely affected a specimen in nature, then that specimen can produce a good Thellier determination of paleointensity providing that the unblocking temperature spectrum is principally distributed below 200° to 300°C. Above those temperatures oxidation generally takes place within the vacuum ovens, which alters the magnetic minerals and thus invalidates the Thellier experiment.

Strong-field thermomagnetic records were made using small cores taken adjacent to each specimen before the Thellier experiments were performed. These records were run both to ascertain the distribution of Curie temperatures for the magnetic mineralogy of each specimen and to see if heating in a 10^{-4} torr vacuum would produce irreversible changes in the Curie temperature distribution or intensity of induced magnetization. The strong-field thermomagnetic record for each specimen upon which the Thellier experiment was performed is reproduced in Appendix 2. An inspection of these records reveals great differences from lava flow to lava flow, though multiple specimens from a given lava flow generally are closely similar. Magnetic oxides found in basic volcanic rocks generally are ulvöspinel-magnetite solid solutions or products of oxidation of such solutions; inflections in the strong-field magnetization records that represent Curie temperatures can be used to identify the Fe/Ti ratio within the solid solution. For instance, Curie temperatures near 580°C indicate essentially pure magnetite is present.

The strong-field thermomagnetic records were inspected for strongly irreversible behavior before the Thellier experiments were performed. Here "strongly irreversible" means changes of 10 percent or more in the total strong-field magnetization measured after cooling to room temperature. Unfortunately it is impossible without several thermomagnetic balance runs to progressively higher maximum temperatures to ascertain at what temperature the irreversibility commenced. As a consequence specimens from some flows for which every specimen showed some irreversibility were used in the Thellier experiment, sometimes with good results and sometimes with very poor results. When another specimen could be substituted for one which showed marked irreversibility, this was done.

The strong-field thermomagnetic records can be used as a guide to the blocking temperature distribution of a given specimen. While not necessarily predicted on theoretical grounds, it turns out that, for basic volcanic rocks with small grain size and simple, rapid cooling history, strong-field magnetization and the thermoremanence have similar temperature distributions. This is due to the fact that there is little magnetic material in these rocks not involved in the remanence. Appendix 3 shows normalized comparisons of the heating portions of strong-field thermomagnetic records and the thermoremanence demagnetization for each specimen upon which the Thellier experiment was performed. Of note is that both the strong-field and remanent magnetization commonly show similar inflections and complete loss of magnetization at similar temperatures. Some of the differences between the records arise because the strong-field

magnetization is measured at temperature, and, although the temperature recorded by the thermomagnetic balance is accurate, the thermocouples in the vacuum ovens typically lead the real temperatures within the specimens by a variable amount which probably does not exceed 10°C at 580°C. These effects can be seen where the strong-field magnetization goes to near zero at a lower temperature than does the remanence. In other words, some of the comparisons seem to suggest that the Curie temperature is on the order of 10°C less than the indicated maximum blocking temperature of NRM, but this is an artifact of the imperfect thermal tracking of the samples by the thermocouples in the vacuum ovens. The imperfect thermal tracking does not affect the precision with which an apparent temperature in the vacuum ovens can be reproduced; this routinely is on the order of ±2°C.

The curves of thermoremanent demagnetization illustrate the general magnetic character of the specimens used in the Thellier experiments. Two quantities have been derived from these curves; the temperature at which remanent magnetization disappeared (maximum unblocking temperature) and the temperature at which the amount of NRM removed per degree of temperature increase is a maximum (the peak of the temperature distribution of partial natural remanent magnetization (PNRM). The maximum unblocking temperature for these fine-grained basic volcanic rocks is probably equal to the Curie temperature for each specimen. Histograms of the maximum unblocking temperature and the peak of the PNRM temperature distribution ($\Delta NRM/\Delta T_{max}$) are shown in Figure 16. Solid bars are for specimens

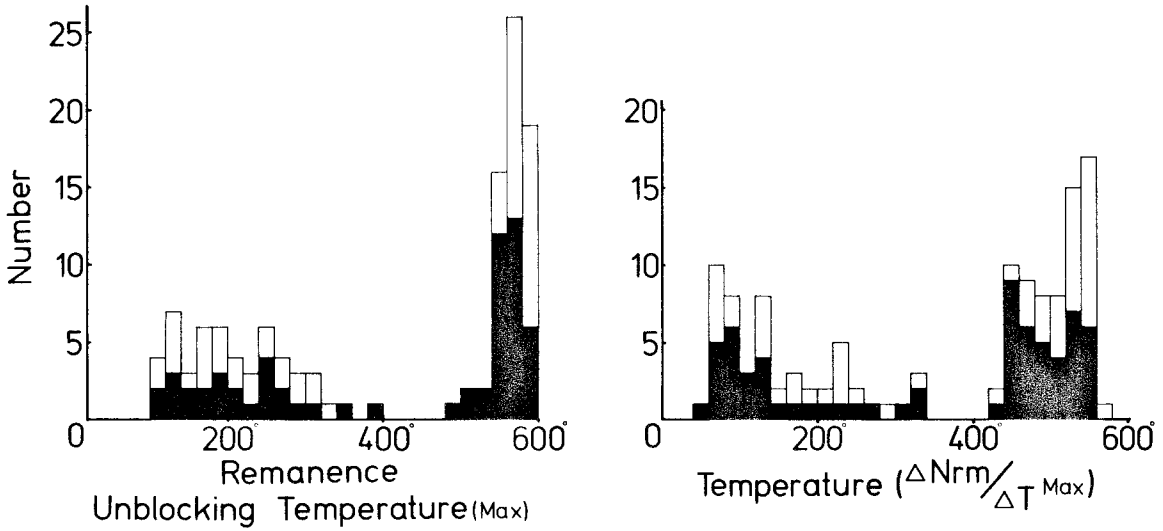

Fig. 16--Histograms of the maximum remanence unblocking temperature and the temperature at which the maximum loss of NRM with change in temperature occurs for 118 specimens from 46 volcanic units in this study. Solid portions of the histograms are for samples thought to display two Curie temperatures.

which display two maxima in their PNRM-temperature distributions. Either the low maxima or high maxima were plotted depending on which represented the largest percentage of the natural remanence.

The histograms show a bimodal distribution for both the maximum unblocking temperatures and the peaks of the PNRM-temperature distributions. This bimodality indicates that two different magnetic phases are common in the collection of specimens studied (Ade-Hall and others, 1965). The histogram of maximum unblocking temperature shows little difference at the lower temperature mode between the distribution for specimens with a single magnetic phase and that for specimens with two magnetic phases but, at the higher temperature mode, specimens with a single magnetic phase tend to have higher maximum unblocking temperatures than specimens with two magnetic phases. This is also shown in the high-temperature mode of the histogram of the peak PNRM-temperature distributions, where double phase specimens have distinctly lower temperature distributions than single phase specimens.

In order to summarize the important characteristics of the thermal demagnetization records, a scatter diagram of the peak of the PNRM-temperature distribution plotted against the maximum unblocking temperature for each specimen was constructed (Fig. 17). Each data point represents a specimen upon which the Thellier experiment was performed. Proximity to the diagonal line of the diagram along the vertical direction indicates a narrow unblocking temperature (PNRM) distribution for a given specimen. The distributions of single and double phase specimens on this diagram are very similar. There is a tendency for samples with 100° to 120°C

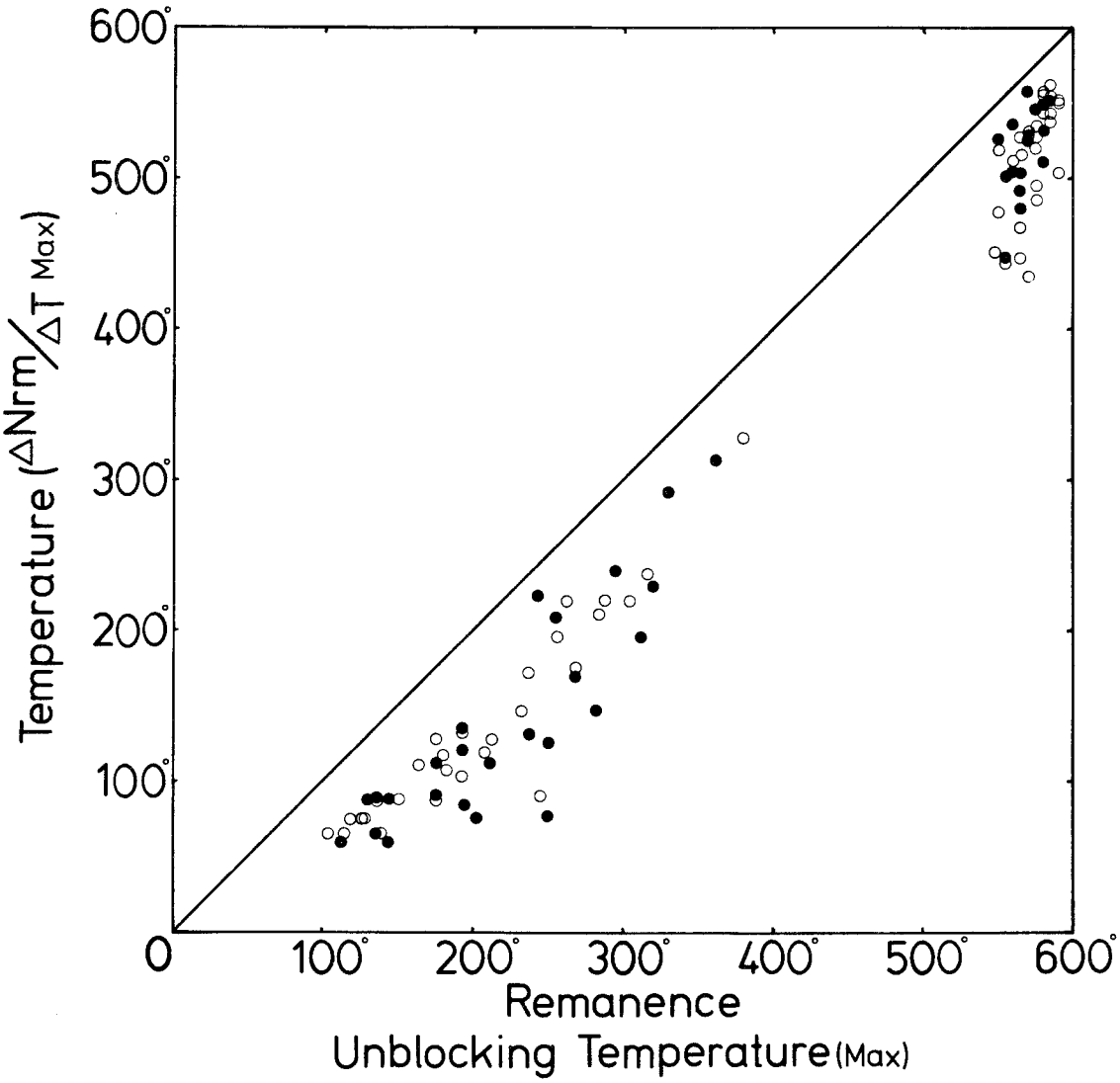

Fig. 17--Temperature at which the maximum loss of NRM with change in temperature occurs plotted as a function of maximum remanence unblocking temperature for 118 samples used in paleointensity determinations. Black data points are for samples thought to display two Curie temperatures.

maximum unblocking temperatures to have their peaks of PNRM-temperature distribution tightly grouped only 50°C lower in temperature than the maximum unblocking temperature. The tightness of the grouping is not an artifact of the proximity of the maximum unblocking temperature to ambient temperature. The first heating steps for these low Curie temperature specimens, typically at 40° to 50°C, remove 3 percent or less of the NRM. For specimens with 150°C and somewhat higher maximum unblocking temperatures, the peaks of the PNRM distributions are more variable and are as much as 75° to 100°C below maximum unblocking temperature. The unblocking temperature distributions are to a first approximation uniform in width from specimen to specimen and as maximum unblocking temperatures increase the unblocking temperature distributions move up with them. This amounts to a broadening of the PNRM-temperature distribution as the maximum unblocking temperature rises in value. The group of specimens with high unblocking temperatures shows the opposite effect. For samples with the very highest maximum unblocking temperatures (580°-590°C), there is little difference between these and the peaks of the PNRM-temperature distributions; in other words nearly all of the PNRM is just below the Curie temperature. But, as the maximum unblocking temperatures fall to 550°C, there is a distinct trend for the unblocking temperature distribution to broaden and peak as much as 110°C lower.

It is necessary at this point to describe in more detail the model of oxidation which produces the phenomena noted thus far. The model is not new, having been developed by Ade-Hall and others

in 1965 and more recently by Haggerty in 1976. Both these references have been drawn on heavily for the details of the model. The magnetic oxides crystallizing from basaltic magma typically are stoichiometric magnetite-ulvöspinel solid solutions with 50 to 80 percent of the ulvöspinel end member. Though ilmenite and Ti-free magnetite can crystallize from some oxidized melts, in general the single phase titanomagnetite is much more common. After extrusion of the basaltic lava this homogeneous oxide phase is subject to a rapid loss of temperature (within hours or days) commonly under conditions of high oxygen fugacity. Under these conditions high-temperature oxidation occurs with two manifestations: cationic and exsolution oxidations (Haggerty, 1976). Cationic oxidation refers to the partial change of Fe^{2+} to Fe^{3+} within the titanomagnetite locally producing diversity of composition with associated distortions and defects in the lattice. Titanomagnetite can accommodate a certain amount of oxidation, but ultimately, ilmenite begins to nucleate on the (111) planes of the cubic phase and nearly Ti-free magnetite exsolves as a second magnetic phase. The ilmenite is paramagnetic above room temperature, so that, while three oxides are present at this point, only two are ferrimagnetic. Oxidation and exsolution of Ti-free magnetite proceeds in many cases until all the original titanomagnetite has been consumed. If the basalt is oxidized still further, hematite and eventually pseudobrookite can develop as additional phases. Due to the short cooling times and elevated temperatures, neither titanomaghemite or maghemite are part of this model. Equilibrium exsolution of magnetite and

ulvöspinel from the initial titanomagnetite is inhibited by the short time of cooling and high oxygen fugacity.

The magnetic oxides of the specimens used for this study commonly did not approach equilibrium under conditions of high-temperature oxidation. The proportion of samples showing two Curie temperatures is larger than in other previous work (Ade-Hall and others, 1965). This appears to be a direct consequence of sampling surfaces of very young flows. The samples are variously quenched and unoxidized, incompletely oxidized, or completely oxidized at high temperature depending on the circumstances of the location of each sample. Under conditions of rapidly falling temperature at the surface or near surface of a flow, the equilibrium oxidation of an ulvospinel-magnetite solid solution phase may lag behind the falling temperature. Thus sometimes magnetite may crystallize below its Curie temperature and possibly below part of its unblocking temperature distribution (Carmichael and Nicholls, 1967; Grommé and others, 1969). Under these conditions the magnetite acquires a high-temperature CRM of small magnitude, followed by a PTRM as the temperature continues to fall. Remanence acquired in this manner does not meet the requirements of the Thellier experiment. The partial NRM removed will not be proportional to the partial TRM gained in the laboratory field because some of the remanence is initial CRM rather than TRM. As long as all the NRM is TRM, however, incomplete oxidation does not necessarily lead to failure of the Thellier experiment.

The distributions of maximum unblocking temperature and peak of the PNRM-temperature distribution indicate the presence or absence of high-temperature oxidation. The samples with two PNRM maxima have undergone incomplete high-temperature oxidation and have two magnetic phases. Single high Curie temperature specimens tend to have higher Curie temperatures than double Curie temperature specimens; this arises because the magnetite first formed from disproportionation still has a small amount of Ti present and a lower Curie temperature as a consequence. The spread of low maximum unblocking temperatures up to 400°C, for both single phase and two phase specimens, and the increasing temperature lag of the peak of the PNRM-temperature distributions behind the maximum unblocking temperatures are both manifestations of cationic oxidation. This oxidation creates a minute distribution of ilmenite and magnetite phases with a variety of Fe/Ti ratios within what optically appears to be a single phase titanomagnetite. The bulk magnetic properties measured in the strong-field magnetization balance or in the thermoremanence would indicate a variety of titanomagnetite compositions in these specimens. When oxidation proceeds to the point of formation of ilmenite and simultaneous exsolution of low Ti magnetite from titanomagnetite the first low Ti magnetite formed has a lower Curie temperature than pure magnetite and a somewhat broad unblocking temperature distribution. As oxidation and exsolution continue a Ti-free magnetite is produced which has a narrow unblocking temperature distribution.

Oxidation occurs within the ovens used in the Thellier experiment, despite the 10^{-5} torr vacuum, but at higher temperatures and

more slowly than it would if the specimens were heated in the Earth's atmosphere. While the reactions in the specimens are subject to some conjecture, certain characteristics of the Thellier experiments indicate that some oxidation commonly takes place. At high temperature steps specimens which have not been naturally oxidized at high temperature and have low Curie temperatures tend to acquire too much laboratory TRM relative to the amount of NRM removed. The expected linear NRM-TRM relationship has instead a curved appearance that is concave up. This is readily accounted for by partial oxidation of the titanomagnetite during the Thellier experiment to form ilmenite and low-Ti magnetite. Specimens with two Curie temperatures frequently yield markedly nonlinear Arai diagrams. This may be due to the formation of more ilmenite lamellae and low-Ti magnetite with a high spontaneous magnetization.

Specimens with single high Curie temperatures can be consistently demagnetized in the Thellier experiment all the way to their Curie temperatures with a linear relationship between PNRM lost and PTRM gained. The success of the Thellier experiment with these specimens suggests that reduction did not occur under the experimental conditions used. Considering the low oxygen fugacities required to reduce ilmenite-magnetite intergrowths to titanomagnetite ($10^{-20.8}$ at 900°K, $10^{-30.6}$ at 700°K, and 10^{-86} at 298°K) (Verhoogen, 1962), this reaction appears unlikely in the 10^{-5} torr ovens.

The information provided by the strong-field thermomagnetic records may be at variance with the high-temperature oxidation model that has been presented and substantiated above. Many specimens

seem to lose part of their saturation magnetization after being heated to 600°C and cooled to room temperature. Specimens with two Curie temperatures and mostly low Curie temperature phases frequently lose much of their higher temperature induced magnetization during the cooling portion of the strong-field measurement. These effects are just the opposite of high-temperature oxidation which would tend to produce grains of purer magnetite with a larger strong-field magnetization and a higher Curie temperature.

There are reasons to think that the conditions within the strong-field thermomagnetic balance are more reducing than those within the vacuum ovens. A powdered specimen of hematite has been partly reduced to magnetite during a run on a strong-field magnetization balance (Shive and Diehl, 1977). This reduction occurred only at the surface of the powder. It is thought that contact with the vacuum pump diffusion oil may allow very reducing conditions to develop locally on the surface and near surface of a specimen in the balance. Considering the large relative surface area of the small 0.4 g, 6 mm diameter cores used in the strong-field balance compared to the 25 g, 25 mm diameter cores used in the Thellier experiment, differences in the oxygen fugacities within the instruments may affect the specimens to different extents. Cores used in the Thellier experiment that initially were slightly red in color turned steely gray after completion of the experiment, but preserved their original color beneath a 1-mm thick or less altered zone. Thus the possibly contradictory information from the strong-field thermo-

magnetic records may not always apply to the conditions of the vacuum ovens during the Thellier experiment.

It is appropriate to discuss whether or not some general rules regarding suitability of specimens for the Thellier experiment are possible in hindsight. The experiment as performed in this study is extremely time consuming, and some specimens gave virtually no useful results. If a method for predicting failure of the experiment could be found it would save much time and effort. To investigate this possibility, the percentage of NRM used to calculate the paleointensity was compared with the maximum unblocking temperature (Fig. 18). The total percentage of NRM interpreted, that is, used for the least squares slope determination, is a useful measure of the response of a specimen in the Thellier experiment. The best determinations of paleointensities are obtained when the relationship of NRM lost to TRM gained is linear over 90 to 100 percent removal of NRM.

Specimens in which the remanence resides only in high-Ti single phase titanomagnetite tend to yield reliable paleointensities. In partially oxidized specimens, with a high Curie temperature, low-Ti magnetite in addition to the high-Ti titanomagnetite, the interpretable fraction of NRM tends to be lower. Specimens which appear to be single phase and unoxidized, yet have lower percentages of interpretable NRM, apparently also carried significant VRM in the lowest unblocking temperature intervals, thus shortening the linear portion of the Arai diagram. This problem is worse for older lava flows.

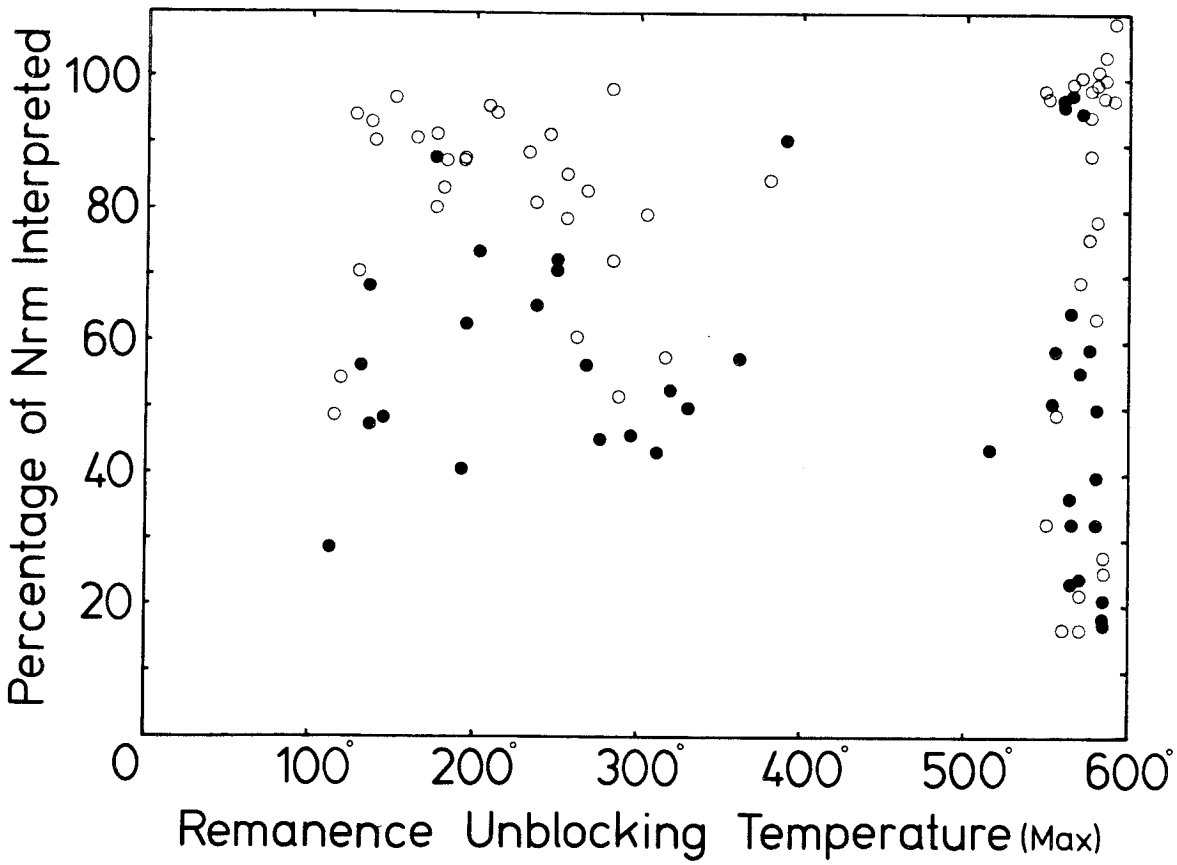

Fig. 18--Percentage of NRM interpreted in the Thellier paleointensity experiment plotted as a function of maximum remanence unblocking temperature for 94 paleointensity determinations. Black data points are for samples thought to display two Curie temperatures.

Specimens which have undergone relatively complete high-temperature oxidation show variable percentages of interpretable NRM in the Thellier experiment. In most specimens that retain a low Curie temperature phase, less than 60 percent of the NRM is interpretable. Where only the high Curie temperature phase is present, more than 90 percent of the NRM is interpretable in the majority of cases. Specimens with narrow unblocking temperature distributions and very high maximum unblocking temperatures tend to produce the best results. However, some specimens with apparent single high Curie temperature phases yield poor paleointensity determinations. This may be due to the presence of an unrecognized lower Curie temperature phase within the specimen. Such a hypothetical magnetite phase may be poorly resolved in the thermal demagnetization record because of the coarse temperature steps through the range of unblocking temperatures for low Curie temperature phases.

In summation, with the use of the 10^{-5} torr experimental vacuum, low Curie temperature specimens can yield reliable paleointensity determinations, if the lowest unblocking temperature intervals are not contaminated with VRM. If natural high-temperature oxidation has occurred, with the partial formation of intergrown ilmenite and low-Ti magnetite, the paleointensity determination will be less reliable. This does not mean, however, that a two-Curie-temperature specimen will not yield useful paleointensity information. If there is a choice between an unoxidized specimen or one that is partially oxidized, the unoxidized specimen is a much better risk in the Thellier experiment. The reliability of paleointensity results is

less variable in specimens in which high-temperature oxidation has produced a single magnetite phase with a narrow blocking temperature distribution and a Curie temperature at or near 580°C. These latter specimens yield the best paleointensity determinations.

Examples of Paleointensity Determination by the Thelliers' Method

As the interpretation of magnetic paleointensity is a less well known technique in paleomagnetism, six examples will be presented in this section illustrating a variety of magnetic properties of the specimens and the process of paleointensity determination using the Thelliers' method. The previous section described the model of the reaction that samples in general have to the environment of heating in the vacuum ovens and this section provides an opportunity to compare this model to individual experiments. Each example presented yields a useful paleointensity determination though each is markedly different from the others, thus confirming the versatility and power of the Thelliers' method.

Specimens from the Little Belknap Flow, Oregon, are representative of rocks with a single magnetic phase with low Curie temperature (Fig. 19). The low Curie temperature indicates that the magnetic phase is titanomagnetite which has escaped high-temperature oxidation during eruption, emplacement and cooling. There is no evidence of any Curie temperature near 550° to 580°C. The strong-field magnetization is fairly reversible during heating in 10^{-5} torr vacuum, with only a 4 percent loss in magnetization measured at room temperature after heating. Without several runs in the thermomagnetic balance to progressively higher maximum temperatures it is virtually impossible to know at which temperature the small irreversible reaction occurs.

The directions of magnetization measured after heating steps in the known applied field follow a smooth great circle path from the 20°C position toward the direction of the applied field for

Fig. 19--Magnetic measurements used in paleointensity determination from sample LtBO 1-1b, Little Belknap Flow, Oregon. Upper diagram shows strong-field magnetization as a function of temperature. Curve with arrow pointing to the right is for heating from room temperature to 600°C, and curve with arrow pointing to left is for cooling from 600°C. Sample was heated and cooled at 10^{-5} torr and in 400 mT applied field. Middle diagram is equal-area projection showing directions of magnetization measured after heating steps in the Thellier experiment. Filled points are on the lower hemisphere and open points are on the upper hemisphere. Squares denote measurements after heating in a known magnetic field and circles denote measurements after heating in a zeroed magnetic field. The letters TRM next to a triangle mark the direction of the applied field. Arrows show the sense of the progressive change in direction after heating in the known field. The lower diagram is an Arai NRM-TRM diagram showing relationship between NRM lost at progressive heating steps compared to TRM gained in a known magnetic field. Filled points are used for determination of the paleointensity for this sample, open points were not included in the interpretation. Lines forming right angle indicate PTRM check of TRM acquisition at earlier lower temperature, and connect to Thellier step at which it was performed (see text for discussion).

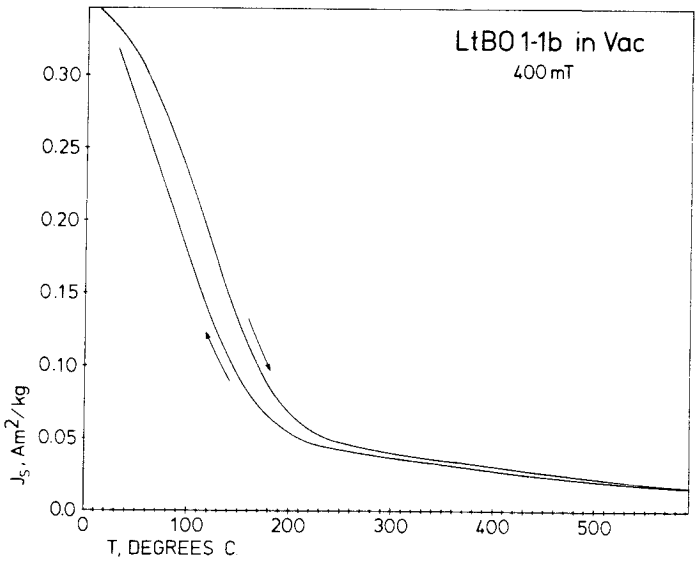
LtB01-1b in Vac
400 mT
0.30
0.25
0.20
0.15
0.10
0.05
0.0
J_S, Am^2/kg
0
100
200
300
400
500
T, DEGREES C

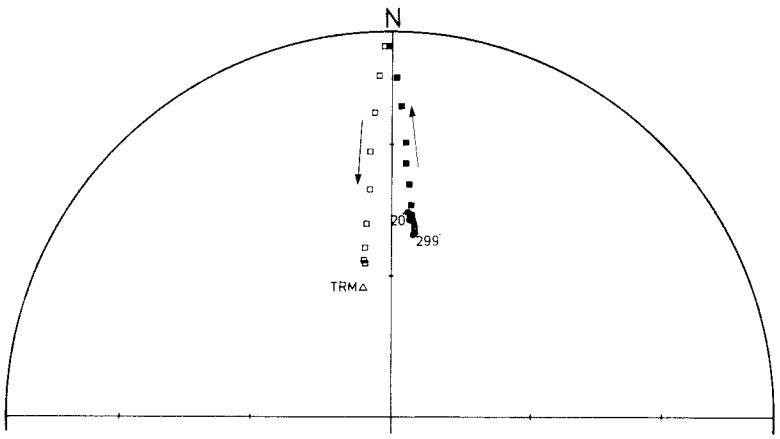
N
20
299
TRM△

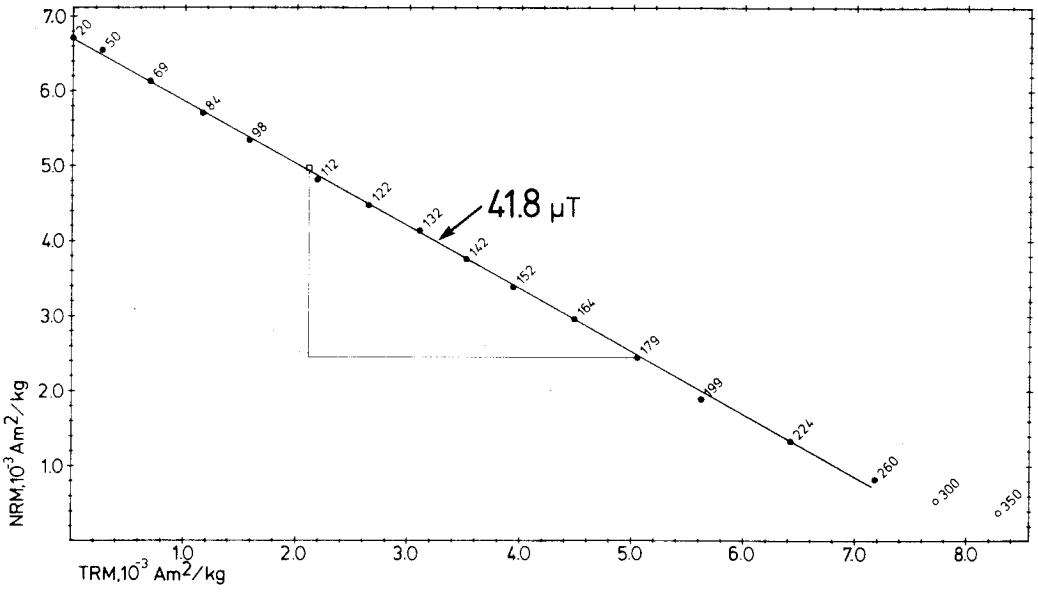
7.0
6.0
5.0
4.0
3.0
2.0
1.0
NRM,10^{-3} Am^2/kg
20
50
69
84
98
112
122
132
142
152
164
179
199
224
260
300
350
41.8 μT
1.0
2.0
3.0
4.0
5.0
6.0
7.0
8.0
TRM,10^{-3} Am^2/kg

progressively higher temperatures. The directions measured after heating steps in a zeroed magnetic field are fairly tightly clustered but shift first to shallower and then gradually to steeper inclinations and somewhat more easterly declinations. This change follows the same great circle as the directions after heating in the applied field. It is likely that the change in direction is due to the formation, by oxidation, of a magnetic phase with CRM having blocking temperatures above the temperature of a given Thellier step. Evidently this oxidation is progressive, beginning in the early steps of the experiment, but does not become appreciable until temperatures of 260°C and above are reached. The direction of magnetization of the new phase is antiparallel to the field in the ovens. The NRM-TRM diagram is linear between 100 percent and about 10 percent of the original NRM with a relative standard deviation of the slope of 0.00783. For heating steps at higher temperatures than 260°C, the ratio of NRM lost to TRM gained diverges from the linear relationship in the sense of gaining too much TRM. A single PTRM check, performed by heating the specimen in the applied field to an earlier temperature step before heating to the temperature of the second stage of the current Thellier step, in this case 179°C, indicates that up to that temperature no alteration of the magnetic phase is perceptible in the remanence (see Appendix of Coe and others (1978) for complete details of PTRM check). While the value of PNRM lost is assumed (calculated by interpolation) for a PTRM check, the reproducibility of the amount of PTRM previously acquired in the applied field is a sensitive measure of possible progressive chemical

alterations. Three specimens from the Little Belknap Flow gave similar results and yielded paleointensities with a precision of 500 nT.

Specimen NoCI 3-4a from the North Crater pahoehoe flow in the Craters of the Moon Lava Field is another rock with a single magnetic phase with a low Curie temperature for which a reliable paleointensity has been obtained (Fig. 20). Reversibility of strong-field magnetization with heating in vacuum and preservation of original magnetic direction through most heating steps is excellent. Above 375°C the directions measured after heating steps in a zeroed magnetic field begin to migrate, but not toward the direction of the laboratory applied field. The Arai diagram is also nonlinear above 375°C. In addition, the relationship between NRM lost and TRM gained is nonlinear as room temperature is approached. For a sample with this low Curie temperature, it is likely that portions of the blocking temperature distribution are within the diurnal temperature range of the surface of the Snake River Plain. Below 42°C, this specimen probably has lost the original TRM and acquired a new component of magnetization either in the field or the laboratory. PTRM checks all confirm preservation of the original magnetic phases. The relationship of NRM lost to TRM gained is linear over 90 percent of the original NRM with a relative standard deviation of 0.01508. Two other specimens gave equally satisfactory results.

Specimen PkDO 2-1a, from the Parkdale Flow on Mt. Hood, Oregon, represents a rock with a single magnetic phase with a high Curie temperature (Fig. 21). Strong-field magnetization for this specimen

Fig. 20--Magnetic measurements used in paleointensity determination from sample NoCI 3-4a, North Crater pahoehoe flow, Craters of the Moon, Idaho. Upper diagram shows strong-field magnetization as a function of temperature. Curve with arrow pointing to the right is for heating from room temperature to 600°C, and curve with arrow pointing to left is for cooling from 600°C. Sample was heated and cooled at 10^{-5} torr and in 300 mT applied field. Middle diagram is equal-area projection showing directions of magnetization measured after heating steps in the Thellier experiment. Filled points are on the lower hemisphere and open points are on the upper hemisphere. Squares denote measurements after heating in a known magnetic field and circles denote measurements after heating in a zeroed magnetic field. The letters TRM next to a triangle mark the direction of the applied field, the letters -TRM mark the antipode of the applied field direction. The arrows show the sense of the progressive change in direction after heating in the known field. The lower diagram is an Arai NRM-TRM diagram showing relationship between NRM lost at progressive heating steps compared to TRM gained in a known magnetic field. Filled points are used for determination of the paleointensity for this sample, open points were not included in the interpretation. Lines forming right angles indicate PTRM checks of TRM acquisition at earlier lower temperatures, and connect to Thellier steps at which they were performed.

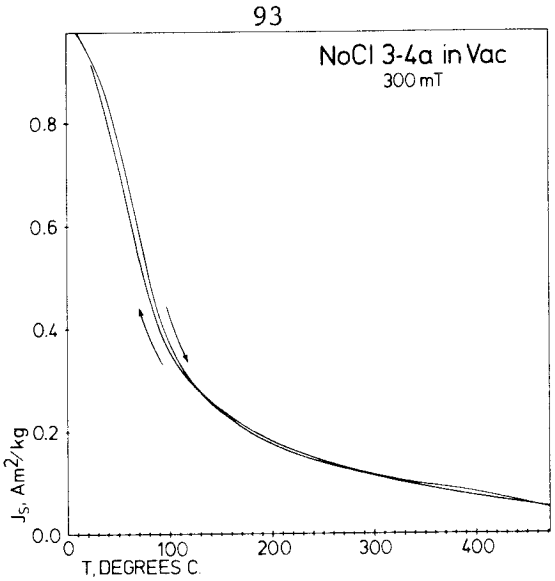
NoCl 3-4a in Vac
300 mT
0.8
0.6
0.4
0.2
0.0
J_s, Am^2/kg
0
100
200
300
400
T, DEGREES C.

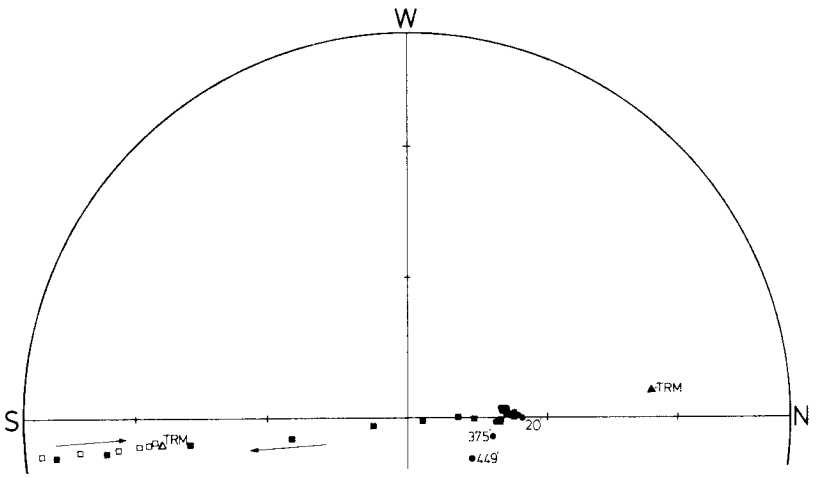
W
S
N
TRM
TRM
375
20
449

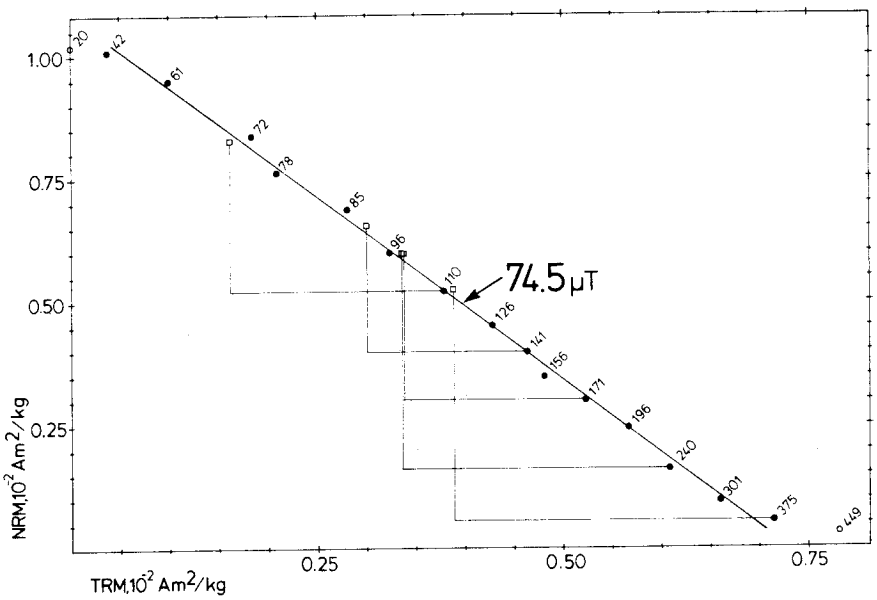
1.00
0.75
0.50
0.25
20
42
61
72
78
85
96
110
126
141
156
171
196
240
301
375
449
74.5 μT
NRM,10^{-2} Am^2/kg
TRM,10^{-2} Am^2/kg
0.25
0.50
0.75

Fig. 21--Magnetic measurements used in paleointensity determination from specimen PkDO 2-1a, Parkdale Flow, Mt. Hood, Oregon. Upper diagram shows strong-field magnetization as a function of temperature. Curve with arrow pointing to the right is for heating from room temperature to 600°C, and curve with arrow pointing to the left is for cooling from 600°C. Sample was heated and cooled at 10^{-5} torr and in 250 mT applied field. Middle diagram is equal-area projection showing directions of magnetization measured after heating steps in the Thellier experiment. Filled points are on the lower hemisphere. Squares denote measurements after heating in a known magnetic field and circles denote measurements after heating in a zeroed magnetic field. The letters TRM next to a black triangle mark the direction of the applied field, the letters -TRM mark the antipode of the applied field direction. The arrow shows the sense of the progressive change in direction after heating in the known field. The lower diagram is an Arai NRM-TRM diagram showing the relationship between NRM lost at progressive heating steps compared to TRM gained in a known magnetic field. Filled points are used for determination of the paleointensity for this sample. Lines forming right angles indicate PTRM checks of TRM acquisition at earlier lower temperatures, and connect to Thellier step at which they were performed.

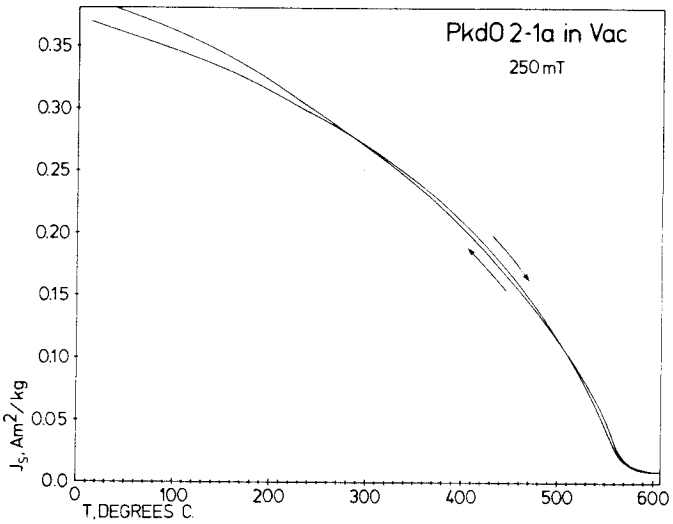
Pkd0 2-1a in Vac
250 mT
0.35
0.30
0.25
0.20
0.15
0.10
0.05
0.0
J_s, Am^2/kg
0
100
200
300
400
500
600
T, DEGREES C.

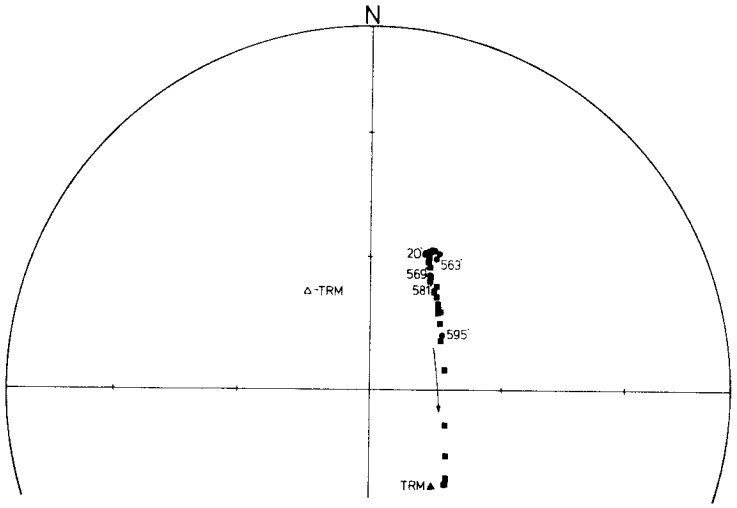
N
Δ-TRM
563
595
TRM

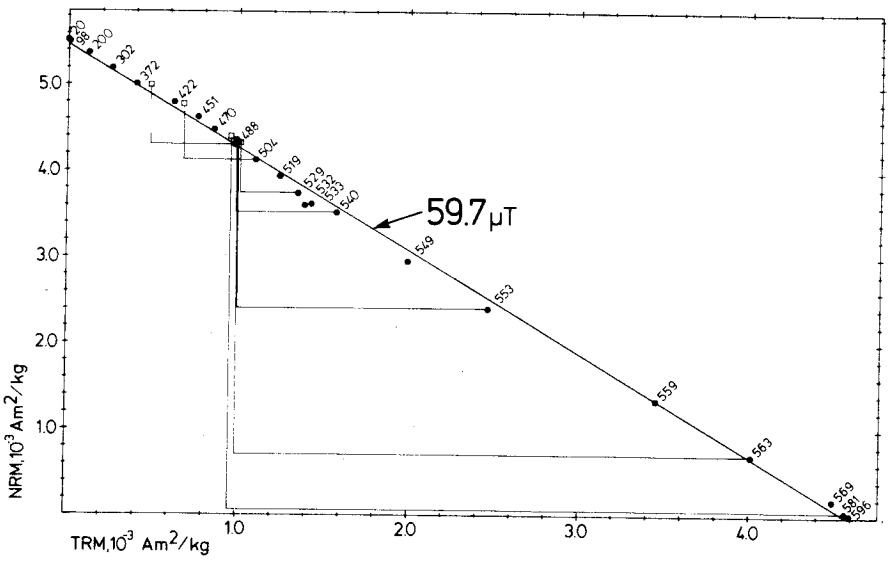
59.7 μT
5.0
4.0
3.0
2.0
1.0
NRM, 10^{-3} Am^2/kg
1.0
2.0
3.0
4.0
TRM, 10^{-3} Am^2/kg

is thermally reversible with only a 5 percent increase in magnetization at room temperature after heating. The Curie temperature is close to 570°C and represents a low-Ti magnetite probably produced by high-temperature oxidation during emplacement of the lava. Directional measurements made after heating in the zeroed magnetic field give consistent results until temperatures above 563°C are reached; above 563°C the PNRM directions shift markedly toward the direction of the applied laboratory field. At these temperatures a CRM that has blocking temperatures above the temperature of a given Thellier step apparently has been produced. While more scattered than the previous examples, the NRM-TRM points for this specimen are distributed linearly, with a relative standard deviation of the slope of 0.00908, and provide a good paleointensity determination. PTRM checks consistently reacquire the same amount of TRM at earlier temperature steps within a few percent and verify that despite the strong directional changes above 563°C, most of the original magnetic phase has been preserved. Two other specimens from this flow were more strongly altered in the Thellier experiment. PTRM checks revealed progressive changes in TRM acquisition at low temperature heating steps. These three specimens contain hematite pigment; their alteration in the Thellier experiment may have been due to reduction of a small amount of hematite to magnetite by reaction with trace amounts of oil from the vacuum pump. Other hematite-free specimens have since been obtained and subsequent experiments will be performed to verify the results from PkDO 2-1a.

Specimen IcSU 2-5c from the Ice Spring Field in Utah provides another example of a rock with a single magnetic phase with a high Curie temperature. A reliable paleointensity can be obtained from this specimen despite the fact that it has a strong component of isothermal remanent magnetization (IRM). The NRM direction included an IRM component which is largely removed after heating to 421°C (Fig. 22). From an af demagnetization experiment, on another specimen from core 5, the IRM component was found to be removed at relatively low fields. As heating in vacuum showed reversible saturation magnetization of the specimen, a decision was made to try the Thellier experiment.

Magnetic directions after heating in a zeroed field for specimen IcSU 2-5c migrate toward the direction of the natural TRM component near 0 deg declination and 65 deg inclination early in the experiment. From room temperature to 421°C, the points on the Arai diagram follow an arc that lies below the linear part of the diagram. Between 421° and 601°C the diagram is linear with a relative standard deviation of 0.00605. At 577°C, the magnetic directions measured after heatings in a zeroed field begin to migrate, in a general way, toward the applied field direction. PTRM checks show fairly good reproduction of original TRM acquisition even after heating at the highest temperature steps. The Arai diagram is linear over about 78 percent of the loss of the NRM. Paleointensity determined from two other specimens from the Ice Springs Field were based on comparable linear fits, including 92 and 94 percent of the NRM with relative standard deviations of 0.00972 and 0.01472 respectively.

Fig. 22--Magnetic measurements used in paleointensity determination from sample IcSU 2-5c, Ice Spring Lava Field, Utah. Upper diagram shows strong-field magnetization as a function of temperature. Curve with arrow pointing to the right is for heating from room temperature to 600°C, and curve with arrow pointing to the left is for cooling from 600°C. Sample was heated and cooled at 10^{-5} torr and in 250 mT applied field. Middle diagram is equal-area projection showing directions of magnetization measured after heating steps in the Thellier experiment. Filled points are on the lower hemisphere. Squares denote measurements after heating in a known magnetic field and circles denote measurements after heating in a zeroed magnetic field. The letters TRM next to a triangle mark the direction of the applied field. The arrows show the sense of the progressive change both in direction after heating in the known field and after heating in the zeroed field. The lower diagram is an Arai NRM-TRM diagram showing relationship between NRM lost at progressive heating steps compared to TRM gained in a known magnetic field. Filled points are used for determination of the paleointensity for this sample, open points were not included in the interpretation. Lines forming right angles indicate PTRM checks of TRM acquisition at earlier lower temperatures, and connect to Thellier steps at which they were performed.

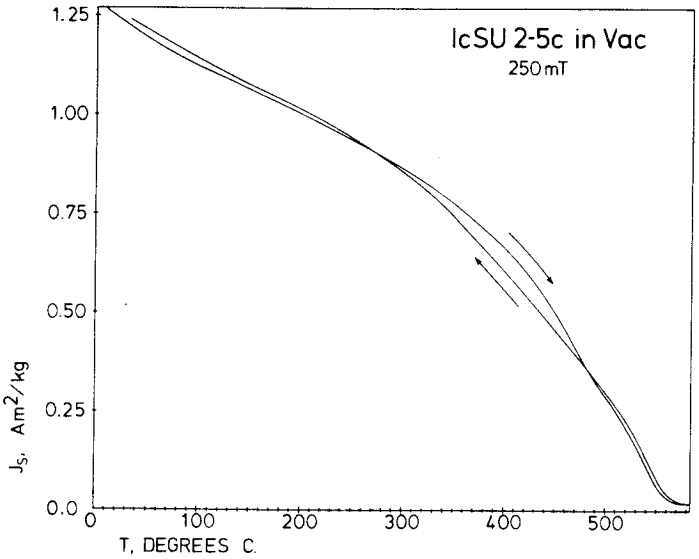
IcSU 2-5c in Vac
250 mT
1.25
1.00
0.75
0.50
0.25
0.0
J_S, Am^2/kg
0
100
200
300
400
500
T, DEGREES C.

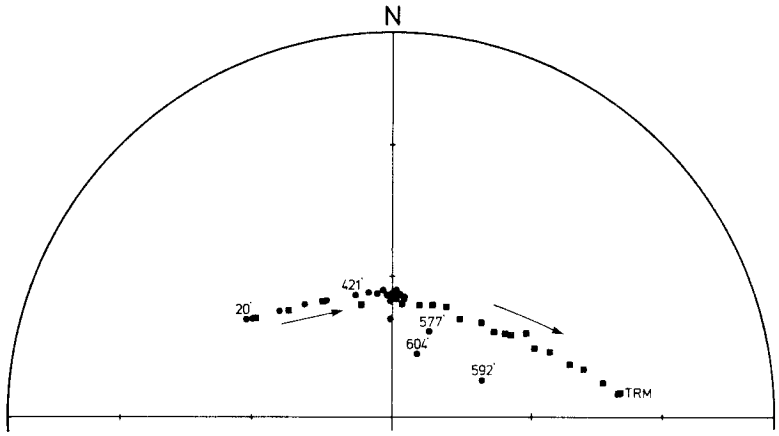
N
20
421
577
604
592
TRM

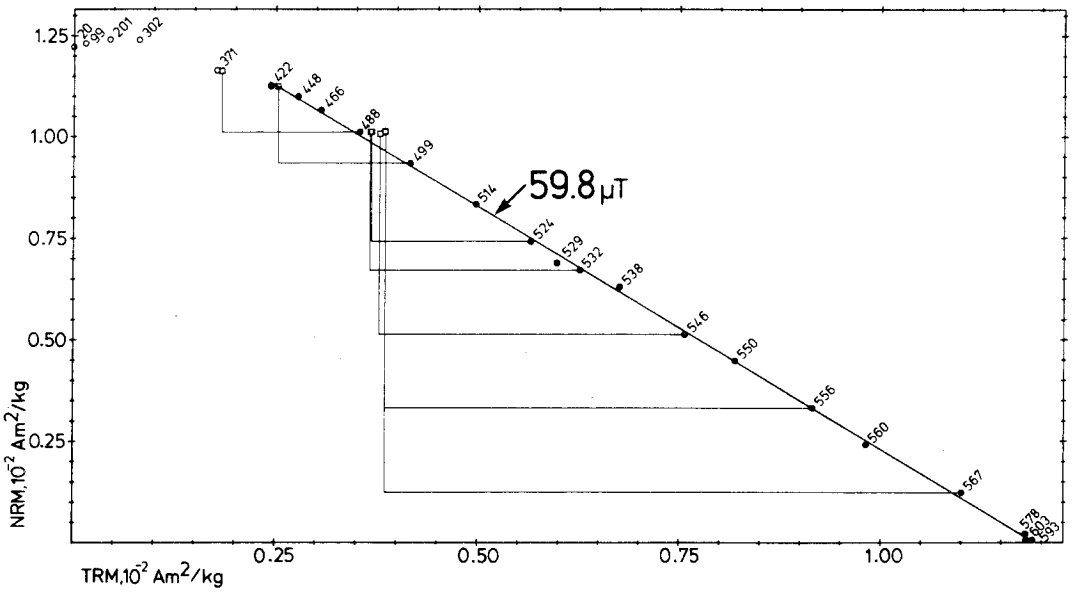
1.25
1.00
0.75
0.50
0.25
NRM,10^{-2} Am^2/kg
0.25
0.50
0.75
1.00
TRM,10^{-2} Am^2/kg
59.8 μT
20
99
201
302
371
422
448
466
488
499
514
524
529
532
538
546
550
556
560
567
578
580
593

Specimen WPiI 1-1a from the Wapi Lava Field is an example of a rock with both a low Curie temperature magnetic phase and a high Curie temperature magnetic phase (Fig. 23). The strong-field thermomagnetic curve for increasing temperature reveals not only a distributed low Curie temperature, but also an additional inflection near 500°C. The cooling branch of the strong-field thermomagnetic curve does not follow the heating curve; apparently the high Curie temperature phase was altered by heating to 600°C in vacuum. The net effect of heating in thermomagnetic balance is an increase of 25 percent in the strong-field magnetization of the specimen. In general, the prospect of obtaining a reliable paleointensity determination from such a specimen is not promising, but the experiment was performed anyway.

The directions of magnetization measured after heating in a zeroed magnetic field for specimen WpiI 1-1a are stable up to 402°C, with a slight tendency to migrate toward the antipode of the TRM direction. Directions of magnetization measured after heating in the applied field follow a smooth great circle path toward the applied field direction with progressive temperature steps. The Arai diagram is linear between 72° and 275°C with a relative standard deviation of 0.01170. Above 275°C, excess laboratory TRM is acquired at each temperature step. All NRM has been lost by 500°C. PTRM checks are consistent and satisfactory up to 329°C, but unsatisfactory at 500°C. At temperatures above 275°C, appreciable oxidation apparently occurs, despite the 10^{-5} torr vacuum. Titanomagnetite probably is replaced by low-Ti magnetite and ilmenite with a resulting decrease in grain

Fig. 23--Magnetic measurements used in paleointensity determination from sample WpiI 1-1a, Wapi Lava Field, Idaho. Upper diagram shows strong-field magnetization as a function of temperature. Curve with arrow pointing to the right is for heating from room temperature to 600°C, and curve with arrow pointing to the left is for cooling from 600°C. Sample was heated and cooled at 10^{-5} torr and in 300 mT applied field. Middle diagram is equal-area projection showing directions of magnetization measured after heating steps in the Thellier experiment. Filled points are on the lower hemisphere and open points are on the upper hemisphere. Squares denote measurements after heating in a known magnetic field and circles denote measurements after heating in a zeroed magnetic field. The letters TRM next to a triangle mark the direction of the applied field, the letters -TRM mark the antipode of the applied field direction. The arrows show the sense of the progressive change in direction after heating in the known field. The lower diagram is an Arai NRM-TRM diagram showing relationship between NRM lost at progressive heating steps compared to TRM gained in a known magnetic field. Filled points are used for determination of the paleointensity for this sample, open points were not included in the interpretation. Lines forming right angles indicate PTRM checks of TRM acquisition at earlier lower temperatures, and connect to Thellier steps at which they were performed.

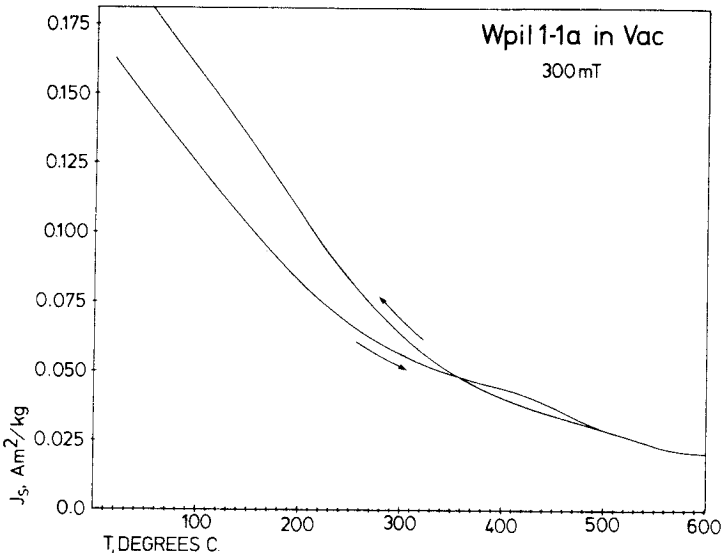
Wpil 1-1a in Vac
300 mT
0.175
0.150
0.125
0.100
0.075
0.050
0.025
0.0
J_s, Am^2/kg
100
200
300
400
500
600
T, DEGREES C.

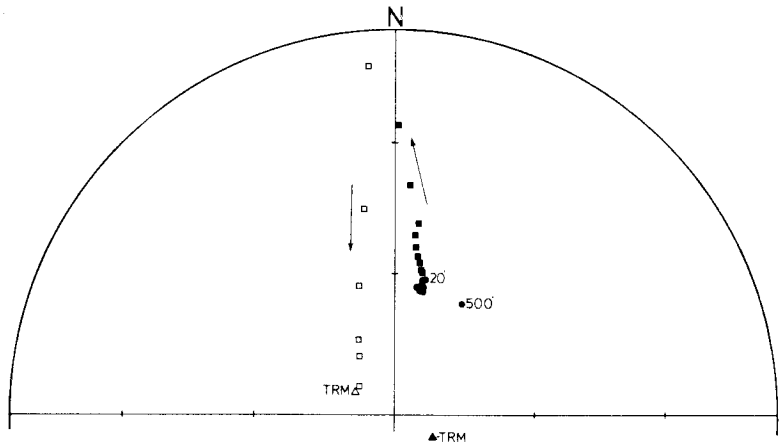
N
20
500
TRM
TRM

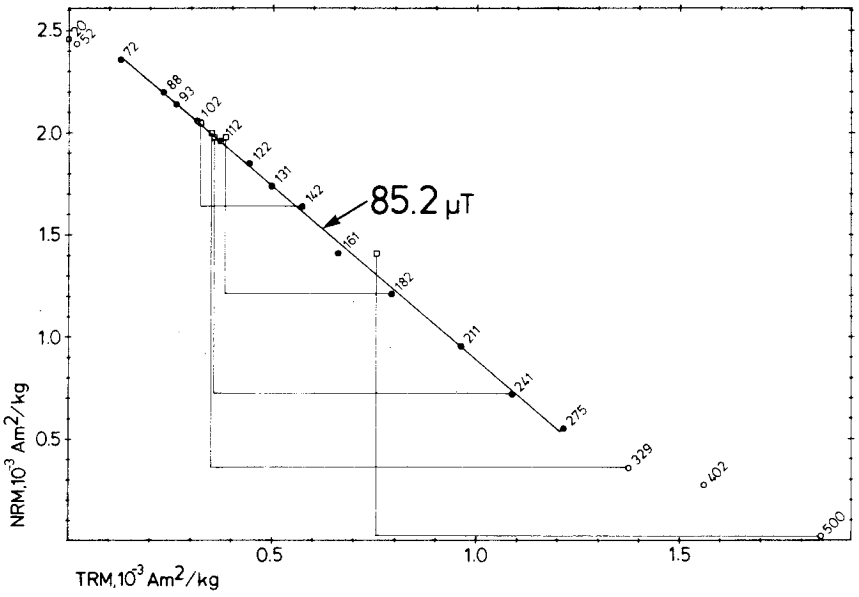
2.5
2.0
1.5
1.0
0.5
72
88
93
102
112
122
131
142
85.2 μT
161
182
211
241
275
329
402
500
0.5
1.0
1.5
NRM, 10^{-3} Am^2/kg
TRM, 10^{-3} Am^2/kg

size of the magnetic phases and increase in spontaneous magnetization, either of which would explain the anomalous gain in TRM. Before this alteration, however, about 71 percent of the NRM has been lost. Similarly satisfactory determinations of paleointensity were obtained for two other specimens from the Wapi Lava Field.

A final example of determination of paleointensity is given for specimen CvBW 2-1 from the Cave Basalt Flow on Mt. St. Helens, Washington (Fig. 24). This rock also has two magnetic phases, as shown by the strong-field magnetization heating curve; the curve for cooling from 600°C does not follow the heating curve. The high Curie temperature phase is altered by heating to 600°C at 10^{-5} torr.

The directions of magnetization measured after heating steps in a zeroed field are tightly grouped. Directions of magnetization measured after heating steps in the applied field show a smooth progression toward the applied field direction with successive temperature steps. The Arai diagram is linear from 20° to 324°C with a relative standard deviation of 0.00940. A single PTRM check after heating to 403°C shows significant alteration of the magnetic characteristics of this specimen. Both the Thellier steps and the PTRM check indicate the alteration allows the specimen to acquire a larger laboratory TRM than expected. The simplest explanation for this alteration is oxidation of titanomagnetite and exsolution of low-Ti magnetite at the higher temperature steps. Only 56 percent of the NRM loss is used for the paleointensity determination, which was the general case for other specimens of the Cave Basalt Flow as well. These other specimens yielded similar paleointensities (Table 2).

Fig. 24--Magnetic measurements used in paleointensity determination from sample CvBW 2-1, Cave Basalt Flow, Mt. St. Helens, Washington. Upper diagram shows strong-field magnetization as a function of temperature. Curve with arrow pointing to the right is for heating from room temperature to 600°C, and curve with arrow pointing to the left is for cooling from 600°C. Sample was heated and cooled at 10^{-5} torr and in 200 mT applied field. Middle diagram is equal-area projection showing directions of magnetization measured after heating steps in the Thellier experiment. Filled points are on the lower hemisphere and open points are on the upper hemisphere. Squares denote measurements after heating in a known magnetic field and circles denote measurements after heating in a zeroed magnetic field. The letters TRM next to a triangle mark the direction of the applied field, the letters -TRM mark the antipode of the applied field direction. The arrows show the sense of the progressive change in direction after heating in the known field. The lower diagram is an Arai NRM-TRM diagram showing relationship between NRM lost at progressive heating steps compared to TRM gained in a known magnetic field. Filled points are used for determination of the paleointensity for this sample, open points were not included in the interpretation. Lines forming right angle indicates PTRM check of TRM acquisition at earlier lower temperatures, and connects to Thellier step at which it was performed.

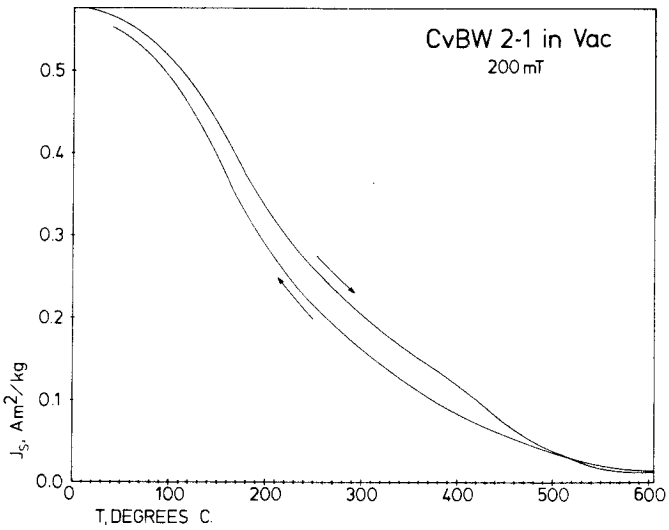
CvBW 2-1 in Vac
200 mT
0.5
0.4
0.3
0.2
0.1
0.0
J_S, Am^2/kg
0
100
200
300
400
500
600
T, DEGREES C.

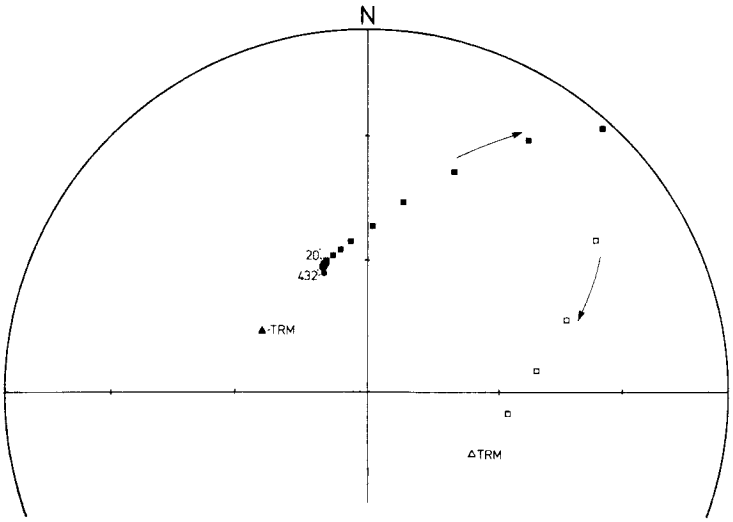
N
20
432
▲-TRM
△TRM

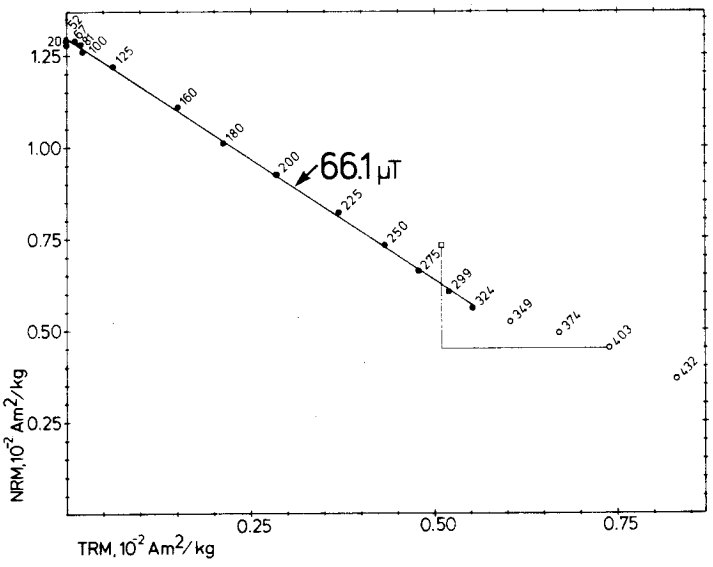
20
100
125
160
180
200
66.1 μT
225
250
275
299
324
349
374
403
432
1.25
1.00
0.75
0.50
0.25
NRM, 10^{-2} Am^2/kg
0.25
0.50
0.75
TRM, 10^{-2} Am^2/kg

Secular Variation of Geomagnetic Field Intensity in Western United States Observed from Holocene Volcanic Rocks and Comparison with Archeointensity Determinations from Snaketown, Arizona

Paleointensity determinations from 30 dated lava flows and one ash flow (Table 2) reveal a complex history of the intensity of the magnetic field in the western United States during latest Pleistocene and Holocene time (Fig. 25). In order to compare the results from different localities in the western United States, the local paleointensities have been reduced to virtual dipole moments of the Earth (VDM) according to the formula

$$VDM = \frac{Fr^3}{(1 + 3\sin^2(\tan^{-1}(\frac{\tan I}{2})))^{1/2}} \quad (1)$$

where F is the local paleointensity, r the radius of the Earth and I the inclination of the paleofield. During the Holocene the VDM corresponding to paleointensities in the western United States has varied by more than a factor of two, ranging from as low as 6.49 to as high as 14.32×10^{22} $A \cdot m^2$. Fluctuations of this VDM by as much as 6×10^{22} $A \cdot m^2$ occurred within periods of time as short as 1000 years. The serial correlation of the measured paleointensities evident in parts of Figure 25 indicates that this fluctuation was a real phenomenon of the ancient geomagnetic field and not an artifact of the measurements.

The observed fluctuations of paleointensity contradict the commonly held impression that local intensity of the geomagnetic field has varied with a period comparable to the duration of the Holocene. This impression is derived from the history of the

Table 2. Paleointensity data for dated Holocene lava flows and volcanic deposits.

	Sample Number	Js/Js	ΔT	N	f	g	σb/b	q	F_ϵ (10^{-4} T)	$\bar{F}_\epsilon \pm \sigma_{\bar{F}_\epsilon}$ (10^{-4} T)	$\frac{\overline{VDM} \pm \sigma_{\overline{VDM}}}{(\overline{VADM} \pm \sigma_{\overline{VADM}})}$ (10^{22} Am^2)
1. Ice Spring Field, Black Rock Desert, Utah	2-1b	0.93	297-573	16	0.950	0.919	.00972	89.7	0.613		
	2-2b	0.96	250-567	24	0.884	0.937	.01472	56.3	0.578	0.600±.010	9.81±0.17
			(450-567	17	0.439	0.900	.01181	33.5	0.657)		(10.53±0.18)
	2-5c	1.02	421-602	18	0.786	0.922	.00605	119.9	0.598		
2. Bonito Flow, San Francisco Volcanic Field, Arizona	1-3c	0.96	20-594	21	1.035	0.922	.01887	50.6	0.784		
	2-2a	0.99	20-566	25	0.994	0.932	.00687	134.8	0.636	0.645±.058	11.34±1.02
	2-5a	0.95	20-582	18	1.014	0.914	.01831	50.6	0.622		(11.82±1.06)
3. Kana-a Flow, San Francisco Volcanic Field, Arizona	1-2b	0.98	Severe Alteration - Results uninterpretable								
	1-6a	0.96	(20-429	9	0.264	0.850	.03128	7.2	0.844)		
			(390-530	16	0.738	0.928	.01359	50.4	0.615)	0.660±(.020)	10.61±0.32
			20-548	24	0.969	0.949	.01349	68.1	0.660		(12.09±0.37)
	2-3a	1.00	20-562	20	0.943	0.930	.01021	85.9	0.660		
4. West Belknap Flow, McKenzie Pass, Oregon	1-6a	1.01	20-323	16	0.970	0.906	.01504	58.5	0.445		
	1-7	0.96	20-243	11	0.909	0.852	.01786	43.3	0.423	0.427±.011	8.09±0.21
	2-4a	0.92	(20-487	10	0.418	0.822	.02276	15.1	0.613)		(7.06±0.18)
			468-560	14	0.638	0.911	.01221	47.6	0.408		
5. South Belknap Cone Flow, McKenzie Pass, Oregon	1-4a	0.99	20-244	11	0.879	0.846	.00603	123.3	0.440		
	1-5a	1.00	20-159	10	0.802	0.866	.00639	108.7	0.386	0.426±.023	8.76±0.48
	2-6a	1.03	20-261	15	0.914	0.905	.00764	108.2	0.462		(7.05±0.38)
6. Cave Basalt Flow, Mt. Saint Helens, Washington	1-1a	0.96	20-354	15	0.499	0.859	.01111	38.6	0.686		
	1-4a	0.97	20-372	16	0.459	0.907	.01799	23.2	0.680	0.670±.009	11.41±0.16
	2-1	0.98	20-324	14	0.563	0.887	.00940	53.1	0.661		(10.87±0.15)
7. Craters of the Moon Flow, near Rattlesnake Butte, Idaho	1-2a	0.92	51-544	14	0.914	0.909	.02121	39.2	0.768		
	2-1	0.84	70-351	15	0.833	0.913	.00747	101.7	0.670	0.708±.035	11.55±0.57
	2-5	0.85	51-352	16	0.874	0.920	.00855	93.9	0.754		(11.83±0.59)
8. Watchman Flow, Craters of the Moon, Idaho	1-1a	0.86	20-408	21	0.905	0.942	.01826	46.7	0.774		
	2-1	0.91	20-541	18	0.973	0.924	.01025	87.7	0.755	0.763±.006	12.37±0.09
	2-2a	0.89	20-552	23	0.982	0.940	.00560	164.9	0.765		(12.74±0.10)
9. Trenchmortar Flat Flow, Craters of the Moon, Idaho	1-1	1.01	52-552	14	0.878	0.905	.02124	37.4	0.811		
	1-3a	1.10	(53-536	21	0.835	0.931	.03091	25.1	0.732)		
			68-228	8	0.288	0.821	.04986	4.7	0.785	0.818±.020	13.17±0.32
	2-1a	1.00	(20-552	19	0.988	0.914	.02816	46.0	0.716)		(13.65±0.33)
			20-422	11	0.491	0.857	.02231	18.9	0.853		
10. Wapi Field, Snake River Plain, Idaho	1-1a	1.25	72-275	13	0.707	0.902	.01170	54.5	0.852		
	1-3	1.17	52-274	12	0.725	0.906	.01951	33.7	0.870	0.865±.030	14.32±0.50
	1-6a	1.13	52-250	11	0.654	0.897	.02163	27.1	0.915		(14.53±0.50)

Table 2. Continued

	Sample Number	Js'/Js	ΔT	N	f	g	σb/b	q	F_ϵ (10^{-4} T)	$\overline{F_\epsilon} \pm \sigma_{\overline{F_\epsilon}}$ (10^{-4} T)	$\frac{\overline{VDM}+\sigma_{\overline{VDM}}}{(\overline{VADM}+\sigma_{\overline{VADM}})}$ (10^{22} Am^2)
11. Kings Bowl Field, Snake River Plain, Idaho	1-1a	0.91	20-391	8	0.397	0.815	.03699	8.8	0.941		
			(20-574	15	1.015	0.903	.02368	38.7	0.736)		
	1-2a	0.95	20-603	23	1.087	0.935	.04228	24.0	0.857	---	---
	2-5a	0.93	(66-378	14	0.456	0.902	.03015	13.7	1.149)		
			20-533	22	0.961	0.939	.02777	32.5	0.898		
12. South Puyallup Block and Bomb Flow, Mt. Rainier, Wash.	2-5a	0.94	Essentially Uninterpretable								
13. Four in One Flow, McKenzie Pass, Oregon	1-2a	1.00	20-452	20	0.847	0.917	.00978	79.5	0.692		
	4-1a	0.99	20-286	9	0.327	0.800	.01520	17.2	0.929		
			(20-548	27	0.989	0.940	.01949	47.7	0.822)	0.690±.138	10.10±2.02
	5-2a	1.03	20-263	18	0.854	0.914	.01340	58.3	0.676		(11.42±2.28)
14. Yapoah Flow, McKenzie Pass, Oregon	1-1a	1.00	20-265	18	0.723	0.923	.01238	53.9	0.681		
	1-5a	0.93	(20-348	8	0.405	0.807	.01773	18.4	1.081)		
			(20-558	20	0.989	0.933	.02380	38.8	0.841)	0.681±.038	11.48±0.64
	2-6a	0.89	(20-496	15	0.480	0.917	.03257	13.5	0.814)		(11.26±0.62)
			323-489	10	0.326	0.882	.05246	5.5	0.735		
15. Little Belknap Flow, McKenzie Pass, Oregon	1-1b	0.96	20-260	15	0.887	0.924	.00783	104.8	0.418		
	1-6a	1.09	20-261	15	0.947	0.899	.00921	92.5	0.403	0.414±.005	8.57±0.10
	2-2a	1.05	20-249	17	0.958	0.915	.00978	89.7	0.420		(6.85±0.08)
16. Clear Lake Flow, Sand Mountain, Oregon	1-5c	0.83	20-374	9	0.573	0.865	.01199	41.3	0.565		
	1-6b	0.89	20-496	10	0.644	0.767	.05462	9.0	0.587	0.568±.009	11.10±0.17
	2-5b	0.91	200-429	8	0.574	0.835	.02320	20.7	0.580		(9.39±0.14)
17. Blue Lake Crater, Santiam Pass, Oregon	1-1a	1.22	20-416	8	0.242	0.747	.04753	3.8	0.536	0.536±(.020)	8.28±0.31
			(20-554	24	0.924	0.926	.01786	47.9	0.673)		(8.85±0.33)
18. Lava Lake Flow, Sand Mountain, Oregon (see table footnotes)	1-2a	0.91	20-501	11	0.514	0.883	.02917	15.6	0.688		
	2-4a	0.94	20-523	13	0.439	0.895	.03043	12.9	0.693	0.702±.010	13.69±0.19
	2-5a	0.93	20-532	15	0.456	0.908	.02489	16.7	0.720		(11.59±0.17)
19. Hell's Half Acre Field, Snake River Plain, Idaho	2-2a	1.01	20-360	16	0.434	0.904	.01702	23.1	0.484	0.500±.014	8.02±0.23
	2-4a	1.27	20-352	17	0.437	0.910	.01440	27.6	0.512		(8.35±0.23)
20. Dotsero Flow, Dotsero, Colorado	1-1b	0.92	208-399	5	0.327	0.732	.08428	2.8	0.577		
			(20-490	13	0.854	0.905	.02885	26.8	0.754)	0.592±.011	10.24±0.19
	2-2c	0.99	194-305	9	0.577	0.853	.03004	16.4	0.824		(10.31±0.19)
	2-4b	0.99	124-332	13	0.787	0.907	.02027	35.2	0.592		
21. Lava Cascade Flow, NW Rift, Newberry Crater, Oregon	1-1	0.98	279-459	10	0.505	0.885	.01823	24.5	0.597		
	2-3	1.06	20-319	14	0.794	0.906	.00744	96.6	0.470	0.466±.059	8.49±1.08
	2-4	1.10	20-373	24	0.529	0.916	.01508	32.1	0.407		(7.75±0.97)

Table 2. Continued

	Sample Number	Js'/Js	ΔT	N	f	g	σb/b	q	F_ϵ (10^{-4} T)	$F_\epsilon \pm$ (10^{-4} T)	$\overline{VDM}+\sigma_{\overline{VDM}}$ ($\overline{VADM}+\sigma_{\overline{VADM}}$) ($10^{22}$ Am^2)
22. Forest Road Flow, NW Rift, Newberry Crater, Oregon	2-1	1.18	20-334	17	0.830	0.919	.00506	150.6	0.547	0.515±.064	9.79±1.22
	2-3	1.13	20-246	17	0.812	0.922	.01032	72.5	0.431		(8.56±1.06)
23. Surveyor Flow, Newberry Crater, Oregon	1-3	1.03	20-379	9	0.468	0.808	.01787	21.2	0.336		
24. Gasline Flow, NW Rift, Newberry Crater, Oregon	1-2b	0.95	20-400	5	0.165	0.623	.11160	0.9	0.440		
	1-5a	0.98	20-578	22	0.995	0.935	.00948	98.0	0.427	0.427±.007	7.61±0.12
	2-5b	0.94	20-447	6	0.156	0.702	.10268	1.1	0.416		(7.09±0.12)
25. Lava Butte Flow, NW Rift, Newberry Crater, Oregon	1-3b	0.95	20-427	10	0.326	0.865	.03334	8.5	0.500		
	1-6b	0.97	(20-502	11	0.244	0.872	.05349	4.0	0.472)	0.412±.036	7.22±0.63
			20-577	21	0.992	0.925	.01134	81.0	0.416		(6.84±0.60)
	2-6b	0.99	20-582	22	0.972	0.932	.01083	83.6	0.408		
26. Lava Cast Forest Flow, NW Rift, Newberry Crater, Oregon	2-4a	1.15	20-243	9	0.607	0.828	.03056	16.4	0.404	0.442±.027	8.34±0.51
	2-5	1.15	20-242	9	0.517	0.850	.00970	45.3	0.448		(7.35±0.44)
27. Crater Lake Ash Flow Deposit Crater Lake, Oregon	1-13a	0.95	20-154	3	0.195	0.441	.12553	0.7	0.568		
	1-14b	0.86	20-427	10	0.591	0.879	.02268	22.9	0.611	0.611±(.020)	8.89±0.29
	1-21b	0.89	20-397	5	0.080	0.718	.05248	1.1	0.564		(10.26±0.33)
28. Parkdale Flow, Mt. Hood, Oregon	1-3a	1.00	20-529	16	0.759	0.897	.00781	87.1	0.540		
	2-1a	1.05	20-595	21	1.004	0.904	.00908	99.9	0.597	0.570±.028	9.63±0.47
	2-6	1.17	20-504	11	0.276	0.825	.03456	6.6	0.516		(9.31±0.46)
			(20-579	21	0.965	0.899	.01806	48.1	0.560)		
29. Cerro Grande Field, Snake River Plain, Idaho	1-5c	1.00	20-242	5	0.288	0.702	.02402	8.4	0.330		
	2-3b	1.01	20-340	7	0.335	0.816	.02744	9.9	0.357	0.364±.019	6.49±0.34
	2-4b	1.01	155-348	5	0.348	0.729	.02135	11.9	0.394		(6.08±0.32)
30. Northeast Sunset Flow, Craters of the Moon, Idaho	1-1b	1.03	20-302	5	0.358	0.725	.04221	6.2	0.456		
	1-4a	1.33	20-302	5	0.311	0.728	.02765	8.2	0.503	0.483±.014	8.32±0.24
	1-6a	1.10	20-298	7	0.410	0.825	.04570	7.4	0.483		(8.05±0.24)
31. North Robbers Flow, Snake River Plain, Idaho	2-3b	1.07	101-426	9	0.218	0.847	.01980	9.3	0.402		
	2-4b	1.14	20-191	6	0.137	0.784	.05228	2.1	0.569	0.419±.026	8.40±0.52
	2-6b	1.08	20-414	11	0.234	0.884	.02772	7.5	0.452		(7.00±0.43)

The Lava Lake Flow was substituted for the Hackleman Creek Flow when no specimens could be found which satisfied the criteria for the Thellier experiment. They are of exactly the same age. Js'/Js is ratio of room temperature strong-field magnetization after and before heating. ΔT and N are temperature range and number of NRM-TRM points used to determine paleointensity; f is fraction of total extrapolated NRM spanned by least squares line segment; g is gap factor for points defining least squares line segment (Coe and others, 1978); σb/b is relative standard deviation of slope of least squares line segment; and q is overall quality factor of individual paleointensity estimate (Coe and others, 1978). F_ϵ is paleointensity estimate for individual specimen. $\overline{F_\epsilon}+\sigma_{\overline{F_\epsilon}}$ is weighted mean paleointensity plus or minus standard error of the mean. $\overline{VDM}+\sigma_{\overline{VDM}}$ ($\overline{VADM}+\sigma_{\overline{VADM}}$) is weighted mean dipole moment plus or minus standard error. Parenthesis around lines of data suggest other interpretations thought not to be correct. The raw data from which these table were constructed, can be found in Appendix 4 for the Arai Diagrams and Appendix 2 for the strong-field thermomagnetic records.

Table 2a. Paleointensity data for lava flows thought to be Holocene or latest Pleistocene in age.

	Sample Number	Js'/Js	ΔT	N	f	g	σb/b	q	F_ϵ (10^{-4} T)	$\overline{F_\epsilon} \pm \sigma_{\overline{F_\epsilon}}$ (10^{-4} T)	$\overline{VDM}+\sigma_{\overline{VDM}}$ ($\overline{VADM}+\sigma_{\overline{VADM}}$) ($10^{22}$ Am^2)
1. Flow near Burnt Lava Flow, Medicine Lake Highlands, California	1-2a	0.99	20-575	22	1.002	0.929	.00415	224.2	0.470		
			(20-505	12	0.308	0.851	.01779	14.7	0.493)		
	2-3	1.05	20-530	31	0.972	0.931	.00468	193.5	0.501	0.483±.010	9.45±0.20
	2-6a	1.01	(20-429	8	0.223	0.762	.03796	4.5	0.506)		(8.23±0.17)
			20-548	22	0.982	0.934	.01307	70.1	0.492		
2. 1915 Dacite Flow, Mt. Lassen, California	1-1	0.98	20-342	14	0.210	0.878	.05579	3.3	0.572	0.570±.002	---
	1-2	0.98	20-339	13	0.173	0.884	.03975	3.9	0.568		
3. Flow from Cinder Cone, Mt. Lassen, California	2-1a	0.98	98-473	12	0.693	0.872	.01969	30.7	0.643		
			(98-572	15	0.952	0.907	.01914	45.1	0.677)	0.627±.017	---
	2-3a	0.99	20-470	13	0.588	0.823	.01725	28.1	0.610		
			(20-559	18	0.978	0.900	.01530	57.5	0.665)		
4. Pahoehoe flow near Carey, Idaho from Craters of the Moon	2-2a	1.05	49-326	15	0.562	0.912	.02184	23.5	0.442	0.442±(.020)	7.57±0.34 (7.39±0.33)
5. Pahoehoe flow near Fingers Butte from Craters of the Moon	1-4b	1.00	(20-266	15	0.515	0.892	.02152	21.3	0.452)	0.396±(.020)	7.07±0.36
			101-328	14	0.406	0.889	.01783	20.2	0.396		(6.61±0.33)
6. South Robbers Flow, Snake River Plain, Idaho	1-1a	1.06	Severe Alteration - Results Uninterpretable								
	1-4b	0.93	20-345	7	0.252	0.810	.06437	3.2	0.488	0.505±.061	9.48±1.14
	1-5b	0.89	20-297	4	0.183	0.666	.07291	1.7	0.590		(8.43±1.02)
7. Grassy Cone Flow, Snake River Plain, Idaho	1-1a	1.01	(50-264	14	0.535	0.881	.01707	27.6	0.694)		
			20-329	17	0.627	0.905	.01569	36.2	0.680	0.634±.028	10.92±0.49
	1-4a	0.98	20-324	15	0.735	0.915	.01393	48.3	0.650		(10.58±0.47)
	1-6a	0.96	20-329	16	0.684	0.914	.01580	39.5	0.586		
8. Highway Flow, Craters of the Moon, Idaho	1-3a	1.05	341-591	24	0.969	0.931	.00534	169.1	0.794	0.804±.040	12.78±0.63
	1-5a	1.02	20-571	21	0.985	0.913	.01178	76.3	0.860		(13.41±0.67)
9. Flow near Inkom, Snake River Plain, Idaho	2-5b	1.01	191-348	11	0.433	0.889	.03313	11.6	0.388		
			(146-319	12	0.539	0.897	.03705	13.0	0.421)	0.337±.052	6.35±0.98
	2-6b	0.99	149-401	8	0.301	0.809	.00956	25.5	0.329		(5.66±0.88)
10. Pahoehoe flow nearest Kimama, Idaho from Craters of the Moon	1-2b	1.00	(20-98	5	0.360	0.737	.01545	17.2	0.416)		
			98-344	9	0.485	0.850	.02817	14.6	0.208	0.231±.019	4.06±0.33
	2-5b	1.00	78-170	8	0.472	0.851	.01855	21.7	0.245		(3.87±0.32)
11. Aa flow near Lava Lake from Craters of the Moon, Idaho	1-1a	0.99	(20-300	15	0.885	0.920	.02072	39.3	0.467)		
			78-240	10	0.545	0.885	.01878	25.7	0.447		
	1-3a	1.00	(20-299	18	0.853	0.928	.01425	55.5	0.460)	0.441±.004	7.52±0.07
			71-299	14	0.706	0.912	.01594	40.4	0.438		(7.37±0.07)
	1-4a	1.04	78-194	9	0.488	0.864	.02894	14.6	0.447		

Table 2a. Continued

	Sample Number	Js'/Js	ΔT	N	f	g	σb/b	q	F_ϵ (10^{-4} T)	$\overline{F_\epsilon} + \sigma_{\overline{F_\epsilon}}$ (10^{-4} T)	$\overline{VDM} + \sigma_{\overline{VDM}}$ ($\overline{VADM} + \sigma_{\overline{VADM}}$) ($10^{22}$ Am^2)
12. Pahoehoe flow nearest Minidoka from Craters of the Moon	1-3a	0.84	43-299	13	0.876	0.895	.01235	63.5	0.638	0.638±(.020)	10.89±0.34 (10.71±0.33)
13. Marsh Valley Flow, Snake River Plain, Idaho	2-1b	1.16	20-299	6	0.450	0.755	.02735	12.4	0.437		
	2-3b	0.98	(20-420	9	0.493	0.871	.03210	13.4	0.608)	0.440±.066	8.31±1.25
			251-439	6	0.309	0.790	.08534	2.9	0.533		(7.41±1.11)
14. North Crater Flow, Craters of the Moon, Idaho	3-1a	0.99	20-330	19	0.943	0.916	.01423	60.7	0.732		
	3-4a	0.99	42-375	15	0.904	0.924	.01508	55.4	0.745	0.741±.005	11.85±0.08
	4-2b	0.99	30-329	18	0.932	0.918	.01215	70.5	0.746		(12.36±0.09)
15. Shoshone Ice Cave Field, Snake River Plain, Idaho	4-1b	0.92	95-374	8	0.366	0.850	.02036	15.3	0.754		
	4-3b	0.92	20-343	7	0.450	0.827	.01330	28.0	0.657	0.535±.103	9.57±1.84
	4-6b	1.03	20-287	6	0.501	0.755	.00755	50.1	0.504		(8.95±1.73)
16. Diamond Craters Field, Diamond, Oregon	1-3a	1.11	20-412	11	0.590	0.886	.01722	30.4	0.525		
			(294-583	13	0.379	0.894	.03139	17.8	0.379)		
	1-5a	1.04	20-396	8	0.500	0.772	.02996	12.9	0.506	0.536±.013	7.97±0.19
			(296-575	10	0.618	0.869	.02741	19.6	0.410)		(8.98±0.22)
	2-1a	1.07	20-399	10	0.609	0.852	.00942	52.2	0.542		
			(343-565	12	0.554	0.889	.01768	27.9	0.329)		

Column headings are identical to those in Table 2 and are explained in footnotes following that table.

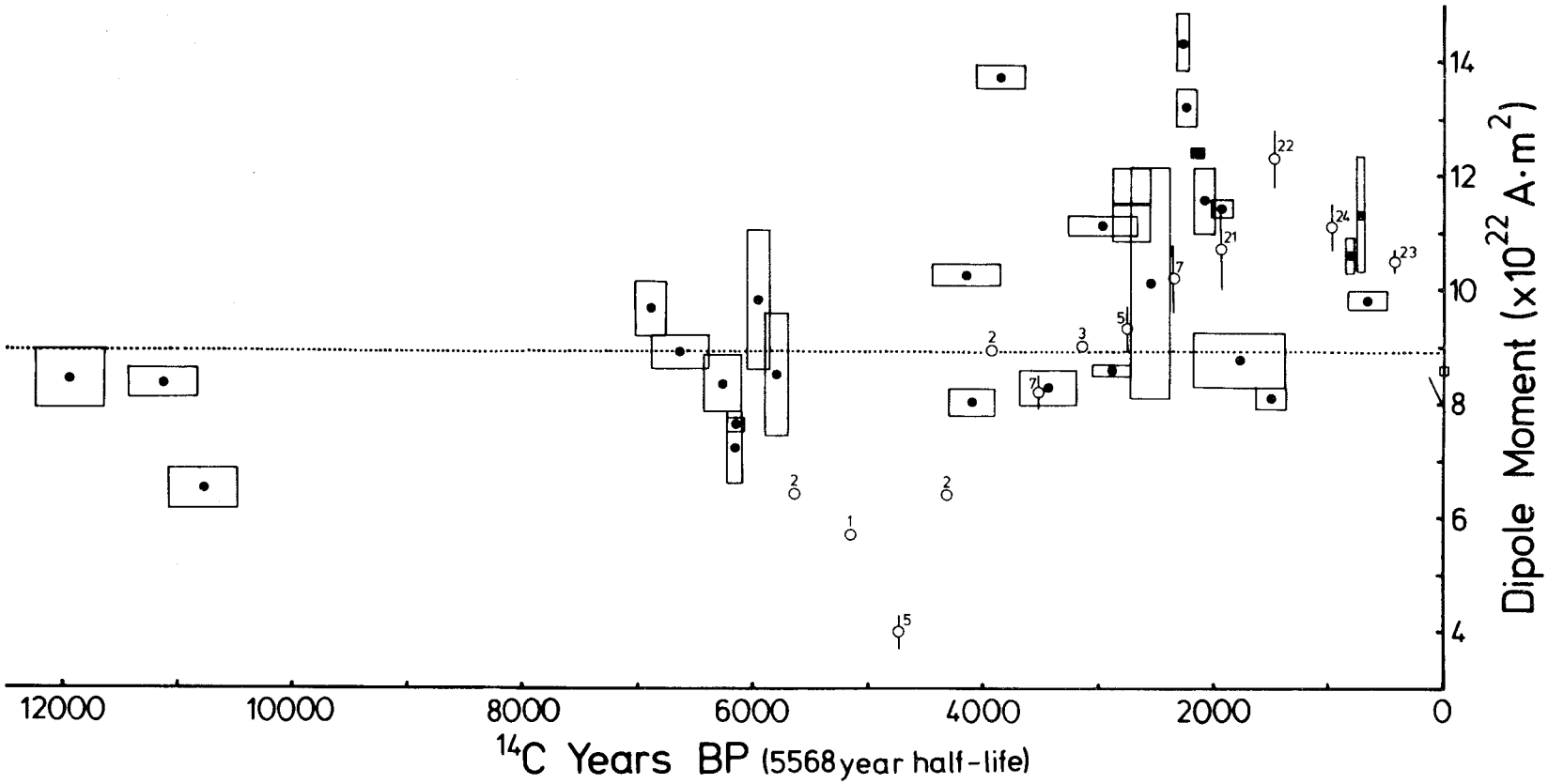

Fig. 25--Dipole moments from dated volcanic rocks in the western United States erupted during the Holocene. Error boxes enclose ^{14}C analytical standard deviations and standard deviation of paleointensity determination for each locality. Dotted line is Pleistocene averaged dipole moment from Kono (1971). Open circles are averaged global dipole moments calculated by Cox (1968). Numbers indicate number of averaged values. Open square on vertical axis is present dipole moment calculated for mean locality from its local inclination and intensity values. Short inclined line segment near vertical axis shows true global dipole moment change during the modern era.

global dipole moment variation (Fig. 25) found by Cox (1968). Even recent discussions of local intensity histories mention periods of variation shorter than 8000 years with a tentative note (Games, 1979). The global dipole moments obtained by Cox were based on world-wide averages for 500-year time windows; such averages were intended to suppress the local fluctuations of intensity due to variations of the nondipole field. It should be noted that a significant difference exists between the data averaged by Cox and the virtual dipole moments computed in the present study. Virtual dipole moments are calculated from the measured paleointensity and paleomagnetic inclination from a given locality, whereas the global dipole moments derived by Cox were based on averaging reduced dipole moments (RDM), calculated from the measured paleointensity of a sample and the present geomagnetic inclination at the sample locality (Smith, 1967a, b, c, 1968). The computed VDM will differ from the RDM by an amount that depends on the difference between the paleomagnetic inclination and the present inclination (see eqn. 1).

Use of the virtual dipole moment calculation to normalize paleointensity determinations from scattered localities assumes that the VGP position is an accurate reflection of the dipole position and that the inclination and intensity variation of the paleomagnetic field are predominantly due to dipole position and moment variation. It was shown in the chapter on the directional history of the western United States that this assumption is not true; the VGP gives only an approximate indication of the dipole position. Other schemes of normalization are the RDM and the

virtual axial dipole moment (VADM) (Barbetti, 1977); the latter is calculated assuming that the paleomagnetic field is that of a geocentric dipole parallel to the spin axis of the Earth. For reasons that will be dealt with in detail in the next chapter, the VADM calculation turns out to be the least inaccurate of the three choices.

Comparison of VDMs and VADMs calculated for each of the volcanic units upon which paleointensity determinations were performed in this study reveals a broad similarity but with minor differences (Fig. 26). The principal differences arise in that the VADM model does not require such rapid apparent changes in dipole moment as the VDM model does at 800, 2600 and 3400 years B.P. The smoother dipole moment variation specified by the VADM model is more in harmony with what stratigraphic and paleodirectional information can be brought to bear on the comparison of VDM and VADM, and with historically observed rates of change of the local geomagnetic field. This probably indicates that at these three points in time nondipole contributions are affecting inclination and intensity in an uncorrelated manner.

A more detailed reconstruction of paleointensity variation for the past 2800 years in the western United States can be made by combining data from the lava flows with data from published archeomagnetic studies (Fig. 27). A substantial number of paleointensity determinations have been made from ceramic material found at Snaketown, Arizona, and vicinity, using the Thellier experiment (Sternberg and Butler, 1978; Bucha and others, 1970). Unlike the

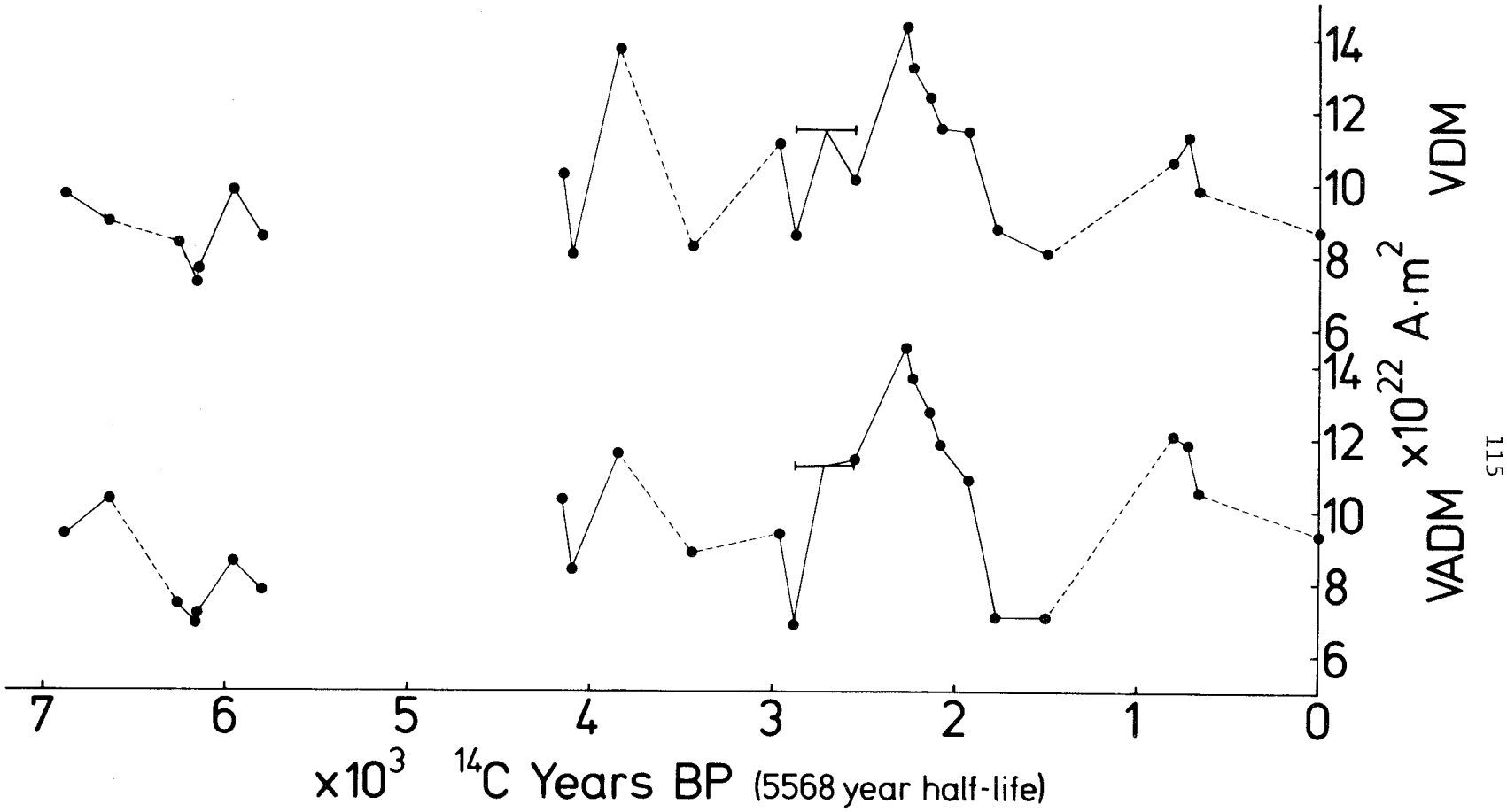

Fig. 26--Comparison of Virtual Dipole Moment (VDM) and Virtual Axial Dipole Moment (VADM) calculated for paleointensity determinations from this study dated between 6900 years B.P. and the present.

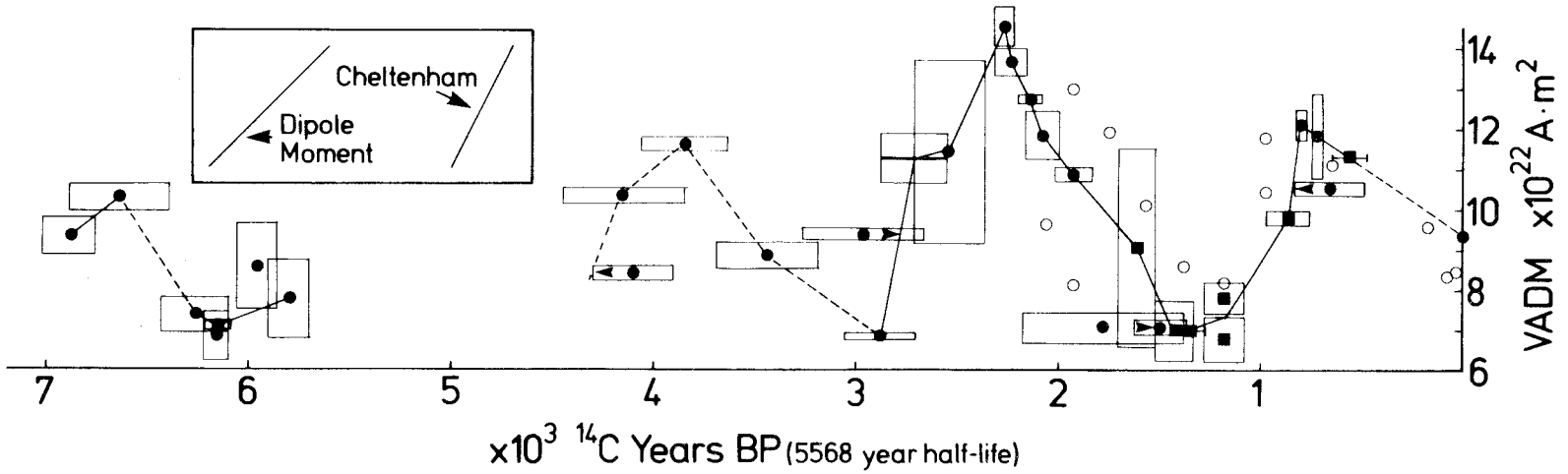

Fig. 27--Paleointensity variation in the western United States calculated as VADM for the past 6900 years B.P. Filled circles from the present study, filled squares from Sternberg and Butler (1978) and open circles from Bucha and others (1970). Boxes indicate error estimates in age and intensity determinations. Box with line for intensity value is for the Yapoah Flow constrianed between 2550 and 2880 years B.P. Arrowheads show preferred shift in age for suspect ^{14}C dates. Line connecting data points is estimated path of intensity variation; dashed where it is uncertain. Rate of change of the historic global dipole moment decay and of the VADM calculated for the Cheltenham Observatory for the period 1905 to 1945, extrapolated for 300 years shown in inset.

present study, the Thellier experiments on ceramics are performed in air and the principal magnetic oxide is ilmenohematite or hematite rather than titanomagnetite. As the ceramics were originally fired and magnetized in air, the low experimental oxygen fugacity discussed earlier in this chapter is unnecessary for such specimens. If the ceramics were completely fired at high temperature when they were made, they can provide excellent archeointensity determinations. The archeointensity determinations have been normalized as VADMs for comparison with the lava flow intensities.

Within the limits of errors in age and intensity, the data from Sternberg and Butler (1978) and the present study are in excellent accord. The data from Bucha and others (1970) on the contrary are mostly not in accord with the two later studies. This discordance is not due to inconsistent dating, as E. W. Haury, the archeologist who headed the excavations of Snaketown, provided the ceramic samples and dates for both studies. Bucha and others (1970) did not publish error estimates for their paleointensity determinations and without the original data, such estimates are impossible to calculate. In the absence of error estimates, the data of Bucha and others have been given little weight in the analysis of the intensity variation which follows.

The intensity determinations are all well defined, with the exception of points from this study at 5960, 5800, 2550 and 720 years B.P. and one from Sternberg and Butler (1978) at 1600 years B.P.; all of the latter have appreciable error boxes. These large error estimates are due to the fact that multiple intensity

determinations yielded different values, typically two similar and one inconsistent with the others. The somewhat high intensity value for the Forest Road flow at 5960 years B.P. (Newberry Crater) has been weighted less for it has one high and one low paleointensity determination. The low value is in close agreement with other determinations from the Northwest Rift of Newberry Crater. The intensity value for the Lava Cascade flow at 5800 years B.P. (Newberry Crater) is also suspect owing to inconsistent determinations. Recalling the arguments presented in Chapter 3 on the age span of the suite of Newberry Crater flows (100-200 years), great variations of the field intensity are not expected. The intensity points at 2550 and 1600 years B.P. have no additional information to help assign preference to the separate intensity determinations and will require additional determinations to resolve the ambiguity. The point at 720 years B.P. includes one very high intensity determination, while the other two determinations agree well with the adjacent point at 800 years B.P. The intensity determinations from Bucha and others (1970) at 30 and 75 years B.P. appear low relative to the VADM calculated for the mean site location. The difference arises from the calculation of the dipole moment using the Earth's axis rather than the present inclined dipole, and indicates the error in dipole moment analysis inherent in the VADM normalization.

The time control used to reconstruct the changes in intensity in the western United States is variable in quality. The analytical standard deviations of the ^{14}C dates grow larger going backward in time. In addition to this trend, certain dates are suspect

for additional reasons. The ^{14}C date of 4100 years B.P. on the Hells Half Acre Field was obtained from the charred content of the A soil horizon directly beneath the lava. Subsequent experience about contamination of such soil samples has revealed that they frequently yield ^{14}C ages too young by as much as 50 percent. The Clear Lake Flow at 2965 years B.P. has ^{14}C ages ranging from 2700 to 3200 years B.P. and is thus not dated precisely. The ^{14}C date for the South Belknap Cone Flow at 1775 years B.P. has a 400-year standard deviation, and on paleodirectional grounds is thought to be close to the West Belknap Flow in age at 1500 years B.P. Lastly, the ^{14}C date on the Ice Spring Field at 660 years B.P. is from a soil sample, and the true age is possibly older than the ^{14}C date. From the archeomagnetic record of DuBois (1974), a date of 840 years B.P. is probable (Fig. 10). Adjustment in the ages of these imprecisely dated lava flows can permit a smoother paleointensity curve to be passed through the data; these preferred adjustments are indicated in Figure 27.

A detailed discussion of the variation in intensity in the western United States can now be made going backward in time. The present VADM for the average locality of the dated volcanic units is calculated from the 1965.0 IGRF as 9.3 (units of 10^{22} $A \cdot m^2$ will be used for the remainder of this discussion). The most recent maximum was 12.1 at 800 years B.P., and the trend from this time toward the present is clear for the interval 800 to 500 years B.P. The minimum of 7.0 between 1500 and 1300 years B.P. is very well established by determinations from both lavas and ceramics. The

increase in VADM from 1500 to 800 years B.P. is probably monotonic but is defined by only two points in time, the earlier of which is represented by ceramic determinations that are in slight disagreement. The maximum VADM of 2300 years B.P. has a value of 14.5, slightly over twice the values of the preceding and succeeding minima. Between 2300 and 1500 years B.P. there are sufficient data to show that the variation is a monotonic decrease, and the average rate is about -1 VADM unit in 100 years or roughly -10 percent in 100 years; this rate is about twice the rate of historic decrease of the global dipole moment in historic time (Harwood and Malin, 1976), but slightly less than the average maximum rates of change in total field intensity at certain geomagnetic observatories. For example, the rate of change of total field intensity at the Cheltenham, Maryland, geomagnetic observatory during the period of time 1905 to 1945 extrapolates to a VADM change of 1.33 for 100 years (Vestine and others, 1947) (Fig. 27).

The earlier minimum of 6.8 at 2900 years B.P. is defined by only one point. The two-fold increase in VADM between 2900 and 2300 years B.P. is probably monotonic but is controlled by only two rather poor data points. Prior to 2900 years B.P. the absolute uncertainties in the ^{14}C ages are greater, so that the VADM variation is less clear. Nevertheless, there is a definite indication of a decrease in VADM from 10.3 to 7.0 between 6700 and 6150 years B.P. with a possible upswing to 7.8 by 5800 years B.P. From 5800 to 4150 years B.P. the VADM variation is unknown. Between 4150 and 2900 years B.P., a broad variation in VADM with a maximum at

3850 years B.P. of 11.6 can be deduced from the data. If errors exist as suspected for the 4100 and 2965 years B.P. points, then this broad variation might be even clearer, and the interpolation is drawn on the assumption that these errors are correctly evaluated. Considering the data at hand and the presently attainable precisions of ^{14}C dating and paleointensity determination, it is likely that the rate of change seen in Figure 27 between 2300 and 1500 years B.P. is the most rapid that these methods can demonstrate. The data in Figure 27 have a peculiar aspect, however, in that the maxima of 2300 and 800 years B.P. seem to be sharply peaked, and the generalized line drawn through the most reliable points looks more like a triangle function than a curve with a continuous first derivative. These abrupt reversals of rate of change of VADM at 2300 and 800 years B.P. are very possibly artifacts of the limited data set; the minimum at 1500 to 1300 years B.P. is not so abrupt-appearing as the maxima.

Where the samples from which the paleointensities were measured are closely spaced in age, the period of fluctuation of paleointensity is found to be similar to the apparent period of variation in paleodirection for the western United States. Moreover, the paleointensity frequently has a positive correlation with paleoinclination for short time intervals. This correlation suggests that, as in the case of variations in paleodirection, the local fluctuations of paleointensity are dominated by nondipole components of the field. However, it is possible that the variation in both intensity and inclination documented in this study for the western United States

may reflect major variations of the dipole component as well. This possibility will be developed more fully in the next chapter.

Chapter 5

GEOMAGNETIC FIELD BEHAVIOR IMPLIED BY OBSERVATIONS OF HOLOCENE SECULAR VARIATION

The nature of secular variation of the geomagnetic field is poorly known for times longer than the past century. A detailed knowledge of the secular variation would provide important evidence about the fluid motions within the outer core of the Earth. If secular variation were understood, other variations of the geomagnetic field such as excursions and polarity reversals would, in turn, become more understandable.

First analyses of secular variation used only geomagnetic observatory data (Vestine and others, 1947; Bullard and others, 1950; Yukutake, 1971; Harwood and Malin, 1976). The observatory record has been found to be too short a length of time to explain many aspects of the past behavior of the field. Later investigations (Cox, 1970; McElhinny and Merrill, 1975) utilized the dispersion of VGPs obtained from paleomagnetic studies to extend the analysis of the geomagnetic field. These workers placed special emphasis on the variation of the VGP dispersion with site latitude, comparing the paleomagnetic data with the similar variation obtained using the present geomagnetic field as a model. Such comparisons allowed preliminary estimates to be made of the relative contributions of the dipole and nondipole fields to the overall dispersion of VGPs. Paleomagnetic observations of the local direction and intensity of

the geomagnetic field during the Holocene from this and other studies may give enough additional data to understand the normal long-term secular variation of the geomagnetic field.

This chapter will present a study of the mean paleomagnetic pole and the dispersion of VGPs derived from 77 Holocene volcanic units from the western United States. The position of the mean paleomagnetic pole and the dispersion of the VGP will be analyzed along the lines of the classic studies (McElhinny and Merrill, 1975) of secular variation. The question of dipole wobble will then be addressed, using principally archeomagnetic data for the past 2000 years from widely spaced regions around the world. The dispersion of VGPs due to nondipole components of the geomagnetic field and dipole wobble will be compared and together found to be equal to the total dispersion of VGPs from the study of the Holocene volcanic units. Lastly, the variation of the magnitude of the dipole moment will be analyzed through spectral studies, which show some evidence of a periodic variation during the past 8000 years.

Previous Models of Secular Variation

Previous studies of secular variation have relied mostly on short-term analyses of trends in the spherical harmonic content of the magnetic field for the past 100 years of so (Vestine and others, 1947; Bullard and others, 1950; Yukutake, 1962; Cox and Doell, 1964). Basic conclusions from this work were that the dipolar component of the geomagnetic field has shown little change other than a decrease of magnitude and that almost all of the observed secular variation of direction was generated by a general westward drift of nondipole features of the field. As we shall see, the limited hindsight available from observatory and repeat station records of the geomagnetic field has led to misunderstanding of the longer term characteristics of secular variation.

With the acquisition of accurate ancient field directions and intensities by paleomagnetic methods, many attempts have been made to analyze secular variation for short segments of geologic time from the dispersion of paleodirections at a given site. From analysis of paleodirections, five models of secular variation have been proposed using different combinations of wobble of the dipole component and fluctuations of the nondipole components of the geomagnetic field (Cox, 1962, 1970; Creer, 1962a, b; Irving and Ward, 1964; Baag and Helsley, 1974). Reviews and comparisons of these models are given by Cox (1970) and Baag and Helsley (1974). The models can be distinguished on the basis of how well they reproduce the angular dispersion of the present geomagnetic field as a function of latitude, upon which it has a strong dependence (Cox, 1970).

A great deal of effort has been expended collecting paleomagnetic data from suites of rocks of Pleistocene age from different latitudes, at least in part to evaluate these models. The angular dispersions calculated as standard deviation statistics have large enough uncertainties, owing principally to insufficient numbers of measured independent field directions at individual sites, that no unambiguous choice of models has been possible. The angular dispersion of paleomagnetic directions from a large number of specimens collected in Hawaii (Doell and Cox, 1972) heavily influenced the analysis of secular variation during these years of study. Because the present field direction at Hawaii corresponds closely with the direction expected for the present inclined dipole component of the geomagnetic field, and because samples obtained from the Kau and Puna series, which were thought to be distributed in age over about 10^4 years, exhibit low angular dispersion, Cox and Doell (1972) concluded that prehistoric secular variation in the central Pacific area primarily reflected variations of the main dipole component of the field. An angular standard deviation of 11 deg found for all Brunhes-age lavas from Hawaii was taken by Cox and Doell as the best estimate of the dispersion due to dipole wobble; on the basis of the Hawaiian data, dipole wobble was thought to have a period greater than 10^4 years. This interpretation was generally accepted until the mid 1970s (McElhinny and Merrill, 1975), though Baag (1974) suggested that the period of dipole wobble might be as great as 10^6 years.

A different interpretation was published by Kawai and others (1965), Kawai and others (1967), and Kawai and Hirooka (1967).

Attracted by the agreement shown between VGP positions for equivalent times from widely separated localities on the Earth, these authors suggested that the major part of secular variation of local direction of the geomagnetic field might be explained by short-period dipole wobble. They additionally postulated the path of motion of the dipole axis to be a quasi-hypotrochoid, a three-cornered figure with elongate loops at the corners. No physical explanation for this motion was presented. These conclusions about the path of dipole wobble were not generally accepted at the time of their presentation nor are they at present.

Recent work (Cox, 1975; McElhinny and Merrill, 1975; Merrill and McElhinny, 1977) based on the increasing volume of paleodirectional data has challenged the commonly used assumption that the mean of a group of VGPs from a common site, averaged over time, will coincide with the spin axis of the Earth. These studies suggest that the average VGP calculated from a sequence of geologic units that had been magnetized at closely spaced but independent times will be in fact displaced "farside," that is lie along a longitude nearly 180 deg from the longitude of the site sampled. In some cases the VGP may tend to be "rightside," that is, to lie near a longitude 90 deg east of the site. Reasons suggested for this "farside" effect include an offset magnetic dipole or alternatively, a lack of zonal (latitudinal) symmetry in the nondipole field. An excess of -Z (upward) nondipole anomalies between 50° N. and 50° S. latitudes, as observed in the present field, would produce an excess of shallow

field directions, and hence a farside mean VGP for any given site between those latitudes, by simple drift, of the nondipole anomalies with time.

Distribution of Holocene Directions of the Magnetic Field and Virtual Geomagnetic Poles from Volcanic Rocks in the Western United States

The paleomagnetic record from Holocene lava flows in the western United States provides a new source of accurate paleodirections against which various models of secular variation can be tested. High-precision paleodirections were obtained from 77 Holocene volcanic units from the western United States. All of the Holocene volcanic units are between 34.5° and 46.8° N. latitude with the majority between 43° and 44° N. latitude. The data are listed in Appendix 5 for these 77 volcanic units. While some of these volcanic units are accurately dated, the majority are not and have been included here on the basis of youthful appearance of the volcanic rocks, lack of superposed soils or other alluvial cover, and lack of vegetation. Most are believed to be younger than 10,000 years. All suspected replications of a single paleomagnetic field direction by multiple flows have been eliminated from the original data set. Virtual geomagnetic poles for each of the 77 units were calculated along with a mean pole and alpha-95 for the group as a whole (Fig. 28). The mean VGP for the 77 Holocene volcanic units sampled in the western United States is at 87.53° N. latitude and 55.81° E. longitude. Assuming a Fisherian distribution for the VGPs, the spin axis of the Earth lies just outside the 95 percent confidence limit of the mean (α_{95} = 2.46 deg). The "farside" displacement of the mean VGP from the spin axis is equivalent to a mean difference in inclination (ΔI anomaly) of -2.94 deg in the paleoinclination at the mean sample site (42.31° N. latitude and 243.30° E. longitude).

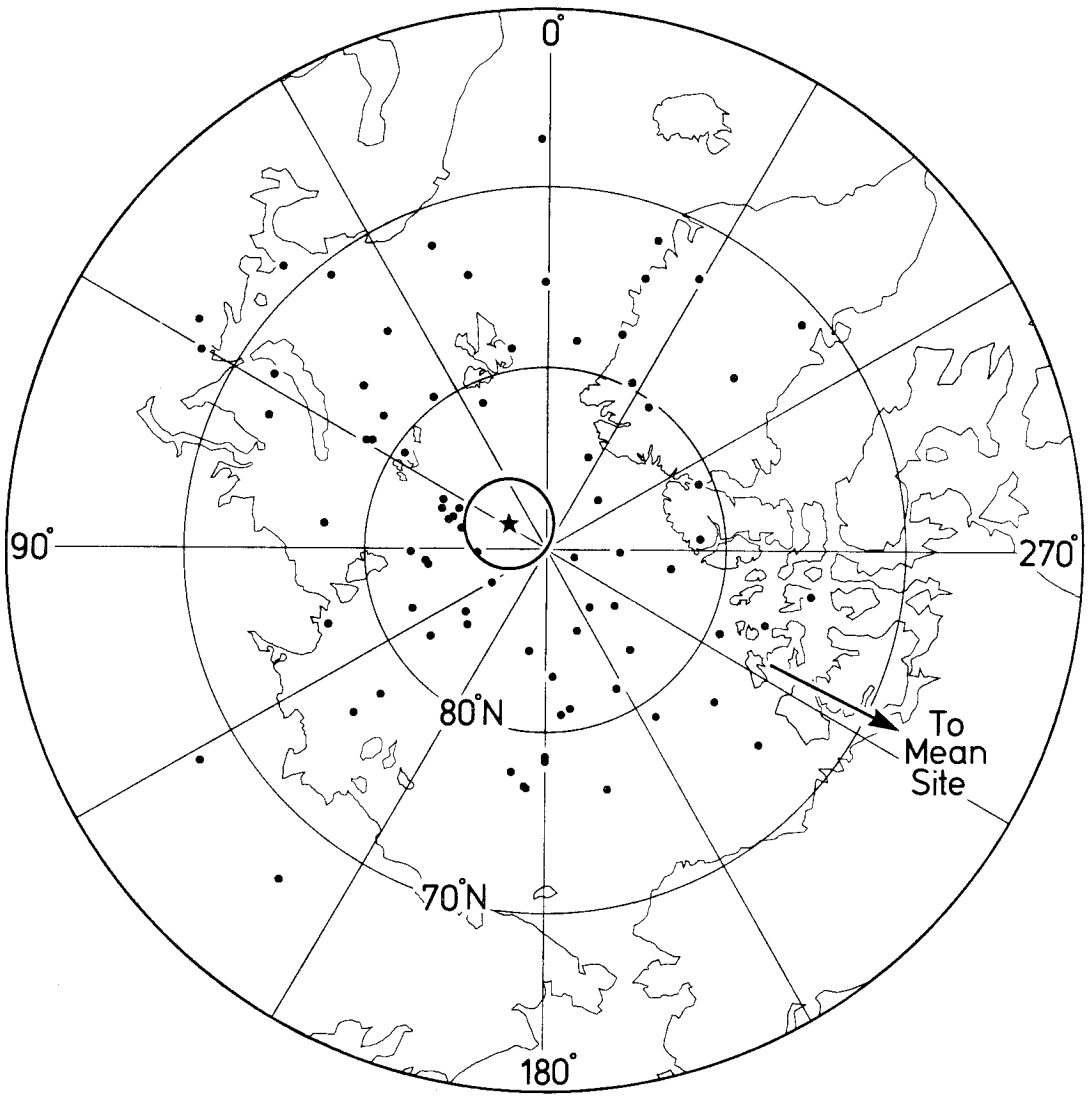

Fig. 28--North polar equal-area plot of VGPs calculated from field directions for 77 Holocene volcanic units from the western United States. Each VGP is thought to be independent in time from all other VGPs. Dark star in center of small circle represents the mean VGP position from these 77 VGPs and circle denotes alpha-95. The alpha-95 does not include the position of the spin axis of the Earth.

Using paleodirections from normal polarity rocks up to 5 m.y. old, Merrill and McElhinny (1977) found a ΔI anomaly of -2.4 ± 1.0 deg for the latitudinal band 40° N. to 50° N. The total time represented in each set of paleodirections used by Merrill and McElhinny individually encompassed on the order of 10^5 to 10^6 years. The present study indicates that a similar ΔI anomaly may occur for paleodirections averaged over as little as 10^4 years.

A subset of the 77 volcanic units was used to determine whether a significant ΔI anomaly might be observed for paleodirections averaged over the last 2000 years. Only units dated as less than 2000 years or comparably youthful in appearance were included. Only 12 volcanic units qualified on these grounds and their mean VGP is located at 87.38° N. and 118.00° E. with an alpha-95 of 6.49 deg. The 12 volcanic units are numbered 1, 3, 5, 9, 11, 12, 34, 64, 67, 72, 75 and 77 in Appendix 5. This mean VGP is "farside" and somewhat "leftside," that is the average magnetic field direction has a westerly declination, but the displacement of the mean VGP from the geographic pole is not significant due to insufficient number of data. The displacement of the mean VGP for this 2000-year subset from the present inclined position of the magnetic dipole is significant, however. Interpretation of this observation will be developed later.

An excellent set of data, presented by Hirooka (1971) for Japan, can also be tested for the ΔI anomaly. Hirooka collected paleodirections from 152 sites, principally from archeological material, spanning the time interval from A.D. 100 to A.D. 1900. The mean

VGP from this set of directions is located at 85.65° N. and 327.85° E. and has a cone of 95 percent confidence with a 2.81 deg radius. The mean VGP position is "farside" from Japan and corresponds to a ΔI anomaly of -4.51 deg. Merrill and McElhinny (1977) predict a ΔI anomaly of -3.4 ± 1.0 deg for the latitudinal band 30° N. to 40° N. which includes Japan. Given the small value of the alpha-95 of the mean VGP, Hirooka's archeomagnetic data significantly satisfy the ΔI anomaly prediction. The mean VGP is also significantly displaced from the present inclined dipole. While the data from Japan constitute only a single example of a ΔI anomaly expressed in so short a total time interval as 2000 years, the volume and quality of the data preclude offhand discounting of the existence of a "farside" effect. Only when equivalent data sets exist for other localities and encompass equally short time intervals can we know whether this result is representative or anomalous.

The 77 Holocene paleodirections from the western United States can be used to test the statistical distribution of field directions and of VGPs. The statistics of Engebretson and Beck (1978) based on the moments of inertia of the paleomagnetic data are here used for this test. The ratio of the major to minor axis of the distribution of paleo field directions is 1.45; this ratio is 1.18 for the distribution of VGPs. The eccentricity (0 signifies perfect circularity; 1 signifies distribution along a great circle) of the paleo field directions is 0.722 and eccentricity of the VGP distribution is 0.532 if they are converted to poles. This result supports the general practice of transforming paleomagnetic field

directions to virtual poles before Fisherian analysis, as the VGPs are more nearly circular in distribution. In addition, it is significant that despite the probable nondipole contribution to the dispersion of these VGPs the distribution appears to be essentially circular.

Wobble of the Dipole Component of the Geomagnetic Field

The concept of wobble of the dipolar component of the geomagnetic field springs from the earliest paleomagnetic work. Despite the present deviation of the dipole from the spin axis, averages of paleomagnetic poles from young rocks are close to the spin axis of the Earth. The conclusion was drawn that, over time, the orientation of the dipole must be more or less uniformly distributed about the spin axis. Estimates of the period of this dipole wobble, based in part on the nearly constant orientation of the dipole over the last 150 years, were 10^4 years or greater (Cox and Doell, 1964).

It has been shown that the average VGP for the last 10^4 years for the western United States is near the spin axis and not at the present inclined position of the geomagnetic pole. This could not be the case if there were a stationary inclined dipole component of the geomagnetic field. The dipole must have wobbled within the last 10^4 years. The 2000-year subset of VGPs from the western United States and the Japanese archeomagnetic data suggest that the dipole wobbled within the last 2000 years.

Barbetti (1977) has suggested, on the basis of comparisons of VGPs for various regions around the world for given intervals of time, that a change in dipole position occurred between A.D. 1400 and A.D. 1650. In an attempt to confirm this result and ascertain if other possible dipole motions were evident, VGPs have been collated predominantly from archeomagnetic studies for the last 2000 years from as many separate localities as could be found. The localities were western North America, Central America, Poland,

Great Britain, Iceland, the Ukraine, Moldavia, Soviet Georgia, Sicily, Africa, Australia and Japan. By taking data from around the globe it was hoped that the effects of the nondipole field could be averaged out. The mean VGP obtained for each short interval of time is assumed to be close to the axis of the dipolar component of the geomagnetic field. This assumption is based on the observation that the average of geomagnetic observatory VGPs from around the world plots very close to the position of the present inclined dipole (Cox and Doell, 1960). Europe was divided into separate northwestern and southeastern regions because of the amount of data available from Europe and also because of its large (30 deg) angular span.

Within each region, the VGPs have been averaged for 100-year intervals (Table 3). For a given 100-year interval the number of separate regions around the world used for this analysis is never more than seven and commonly is as low as four. The mean VGP for each 100-year interval is shown on a north polar equal-area plot (Fig. 29). Circles of 95 percent confidence around these century means are shown only for A.D. 1965, 1700, 1300 and 900 for simplicity of the diagram and to illustrate salient points for the following discussion. The mean for 1965 with its circle of 95 percent confidence was calculated from the 1965.0 IGRF for the seven localities used in this analysis. This mean VGP is not significantly different from the present inclined dipole and neither is the mean for A.D. 1700 significantly different from the present inclined

Table 3 - Regionalized Records of VGP Variation and Global Dipole Wobble for the Past 2000 Years

Century (AD)	Northern Europe PLA	PLO	(ref,n)	Southern Europe PLA	PLO	(ref,n)	Africa (0N,40E) PLA	PLO(ref,n)	Japan PLA	PLO(ref,n)	Australia PLA	PLO(ref,n)	W. North America PLA	PLO(ref,n)	Central America PLA	PLO(ref,n)	Dipole Position n	k	95	PLA	PLO
(1965)	85.1	253.4	(m,1)	86.4	172.3	(m,1)	77.6	227.8 (m,1)	82.2	359.4 (m,1)	75.3	298.1 (m,1)	76.5	295.8 (m,1)	76.7	292.2 (m,1)	7	91	6.4	82.5	283.6
1900	80.1	265.4	(a,*;c,*) (e,*)	82.9	121.5	(h,*;k,2)	76.4	248.1 (j,*)	83.5	356.0 (g,*)	76.8	297.8 (b,3)	77.3	297.9 (d,*)	79.5	305.0 (1,*)	7	87	6.5	82.7	287.3
1800	76.0	285.4	(a,*;c,*) (e,*)	84.2	106.2	(h,*;k,4)	74.0	276.8 (j,*)	83.0	312.0 (g,*)	73.3	313.2 (b,4)	79.0	296.0 (d,*)	82.0	317.5 (1,*)	7	97	6.2	80.8	298.7
1700	81.5	309.1	(a,*;c,*) (e,*)	84.7	60.4	(h,*;k,1)	73.0	313.4 (j,*)	78.0	288.0 (g,*)	73.0	318.0 (b,6)	81.7	292.1 (d,*)			6	109	6.4	80.1	311.1
1600	84.0	45.0	(a,*;c,*) (e,*)	87.2	75.9	(h,*;k,1)			74.5	287.0 (g,*)			83.0	338.0 (d,*)			4	82	10.2	85.2	327.0
1500	85.7	114.6	(a,*;c,*) (e,*)	84.6	186.2	(h,*;i,1) (k,1)			75.0	312.5 (g,*)	81.0	293.0 (b,9)	83.4	7.9 (f,*)			5	83	8.5	86.0	310.8
1400	76.2	195.1	(a,*;c,*)	84.6	160.5	(h,*;i,4) (k,1)			79.5	305.5 (g,*)			84.8	254.5 (f,*)			4	79	10.4	84.8	228.3
1300	78.4	171.8	(a,*;c,*)	87.1	175.3	(h,*;i,4)			79.0	223.0 (g,*)			85.3	164.3 (f,*)			4	198	6.6	83.2	189.1
1200	78.3	140.4	(a,*;c,*)	82.9	112.0	(h,*;i,2)			86.5	215.0 (g,*)	78.0	61.0 (b,8)	78.2	191.7 (f,*)			5	83	8.5	84.3	135.2
1100	78.0	116.2	(a,*;c,*)	81.2	94.6	(h,*;i,2)			85.0	11.5 (g,*)			83.9	210.2 (f,*)			4	100	9.2	85.3	110.0
1000	77.5	93.2	(a,*;c,*)	78.4	85.4	(h,*;i,3)			79.5	16.0 (g,*)	77.0	57.0 (b,7)	82.2	64.6 (f,*)	80.0	144.5 (1,*)	6	120	6.1	81.3	76.0
900	81.0	49.0	(c,*)	76.6	11.7	(h,*;i,2)			76.5	19.5 (g,*)			80.0	44.7 (f,*)	81.0	92.0 (1,*)	5	181	5.7	80.2	38.0
800				79.1	7.8	(h,*;i,3)			77.0	15.0 (g,*)			84.0	54.7 (f,*)	84.0	69.5 (1,*)	4	216	6.3	81.8	28.0
700				77.9	356.8	(h,*;i,3)			82.0	69.0 (g,*)			83.9	321.5 (f,*)	80.0	90.0 (1,*)	4	80	10.4	85.0	8.6
600				81.5	20.4	(h,*;i,3)			76.5	60.5 (g,*)	79.0	296.0 (b,5)	78.8	325.9 (f,*)	82.0	150.0 (1,*)	5	56	10.3	85.6	6.6
500				83.3	282.7	(i,1)			79.0	2.5 (g,*)			85.2	60.8 (d,*)	87.5	269.0 (1,*)	4	145	7.7	86.1	343.5
400				83.4	239.4	(i,1)			82.5	270.0 (g,*)			74.6	58.2 (d,*)	77.5	302.0 (1,*)	4	43	14.1	87.0	343.9
300				89.0	270.0	(i,3)			78.5	211.5 (g,*)			75.6	70.4 (d,*)	86.0	303.0 (1,*)	4	57	12.3	88.7	124.2
200				84.6	34.6	(h,*;i,3)			82.0	199.0 (g,*)			78.2	87.4 (d,*)	79.0	236.0 (1,*)	4	60	12.0	87.7	160.3
100	86.5	207.0	(a,*)						85.5	341.5 (g,*)			78.9	111.0 (d,*)	85.0	202.0 (1,*)	4	124	8.3	87.7	143.9
0	84.0	319.5	(a,*)										77.9	131.4 (d,*)	85.5	118.5 (1,*)	3	80	13.9	86.4	121.4
Statistics for VGP mean of 20 centurys ->																	20	181	2.4	88.5	358.6

PLA and PLO are north paleolatitude and east paleolongitude of virtual geomagnetic pole for each century in each region. (ref,n) denotes source of VGP information and number of poles used to calculate each century's VGP. Asterisks indicate information derived from VGP plot or declination-inclination graph in reference. (a,*) compiled from VGP plot in Aitken and Weaver (1965); (b,n) from Barbetti (1977); (c,*) compiled from VGP plot in Brynjolfsson (1957); (d,*) compiled from VGP plot it this study; (e,*) compiled from declination-inclination graphs in Czyszek (1973); (f,*) compiled from VGP plot in DuBois (1974); (g,*) compiled from VGP plot in Hirooka (1971); (h,*) compiled from declination-inclination graphs in Nadia and Chelidze (1972); (i,n) from Rusakov and Zagniy (1973); (j,*) compiled from declination-inclination graphs in Skinner and others (1970); (k,n) from Tanguy and Wilson (1973); (l,*) compiled from VGP plot in Wolfman (1973); (m,n) from 1965.0 I.G.R.F.

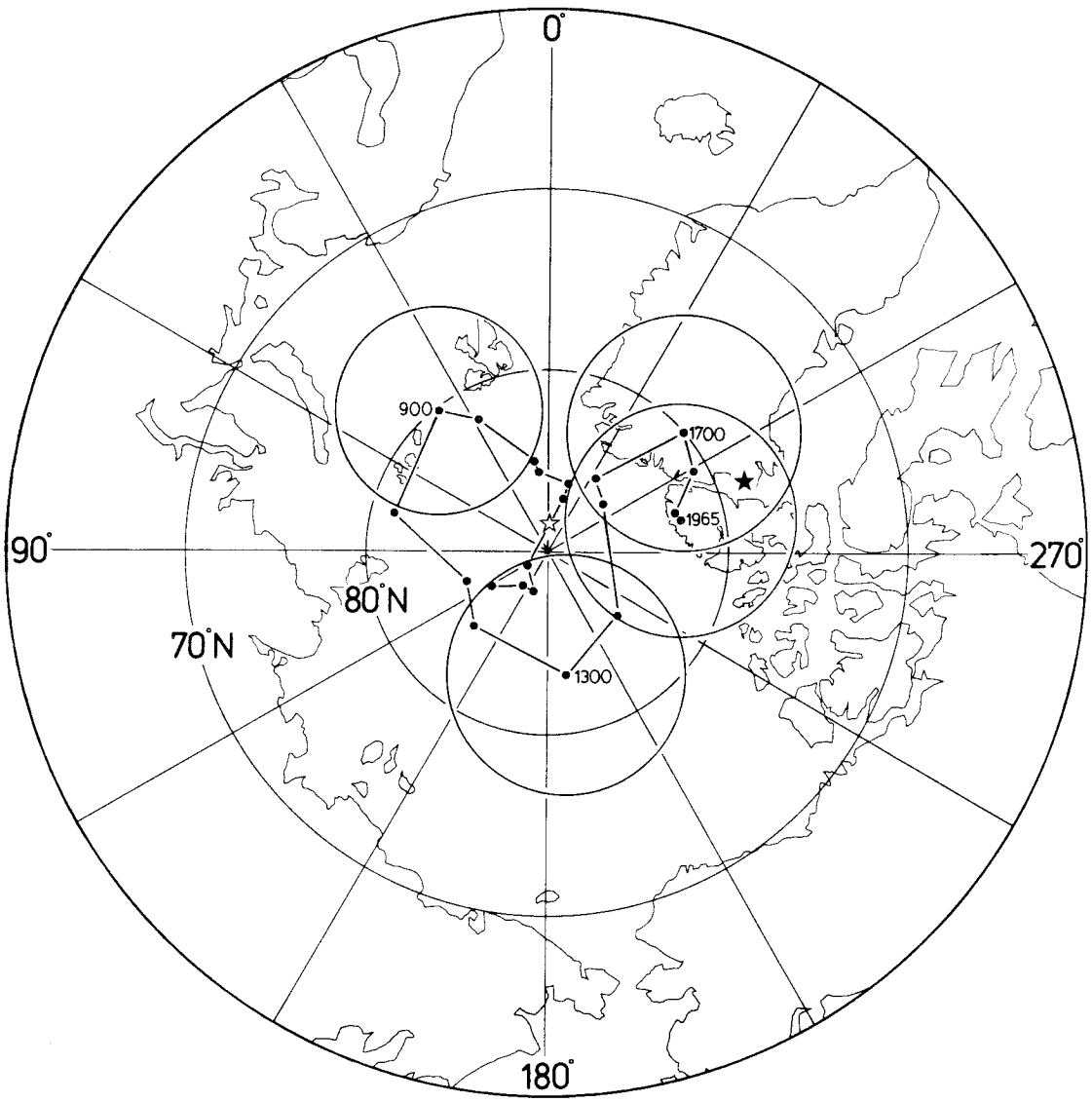

Fig. 29--North polar equal-area plot of mean VGP track for the last 2000 years from globally distributed directional data. Circles of 95 percent confidence shown for A.D. 1965, 1700, 1300 and 900. Black star denotes position of present inclined dipole. Open star near spin axis represents the mean VGP position for the 2000-year period of analysis of global directional data.

dipole. Thus the present analysis is consistent with the analyses of dipole movement from historic measurements (Barraclough, 1974).

Previous to A.D. 1700, mean VGP shifted more rapidly than during the last 250 years. The VGP for A.D. 1300 is significantly distinct from both the A.D. 1700 VGP and the present inclined dipole. Going backward in time yet another 400 years to A.D. 900, another distinct VGP position is disclosed. Continuing further back in time, a relatively smooth VGP track is found, though there is less confidence in this track because of decreasing amounts of paleomagnetic data. The mean VGP for A.D. 100 is significantly different from the VGP for A.D. 900. The mean VGP track illustrated in Figure 29 strongly indicates significant dipole wobble over a short (2000 year) period of time.

The principal weakness of the above analysis lies in the small number of regions for which data are available. Preliminary paleomagnetic data for the past 2000 years from the island of Hawaii have recently become available (Holcomb, Champion, and McWilliams, unpubl.). Initial indications are that the Hawaiian data will fit well with the existing data, preserving the position and sense of the mean VGP track and increasing the level of statistical confidence in it. The mean VGP for all 20 centuries of VGP data, with an alpha-95 of 2.4 deg, is only 1.5 deg from the spin axis. This confirms that the inclination of the dipole averages out in 2000 years or less. It also suggests that if there is any periodic character to the dipole wobble, it is 2000 years or less.

Sources of Directional Dispersion of the Local Geomagnetic Field

Angular standard deviation of directions converted to VGP commonly has been used to describe secular variation for various locations on the Earth. For each region, the angular variance of VGP is taken to be the sum of the variances from dipole and nondipole sources, as given by:

$$S_T^2 = S_D^2 + S_{ND}^2, \quad (2)$$

where S_T equals the total angular standard deviation of VGPs and S_D and S_{ND} equal the dipole and nondipole angular standard deviation components respectively. Summing the various sources of angular dispersion due to secular variation is performed after the directions have been converted to VGPs on the presumption that VGPs are more circularly distributed. Different combinations and amounts of the dipole and nondipole components have been invoked to explain the observed dependence of secular variation on latitude (McElhinny and Merrill, 1975). It has proven difficult to obtain objective figures for S_D. The total angular standard deviation of VGPs for Hawaii of 11 deg has been widely used for S_D. From the 20 inferred dipole positions given in Table 3 the dipole component of the angular standard deviation of VGP is estimated to be 6.02 deg with a 95 percent confidence range (Cox, 1969) from 4.94 to 7.71 deg. This dispersion is about a mean close to the spin axis of the Earth.

Secular variation due to nondipole sources can be estimated in a variety of ways. Cox (1970), in constructing his model D, chose to estimate S_{ND} from the 1945.0 Epoch mean equatorial nondipole component (8 deg angular standard deviation of VGPs), multiplied

by the function

$$W_{NP} = \left(5 \frac{1 + 3\sin^2\lambda}{5 + 3\sin^2\lambda} \right)^{1/2}, \qquad (3)$$

where λ is the geomagnetic latitude of the site. The form of the latitude dependence of S_{ND} used is based on the assumptions that the average intensity of the nondipole field is latitude invariant and that the VGP distribution is Fisherian. This last assumption is consistent with results obtained for 77 Holocene flows in this study. Another estimate of S_{ND} can be derived from sampling the present field at uniform intervals of longitude along lines of constant geomagnetic latitude. At the mean latitude of 42.31° N. for sites studied in western United States, Cox's method and the latter method coincidentally yield the same estimate of 10.90 deg for S_{ND} . The method of sampling along lines of geomagnetic latitude gives S_{ND} with 95 percent confidence limits of 10.08 to 11.87 deg. The sampling of the present field along constant magnetic latitude was done for northern and southern hemispheres combined; it is assumed that the present north-south asymmetry of the field is short-lived (McElhinny and Merrill, 1975).

For the 77 Holocene flows reported here the total angular standard deviation of VGPs for the past 10,000 years is 12.23 deg, with 95 percent confidence limits of 11.01 to 13.76 deg. The dispersion in the western United States during the last 2000 years is essentially equal (S_T = 11.98) to that observed for the last 10,000 years, suggesting that secular variation is dominated by frequencies shorter than 2000 years. Using equation 2, and the

estimates of 6.02 deg for S_D and 10.90 deg for S_{ND} we obtain S_T = 12.45 deg, which is well within the confidence limit of the observed value of S_T. This close agreement suggests that the dipole wobble observed in the past 2000 years may be representative of the Holocene.

Greater local dispersion of VGPs has generally been reported from other sites at temperate latitudes than found for the western U.S. Holocene (Fig. 10, McElhinny and Merrill, 1975). Reported angular standard deviations of VGPs average near 15 deg for rocks of Brunhes age, with some sites yielding S_T as high as 18 deg. This disparity exists despite the subtraction of within-site dispersions of 10 deg. The difference is not trivial for it requires an unidentified source of VGP dispersion with an angular standard deviation of approximately 9 deg. An explanation of the difference could lie in the much broader span of time sampled (10^5 to 10^6 years) in many studies as compared to 10^4 years of the present study. There may be low frequency nondipole or dipole sources of dispersion not sampled in the Holocene. This would be consistent with the observation that all Holocene data show lower total dispersion than Brunhes Epoch data (McElhinny and Merrill, 1975).

It is difficult to explain the close agreement between the mean VGP for the Holocene and the spin axis, if only limited portions of some longer period of secular variation have been sampled, unless the amplitude of this long period component happened to be very small during the last 10^4 years. Alternatively, there may be temporal variations of S_T as recorded over given intervals of time.

In other words, other periods of 10^4 years in the Pleistocene might show significantly different dispersion of VGPs for the same location. Excursions of the magnetic field are examples of this kind of temporal variability, as they are usually quick events, shorter than 10^4 years. McElhinny and Merrill (1975) discuss this possibility, pointing out that removal of single VGPs, particularly from small sets of data, can sometimes vastly reduce the dispersion within the set. Doell and Dalrymple (1973) have pointed out that the dispersion of VGPs for all localities increases with age. They suggested three possible causes for this: (1) weathering, tectonism, and geomorphic processes leading to dispersion of magnetic directions; (2) long-term increase in the ratio of dipole to nondipole field strengths; and (3) decreasing wobble of a constant strength dipole with a constant ratio of dipole to nondipole strengths. A final possibility is that some asymmetry exists in the geomagnetic field such that the western United States has less total dispersion than other locations at equivalent latitudes. A previous figure for total VGP dispersion from 21 Plio-Pleistocene flows in the western United States was 12.5 deg (Doell and Cox, 1972). The true reason for the comparatively low dispersion of Holocene-aged paleomagnetic data sets is unknown.

Variation of the Geomagnetic Dipole Moment

Variation of the geomagnetic dipole moment as a function of time can be analyzed in a manner similar to that used to analyze wobble of the dipole component of the field. There is excellent evidence from harmonic analysis of total field intensity measurements at geomagnetic observatories that the dipole moment has decreased rapidly in the recent past (Harwood and Malin, 1976). Considering the frequency of variation deduced from the analysis of dipole wobble, it is interesting to see whether similar frequencies occur in the variation of amplitude of the dipole moment. A previous analysis by Cox (1968) on approximately one-third of the data currently available, suggested an approximately sinusoidal variation of the dipole moment with a period of about 8000 years, a period slightly longer than the time span of the data.

A new compilation has been made of all paleointensity and archeointensity data available for the past 12,000 years (Table 4). The data have been grouped according to region in a manner analogous to that used in the dipole wobble analysis. As in the wobble analysis, this was done to minimize the effect of the nondipole field on the dipole moment estimation. As demonstrated from harmonic analysis of the present field and by the history of the intensity of the field in the western United States during the Holocene, the nondipole field commonly is a significant component of the total field at a given place. The data in Table 4 are reported either as Virtual Dipole Moment (VDM), or as Virtual Axial Dipole Moment (VADM, Barbetti, 1977) in the absence of paleoinclination data. Calculation

Table 4 - Regionalized Records of Dipole Moments and 100 and 500 Year Average Global Dipole Moments

Years BP	Ontario, Canada	(ref,n)	Western United States	(ref,n)	Central America Mexico	(ref,n)	Bolivia-Peru	(ref,n)	Hawaii	(ref,n)	Australia	(ref,n)	Japan	(ref,n)
(-15)	8.33		8.60		8.84		6.87		8.00		9.36		9.27	
100													10.24	(u,1;x,1)
200	6.8	(y,2)			11.59	(r,1)								
300					10.61	(r,1)								
400							12.08	(r,1)					10.62	(u,1)
500							10.16	(v,1)					11.26	(u,1;x,1)
600			11.16	(aa,1)	11.81±1.59	(e,2;r,2)	11.18	(r,2)					9.64	(u,1)
700	9.65	(y,1)	9.81	(j,1)										
800	6.98	(y,1)	10.61	(j,1)	14.35	(r,2)	8.61	(m,1)					10.50	(x,1)
900			9.67	(aa,1)									8.61	(u,1)
1000	7.10	(y,1)			12.50±1.20	(e,2;r,1)							11.58	(x,2)
1100			7.26	(aa,2)	10.99	(e,1;r,1)								
1200					9.91±0.44	(r,7)	11.91±1.38	(r,5)					10.95±1.58	(u,2;x,2)
1300							10.16	(m,1)					11.83±1.24	(x,3)
1400			6.88	(aa,2)	11.11±0.23	(e,2;r,2)	12.58±0.98	(r,1;v,2)					11.32±1.46	(u,2;x,1)
1500	8.16	(y,1)	8.09	(j,1)	10.77	(r,1)	15.60	(v,1)					12.39	(x,1)
1600	7.18	(y,1)	8.85	(aa,1;j,1)	11.01	(r,1)	9.74	(m,1;v,1)					11.61	(x,1)
1700			8.93	(aa,1)	9.91	(r,1)							12.53	(u,1;x,1)
1800	10.56	(y,1)			8.34	(r,1)							13.14	(x,2)
1900			11.41	(j,1)			8.20	(v,1)						
2000					10.67±0.99	(e,2;r,2)								
2100			12.37	(j,1)	11.32±0.95	(e,1;r,3;v,1)	7.34	(m,1)					13.08	(u,1)
2200			13.17	(j,1)	12.40	(r,2)							12.77	(n,1;u,1)
2300			14.32	(j,1)									12.15	(1,1)
2400	8.94	(y,2)					8.30	(r,1)						
2500							8.57	(m,1)						
2600			10.10	(j,1)	11.08	(e,2)	10.19	(r,1)	12.34	(k,1)				
2700			11.48	(j,1)									8.20	(u,1;x,1)
2800													8.77±2.43	(1,4)
2900			8.57	(j,1)										
3000			11.10	(j,1)										
3100														
3200														
3300														
3400			8.28	(j,1)										
3500													9.75	(u,1;x,1)
3600														
3700														
3800									13.04	(k,1)				
3900			13.69	(j,1)									7.33±0.77	(1,2;u,1)
4000														

Table 4 - Continued

Years BP	Ontario, Canada(ref,n)	Western United States	(ref,n)	Central America Mexico	(ref,n)	Bolivia-Peru (ref,n)	Hawaii(ref,n)	Australia	(ref,n)	Japan	(ref,n)
4100		8.02	(j,1)								
4200		10.24	(j,1)								
4300										4.18	(1,1)
4400										6.04	(1,1;u,1)
4500								8.20	(b,1)		
4600							12.92 (k,1)	9.30	(b,1)		
4700										5.57	(1,1)
4800											
4900											
5000											
5100											
5200											
5300											
5400											
5500										4.19	(1,1)
5600											
5700											
5800		8.49	(j,1)								
5900											
6000		9.79	(j,1)								
6100											
6200		7.72	(j,1)								
6300											
6400										5.39	(1,1)
6500											
6600		8.89	(j,1)								
6700											
6800											
6900		9.63	(j,1)								
7000											
7100											
7200											
7300										5.75	(1,1)
7400											
7500											
7600											
7700											
7800											
7900											
8000											

8200										7.13	(1,1)

9300										6.95	(1,1)

10400							8.72 (k,1)				

10800		6.49	(j,1)								

11100		8.32	(j,1)								

11900		8.40	(j,1)								

Table 4 - Continued

Years BP (-15)	Mongolia (ref,n)	Uzbek,USSR (ref,n)	Southeastern Europe (ref,n)	Northwestern Europe (ref,n)	100 Year Average n	500 Year Average n
	9.24	9.03	7.85	7.45	8.44±0.82 11	-------
100	9.27±2.23 (i,5)	7.93±0.77 (i,5)	8.17±0.70 (g,5;p,5;s,9) (t,1;w,1)	7.53±0.71 (h,3;cc,2)	8.62±1.11 5	
200	10.91±2.01 (i,5)	8.29±0.42 (i,3)	8.23±0.77 (g,3;s,8;t,1) (w,1)		9.16±2.01 5	
300	8.93±1.75 (i,7)	8.39±0.73 (f,3;i,7)	9.17±0.63 (g,3;i,1;s,3)	8.53 (h,1)	9.12±0.89 5	9.33±1.39 26
400	10.64 (i,1)	8.44 (i,2)	8.62±0.83 (p,1;s,4;t,2)	7.34 (h,1;cc,1)	9.62±1.77 6	
500		9.09±0.94 (f,4;i,2)	9.97±0.96 (g,1;i,2;p,1) (t,3)	9.69±0.83 (h,3;bb,1)	10.03±0.80 5	
600	10.33±1.90 (i,3)	8.66±1.50 (f,3;i,2)	10.15±0.86 (g,4;p,5;t,1) (w,3)	9.81 (cc,1)	10.34±1.01 8	
700	10.07±1.27 (i,3)	8.18 (f,1;i,1)	10.01±1.43 (g,2;w,1)	10.18±0.26 (h,3)	9.77±0.75 7	
800		9.54 (i,1)	11.33±1.11 (g,8;p,1;t,1) (w,2)		10.24±2.53 6	10.13±1.48 31
900		11.41 (f,1)	10.80±1.86 (g,4;i,3;t,1) (w,2)		10.12±1.24 4	
1000	9.43±1.22 (i,7)	9.86 (f,1)	10.53±1.18 (g,2;t,2;w,2)		10.17±1.88 6	
1100	10.11 (i,2)	9.88 (f,1;i,1)	11.52±1.63 (g,3;i,1;p,3) (t,1;w,1)	9.52 (c,1;d,1)	9.88±1.48 6	
1200	10.59±0.30 (i,5)		11.38±1.49 (g,8;w,7)		10.80±0.58 5	
1300	9.54±1.17 (i,4)		10.14±2.86 (g,1;p,1;t,1) (w,3)	9.89 (d,1)	10.31±0.88 5	10.55±1.76 27
1400			11.94±1.42 (g,3;i,1;w,2)		10.77±2.25 5	
1500			11.25±1.38 (g,1;i,1;p,5)		11.04±2.82 6	
1600			11.75±1.63 (g,2;i,2;p,2) (w,2)	10.84±1.00 (d,1;h,1;cc,1)	10.14±1.66 7	
1700			10.57±1.16 (g,2;i,2;t,1) (p,10;w,5)	11.41±1.23 (bb,1;cc,2)	10.67±1.38 5	
1800	8.28±0.54 (i,4)		10.71±1.04 (g,1;p,4;w,1)	11.85 (bb,1)	10.48±1.92 6	10.44±1.49 24
1900			11.62±2.81 (g,2;p,1;w,1)	11.05 (bb,1)	10.57±1.60 4	
2000			10.47±1.61 (g,3)		10.57 2	
2100			9.34±0.47 (i,2;q,1)	11.72 (c,1;bb,1)	10.86±2.14 6	
2200			11.01±1.04 (i,4;p,1;w,1)	12.43 (d,1)	12.36±0.81 5	
2300			8.49 (i,2)	15.03 (d,1)	12.49±2.94 4	11.34±2.14 20
2400			11.89±1.63 (q,1;w,2)	12.23 (d,1;bb,1)	10.34±2.01 4	
2500					8.57 1	
2600			11.42±1.00 (g,2;q,1)		11.03±0.93 5	
2700			10.50 (g,1;q,1)	9.22 (c,1;d,1)	9.85±1.44 4	
2800			12.02 (w,1)		10.40 2	10.34±1.27 15
2900			10.49 (q,1)	9.63 (d,1)	9.56±0.96 3	
3000					11.10 1	
3100				8.37 (c,1;d,1)	8.37 1	
3200			10.94 (q,1)		10.94 1	
3300					(9.68)	8.98±1.14 6
3400				8.54 (c,1)	8.41 2	
3500			7.97 (a,1)		8.86 2	
3600			8.61 (w,1)		8.61 1	
3700			7.20 (p,1)		7.20 1	
3800			10.70±0.59 (q,2;w,1)		11.87 2	10.04±2.47 8
3900			11.00 (w,1)		10.67±3.19 3	
4000			8.75±0.39 (g,1;w,4)		8.75 1	

Table 4 - Continued

Years BP	Mongolia (ref,n)	Uzbek,USSR (ref,n)	Southeastern Europe	(ref,n)	Northwestern Europe	(ref,n)	100 Year Average	n	500 Year Average	n
4100			8.14±2.03	(g,2;q,1;w,1)	5.68	(d,1)	7.28±1.39	3		
4200			7.86±0.68	(q,1;t,1;w,7)			9.05	2		
4300			10.33	(t,1)	6.39	(c,1;d,1)	6.97±3.12	3	7.17±1.79	14
4400			7.05	(q,1)	6.75	(d,1)	6.61±0.52	3		
4500			6.64	(a,1)	4.82	(d,1)	6.55±1.69	3		
4600			9.18±0.09	(q,1;w,2)	4.73	(c,1;d,1)	9.03±3.35	4		
4700			9.49	(q,1)			7.53	2		
4800					3.72	(c,1;d,1)	3.72	1	7.81±3.04	9
4900					5.48	(d,1)	5.48	1		
5000			9.92	(p,1;w,1)			9.92	1		
5100			9.41	(q,1)	6.96	(d,1)	8.19	2		
5200					6.37	(c,1)	6.37	1		
5300			9.76	(q,1)			9.76	1	7.29±1.89	8
5400			8.83	(q,2)			6.51	2		
5500			6.55	(q,2)	6.28	(c,1;d,1)	6.42	2		
5600			7.54±0.89	(q,4)			7.54	1		
5700			8.35	(q,2)			8.35	1		
5800			8.21	(q,1)			8.35	2	8.58±0.77	6
5900			9.07	(q,2)			9.07	1		
6000							9.79	1		
6100							(9.63)			
6200			11.21	(q,1)			9.47	2		
6300							5.39	1	7.74±2.20	5
6400			7.99	(q,1)			7.99	1		
6500			6.41	(q,1)			6.41	1		
6600							8.89	1		
6700			7.41	(q,1)			7.41	1		
6800			7.37	(q,2)			7.37	1	8.16±1.04	5
6900			7.51	(q,1)			8.57	2		
7000							(8.15)			
7100			7.73	(q,1)			7.73	1		
7200							5.75	1		
7300							(7.70)		8.17±1.84	4
7400			9.64	(q,1)			9.64)	1		
7500			9.58±0.61	(z,3)			9.58	1		
7600			8.43	(z,2)			8.43	1		
7700			9.72±1.72	(z,6;q,1)			9.72	1		
7800			8.96±1.16	(z,4)			8.96	1	9.62±0.98	5
7900			10.99±0.92	(z,3)			10.99	1		
8000			9.99±1.48	(z,3)			9.99	1		

100 year intervals have been divided at the midpoints between centuries. (ref,n) denotes source of dipole moment data and the number of separate paleointensity determinations used to calculate that number. (a,n) from Athavale (1969); (b,n) from Barbetti, McElhinny, Edwards and Schmidt (1977); (c,n) from Bucha (1965); (d,n) from Bucha (1967); (e,n) from Bucha, Taylor, Berger and Haury (1970); (f,n) from Burlatskaya, Nechaeva and Petrova (1965); (g,n) from Burlatskaya, Nachasova and Petrova (1969); (h,n) from Burlatskaya, Nachasova, Nachaeva, Rusakov, Zagniy, Tarhov and Tchelidze (1970); (i,n) from Burlatskaya, Nachasova and Burakov (1975); (j,n) from Champion (this study); (k,n) from Coe, Gromme and Mankinen (1978); (l,n) from Kitazawa (1970); (m,n) from Kitazawa and Kobayashi (1968); (n,n) from Kono (1978); (o,n) from Kovacheva (1973); (p,n) from Kovacheva (1977); (q,n) from Kovacheva and Veljovich (1977); (r,n) from Lee (1975); (s,n) from Nachasova (1972); (t,n) from Nadia and Chelidze (1972); (u,n) from Nagata, Arai and Momose (1963); (v,n) from Nagata, Kobayashi and Schwarz (1965); (w,n) from Rusakov and Zagniy (1973); (x,n) from Sasajima and Maenaka (1966); (y,n) from Schwarz and Christie (1967); (z,n) from Smith (1968); (aa,n) from Sternberg and Butler (1978); (bb,n) from Thellier and Thellier (1959); and (cc,n) from Weaver (1966).

of a VADM assumes that the best average position to assume for the dipole is centered and parallel to the spin axis of the Earth, while the VDM is calculated using the observed paleoinclination. For each 100-year interval, an average of the dipole moments from all regions was calculated, as well as the standard deviation where moments are available for three regions or more in a given 100-year interval. For comparison with the study of Cox (1968) 500-year averages of the dipole moment data were calculated as well; all 100-year means within each 500-year span of time from all regions available were averaged. Thus the 500-year averages tend to be weighted with respect to regions for which the most 100-year means are available. This was judged to be preferable to weighting all regions equally and letting a single, possibly poor dipole moment from a region bias the 500-year average for the whole world. It was done also assuming that a nondipole feature would affect a region for less than a 500-year span of time.

As a test of whether an average from the 11 regions can yield an accurate estimate of the dipole moment, the 1965.0 IGRF was used to generate the VDM at each of the 11 regions represented in Table 4. The mean moment, $8.44 \pm 0.82 \times 10^{22}$ A·m^2 obtained for the 11 regions is statistically indistinguishable, at the 95 percent confidence level, from the dipole moment of 8.00×10^{22} A·m^2 found from global geomagnetic observations used in the 1965.0 IGRF. Given sufficient data, it appears that useful estimates of the dipole moment can be made from the 11 regions used.

The dipole moment, computed from 100-year averages, ranged from about 6 x 10^{22}A·m^2 to about 12 x 10^{22} A·m^2 during the Holocene (Fig. 30). Over the last 2000 years there has been a general decrease of the dipole moment with time. Previous to about 2500 years B.P. the data are too sparse to obtain reliable 100-year averages. Most of these scattered 100-year means are comprised of data only from a single region and likely are still manifesting the effects of the nondipole field on that region.

By averaging over 500-year intervals it is possible to reduce the scatter of the averages by grouping more data from separate regions (Fig. 31). The 500-year averages show a broad quasi-sinusoidal pattern in the dipole moment with a period of the order of 8000 years, similar to that found by Cox (1968). The dipole moment has been above the mean value for the past 4000 years and generally below it for the previous 4000 years. The half amplitude of this fluctuation is comparable to the mean standard deviation of the 500-year averages. The amplitude of fluctuation, 4.1 x 10^{22} A·m^2, is substantially less for the regionalized data than the amplitude found by Cox. The earliest 500-year average at 7800 years B.P. is comprised of data only from southeastern Europe (Bulgaria and Turkey). If the downward trend with time denoted by the question-marked line on Figure 31 is a nondipole field effect, then this average should not be on this diagram. But if, in fact, it is a dipole field effect, then it is a very important 500-year average, as will be shown in the following analysis.

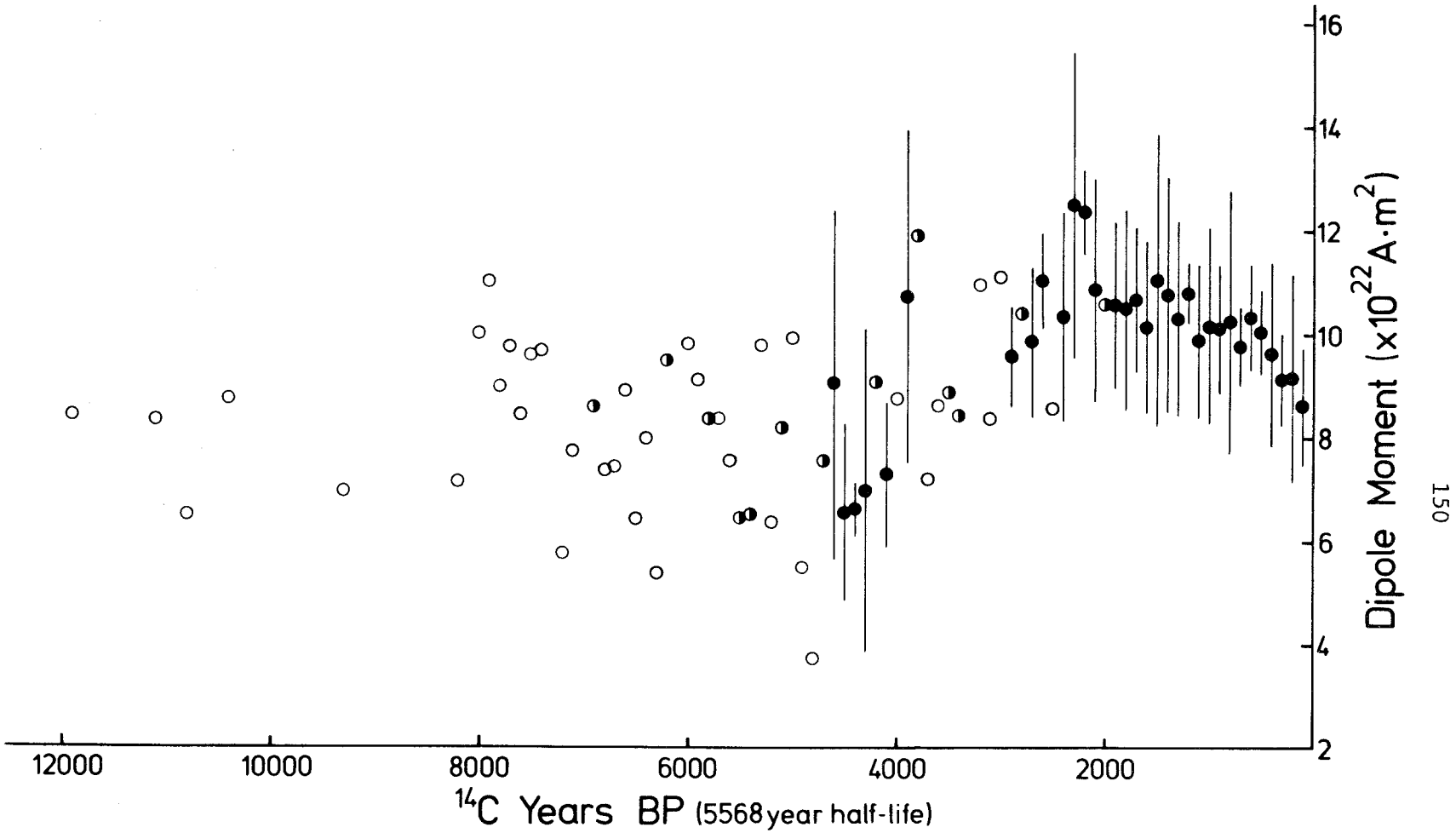

Fig. 30--Geomagnetic dipole moment estimated from 100-year global averages. Vertical lines indicate an interval of ±1 standard deviation. Filled circles indicate three or more regions included in the average. Half-filled circles indicate two regions included in the average and open circles indicate data from a single region.

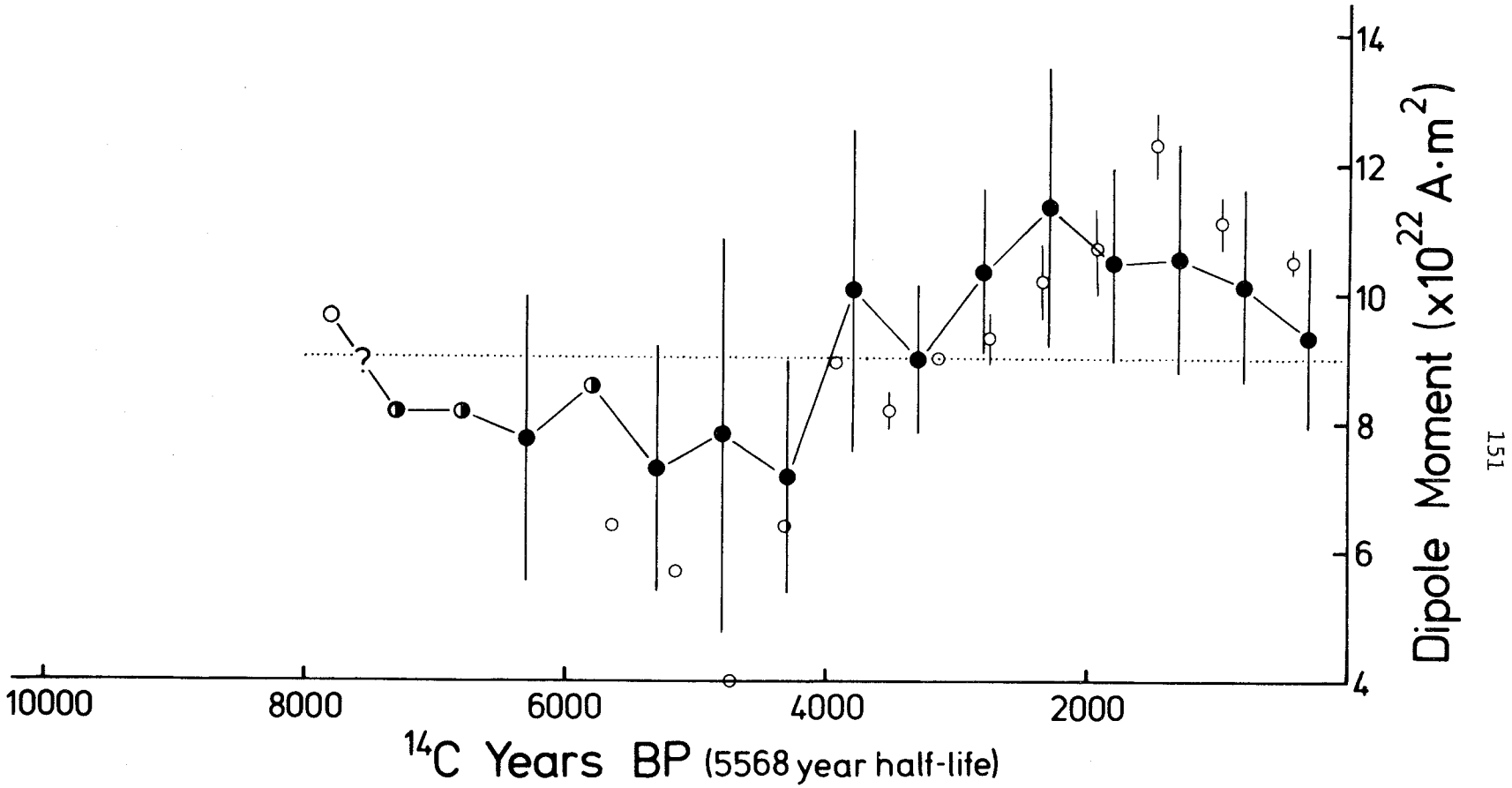

Fig. 31--Geomagnetic dipole moment estimated from 500-year global averages. Vertical lines indicate an interval of ±1 standard deviation. Filled circles with standard deviations indicate three or more regions included in the average. Half-filled circles indicate two regions included in the average and open circles indicate data from a single region. The dotted line represents the grand average of 9.03 x 10^{22} A·m^2.

An analysis of the power spectral density for the time variation of the geomagnetic dipole moment was performed to ascertain whether the fluctuation is periodic. The data used for this analysis were the 100-year interval averages from Table 4. While a variety of spectral analysis techniques exist, most yield incoherent results from initial data as noisy as the 100-year averages. The spectral analysis used was the maximum entropy method (MEM) or Burg's power spectrum (Burg, 1967, 1972). MEM analysis is particularly useful when the input data are noisy and when the time span of the data is on the order of the wavelength of the largest period of variation. It was hoped that despite the shortness of the record relative to the possible 8000-year period within it, and despite the noise from the nondipole field, the MEM would deliver a useful analysis of the spectral characteristics of the 100-year dipole moment averages. The MEM technique has been used by Yukutake (1973) and Jin and Thomas (1977) to analyze the last few decades of dipole moment variation with satisfactory results.

Central to the MEM procedure is the choice of the length of the prediction error filter (PEF). The PEF passes only random noise, so that all "predictable" information about the data is contained in the filter. Inversion of the spectrum of the filter is a spectrum of the predictable part of the input data. The shape of the power spectrum calculated from a sequence of data using the MEM depends on the number of terms of the PEF. A PEF with only a few terms produces a smooth spectrum at the expense of resolution. Longer PEFs improve the spectral resolution but at the hazard of introducing

split peaks produced by the Burg algorithm. Although the length of the filter influences the details of a spectrum, the general properties of a spectrum are not strongly dependent on filter length unless the lengths are very long or very short.

A variety of PEF lengths were used to study the 100-year averages of the dipole moment. As no dipole moment information exists for 100-year intervals centered at 3300, 6100, 7000 or 7300 years B.P., these gaps were filled by linear interpolation. The 100-year averages were differenced from the grand average to remove the offset from zero, a procedure required for most spectral analyses. It quickly became clear that the choice of PEF was crucial (Fig. 32). For short PEFs, up to 21 of the 80 terms, the MEM yields a rather weak spectrum with the greatest power at zero frequency (infinite period). Some power is found at shorter periods but, as these periods represent the Nyquist frequency (200 years) or harmonics of the Nyquist frequency, it is likely they are artifacts of the sampling interval and of the noise in the data. If 21 or more terms are used in the PEF, the period of greatest power shifts to approximately 6600 years, settling to between 7000 to 8000 years for filters longer than 30 terms. Shorter periods containing some power proliferate with the use of longer PEFs, both through the process of line splitting and through nucleation from the shoulders of existing peaks. Though it is not known definitely why line splitting occurs, Fougere (1975) maintains that it is a consequence of the Burg algorithm and not a function of the input data. Because of this, the shorter periods resolved by longer PEFs are not considered to

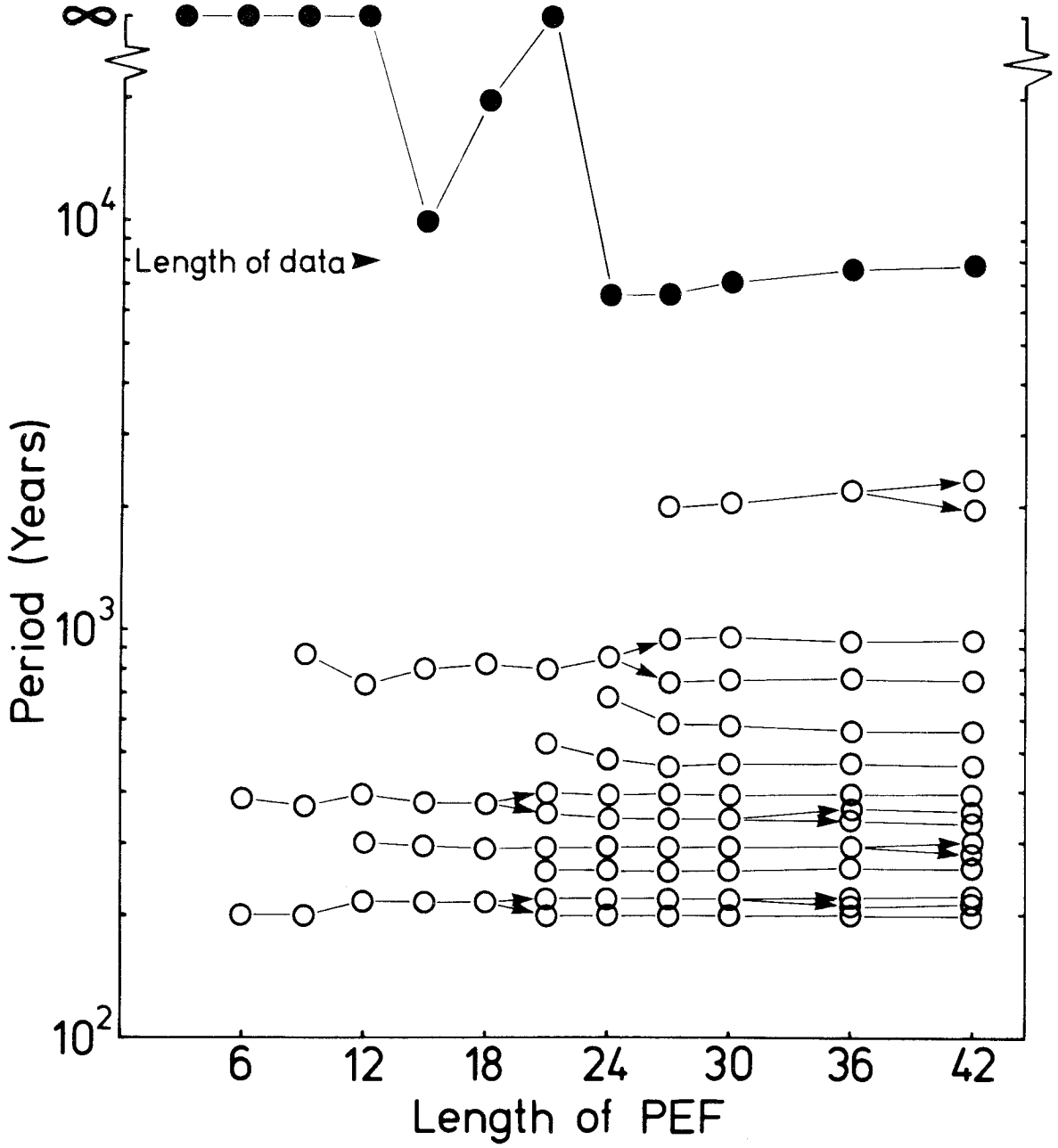

Fig. 32--Periods of variation of the dipole moment of the Earth determined by power spectral analysis using the maximum entropy method. The periods resolved are a function of the length of the prediction error filter (PEF) used. Filled circles denote period with greatest power. Arrows show single periods which split into two periods when longer PEFs are used.

be valid. The 7000- to 8000-year period with maximum power does not split, even at PEF lengths up to the length of the input data (80 terms). A PEF of 30-term length was chosen as the most appropriate for the MEM analysis as it is the smallest PEF which produces the 7000- to 8000-year period and minimizes the line splitting problem.

The power spectrum for the 100-year averages of dipole moment shows how completely the 7000- to 8000-year period dominates the spectral power (Fig. 33). None of the shorter periods contains more than 10 percent as much power as that found at 7270 years. These shorter periods are possibly all artifacts. The 750 and 960 peaks, for instance, represent line splits from a peak at 860 years. The 7000- to 8000-year dominant period confirms the apparent ≃8000-year period found from the graph of the 500-year averages.

An additional analysis using the MEM technique was performed using only the last 7200 years of dipole moment data (Fig. 34). Again a PEF of 30-term length was used to study the 100-year averages of the dipole moment. The shorter time span was investigated in order to ascertain the effect of the data from 7400 to 8000 years, which are exclusively from southeastern Europe. The apparent decrease of the dipole moment during those centuries in southeastern Europe may be due to changes in the nondipole field. The deletion of this southeastern European data has the effect of lengthening the period with dominant power to 8700 years and broadening the peak so that 10 percent power returns to infinite period.

The global dipole moment clearly varied during the Holocene with approximately an 8000-year period. Whether or not there are

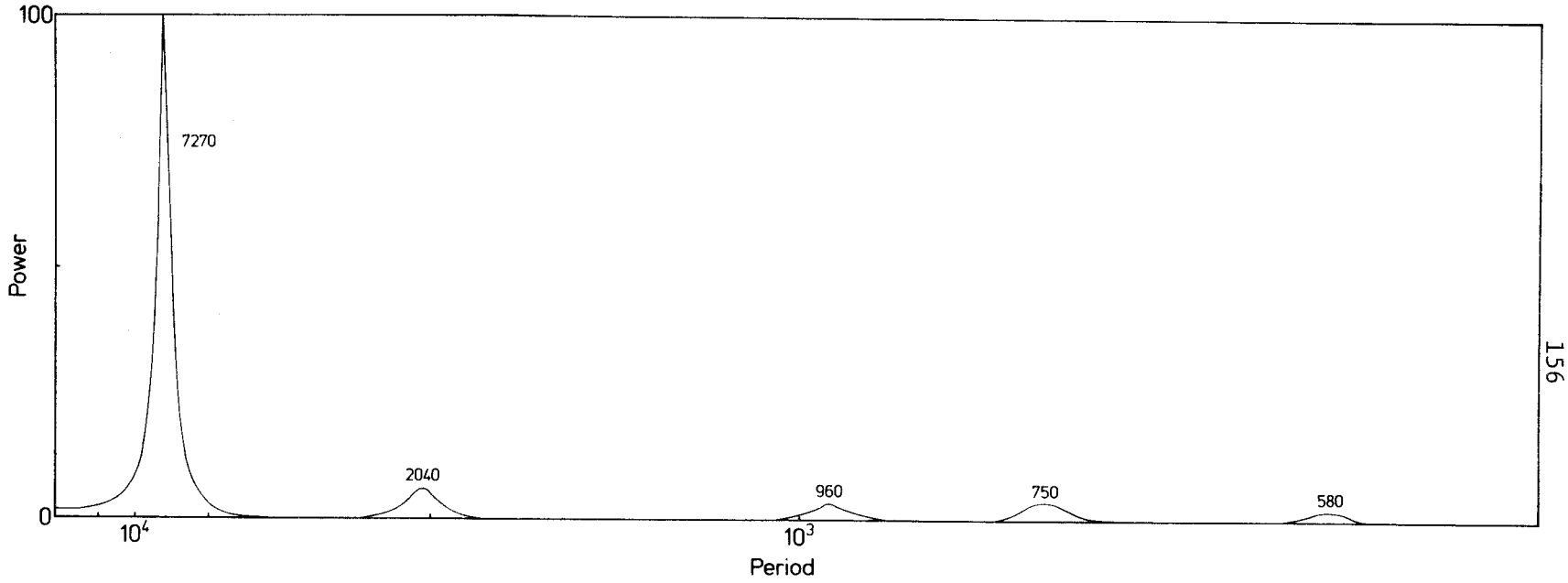

Fig. 33--Power spectrum for 8000 years of dipole moment data averaged at 100-year intervals. Spectrum obtained using the maximum entropy method (MEM) with a prediction error filter (PEF) equal to 30 terms of the data. Power has been normalized to the largest peak; the numbers denote the period in years.

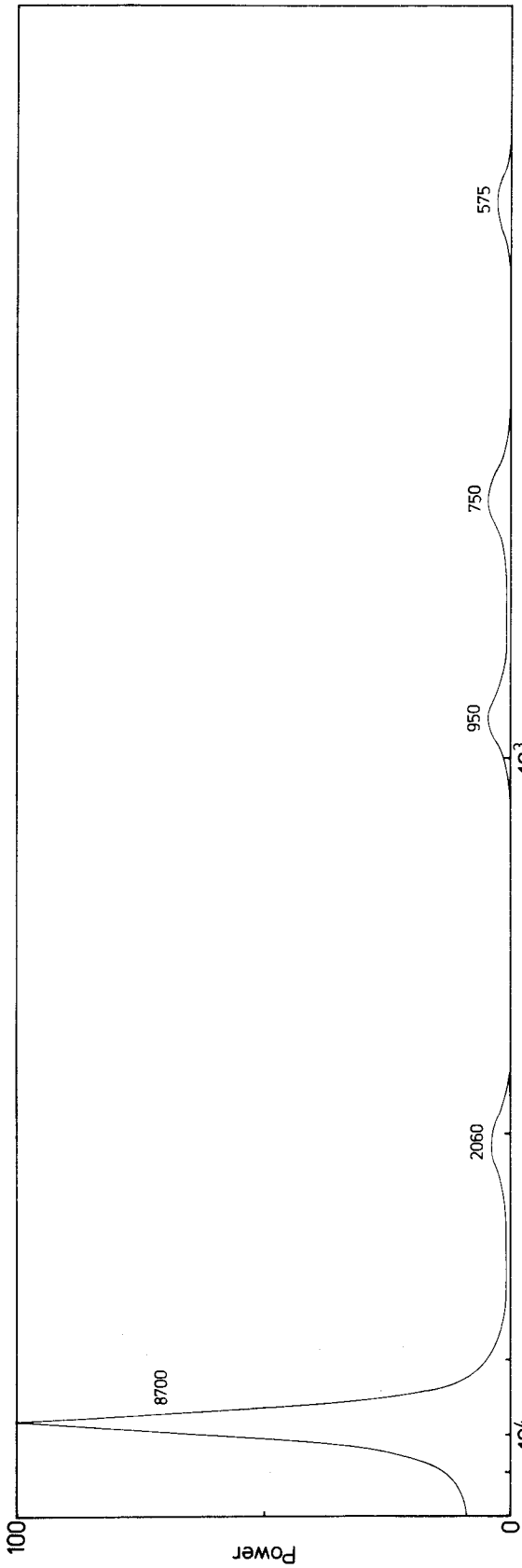

Fig. 34--Power spectrum for 7200 years of dipole moment data averaged at 100-year intervals. Spectrum obtained using the maximum entropy method (MEM) with a prediction error filter (PEF) equal to 30 terms of the data. Power has been normalized to the largest peak; the numbers denote the period in years.

significant shorter periodic variations appears unanswerable with the available data. An MEM analysis of the 100-year interval averages for only the past 2500 years, for which the scatter in the data is much less, surprisingly gave no reliable indication of high frequency periodic variation of the global dipole moment, but rather a very similar result to the MEM analysis on 80 centuries of data. Thus there is no indication at this time that the variation of dipole position and the dipole magnitude are correlated in any manner.

If the fluctuation of the dipole moment has been truly periodic over a time span greater than 8000 years, then the average dipole moment between 8000 and 11,000 years B.P. should have been above 10×10^{22} A·m^2. Four paleointensity determinations available for this span of time however, are all less than 9×10^{22} A·m^2 (Fig. 30, Table 4). Thus there is no evidence that the apparent ≈8000-year period variation can be extrapolated to times earlier than 8000 years B.P. The high global dipole moment observed between 3000 and 1000 years B.P. may simply be a surge in the amplitude of the dipole moment that is irregularly spaced in time from other surges.

REFERENCES

Abokhodair, A. A., 1977, The accuracy of the Thelliers' technique for the determination of paleointensity of the Earth's magnetic field: University of California, Santa Cruz, Ph.D. thesis, 164 p.

Ade-Hall, J. M., Wilson, R. L., and Smith, P. J., 1965, The petrology, Curie points and natural magnetization of basic lavas: Geophysical Journal of the Royal Astronomical Society, v. 9, p. 323-336.

Aitken, M. J., and Weaver, G. H., 1965, Recent archaeomagnetic results in England: Journal of Geomagnetism and Geoelectricity, v. 17, p. 391-394.

Arai, Y., 1963, Secular variation in the intensity of the past geomagnetic field: University of Tokyo, Japan, M.S. thesis, 84 p.

Athavale, R. N., 1966, Intensity of the geomagnetic field in India over the past 4,000 years: Nature, v. 210, p. 1310-1312.

Athavale, R. N., 1969, Intensity of the geomagnetic field in prehistoric Egypt: Earth and Planetary Science Letters, v. 6, p. 221-224.

Baag, C., 1974, Discussion on quiet secular variation in Japan during the last 9500 years: Journal of Geomagnetism and Geoelectricity, v. 26, p. 83-86.

Baag, Czang-go, and Helsley, C. E., 1974, Geomagnetic secular variation model E: Journal of Geophysical Research, v. 79, p. 4918-4922.

Banerjee, S. K., and Mellema, J. P., 1974, A new method for the determination of paleointensity from the ARM properties of rocks: Earth and Planetary Science Letters, v. 23, p. 177-184.

Barbetti, M., 1977, Measurements of recent geomagnetic secular variation in southeastern Australia and the question of dipole wobble: Earth and Planetary Science Letters, v. 36, p. 207-218.

Barbetti, M. F., McElhinny, M. W., Edwards, D. J., and Schmidt, P. W., 1977, Weathering processes in baked sediments and their effects on archaeomagnetic field-intensity measurements: Physics of the Earth and Planetary Interiors, v. 13, p. 346-354.

Barraclough, D. R., 1974, Spherical harmonic analysis of the geomagnetic field for eight epochs between 1600 and 1910: Geophysical Journal of the Royal Astronomical Society, v. 36, p. 497-513.

Benson, G. T., 1965, The age of Clear Lake, Oregon: The Ore Bin, v. 27, p. 37-40.

Breternitz, D. A., 1967, The eruption(s) of Sunset Crater: dating and effects: Plateau, v. 40, p. 72-76.

Brynjolfsson, Ari, 1957, Studies of remanent magnetism and viscous magnetism in the basalts of Iceland: Advances in Physics, v. 6, p. 247-254.

Bucha, V., 1965, Archaeomagnetic research into the total geomagnetic field intensity and its changes in Czechoslovakia: Studia Geophysica et Geodaetica, v. 9, p. 272-289.

Bucha, V., 1967, Intensity of the Earth's magnetic field during archaeological times in Czechoslovakia: Archaeometry, v. 10, p. 12-22.

Bucha, V., Taylor, R. E., Berger, R., and Haury, E. W., 1970, Geomagnetic intensity: changes during the past 3000 years in the western hemisphere: Science, v. 168, p. 111-114.

Buckley, J. D., Trautman, M. A., and Willis, E. H., 1968, Isotopes radiocarbon measurements VI: Radiocarbon, v. 10, p. 246-294.

Buddington, A. F., and Lindsley, D. H., 1964, Iron-titanium oxide minerals and synthetic equivalents: Journal of Petrology, v. 5, p. 310-357.

Bullard, F. M., 1971, Volcanic history of the Great Rift, Craters of the Moon National Monument, south-central Idaho [abs.]: Geological Society of America Meeting, v. 3, no. 3, p. 234.

Bullard, E. C., Freedman, C., Gellman, H., and Nixon, J., 19 The westward drift of the Earth's magnetic field: Royal Society of London, Philosophical Transactions, v. 243, p. 67-92.

Bullard, F. M., and Rylander, D. L., 1970, Holocene volcanism in Craters of the Moon National Monument and adjacent areas, south-central Idaho [abs.]: Geological Society of America Meeting, v. 2, no. 4, p. 273-274.

Burg, J. P., 1967, Maximum entropy spectral analysis: Paper presented at the 37th Annual Meeting, Society of Exploration Geophysics, Oklahoma City, Oct. 31.

Burg, J. P., 1972, The relationships between maximum entropy spectra and maximum likelihood spectra: Geophysics, v. 37, p. 375-376.

Burlatskaya, S. P., Nechaeva, T. B., and Petrova, G. N., 1965, The westward drift of the secular variation of magnetic inclination and variations of the Earth's magnetic moment according to archeomagnetic data: Izvestia Akadamia nauk SSSR, Fizika Zemli, v. 6, p. 31-42.

Burlatskaya, S. P., Nechaeva, T., and Petrova, G., 1969, Some archaeomagnetic data indicative of the westward drift of the geomagnetic field: Archaeometry, v. 11, p. 115-130.

Burlatskaya, S. P., Nachasova, I. E., Nachaeva, T. B., Rusakov, O. M., Zagniy, G. F., Tarhov, E. N., and Tchelidze, Z. A., 1970, Archaeomagnetic research in the USSR: recent results and spectral analysis: Archaeometry, v. 12, p. 73-85.

Burlatskaya, S. P., Kruchik, Y. A., Malkovskiy, Z., Nechayeva, T. B., and Petrova, G. N., 1970, Comparison of secular variation in inclination in Poland and the Ukraine: Geomagnetism and Aeronomy, v. 10, p. 243-245.

Burlatskaya, S. P., Nachasova, I. E., and Burakov, K. S., 1975, New determinations of the parameters of the ancient geomagnetic field for Mongolia, Soviet Central Asia, and Abhazia: Geomagnetism and Aeronomy, v. 16, p. 447-450.

Carmichael, I. S. E., and Nicholls, J., 1967, Iron-titanium oxides and oxygen fugacities in volcanic rocks: Journal of Geophysical Research, v. 72, p. 4665-4687.

Champion, D. E., 1973, The relationship of large scale surface morphology to lava flow direction, Wapi Lava Field, southeast Idaho: State University of New York, Buffalo, M.A. thesis, 44 p.

Champion, D. E., and Greeley, R., 1977, Geology of the Wapi Lava Field, Snake River Plain, Idaho, in Volcanism of the Eastern Snake River Plain, Idaho: A Comparative Planetary Geology Guidebook, Ch. 8, p. 133-152.

Chatters, R. M., 1968, Washington State University Natural Radiocarbon Measurements I: Radiocarbon, v. 10, p. 479-498.

Chitwood, L. A., Jensen, R. A., and Groh, E. A., 1977, The age of Lava Butte: The Ore Bin, v. 39, p. 157-164.

Coe, R. S., 1967, Paleointensities of the Earth's magnetic field determined from Tertiary and Quaternary rocks: Journal of Geophysical Research, v. 72, p. 3247-3262.

Coe, R. S., 1967, The determination of paleointensity of the Earth's magnetic field with emphasis on mechanisms which could cause non-ideal behavior in Thelliers' method: Journal of Geomagnetism and Geoelectricity, v. 19, p. 157-179.

Coe, R. S., and Grommé, C. S., 1973, A comparison of three methods for determining geomagnetic paleointensities: Journal of Geomagnetism and Geoelectricity, v. 25, p. 415-435.

Coe, R. S., Grommé, C. S., and Mankinen, E. A., 1978, Geomagnetic paleointensities by the Thelliers' method from radiocarbon dated lava flows on Hawaii: Journal of Geophysical Research, v. 83, p. 1740-1756.

Colton, H. S., 1932, A possible Hopi tradition of the eruption of Sunset Crater: Northern Arizona Museum Notes, v. 5, no. 4, p. 23.

Colton, H. S., 1937, The eruption of Sunset Crater as an eyewitness might have observed it: Northern Arizona Museum Notes, v. 10, no. 4, p. 9-12.

Colton, H. S., 1945, A revision of the date of the eruption of Sunset Crater: Southwestern Journal of Anthropology, v. 1, no. 3, p. 345-355.

Condie, K., and Barsky, C., 1972, Origin of Quaternary basalts from the Black Rock Desert region, Utah: Geological Society of America Bulletin, v. 83, p. 333-352.

Cox, Allan, 1962, Analysis of present geomagnetic field comparison with paleomagnetic results: Journal of Geomagnetism and Geoelectricity, v. 13, p. 101-112.

Cox, Allan, 1968, Lengths of geomagnetic polarity intervals: Journal of Geophysical Research, v. 73, p. 3247-3260.

Cox, Allan, 1969, Research note confidence limits for the precision parameter k: Geophysical Journal of the Royal Astronomical Society, v. 18, p. 545-549.

Cox, Allan, 1970, Latitude dependence of the angular dispersion of the geomagnetic field: Geophysical Journal of the Royal Astronomical Society, v. 20, p. 253-269.

Cox, Allan, 1975, The frequency of geomagnetic reversals and the symmetry of the nondipole field: Reviews of Geophysics and Space Physics, v. 13, p. 35-51.

Cox, Allan, and Doell, R. R., 1960, Review of paleomagnetism: Geological Society of America Bulletin, v. 71, p. 645-768.

Cox, A., and Doell, R. R., 1964, Long period variations of the geomagnetic field: Seismological Society of America Bulletin, v. 54, p. 2243-2270.

Crandell, D. R., 1971, Postglacial lahars from Mount Rainier volcano, Washington: U.S. Geological Survey Professional Paper 677, 75 p.

Creer, K. M., 1962a, The dispersion of the geomagnetic field due to secular variation and its determination for remote times from paleomagnetic data: Journal of Geophysical Research, v. 67, p. 3461-3476.

Creer, K. M., 1962b, An analysis of the geomagnetic field using paleomagnetic methods: Journal of Geomagnetism and Geoelectricity, v. 13, p. 113-119.

Czyszek, Waclaw, 1973, Archaeomagnetism: a preliminary report: Publication of the Institute of Geophysics, Polish Academy of Sciences, v. 76, p. 59-73.

Damon, P. E., Long, A., and Wallick, E. I., 1972, Dendrochronologic calibration of the carbon-14 time scale, in Proceedings of 8th International Conference on Radiocarbon Dating: Royal Society of New Zealand, v. 1, p. 45-59.

Dodson, R., Day, R., Dunn, J. P., Fuller, M., Henyey, T. L., and Kean, W., 1977, Continuous records of secular variation [abs.]: American Geophysical Union Fall Meeting, EOS, v. 58, no. 6, p. 380.

Doell, R. R., and Cox, A. V., 1963, The accuracy of the paleomagnetic method as evaluated from historic Hawaiian lava flows: Journal of Geophysical Research, v. 68, p. 1997-2099.

Doell, R. R., and Cox, A. V., 1965, Measurement of the remanent magnetization of igneous rocks: U.S. Geological Survey Bulletin 1203-A, p. 1-32.

Doell, R. R., and Cox, A. V., 1967, Analysis of spinner magnetometer operation, in Collinson, D. W., Creer, K. M., and Runcorn, S. K., eds., Methods in Paleomagnetism: p. 196-206.

Doell, R. R., and Cox, A. V., 1967, Recording magnetic balance, in Collinson, D. W., Creer, K. M., and Runcorn, S. K., eds., Methods in Paleomagnetism: p. 440-444.

Doell, R. R., and Cox, A., 1972, The Pacific geomagnetic secular variation anomaly and the question of lateral uniformity in the lower mantle, in Richardson, E. C., ed., Nature of the Solid Earth: New York, McGraw-Hill, 245 p.

Doell, R. R., and Dalrymple, G. B., 1973, Potassium-argon ages and paleomagnetism of the Waianae and Koolau volcanic series, Oahu, Hawaii: Geological Society of America Bulletin, v. 84, p. 1217-1242.

DuBois, R. L., 1974, Secular variation in southwestern United States as suggested by archeomagnetic studies, in Fisher, R. M., Fuller, M., Schmidt, V. A., and Wasilewski, P. J., eds., Proceedings of the Takesi Nagata Conference: University of Pittsburgh, p. 133-144.

Engebretson, D., and Beck, M., in press, On the shape of directional data set: Journal of Geophysical Research, v. 83.

Fisher, R. A., 1953, Dispersion on a sphere: Proceedings of the Royal Society of London, Series A, v. 217, p. 295-305.

Fougere, P. F., 1975, A solution to the problem of spontaneous line splitting in maximum entropy power spectrum analysis [abs.]: American Geophysical Union, EOS Transactions, v. 56, p. 1054.

Games, K. P., 1979, Short period fluctuations in the Earth's magnetic field: Nature, v. 277, p. 600-601.

Giegengack, R. F., 1962, Recent volcanism near Dotsero, Colorado: University of Colorado, M.S. thesis, 43 p.

Greeley, R., and Hyde, J. H., 1972, Lava tubes of the Cave Basalt, Mt. St. Helens, Washington: Geological Society of America Bulletin, v. 83, p. 2397-2418.

Greeley, R., and King, J. S., 1975, Rift zones in the south-central Snake River Plain, Idaho [abs.]: Geological Society of America Meeting, Rocky Mountain Section, v. 7, p. 610.

Grommé, C. S., Wright, T. L., and Peck, D. L., 1969, Magnetic properties and oxidation of iron-titanium oxide minerals in Alae and Makapuhi Lava Lakes, Hawaii: Journal of Geophysical Research, v. 74, p. 5277-5293.

Haggerty, S. E., 1976, Oxidation of opaque mineral oxides in basalts, in Short course notes "Oxide Minerals": Mineralogical Society of America, v. 3, Ch. 4, p. Hg1-Hg100.

Harris, B. L., 1973, Genesis, mineralogy and properties of Parkdale soils, Oregon: Oregon State University, Ph.D. thesis.

Harwood, J. M., and Malin, S. R. C., 1976, Present trends in the Earth's magnetic field: Nature, v. 259, p. 469-471.

Henyey, T. L., Liddicoat, J. C., Day, R., Dodson, R., Fuller, M., and Palmer, D. F., 1977, Ages of Lake Tahoe cores and comparison of paleomagnetic curves for Lake Tahoe with those of Mono Lake and Lake Lahontan [abs.]: American Geophysical Union, Fall Meeting, EOS Transactions, v. 58, p. 1124.

Hirooka, K., 1971, Archaeomagnetic study for the past 2,000 years in southwest Japan: Memoirs of the Faculty of Science, Kyoto University, Series of Geology and Mineralogy, v. XXXVIII, p. 167-207.

Hoover, J. D., 1975, Periodic Quaternary volcanism in the Black Rock Desert, Utah: Brigham Young Geologic Studies, v. 22, p. 3-72.

Hsing-Huei, T., and Tung-chieh, L., 1965, The geomagnetic field in Peking region and its secular variation during the last 2000 years: Acta Geophysica Sinica, v. 14, p. 181-195.

Irving, E., and Ward, M. A., 1964, A statistical model of the geomagnetic field: Pure Applied Geophysics, v. 57, p. 47-52.

Ives, P. C., Levin, B., Robinson, R. D., and Rubin, M., 1964, Geological Survey Radiocarbon Dates VIII: Radiocarbon, v. 6, p. 37-76.

Ives, P. C., Levin, B., Oman, C. L., Rubin, M., 1967, U.S. Geological Survey Radiocarbon Dates IX: Radiocarbon, v. 9, p. 505-529.

Jin, R. S., and Thomas, D. M., 1977, Spectral line similarity in the geomagnetic field variation and length of day fluctuations: Journal of Geophysical Research, v. 82, p. 828-834.

Karlo, J. F., 1977, Geology of the Hell's Half Acre Lava Field, in Volcanism of the Eastern Snake River Plain, Idaho: A Comparative Planetary Geology Guidebook, Ch. 7, p. 123-131.

Kawai, N., Hirook, K., and Sasajima, S., 1965, Counterclockwise rotation of the geomagnetic dipole axis revealed in the world-wide archaeosecular variations: Proceedings of the Japan Academy, v. 41, p. 398-403.

Kawai, N., Hirooka, K., and Tokieda, K., 1967, A vibration of geomagnetic axis around the geographic North Pole in the historic time: Earth and Planetary Science Letters, v. 3, p. 48-50.

Kawai, N., and Hirooka, K., 1967, Wobbling motion of the geomagnetic dipole field in historic time during these 2000 years: Journal of Geomagnetism and Geoelectricity, v. 19, p. 217-227.

Khodair, A. A., and Coe, R. S., 1975, Determination of geomagnetic paleointensities in vacuum: Geophysical Journal of the Royal Astronomical Society, v. 42, p. 107-115.

King, J. S., 1977, Crystal Ice Cave and Kings Bowl Crater, Snake River Plain, Idaho, in Volcanism of the Eastern Snake River Plain, Idaho: A Comparative Planetary Geology Guidebook, Ch. 9, p. 153-164.

Kinoshita, H., 1970, Lists of archeomagnetic and paleomagnetic results: Journal of Geomagnetism and Geoelectricity, v. 22, p. 507-550.

Kitazawa, K., 1970, Intensity of the geomagnetic field in Japan for the past 10,000 years: Journal of Geophysical Research, v. 75, p. 7403-7411.

Kitazawa, K., and Kobayashi, K., 1968, Intensity variation of the geomagnetic field during the past 4000 years in South America: Journal of Geomagnetism and Geoelectricity, v. 20, p. 7-19.

Kittleman, L. R., 1973, Mineralogy, correlation and grain size distribution of Mazama tephra and other postglacial pyroclastic layers, Pacific northwest: Geological Society of America Bulletin, v. 84, p. 2957-2980.

Kono, M., 1971, Intensity of the earth's magnetic field during the Pliocene and Pleistocene in relation to the amplitude of mid-ocean ridge magnetic anomalies: Earth and Planetary Science Letters, v. 11, p. 10-17.

Kono, Masaru, 1978, Reliability of paleointensity methods using alternating field demagnetization and anhysteretic remanence: Geophysical Journal of the Royal Astronomical Society, v. 54, p. 241-261.

Kovacheva, M., 1973, Secular variation of the ancient magnetic fields intensity during the last 2400 years in Bulgaria: Bulgarska Akademiia na Naukite, Sofia, Comptes rendes (Doklady), v. 26, p. 747-749.

Kovacheva, M.,1977, Archaeomagnetic investigations in Bulgaria: field intensity determinations: Physics of the Earth and Planetary Interiors, v. 13, p. 355-359.

Kovacheva, M., and Veljovich, D., 1977, Geomagnetic field variations in southeastern Europe between 6500 and 100 years B.C.: Earth and Planetary Science Letters, v. 37, p. 131-138.

Kuntz, M. A., 1977, Extensional faulting and volcanism along the Arco Rift Zone, eastern Snake River Plain, Idaho [abs.]: Geological Society of America Meeting, Rocky Mountain Section, v. 9, p. 740-741.

Landon, R. E., 1933, Date of recent volcanism in Colorado: American Journal of Science, v. 25, p. 20-24.

Lefebvre, R. H., 1975, Mapping in the Craters of the Moon Volcanic Field, Idaho with LANDSAT (ERTS) imagery: Proceedings of the 19th International Symposium on Remote Sensing of the Environment, 6-10 Oct., Ann Arbor, Michigan, p. 951-963.

Levi, Shaul, 1975, Comparison of two methods of performing the Thellier experiment or how the Thellier experiment should not be done: Journal of Geomagnetism and Geoelectricity, v. 27, p. 245-255.

Libby, W. F., 1955, Chicago radiocarbon dates III: Science, v. 116, p. 673-681.

Lingenfelter, R. E., and Ramaty, R., 1970, Astrophysical and geophysical variations in C-14 production, in Olsson, I. U., ed., Radiocarbon Variation and Absolute Chronology: New York, Wiley.

Lund, S., Bogdan, D., Levi, S., Banerjee, S., and Long, A., 1976, Continuous geomagnetic record for the past 10,000 years from Lake St. Croix, Minnesota: American Geophysical Union, Fall Meeting, EOS Transactions, v. 57, p. 910.

McElhinny, M. W., and Merrill, R. T., 1975, Geomagnetic secular variation over the past 5 m.y.: Reviews of Geophysics and Space Physics, v. 13, p. 687-708.

Mehringer, P. J., Blinman, E., and Petersen, K. L., 1977, Pollen influx and volcanic ash: Science, v. 198, p. 257-261.

Merrill, R. T., and McElhinny, M. W., 1977, Anomalies in the time-averaged paleomagnetic field and their implication for the lower mantle: Reviews of Geophysics and Space Physics, v. 15, p. 309-323.

Moore, R. B., Wolfe, E. W., and Ulrich, G. E., 1976, Volcanic rocks of the eastern and northern parts of the San Francisco volcanic field, Arizona: U.S. Geological Survey Journal of Research, v. 4, p. 549-560.

Murtaugh, J. G., 1961, Geology of Craters of the Moon National Monument, Idaho: University of Idaho, Moscow, M.S. thesis, 99 p.

Nachasova, I. Ye., 1972, Magnetic field in the Moscow area from 1480 to 1840: Geomagnetism and Aeronomy, v. 12, p. 277-280.

Nadia, M. Z., and Chelidze, Z. A., 1972, Position of the geomagnetic pole in the past: Geomagnetism and Aeronomy, v. 12, p. 518-519.

Nagata, T., Arai, Y., and Momose, K., 1963, Secular variation of the geomagnetic total force during the last 5000 years: Journal of Geophysical Research, v. 68, p. 5277-5281.

Nagata, T., Kobayashi, K., and Schwarz, E. J., 1965, Archeomagnetic intensity studies of South and Central America: Journal of Geomagnetism and Geoelectricity, v. 17, p. 399-405.

Nieland, J., 1967, Spatter cone pits, Sand Mountain Lava Field, Oregon Cascades: The Ore Bin, v. 32, p. 231-236.

Palmer, D. F., Hanyey, T. L., and Dodson, R. E., 1979, Paleomagnetic and sedimentological studies at Lake Tahoe, California-Nevada: Earth and Planetary Science Letters, v. 46, p. 125-137.

Peterson, N. V., and Groh, E. A., eds., 1965, Lunar Geological Field Conference Guidebook: p. 8-9.

Peterson, N. V., and Groh, E. A., 1969, The ages of some Holocene volcanic eruptions in the Newberry volcano area, Oregon: The Ore Bin, v. 31, p. 73-87.

Prinz, M., 1970, Idaho rift systems, Snake River Plain, Idaho: Geological Society of America Bulletin, v. 81, p. 941-948.

Robertson, W. A., 1963, The paleomagnetism of some Mesozoic extrusions and tuffs from eastern Australia: Journal of Geophysical Research, v. 68, p. 2299-2312.

Robinson, S. W., 1977, U.S. Geological Survey, Menlo Park, California, Radiocarbon Dates I: Radiocarbon, v. 19, p. 460-464.

Rubin, M., and Alexander, C., 1960, Geological Survey Radiocarbon Dates V: American Journal of Science Radiocarbon Supplement, v. 2, p. 129-185.

Rusakov, O. M., and Zagniy, G. F., 1973, Intensity of the geomagnetic field in the Ukraine and Moldavia during the past 6000 years: Archaeometry, v. 15, p. 275-285.

Sasajima, S., and Maenaka, K., 1966, Intensity studies of the archaeo-secular variation in West Japan with special reference to the hypothesis of the dipole axis rotation: University of Kyoto, Memoirs of the College of Science, Series B, v. XXXIII, p. 53-67.

Schwarz, E. J., and Christie, K. W., 1967, Original remanent magnetization of Ontario potsherds: Journal of Geophysical Research, v. 72, p. 3263-3269.

Shaw, J., 1974, A new method for determining ancient geomagnetic field strengths: applications to five historic lavas: Geophysical Journal of the Royal Astronomical Society, v. 39, p. 133-141.

Shive, P. N., and Diehl, J. F., 1977, Thermomagnetic analysis of natural and synthetic hematite: Geophysical Research Letters, v. 4, no. 4, p. 159-162.

Shuey, R. T., Cole, E. R., and Mikulich, M. J., 1970, Geographic correction of archeomagnetic data: Journal of Geomagnetism and Geoelectricity, v. 22, p. 485-489.

Shuey, R. T., Ugland, R. O., and Schmidt, C. R., 1977, Magnetic properties and secular variation in cores from Yellowstone and Jackson Lakes, Wyoming: Journal of Geophysical Research, v. 82, p. 3739-3746.

Skinner, N. J., Iles, W., and Brock, A., 1975, The recent secular variation of declination and inclination in Kenya: Earth and Planetary Science Letters, v. 25, p. 338-346.

Smiley, T. L., 1958, The geology and dating of Sunset Crater, Flagstaff, Arizona, in Anderson, R. Y., and Harshbarger, J. W., eds., Guidebook of the Black Mesa Basin, Northeastern Arizona: New Mexico Geological Society 9th Field Conference, Socorro, p. 186-190.

Smith, P. J., 1967, The intensity of the ancient geomagnetic field: a review and analysis: Geophysical Journal of the Royal Astronomical Society, v. 12, p. 321-362.

Smith, P. J., 1967, Ancient geomagnetic field intensities I, Historic and archaeological data, Sets H1-H9: Geophysical Journal of the Royal Astronomical Society, v. 13, p. 417-419.

Smith, P. J., 1967, Ancient geomagnetic field intensities II, Geological data, Sets G1-G21; Historic and archaeological data, H10-H13: Geophysical Journal of the Royal Astronomical Society, v. 13, p. 483-486.

Smith, P. J., 1968, Ancient geomagnetic field intensities III, Historic and archeological data, H13X and H14-15; Geological data G22-G29: Geophysical Journal of the Royal Astronomical Society, v. 16, p. 457-460.

Stearns, H. T., 1928, Craters of the Moon National Monument, Idaho: Idaho Bureau Mines Geology Bulletin, no. 13, p. 1-57.

Sternberg, R. S., and Butler, R. F., 1978, Archaeomagnetic paleo-intensity study of some Hohokam potsherds from Snaketown, Arizona: Geophysical Research Letters, v. 5, p. 101-104.

Sternberg, R. S., Butler, R. F., and Eighmy, J. L., 1978, Use of Southwest Indian hearths in reconstructing paleosecular variation [abs.]: American Geophysical Union, Fall Meeting, EOS Transactions, v. 59, no. 12, p. 1059.

Symons, D. T. A., 1975, Age and flow direction from magnetic measurements on the historic Aiyansh flow, British Columbia: Journal of Geophysical Research, v. 80, p. 2622-2626.

Tanguy, J. C., and Wilson, R. L., 1973, Paleomagnetism of Mount Etna: Royal Society of London Philosophical Transactions A, v. 274, p. 163.

Taylor, E. M., 1965, Recent volcanism between Three Fingered Jack and North Sister, Oregon, Cascade Range: The Ore Bin, v. 27, p. 121.

Taylor, E. M., 1967, Recent volcanism between Three Fingered Jack and North Sister, Oregon, Cascade Range: Washington State University, Ph.D. thesis, 84 p.

Taylor, E. M., 1968, Roadside geology, Santiam and McKenzie Pass Highway, Oregon, in Dole, H. M., ed., Andesite Conference Guidebook: Oregon Department of Geology and Mineral Resources Bulletin 62, p. 3-34.

Thellier, E., 1938, Sur l'amantation des ternes cuites et ses applications géophysiques: Annals Institute Physique du Globe, v. 16, p. 157-302.

Thellier, E., and Thellier, O., 1959, Sur l'intensité du Champ magnétique terrestre dans le passé historique et géologique: Annals Géophysique, v. 15, p. 285-376.

Valastro, S., Davis, E. M., and Varela, A. G., 1972, University of Texas at Austin, Radiocarbon: v. 14, p. 468-470.

Van Zijl, J. S. V., Graham, V. W. T., and Hales, A. L., 1962, The paleomagnetism of the Stormberg lavas of South Africa, Parts 1 and 2: Geophysical Journal of the Royal Astronomical Society, v. 7, p. 23-39.

Verhoogen, J., 1962, Oxidation of iron-titanium oxides in igneous rocks: Journal of Geology, v. 70, p. 168-181.

Vestine, E. H., LaPorte, L., Cooper, C., Lange, I., and Hendrix, W. C., 1947, Description of the earth's main magnetic field and its secular change, 1905-1945: Carnegie Institute of Washington Publication, 532 p.

Weaver, G. H., 1966, Measurement of the past intensity of the Earth's magnetic field: Archaeometry, v. 9, p. 174-186.

Williams, H., 1942, The geology of Crater Lake National Park, Oregon: Carenegie Institute of Washington Publication 540, 162 p.

Wilson, R. L., 1961, Paleomagnetism in Northern Ireland, Part 1--The thermal demagnetization of natural magnetic moments in rocks: Geophysical Journal of the Royal Astronomical Society, v. 5, p. 45-58.

Wolfman, D., 1973, A re-evaluation of mesoamerican chronology: A.D. 1-1200: University of Colorado, Ph.D. thesis, 293 p.

Yukutake, T., 1962, The westward drift of the magnetic field of the earth: Earthquake Research Institute Bulletin, v. 40, p. 1-65.

Yukutake, T., 1971, Spherical harmonic analysis of the Earth's magnetic field for the 17th and the 18th centuries: Journal of Geomagnetism and Geoelectricity, v. 23, p. 11-23.

Yukutake, T., 1973, Fluctuations in the Earth's rate of rotation related to changes in the geomagnetic dipole field: Journal of Geomagnetism and Geoelectricity, v. 25, p. 195-212.

Appendix 1

Location of Sites and Sources of Age and Geologic Control

1. Ice Spring Field, Black Rock Desert, Utah; 38.96 N., 247.49 E.

   Site location: Within the complex of vents presently worked for cinder production. Two sites 150 m southwest of VABM 4996 and two sites 500 m south.
   Age control: ^{14}C date (Tx-1166) on uncharred root fragments under edge of flow about 5 km northeast of vent area reported by Valastro and others (1972). Date assumes entire field represents a single short episode.
   Geologic references: Condie and Barsky (1972); Hoover (1975).

2. Sunset Crater, San Francisco Volcanic Field, Arizona; 35.36 N., 248.50 E.

   Site location: On the rim of the crater itself, at elevation 8029 and around the east rim to the south.
   Age control: Dendrochronologic control, Smiley (1958); Breternitz (1967), establishes general time framework, proximity to DuBois' VGP path provides exact date. Date assumes DuBois' VGP path is valid.
   Geologic references: Moore and others (1976); field work during this study.

3. Bonito Flow, San Francisco Volcanic Field, Arizona; 35.38 N., 248.48 E.

   Site location: Two sites located 100 m from west base of Sunset Cone, two sites on northern periphery of flow 500 m southwest of hill 7050, and two sites on southern periphery 350 m northeast of section corner at elevation 6915.
   Age control: Dendrochronologic control, Smiley (1958); Breternitz (1967), establish general time framework, proximity to DuBois' VGP path provides exact date. Date assumes DuBois' VGP path is valid.
   Geologic references: Moore and others (1976); field work during this study.

4. Gyp Crater, San Francisco Volcanic Field, Arizona; 35.35 N., 248.54 E.

   Site location: On the northeast rim of Gyp Crater in exposed rootless flows and welded spatter deposits, approximately

450 m south-southwest from road juction 7332.
Age control: Dendrochronologic control, Smiley (1958); Breternitz (1967), establishes general time framework, proximity to DuBois' VGP path provides exact date. Date assumes DuBois' VGP path is valid.
Geologic references: Moore and others (1976); field work during this study.

5. Vent 512, San Francisco Volcanic Field, Arizona; 35.33 N., 248.58 E.

Site location: At moderately sized spatter rampart structure about 400 m east of hill 6859.
Age control: Dendrochronologic control, Smiley (1958); Breternitz (1967), establishes general time framework, proximity to DuBois' VGP path provides exact date. Date assumes DuBois' VGP path is valid.
Geologic references: Moore and others (1976); and field work during this study. Care must be taken not to confuse red spatter deposits with earlier underlying flow, possibly not associated with spatter at all.

6. Kana-a Flow, San Francisco Volcanic Field, Arizona; 35.39 N., 248.57 E.

Site location: On both sides of leveed channel aa flow about 200 to 300 m down road to east of entrance of Painted Desert Vista picnic area.
Age control: Dendrochronologic control, Smiley (1958); Breternitz (1967) establishes general time frame , proximity to DuBois' VGP path provides exact date. Date assumes DuBois' VGP path is valid.
Geologic references: Moore and others (1976); field work during this study.

7. West Belknap Flow, McKenzie Pass, Mt. Belknap, Oregon; 44.32 N., 238.01 E.

Site location: At point where flow crosses Oregon Highway 126, in borrow pit probably from construction of the modern roadbed about 100 m east of the highway in four different sites.
Age control: ^{14}C dates (WSU-292, 270) on charred roots in tree molds about 1.75 km southeast of the sampling area reported by Chatters (1968). Date assumes flow unit sampled and tree mold unit are the same.
Geologic references: Taylor (1965, 1967, 1968).

8. South Belknap Cone Flow, McKenzie Pass, Mt. Belknap, Oregon; 44.24 N., 238.14 E.

Site location: On northern edge of Oregon Highway 242 at pull-off

about 400 m west of BM 5036.
Age control: ^{14}C date (Taylor, unpubl.) on charred roots in tree mold about 800 m west of sampling site on east edge of kipuka. Date assumes flow unit of tree mold and sampling site are the same.
Geologic references: Taylor (1965, 1967, 1968).

9. Cave Basalt Flow, Mt. Saint Helens, Washington; 46.11 N., 237.79 E.

Site location: On north side of road before road ascends hillslope which constrained lava flow about 500 m north of Ape Cave.
Age control: ^{14}C dates (W-2277, Gx-1673) on charred roots in tree molds near Ape Cave and Lake Cave. Because only the Ape Cave area was sampled, only that date was used. Date assumes dated flow unit was sampled for paleomagnetic measurement.
Geologic references: Greeley and Hyde (1972).

10. Rattlesnake Butte Flow, Craters of the Moon Lava Field, Idaho; 43.30 N., 246.68 E.

Site location: On east periphery of COM Field in very young appearing pahoehoe. Four sites, two 350 m southwest of hill 5123 at site of Bullard's tunnel and another two 200 m westsouthwest from there.
Age control: ^{14}C dates (Tx-899, Tx-900) on carbonized plant material in soil uncovered by digging under edge of flow, reported by Valastro and others (1972).
Geologic reference: Bullard and Rylander (1970); field work during this study.

11. Watchman Flow, Craters of the Moon Lava Field, Idaho; 43.39 N., 246.51 E.

Site location: In fresh pahoehoe flow units about 250 m northwest of base of the Watchman Cone, near group of tree molds.
Age control: ^{14}C date (Tx-1163) on charcoal from tree mold reported by Valastro and others (1972).
Geologic references: Bullard (1971), Stearns (1978), Murtaugh (1961); field work during this study.

12. Trenchmortar Flat Flow, Craters of the Moon Lava Field, Idaho; 43.41 N., 246.47 E.

Site location: In area of tree molds at southwest edge of Trenchmortar Flat along conspicuous crack in the flow.
Age control: From six ^{14}C dates (Tx-1157 through Tx-1162) ranging in age from 2130 to 2310 B.P. reported by Valastro and others (1972). Age quoted on Table 1 is mean of ages with largest standard deviation reported.

Geologic references: Bullard (1971, Stearns (1928), Murtaugh (1961) and geologic field work during this study.

13. Wapi Field, Snake River Plain, Idaho; 42.85 N., 246.83 E.

Site location: Four sites, two sites 300 m south of section corner 4521 and two sites on west side of Wapi Park where road makes closest approach to margin, 325 m north of elevation 5087.
Age control: ^{14}C date on charred sagebrush roots from under flow unit on east side of Wapi Park, Robinson (unpubl.). Date assumes flow unit dated as in same time episode as flow unit sampled.
Geologic references: Champion (1973), Champion and Greeley (1977).

14. Kings Bowl Field, Snake River Plain, Idaho; 42.96 N., 246.78 E.

Site location: Four sites, two sites located on southeast edge of Kings Bowl Crater about 25 m down walkway on east side which descends to the bottom of the crater, and two sites at point where Bear Trap Cave Road crosses the Great Rift, about 150 m southwest of BM 4927.
Age control: ^{14}C dates (Tx-1164, Tx-1165, Olsen, unpubl.) on charred sagebrush roots underneath bottom flow unit of Kings Bowl eruption reported by Valastro and others (1972). Date assumes eruptive event is very short lived. In calculating mean date Tx-1164 was left out due to extremely large standard deviation.
Geologic references: Prinz (1970), King (1977), Greeley and King (1975).

15. South Puyallup River Block and Bomb Flow, Mt. Rainier, Washington; 46.81 N., 238.10 E.

Site location: On the Round Pass Road 100 m after it crosses South Puyallup River headed north, on north side of the road. Samples from bombs exposed high in outcrop. Site may be subject to slumping to south and also relatively low-temperature TRM.
Age control: ^{14}C date (W-1587) on sample of charred log found within block and bomb deposit reported by Ives and others (1967). Date assumes deposit developed TRM magnetization after its emplacement as an ashflow.
Geologic reference: Crandell (1971).

16. Four in One Flow, McKenzie Pass, Oregon; 44.21 N., 238.19 E.

Site location: Adjacent to Scott Trail at southern end of line of vent structures about 200 m southwest of hill 6258 on east rim of small crater.

Age control: ^{14}C date (WSU-365) on charcoal found under ash blanket originating from Four in One Cone eruption reported by Chatters (1968). Date assumes charcoal was carbonized at time of Four in One eruption and not earlier. Large alpha 95 is due to inability to use rock drill in wilderness areas. Block samples were taken with much less precision. Date assumes flow unit dated is in same time episode as flow unit sampled.
Geologic references: Taylor (1965, 1967, 1968).

17. Yapoah Flow, McKenzie Pass, Oregon; 44.26 N., 238.20 E.

Site location: Along Oregon Highway 242 in four sites, two in road cut about 300 m east of Dee Wright Observatory, and two in north-south crack in flow erroneously marked as lava channel about 100 m east of Observatory along nature trail.
Age control: None specific to this flow but flows above and below are ^{14}C dated and constrain age of this flow between that of Four in One Flow and Little Belknap Flow.
Geologic references: Taylor (1965, 1967, 1968).

18. Little Belknap Flow, McKenzie Pass, Mt. Belknap, Oregon; 44.26 N., 238.18 E.

Site location: Along Oregon Highway 242 in four sites, two about 100 m west of BM 5260 and two more about 100 m farther west.
Age control: ^{14}C date (WSU-364) on charred roots found in tree mold along Skyline Trail reported by Chatters (1968). Date assumes flow unit which is dated is same age as flow unit sampled.
Geologic references: Taylor (1965, 1967, 1968).

19. Clear Lake Flow, Sand Mountain, Oregon; 44.36 N., 238.01 E.

Site location: Four sites along Oregon Highway 126, two sites on east side of road at bridge crossing McKenzie River at south end of Clear Lake and two sites about 1 km south of bridge in large roadcut through flow.
Age control: ^{14}C dates (all unpubl.) on charred log found under flows on east side of Clear Lake and on drowned snags found in Clear Lake killed at time lake was formed by flow. Date assumes Clear Lake eruption was quick episode and all flow units record same direction.
Geologic references: Taylor (1965, 1967, 1968), Benson (1965), Nieland (1967).

20. Blue Lake Crater, Santiam Pass, Oregon; 44.41 N., 238.23 E.

Site location: Three sites on rim of crater at south end of the lake adjacent to horse trail at edge of welded spatter cliffs.

Age control: ^{14}C date (WSU-291) on charcoal found under thick ash and cinder blanket downwind from crater reported by Chatters (1968).
Geologic references: Taylor (1965, 1967, 1968).

21. Hackleman Creek Flow, Sand Mountain, Oregon; 44.40 N., 238.00 E.

Site location: On east shore of Fish Lake, where pahoehoe flow outcrops from under later aa flows, about 100 m southwest of picnic area. If lake is reasonably full site will be under water.
Age control: ^{14}C date (WSU-372) on charred roots in tree mold next to old Santiam Wagon Road. Date assumes flow unit dated and flow unit sampled are the same.
Geologic references: Taylor (1965, 1967, 1968).

22. Hell's Half Acre Field, Snake River Plain, Idaho; 43.40 N., 247.55 E.

Site location: Four sites, two sites on west side of Lemhi Pass Road about 2 km north of U.S. 26 and two sites in northern edge of field about 1300 m southwest of Twentymile Rock, on high pressure plateau at edge of small wheat field.
Age control: ^{14}C date (W-3662) on organic-rich sediment in aeolian deposit under edge of lava flow. Application of date to age of lava flow assumes living material carbonized at time of eruption of flow. If assumption is incorrect, then true age could be older or younger by different models. Date assumes flow unit dated and flow units sampled are the same age.
Geologic references: Karlo (1977), Kuntz (1977).

23. Dotsero Flow, Dotsero, Colorado; 39.64 N., 252.95 E.

Site location: On north bank of Eagle River in massive outcrop farthest west in flow along bulldozed road about 1 km southeast of town of Dotsero.
Age control: ^{14}C date (W-1129) on small pinon or juniper tree charred by ash erupted from East Rim Blowout, reported by Ives and others (1964). Date assumes ash and flow sampled belong to same episode of eruption.
Geologic references: Giegengack (1962), Landon (1933).

24. Lava Cascade Flow, Northwest Rift, Newberry Crater, Oregon; 43.79 N., 238.71 E.

Site location: At end of forest road 2045 where it approaches south edge of flow, about 1100 m northwest of hill 6637.
Age control: ^{14}C date, Gakushuin (unpubl.), on charcoal from bottom of tree mold. Date assumes flow unit dated and flow units sampled are the same age.

Geologic references: Peterson and Groh (1965, 1969); field work during this study.

25. Sugar Pine Butte Flow, Northwest Rift, Newberry Crater, Oregon; 43.83 N., 238.64 E.

Site location: Along forest road 10006 as it approaches south margin of small aa flow about 700 m north-northeast of hill 5094. Site is in area of tree molds on north side of flow.
Age control: ^{14}C date (USGS-106, Robinson (unpubl.)) on charred root material found in bottom of 3-ft diameter tree mold.
Geologic references: Field work performed during this study.

26. Forest Road Flow, Northwest Rift, Newberry Crater, Oregon; 43.82 N., 238.71 E.

Site location: Four sites on north side of forest road 195 to Lava Cast Forest, two sites at point of closest approach to road and two sites 300 m east-northeast in vicinity of vent structure along rift itself.
Age control: ^{14}C date, Gakushuin (unpubl.), on charcoal from bottom of tree mold. Date assumes flow unit dated and flow units sampled are the same age.
Geologic references: Peterson and Groh (1965, 1969); and field work performed during the course of this study.

27. Surveyor Flow, Newberry Crater, Oregon; 43.64 N., 238.75 E.

Site location: West of forest road 2262 along north margin of the flow about 400 m southwest of Surveyor Cave in area of tree molds.
Age control: ^{14}C date, Gakushuin (unpubl.), on charcoal from bottom of tree mold. Date assumes flow unit dated and flow units sampled are the same age.
Geologic references: Peterson and Groh (1965, 1969); and field work performed during the course of this study.

28. North Summit Flow, Northwest Rift, Newberry Crater, Oregon; 43.75 N., 238.76 E.

Site location: At two separate localities in vent area to south and long east side of flow margin about 1 km northeast of North Paulina Peak.
Age control: ^{14}C date (USGS-105, Robinson (unpubl.)) on charred roots found in bottom of tree mold. Date assumes flow unit dated and flow units sampled are the same age.
Geologic references: Peterson and Groh (1965, 1969); and field work performed during this study.

29. Gasline Flow, Northwest Rift, Newberry Crater, Oregon; 43.91 N., 238.65 E.

Site location: Along gas pipeline maintenance road where it crosses south Gasline Flow in spatter rampart structure south of the road, about 100 m from the road.
Age control: ^{14}C date (USGS-80) on charred roots found in bottom of tree mold, reported by Robinson (1977). Date assumes Gasline Flow is one short episode in time. Earlier age report by Peterson and Groh (1965) is incorrect.
Geologic references: Peterson and Groh (1965, 1969); and field work performed during this study.

30. Lava Butte Flow, Northwest Rift, Newberry Crater, Oregon; 43.92 N., 238.62 E.

Site location: Four sites, two in large levee complex south of the cone about 400 m northwest of Lava Butte Visitor Center and two in large railroad cut where it emerges from the flow about 500 m southeast of Benham Falls campground.
Age control: ^{14}C date (USGS-107, Robinson (unpubl.)) on charred material found beneath thick layer of cinders from the formation of Lava Butte itself. Date assumes formation of flows and Cone occurred in one short event.
Geologic references: Peterson and Groh (1965, 1969), Chitwood and others (1977); and field work during this study.

31. Lava Cast Forest Flow, Northwest Rift, Newberry Crater, Oregon; 43.82 N., 238.71 E.

Site location: Four sites all in area immediately west of nature walk in tree molds or flat areas of flow, about 200 m southwest of campground.
Age control: ^{14}C dates (GaK-845, I-1505) on charred roots found in the bottom of tree molds reported by Buckley and others (1968). Dates assume flow unit sampled and flow unit dated are the same.
Geologic references: Peterson and Groh (1965, 1969).

32. Crater Lake Ash Flow Deposit, Crater Lake, Oregon; 42.88 N., 237.91 E.

Site location: Two sites at widely separated locations. One in Sand Creek valley, along Pinnacles Road about 550 m north of Lost Creek Campground, and another in Munson Creek valley along Duwee Falls nature trail about 100 m southeast of trailhead.
Age control: ^{14}C dates (C-247, W-858) on charred wood found in the Mazama ash deposit and on other assorted organic materials found in close proximity to Crater Lake pumice. Some time

control has been ignored as irrelevant. Entire eruption represents one geologically short event, Mehringer and others (1977).
Geologic references: Howell (1942), Kittleman (1973).

33. Parkdale Flow, Mt. Hood, Oregon; 45.49 N., 238.37 E.

Site location: Four sites, two in vent area of flow on east rim of crater about 150 m east-southeast of hill 2825, and two on east bank of Middle Fork Hood River where road makes closest approach to stream bed and margin of flow.
Age control: ^{14}C date (unpubl.) on charred material found under flow in drainage of the Middle Fork Hood River reported by Harris (1973). Date assumes that flow unit dated and flow unit sampled are the same.
Geologic references: Harris (1973); field work during this study.

34. Cerro Grande Lava Field, Snake River Plain, Idaho; 43.35 N., 247.20 E.

Site location: Four sites, two located on road from Atomic City to Big Southern Butte where road crosses Cerro Grande Field, about 200 m from west edge of the field, and two in Taber area 1 km west-northwest of section corner 4656.
Age control: ^{14}C date (W-3673) on charred organic-rich soil dug from under edge of lava flow. Date assumes entire field is one age. Date assumes living material was carbonized at time of eruption of the basalt.
Geologic references: Kuntz (1977); field work during this study.

35. Northeast Sunset Flow, Craters of the Moon Lava Field, Idaho; 43.53 N., 246.50 E.

Site location: Four sites, two along Highways 20 and 26, 1 to 1.5 km northeast from monument boundary, and two 4 km northeast from there opposite corner 5415 about 100 m.
Age control: ^{14}C date (W-3674) on organic soil containing visible charcoal dug from under edge of lava flow. Date assumes living material carbonized at time of eruption of lava flow and that unit sampled was unit dated.
Geologic references: Lefebvre (1976), Kuntz (1977); field work during this study.

36. North Robbers Flow, Snake River Plain, Idaho; 43.38 N., 247.02 E.

Site location: Four sites, two 100 m east of BM 5155 and two others on west side of leveed flow 200 m north of vent structure labelled 5259.
Age control: ^{14}C date (W-3672) on charred organic soil layer under edge of lava flow. Date assumes living material was

carbonized at time of eruption of basalt, and that unit is one single time event.

Geologic references: Kuntz (1977); field work performed during this study.

Appendix 2

Strong Field Magnetization Records

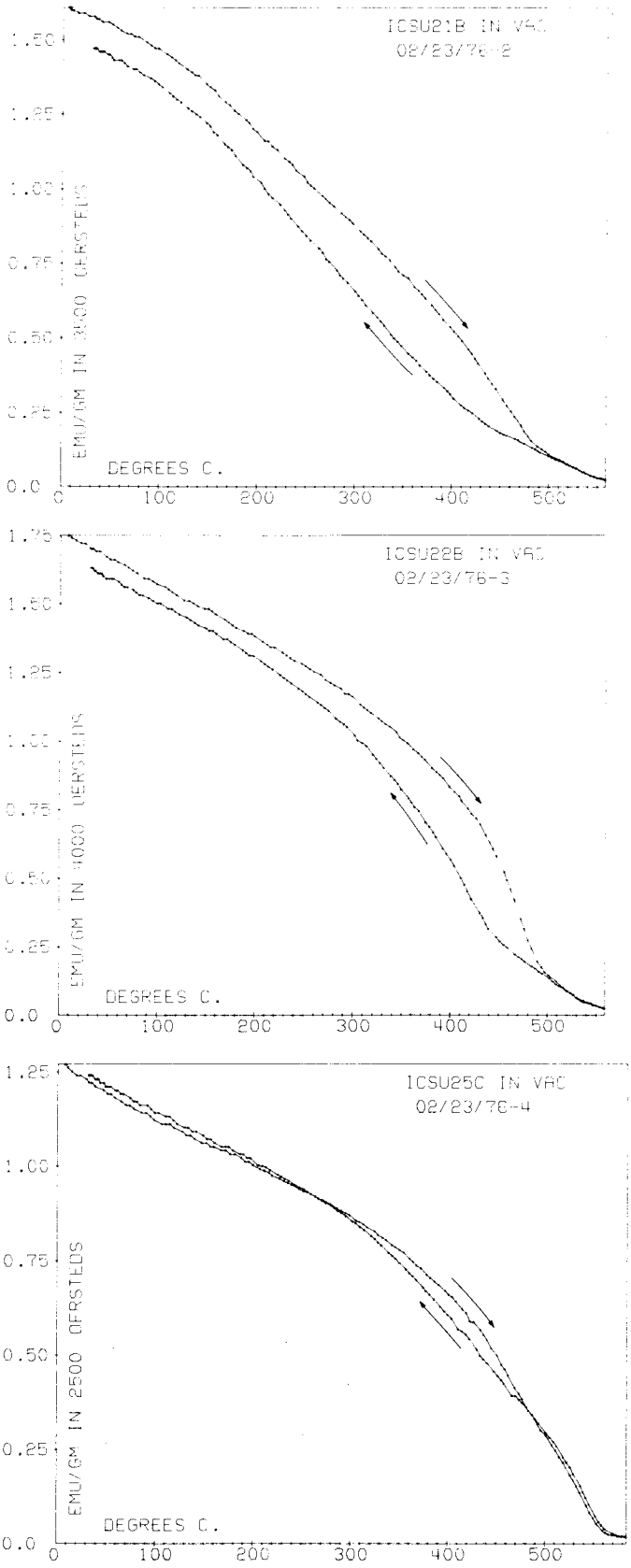
ICSU21B IN VAC
02/23/76-2
EMU/GM IN 3400 OERSTEDS
DEGREES C.
0.0
0.25
0.50
0.75
1.00
1.25
1.50
0
100
200
300
400
500
ICSU22B IN VAC
02/23/76-3
EMU/GM IN 4000 OERSTEDS
DEGREES C.
ICSU25C IN VAC
02/23/76-4
EMU/GM IN 2500 OERSTEDS
DEGREES C.

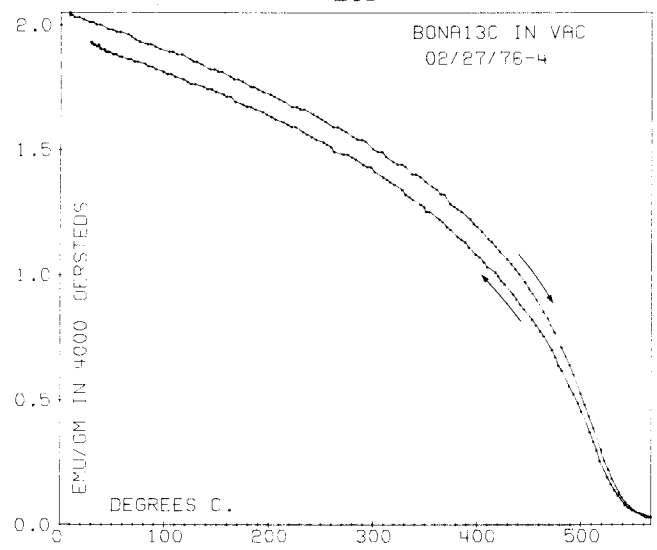
BONA13C IN VAC
02/27/76-4
EMU/GM IN 4000 OERSTEDS
DEGREES C.
2.0
1.5
1.0
0.5
0.0
0
100
200
300
400
500

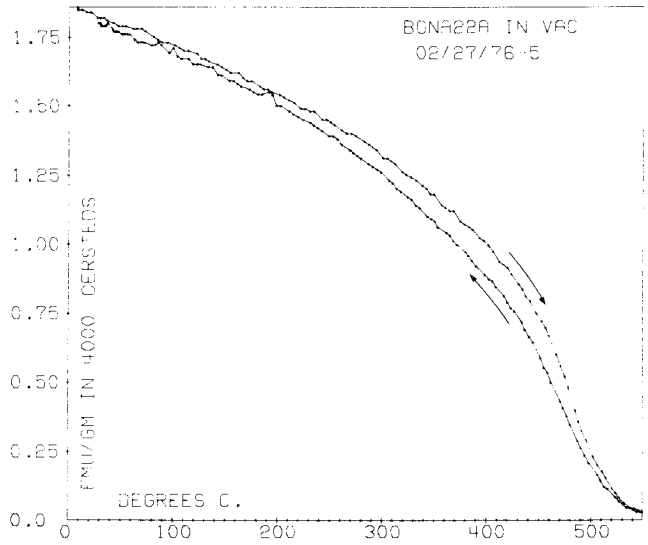
BONA22A IN VAC
02/27/76-5
EMU/GM IN 4000 OERSTEDS
DEGREES C.
1.75
1.50
1.25
1.00
0.75
0.50
0.25
0.0
0
100
200
300
400
500

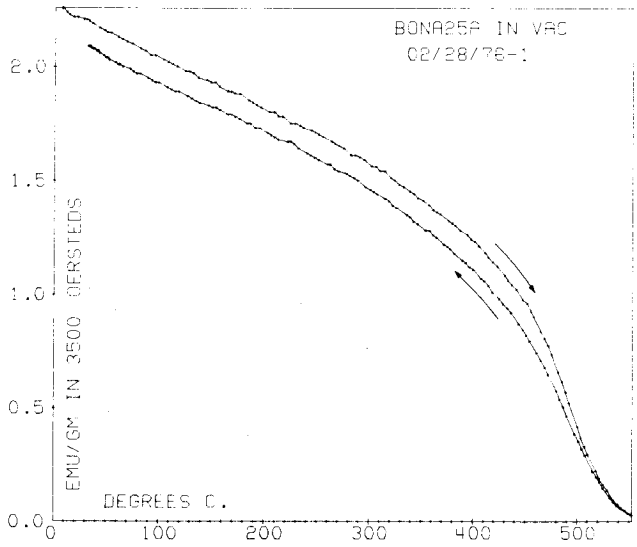
BONA25A IN VAC
02/28/76-1
EMU/GM IN 3500 OERSTEDS
DEGREES C.
2.0
1.5
1.0
0.5
0.0
0
100
200
300
400
500

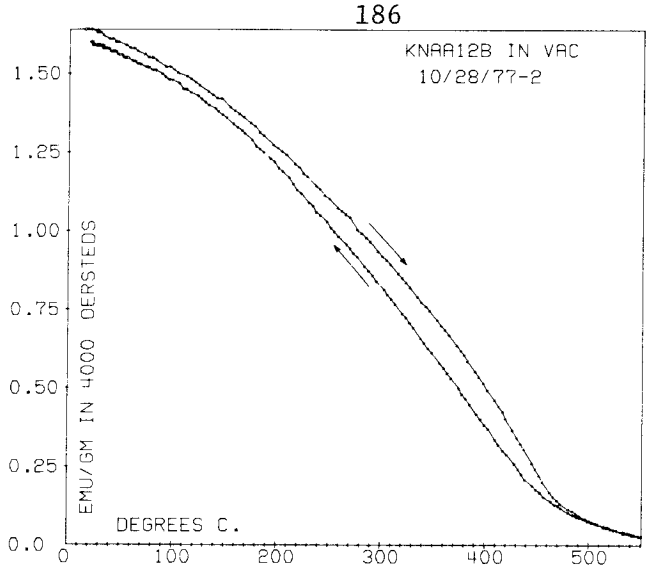
KNAA12B IN VAC
10/28/77-2
EMU/GM IN 4000 OERSTEDS
DEGREES C.
1.50
1.25
1.00
0.75
0.50
0.25
0.0
0
100
200
300
400
500

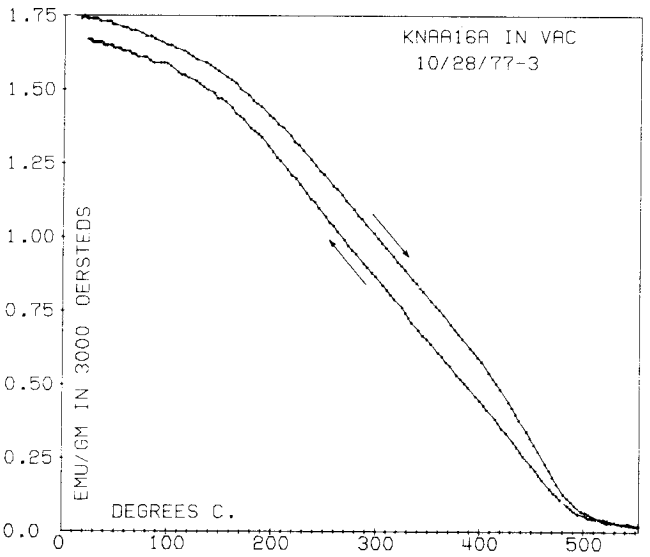
KNAA16A IN VAC
10/28/77-3
EMU/GM IN 3000 OERSTEDS
DEGREES C.
1.75
1.50
1.25
1.00
0.75
0.50
0.25
0.0
0
100
200
300
400
500

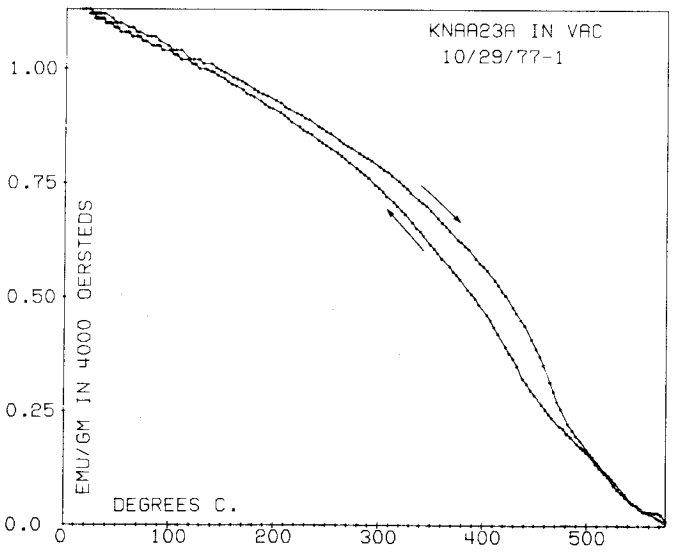
KNAA23A IN VAC
10/29/77-1
EMU/GM IN 4000 OERSTEDS
DEGREES C.
1.00
0.75
0.50
0.25
0.0
0
100
200
300
400
500

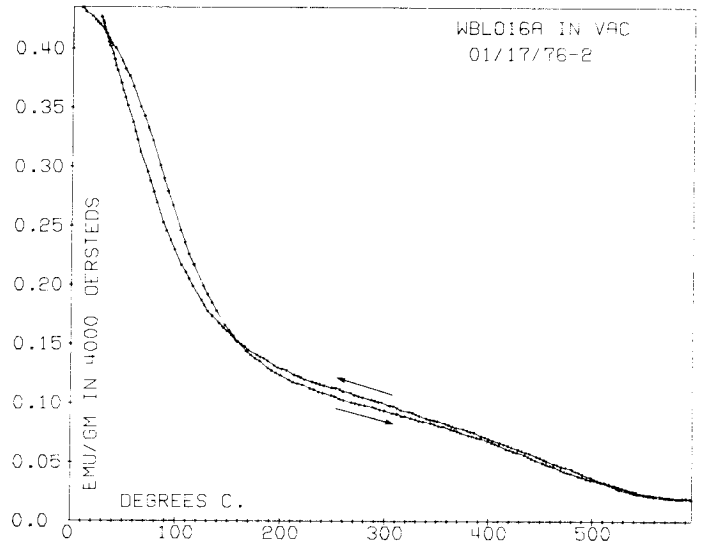
WBL016A IN VAC
01/17/76-2
EMU/GM IN 4000 OERSTEDS
DEGREES C.
0.0
0.05
0.10
0.15
0.20
0.25
0.30
0.35
0.40
0
100
200
300
400
500

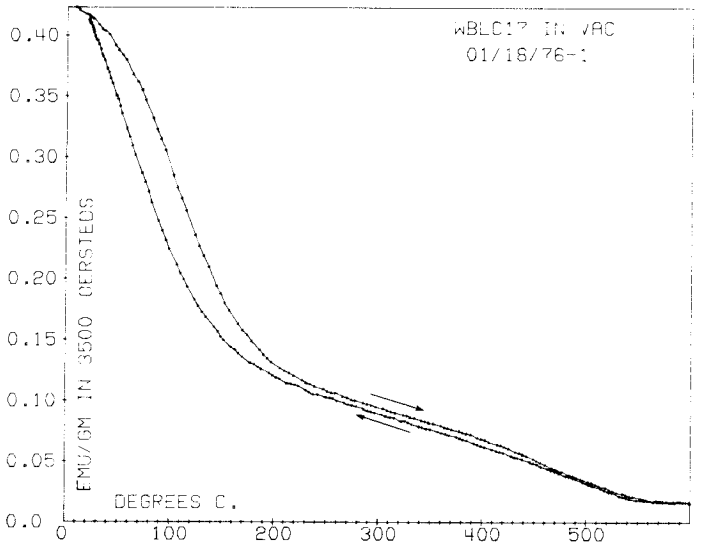
WBL017 IN VAC
01/18/76-1
EMU/GM IN 3500 OERSTEDS
DEGREES C.
0.0
0.05
0.10
0.15
0.20
0.25
0.30
0.35
0.40
0
100
200
300
400
500

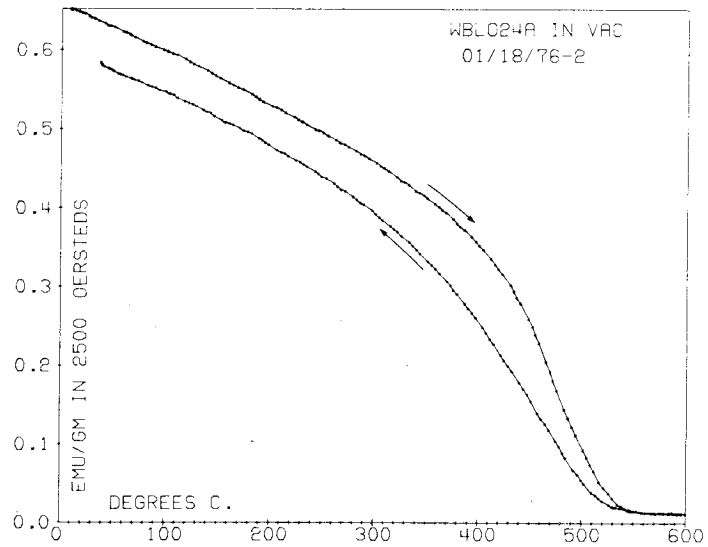
WBL024A IN VAC
01/18/76-2
EMU/GM IN 2500 OERSTEDS
DEGREES C.
0.0
0.1
0.2
0.3
0.4
0.5
0.6
0
100
200
300
400
500
600

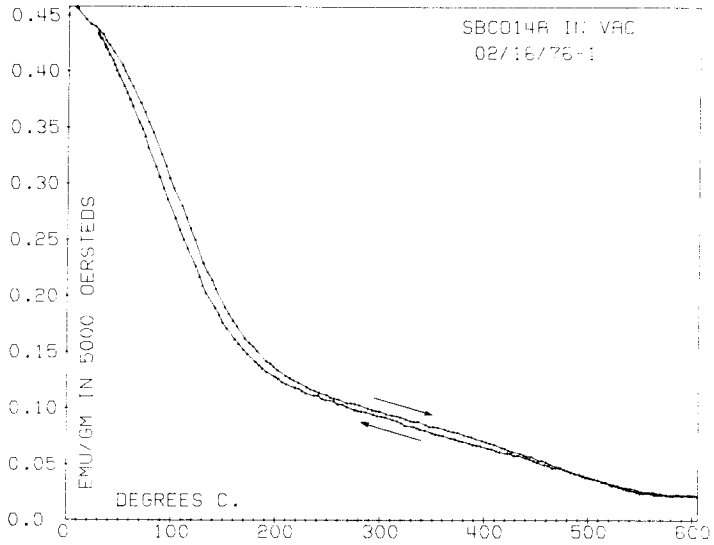
SBC014A IN VAC
02/16/76-1
EMU/GM IN 5000 OERSTEDS
DEGREES C.
0.45
0.40
0.35
0.30
0.25
0.20
0.15
0.10
0.05
0.0
0
100
200
300
400
500
600

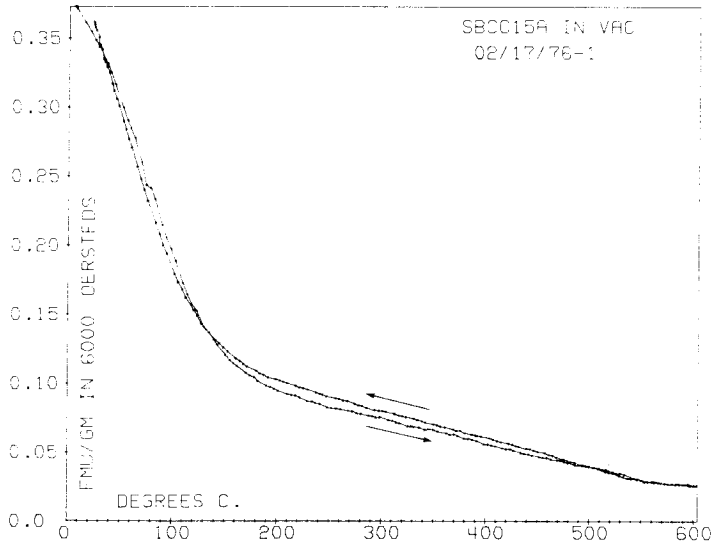
SBC015A IN VAC
02/17/76-1
EMU/GM IN 6000 OERSTEDS
DEGREES C.
0.35
0.30
0.25
0.20
0.15
0.10
0.05
0.0
0
100
200
300
400
500
600

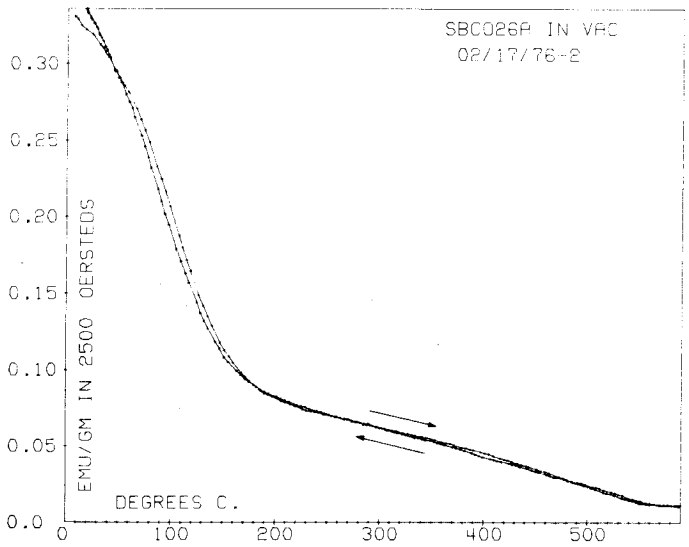
SBC026A IN VAC
02/17/76-2
EMU/GM IN 2500 OERSTEDS
DEGREES C.
0.30
0.25
0.20
0.15
0.10
0.05
0.0
0
100
200
300
400
500

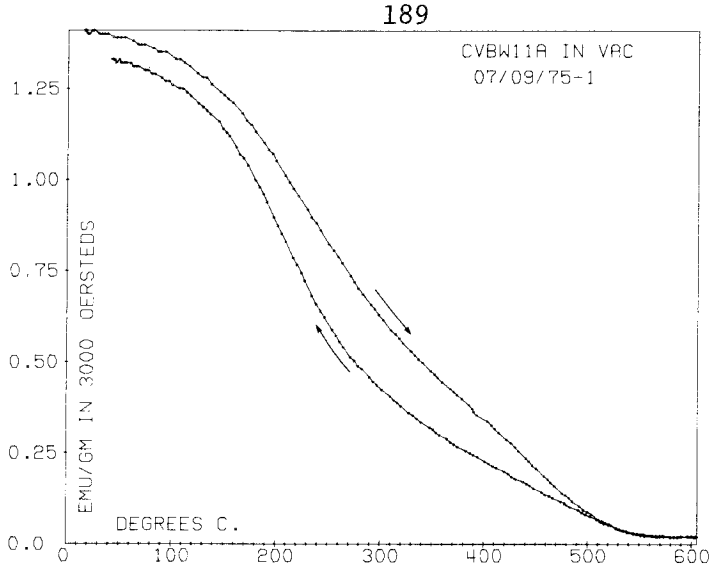
CVBW11A IN VAC
07/09/75-1
EMU/GM IN 3000 OERSTEDS
DEGREES C.
1.25
1.00
0.75
0.50
0.25
0.0
0
100
200
300
400
500
600

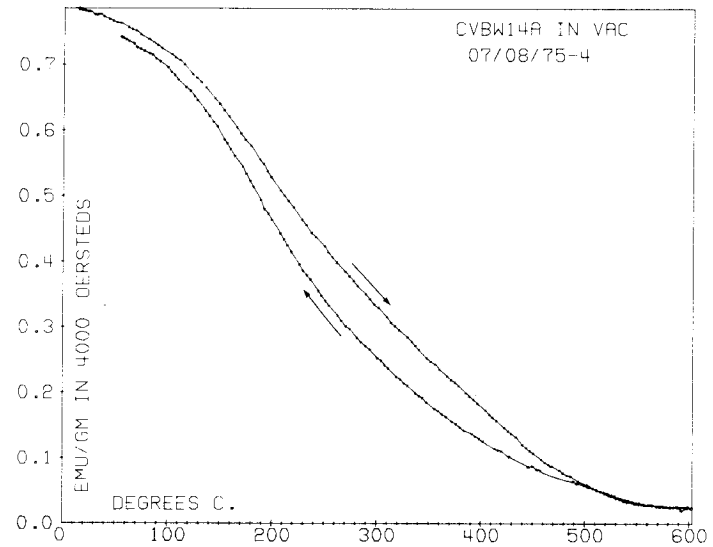
CVBW14A IN VAC
07/08/75-4
EMU/GM IN 4000 OERSTEDS
DEGREES C.
0.7
0.6
0.5
0.4
0.3
0.2
0.1
0.0
0
100
200
300
400
500
600

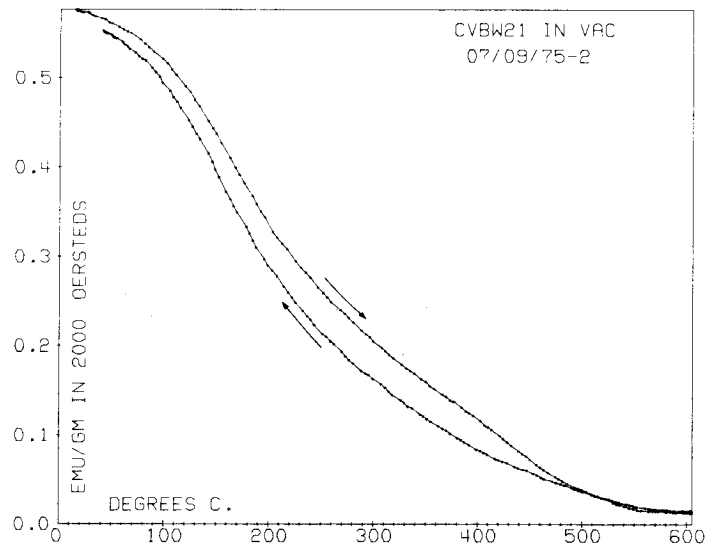
CVBW21 IN VAC
07/09/75-2
EMU/GM IN 2000 OERSTEDS
DEGREES C.
0.5
0.4
0.3
0.2
0.1
0.0
0
100
200
300
400
500
600

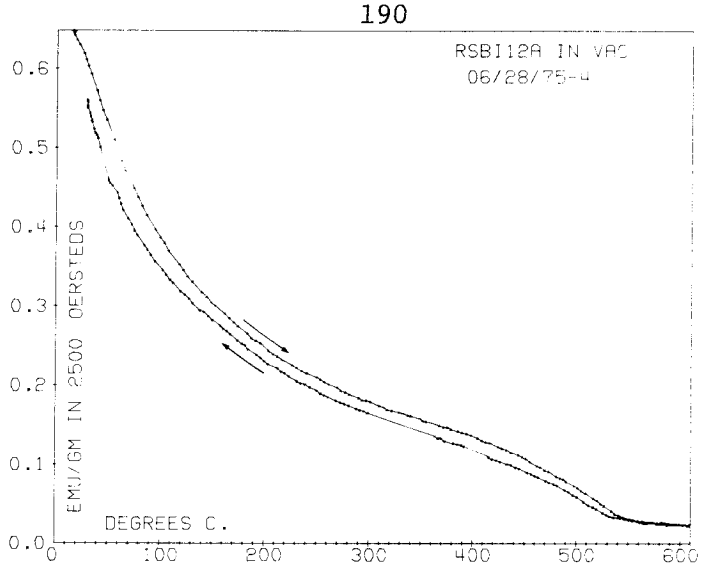
RSBI12A IN VAC
06/28/75-4
EMU/GM IN 2500 OERSTEDS
DEGREES C.
0.0
0.1
0.2
0.3
0.4
0.5
0.6
0
100
200
300
400
500
600

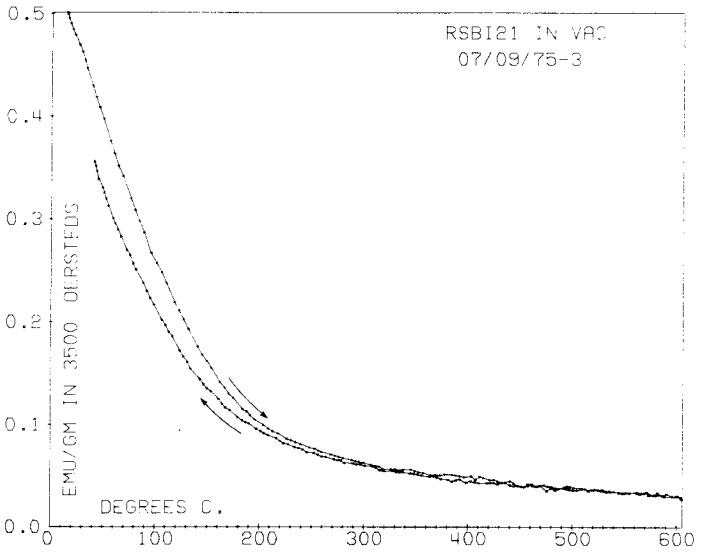
RSBI21 IN VAC
07/09/75-3
EMU/GM IN 3500 OERSTEDS
DEGREES C.
0.0
0.1
0.2
0.3
0.4
0.5
0
100
200
300
400
500
600

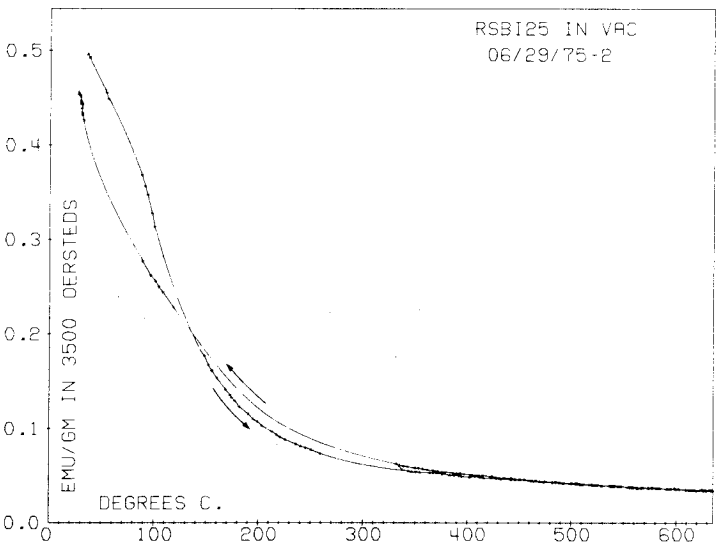
RSBI25 IN VAC
06/29/75-2
EMU/GM IN 3500 OERSTEDS
DEGREES C.
0.0
0.1
0.2
0.3
0.4
0.5
0
100
200
300
400
500
600

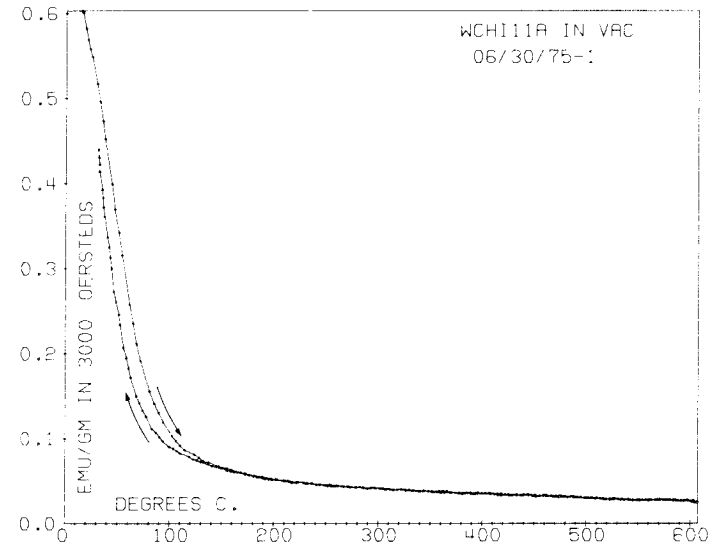
WCHI11A IN VAC
06/30/75-1
EMU/GM IN 3000 OERSTEDS
DEGREES C.
0.6
0.5
0.4
0.3
0.2
0.1
0.0
0
100
200
300
400
500
600

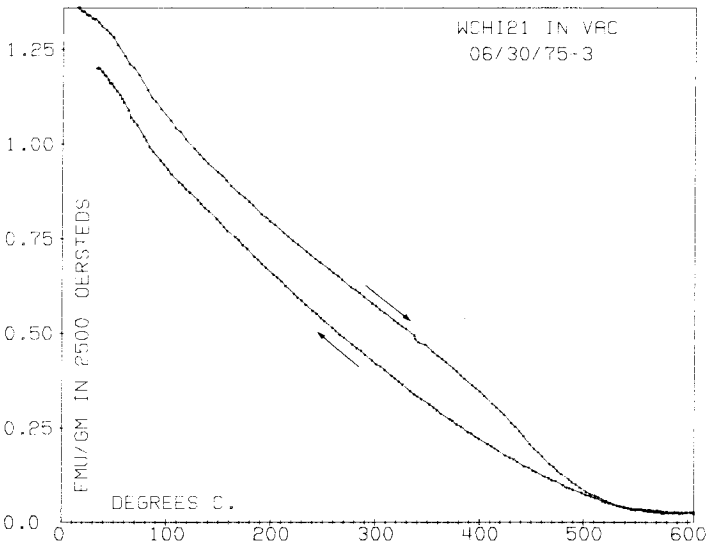
WCHI21 IN VAC
06/30/75-3
EMU/GM IN 2500 OERSTEDS
DEGREES C.
1.25
1.00
0.75
0.50
0.25
0.0
0
100
200
300
400
500
600

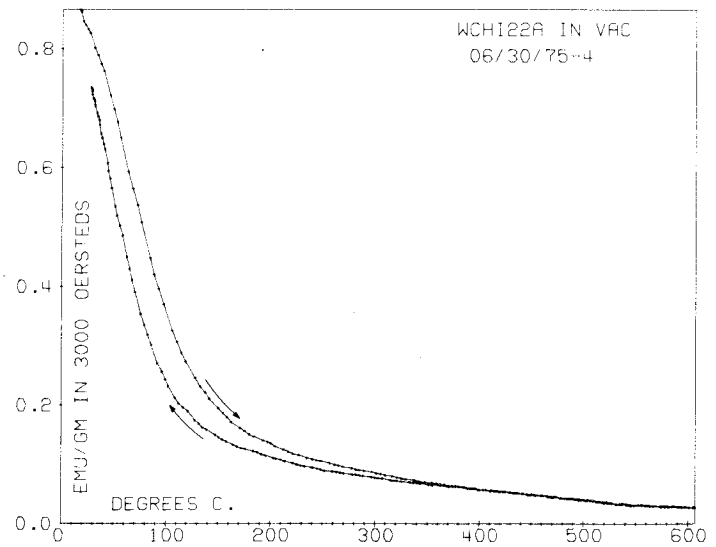
WCHI22A IN VAC
06/30/75-4
EMU/GM IN 3000 OERSTEDS
DEGREES C.
0.8
0.6
0.4
0.2
0.0
0
100
200
300
400
500
600

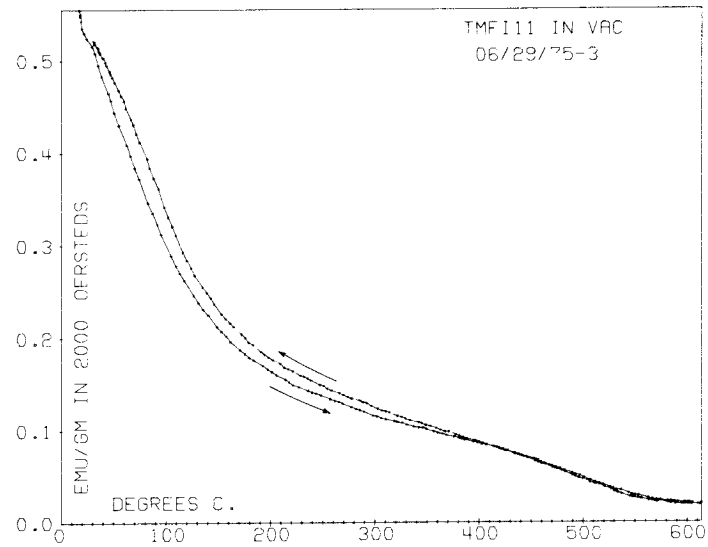
TMFI11 IN VAC
06/29/75-3
EMU/GM IN 2000 OERSTEDS
DEGREES C.
0.0
0.1
0.2
0.3
0.4
0.5
0
100
200
300
400
500
600

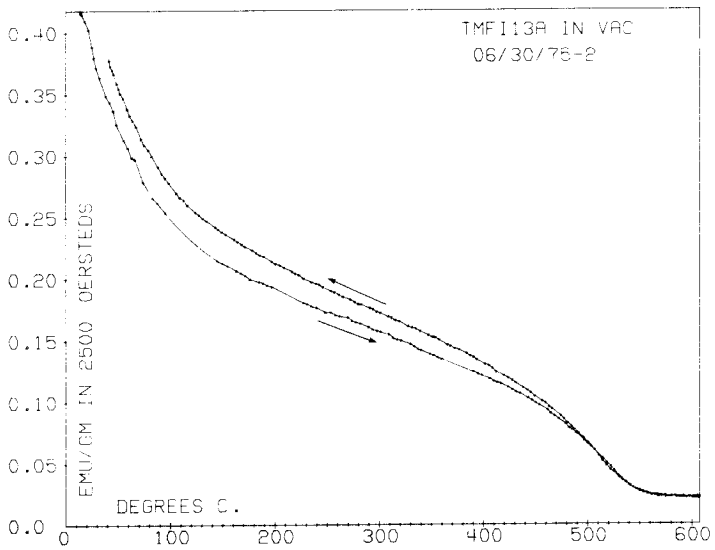
TMFI13A IN VAC
06/30/75-2
EMU/GM IN 2500 OERSTEDS
DEGREES C.
0.0
0.05
0.10
0.15
0.20
0.25
0.30
0.35
0.40
0
100
200
300
400
500
600

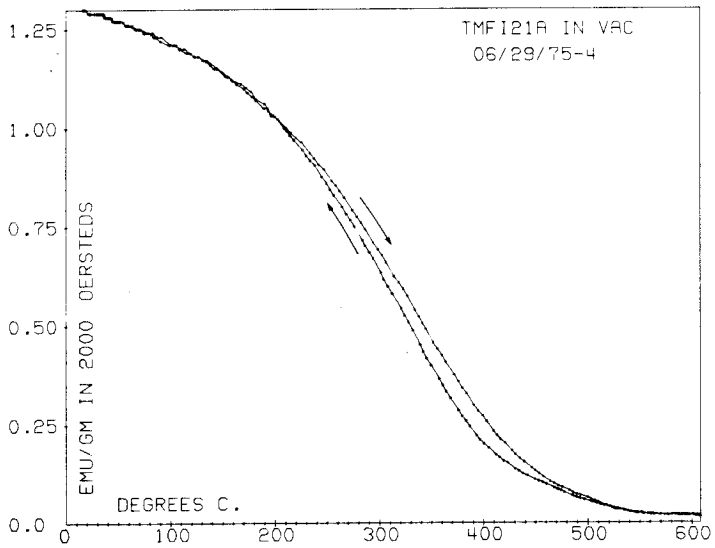
TMFI21A IN VAC
06/29/75-4
EMU/GM IN 2000 OERSTEDS
DEGREES C.
0.0
0.25
0.50
0.75
1.00
1.25
0
100
200
300
400
500
600

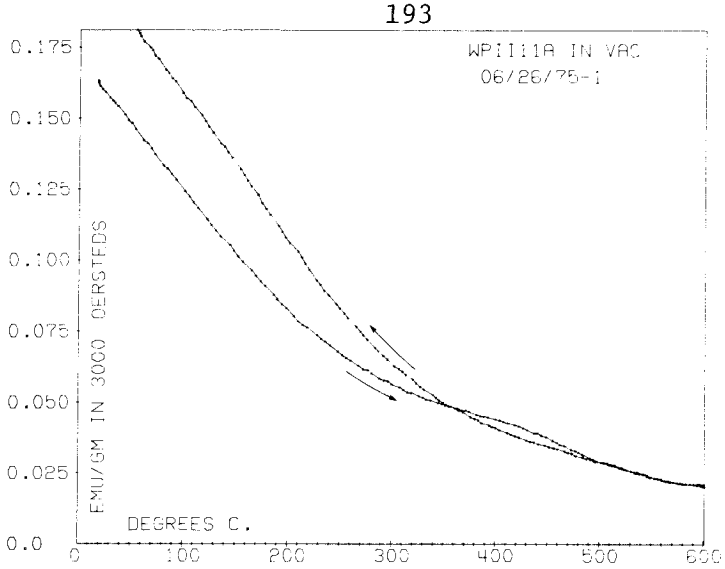
WPIII1A IN VAC
06/26/75-1
EMU/GM IN 3000 OERSTEDS
DEGREES C.
0.175
0.150
0.125
0.100
0.075
0.050
0.025
0.0
0
100
200
300
400
500
600

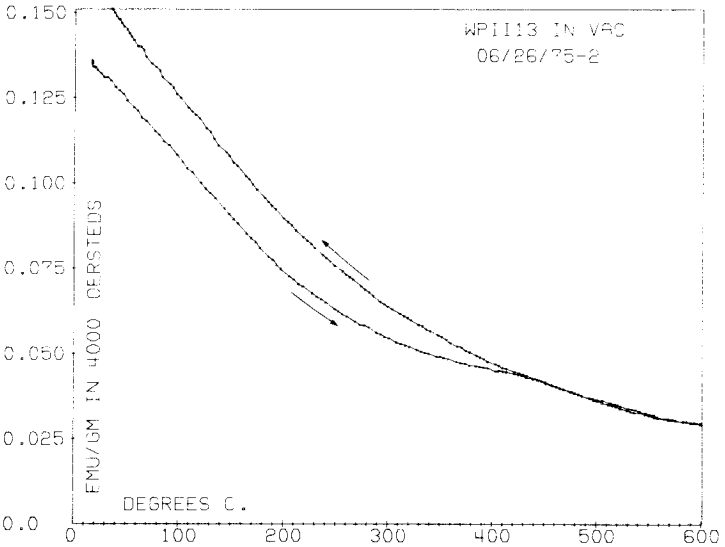
WPII13 IN VAC
06/26/75-2
EMU/GM IN 4000 OERSTEDS
DEGREES C.
0.150
0.125
0.100
0.075
0.050
0.025
0.0
0
100
200
300
400
500
600

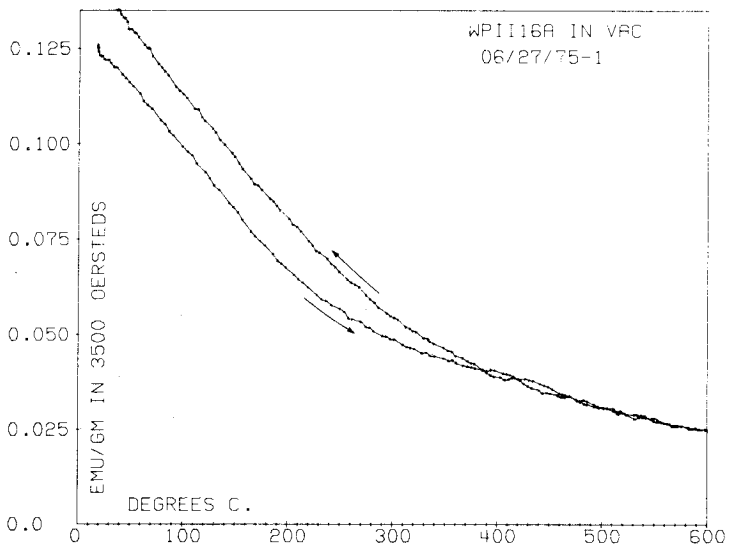
WPII16A IN VAC
06/27/75-1
EMU/GM IN 3500 OERSTEDS
DEGREES C.
0.125
0.100
0.075
0.050
0.025
0.0
0
100
200
300
400
500
600

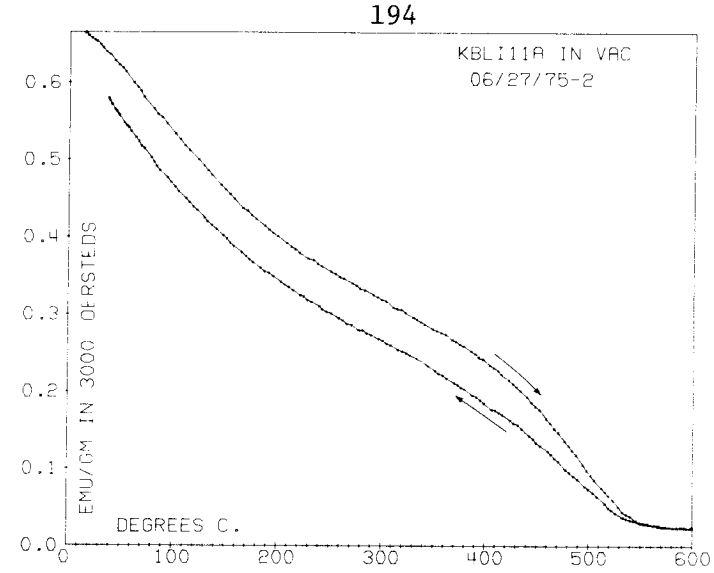
KBLI11A IN VAC
06/27/75-2
EMU/GM IN 3000 OERSTEDS
DEGREES C.
0.0
0.1
0.2
0.3
0.4
0.5
0.6
0
100
200
300
400
500
600

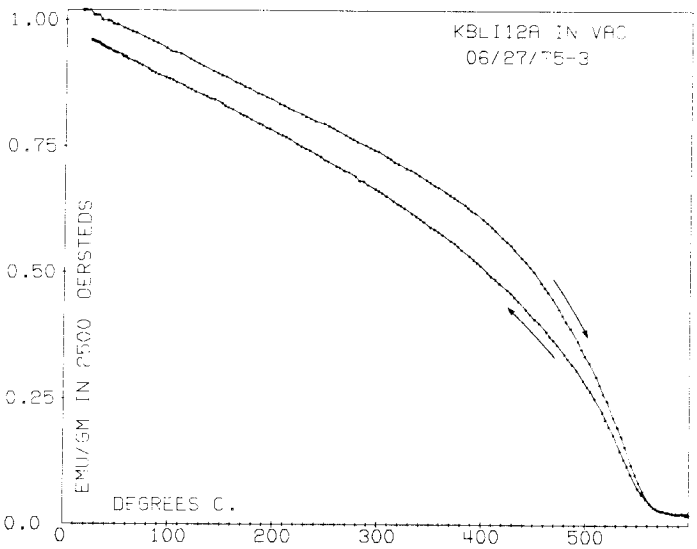
KBLI12A IN VAC
06/27/75-3
EMU/GM IN 2500 OERSTEDS
DEGREES C.
0.0
0.25
0.50
0.75
1.00
0
100
200
300
400
500

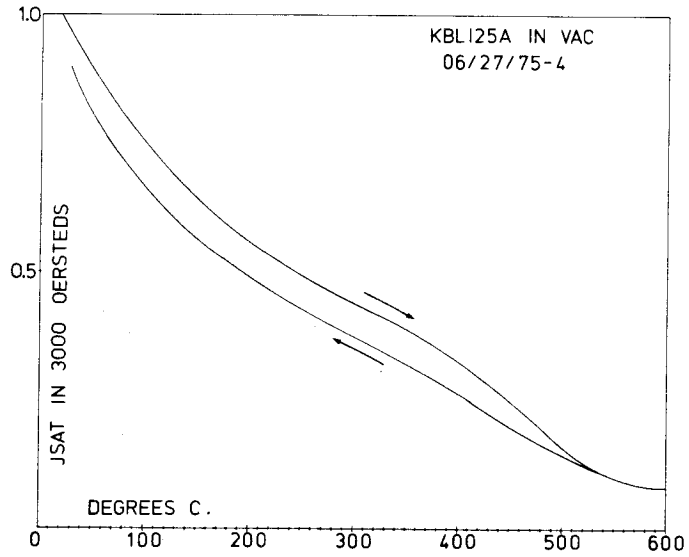
KBLI25A IN VAC
06/27/75-4
JSAT IN 3000 OERSTEDS
DEGREES C.
0.5
1.0
0
100
200
300
400
500
600

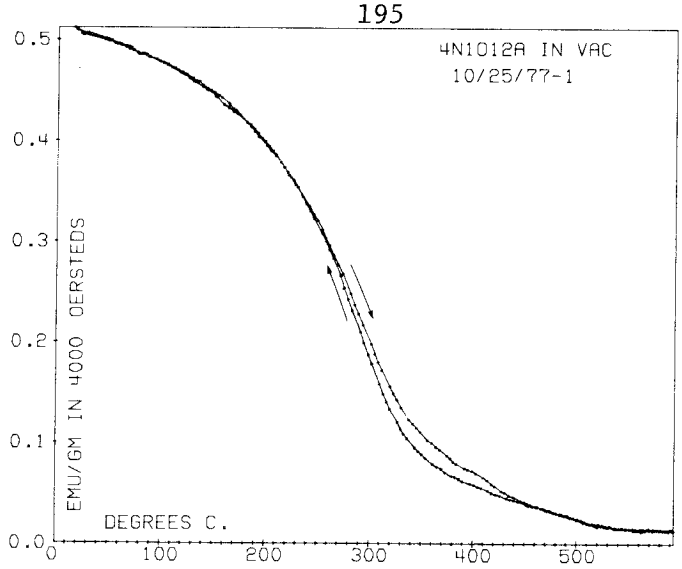
4N1012A IN VAC
10/25/77-1
EMU/GM IN 4000 OERSTEDS
DEGREES C.
0.0
0.1
0.2
0.3
0.4
0.5
0
100
200
300
400
500

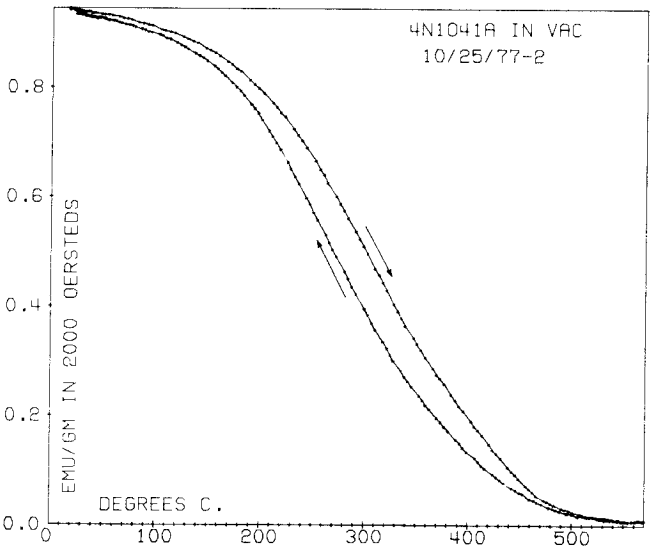
4N1041A IN VAC
10/25/77-2
EMU/GM IN 2000 OERSTEDS
DEGREES C.
0.0
0.2
0.4
0.6
0.8
0
100
200
300
400
500

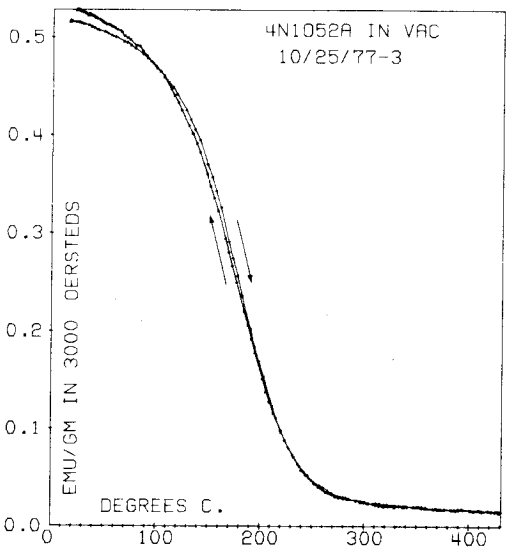
4N1052A IN VAC
10/25/77-3
EMU/GM IN 3000 OERSTEDS
DEGREES C.
0.0
0.1
0.2
0.3
0.4
0.5
0
100
200
300
400

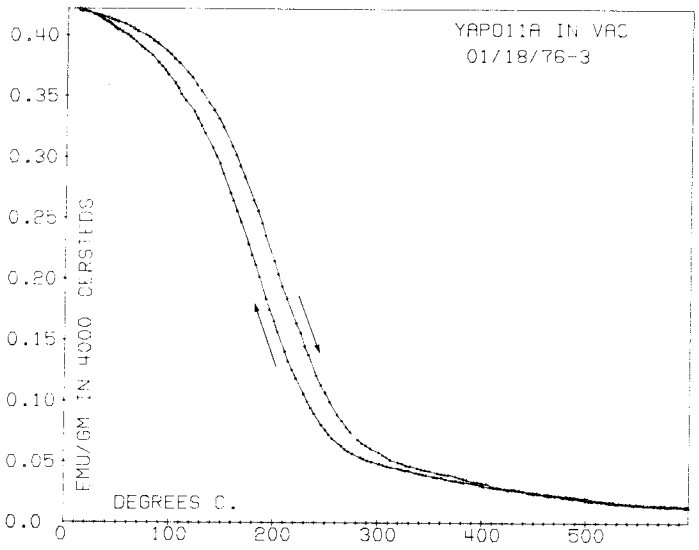
YAP011A IN VAC
01/18/76-3
EMU/GM IN 4000 OERSTEDS
DEGREES C.
0.40
0.35
0.30
0.25
0.20
0.15
0.10
0.05
0.0
0
100
200
300
400
500

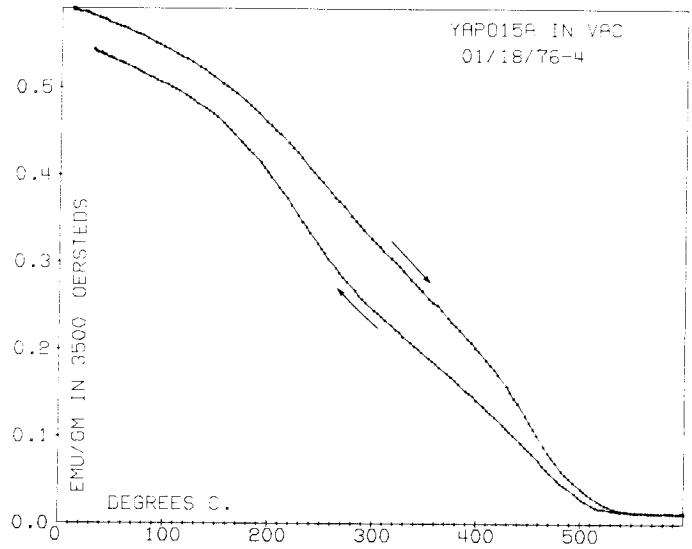
YAP015A IN VAC
01/18/76-4
EMU/GM IN 3500 OERSTEDS
DEGREES C.
0.5
0.4
0.3
0.2
0.1
0.0
0
100
200
300
400
500

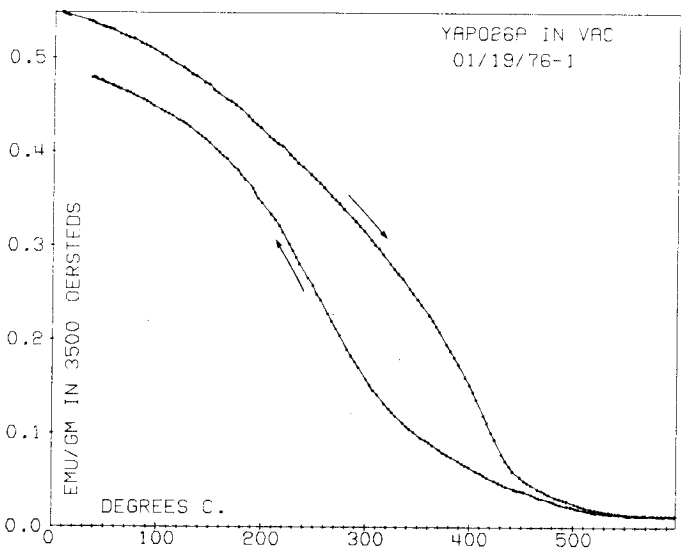
YAP026A IN VAC
01/19/76-1
EMU/GM IN 3500 OERSTEDS
DEGREES C.
0.5
0.4
0.3
0.2
0.1
0.0
0
100
200
300
400
500

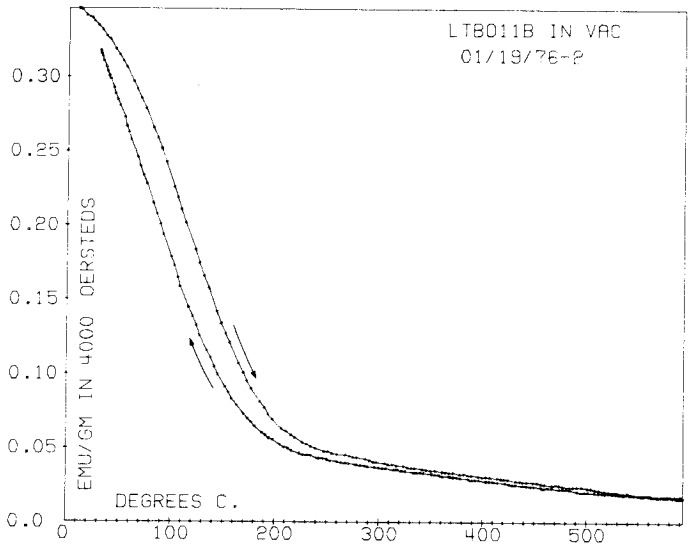
LTB011B IN VAC
01/19/76-2
EMU/GM IN 4000 OERSTEDS
DEGREES C.
0.0
0.05
0.10
0.15
0.20
0.25
0.30
0
100
200
300
400
500

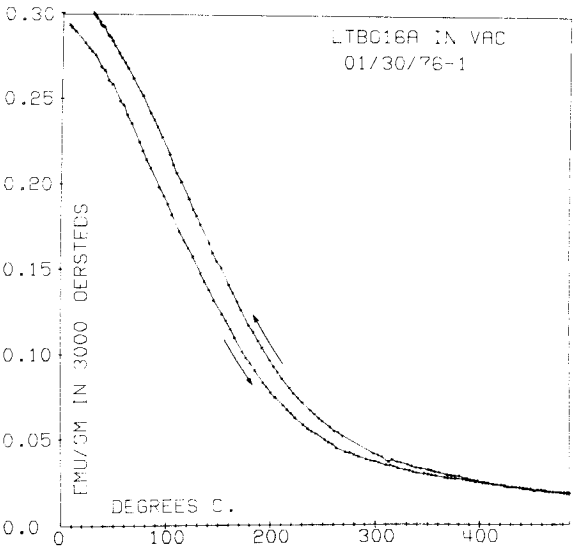
LTB016A IN VAC
01/30/76-1
EMU/GM IN 3000 OERSTEDS
DEGREES C.
0.0
0.05
0.10
0.15
0.20
0.25
0.30
0
100
200
300
400

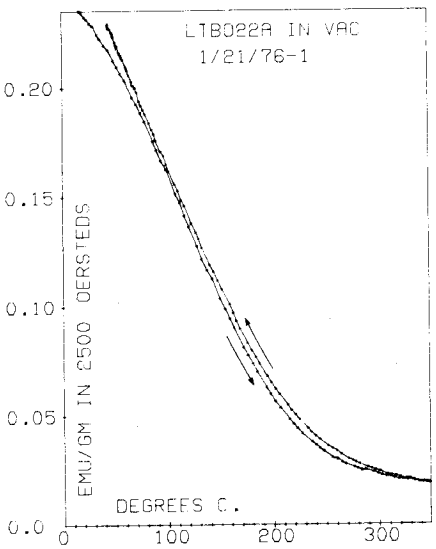
LTB022A IN VAC
1/21/76-1
EMU/GM IN 2500 OERSTEDS
DEGREES C.
0.0
0.05
0.10
0.15
0.20
0
100
200
300

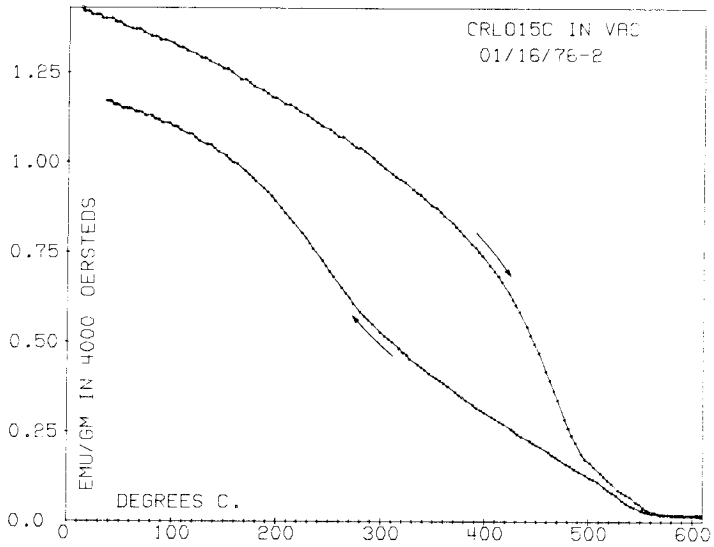
CRL015C IN VAC
01/16/76-2
EMU/GM IN 4000 OERSTEDS
DEGREES C.
0.0
0.25
0.50
0.75
1.00
1.25
0
100
200
300
400
500
600

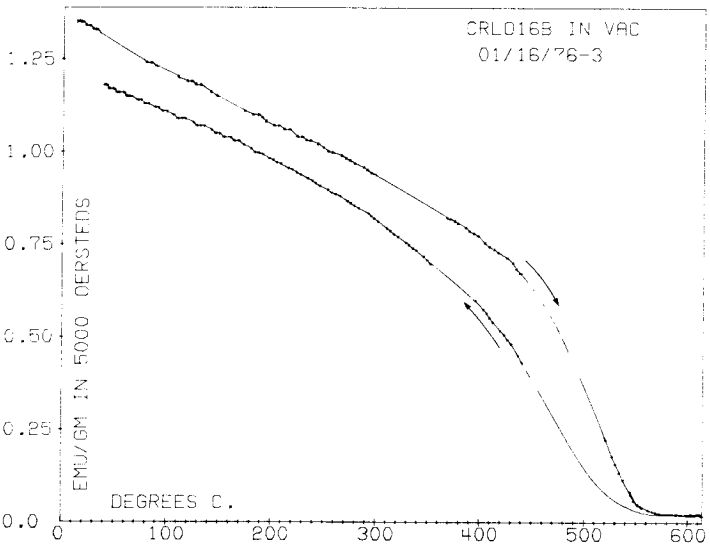
CRL016B IN VAC
01/16/76-3
EMU/GM IN 5000 OERSTEDS
DEGREES C.
0.0
0.25
0.50
0.75
1.00
1.25
0
100
200
300
400
500
600

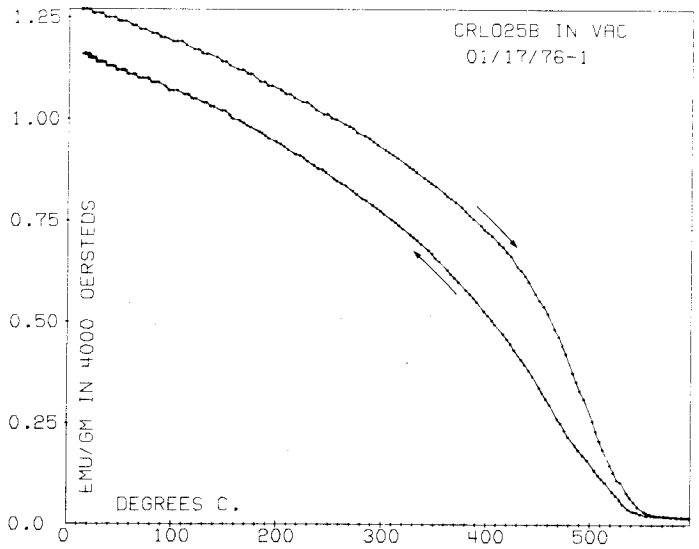
CRL025B IN VAC
01/17/76-1
EMU/GM IN 4000 OERSTEDS
DEGREES C.
0.0
0.25
0.50
0.75
1.00
1.25
0
100
200
300
400
500

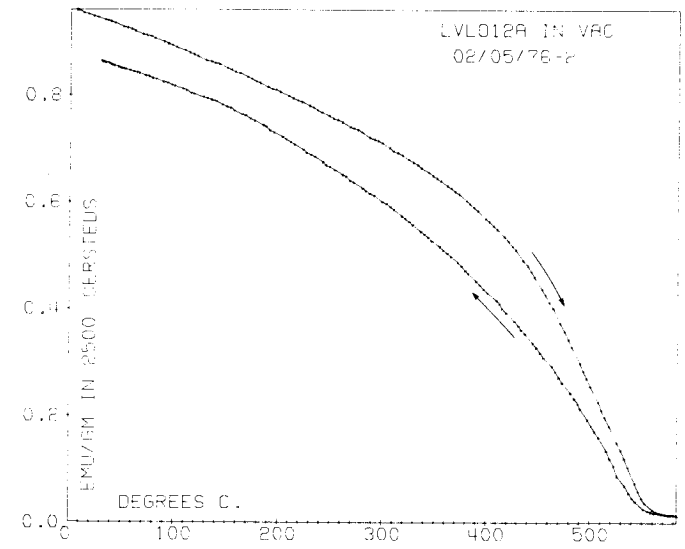
LVL012A IN VAC
02/05/76-2
EMU/GM IN 2500 OERSTEDS
DEGREES C.
0.0
0.2
0.4
0.6
0.8
0
100
200
300
400
500

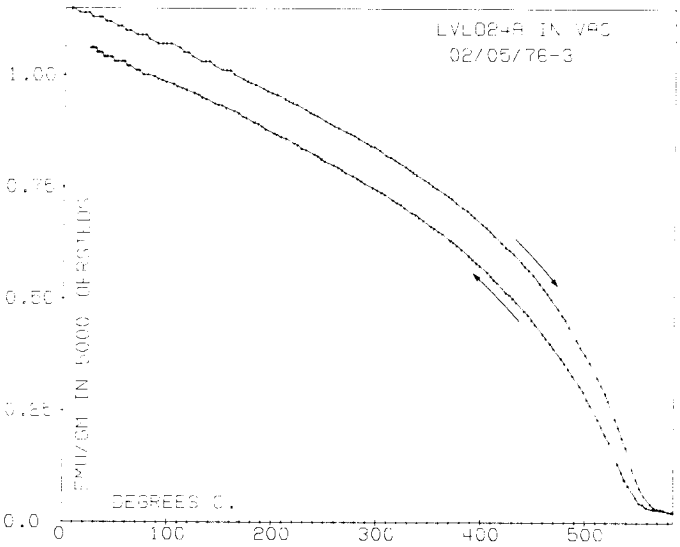
LVL024A IN VAC
02/05/76-3
EMU/GM IN 5000 OERSTEDS
DEGREES C.
0.0
0.25
0.50
0.75
1.00
0
100
200
300
400
500

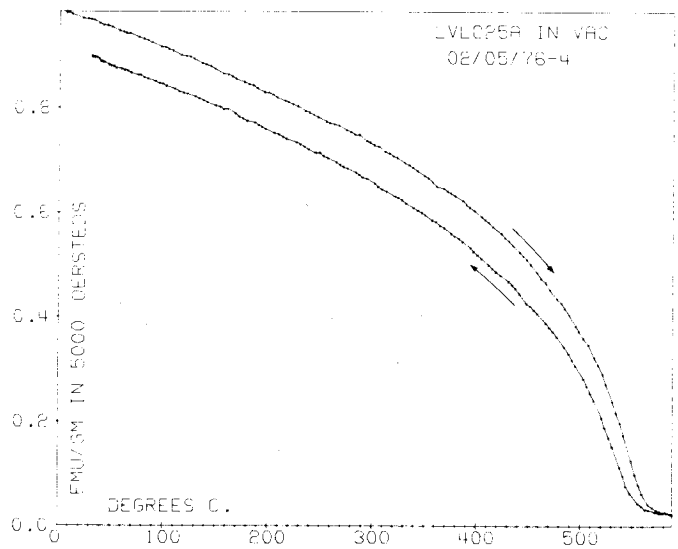
LVL025A IN VAC
02/05/76-4
EMU/GM IN 5000 OERSTEDS
DEGREES C.
0.0
0.2
0.4
0.6
0.8
0
100
200
300
400
500

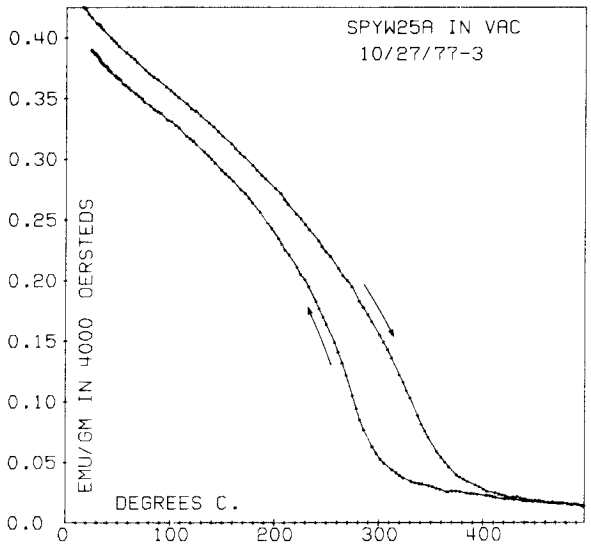
SPYW25A IN VAC
10/27/77-3
EMU/GM IN 4000 OERSTEDS
DEGREES C.
0.0
0.05
0.10
0.15
0.20
0.25
0.30
0.35
0.40
0
100
200
300
400

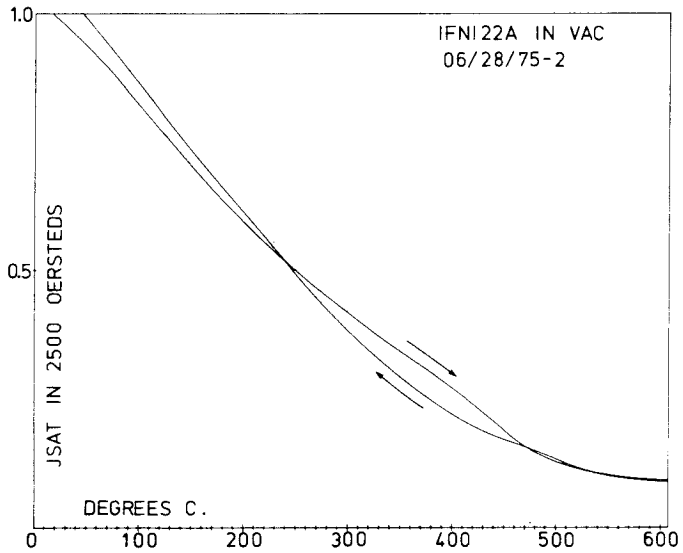
IFN122A IN VAC
06/28/75-2
JSAT IN 2500 OERSTEDS
DEGREES C.
0.5
1.0
0
100
200
300
400
500
600

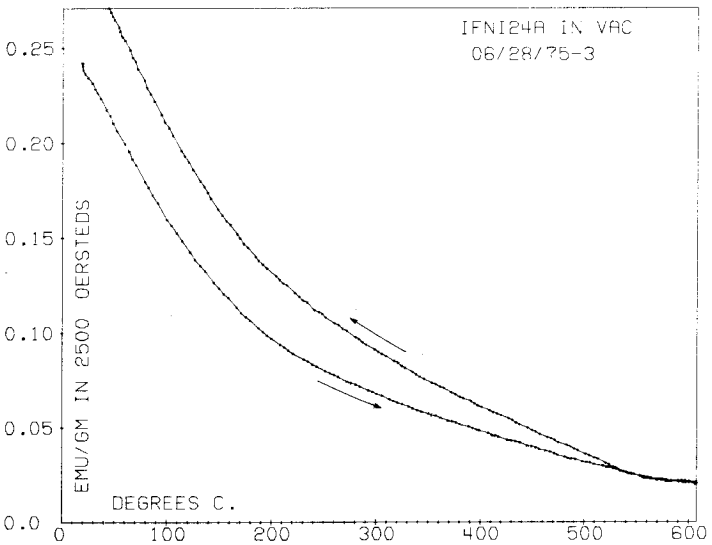
IFN124A IN VAC
06/28/75-3
EMU/GM IN 2500 OERSTEDS
DEGREES C.
0.0
0.05
0.10
0.15
0.20
0.25
0
100
200
300
400
500
600

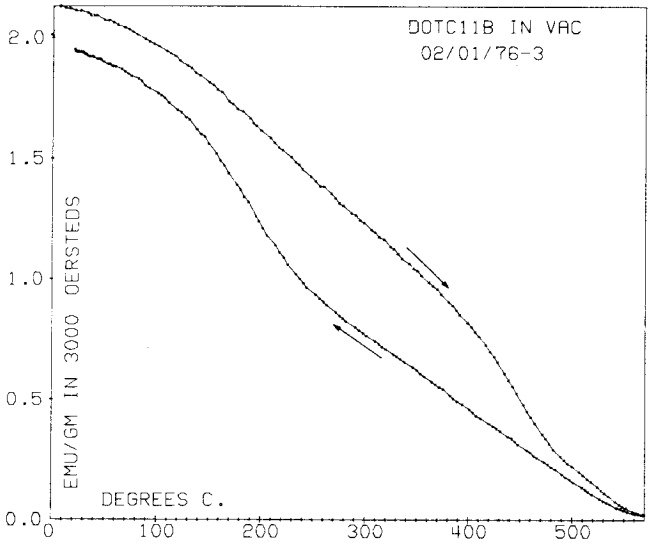
DOTC11B IN VAC
02/01/76-3
EMU/GM IN 3000 OERSTEDS
DEGREES C.
2.0
1.5
1.0
0.5
0.0
0
100
200
300
400
500

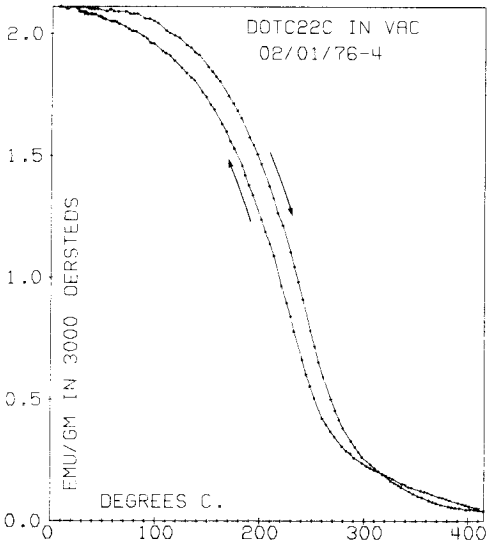
DOTC22C IN VAC
02/01/76-4
EMU/GM IN 3000 OERSTEDS
DEGREES C.
2.0
1.5
1.0
0.5
0.0
0
100
200
300
400

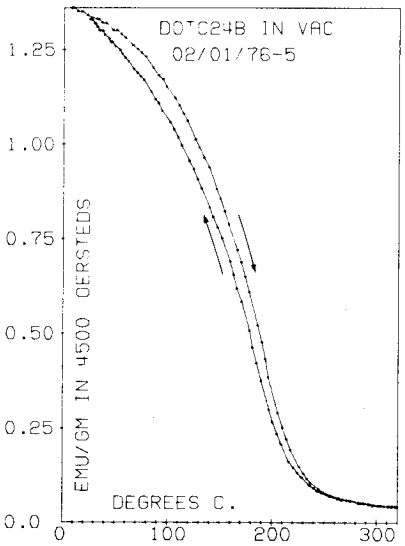
DOTC24B IN VAC
02/01/76-5
EMU/GM IN 4500 OERSTEDS
DEGREES C.
1.25
1.00
0.75
0.50
0.25
0.0
0
100
200
300

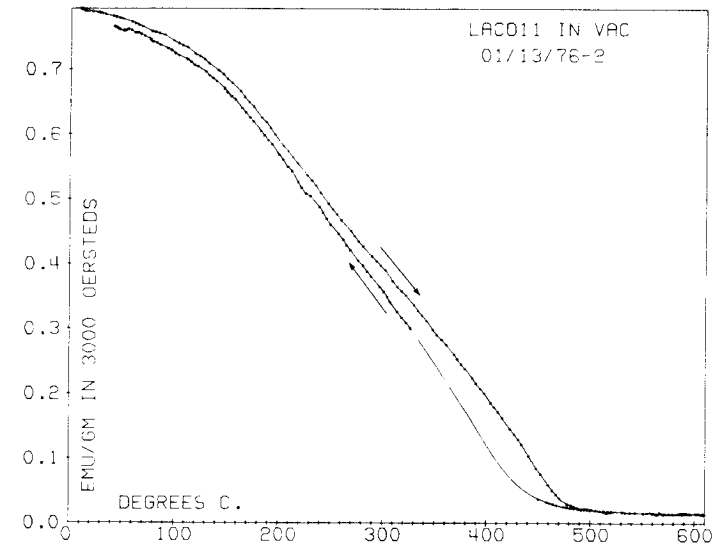
LAC011 IN VAC
01/13/76-2
EMU/GM IN 3000 OERSTEDS
DEGREES C.
0.0
0.1
0.2
0.3
0.4
0.5
0.6
0.7
0
100
200
300
400
500
600

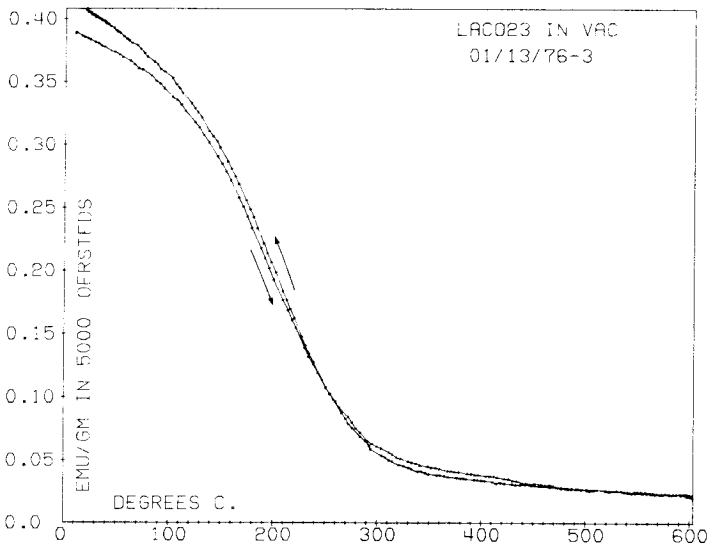
LAC023 IN VAC
01/13/76-3
EMU/GM IN 5000 OERSTEDS
DEGREES C.
0.0
0.05
0.10
0.15
0.20
0.25
0.30
0.35
0.40
0
100
200
300
400
500
600

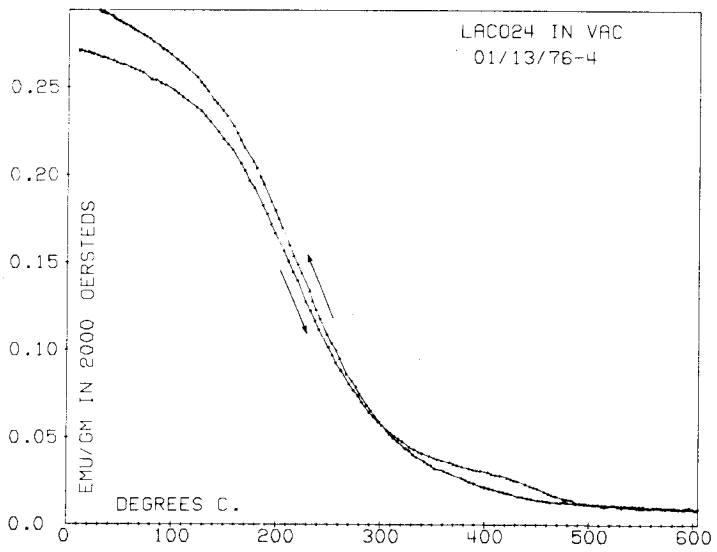
LAC024 IN VAC
01/13/76-4
EMU/GM IN 2000 OERSTEDS
DEGREES C.
0.0
0.05
0.10
0.15
0.20
0.25
0
100
200
300
400
500
600

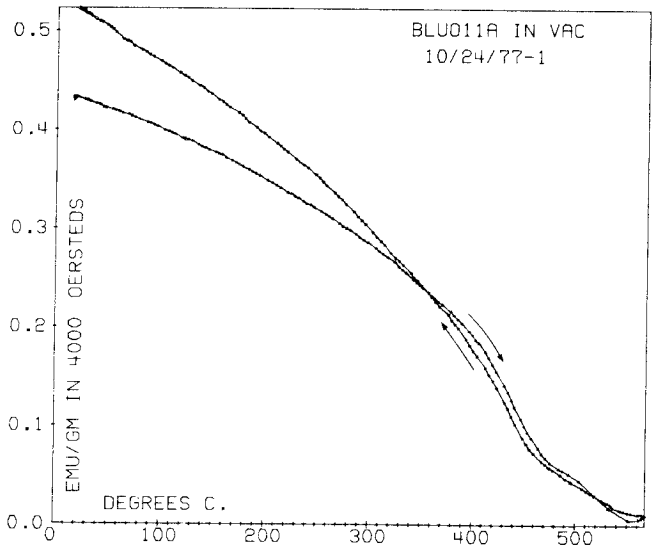
BLU011A IN VAC
10/24/77-1
EMU/GM IN 4000 OERSTEDS
DEGREES C.
0.0
0.1
0.2
0.3
0.4
0.5
0
100
200
300
400
500

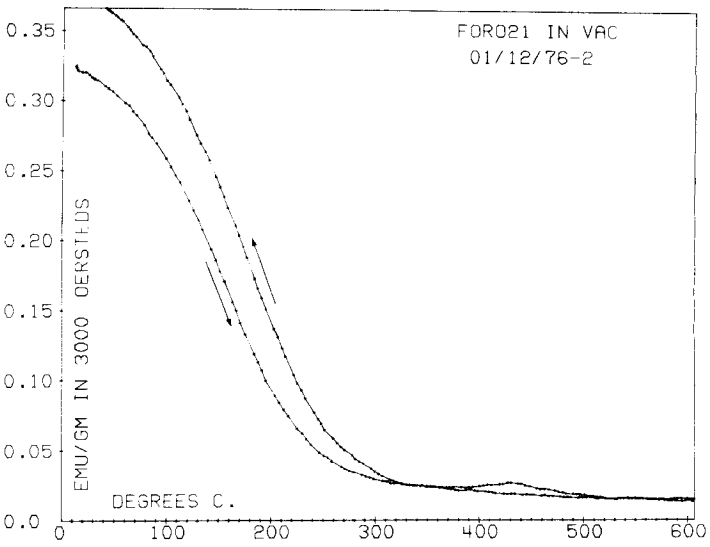
FOR021 IN VAC
01/12/76-2
EMU/GM IN 3000 OERSTEDS
DEGREES C.
0.0
0.05
0.10
0.15
0.20
0.25
0.30
0.35
0
100
200
300
400
500
600

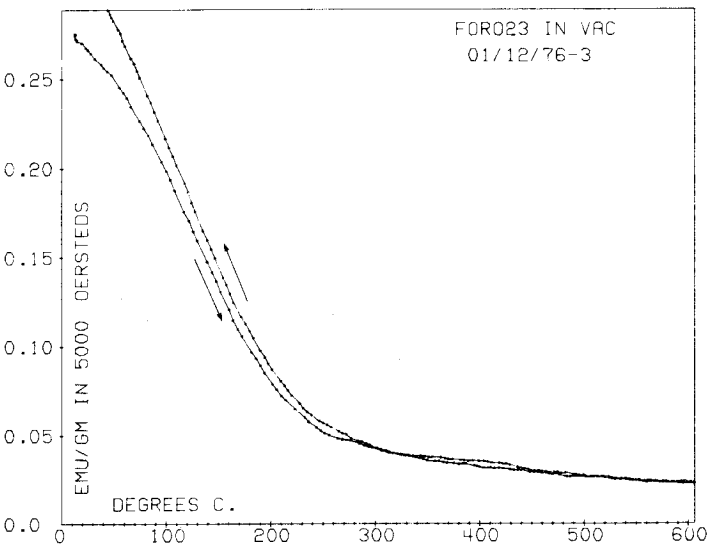
FOR023 IN VAC
01/12/76-3
EMU/GM IN 5000 OERSTEDS
DEGREES C.
0.0
0.05
0.10
0.15
0.20
0.25
0
100
200
300
400
500
600

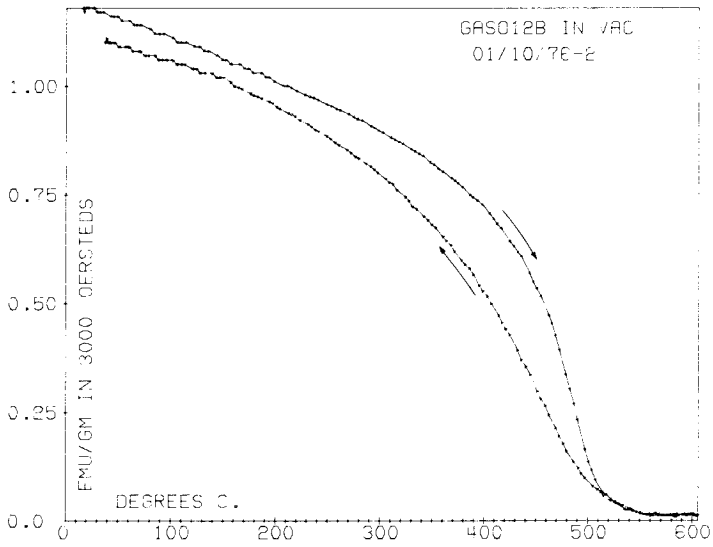
GAS012B IN VAC
01/10/76-2
1.00
0.75
0.50
0.25
0.0
EMU/GM IN 3000 OERSTEDS
DEGREES C.
0
100
200
300
400
500
600

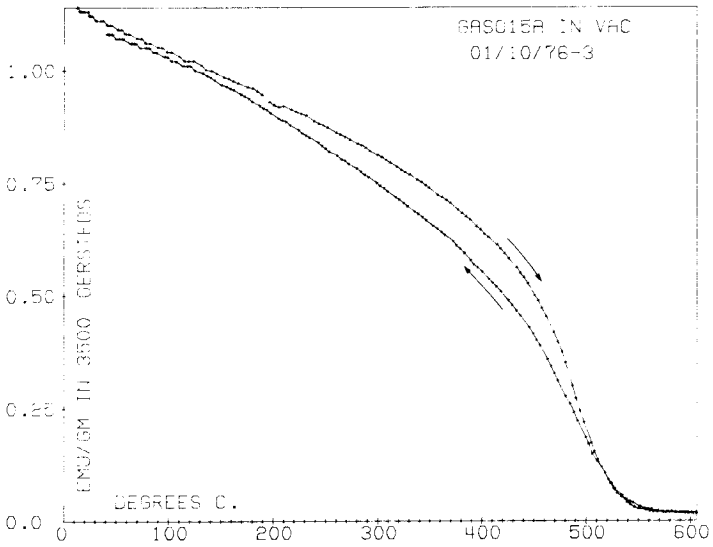
GAS015A IN VAC
01/10/76-3
1.00
0.75
0.50
0.25
0.0
EMU/GM IN 3500 OERSTEDS
DEGREES C.
0
100
200
300
400
500
600

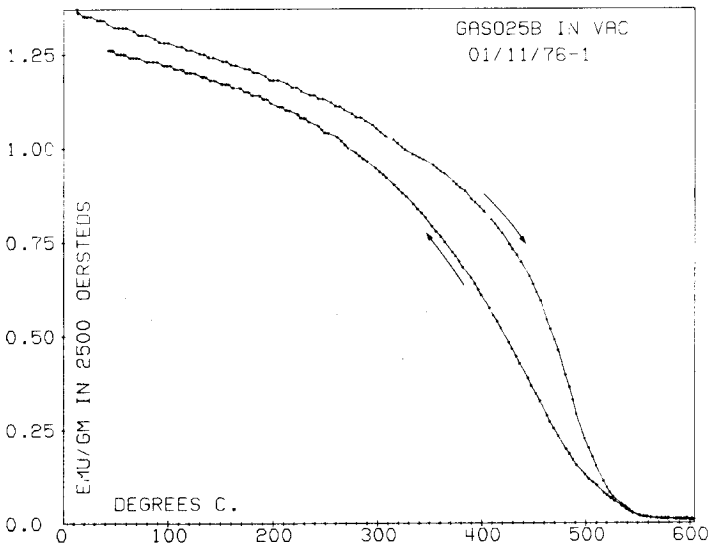
GAS025B IN VAC
01/11/76-1
1.25
1.00
0.75
0.50
0.25
0.0
EMU/GM IN 2500 OERSTEDS
DEGREES C.
0
100
200
300
400
500
600

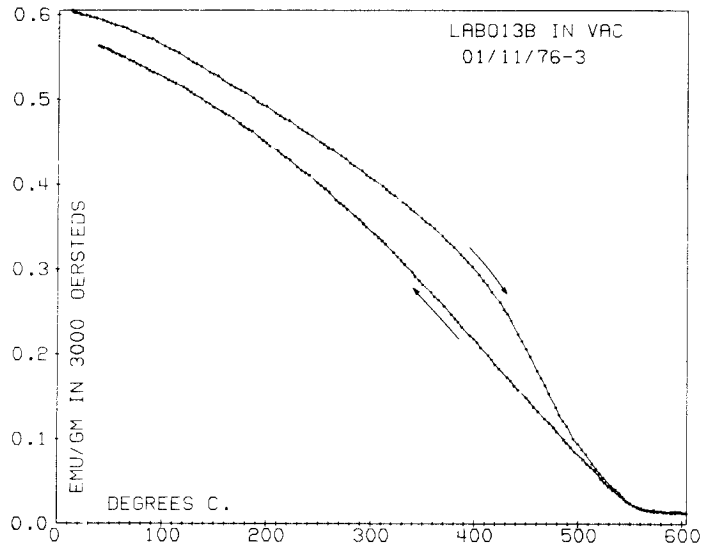
LAB013B IN VAC
01/11/76-3
EMU/GM IN 3000 OERSTEDS
DEGREES C.
0.6
0.5
0.4
0.3
0.2
0.1
0.0
0
100
200
300
400
500
600

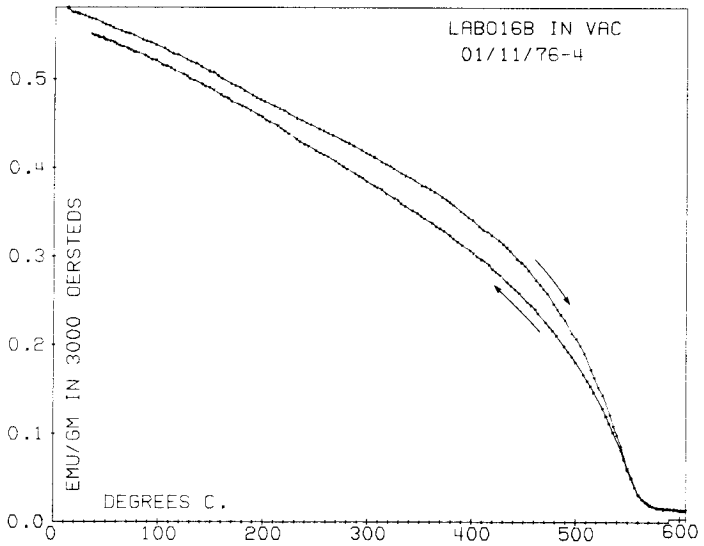
LAB016B IN VAC
01/11/76-4
EMU/GM IN 3000 OERSTEDS
DEGREES C.
0.5
0.4
0.3
0.2
0.1
0.0
0
100
200
300
400
500
600

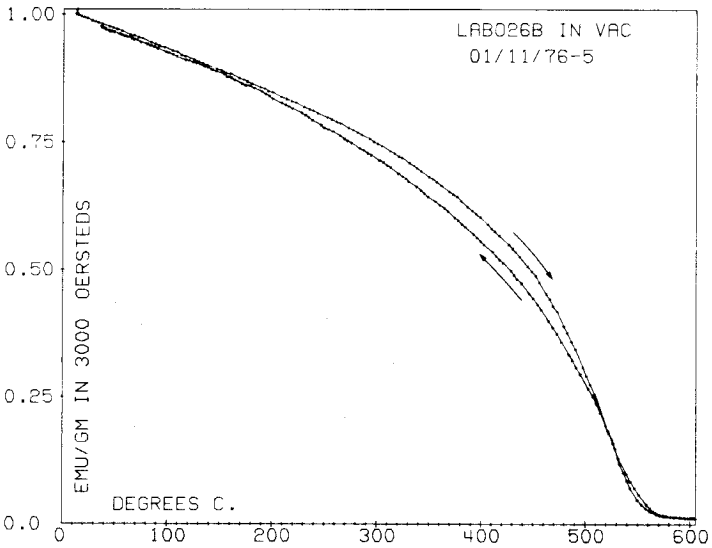
LAB026B IN VAC
01/11/76-5
EMU/GM IN 3000 OERSTEDS
DEGREES C.
1.00
0.75
0.50
0.25
0.0
0
100
200
300
400
500
600

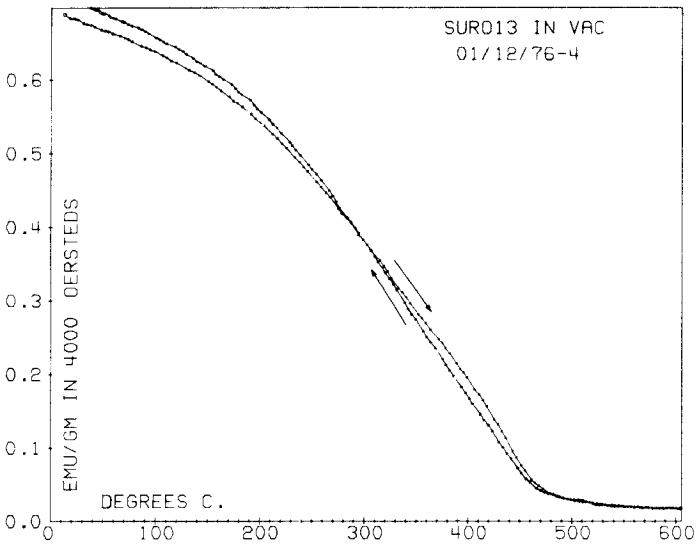
SUR013 IN VAC
01/12/76-4
EMU/GM IN 4000 OERSTEDS
DEGREES C.
0.0
0.1
0.2
0.3
0.4
0.5
0.6
0
100
200
300
400
500
600

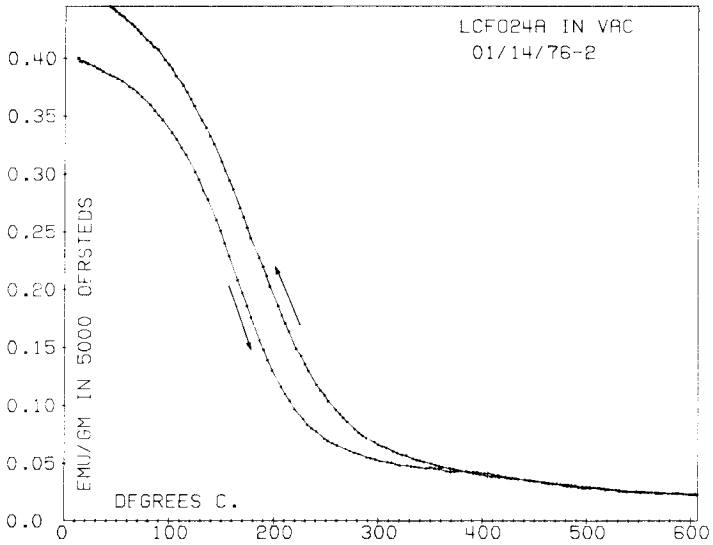
LCF024A IN VAC
01/14/76-2
EMU/GM IN 5000 OERSTEDS
DEGREES C.
0.0
0.05
0.10
0.15
0.20
0.25
0.30
0.35
0.40
0
100
200
300
400
500
600

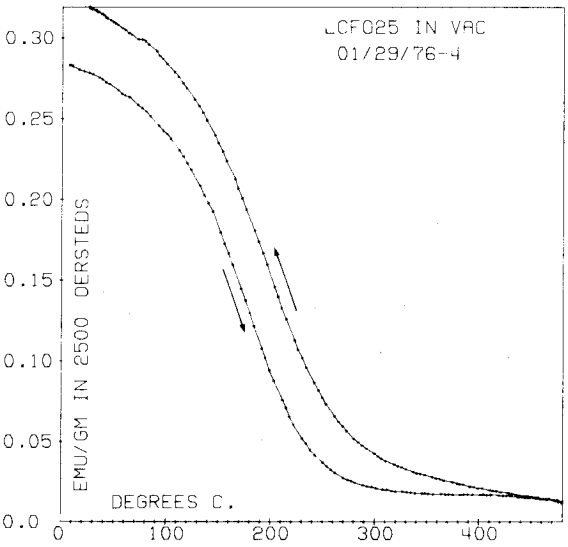
LCF025 IN VAC
01/29/76-4
EMU/GM IN 2500 OERSTEDS
DEGREES C.
0.0
0.05
0.10
0.15
0.20
0.25
0.30
0
100
200
300
400

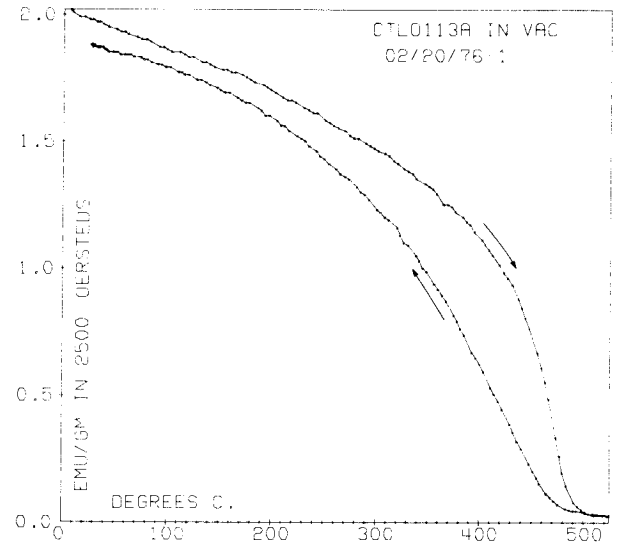
CTL0113A IN VAC
02/20/76-1
EMU/GM IN 2500 OERSTEDS
DEGREES C.
2.0
1.5
1.0
0.5
0.0
0
100
200
300
400
500

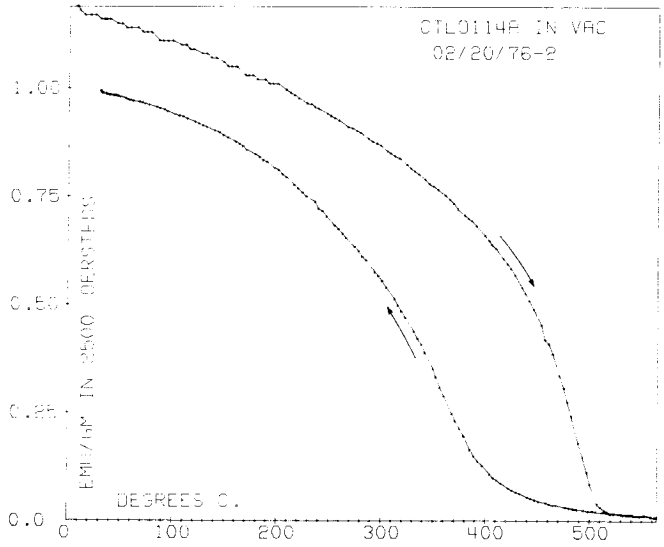
CTL0114B IN VAC
02/20/76-2
EMU/GM IN 2500 OERSTEDS
DEGREES C.
1.00
0.75
0.50
0.25
0.0
0
100
200
300
400
500

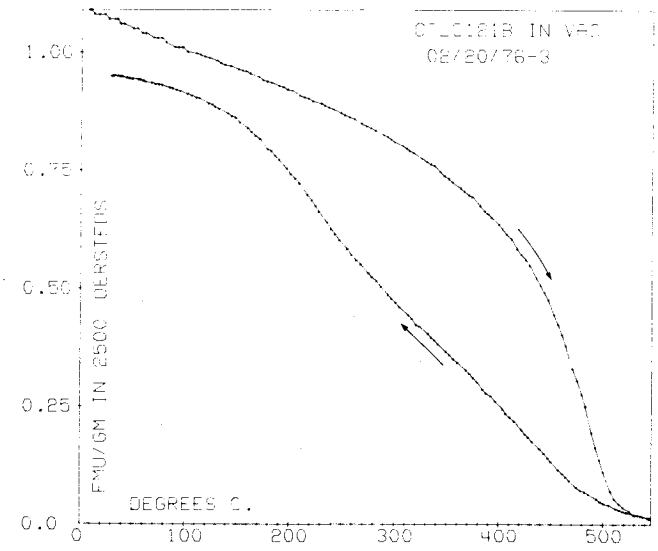
CTL0181B IN VAC
02/20/76-3
EMU/GM IN 2500 OERSTEDS
DEGREES C.
1.00
0.75
0.50
0.25
0.0
0
100
200
300
400
500

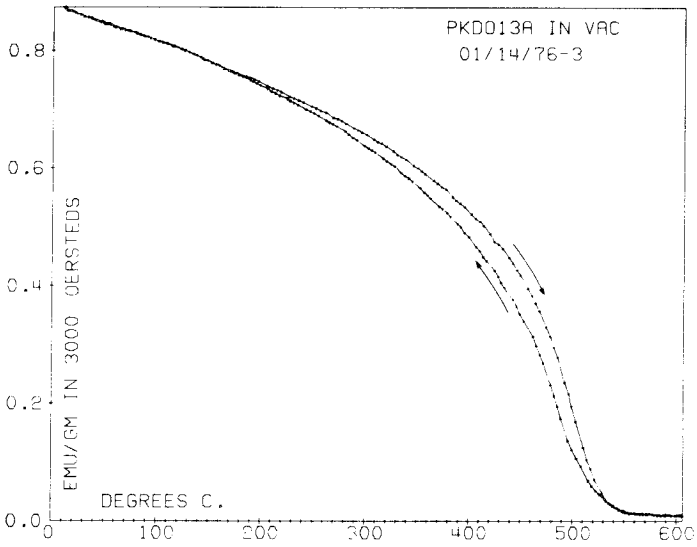
PKD013A IN VAC
01/14/76-3
EMU/GM IN 3000 OERSTEDS
DEGREES C.
0.0
0.2
0.4
0.6
0.8
0
100
200
300
400
500
600

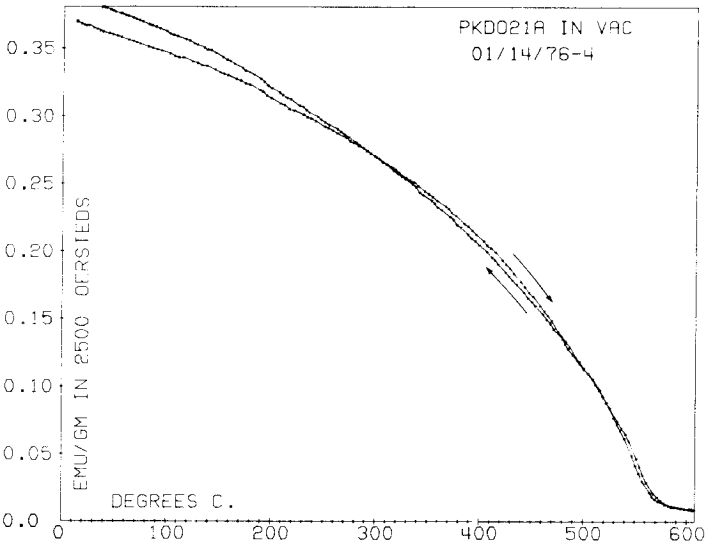
PKD021A IN VAC
01/14/76-4
EMU/GM IN 2500 OERSTEDS
DEGREES C.
0.0
0.05
0.10
0.15
0.20
0.25
0.30
0.35
0
100
200
300
400
500
600

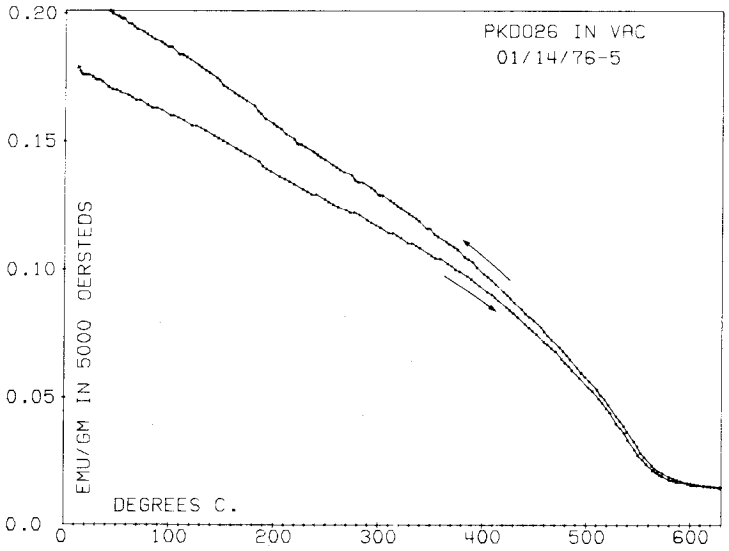
PKD026 IN VAC
01/14/76-5
EMU/GM IN 5000 OERSTEDS
DEGREES C.
0.0
0.05
0.10
0.15
0.20
0
100
200
300
400
500
600

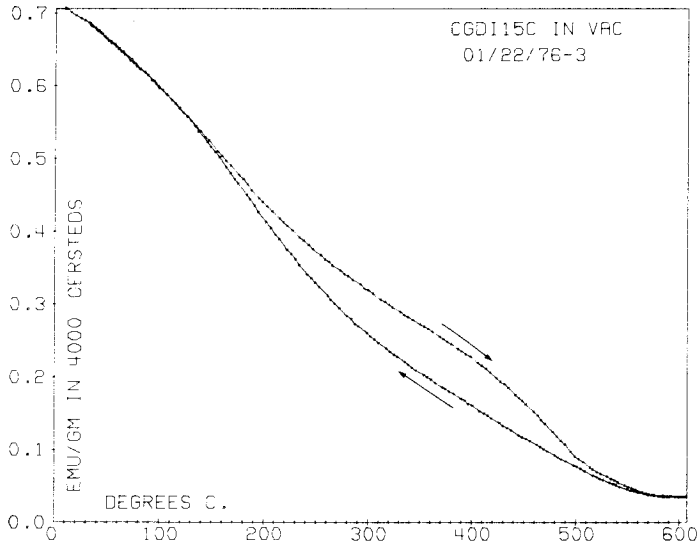
CGDI15C IN VAC
01/22/76-3
EMU/GM IN 4000 OERSTEDS
DEGREES C.
0.0
0.1
0.2
0.3
0.4
0.5
0.6
0.7
0
100
200
300
400
500
600

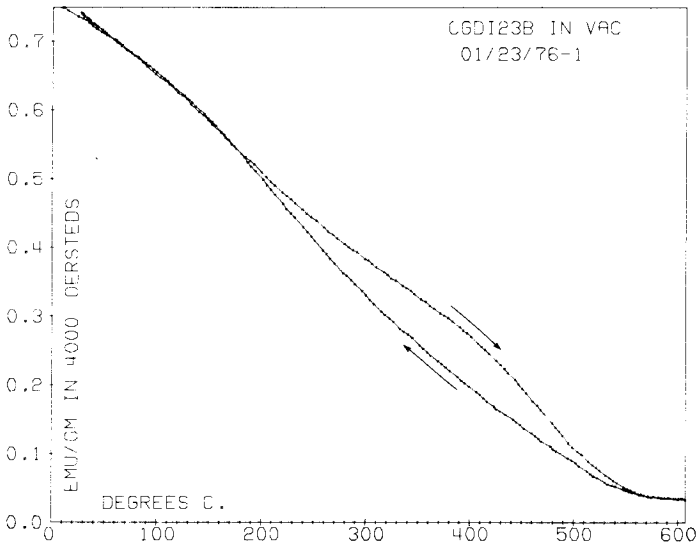
CGDI23B IN VAC
01/23/76-1
EMU/GM IN 4000 OERSTEDS
DEGREES C.
0.0
0.1
0.2
0.3
0.4
0.5
0.6
0.7
0
100
200
300
400
500
600

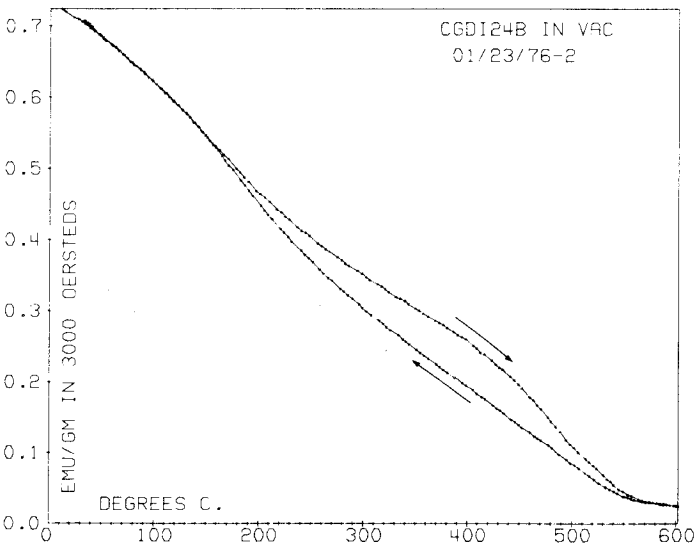
CGDI24B IN VAC
01/23/76-2
EMU/GM IN 3000 OERSTEDS
DEGREES C.
0.0
0.1
0.2
0.3
0.4
0.5
0.6
0.7
0
100
200
300
400
500
600

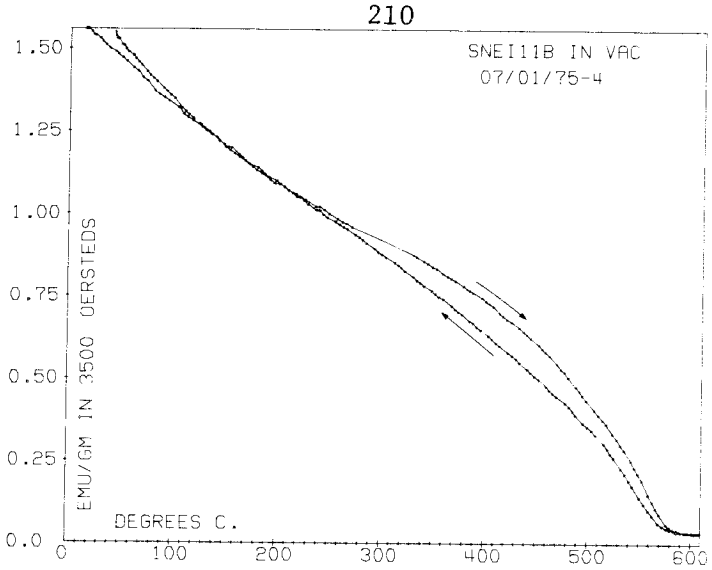
SNEI11B IN VAC
07/01/75-4
EMU/GM IN 3500 OERSTEDS
DEGREES C.
1.50
1.25
1.00
0.75
0.50
0.25
0.0
0
100
200
300
400
500
600

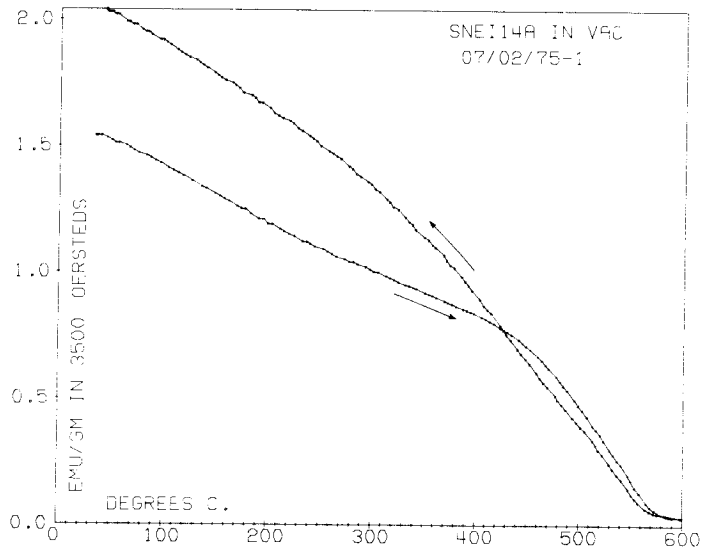
SNEI14A IN VAC
07/02/75-1
EMU/GM IN 3500 OERSTEDS
DEGREES C.
2.0
1.5
1.0
0.5
0.0
0
100
200
300
400
500
600

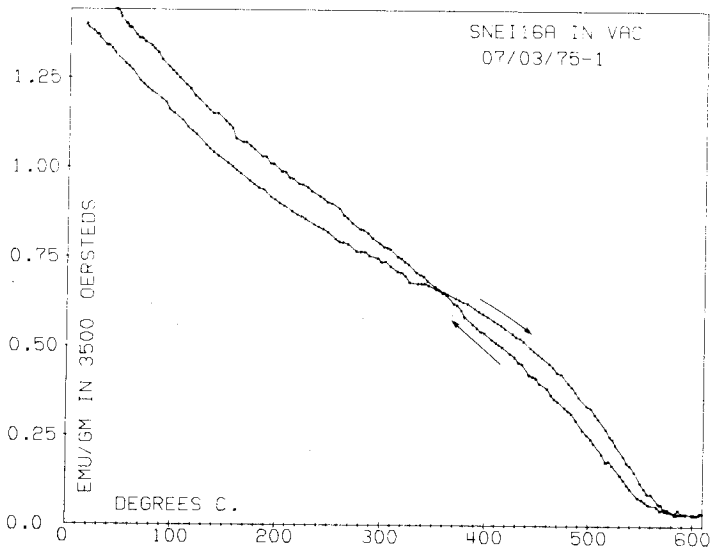
SNEI16A IN VAC
07/03/75-1
EMU/GM IN 3500 OERSTEDS
DEGREES C.
1.25
1.00
0.75
0.50
0.25
0.0
0
100
200
300
400
500
600

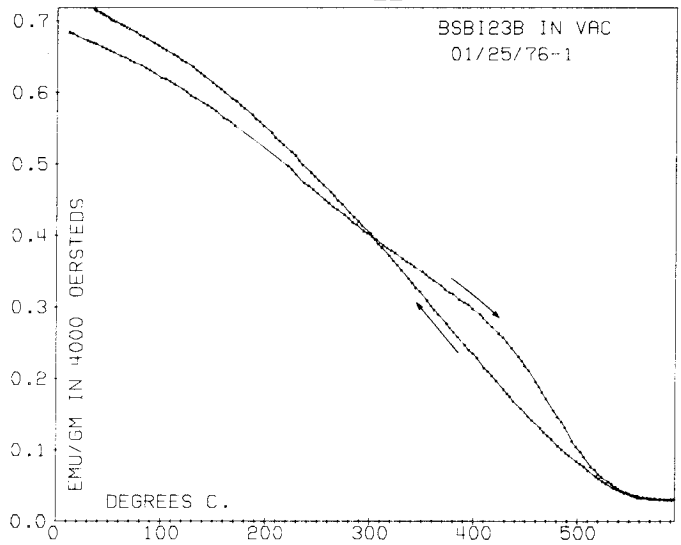
BSBI23B IN VAC
01/25/76-1
EMU/GM IN 4000 OERSTEDS
DEGREES C.
0.0
0.1
0.2
0.3
0.4
0.5
0.6
0.7
0
100
200
300
400
500

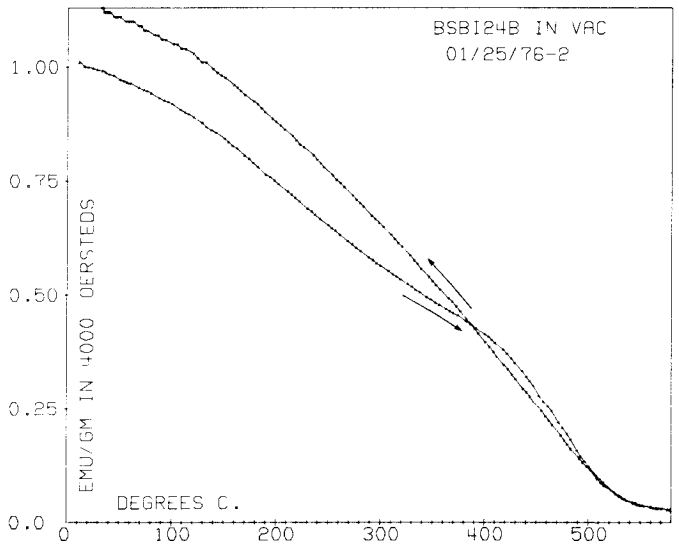
BSBI24B IN VAC
01/25/76-2
EMU/GM IN 4000 OERSTEDS
DEGREES C.
0.0
0.25
0.50
0.75
1.00
0
100
200
300
400
500

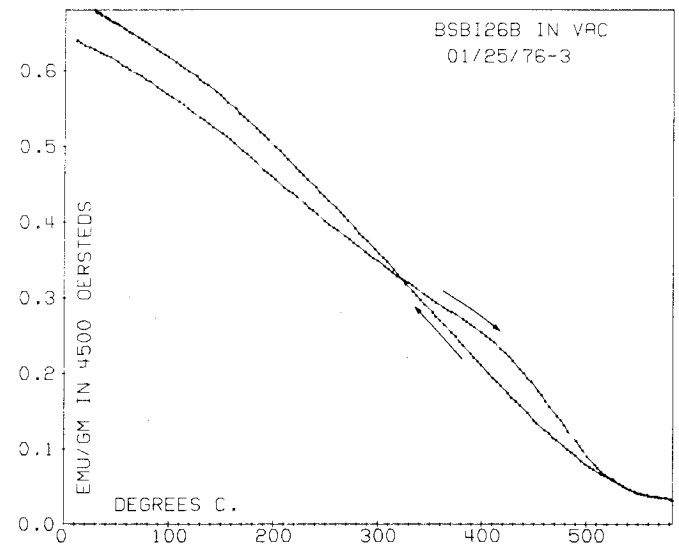
BSBI26B IN VAC
01/25/76-3
EMU/GM IN 4500 OERSTEDS
DEGREES C.
0.0
0.1
0.2
0.3
0.4
0.5
0.6
0
100
200
300
400
500

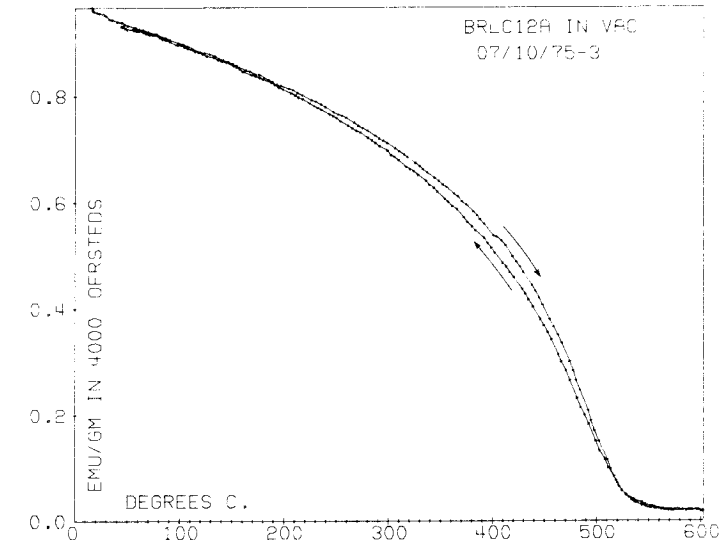
BRLC12A IN VAC
07/10/75-3
EMU/GM IN 4000 OERSTEDS
DEGREES C.
0.0
0.2
0.4
0.6
0.8
0
100
200
300
400
500
600

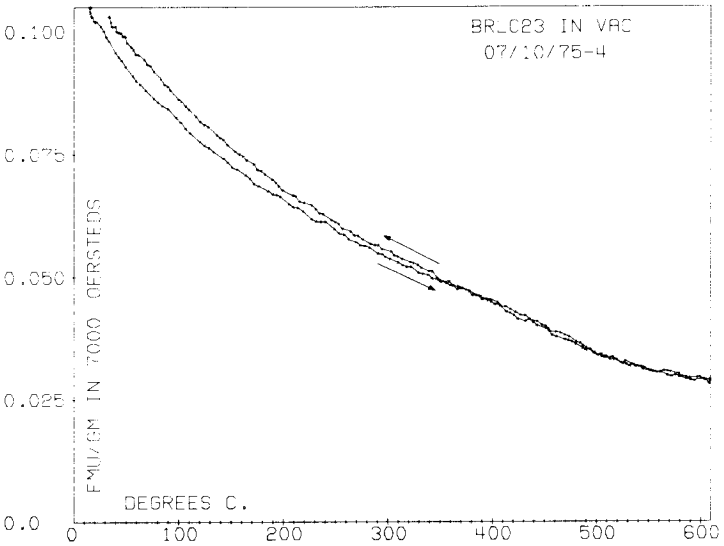
BRLC23 IN VAC
07/10/75-4
EMU/GM IN 7000 OERSTEDS
DEGREES C.
0.0
0.025
0.050
0.100
0
100
200
300
400
500
600

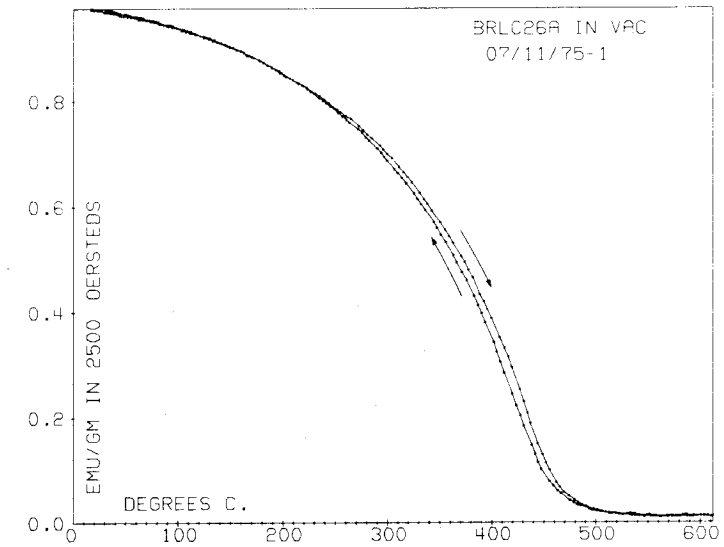
BRLC26A IN VAC
07/11/75-1
EMU/GM IN 2500 OERSTEDS
DEGREES C.
0.0
0.2
0.4
0.6
0.8
0
100
200
300
400
500
600

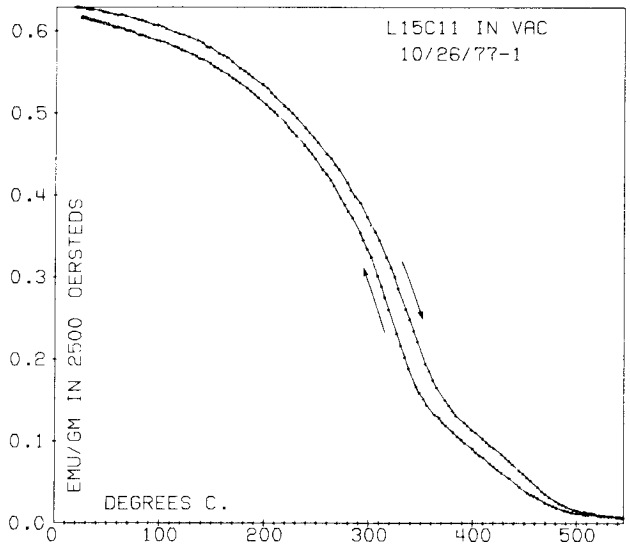
L15C11 IN VAC
10/26/77-1
EMU/GM IN 2500 OERSTEDS
DEGREES C.
0.0
0.1
0.2
0.3
0.4
0.5
0.6
0
100
200
300
400
500

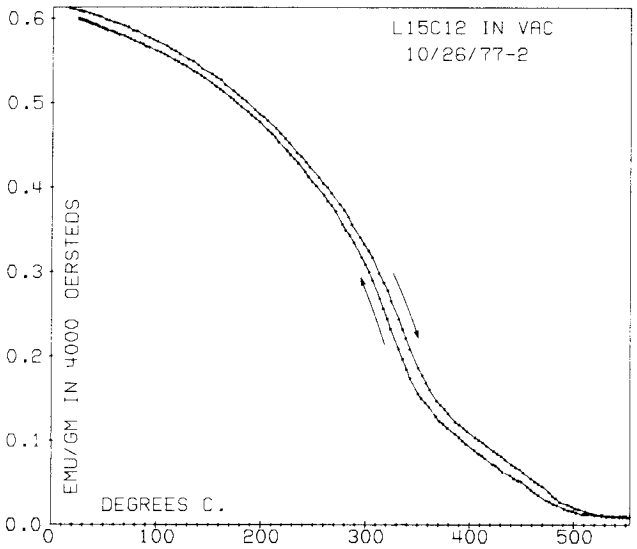
L15C12 IN VAC
10/26/77-2
EMU/GM IN 4000 OERSTEDS
DEGREES C.
0.0
0.1
0.2
0.3
0.4
0.5
0.6
0
100
200
300
400
500

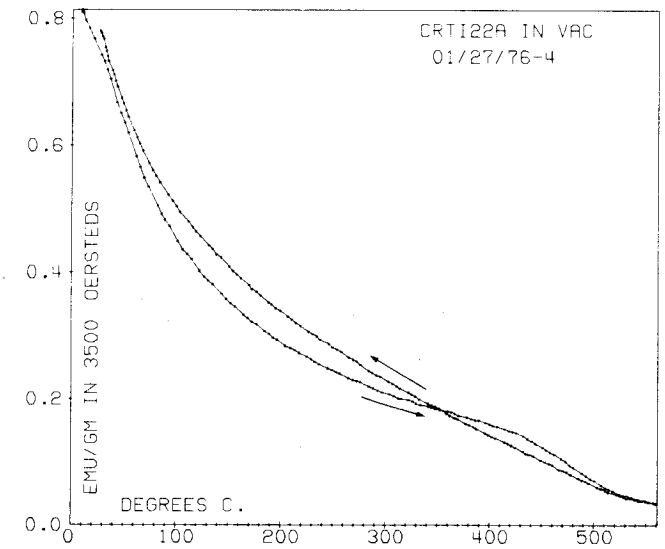
CRTI22A IN VAC
01/27/76-4
EMU/GM IN 3500 OERSTEDS
DEGREES C.
0.0
0.2
0.4
0.6
0.8
0
100
200
300
400
500

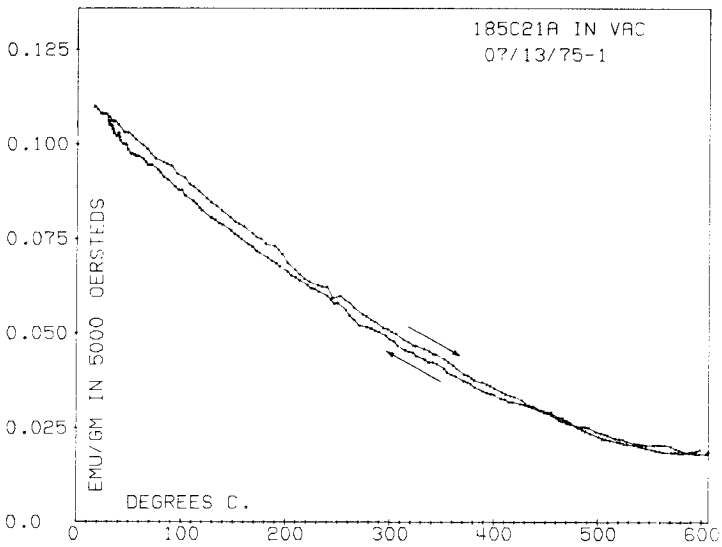
185C21A IN VAC
07/13/75-1
EMU/GM IN 5000 OERSTEDS
DEGREES C.
0.125
0.100
0.075
0.050
0.025
0.0
0
100
200
300
400
500
600

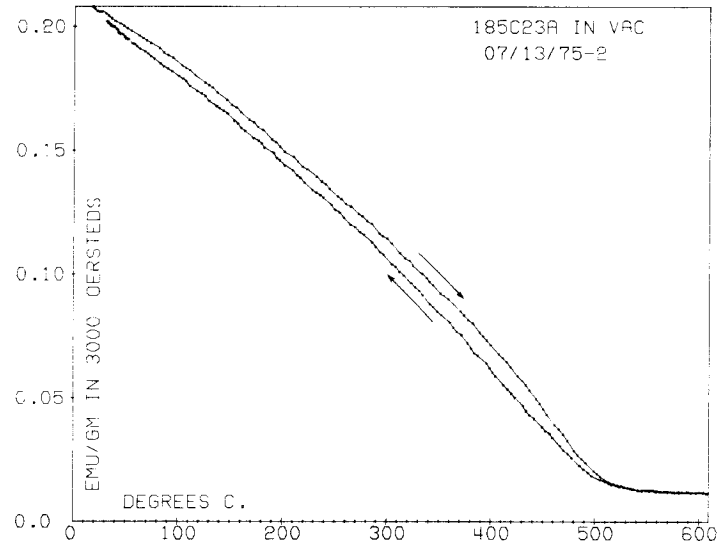
185C23A IN VAC
07/13/75-2
EMU/GM IN 3000 OERSTEDS
DEGREES C.
0.20
0.15
0.10
0.05
0.0
0
100
200
300
400
500
600

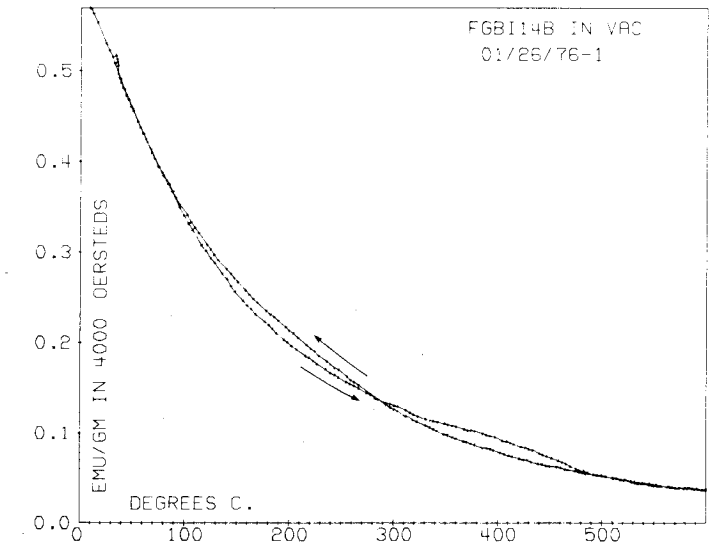
FGBI14B IN VAC
01/26/76-1
EMU/GM IN 4000 OERSTEDS
DEGREES C.
0.5
0.4
0.3
0.2
0.1
0.0
0
100
200
300
400
500

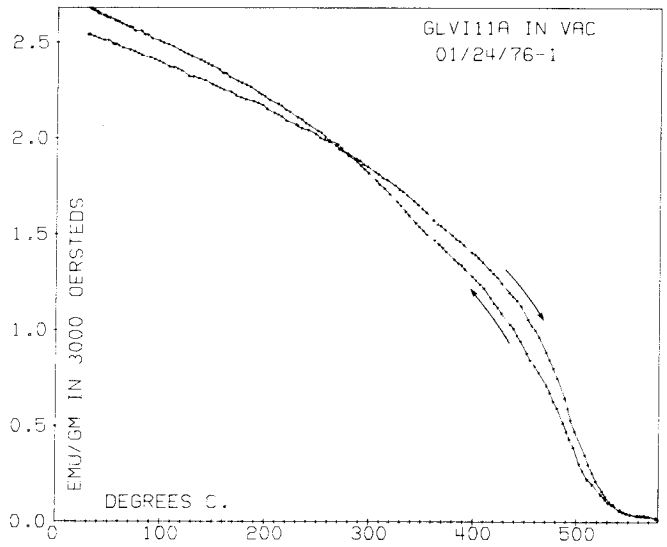
GLVI11A IN VAC
01/24/76-1
EMU/GM IN 3000 OERSTEDS
DEGREES C.
0.0
0.5
1.0
1.5
2.0
2.5
0
100
200
300
400
500

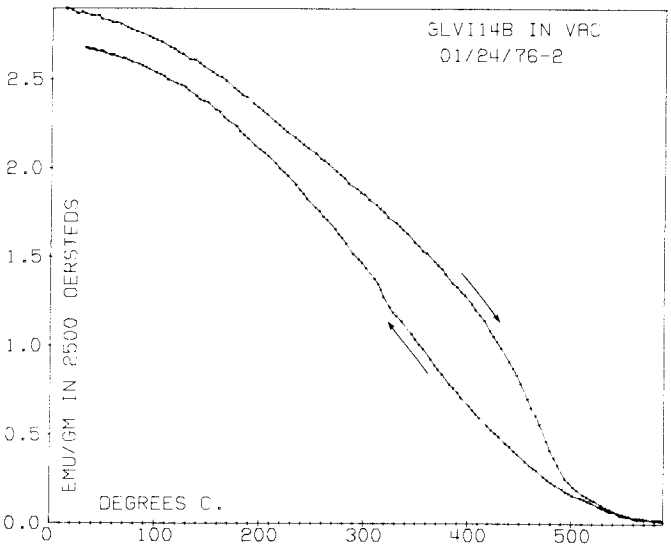
GLVI14B IN VAC
01/24/76-2
EMU/GM IN 2500 OERSTEDS
DEGREES C.
0.0
0.5
1.0
1.5
2.0
2.5
0
100
200
300
400
500

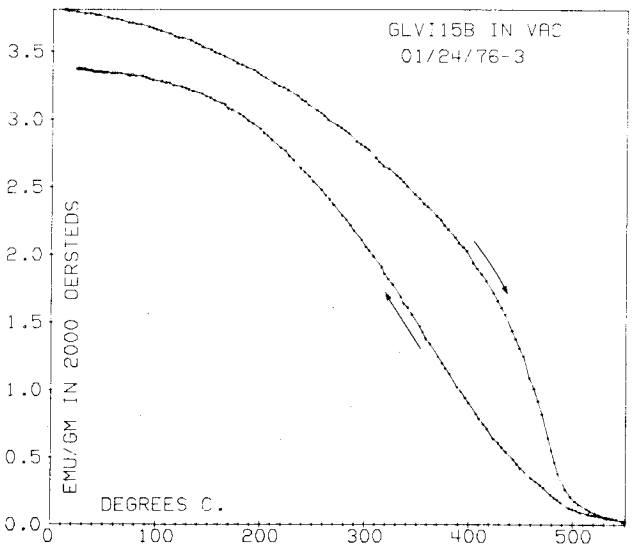
GLVI15B IN VAC
01/24/76-3
EMU/GM IN 2000 OERSTEDS
DEGREES C.
0.0
0.5
1.0
1.5
2.0
2.5
3.0
3.5
0
100
200
300
400
500

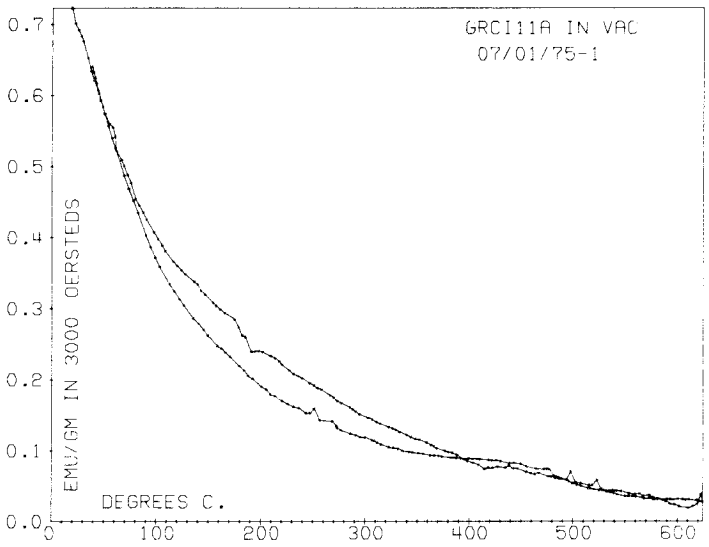
GRCI11A IN VAC
07/01/75-1
EMU/GM IN 3000 OERSTEDS
DEGREES C.
0.0
0.1
0.2
0.3
0.4
0.5
0.6
0.7
0
100
200
300
400
500
600

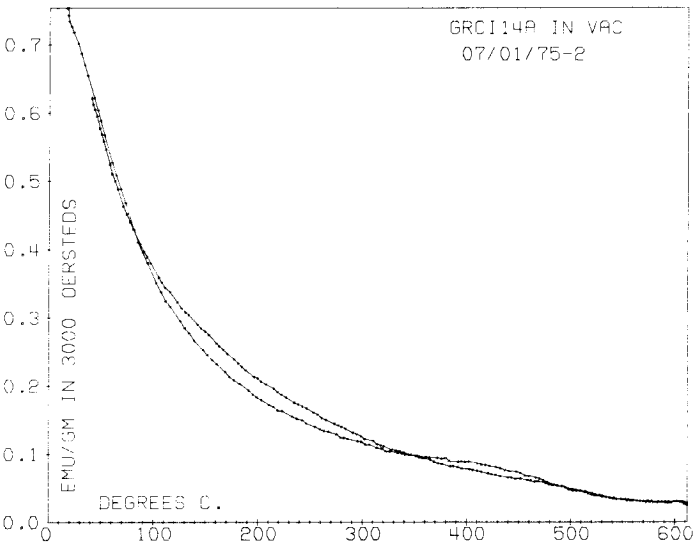
GRCI14A IN VAC
07/01/75-2
EMU/GM IN 3000 OERSTEDS
DEGREES C.
0.0
0.1
0.2
0.3
0.4
0.5
0.6
0.7
0
100
200
300
400
500
600

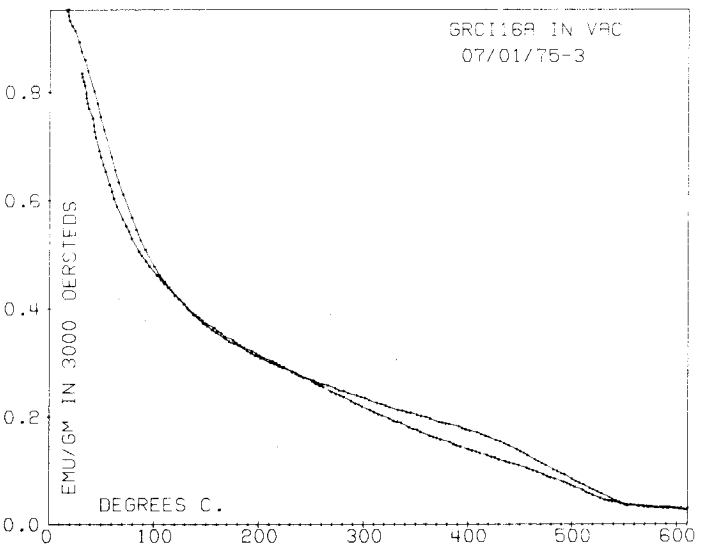
GRCI16A IN VAC
07/01/75-3
EMU/GM IN 3000 OERSTEDS
DEGREES C.
0.0
0.2
0.4
0.6
0.8
0
100
200
300
400
500
600

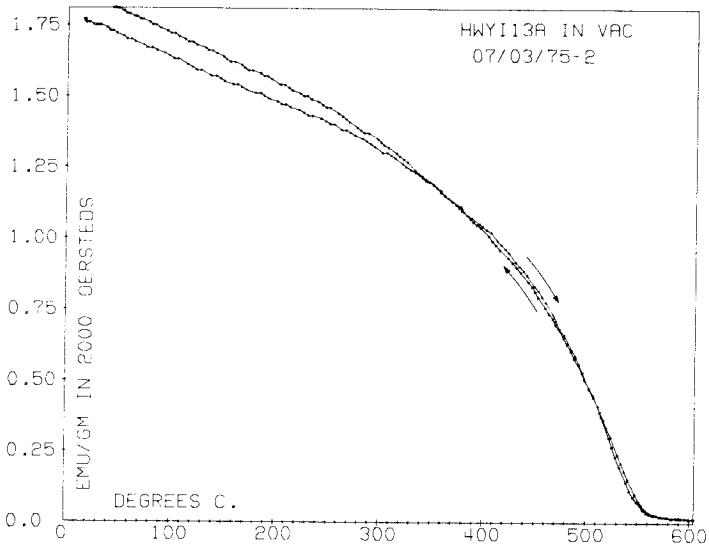
HWYI13A IN VAC
07/03/75-2
EMU/GM IN 2000 OERSTEDS
DEGREES C.
1.75
1.50
1.25
1.00
0.75
0.50
0.25
0.0
0
100
200
300
400
500
600

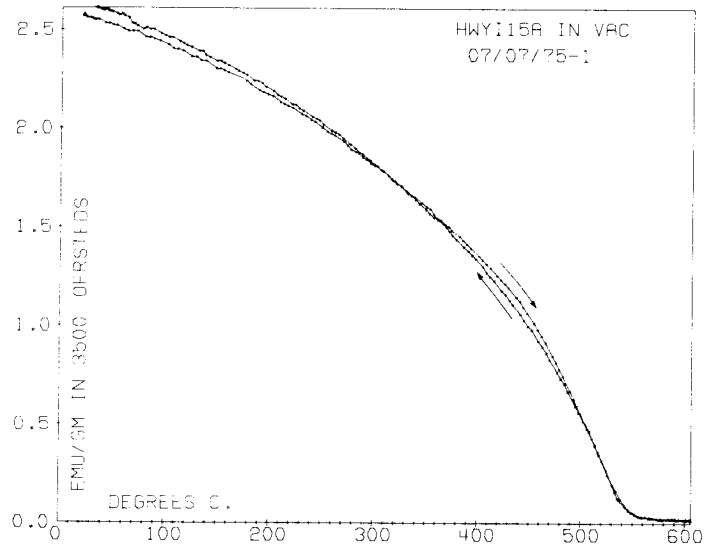
HWYI15A IN VAC
07/07/75-1
EMU/GM IN 3500 OERSTEDS
DEGREES C.
2.5
2.0
1.5
1.0
0.5
0.0
0
100
200
300
400
500
600

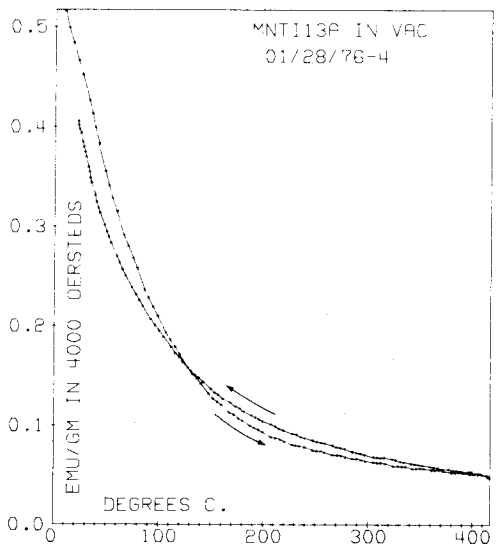
MNTI13A IN VAC
01/28/76-4
EMU/GM IN 4000 OERSTEDS
DEGREES C.
0.5
0.4
0.3
0.2
0.1
0.0
0
100
200
300
400

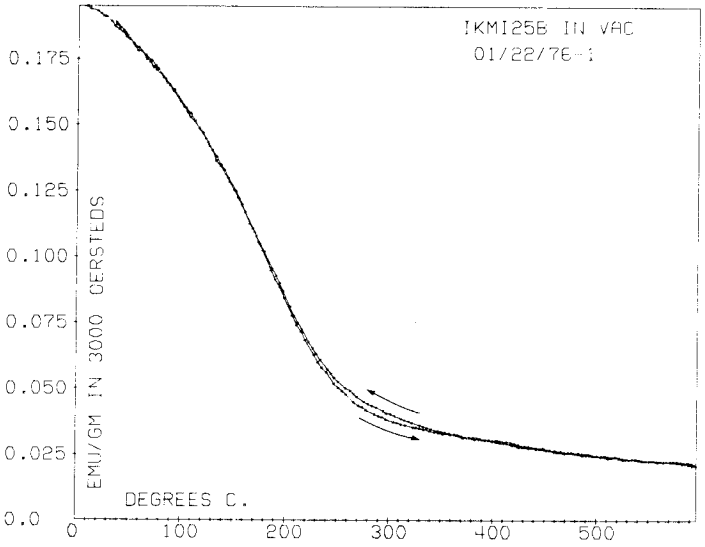
IKMI25B IN VAC
01/22/76-1
EMU/GM IN 3000 OERSTEDS
DEGREES C.
0.175
0.150
0.125
0.100
0.075
0.050
0.025
0.0
0
100
200
300
400
500

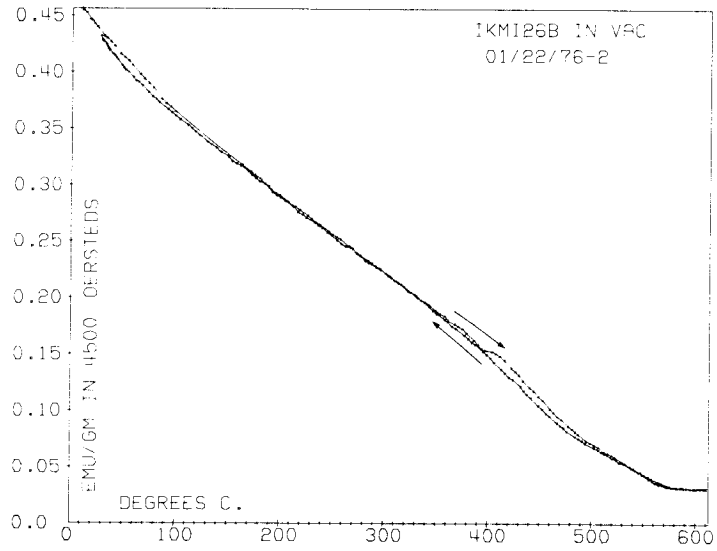
IKMI26B IN VAC
01/22/76-2
EMU/GM IN 4500 OERSTEDS
DEGREES C.
0.45
0.40
0.35
0.30
0.25
0.20
0.15
0.10
0.05
0.0
0
100
200
300
400
500
600

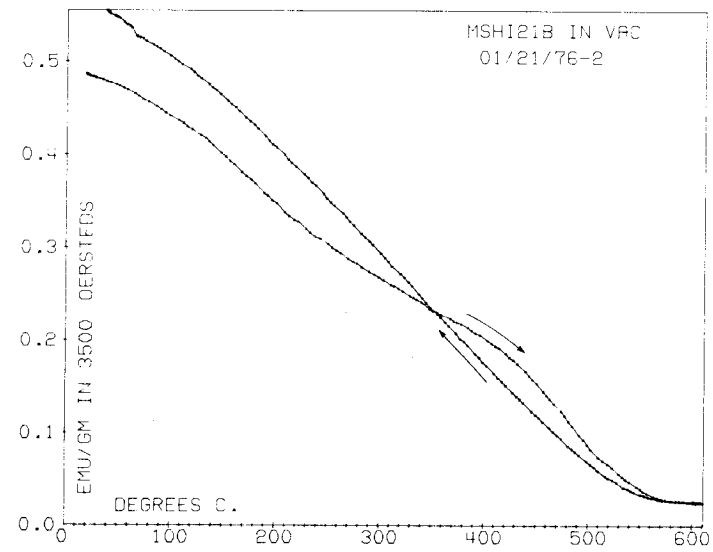
MSHI21B IN VAC
01/21/76-2
EMU/GM IN 3500 OERSTEDS
DEGREES C.
0.5
0.4
0.3
0.2
0.1
0.0
0
100
200
300
400
500
600

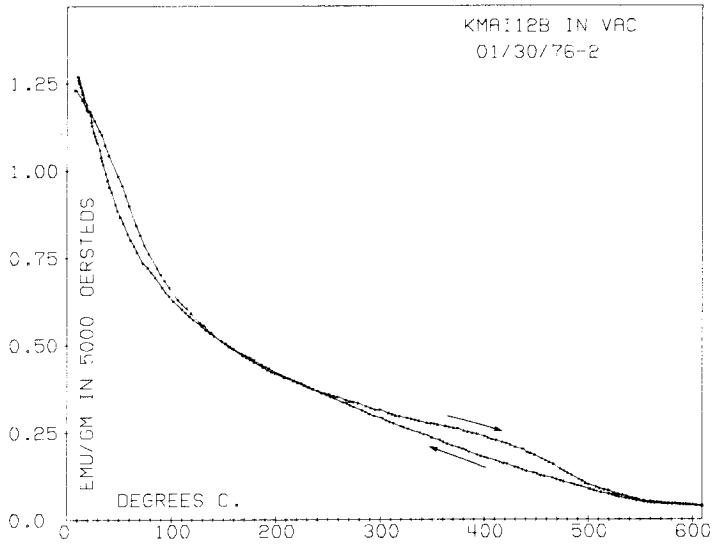
KMAI12B IN VAC
01/30/76-2
EMU/GM IN 5000 OERSTEDS
DEGREES C.
1.25
1.00
0.75
0.50
0.25
0.0
0
100
200
300
400
500
600

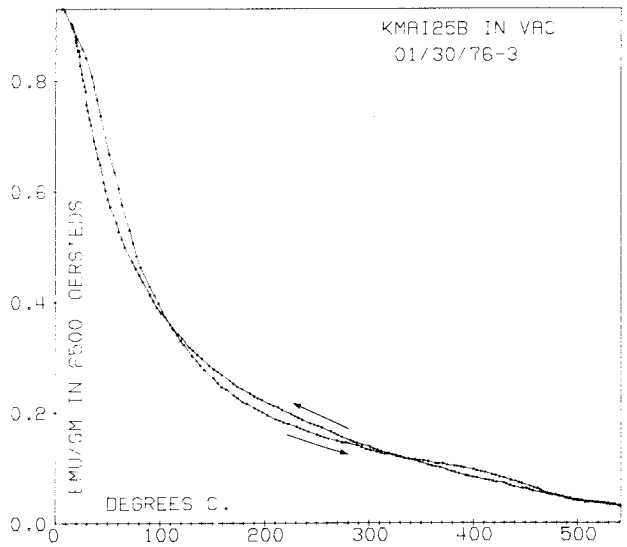
KMAI25B IN VAC
01/30/76-3
EMU/GM IN 2500 OERSTEDS
DEGREES C.
0.8
0.6
0.4
0.2
0.0
0
100
200
300
400
500

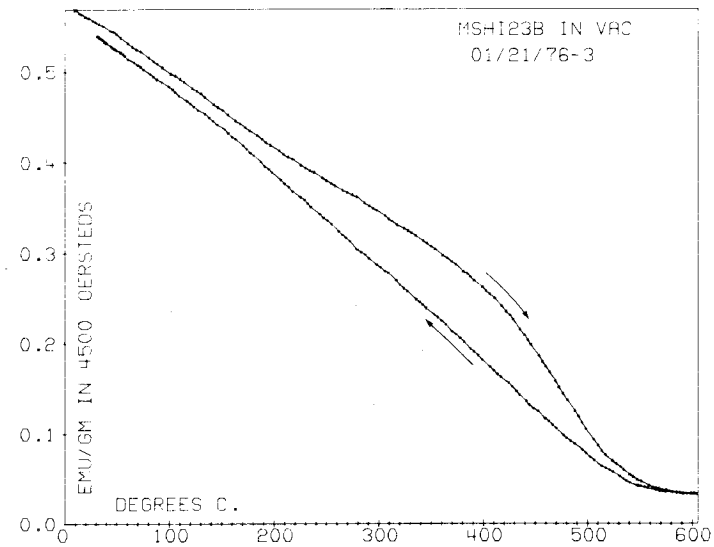
MSHI23B IN VAC
01/21/76-3
EMU/GM IN 4500 OERSTEDS
DEGREES C.
0.5
0.4
0.3
0.2
0.1
0.0
0
100
200
300
400
500
600

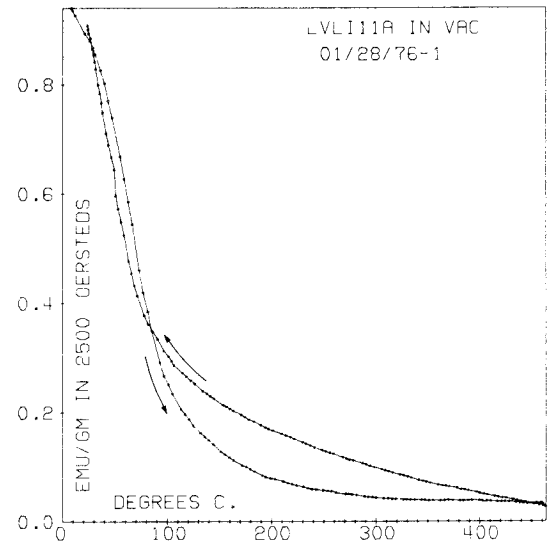
LVLI11A IN VAC
01/28/76-1
EMU/GM IN 2500 OERSTEDS
DEGREES C.
0.0
0.2
0.4
0.6
0.8
0
100
200
300
400

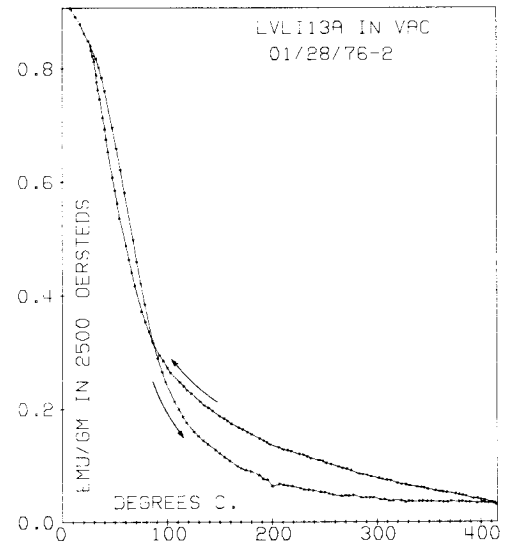
LVLI13A IN VAC
01/28/76-2
EMU/GM IN 2500 OERSTEDS
DEGREES C.
0.0
0.2
0.4
0.6
0.8
0
100
200
300
400

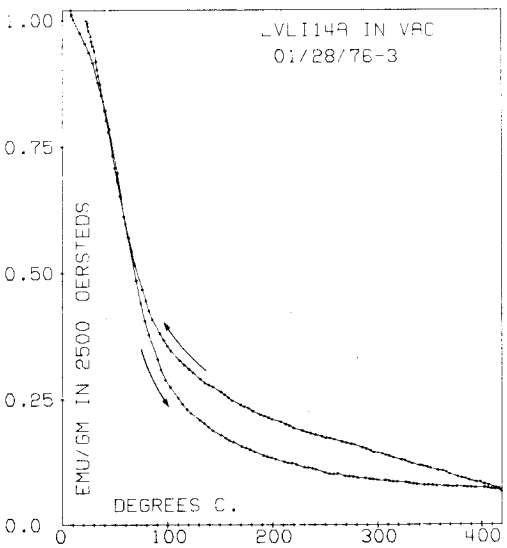
LVLI14A IN VAC
01/28/76-3
EMU/GM IN 2500 OERSTEDS
DEGREES C.
0.0
0.25
0.50
0.75
1.00
0
100
200
300
400

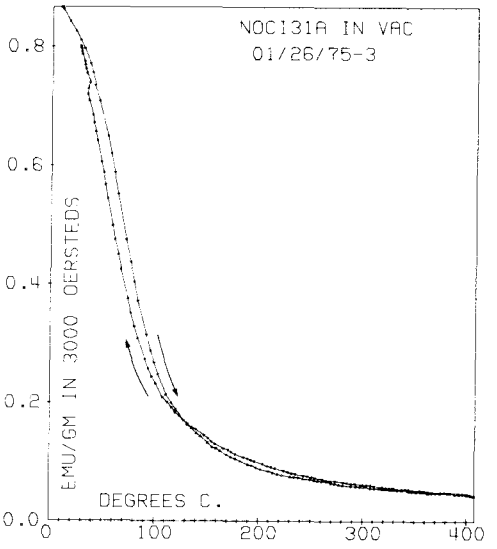
NOC131A IN VAC
01/26/75-3
EMU/GM IN 3000 OERSTEDS
DEGREES C.
0.0
0.2
0.4
0.6
0.8
0
100
200
300
400

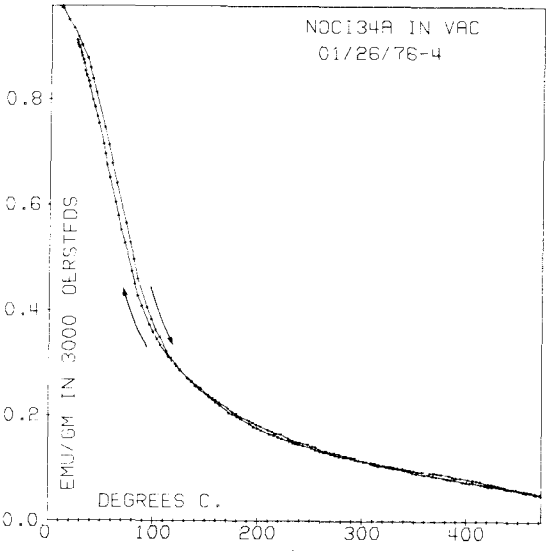
NOC134A IN VAC
01/26/76-4
EMU/GM IN 3000 OERSTEDS
DEGREES C.
0.0
0.2
0.4
0.6
0.8
0
100
200
300
400

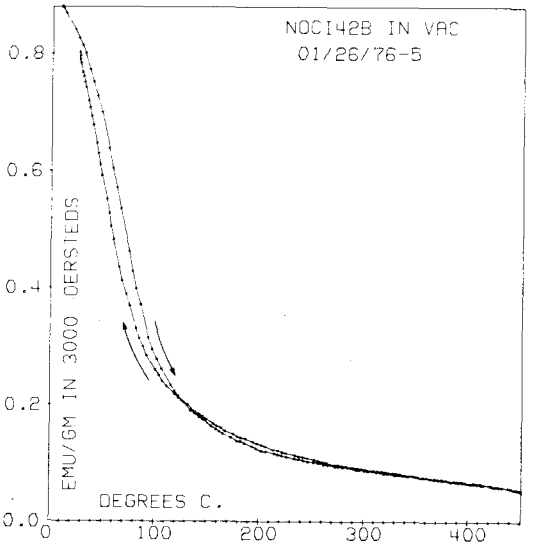
NOC142B IN VAC
01/26/76-5
EMU/GM IN 3000 OERSTEDS
DEGREES C.
0.0
0.2
0.4
0.6
0.8
0
100
200
300
400

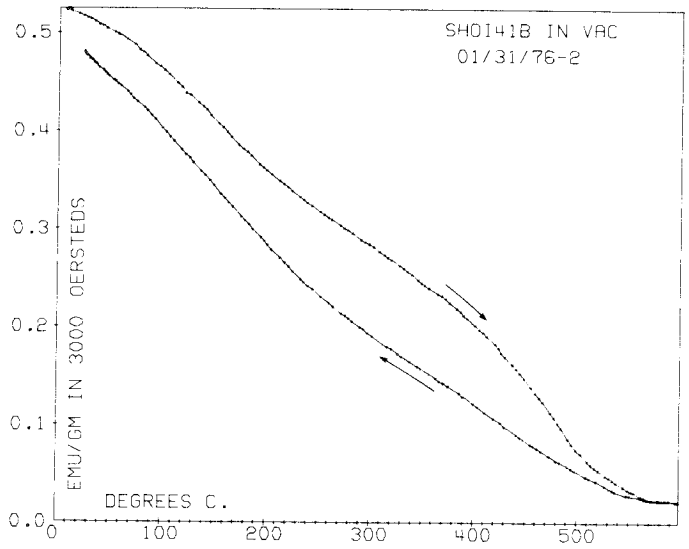
SHOI41B IN VAC
01/31/76-2
EMU/GM IN 3000 OERSTEDS
DEGREES C.
0.0
0.1
0.2
0.3
0.4
0.5
0
100
200
300
400
500

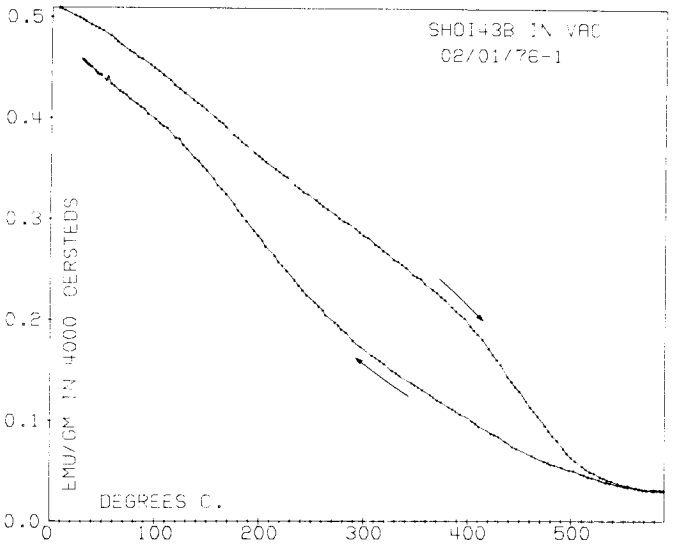
SHOI43B IN VAC
02/01/76-1
EMU/GM IN 4000 OERSTEDS
DEGREES C.
0.0
0.1
0.2
0.3
0.4
0.5
0
100
200
300
400
500

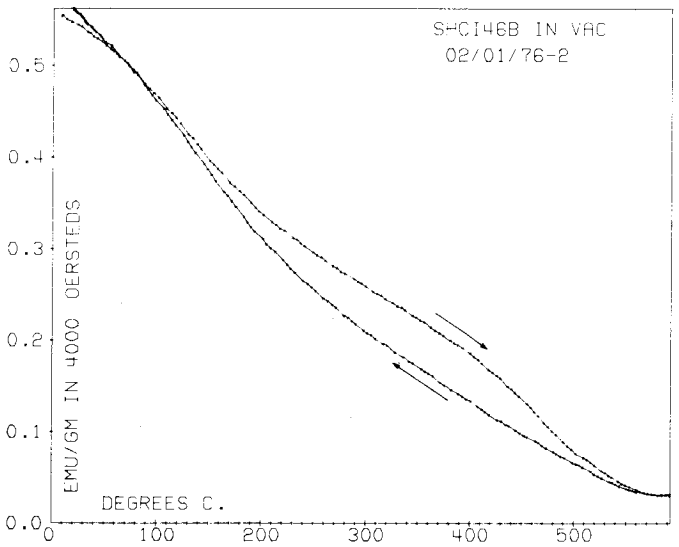
SHCI46B IN VAC
02/01/76-2
EMU/GM IN 4000 OERSTEDS
DEGREES C.
0.0
0.1
0.2
0.3
0.4
0.5
0
100
200
300
400
500

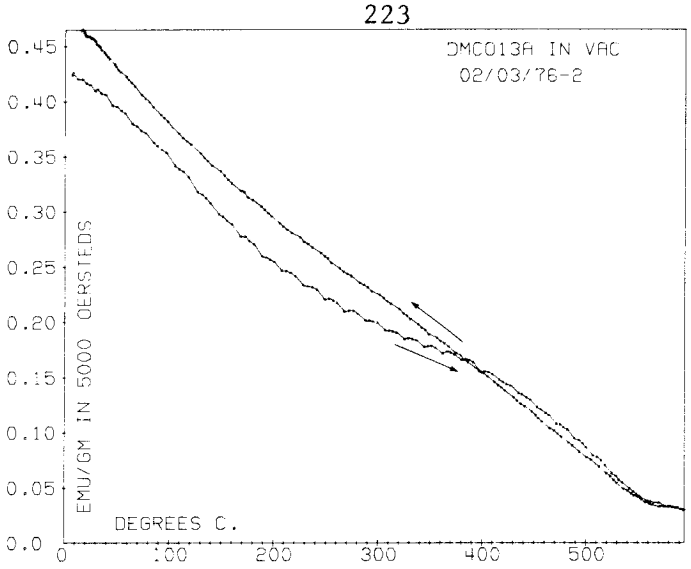
DMC013A IN VAC
02/03/76-2
EMU/GM IN 5000 OERSTEDS
DEGREES C.
0.45
0.40
0.35
0.30
0.25
0.20
0.15
0.10
0.05
0.0
0
100
200
300
400
500

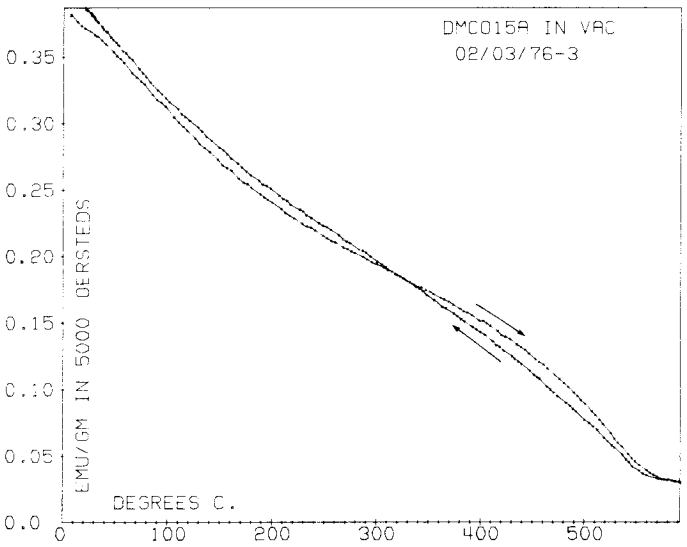
DMC015A IN VAC
02/03/76-3
EMU/GM IN 5000 OERSTEDS
DEGREES C.
0.35
0.30
0.25
0.20
0.15
0.10
0.05
0.0
0
100
200
300
400
500

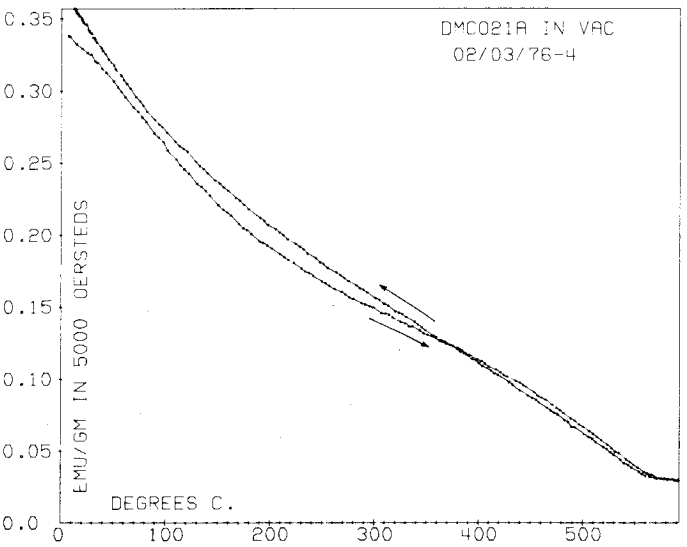
DMC021A IN VAC
02/03/76-4
EMU/GM IN 5000 OERSTEDS
DEGREES C.
0.35
0.30
0.25
0.20
0.15
0.10
0.05
0.0
0
100
200
300
400
500

Appendix 3

Normalized Comparisons between Remanence and Strong Field Magnetization Records

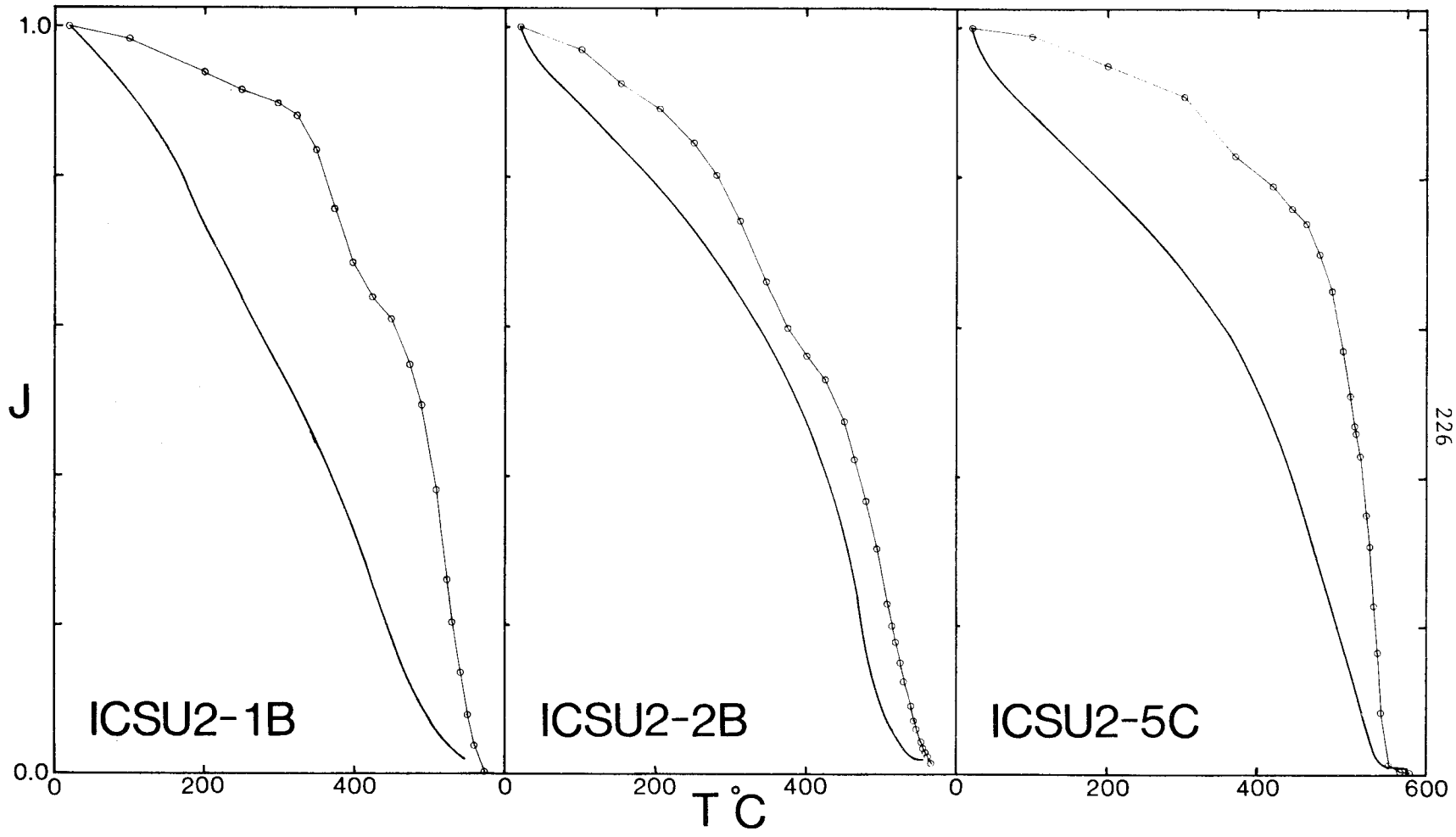
1.0
0.0
J
ICSU2-1B
ICSU2-2B
ICSU2-5C
0
200
400
0
200
400
0
200
400
600
T °C

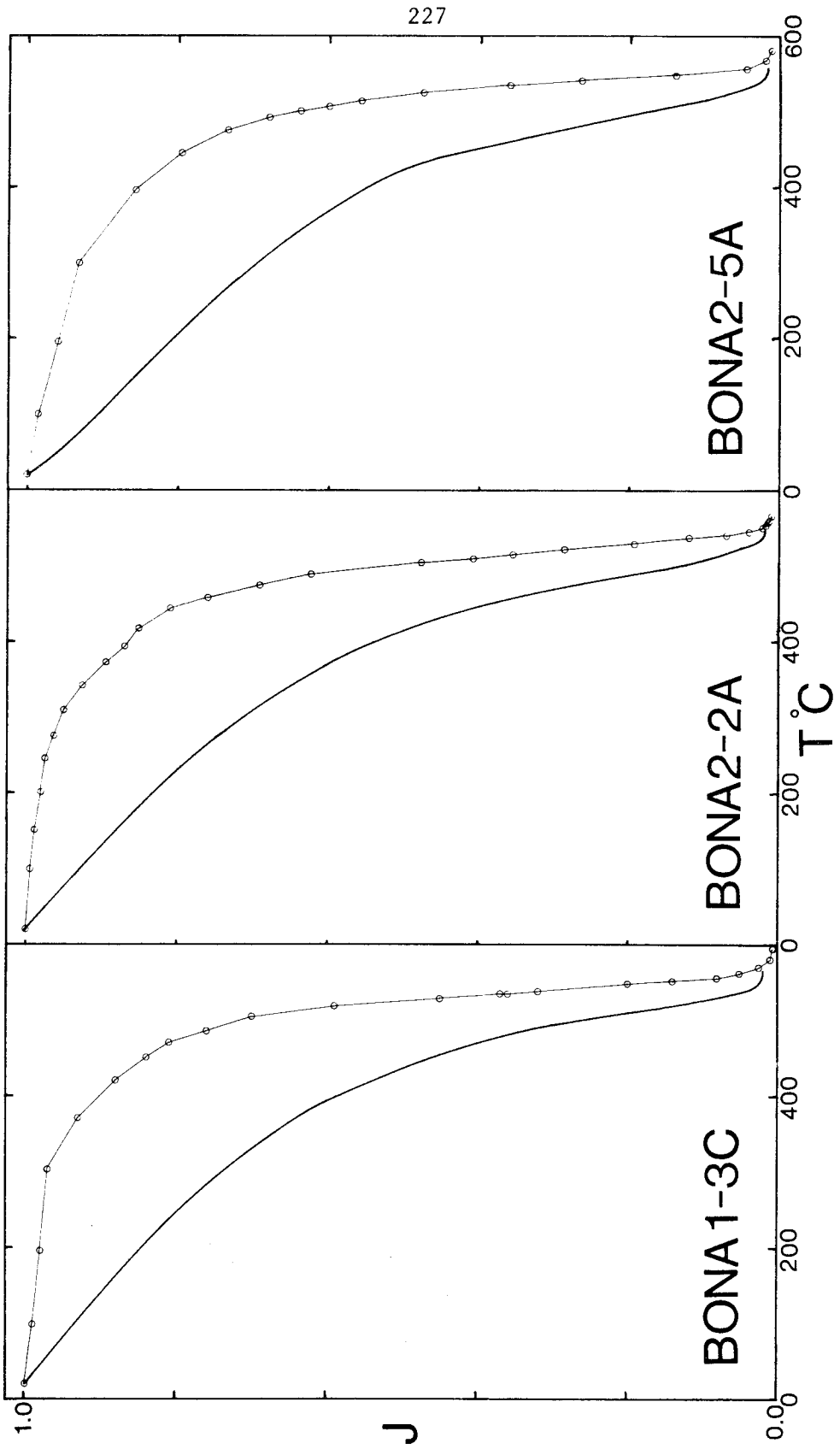
BONA1-3C
BONA2-2A
BONA2-5A
J
T°C
1.0
0.0
0
200
400
600

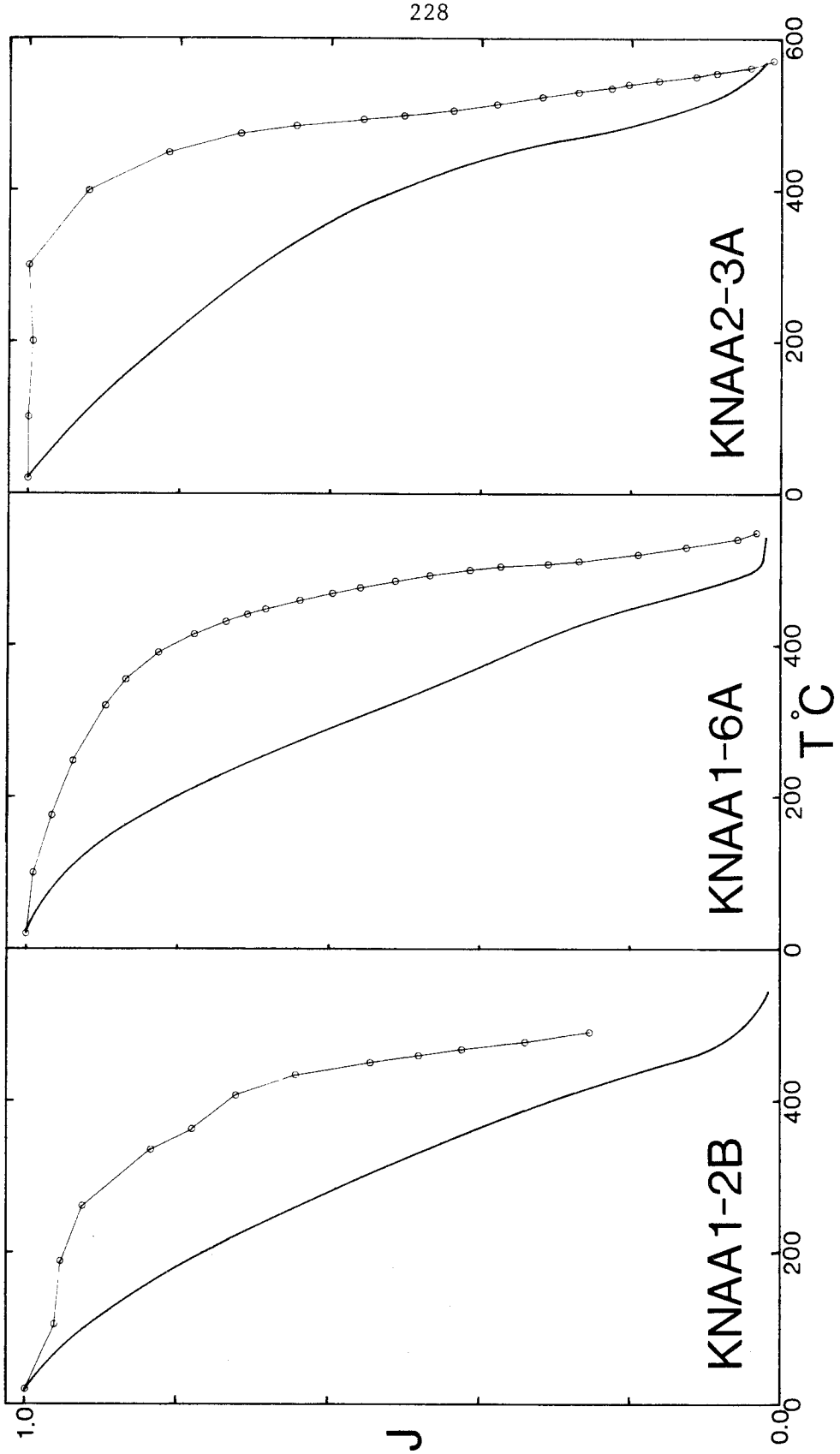
KNAA1-2B
KNAA1-6A
KNAA2-3A
J
T°C
1.0
0.0
0
200
400
600

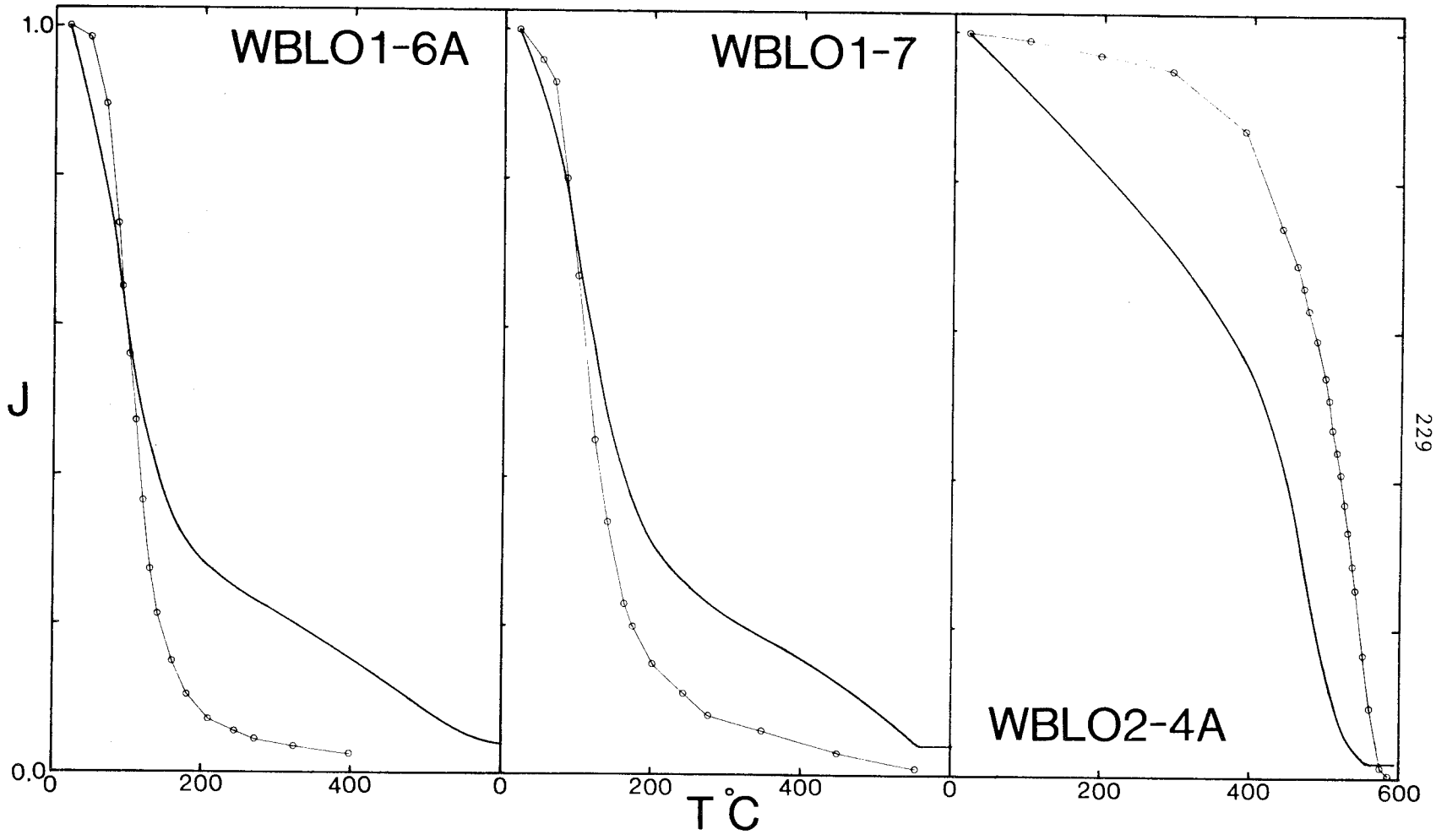
WBLO1-6A
WBLO1-7
WBLO2-4A
J
1.0
0.0
0
200
400
0
200
400
0
200
400
600
T°C

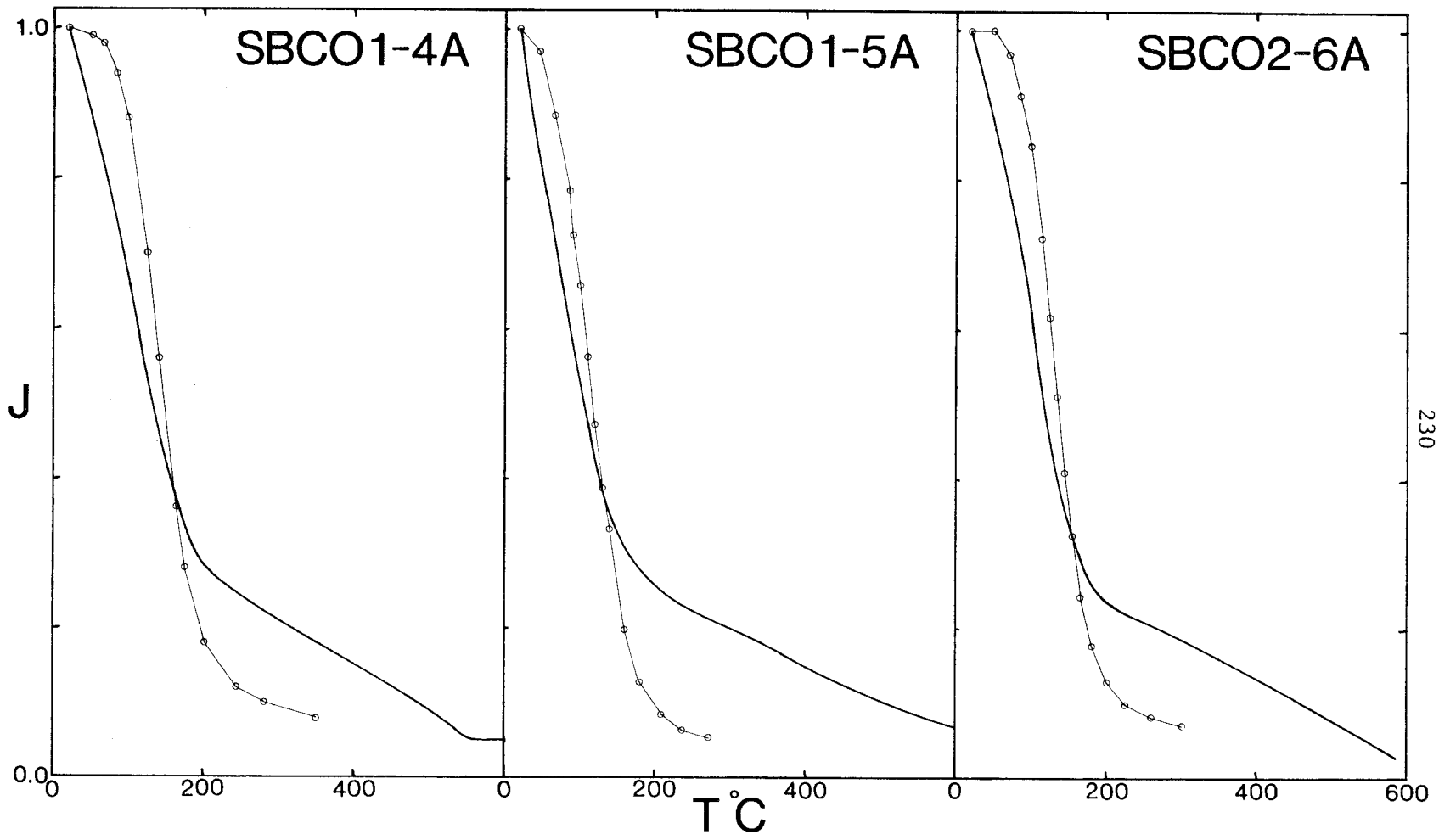
SBCO1-4A
SBCO1-5A
SBCO2-6A
1.0
0.0
J
0
200
400
0
200
400
0
200
400
600
T °C

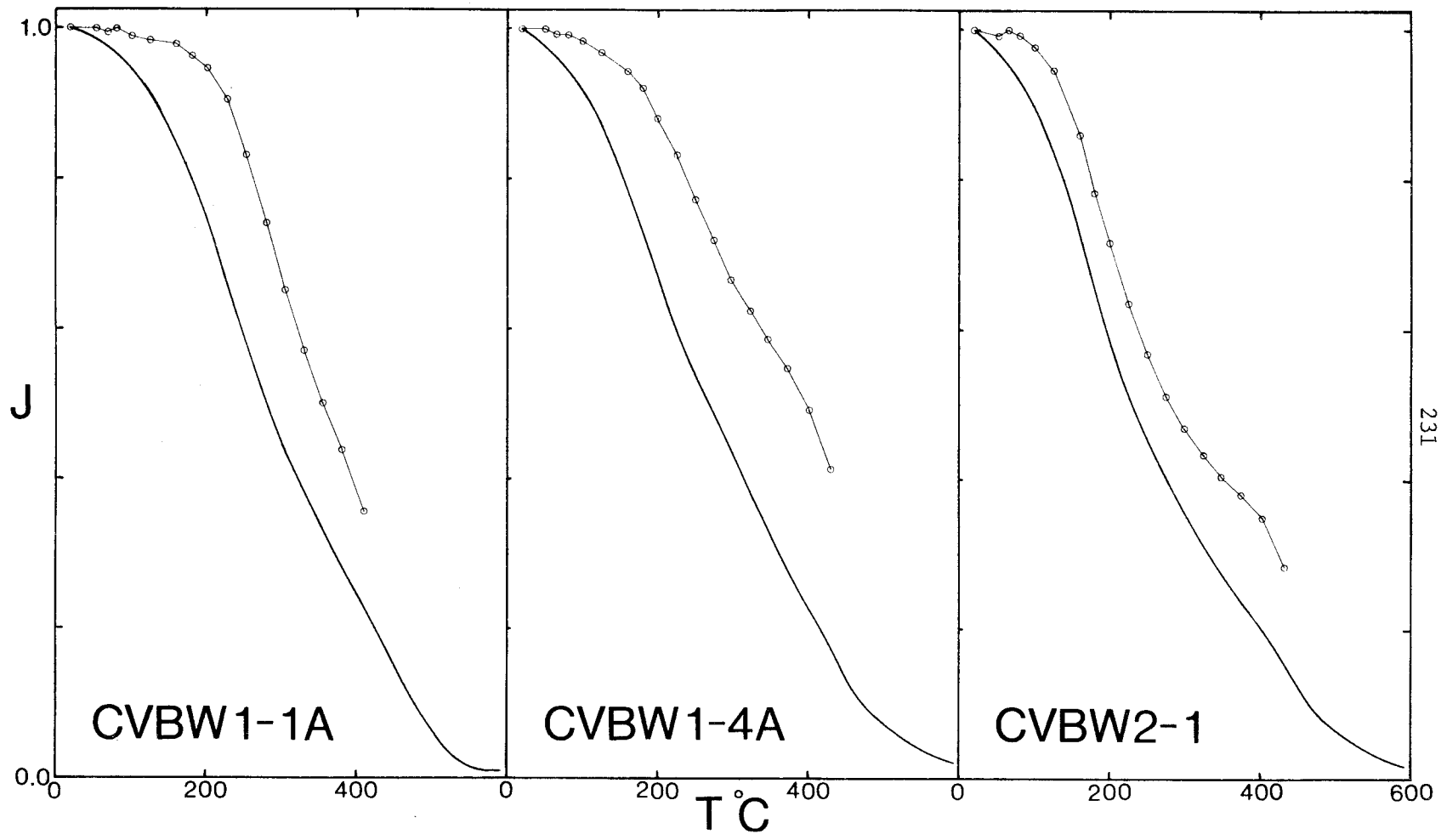
1.0
0.0
J
CVBW1-1A
CVBW1-4A
CVBW2-1
0
200
400
0
200
400
0
200
400
600
T °C

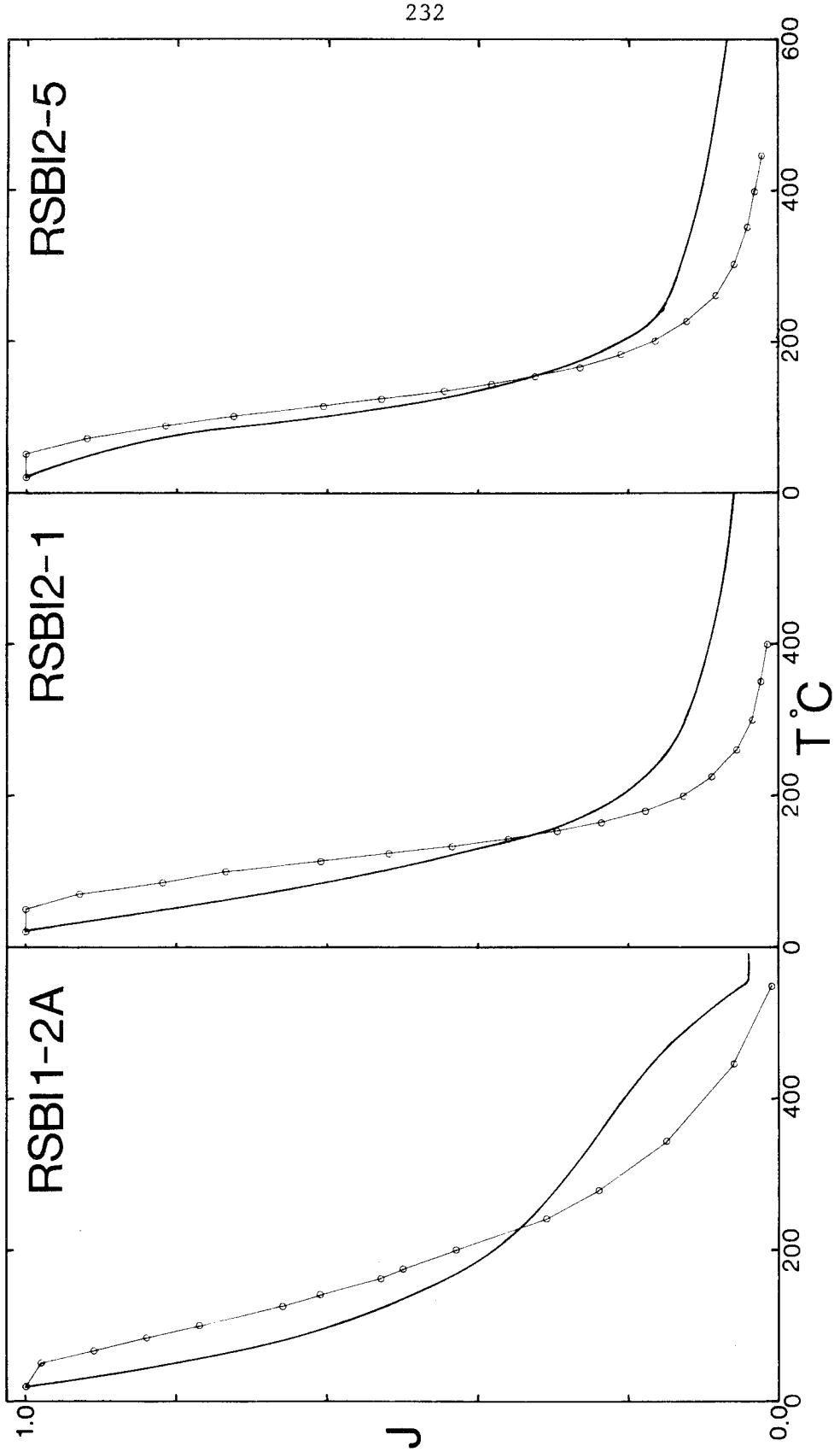
RSBI1-2A
RSBI2-1
RSBI2-5
J
T°C
1.0
0.0
0
200
400
600

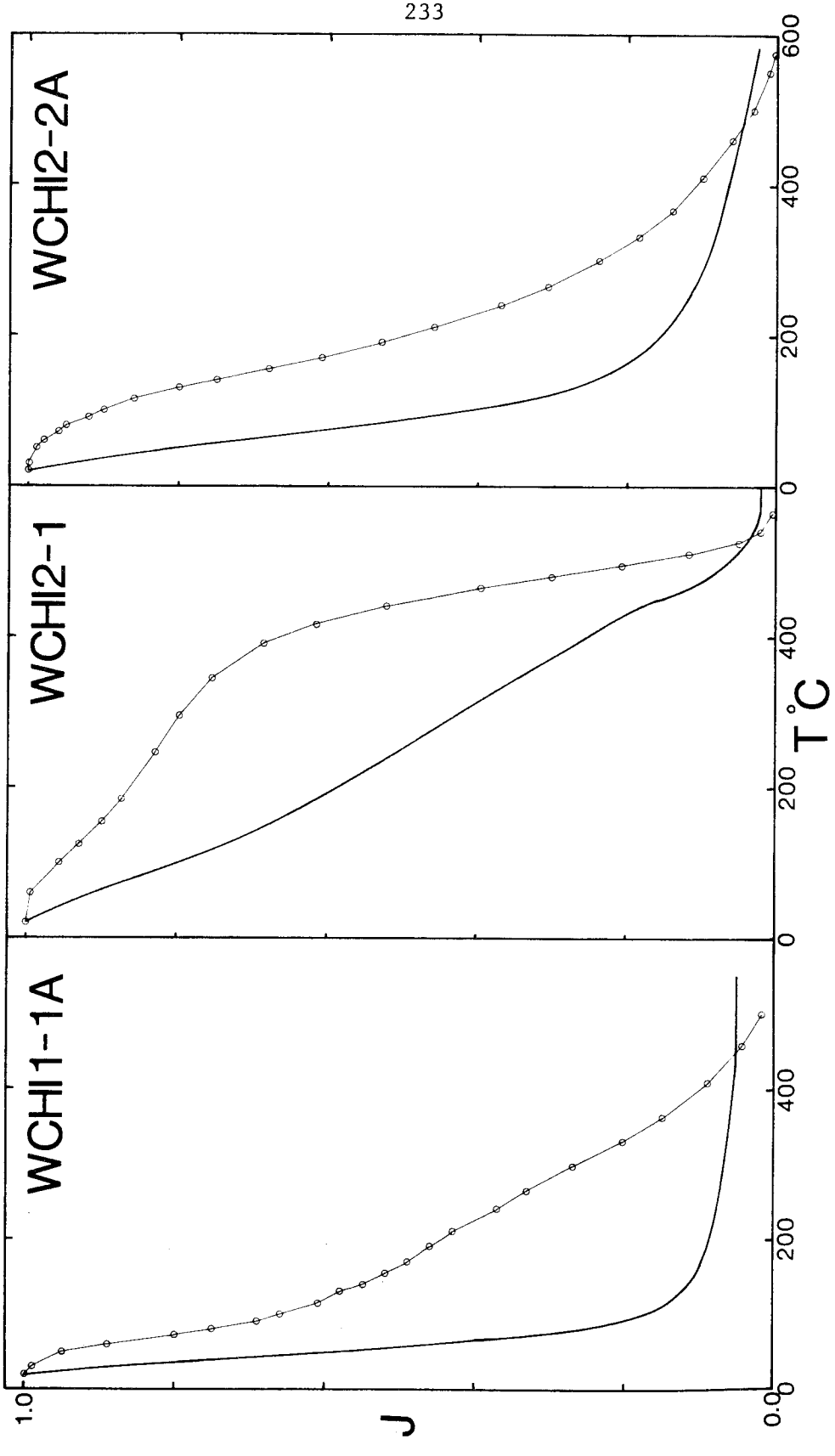
WCHI1-1A
WCHI2-1
WCHI2-2A
J
T °C
1.0
0.0
0
200
400
600

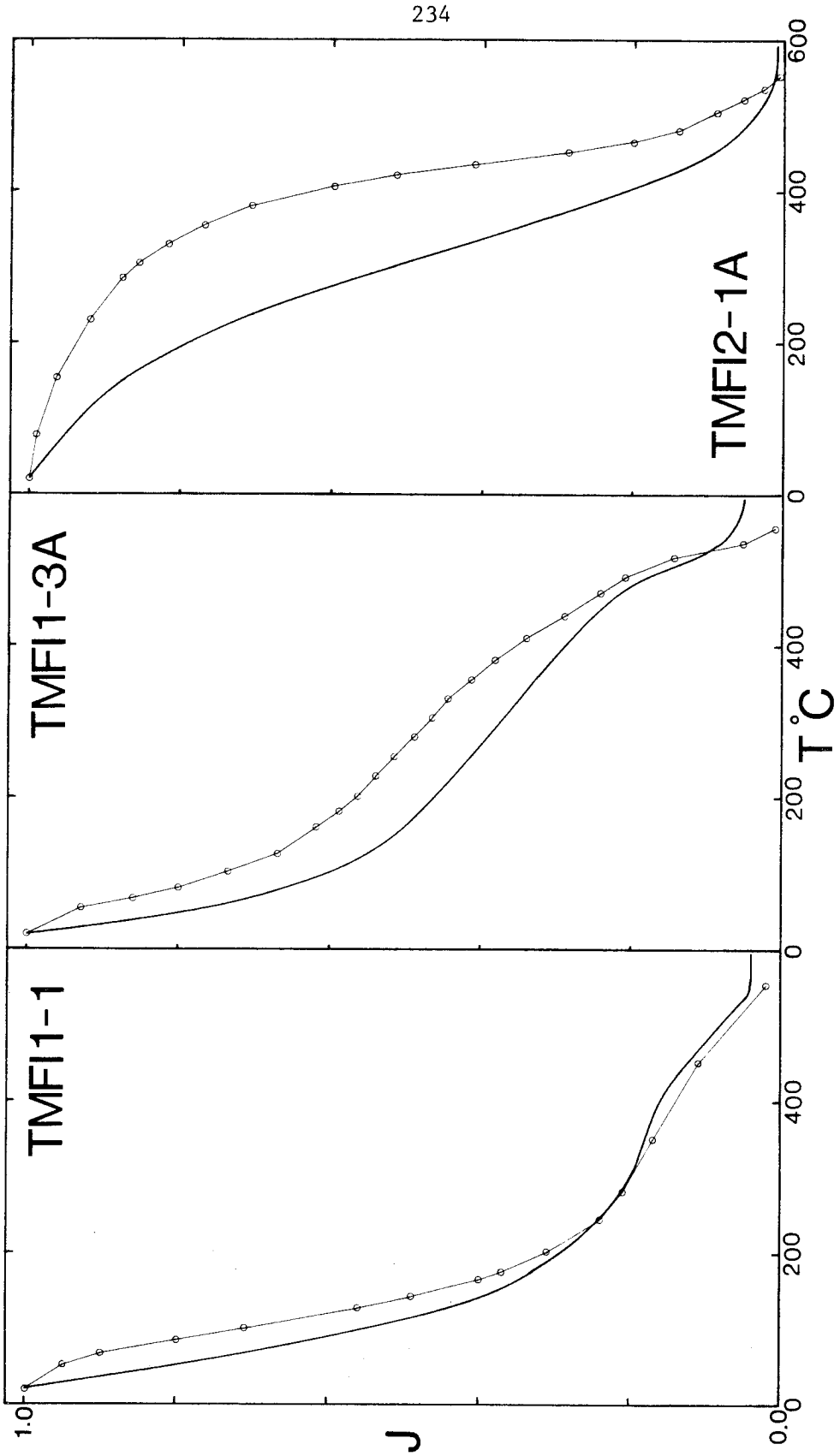
TMFI1-1
TMFI1-3A
TMFI2-1A
J
T °C
1.0
0.0
0
200
400
600

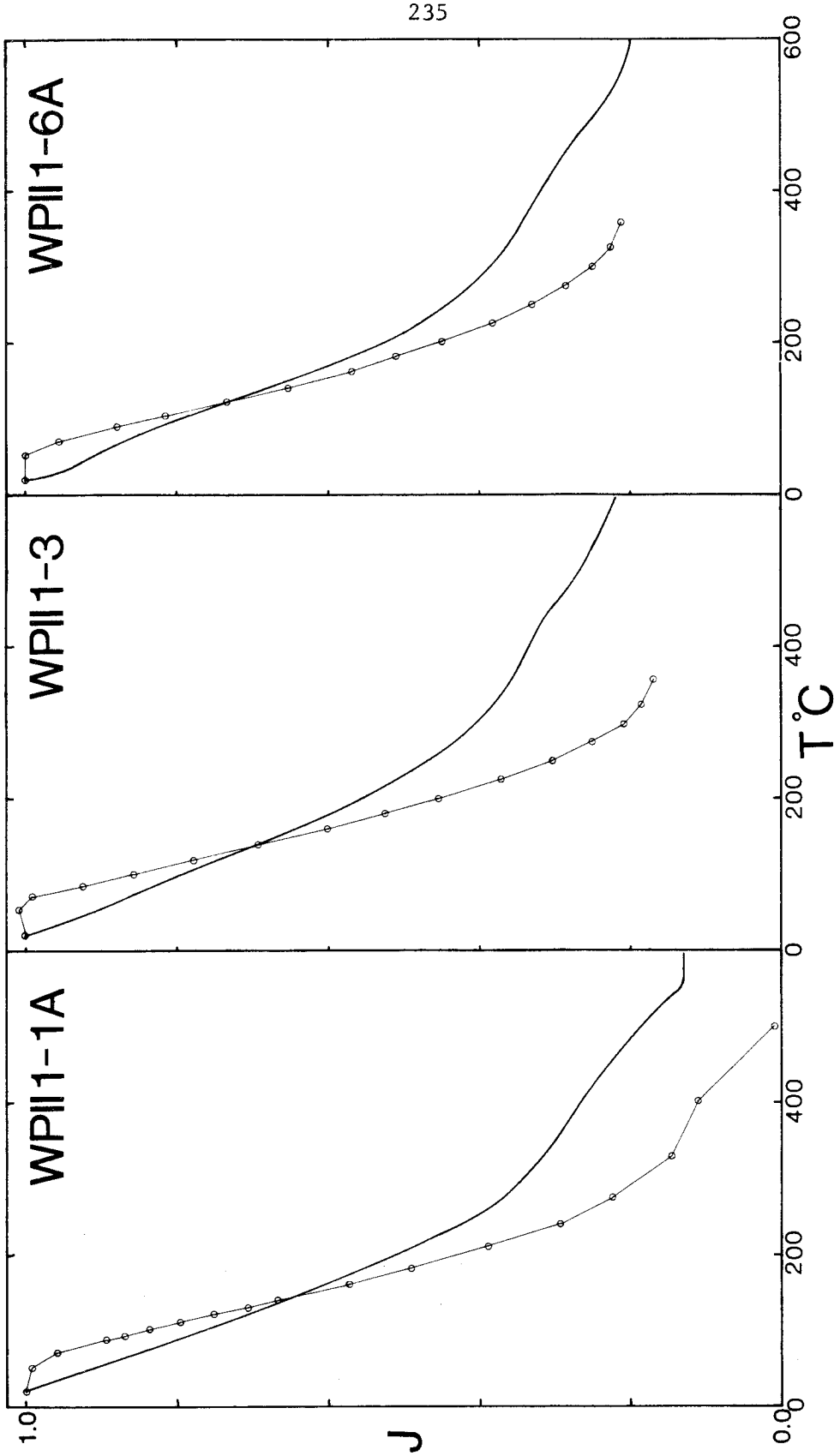
WPII1-1A
WPII1-3
WPII1-6A
J
T°C
1.0
0.0
0
200
400
600

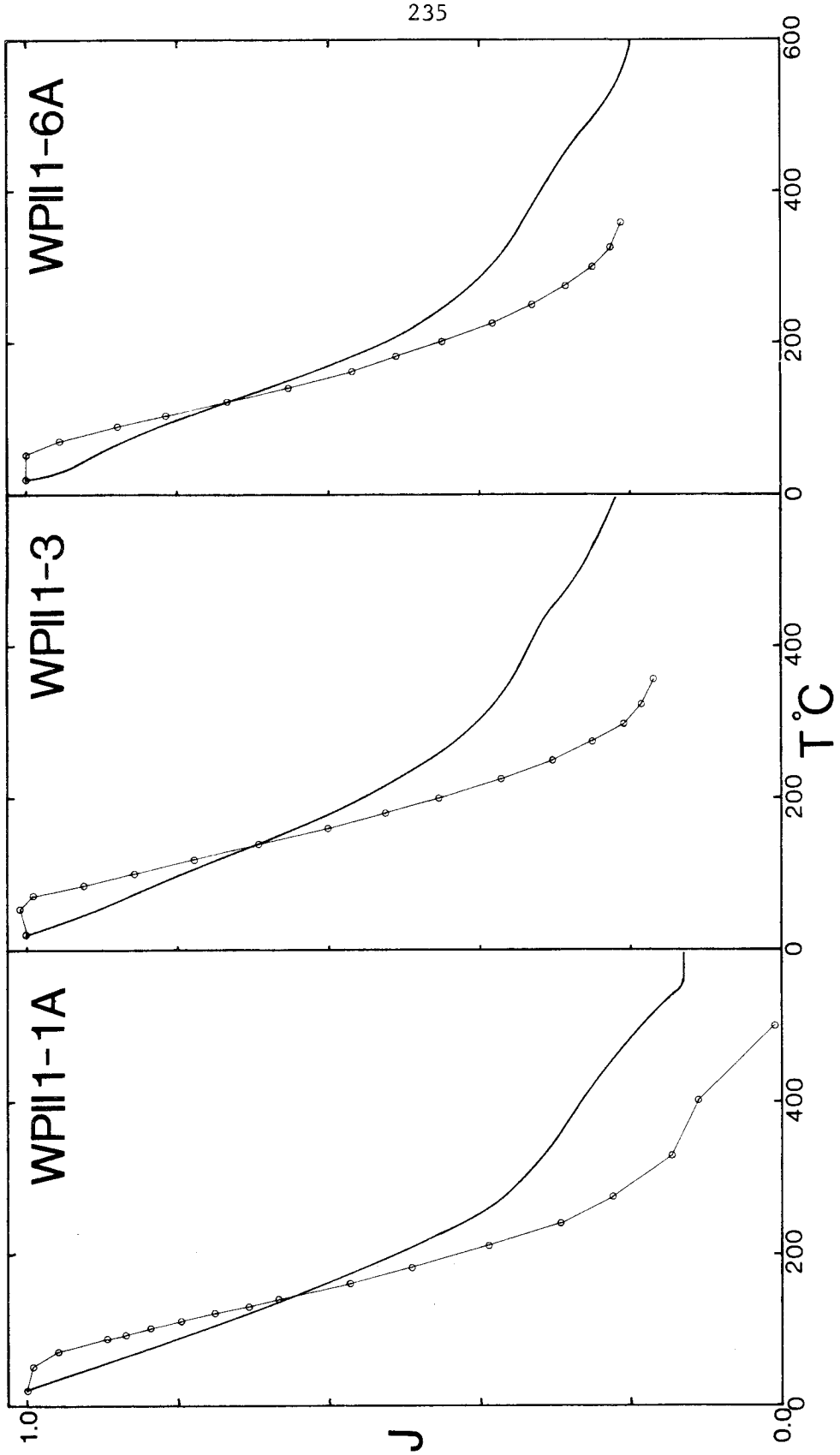
WPII1-1A
WPII1-3
WPII1-6A
J
T°C
1.0
0.0
0
200
400
600

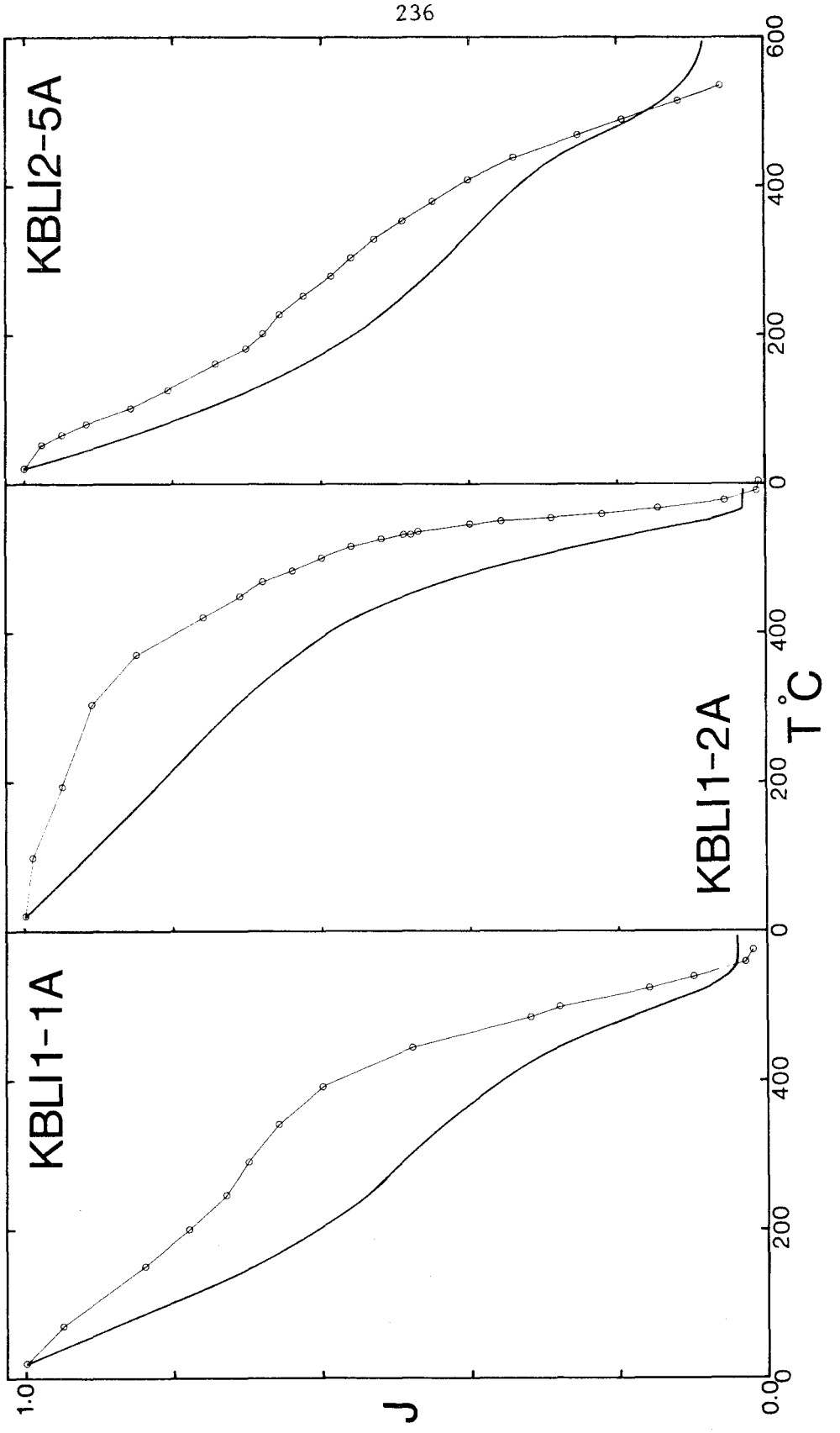
KBLI1-1A
KBLI1-2A
KBLI2-5A
J
T °C
1.0
0.0
0
200
400
600

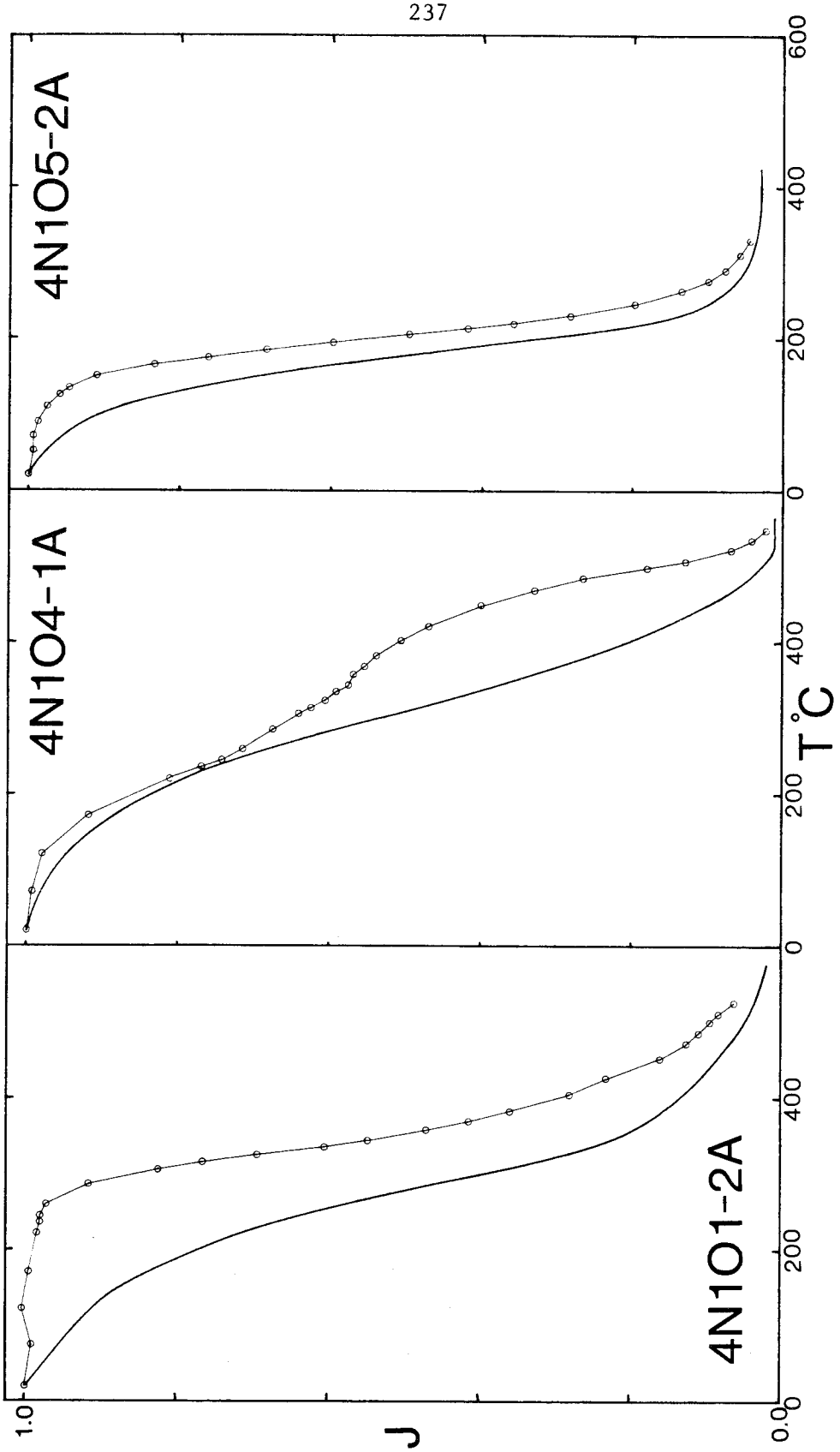
4N1O5-2A
4N1O4-1A
4N1O1-2A
J
T°C
1.0
0.0
0
200
400
600

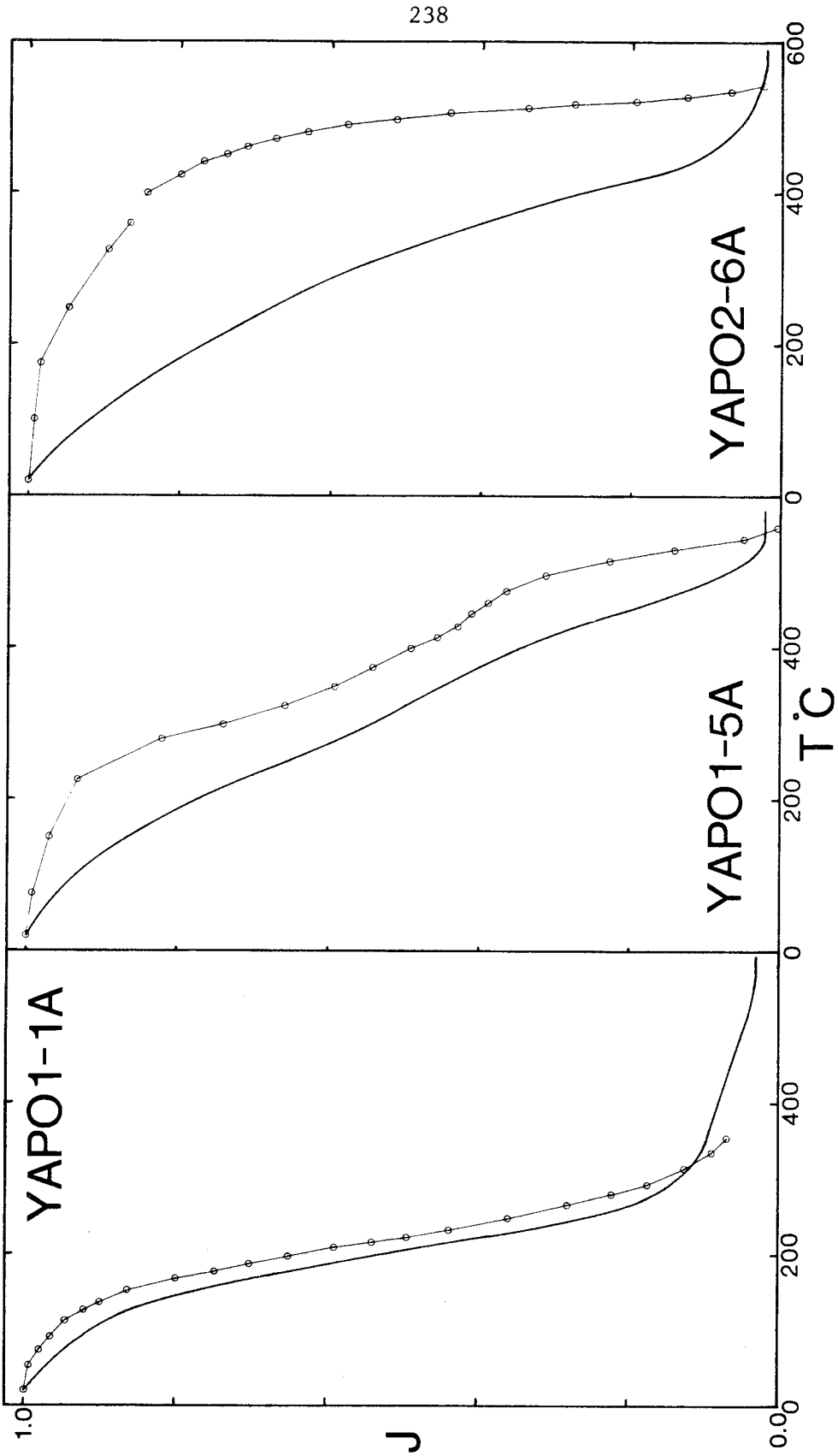
YAPO1-1A
YAPO1-5A
YAPO2-6A
J
T°C
1.0
0.0
0
200
400
600

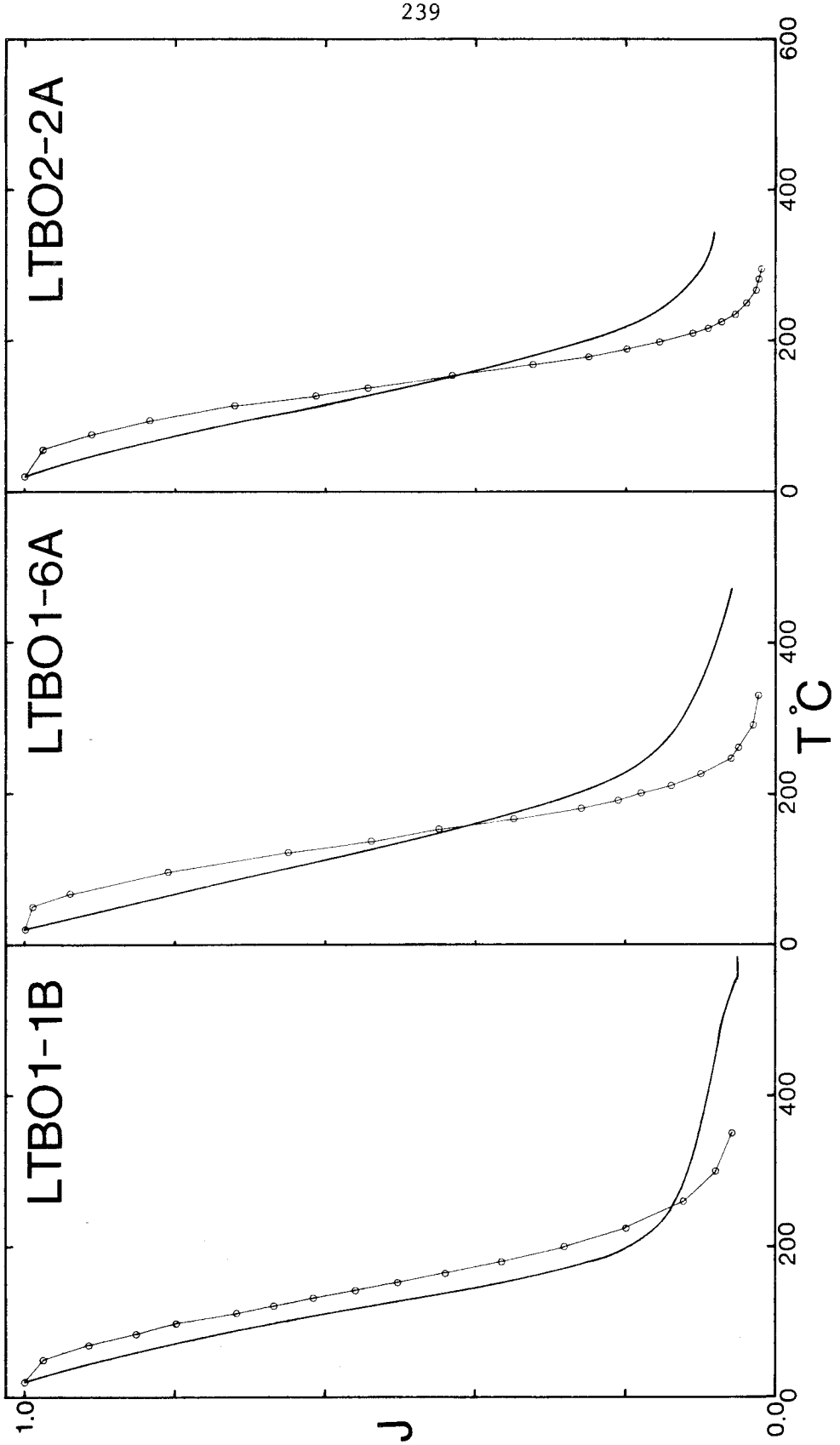
LTBO1-1B
LTBO1-6A
LTBO2-2A
J
T°C
1.0
0.0
0
200
400
600

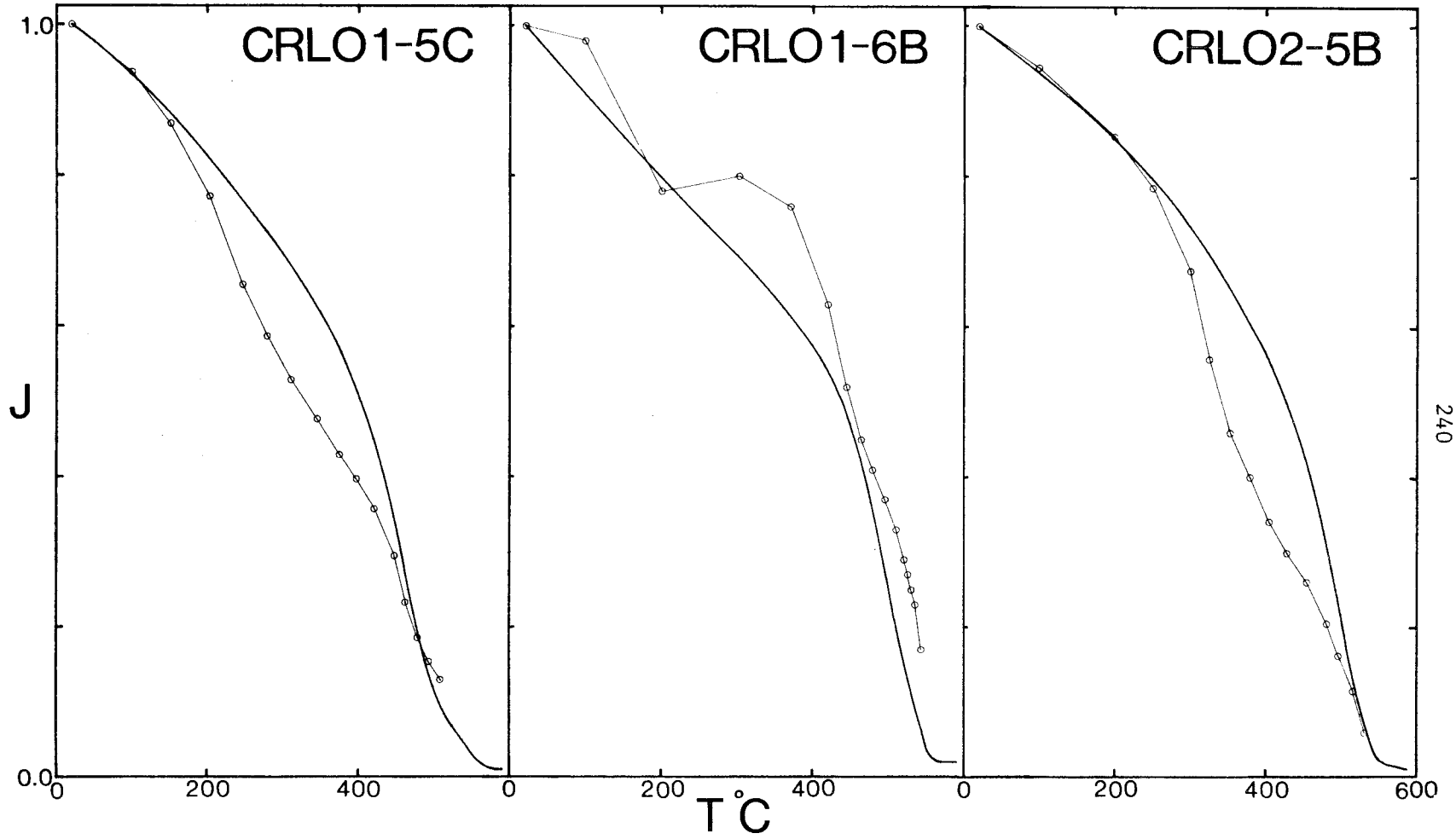
CRLO1-5C
CRLO1-6B
CRLO2-5B
1.0
0.0
J
0
200
400
0
200
400
0
200
400
600
T°C

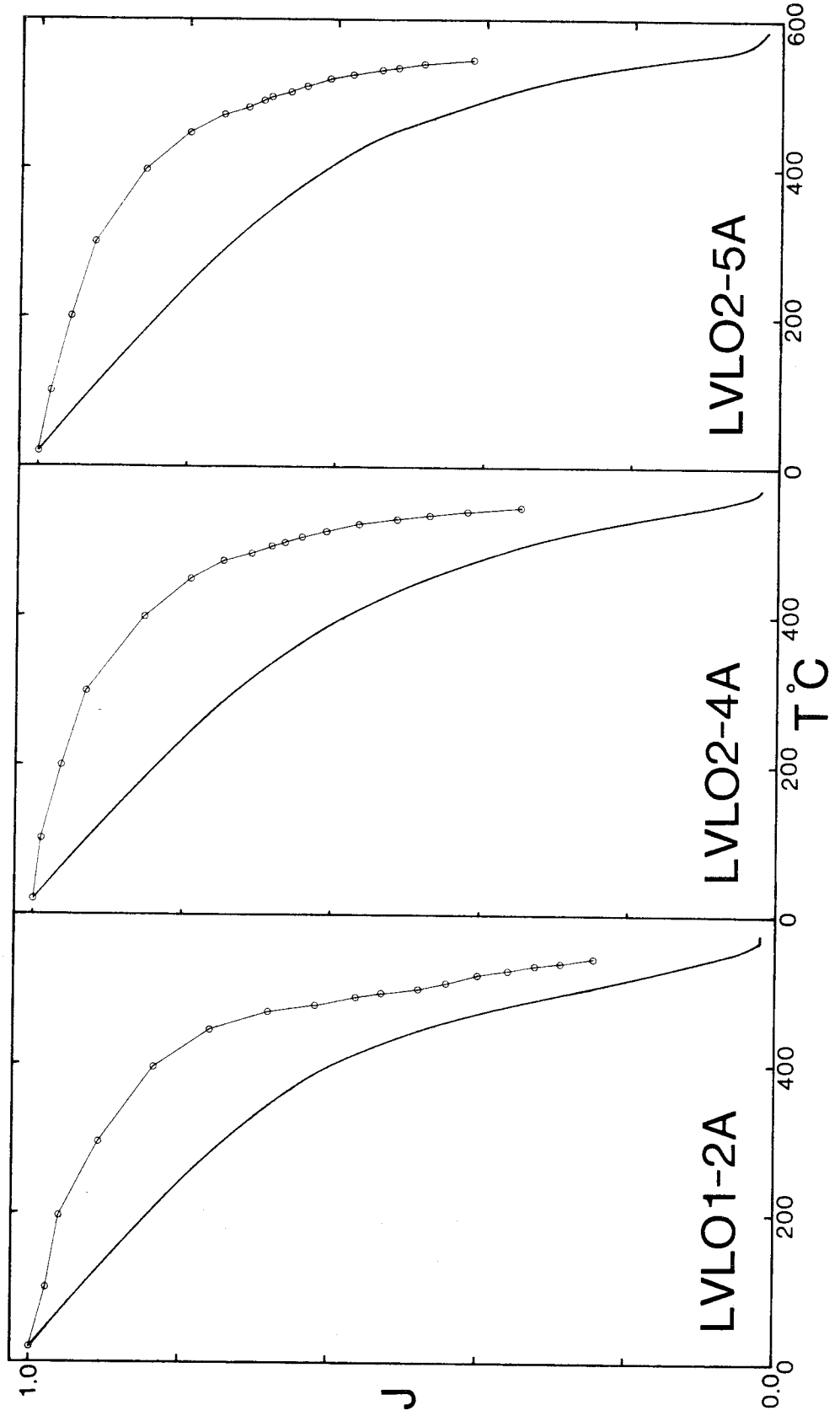
LVLO1-2A
LVLO2-4A
LVLO2-5A
J
T°C
0.0
1.0
0
200
400
600

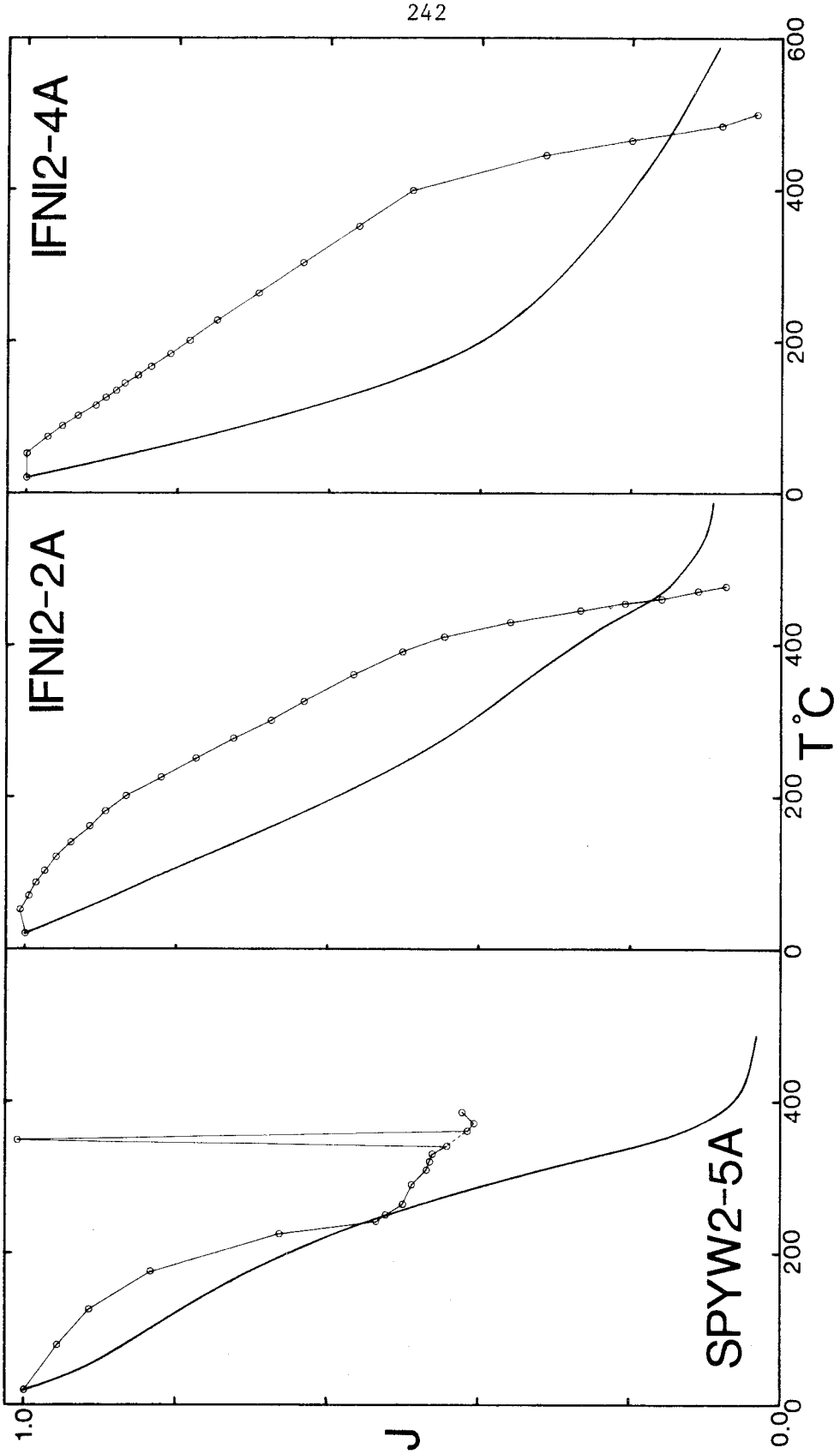
SPYW2-5A
IFNI2-2A
IFNI2-4A
J
T°C
1.0
0.0
0
200
400
600

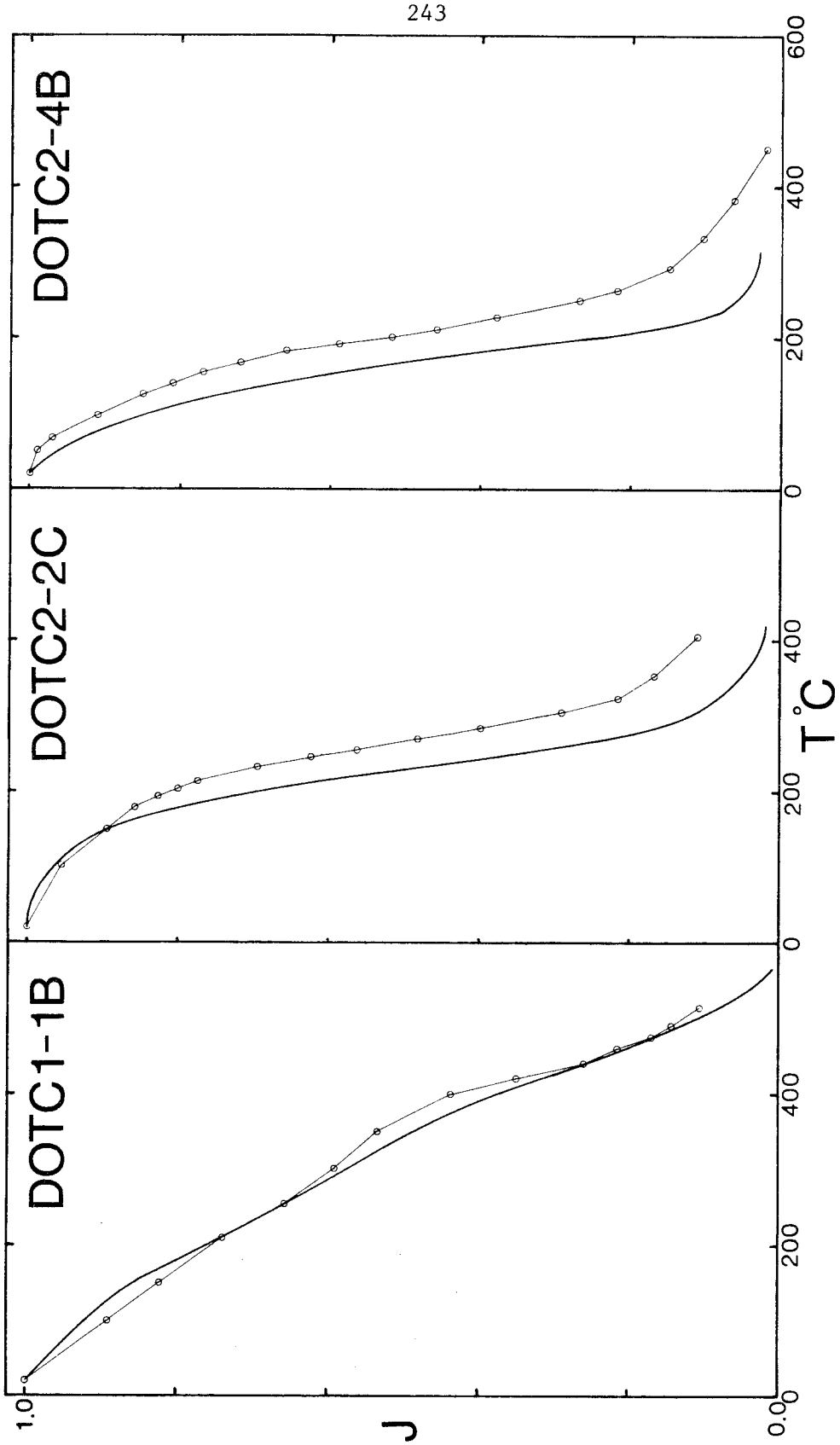
DOTC1-1B
DOTC2-2C
DOTC2-4B
J
1.0
0.0
0
200
400
600
T°C

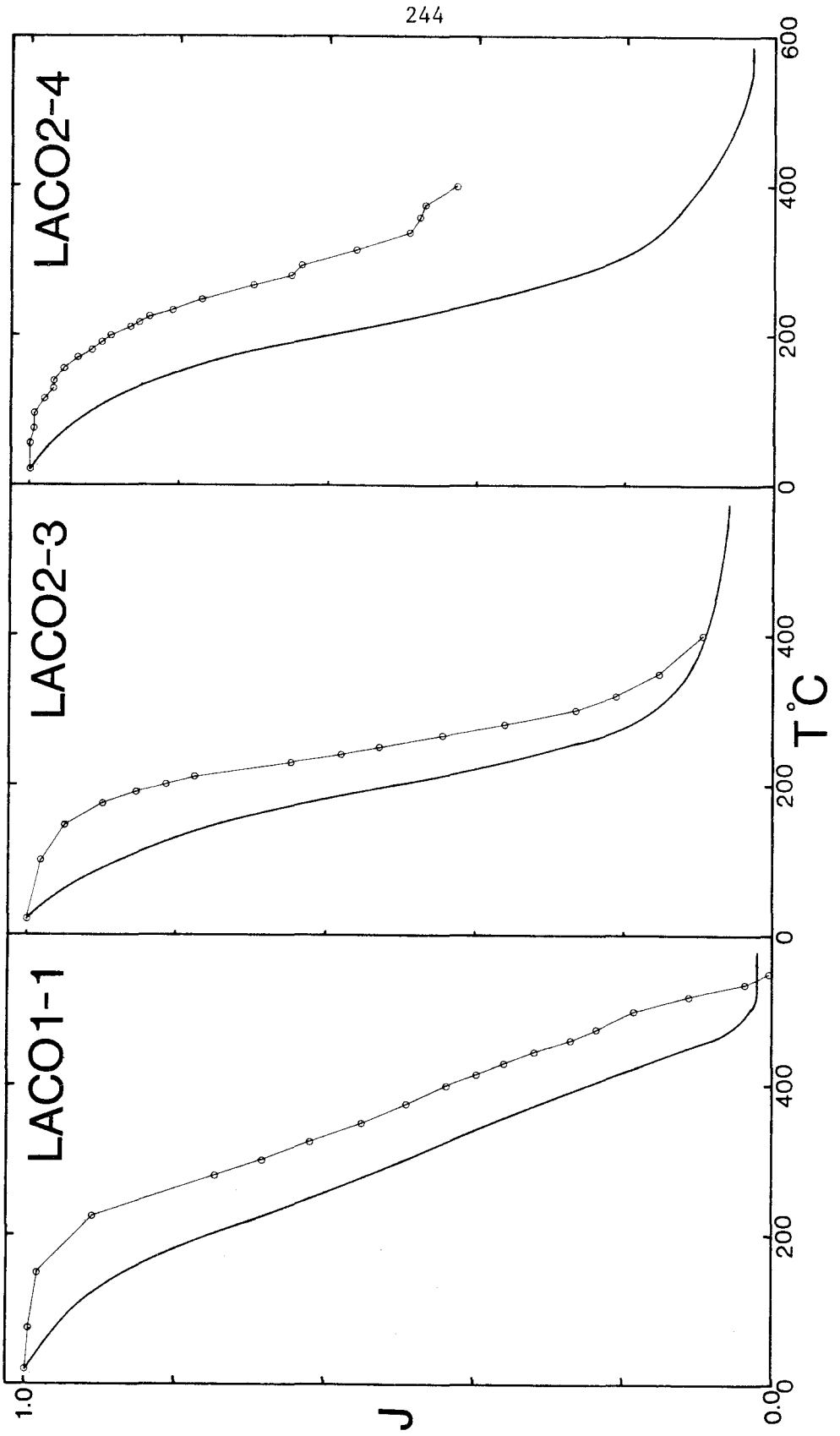
LACO1-1
LACO2-3
LACO2-4
J
T°C
1.0
0.0
0
200
400
600

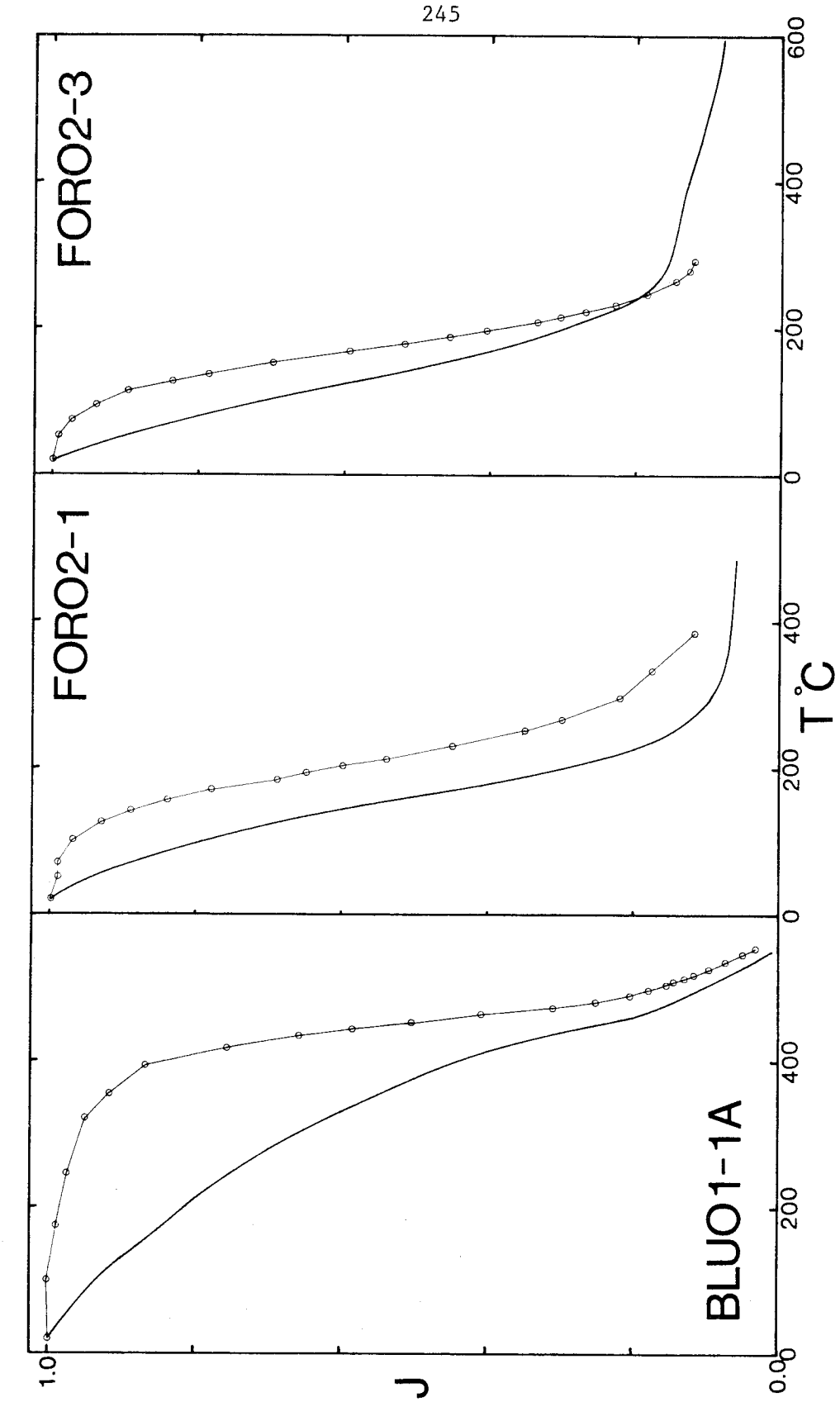
BLUO1-1A
FORO2-1
FORO2-3
J
T°C
1.0
0.0
0
200
400
600

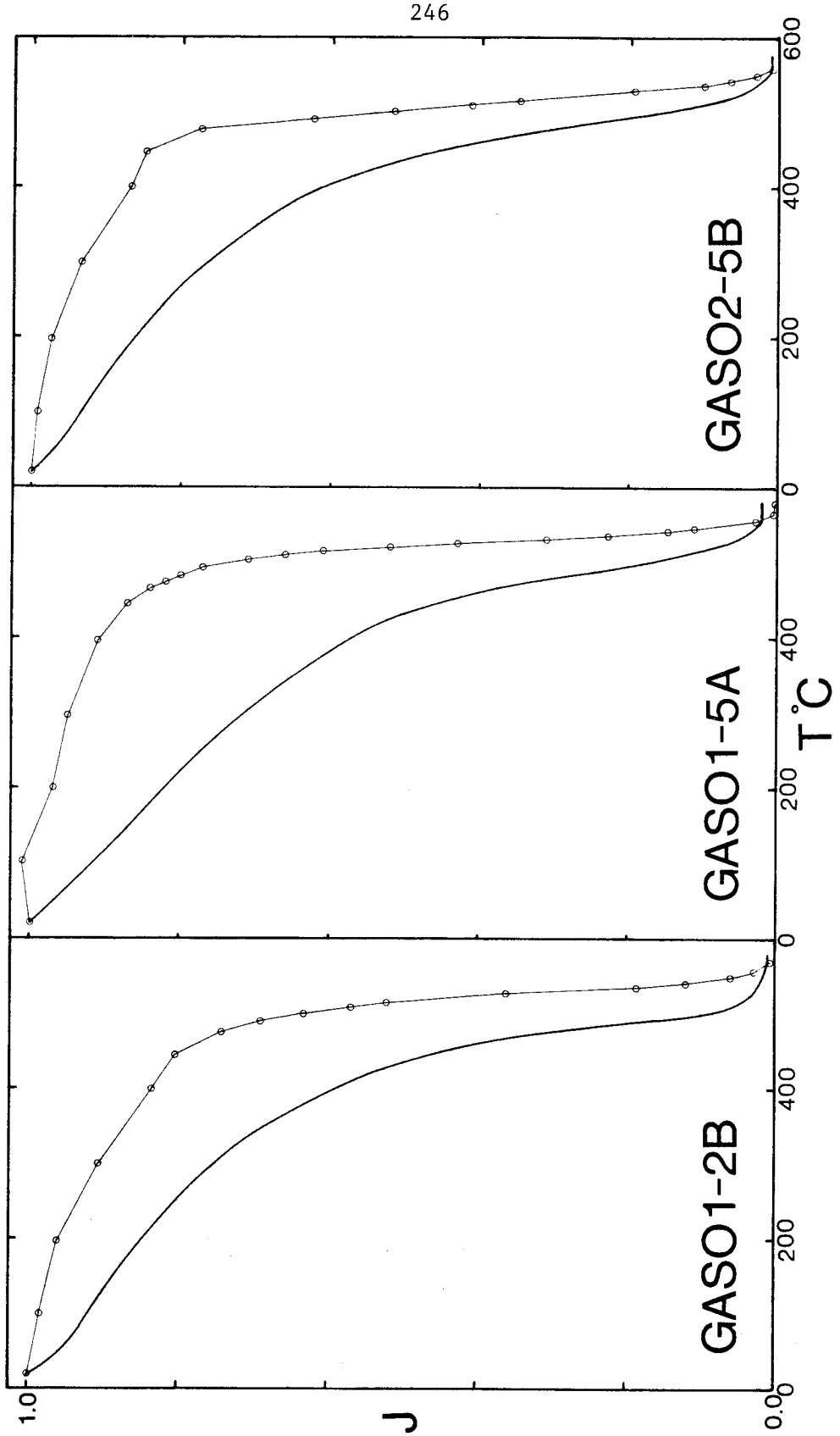
GASO1-2B
GASO1-5A
GASO2-5B
J
1.0
0.0
0
200
400
600
T°C

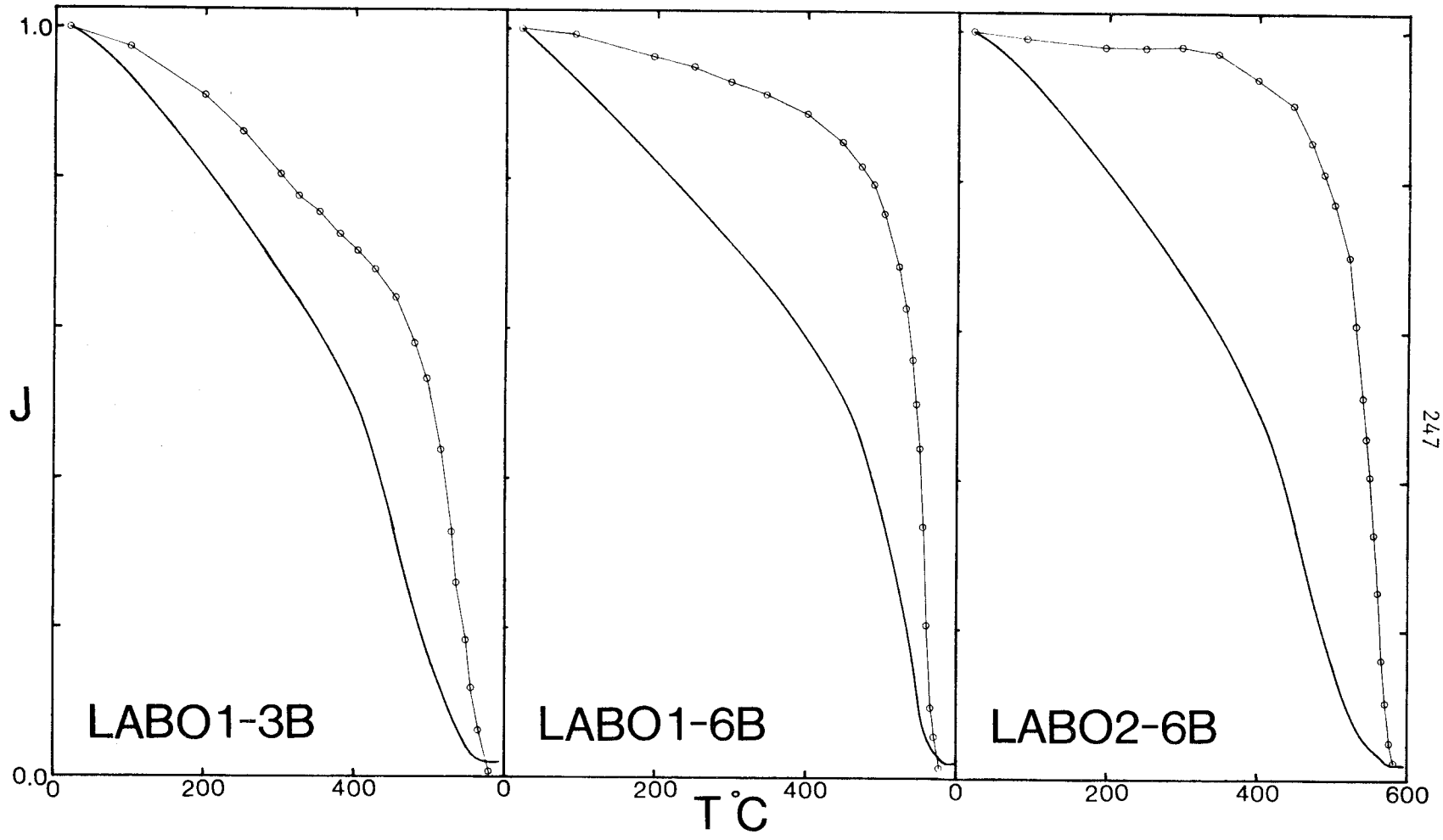
1.0
0.0
J
LABO1-3B
LABO1-6B
LABO2-6B
0
200
400
0
200
400
0
200
400
600
T°C

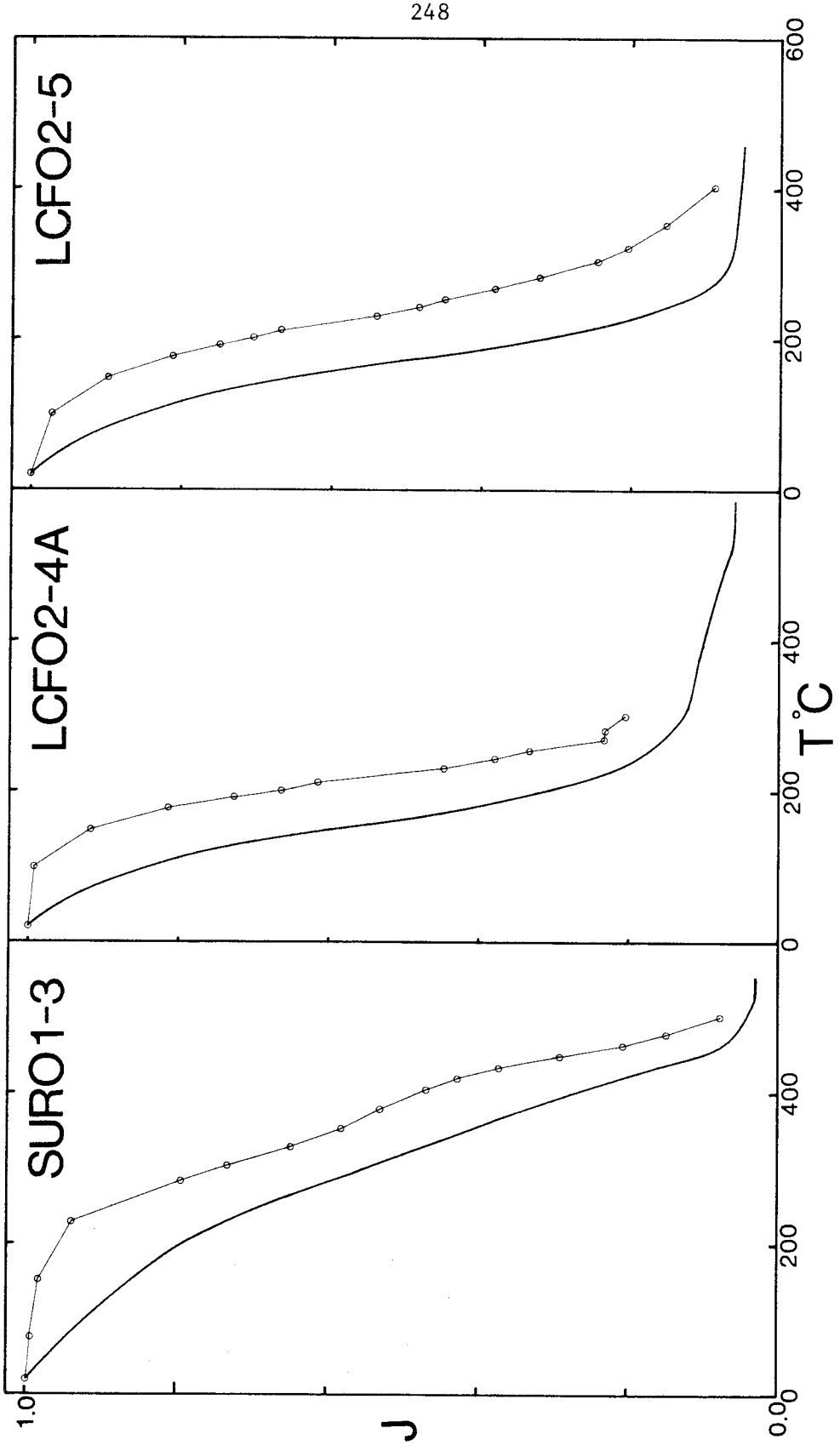
SURO1-3
LCFO2-4A
LCFO2-5
J
T°C
1.0
0.0
0
200
400
600

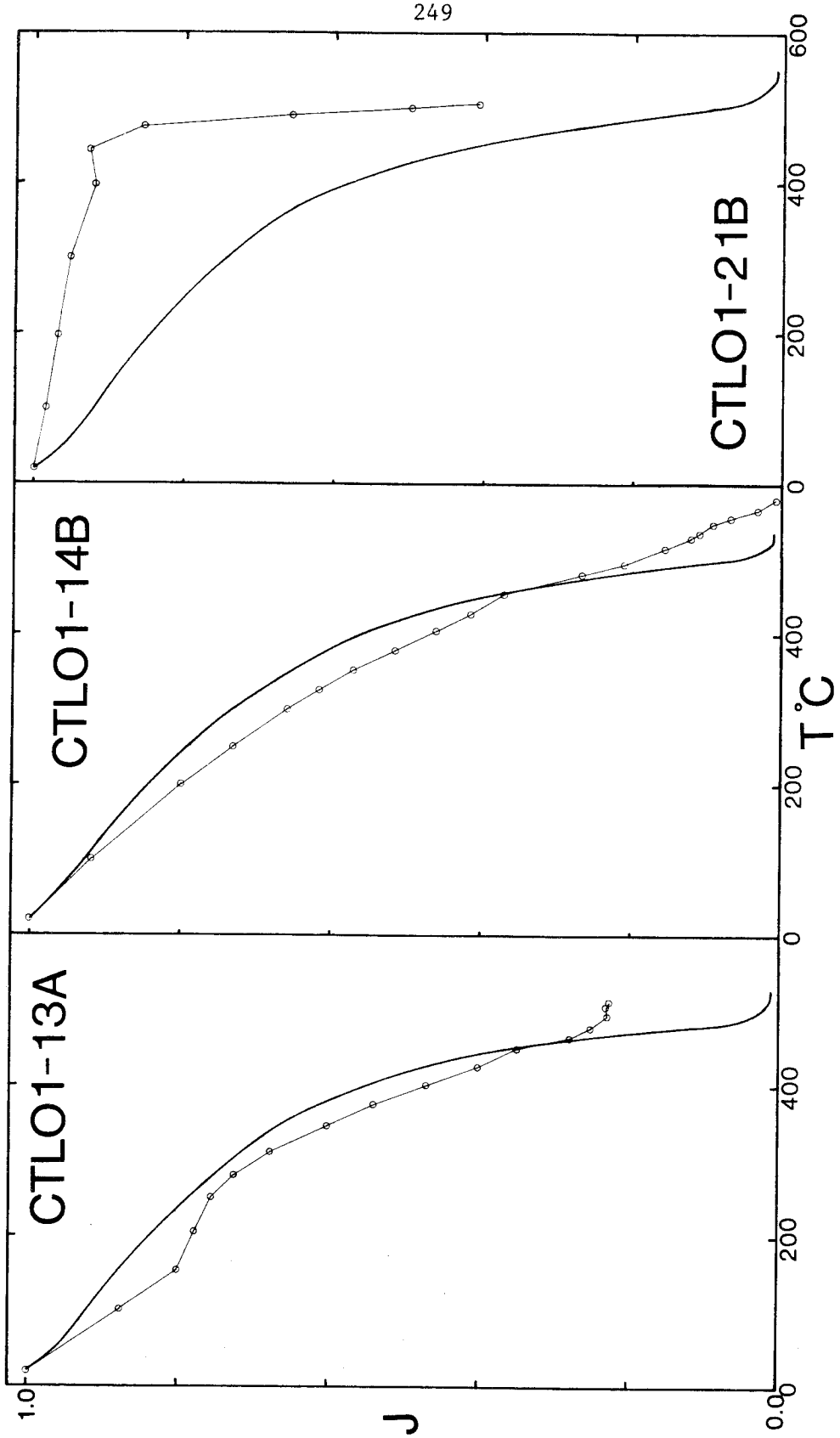
CTLO1-13A
CTLO1-14B
CTLO1-21B
J
T °C
1.0
0.0
0
200
400
600

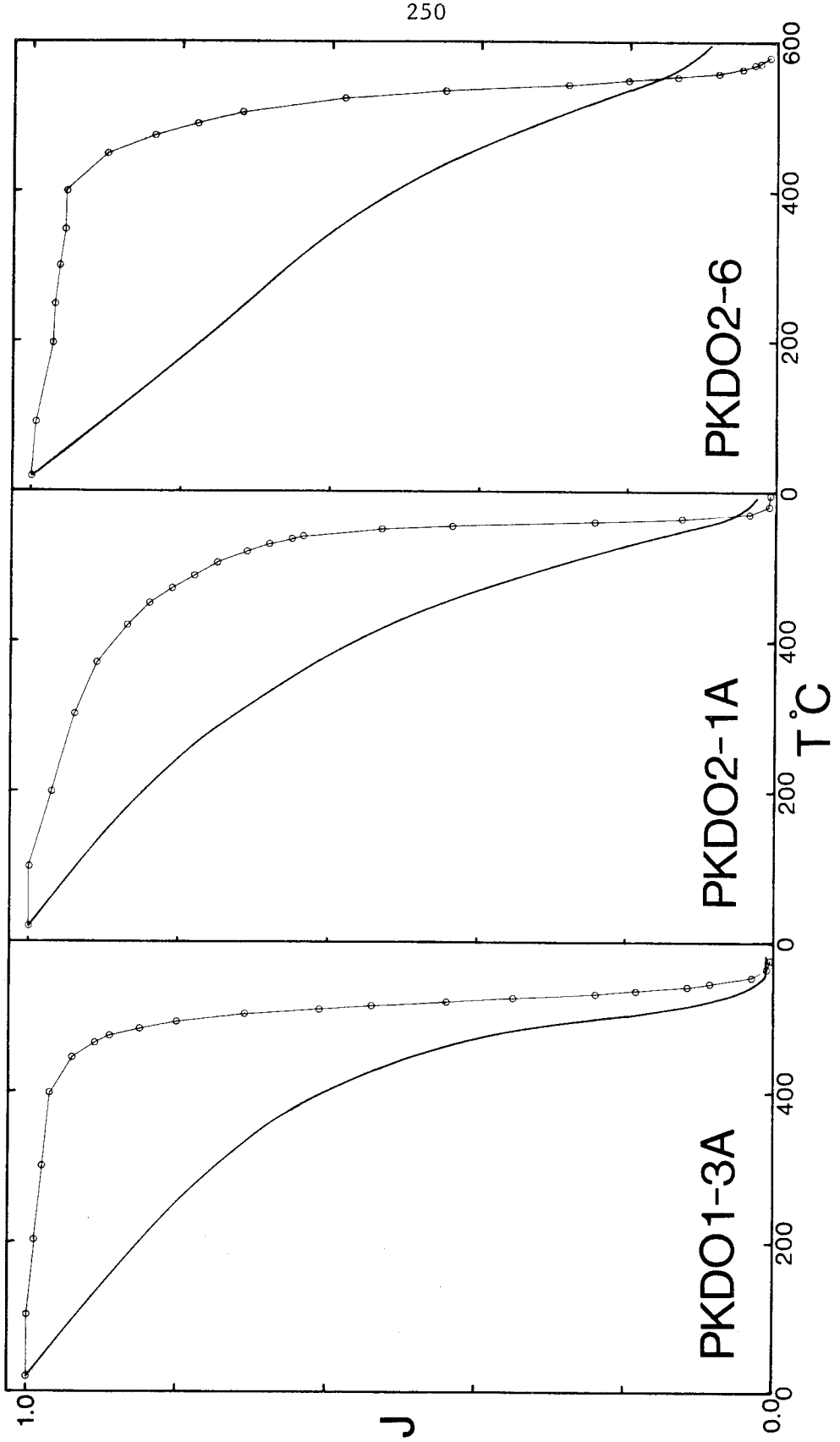
PKDO1-3A
PKDO2-1A
PKDO2-6
J
T°C
1.0
0.0
0
200
400
600

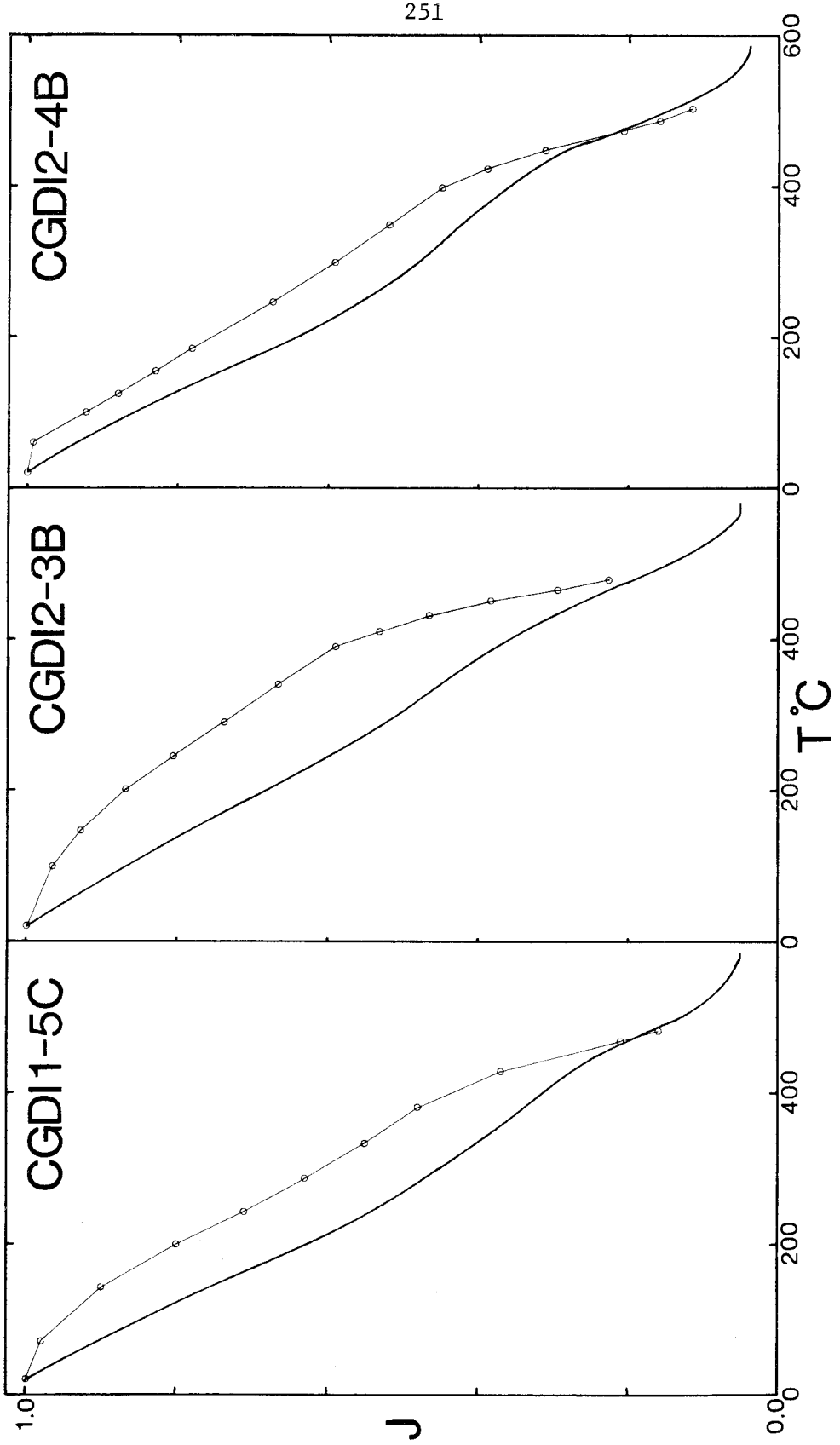
CGDI1-5C
CGDI2-3B
CGDI2-4B
J
1.0
0.0
0
200
400
600
T°C

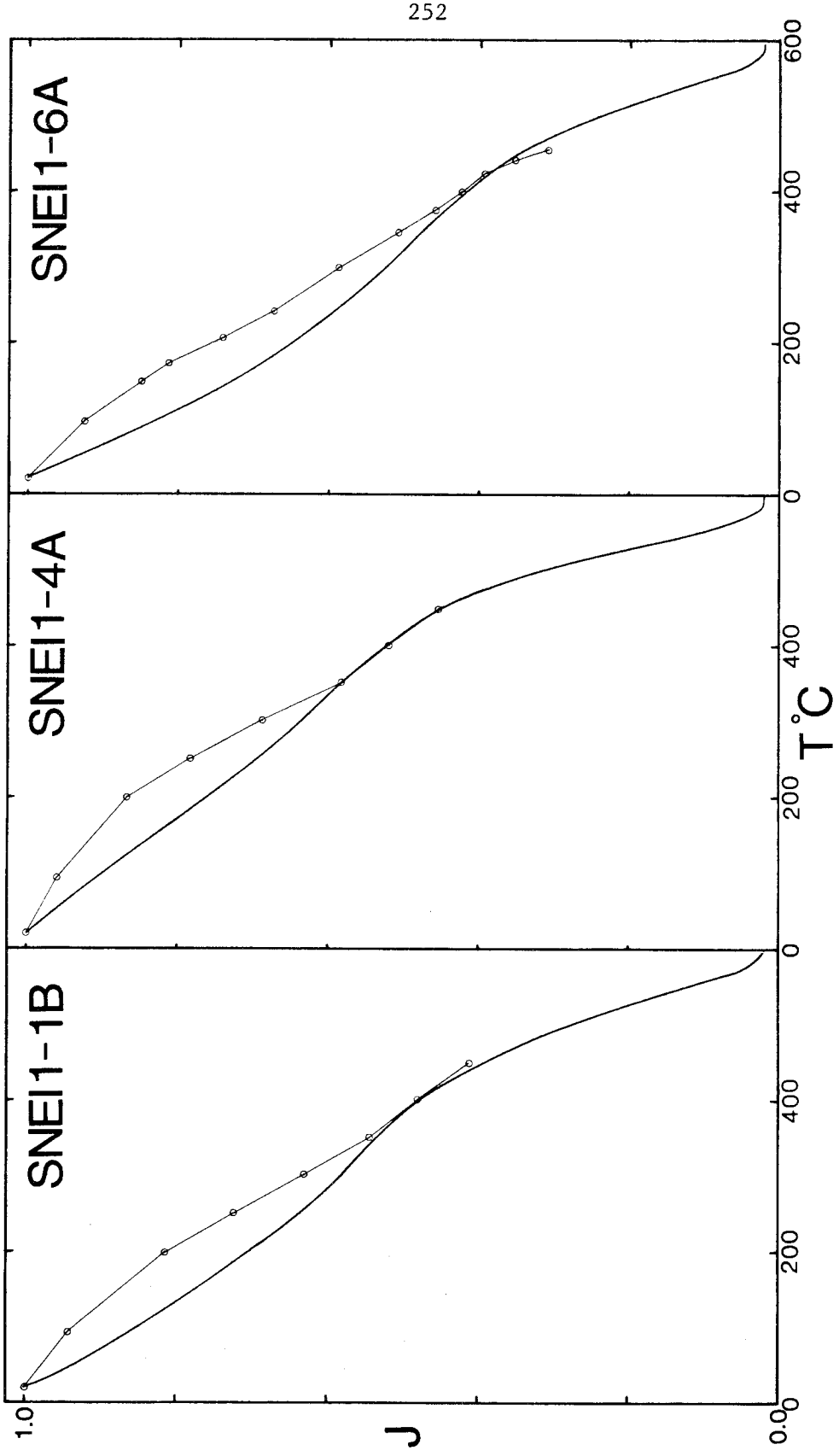
SNEI1-1B
SNEI1-4A
SNEI1-6A
J
T°C
1.0
0.0
0
200
400
600

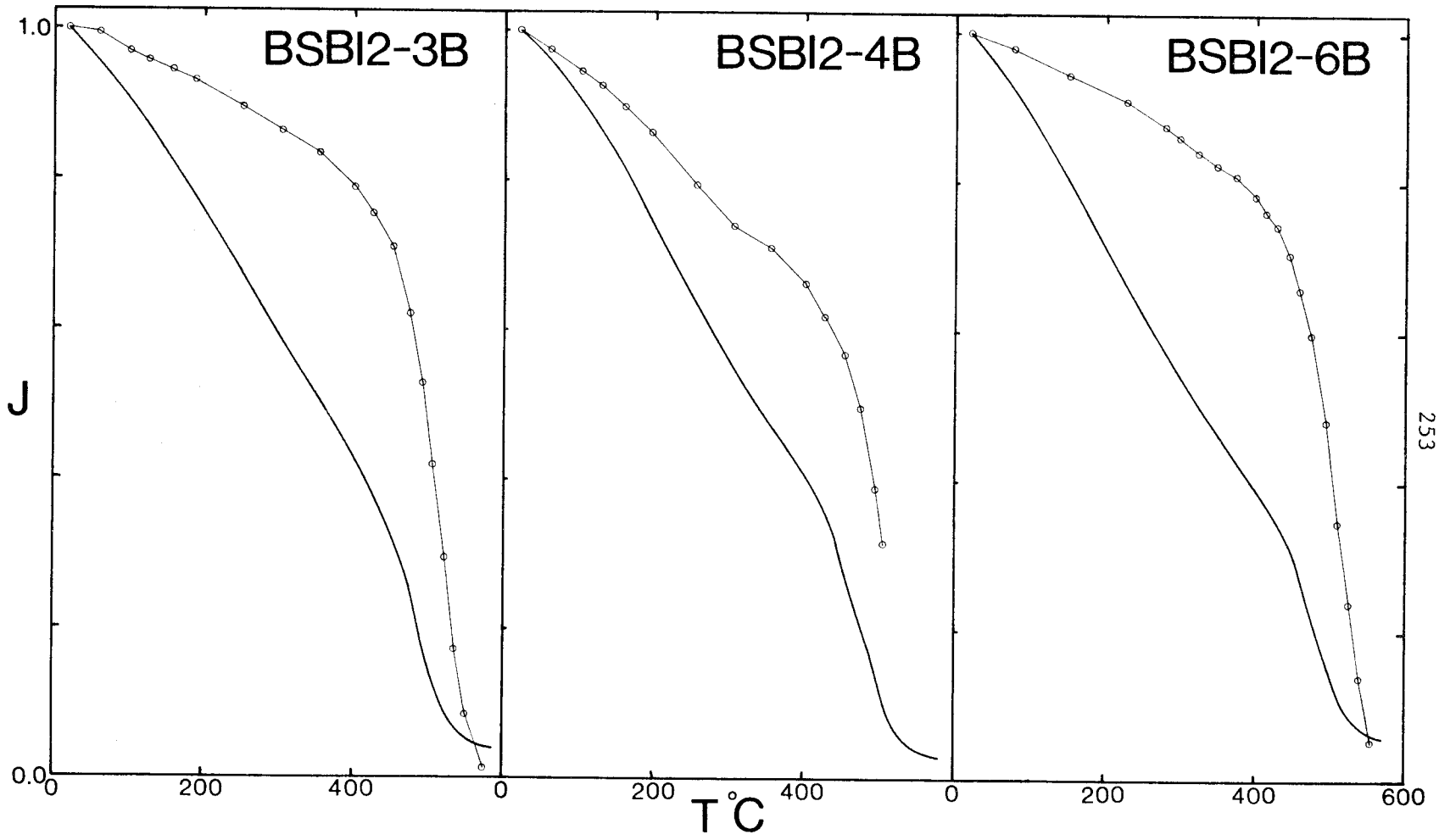
BSBI2-3B
BSBI2-4B
BSBI2-6B
1.0
0.0
J
0
200
400
600
T °C

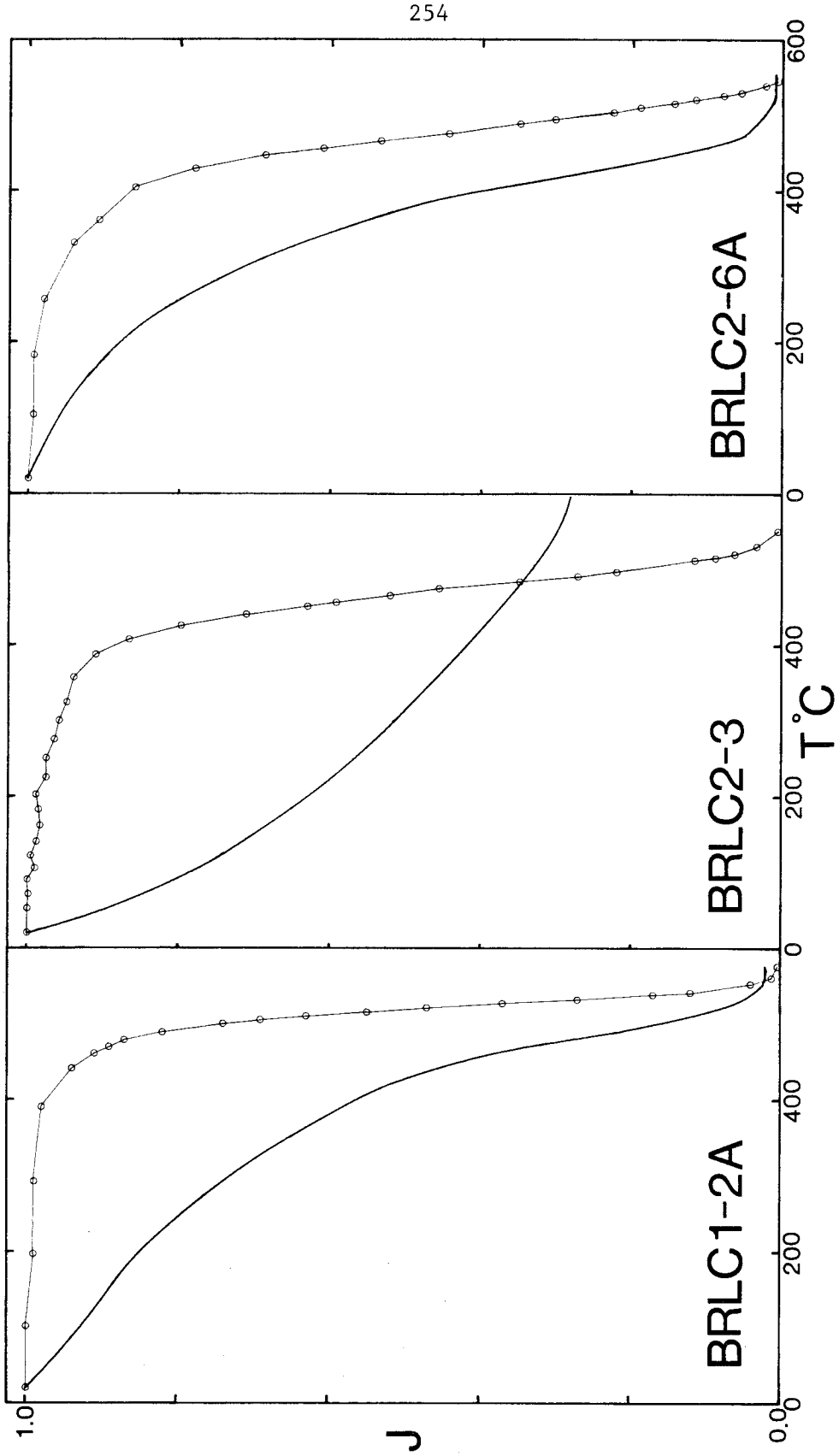
BRLC1-2A
BRLC2-3
BRLC2-6A
J
T°C
1.0
0.0
0
200
400
600

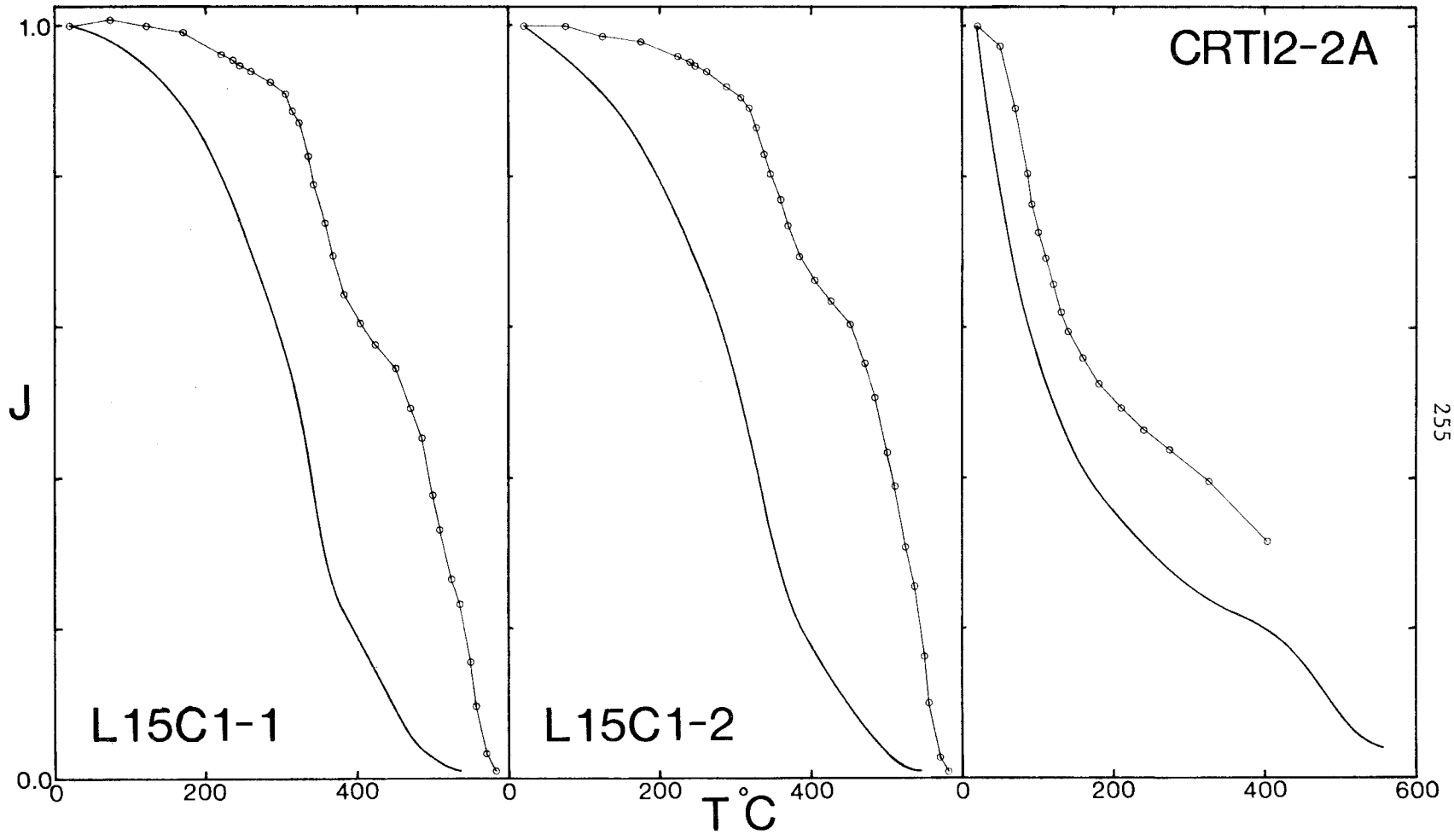
1.0
0.0
J
L15C1-1
L15C1-2
CRTI2-2A
0
200
400
0
200
400
0
200
400
600
T °C

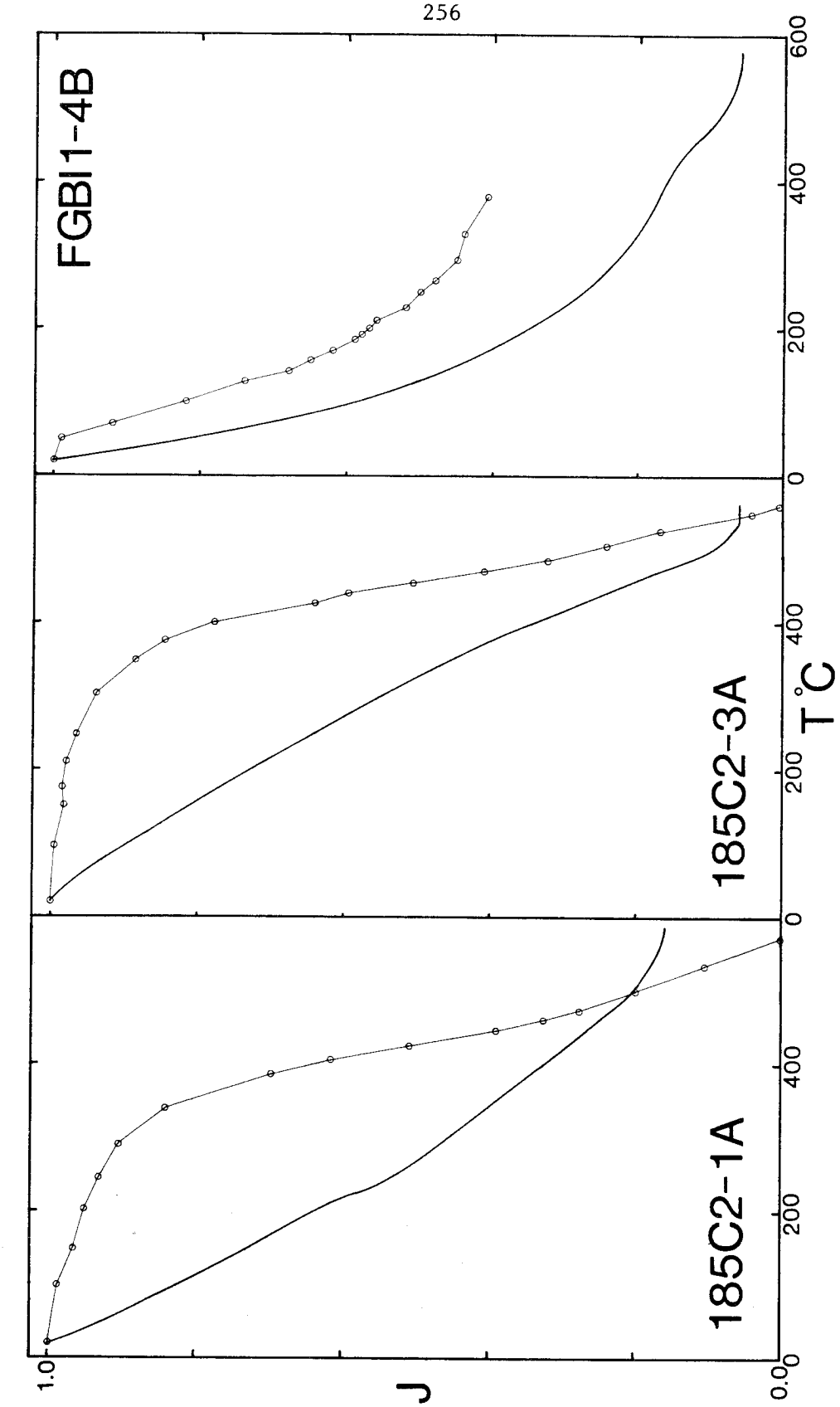
FGBI1-4B
185C2-3A
185C2-1A
J
T°C
1.0
0.0
0
200
400
600

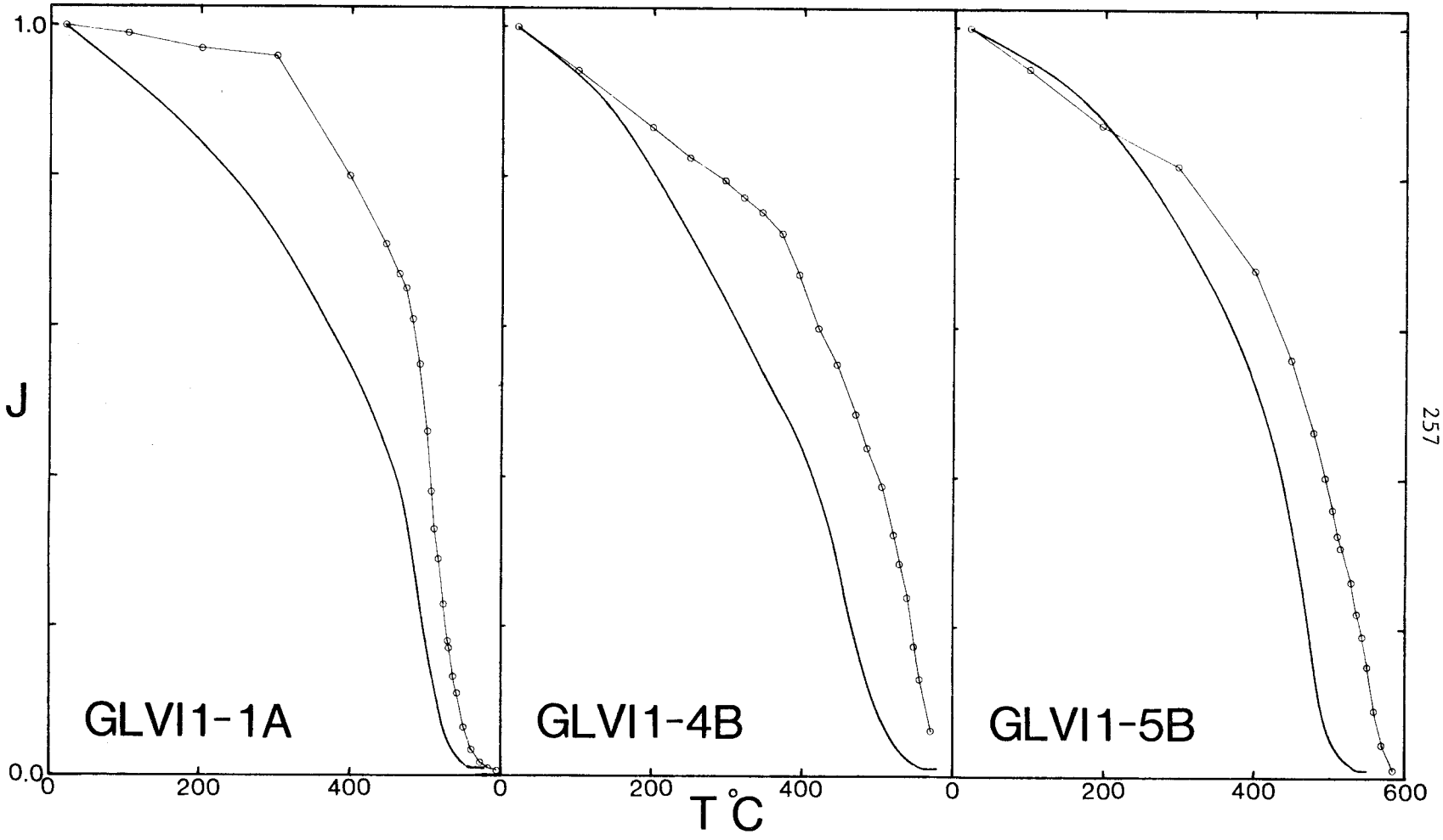
1.0
0.0
J
GLVI1-1A
GLVI1-4B
GLVI1-5B
0
200
400
0
200
400
0
200
400
600
T °C

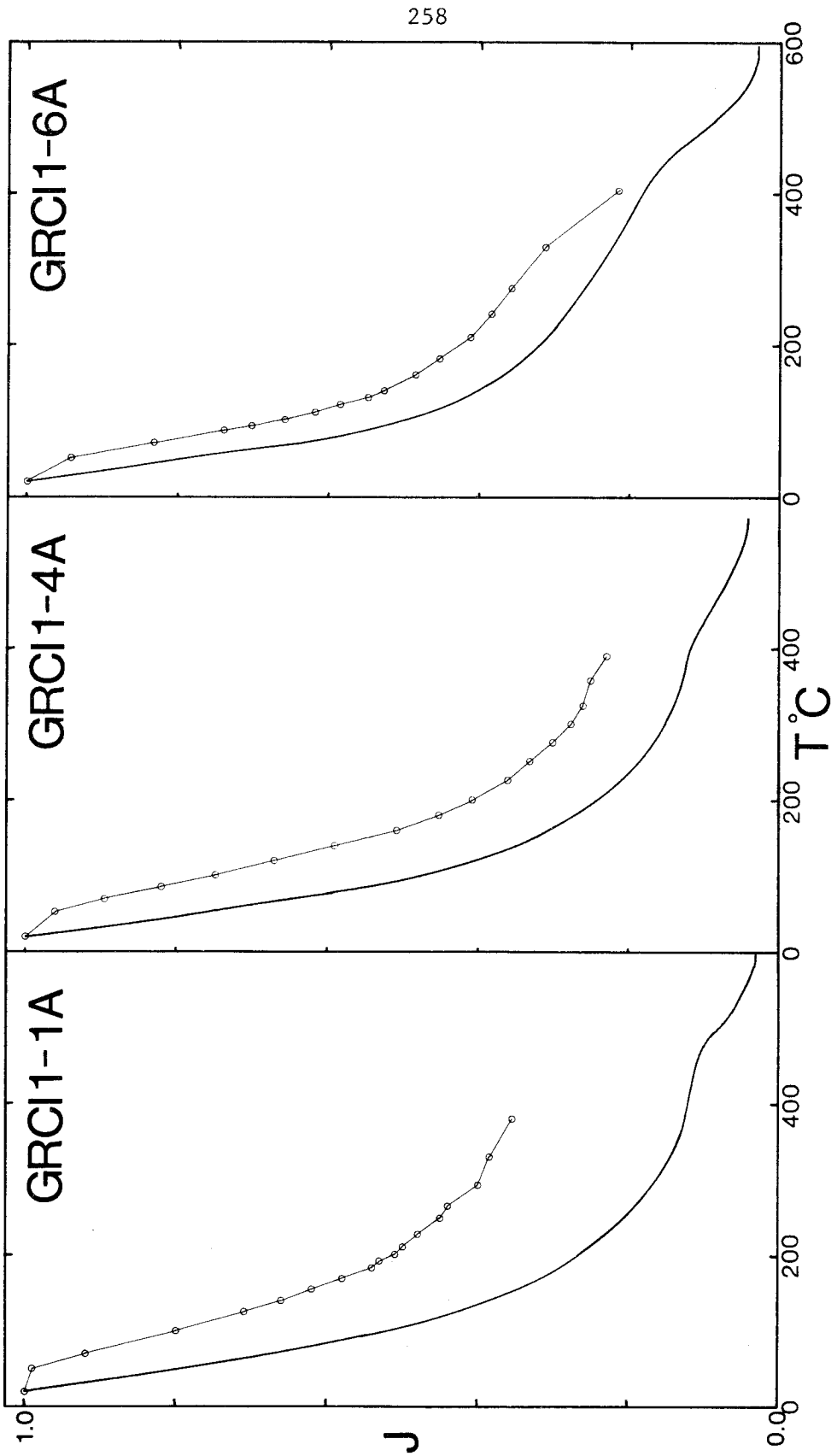
GRCI1-1A
GRCI1-4A
GRCI1-6A
J
T°C
1.0
0.0
0
200
400
600

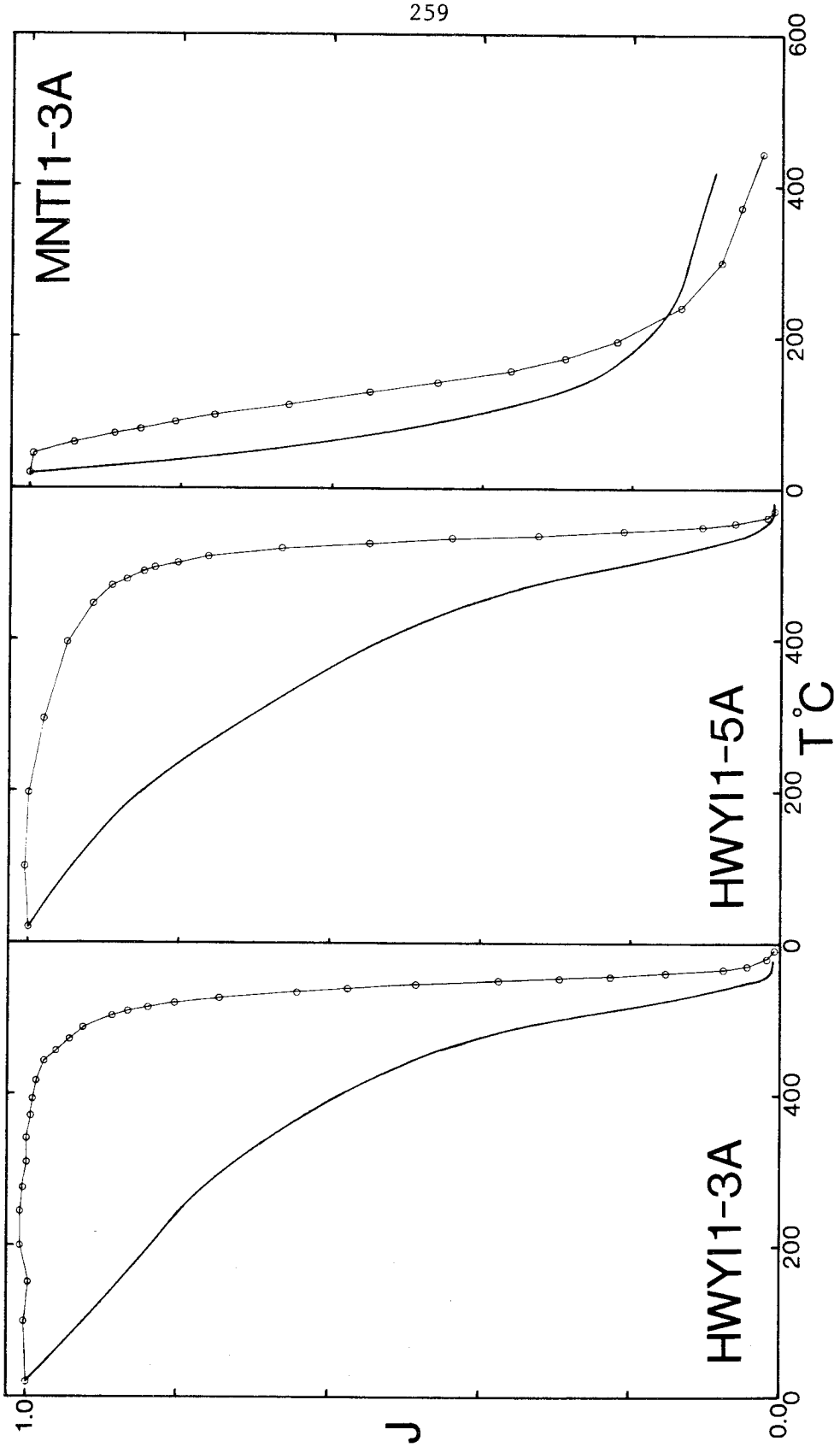
MNTI1-3A
HWYI1-5A
HWYI1-3A
J
T°C
1.0
0.0
0
200
400
600

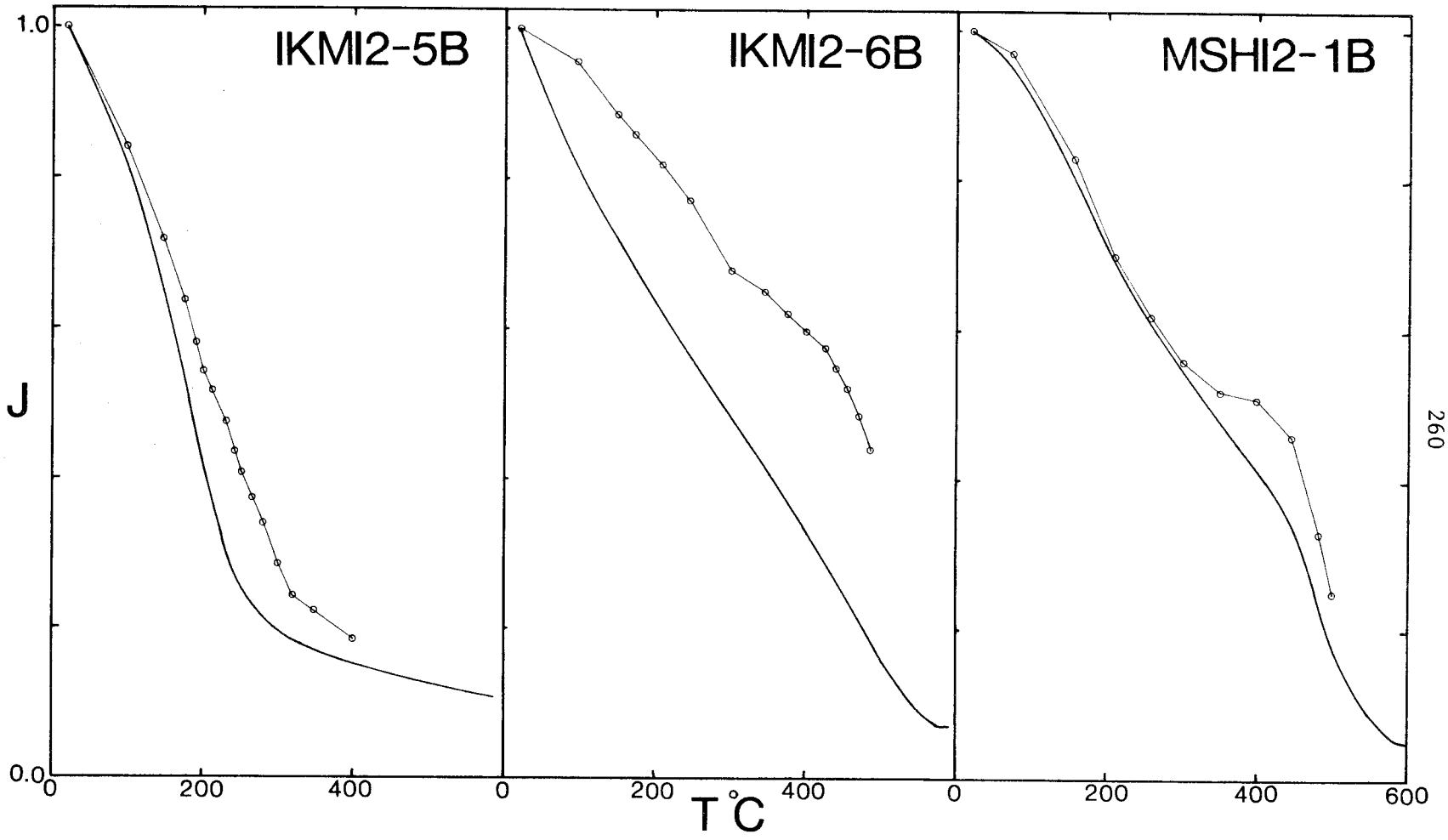
IKMI2-5B
IKMI2-6B
MSHI2-1B
1.0
0.0
J
0
200
400
600
T °C
260

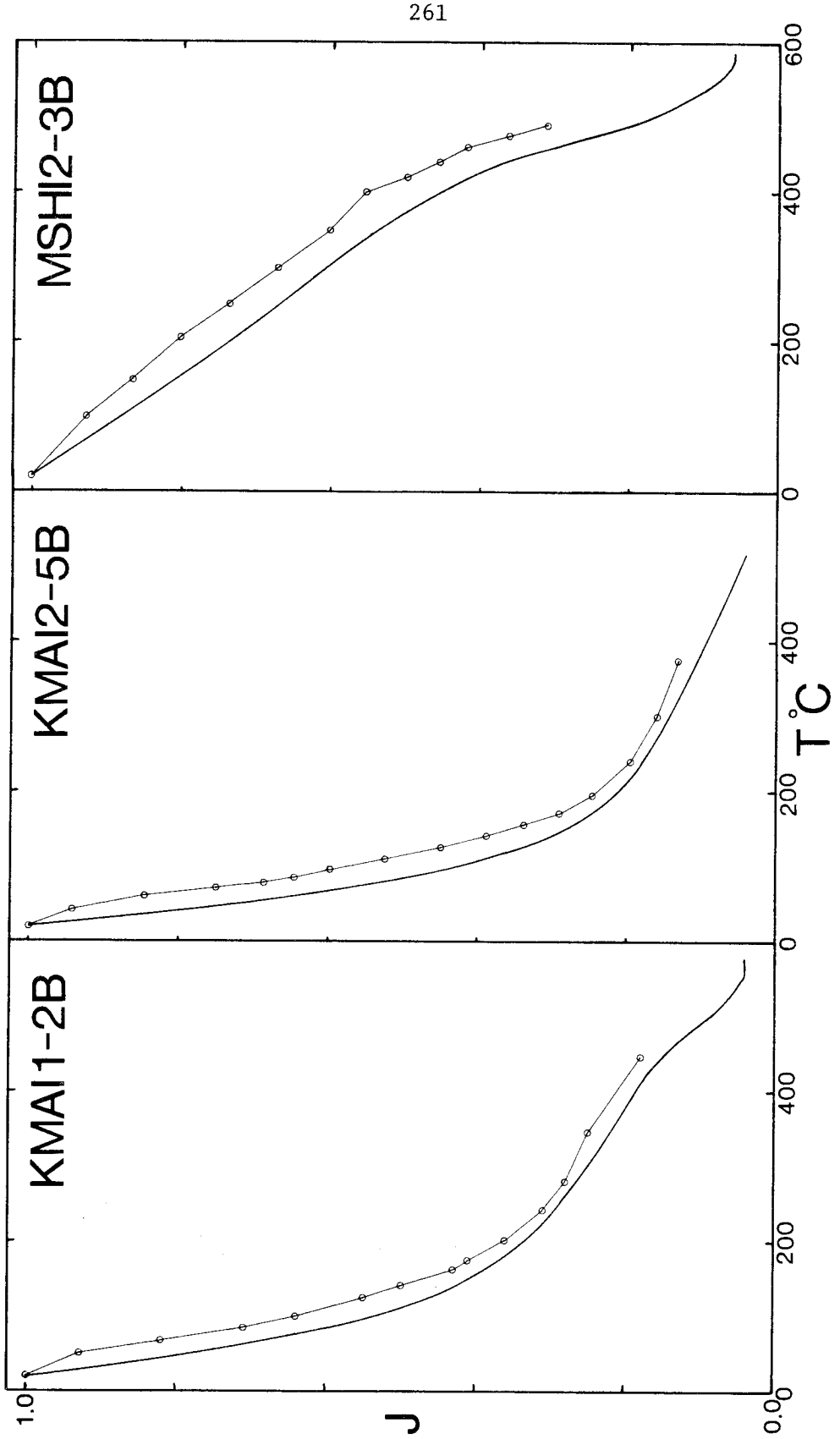
KMAI1-2B
KMAI2-5B
MSHI2-3B
J
1.0
0.0
0
200
400
600
T°C

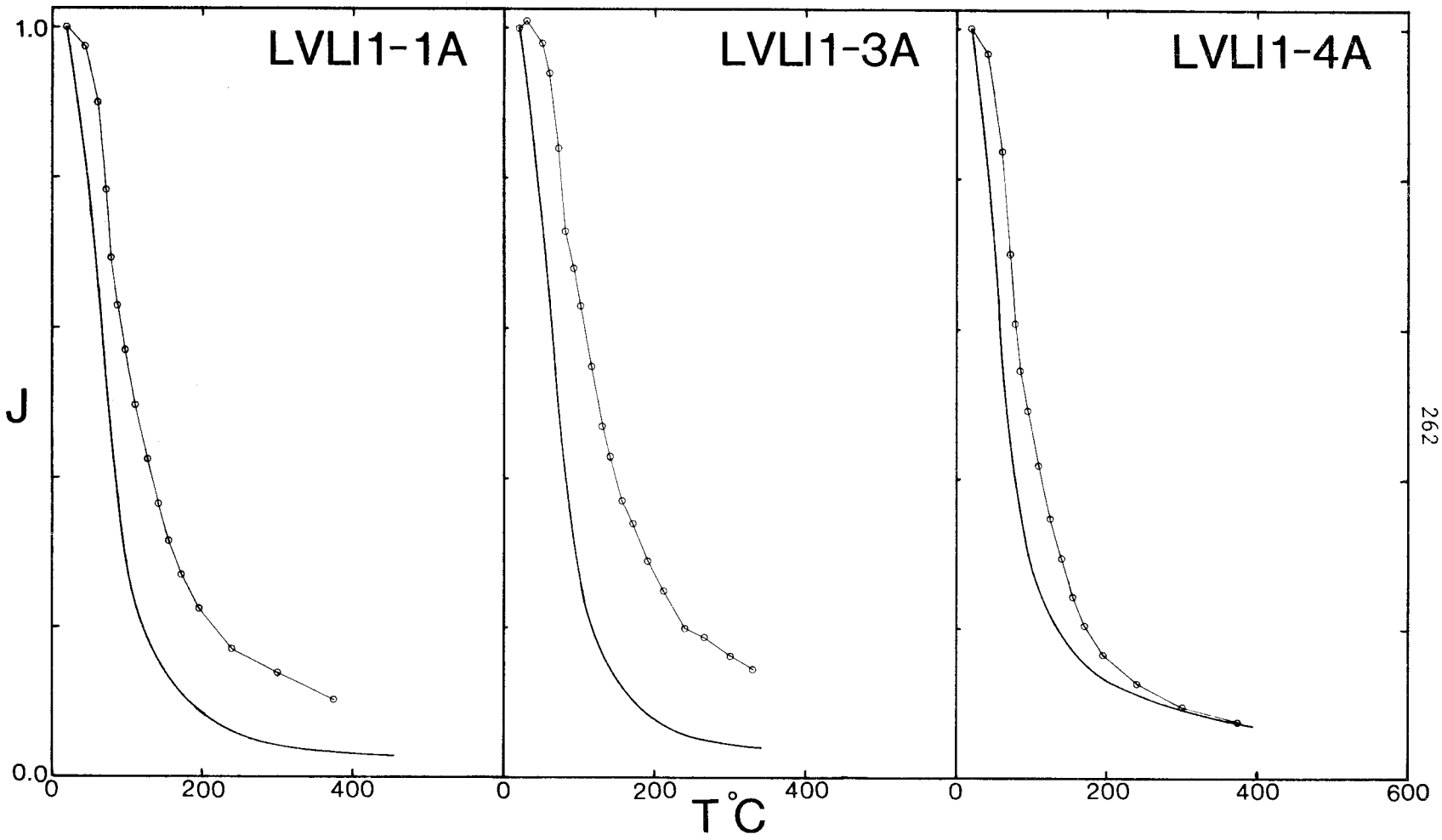
LVLI1-1A
LVLI1-3A
LVLI1-4A
1.0
0.0
J
0
200
400
0
200
400
0
200
400
600
T °C

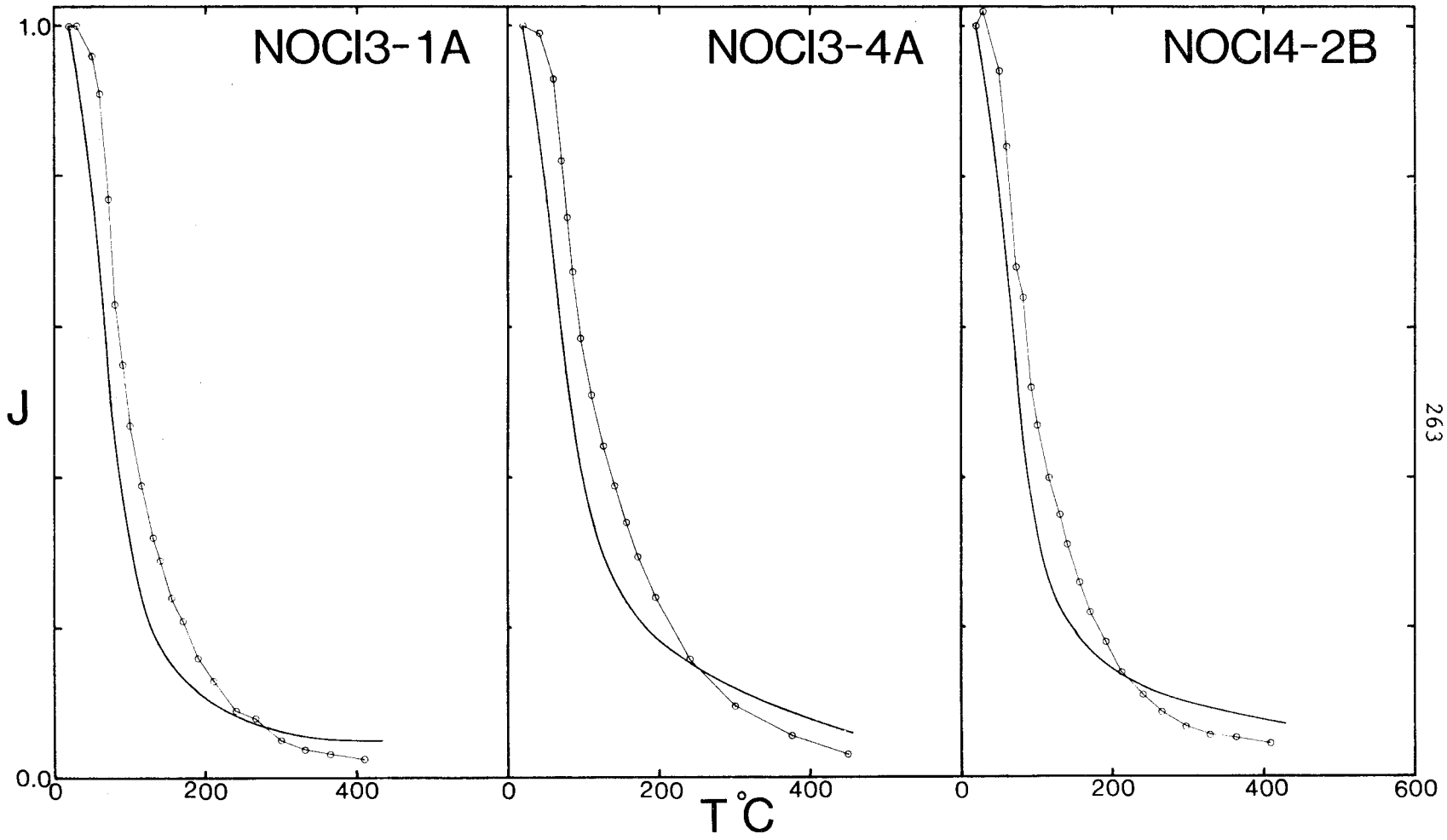
NOCl3-1A
NOCl3-4A
NOCl4-2B
1.0
0.0
J
0
200
400
600
T °C

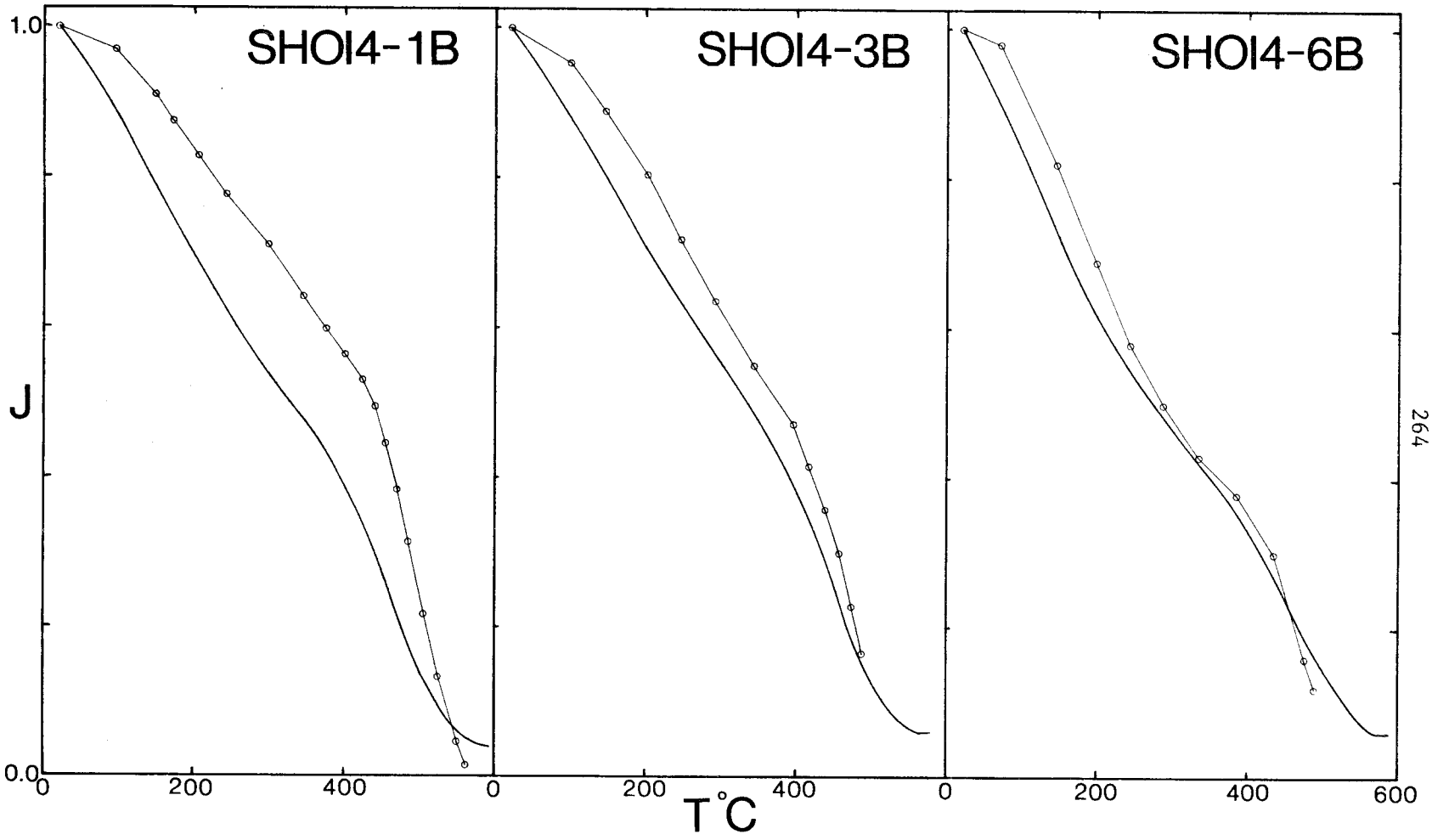
SHOI4-1B
SHOI4-3B
SHOI4-6B
1.0
0.0
J
0
200
400
0
200
400
0
200
400
600
T°C

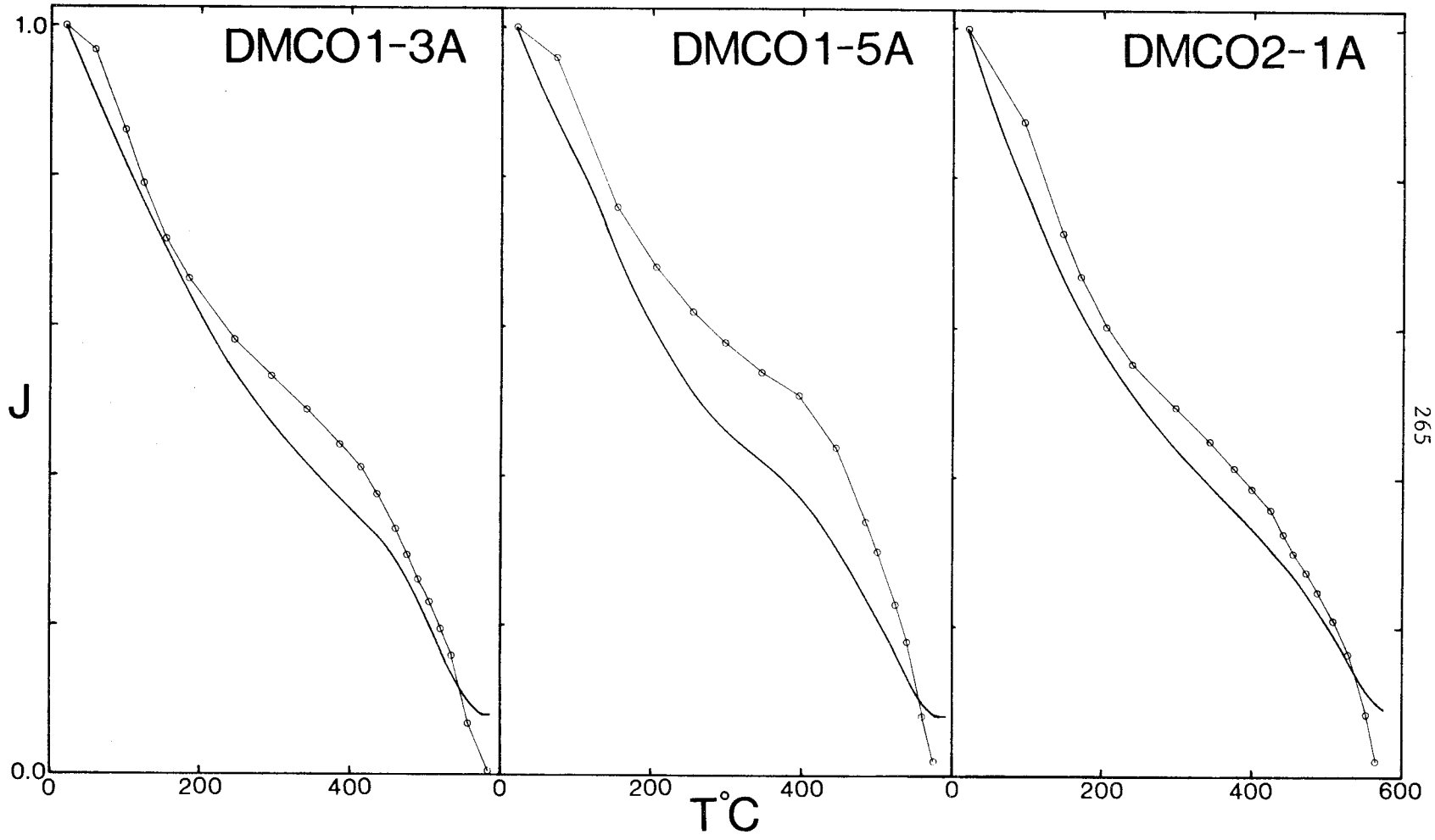
DMCO1-3A
DMCO1-5A
DMCO2-1A
1.0
0.0
J
0
200
400
0
200
400
0
200
400
600
T°C

Appendix 4

Thellier Diagrams

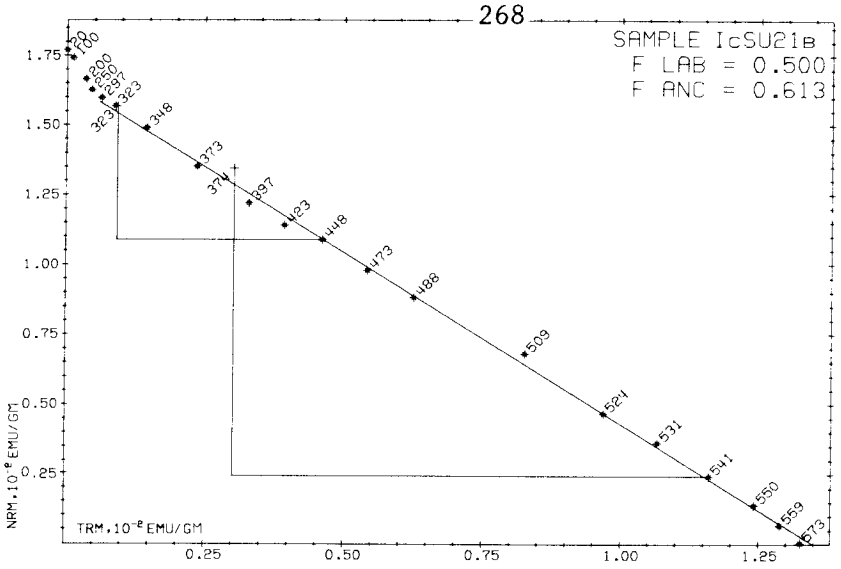
SAMPLE IcSU21B
F LAB = 0.500
F ANC = 0.613
NRM,10⁻⁶EMU/GM
TRM,10⁻⁶EMU/GM

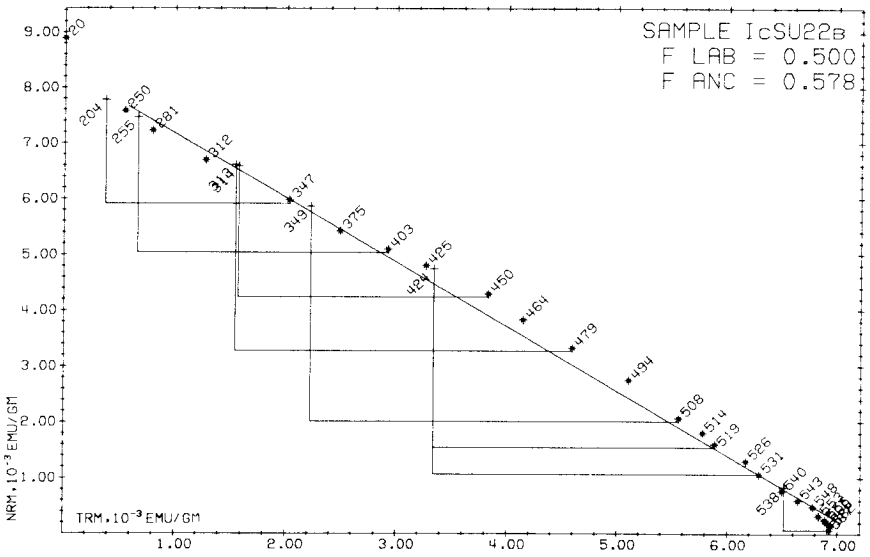
SAMPLE IcSU22B
F LAB = 0.500
F ANC = 0.578
NRM,10⁻³EMU/GM
TRM,10⁻³EMU/GM

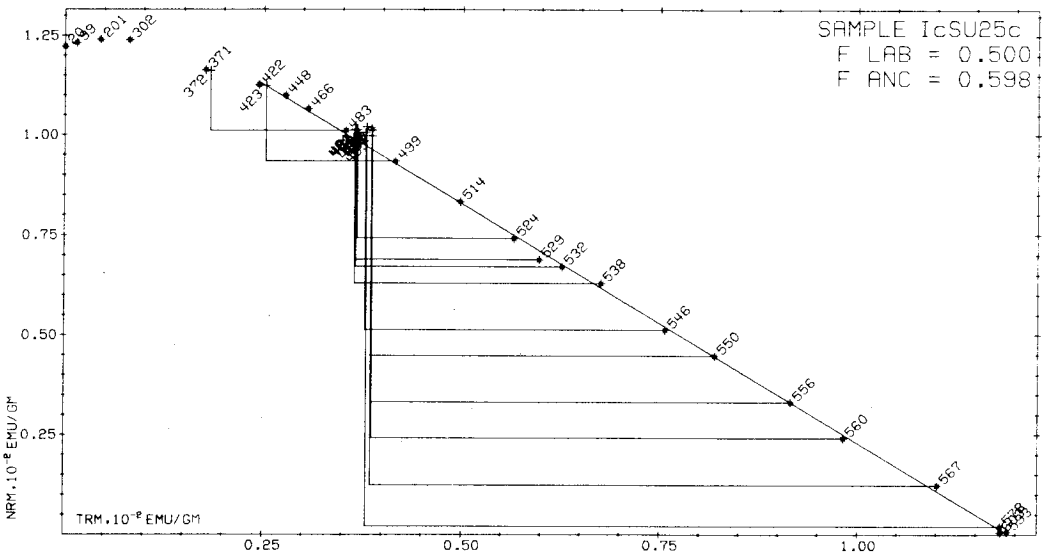
SAMPLE IcSU25c
F LAB = 0.500
F ANC = 0.598
NRM,10⁻⁶EMU/GM
TRM,10⁻⁶EMU/GM

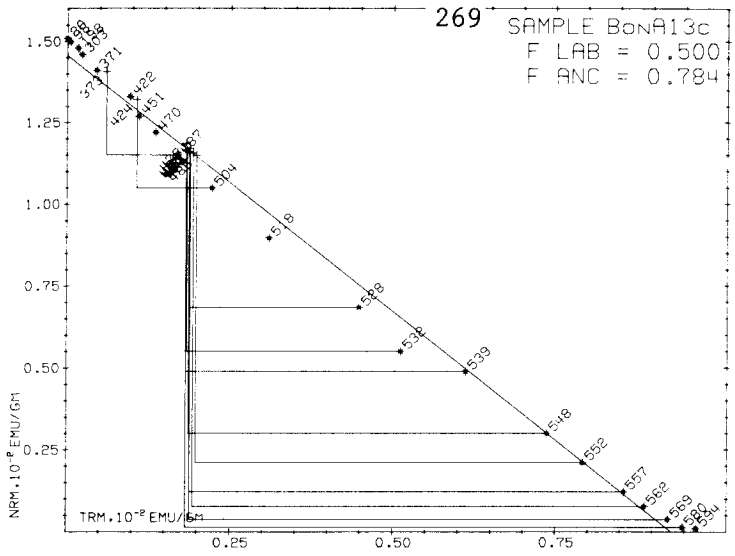
SAMPLE BONA13C
F LAB = 0.500
F ANC = 0.784
NRM,10⁻⁸ EMU/GM
TRM,10⁻⁸ EMU/GM
0.25
0.50
0.75
1.00
1.25
1.50

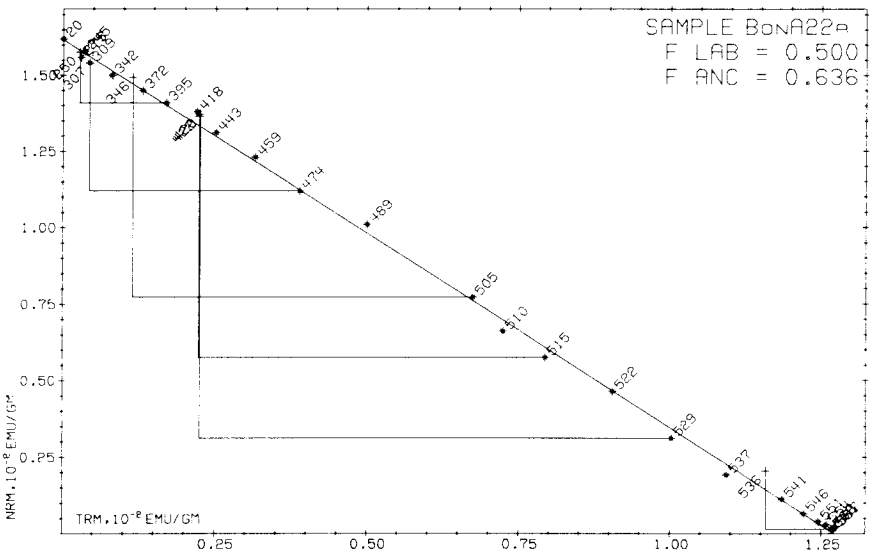
SAMPLE BONA22A
F LAB = 0.500
F ANC = 0.636
NRM,10⁻⁸ EMU/GM
TRM,10⁻⁸ EMU/GM
0.25
0.50
0.75
1.00
1.25
1.50

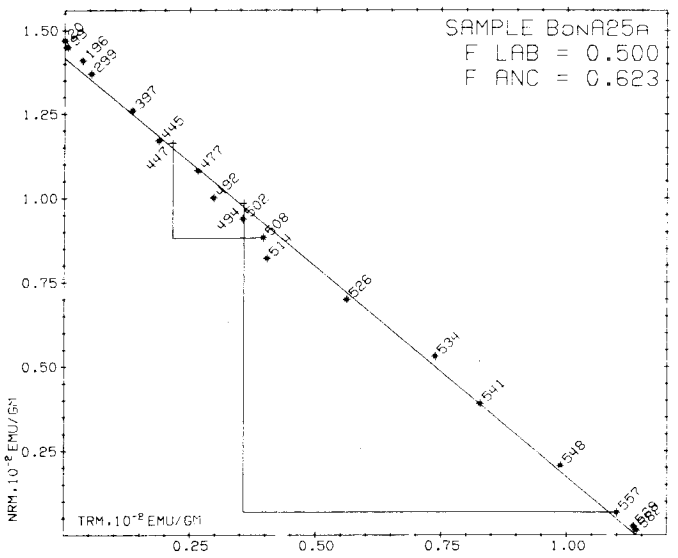
SAMPLE BONA25A
F LAB = 0.500
F ANC = 0.623
NRM,10⁻⁸ EMU/GM
TRM,10⁻⁸ EMU/GM
0.25
0.50
0.75
1.00
1.25
1.50

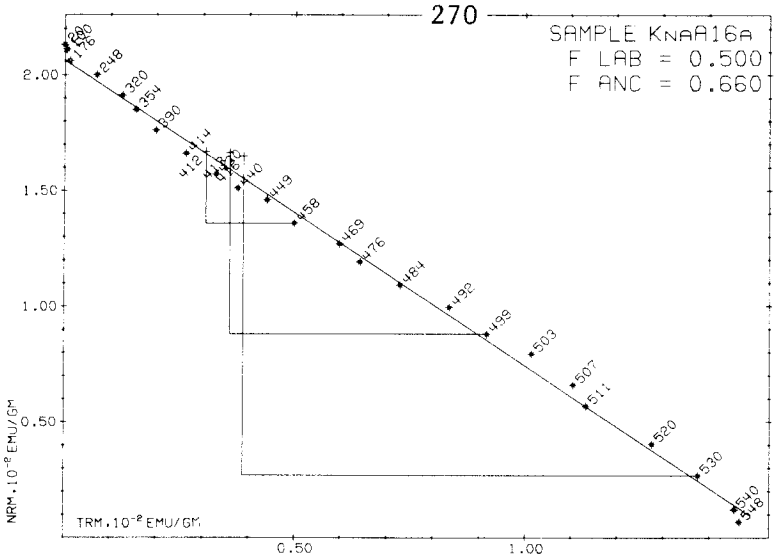
SAMPLE KNAA16A
F LAB = 0.500
F ANC = 0.660
NRM.10⁻³ EMU/GM
TRM.10⁻³ EMU/GM
0.50
1.00
1.50
2.00
176
248
320
354
390
414
440
443
458
469
476
484
492
498
503
507
511
520
530
540
548

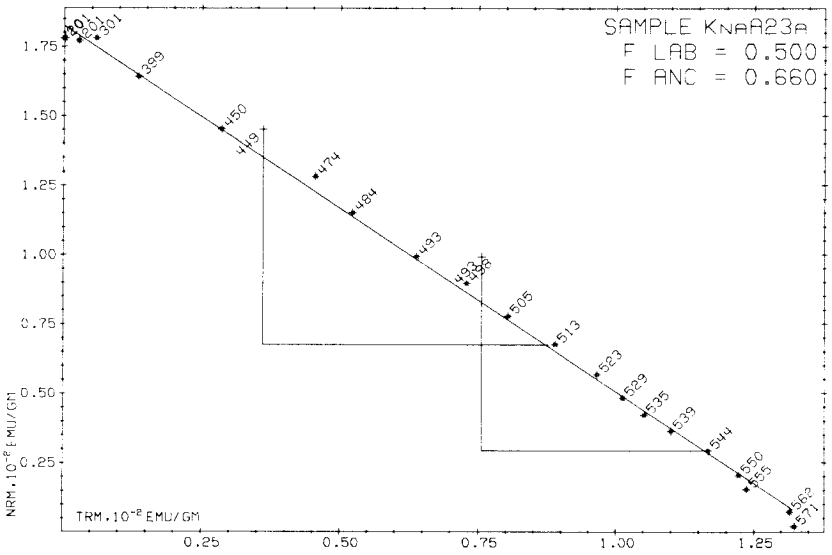
SAMPLE KNAA23A
F LAB = 0.500
F ANC = 0.660
NRM.10⁻³ EMU/GM
TRM.10⁻³ EMU/GM
0.25
0.50
0.75
1.00
1.25
1.50
1.75
301
399
450
449
474
484
493
505
513
523
529
535
539
544
550
555
562
571

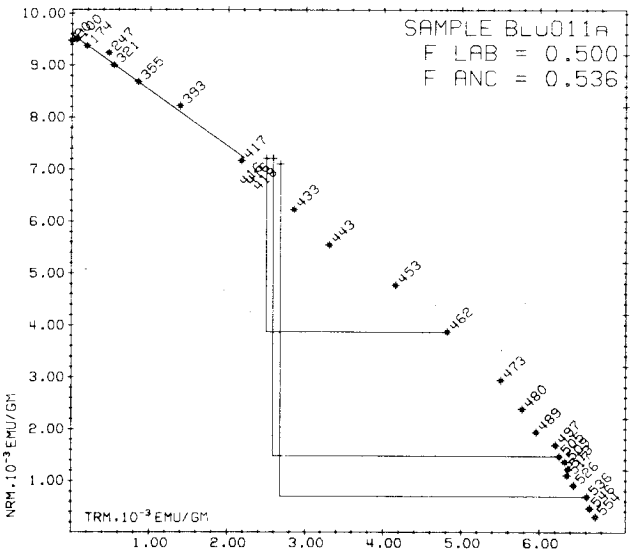
SAMPLE BLU011A
F LAB = 0.500
F ANC = 0.536
NRM.10⁻³ EMU/GM
TRM.10⁻³ EMU/GM
1.00
2.00
3.00
4.00
5.00
6.00
7.00
8.00
9.00
10.00
247
321
355
393
417
433
443
453
462
473
480
489
497
526
536
541

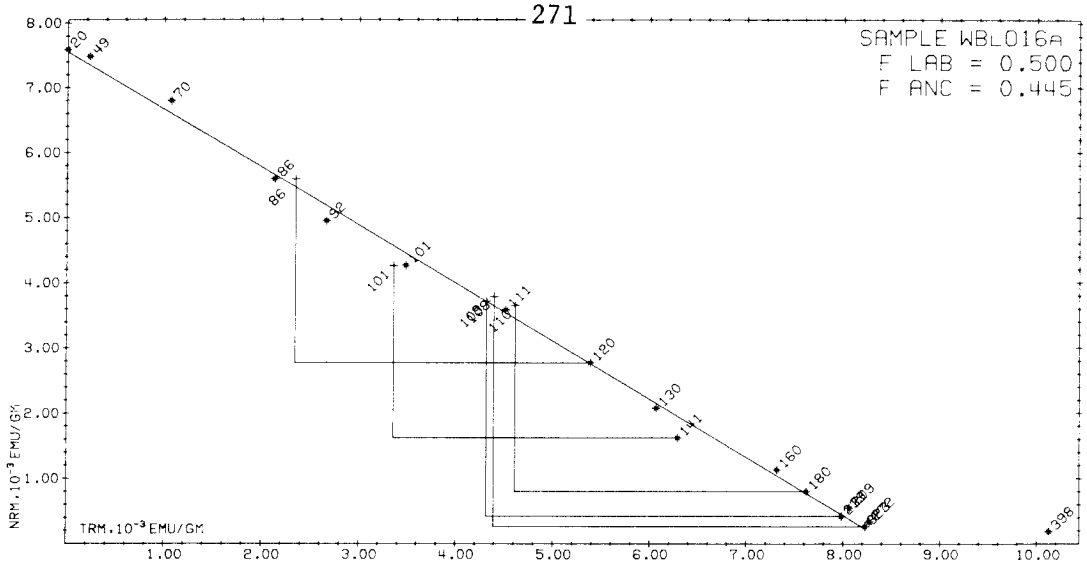
SAMPLE WBL016A
F LAB = 0.500
F ANC = 0.445
NRM,10⁻³EMU/GM
TRM,10⁻³EMU/GM

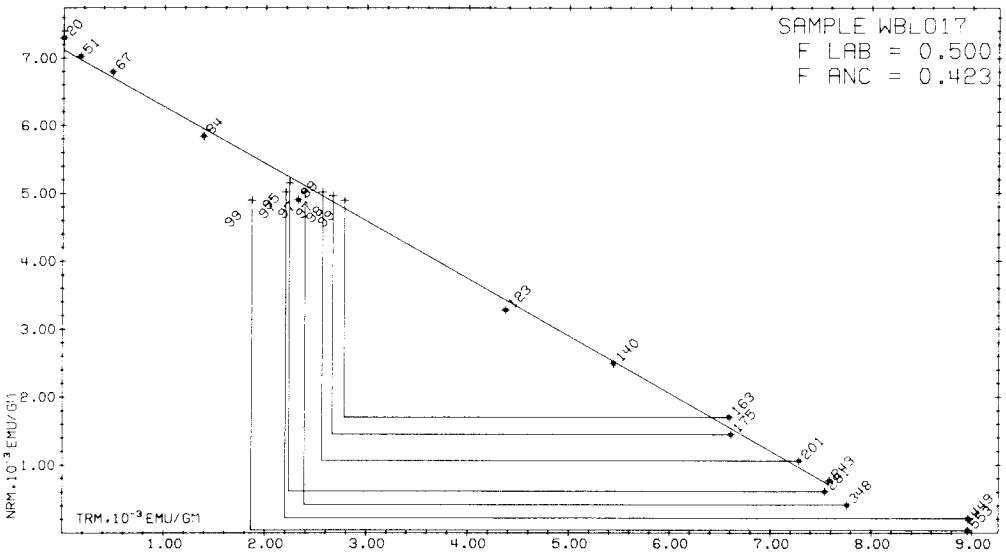
SAMPLE WBL017
F LAB = 0.500
F ANC = 0.423
NRM,10⁻³EMU/GM
TRM,10⁻³EMU/GM

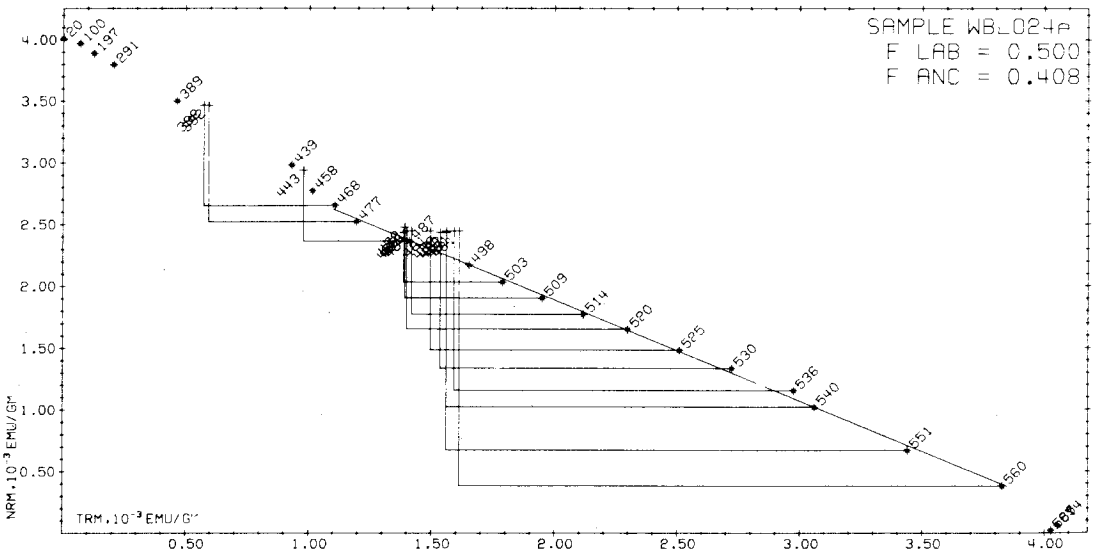
SAMPLE WBL024A
F LAB = 0.500
F ANC = 0.408
NRM,10⁻³EMU/GM
TRM,10⁻³EMU/GM

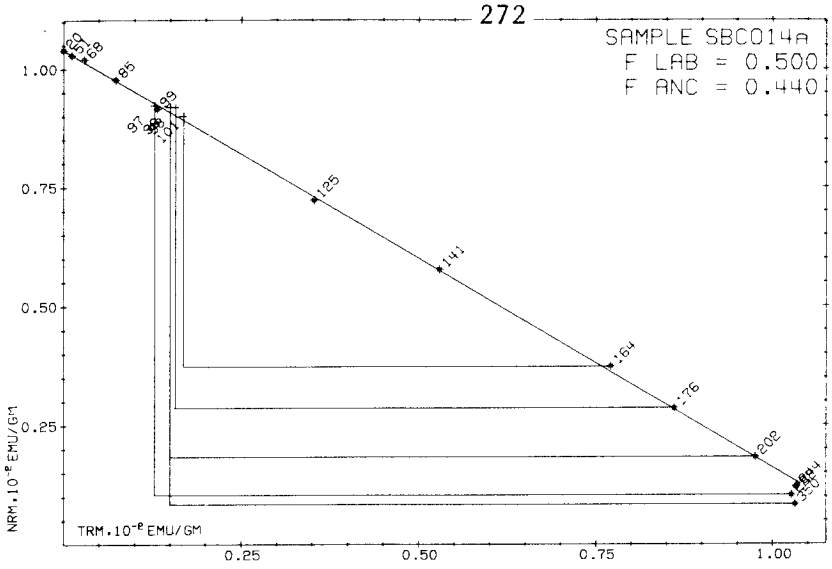
SAMPLE SBC014A
F LAB = 0.500
F ANC = 0.440
NRM,10⁻² EMU/GM
TRM,10⁻² EMU/GM
1.00
0.75
0.50
0.25
0.25
0.50
0.75
1.00

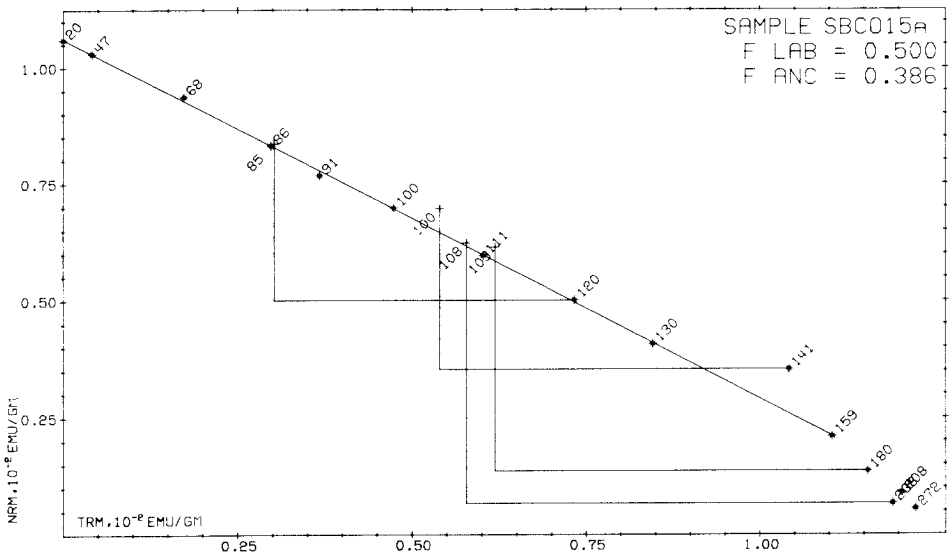
SAMPLE SBC015A
F LAB = 0.500
F ANC = 0.386
NRM,10⁻² EMU/GM
TRM,10⁻² EMU/GM
1.00
0.75
0.50
0.25
0.25
0.50
0.75
1.00

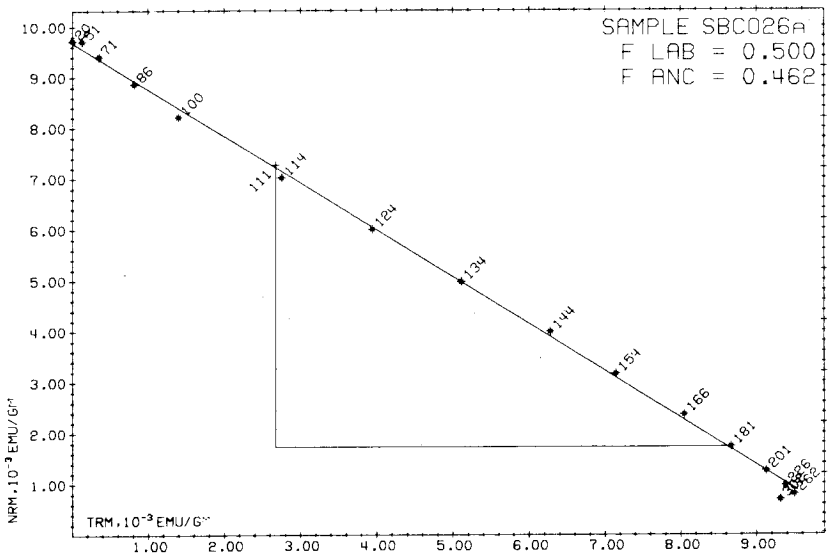
SAMPLE SBC026A
F LAB = 0.500
F ANC = 0.462
NRM,10⁻³ EMU/GM
TRM,10⁻³ EMU/GM
10.00
9.00
8.00
7.00
6.00
5.00
4.00
3.00
2.00
1.00
1.00
2.00
3.00
4.00
5.00
6.00
7.00
8.00
9.00

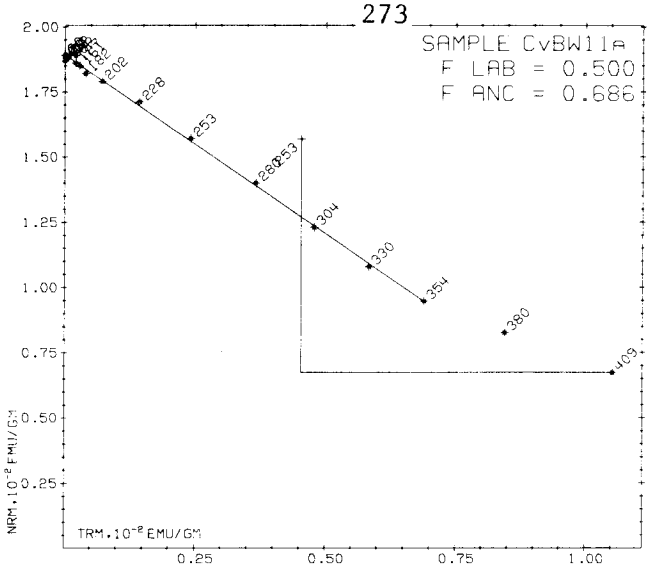
SAMPLE CvBW11a
F LAB = 0.500
F ANC = 0.686
NRM,10⁻² EMU/GM
TRM,10⁻² EMU/GM
202
228
253
280
304
330
354
380
409

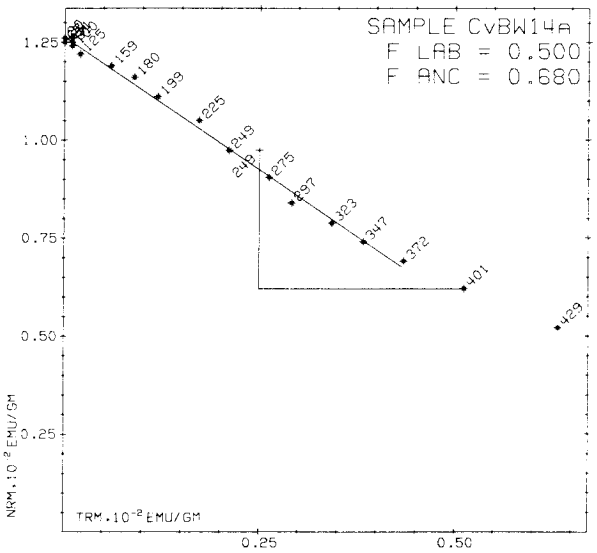
SAMPLE CvBW14a
F LAB = 0.500
F ANC = 0.680
NRM,10⁻² EMU/GM
TRM,10⁻² EMU/GM
159
180
199
225
249
275
297
323
347
372
401
429

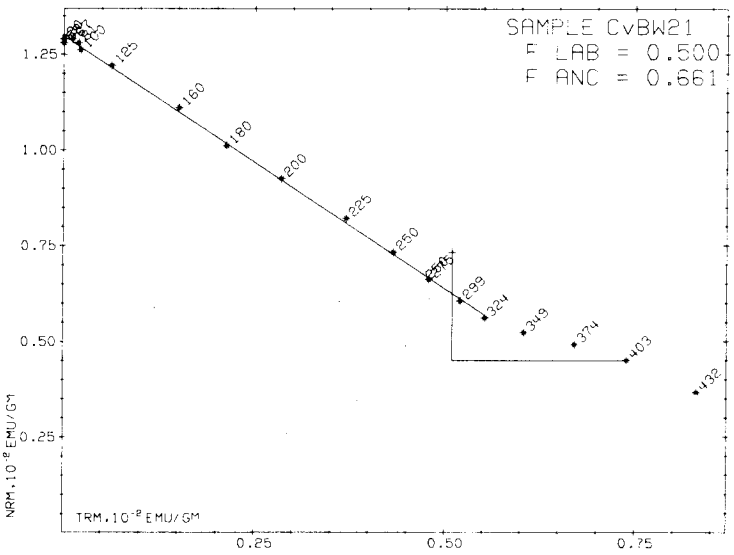
SAMPLE CvBW21
F LAB = 0.500
F ANC = 0.661
NRM,10⁻² EMU/GM
TRM,10⁻² EMU/GM
125
160
180
200
225
250
299
324
349
374
403
432

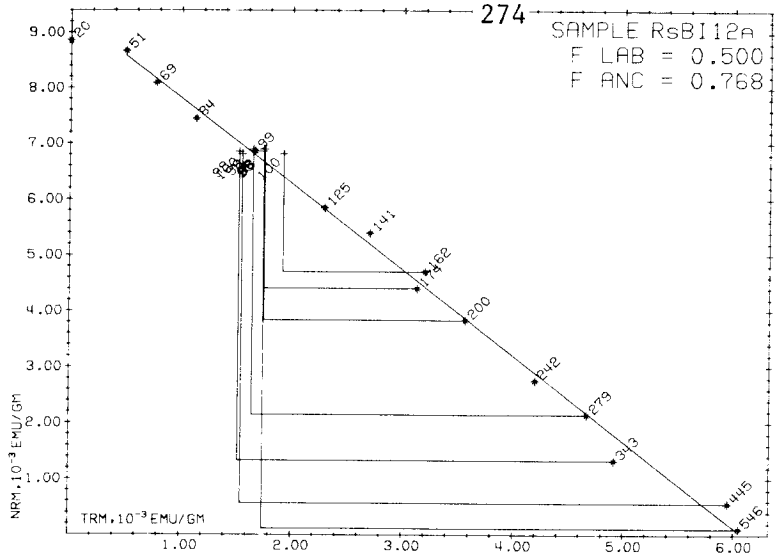
SAMPLE RsBI12a
F LAB = 0.500
F ANC = 0.768
NRM, 10^{-3} EMU/GM
TRM, 10^{-3} EMU/GM
20
51
69
84
89
98
100
125
141
162
200
242
279
313
445
546

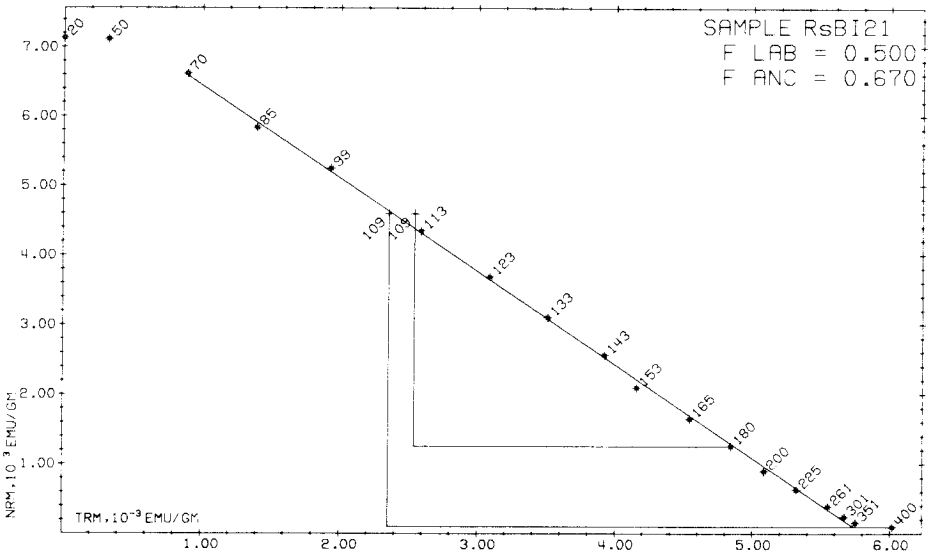
SAMPLE RsBI21
F LAB = 0.500
F ANC = 0.670
NRM, 10^{-3} EMU/GM
TRM, 10^{-3} EMU/GM
20
50
70
85
99
109
109
113
123
133
143
153
165
180
200
225
261
301
351
400

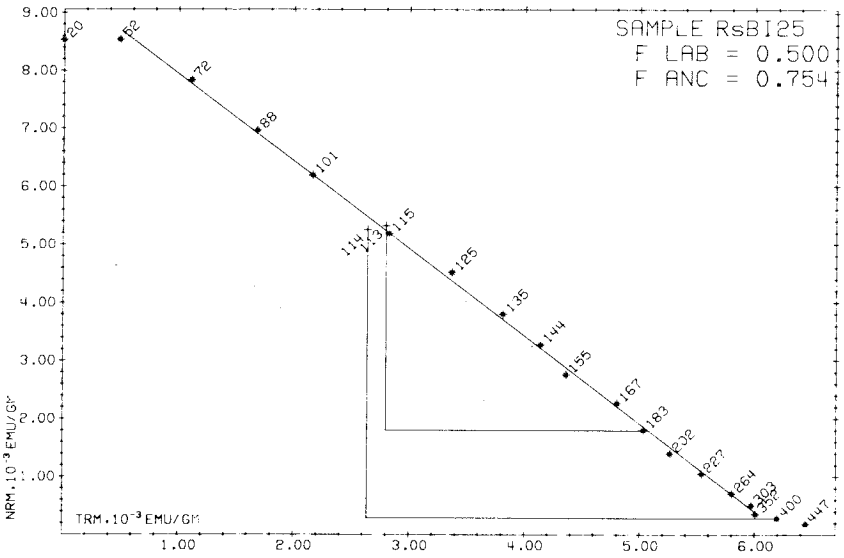
SAMPLE RsBI25
F LAB = 0.500
F ANC = 0.754
NRM, 10^{-3} EMU/GM
TRM, 10^{-3} EMU/GM
20
52
72
88
101
113
113
115
125
135
144
155
167
183
202
227
264
383
400
447

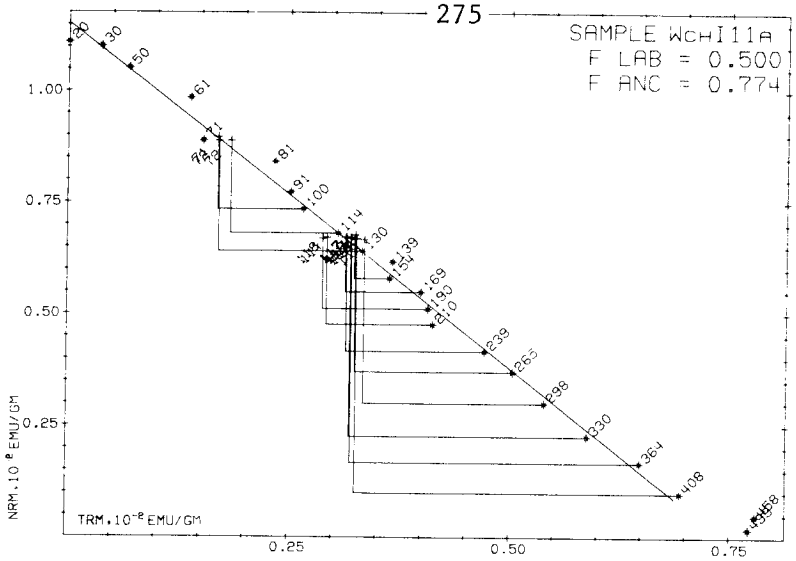
SAMPLE WCHI11A
F LAB = 0.500
F ANC = 0.774
NRM,10⁻³ EMU/GM
TRM,10⁻³ EMU/GM
0.25
0.50
0.75
1.00

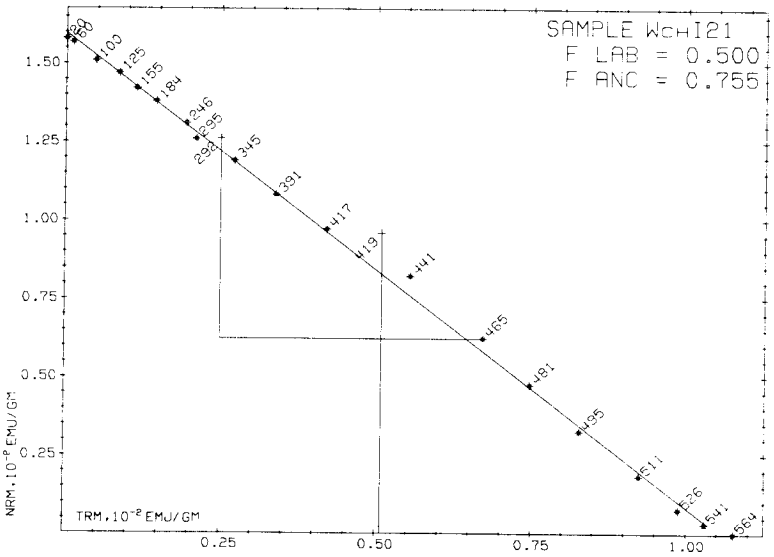
SAMPLE WCHI21
F LAB = 0.500
F ANC = 0.755
NRM,10⁻³ EMU/GM
TRM,10⁻³ EMU/GM
0.25
0.50
0.75
1.00
1.25
1.50

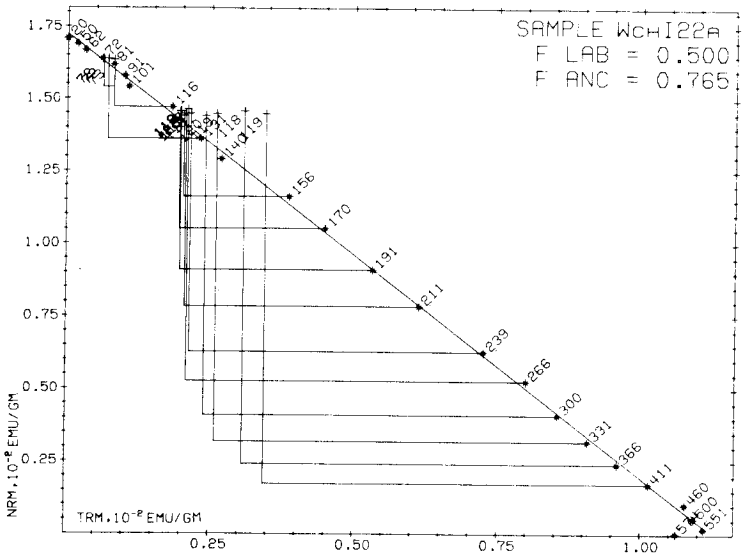
SAMPLE WCHI22A
F LAB = 0.500
F ANC = 0.765
NRM,10⁻³ EMU/GM
TRM,10⁻³ EMU/GM
0.25
0.50
0.75
1.00
1.25
1.50
1.75

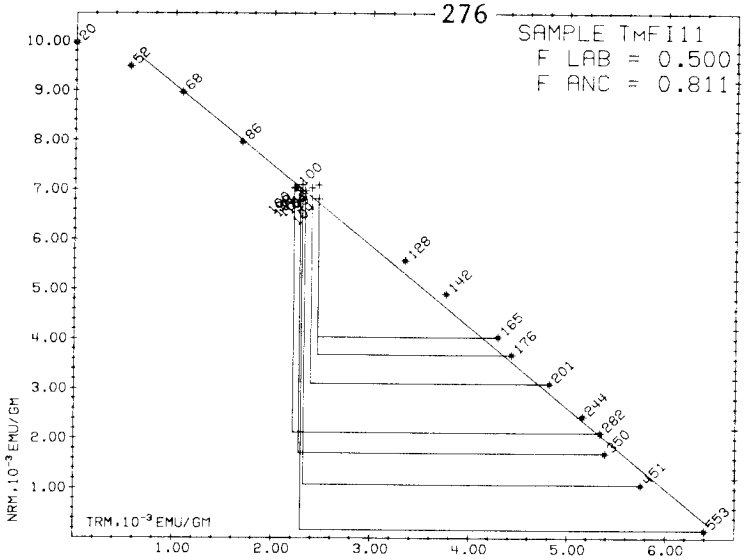
SAMPLE TmFI11
F LAB = 0.500
F ANC = 0.811
NRM,10⁻³EMU/GM
TRM,10⁻³EMU/GM

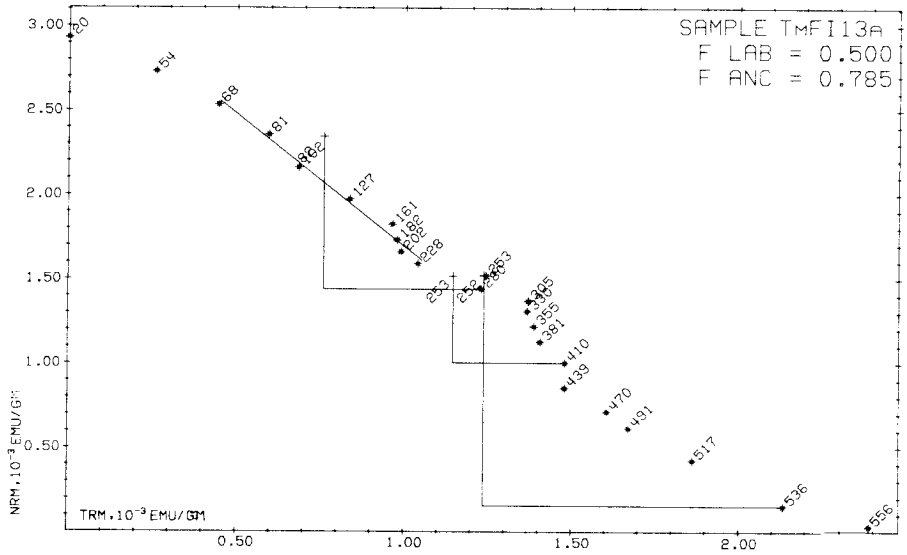
SAMPLE TmFI13a
F LAB = 0.500
F ANC = 0.785
NRM,10⁻³EMU/GM
TRM,10⁻³EMU/GM

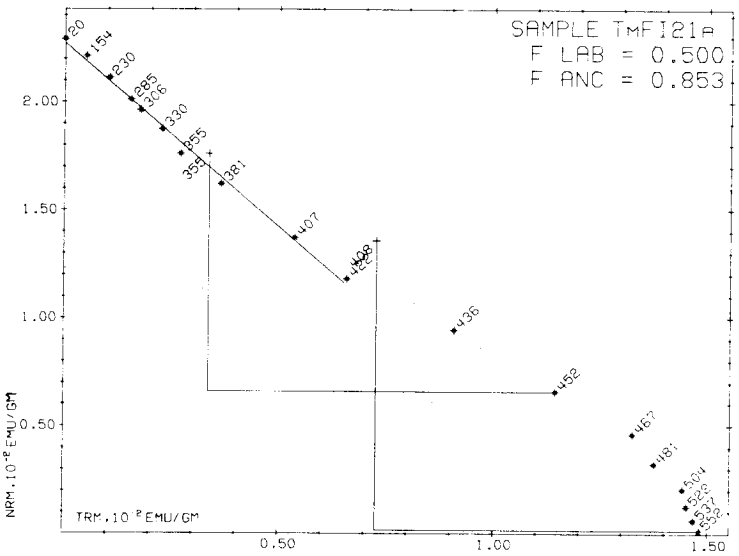
SAMPLE TmFI21a
F LAB = 0.500
F ANC = 0.853
NRM,10⁻³EMU/GM
TRM,10⁻³EMU/GM

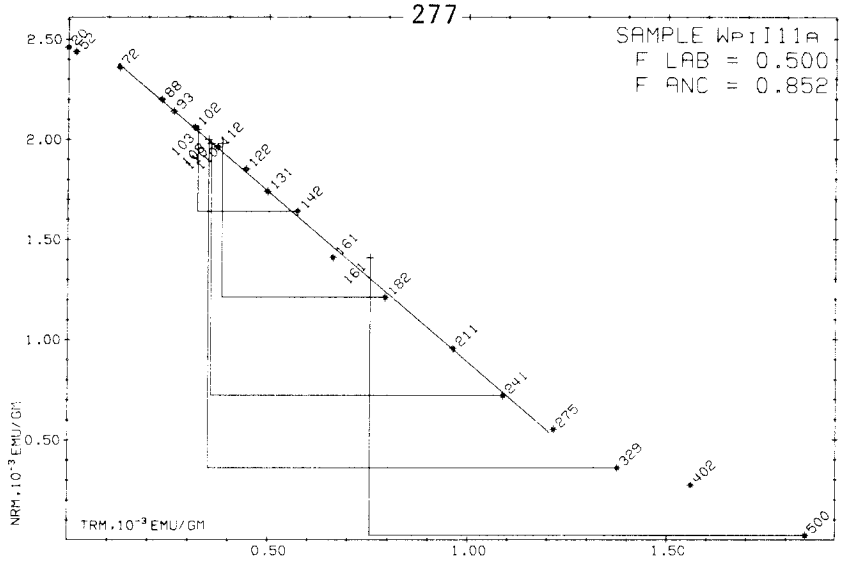
SAMPLE WPI11A
F LAB = 0.500
F ANC = 0.852
NRM,10⁻³EMU/GM
TRM,10⁻³EMU/GM
2.50
2.00
1.50
1.00
0.50
0.50
1.00
1.50
50
52
72
88
93
102
103
112
122
131
142
161
182
211
241
275
329
402
500

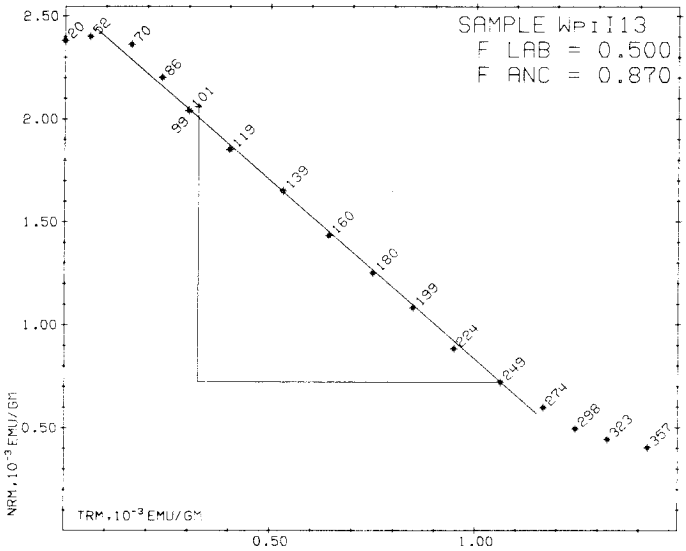
SAMPLE WPI13
F LAB = 0.500
F ANC = 0.870
NRM,10⁻³EMU/GM
TRM,10⁻³EMU/GM
2.50
2.00
1.50
1.00
0.50
0.50
1.00
20
52
70
86
99
101
119
139
160
180
199
224
249
274
298
323
357

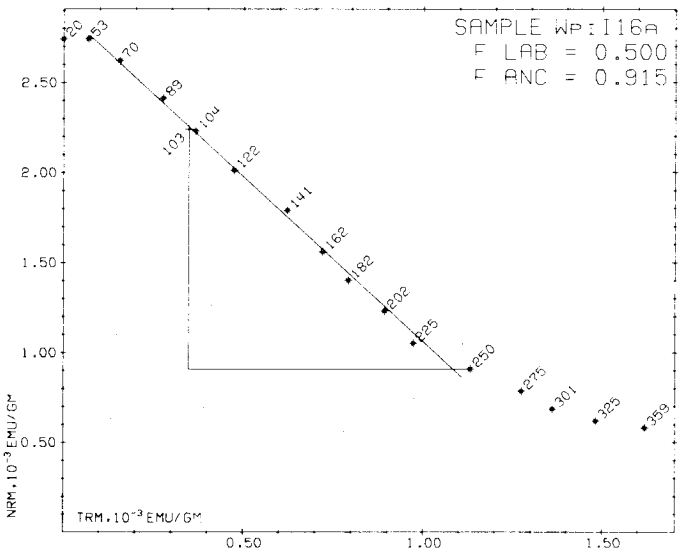
SAMPLE WPI16A
F LAB = 0.500
F ANC = 0.915
NRM,10⁻³EMU/GM
TRM,10⁻³EMU/GM
2.50
2.00
1.50
1.00
0.50
0.50
1.00
1.50
20
53
70
89
104
103
122
141
162
182
202
225
250
275
301
325
359

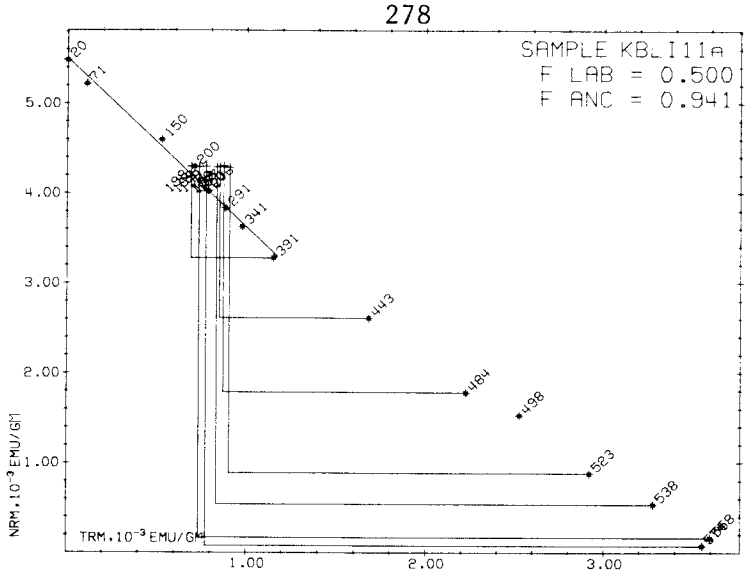
SAMPLE KBLI11A
F LAB = 0.500
F ANC = 0.941
NRM,10⁻³ EMU/GM
TRM,10⁻³ EMU/GM
20
71
150
200
291
341
391
443
484
498
523
538
1.00
2.00
3.00
4.00
5.00

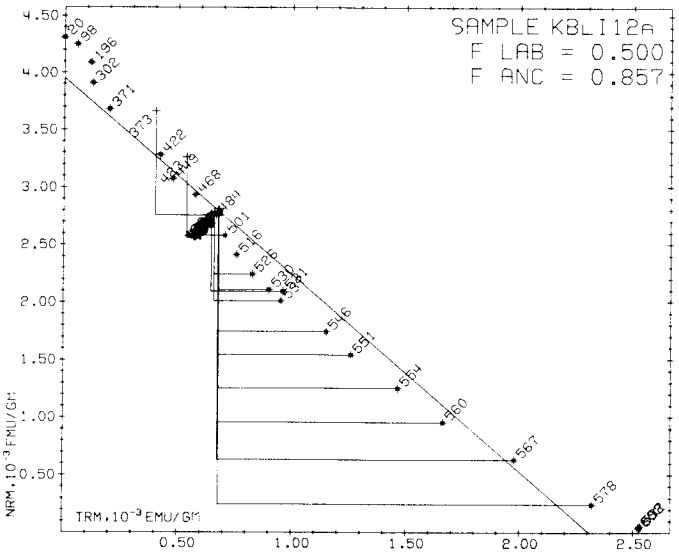
SAMPLE KBLI12A
F LAB = 0.500
F ANC = 0.857
NRM,10⁻³ EMU/GM
TRM,10⁻³ EMU/GM
20
98
196
302
371
422
468
516
526
530
546
551
564
560
567
578
0.50
1.00
1.50
2.00
2.50
3.00
3.50
4.00
4.50

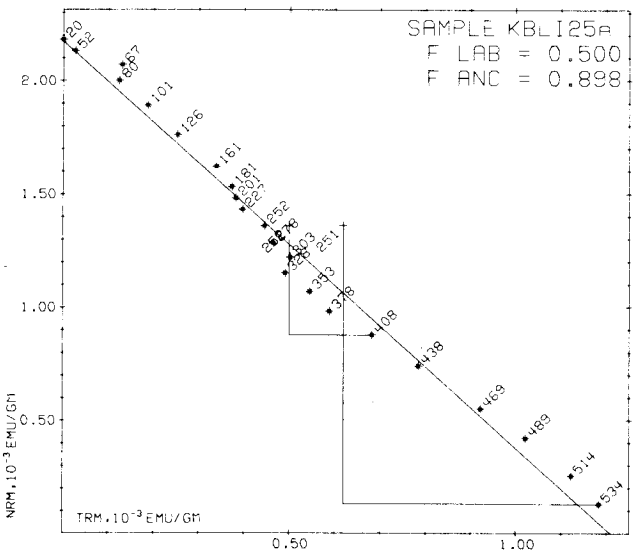
SAMPLE KBLI25A
F LAB = 0.500
F ANC = 0.898
NRM,10⁻³ EMU/GM
TRM,10⁻³ EMU/GM
20
52
67
80
101
126
161
181
201
252
251
343
358
408
438
469
489
514
534
0.50
1.00
1.50
2.00

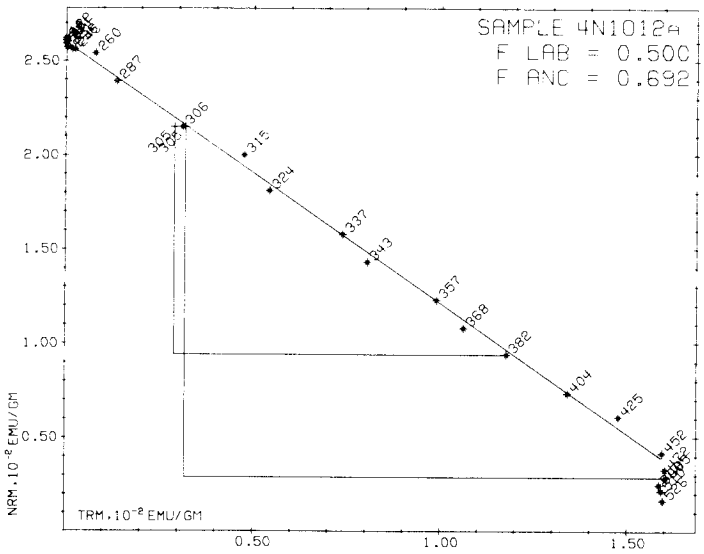
SAMPLE 4N1012A
F LAB = 0.500
F ANC = 0.692
NRM,10⁻² EMU/GM
TRM,10⁻² EMU/GM
2.50
2.00
1.50
1.00
0.50
0.50
1.00
1.50
260
287
306
315
324
337
343
357
368
382
404
425
452

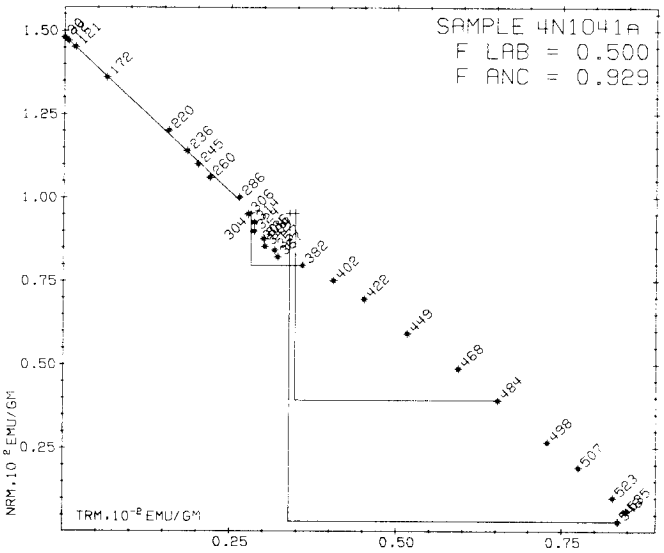
SAMPLE 4N1041A
F LAB = 0.500
F ANC = 0.929
NRM,10⁻² EMU/GM
TRM,10⁻² EMU/GM
1.50
1.25
1.00
0.75
0.50
0.25
0.25
0.50
0.75
172
220
236
245
260
286
304
382
402
422
449
468
484
498
507
523

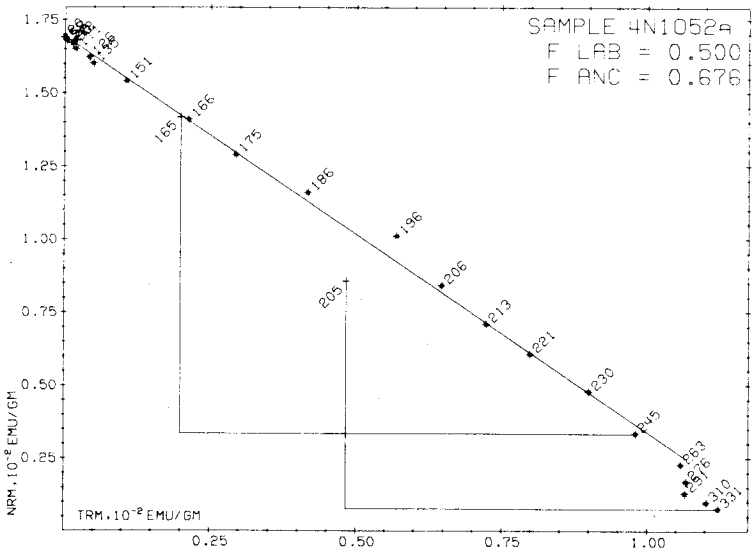
SAMPLE 4N1052A
F LAB = 0.500
F ANC = 0.676
NRM,10⁻² EMU/GM
TRM,10⁻² EMU/GM
1.75
1.50
1.25
1.00
0.75
0.50
0.25
0.25
0.50
0.75
1.00
151
165
166
175
186
196
205
206
213
221
230
245
263
276
310
331

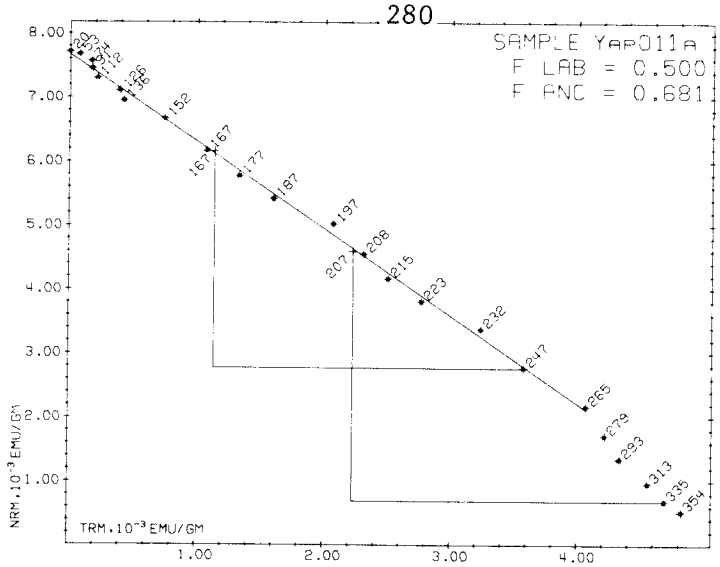
SAMPLE YAP011A
F LAB = 0.500
F ANC = 0.681
NRM, 10^{-3} EMU/GM
TRM, 10^{-3} EMU/GM
8.00
7.00
6.00
5.00
4.00
3.00
2.00
1.00
1.00
2.00
3.00
4.00

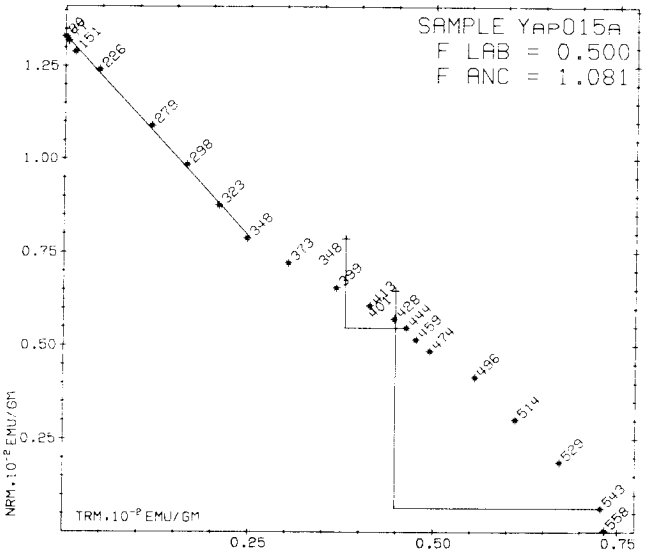
SAMPLE YAP015A
F LAB = 0.500
F ANC = 1.081
NRM, 10^{-2} EMU/GM
TRM, 10^{-2} EMU/GM
1.25
1.00
0.75
0.50
0.25
0.25
0.50
0.75

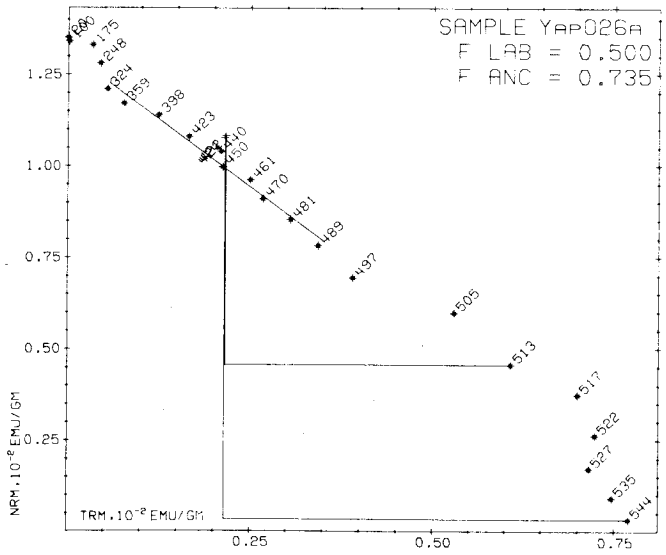
SAMPLE YAP026A
F LAB = 0.500
F ANC = 0.735
NRM, 10^{-2} EMU/GM
TRM, 10^{-2} EMU/GM
1.25
1.00
0.75
0.50
0.25
0.25
0.50
0.75

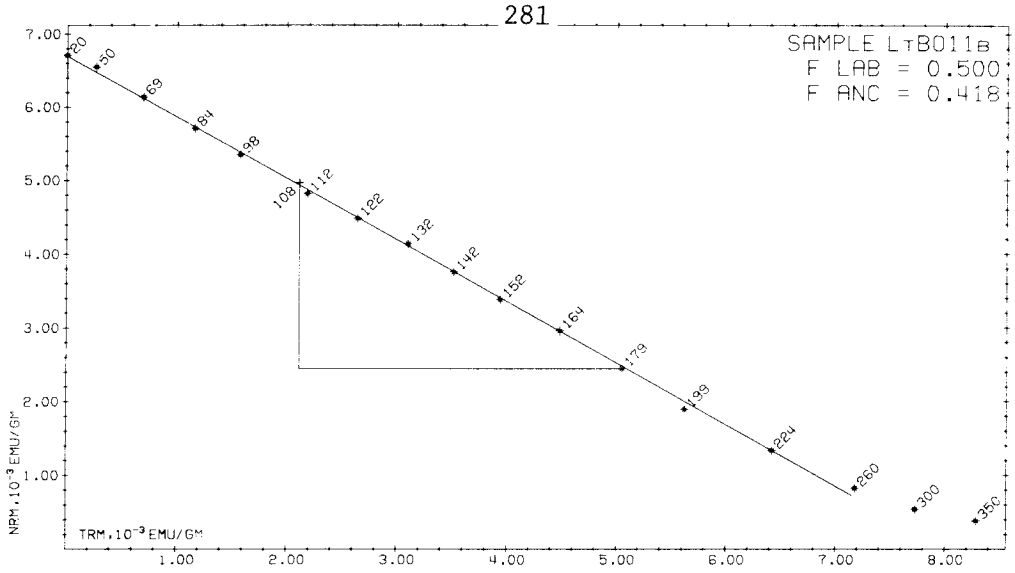
SAMPLE LTB011B
F LAB = 0.500
F ANC = 0.418
NRM,10⁻³ EMU/GM
TRM,10⁻³ EMU/GM

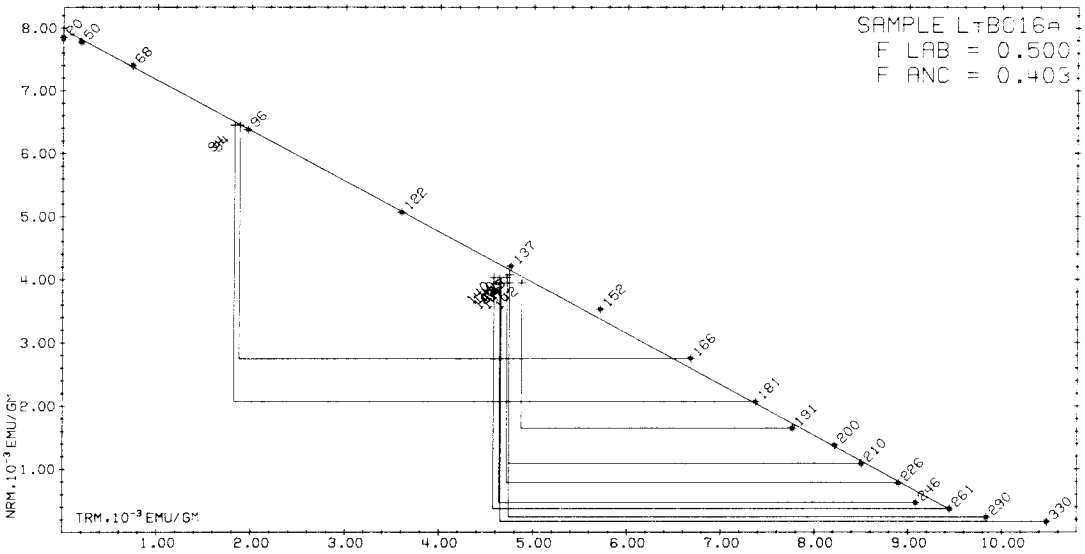
SAMPLE LTB016A
F LAB = 0.500
F ANC = 0.403
NRM,10⁻³ EMU/GM
TRM,10⁻³ EMU/GM

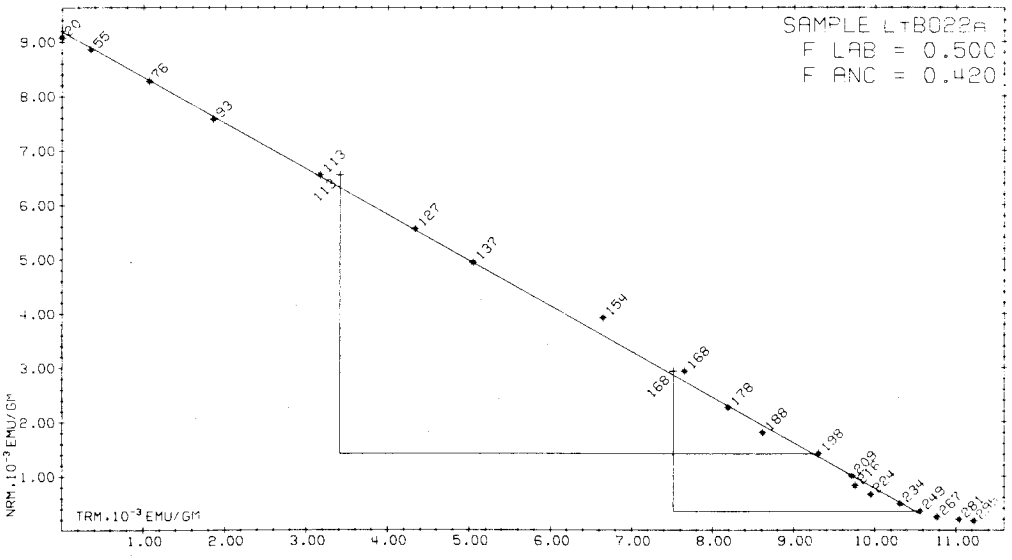
SAMPLE LTB022A
F LAB = 0.500
F ANC = 0.420
NRM,10⁻³ EMU/GM
TRM,10⁻³ EMU/GM

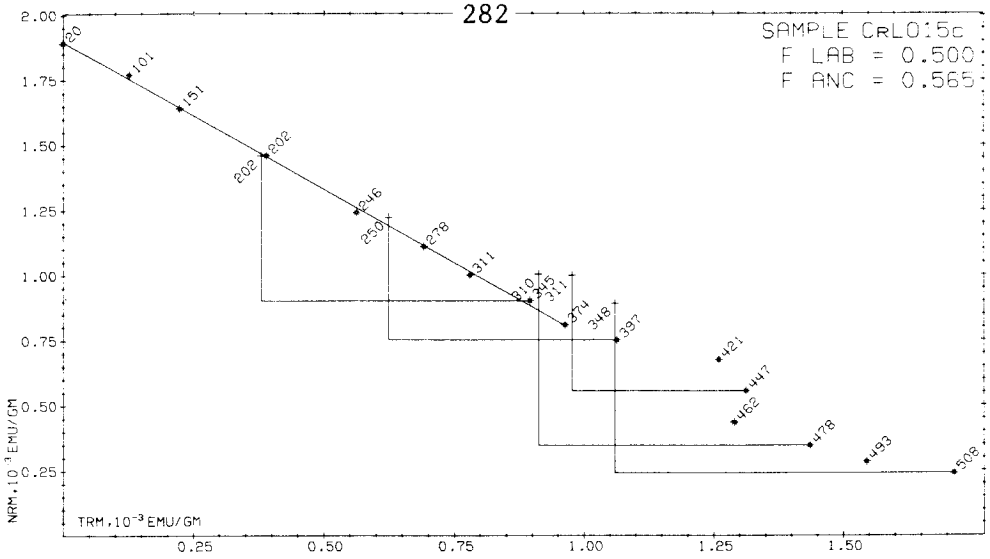
SAMPLE CRL015C
F LAB = 0.500
F ANC = 0.565
NRM,10⁻³ EMU/GM
TRM,10⁻³ EMU/GM

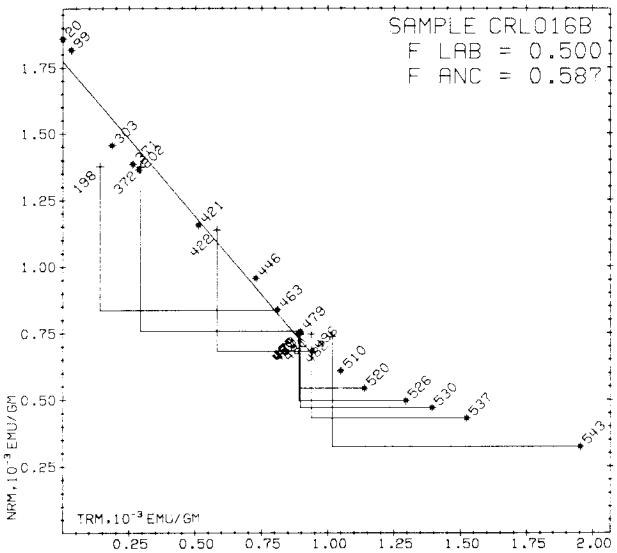
SAMPLE CRL016B
F LAB = 0.500
F ANC = 0.587
NRM,10⁻³ EMU/GM
TRM,10⁻³ EMU/GM

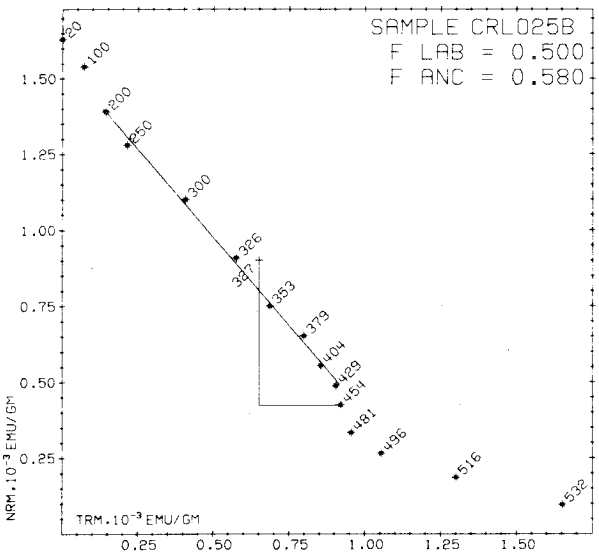
SAMPLE CRL025B
F LAB = 0.500
F ANC = 0.580
NRM,10⁻³ EMU/GM
TRM,10⁻³ EMU/GM

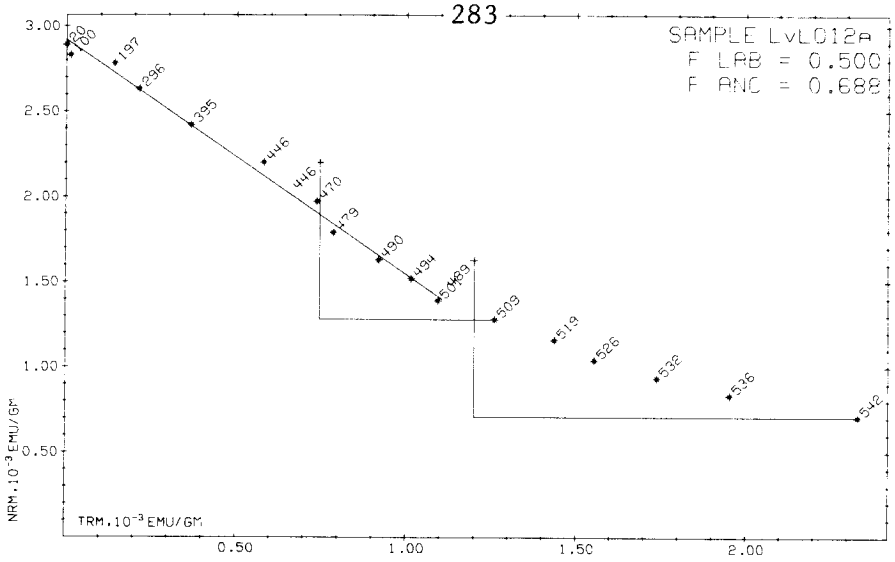
SAMPLE LvL012A
F LAB = 0.500
F ANC = 0.688
NRM,10⁻³EMU/GM
TRM,10⁻³EMU/GM
3.00
2.50
2.00
1.50
1.00
0.50
0.50
1.00
1.50
2.00
20
100
197
296
395
446
446
470
479
490
494
509
519
526
532
536
542

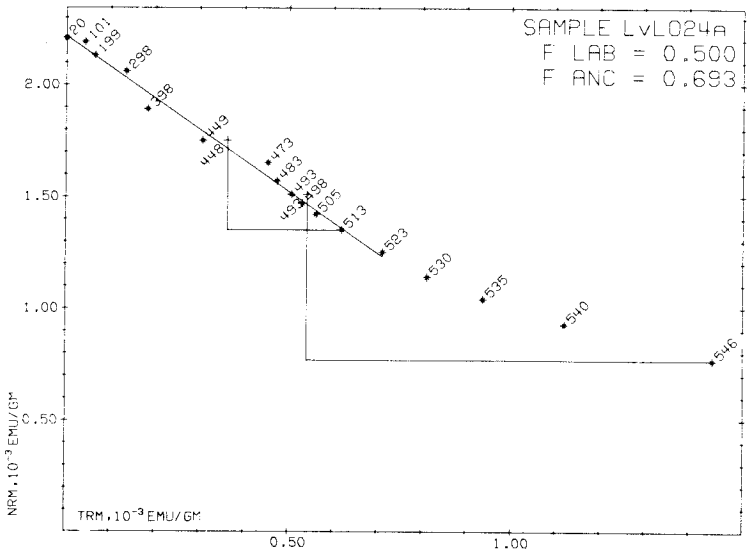
SAMPLE LvL024A
F LAB = 0.500
F ANC = 0.693
NRM,10⁻³EMU/GM
TRM,10⁻³EMU/GM
2.00
1.50
1.00
0.50
0.50
1.00
20
101
199
298
398
448
473
483
493
505
513
523
530
535
540
546

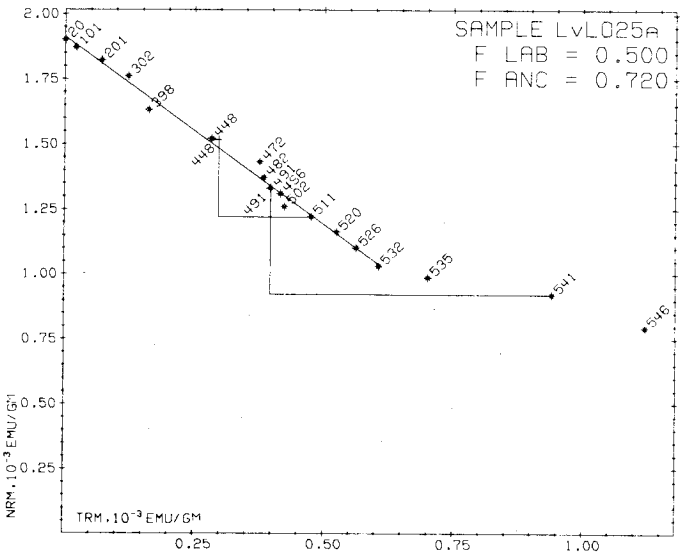
SAMPLE LvL025A
F LAB = 0.500
F ANC = 0.720
NRM,10⁻³EMU/GM
TRM,10⁻³EMU/GM
2.00
1.75
1.50
1.25
1.00
0.75
0.50
0.25
0.25
0.50
0.75
1.00
20
101
201
302
398
448
472
482
491
502
511
520
526
532
535
541
546

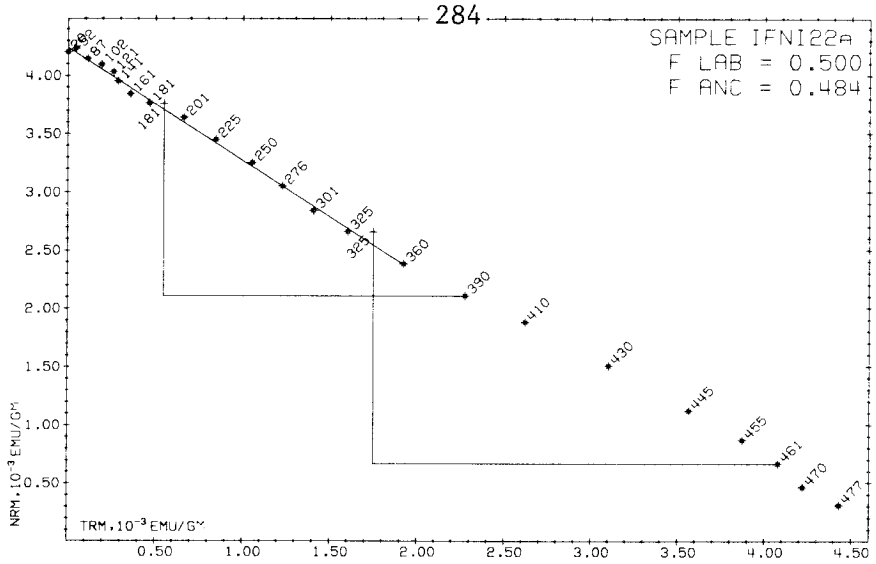
SAMPLE IFNI22A
F LAB = 0.500
F ANC = 0.484
NRM, 10^{-3} EMU/GM
TRM, 10^{-3} EMU/GM

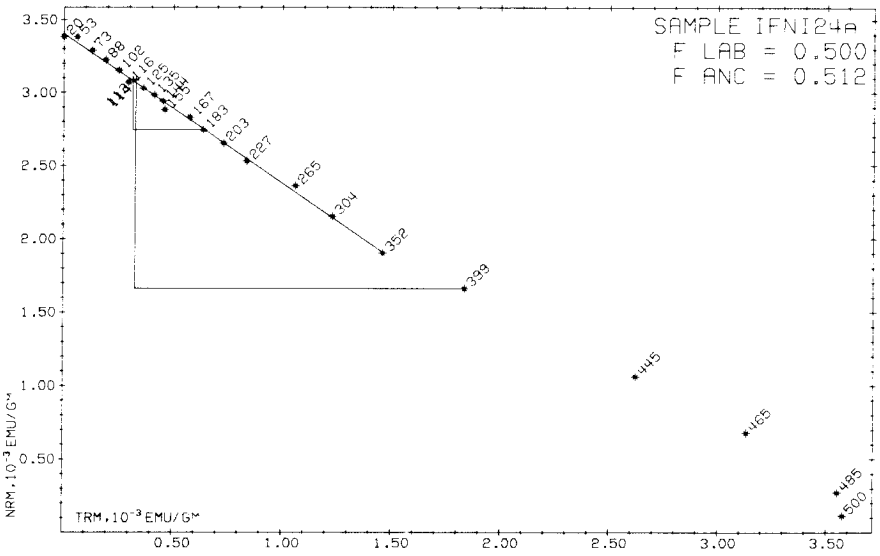
SAMPLE IFNI24A
F LAB = 0.500
F ANC = 0.512
NRM, 10^{-3} EMU/GM
TRM, 10^{-3} EMU/GM

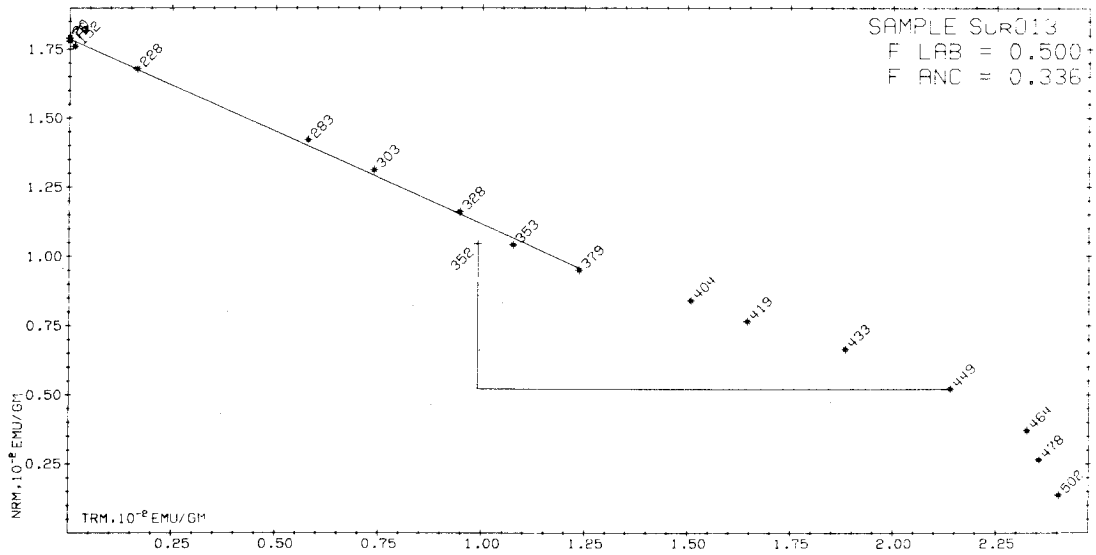
SAMPLE SUR013
F LAB = 0.500
F ANC = 0.336
NRM, 10^{-6} EMU/GM
TRM, 10^{-6} EMU/GM

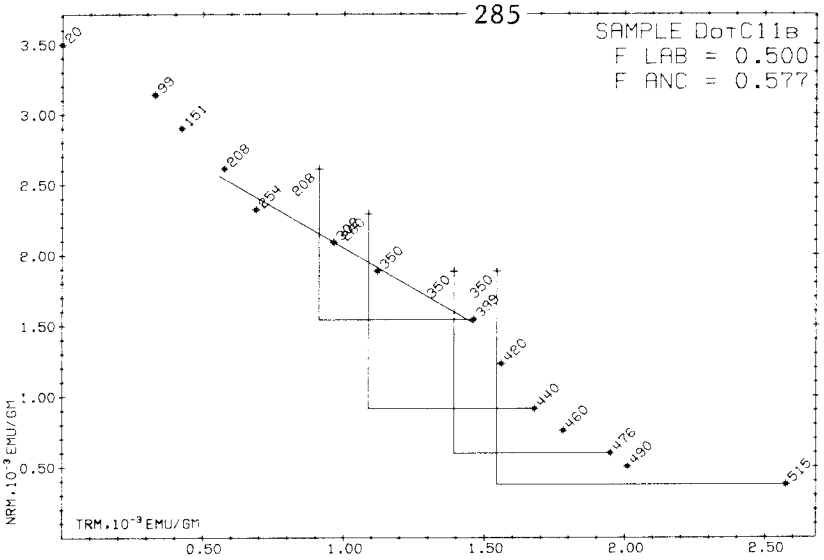
SAMPLE DoTC11B
F LAB = 0.500
F ANC = 0.577
NRM,10⁻³ EMU/GM
TRM,10⁻³ EMU/GM
20
99
151
208
254
208
308
350
350
350
399
420
440
460
476
490
515
0.50
1.00
1.50
2.00
2.50
3.00
3.50

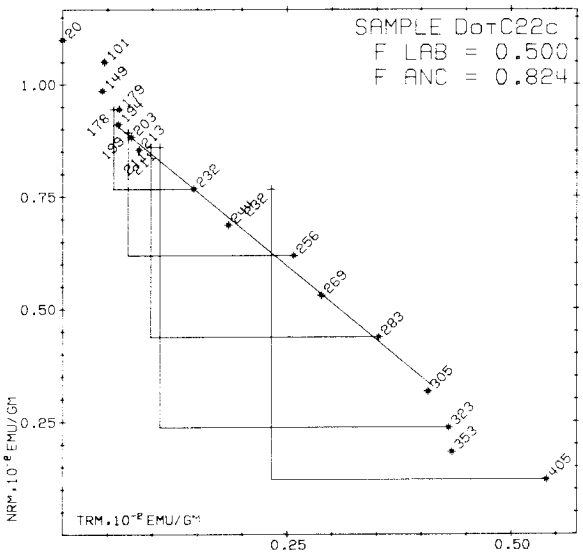
SAMPLE DoTC22c
F LAB = 0.500
F ANC = 0.824
NRM,10⁻⁶ EMU/GM
TRM,10⁻⁶ EMU/GM
20
101
149
178
203
213
232
256
269
283
305
323
353
405
0.25
0.50
0.75
1.00

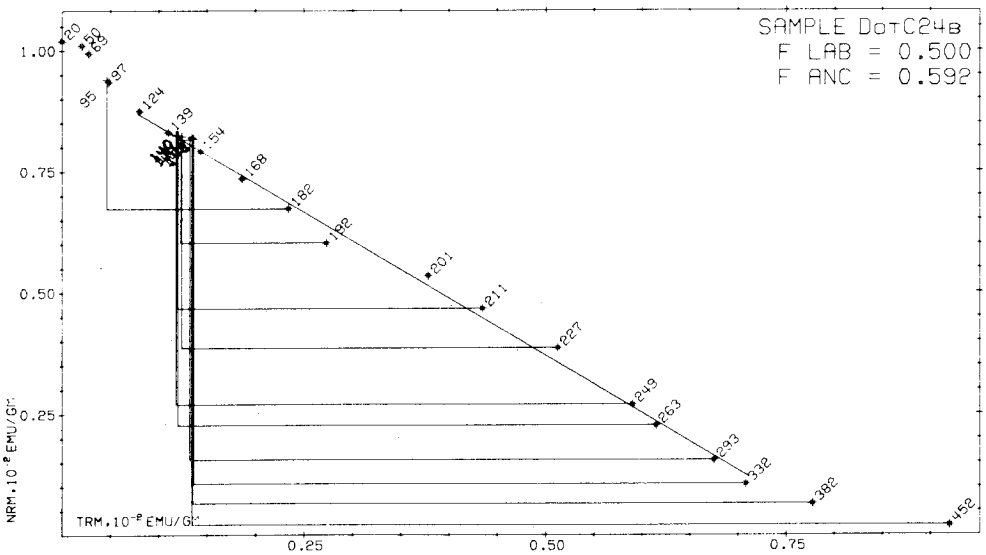
SAMPLE DoTC24B
F LAB = 0.500
F ANC = 0.592
NRM,10⁻⁶ EMU/GM
TRM,10⁻⁶ EMU/GM
20
50
69
97
95
124
139
154
168
182
192
201
211
227
249
263
293
332
382
452
0.25
0.50
0.75
1.00

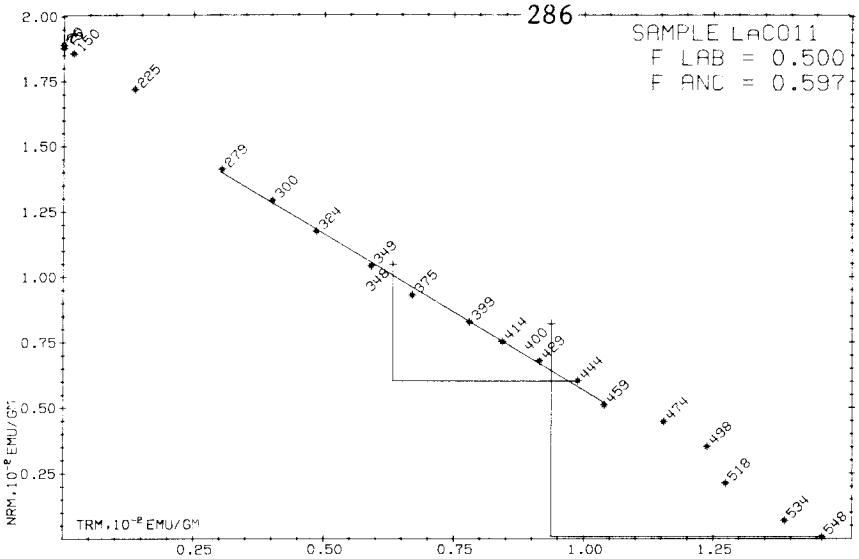
SAMPLE LaC011
F LAB = 0.500
F ANC = 0.597
NRM, 10^{-8} EMU/GM
TRM, 10^{-8} EMU/GM

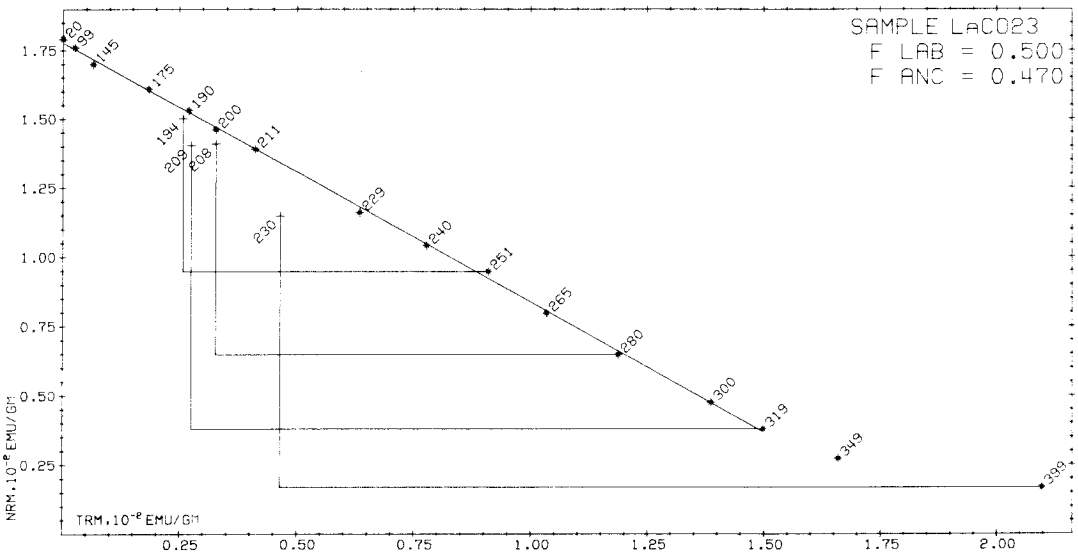
SAMPLE LaC023
F LAB = 0.500
F ANC = 0.470
NRM, 10^{-8} EMU/GM
TRM, 10^{-8} EMU/GM

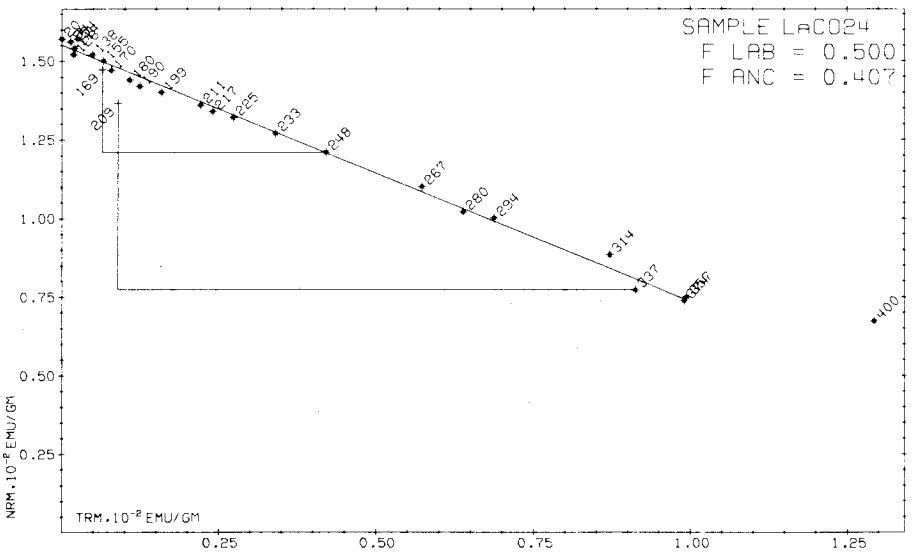
SAMPLE LaC024
F LAB = 0.500
F ANC = 0.407
NRM, 10^{-8} EMU/GM
TRM, 10^{-8} EMU/GM

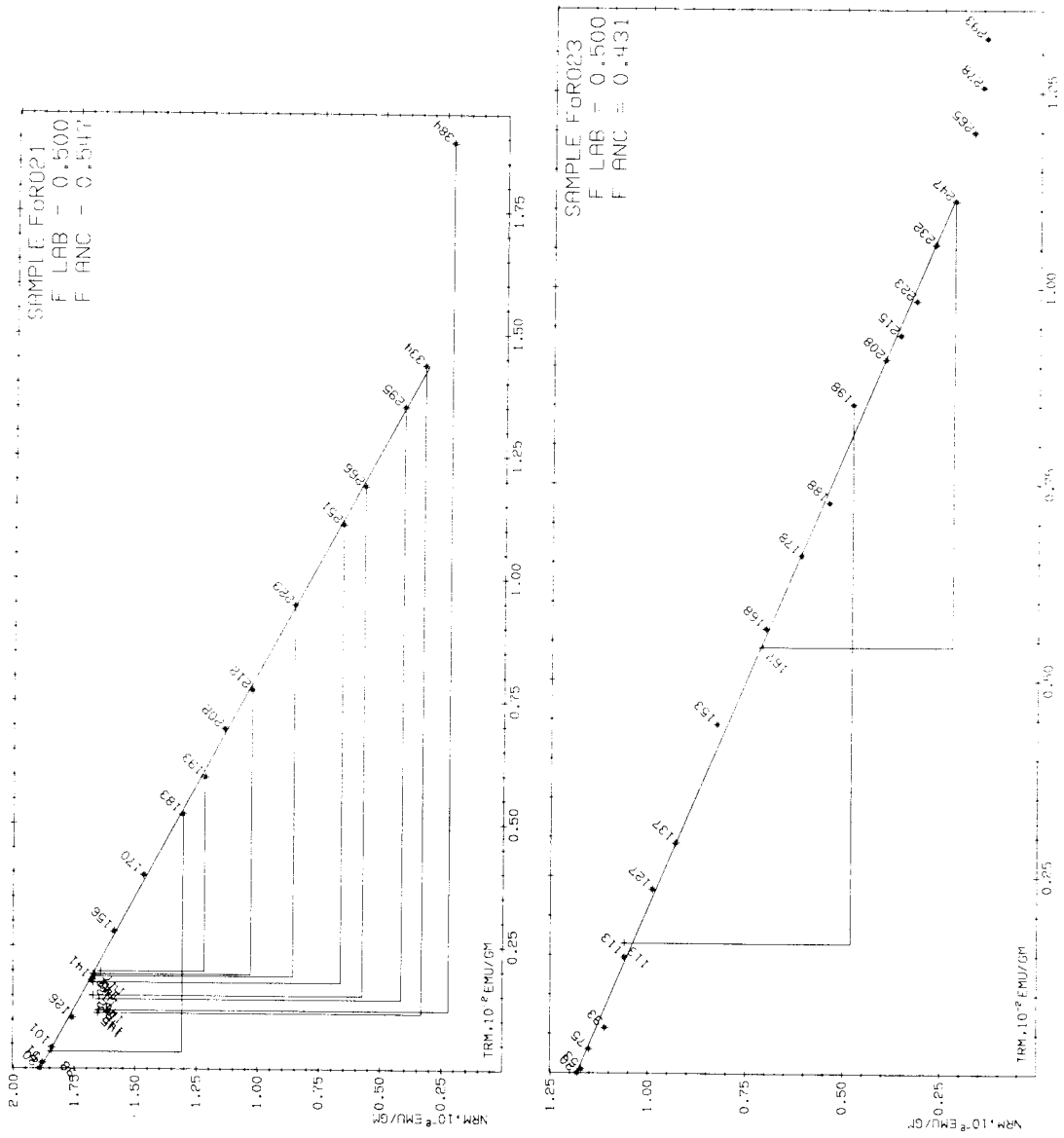
SAMPLE FoR021
F LAB = 0.500
F ANC = 0.5417
NRM,10⁻³ EMU/GM
TRM,10⁻³ EMU/GM
SAMPLE FoR023
F LAB = 0.500
F ANC = 0.431
NRM,10⁻³ EMU/GM
TRM,10⁻³ EMU/GM

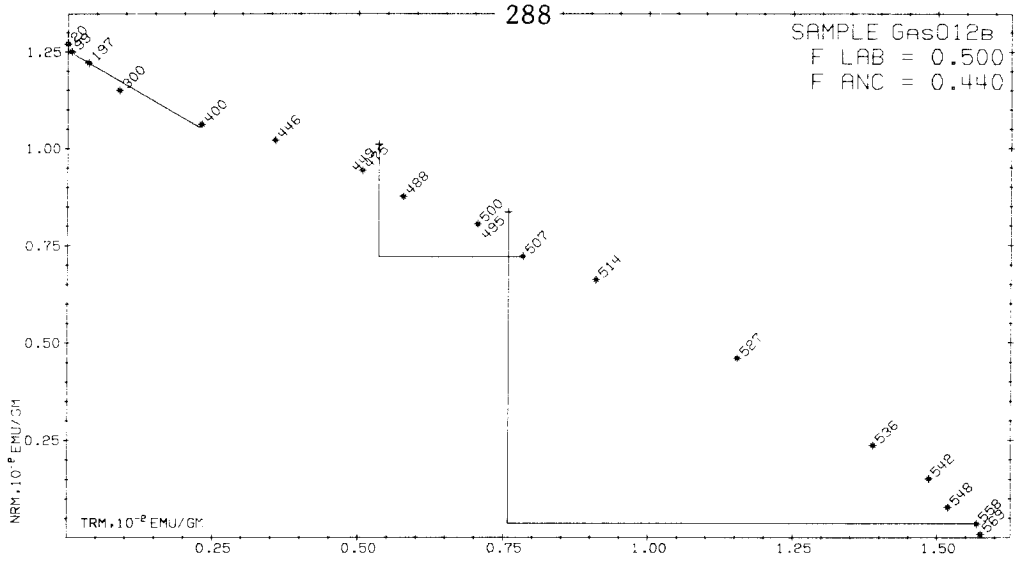
SAMPLE GAS012B
F LAB = 0.500
F ANC = 0.440
NRM,10⁻³ EMU/GM
TRM,10⁻³ EMU/GM

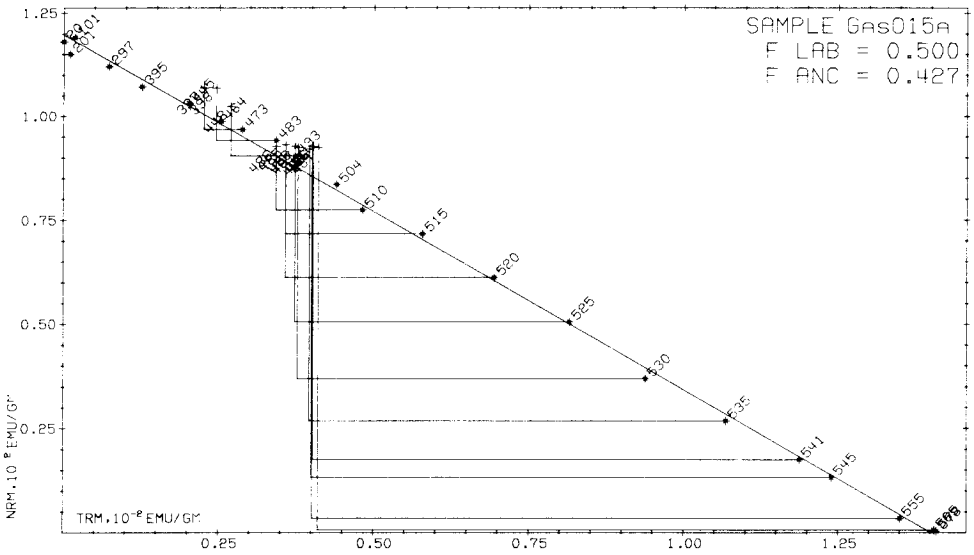
SAMPLE GAS015A
F LAB = 0.500
F ANC = 0.427
NRM,10⁻³ EMU/GM
TRM,10⁻³ EMU/GM

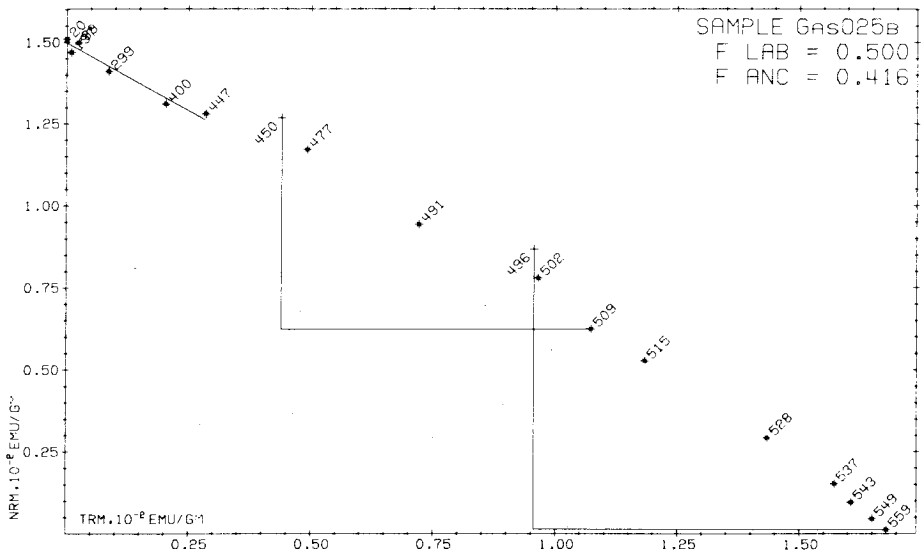
SAMPLE GAS025B
F LAB = 0.500
F ANC = 0.416
NRM,10⁻³ EMU/GM
TRM,10⁻³ EMU/GM

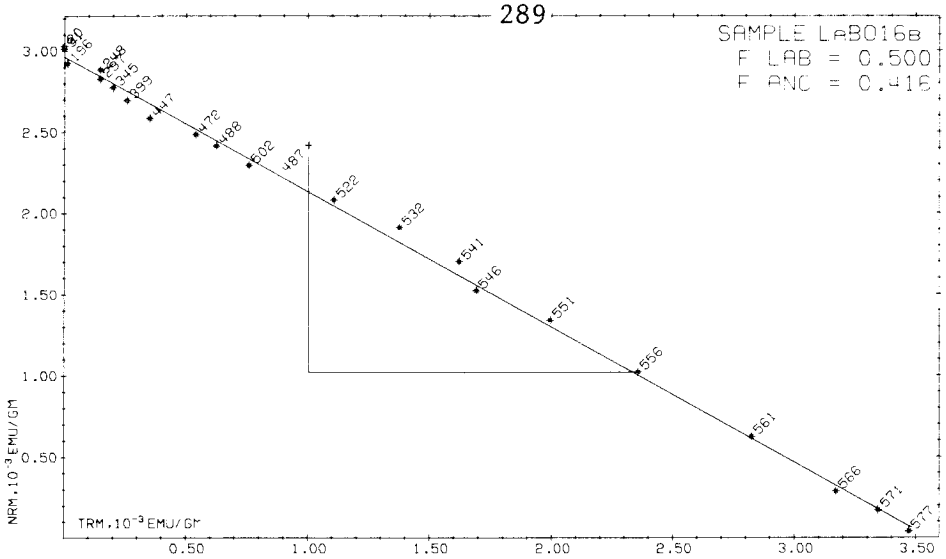
SAMPLE LaB016B
F LAB = 0.500
F ANC = 0.416
NRM,10⁻³EMU/GM
TRM,10⁻³EMU/GM
3.00
2.50
2.00
1.50
1.00
0.50
0.50
1.00
1.50
2.00
2.50
3.00
3.50
487
522
532
541
546
551
556
561
566
571
577

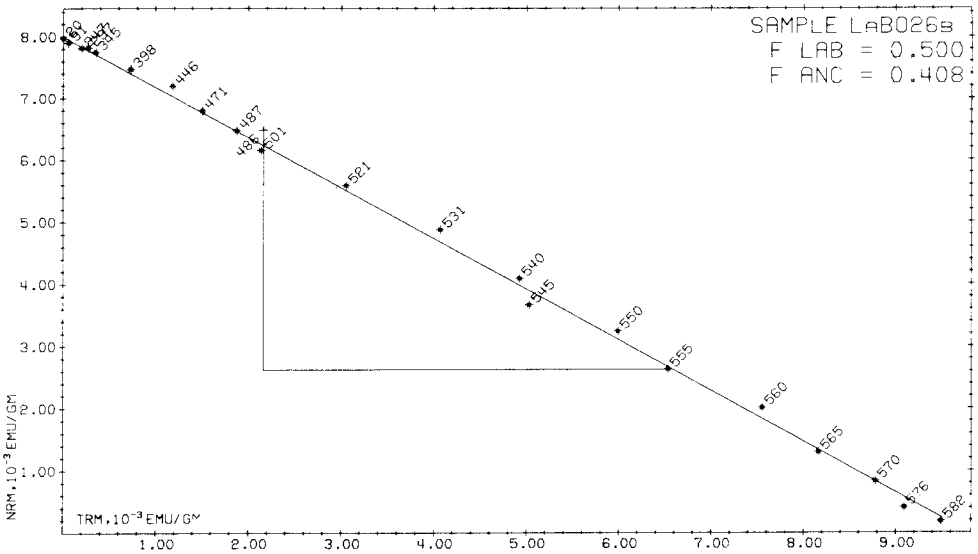
SAMPLE LaB026B
F LAB = 0.500
F ANC = 0.408
NRM,10⁻³EMU/GM
TRM,10⁻³EMU/GM
8.00
7.00
6.00
5.00
4.00
3.00
2.00
1.00
1.00
2.00
3.00
4.00
5.00
6.00
7.00
8.00
9.00
487
501
521
531
540
545
550
555
560
565
570
576
582

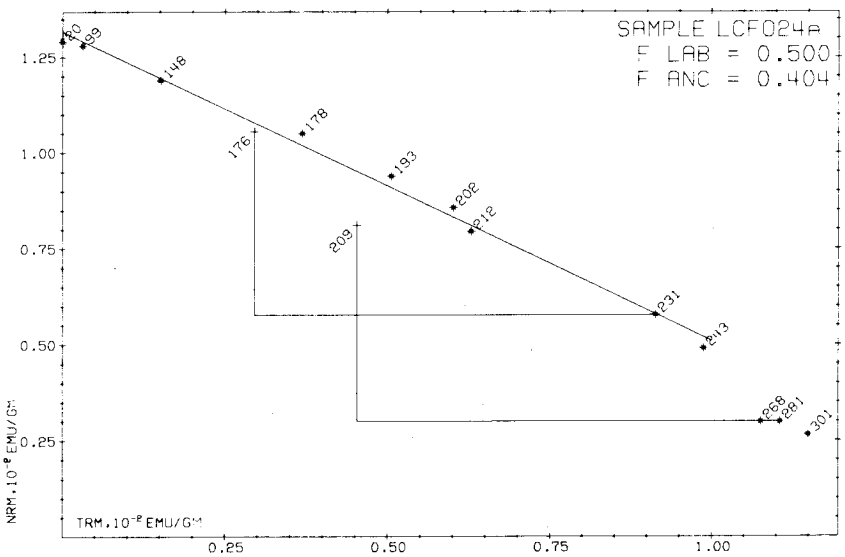
SAMPLE LCF024A
F LAB = 0.500
F ANC = 0.404
NRM,10⁻⁸EMU/GM
TRM,10⁻⁸EMU/GM
1.25
1.00
0.75
0.50
0.25
0.25
0.50
0.75
1.00
176
178
193
202
212
209
231
213
268
281
301

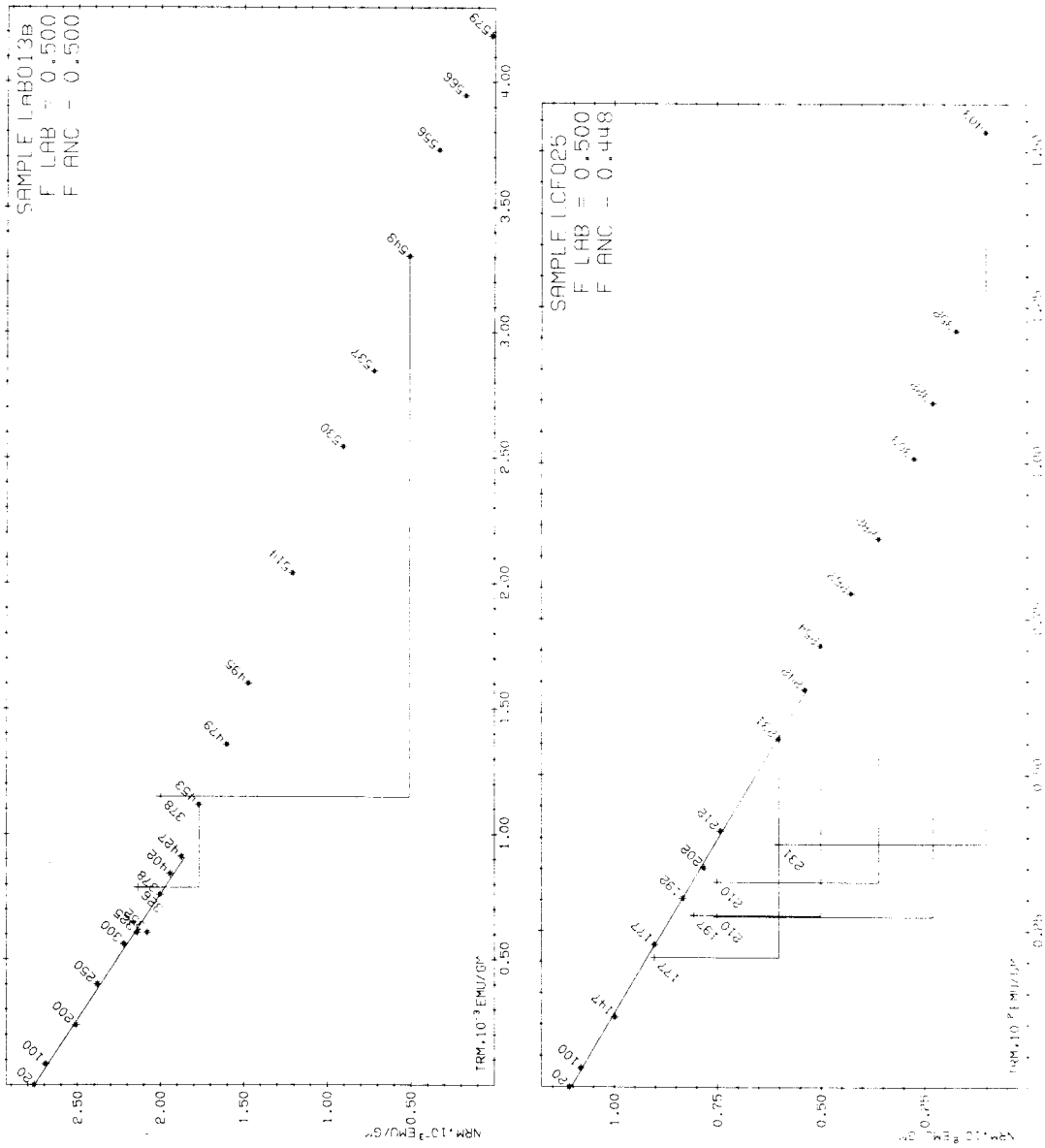
SAMPLE LAB013B
F LAB = 0.500
F ANC = 0.500
SAMPLE LCF025
F LAB = 0.500
F ANC = 0.448

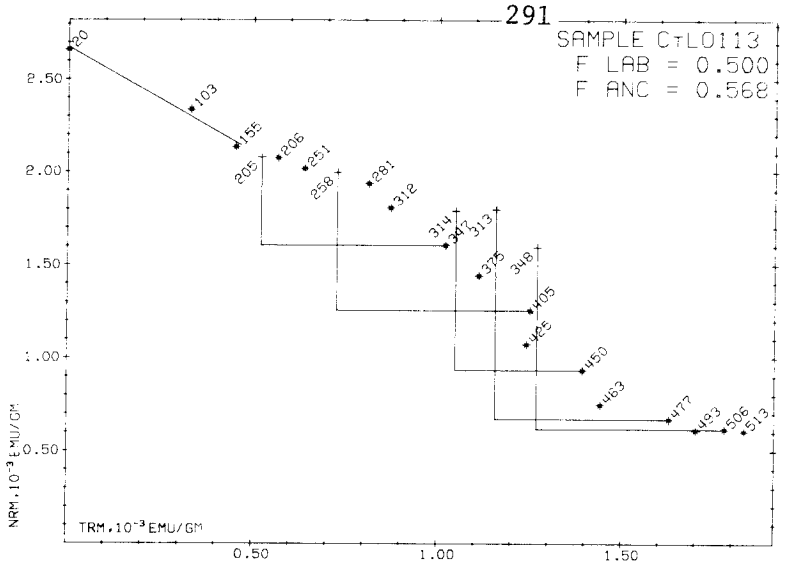
SAMPLE CTL0113
F LAB = 0.500
F ANC = 0.568
NRM,10⁻³EMU/GM
TRM,10⁻³EMU/GM
20
103
155
205
206
251
258
281
312
314
347
313
375
348
405
425
450
463
477
493
506
513
2.50
2.00
1.50
1.00
0.50
0.50
1.00
1.50

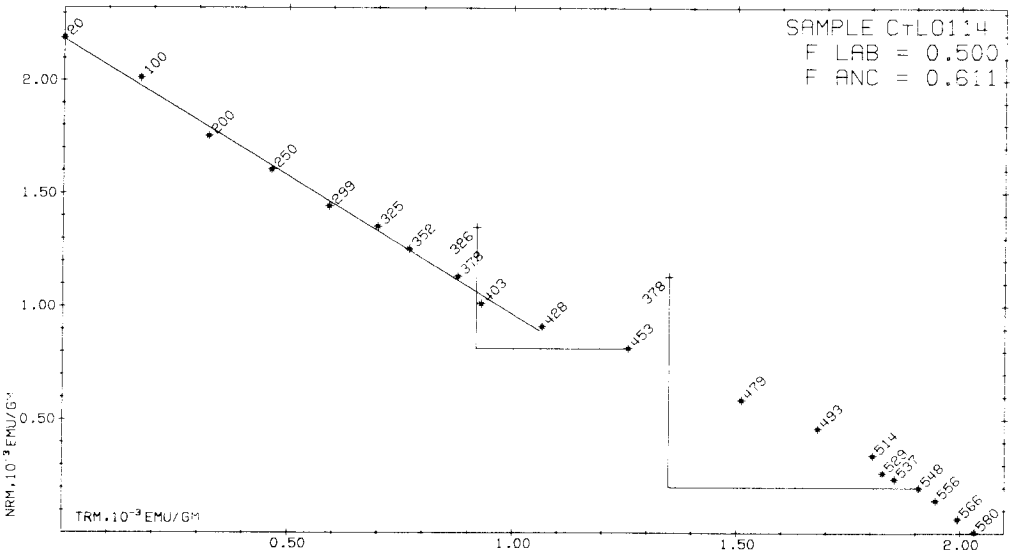
SAMPLE CTL0114
F LAB = 0.500
F ANC = 0.611
NRM,10⁻³EMU/GM
TRM,10⁻³EMU/GM
20
100
200
250
299
325
352
326
378
403
428
453
378
479
493
514
529
537
548
556
566
580
2.00
1.50
1.00
0.50
0.50
1.00
1.50
2.00

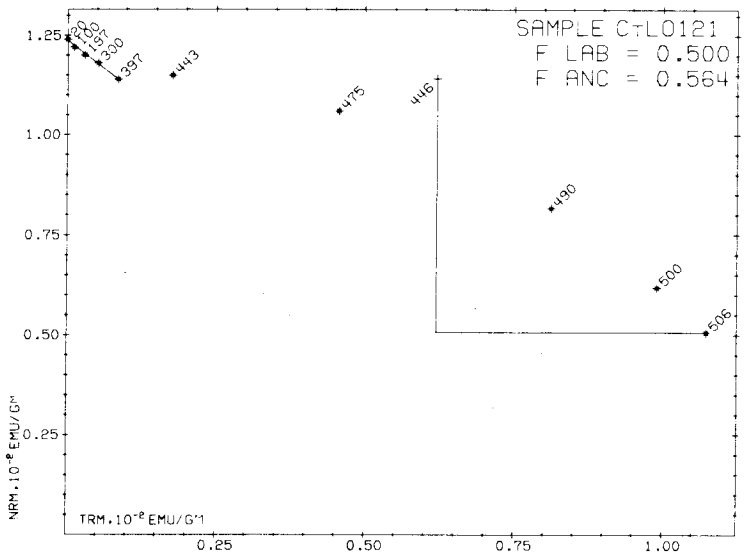
SAMPLE CTL0121
F LAB = 0.500
F ANC = 0.564
NRM,10⁻³EMU/GM
TRM,10⁻³EMU/GM
20
100
157
300
397
443
475
446
490
500
506
1.25
1.00
0.75
0.50
0.25
0.25
0.50
0.75
1.00

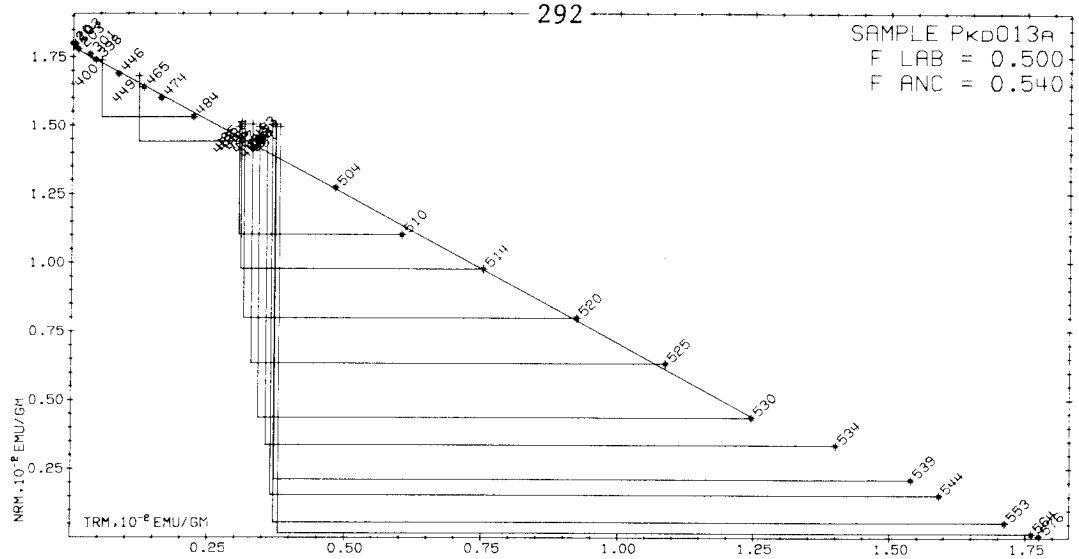
SAMPLE PKD013A
F LAB = 0.500
F ANC = 0.540
NRM,10⁻⁶ EMU/GM
TRM,10⁻⁶ EMU/GM
0.25
0.50
0.75
1.00
1.25
1.50
1.75
400
446
449
465
474
484
504
510
514
520
525
530
534
539
544
553

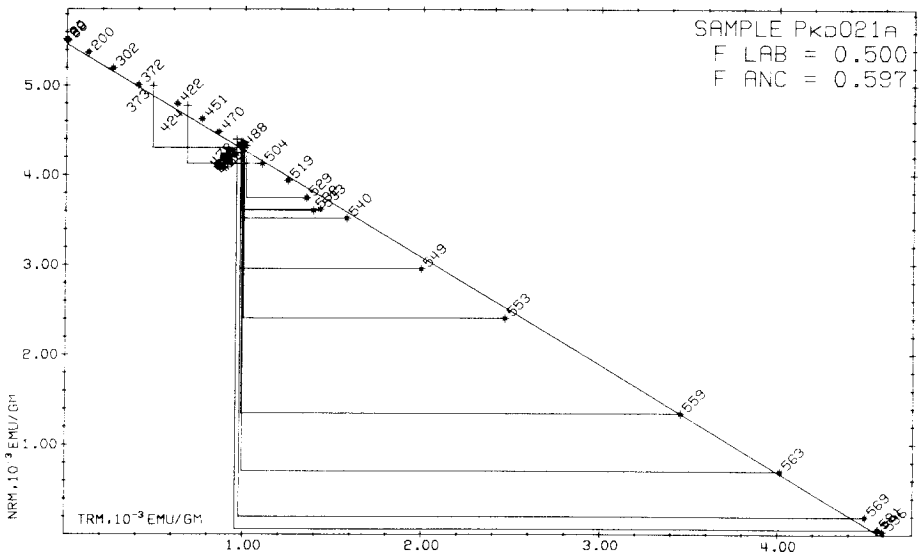
SAMPLE PKD021A
F LAB = 0.500
F ANC = 0.597
NRM,10⁻³ EMU/GM
TRM,10⁻³ EMU/GM
1.00
2.00
3.00
4.00
5.00
200
302
372
373
422
451
470
488
504
519
529
540
549
553
559
563
569

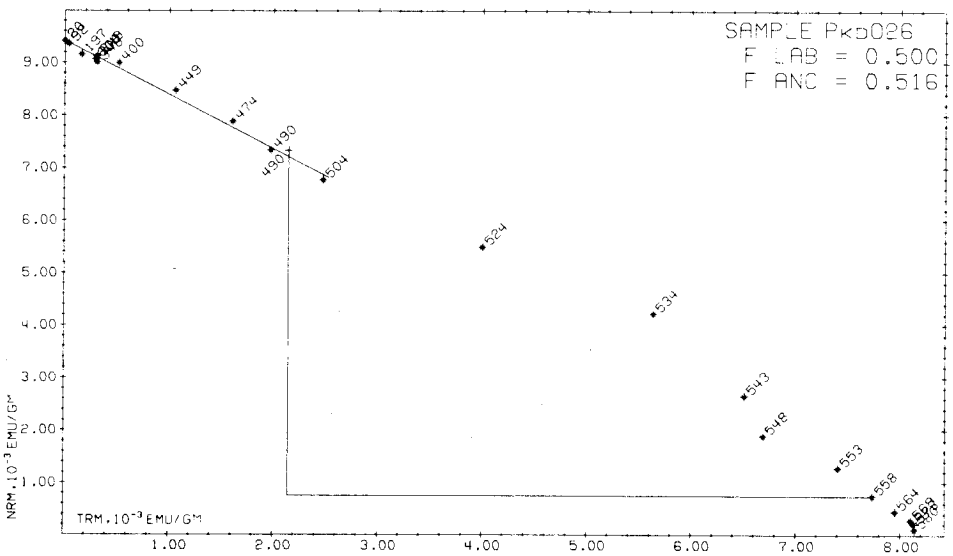
SAMPLE PKD026
F LAB = 0.500
F ANC = 0.516
NRM,10⁻³ EMU/GM
TRM,10⁻³ EMU/GM
1.00
2.00
3.00
4.00
5.00
6.00
7.00
8.00
9.00
400
449
474
490
490
504
524
534
543
548
553
558
564

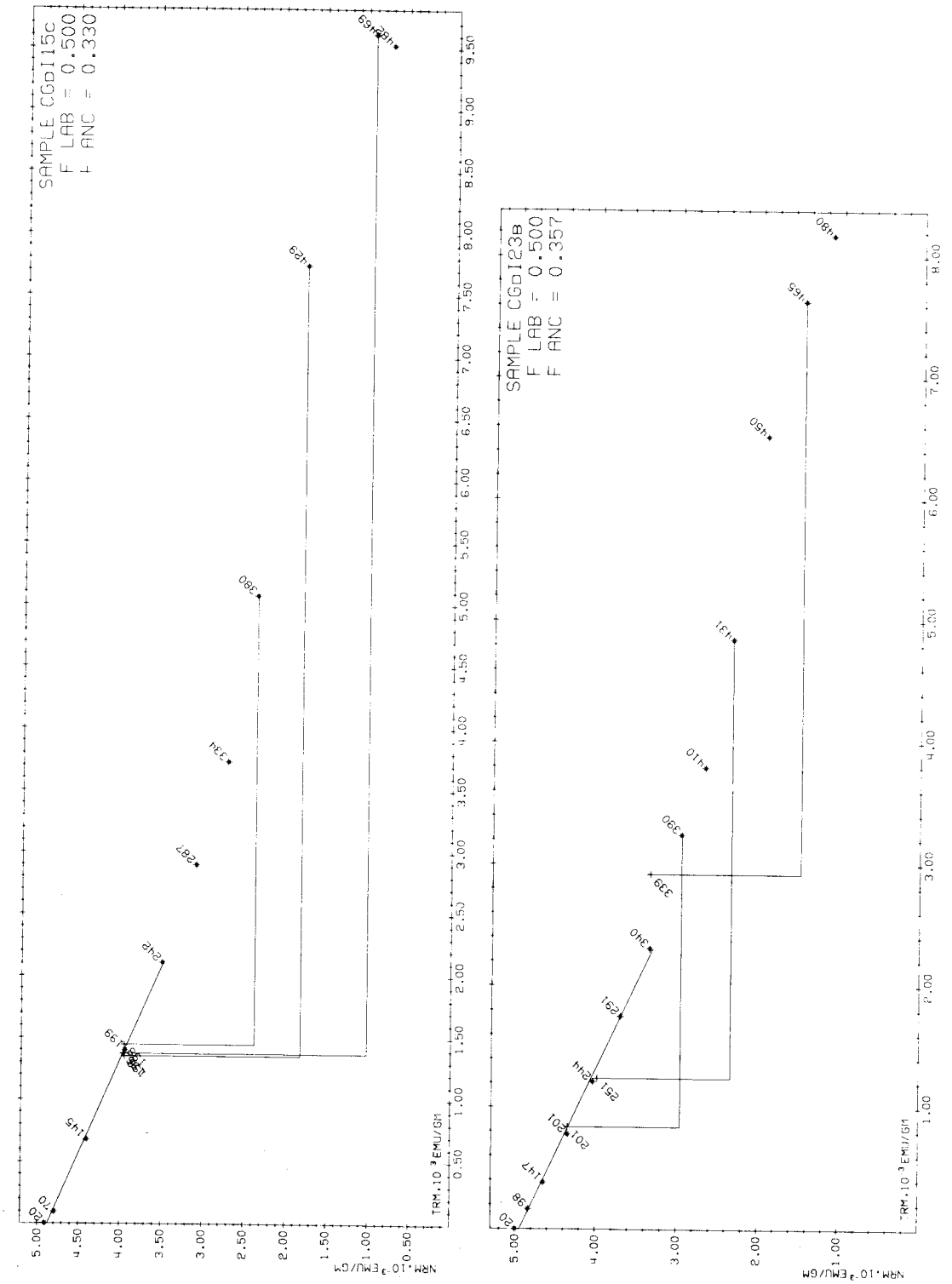
SAMPLE CGDI15c
F LAB = 0.500
F ANC = 0.330
NRM.10⁻³EMU/GM
TRM.10⁻³EMU/GM
SAMPLE CGDI23B
F LAB = 0.500
F ANC = 0.357
NRM.10⁻³EMU/GM
TRM.10⁻³EMU/GM

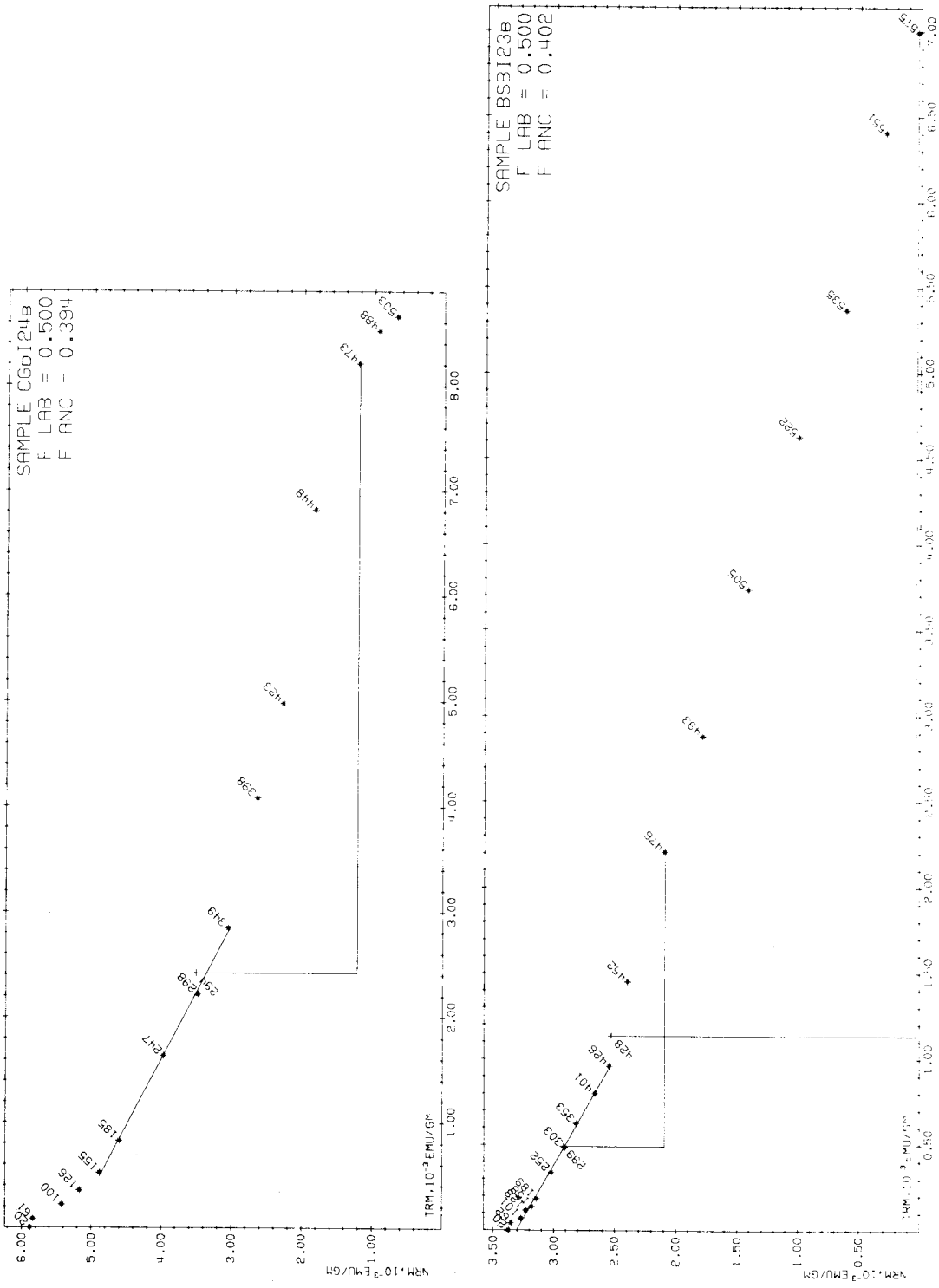
SAMPLE CGbI24B
F LAB = 0.500
F ANC = 0.394
SAMPLE BSBI23B
F LAB = 0.500
F ANC = 0.402
NRM,10⁻³EMU/GM
TRM,10⁻³EMU/GM

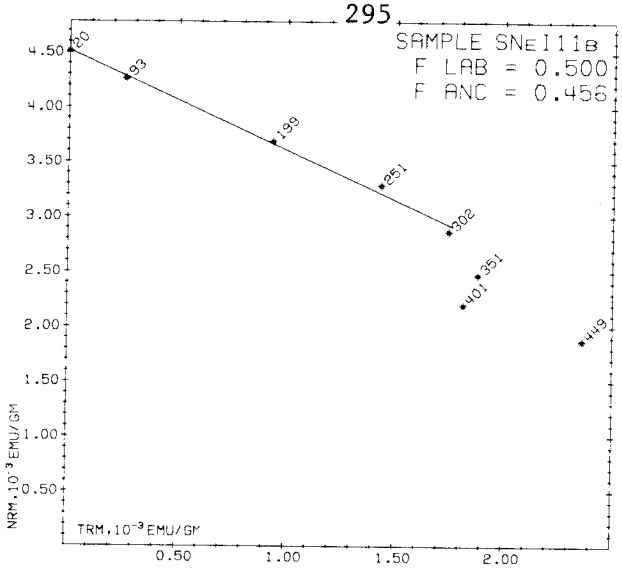
SAMPLE SNEI11B
F LAB = 0.500
F ANC = 0.456
20
93
199
251
302
351
401
449
NRM,10⁻³EMU/GM
TRM,10⁻³EMU/GM
0.50
1.00
1.50
2.00
2.50
3.00
3.50
4.00
4.50

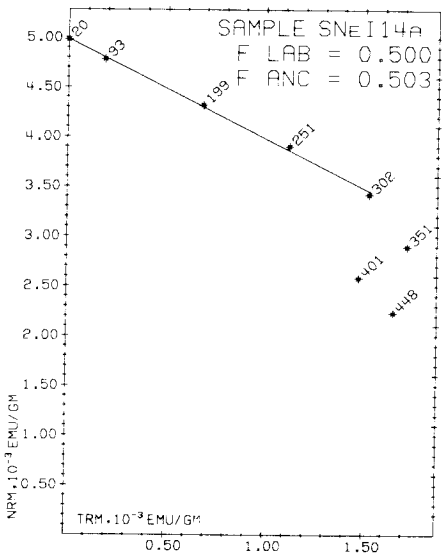
SAMPLE SNEI14A
F LAB = 0.500
F ANC = 0.503
20
93
199
251
302
351
401
448
NRM,10⁻³EMU/GM
TRM,10⁻³EMU/GM
0.50
1.00
1.50
2.00
2.50
3.00
3.50
4.00
4.50
5.00

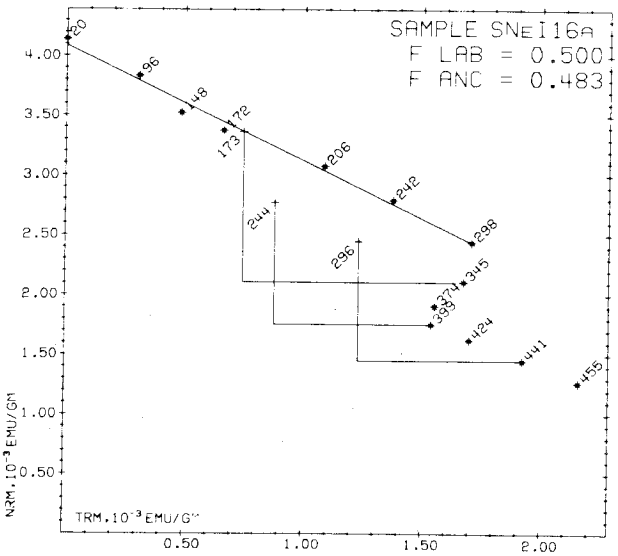
SAMPLE SNEI16A
F LAB = 0.500
F ANC = 0.483
20
96
148
172
173
206
242
244
296
298
345
374
399
424
441
455
NRM,10⁻³EMU/GM
TRM,10⁻³EMU/GM
0.50
1.00
1.50
2.00
2.50
3.00
3.50
4.00

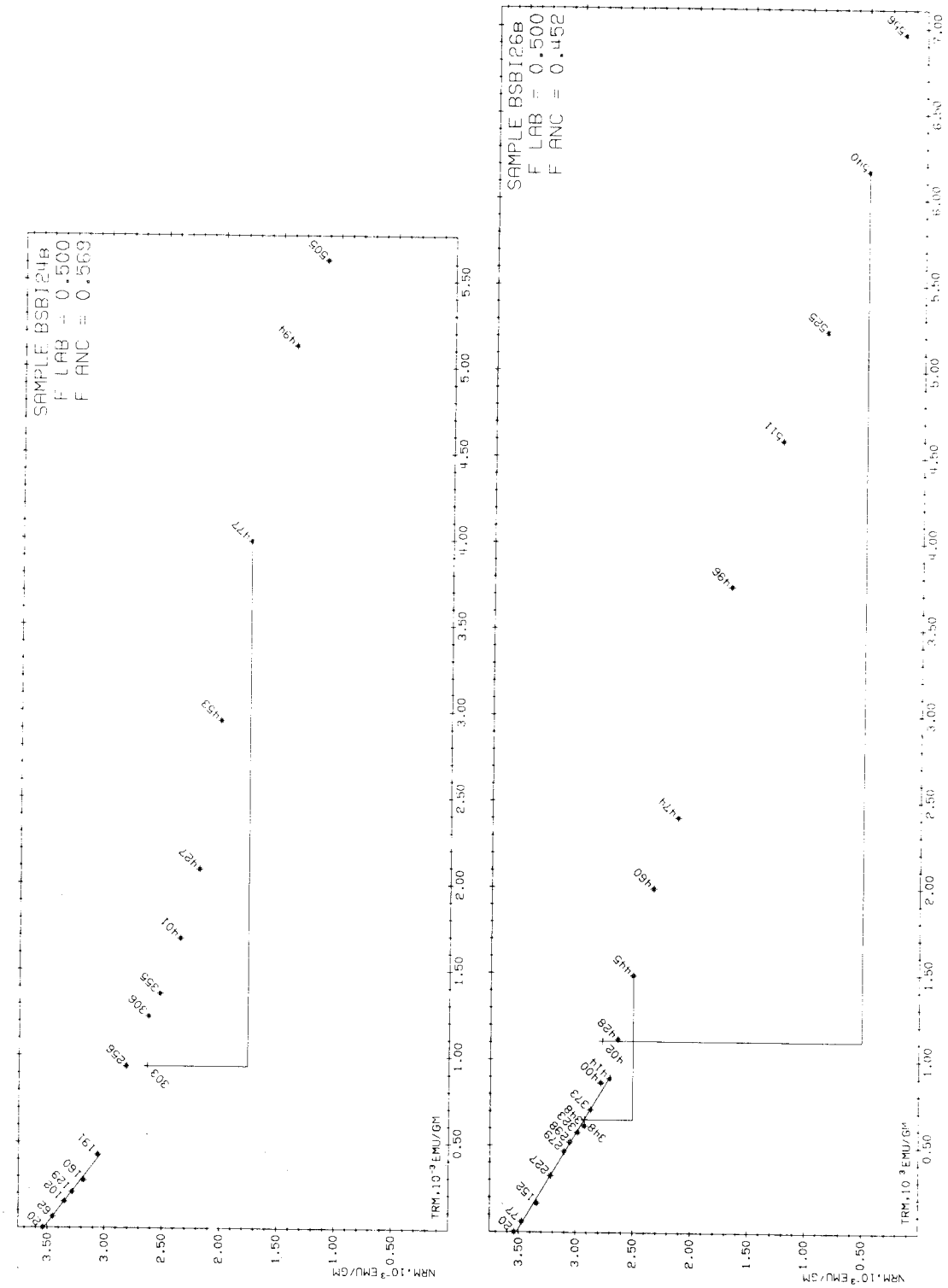
SAMPLE BSBI24B
F LAB = 0.500
F ANC = 0.569
NRM.10⁻³EMU/GM
TRM.10⁻³EMU/GM
SAMPLE BSBI26B
F LAB = 0.500
F ANC = 0.452
NRM.10⁻³EMU/GM
TRM.10⁻³EMU/GM

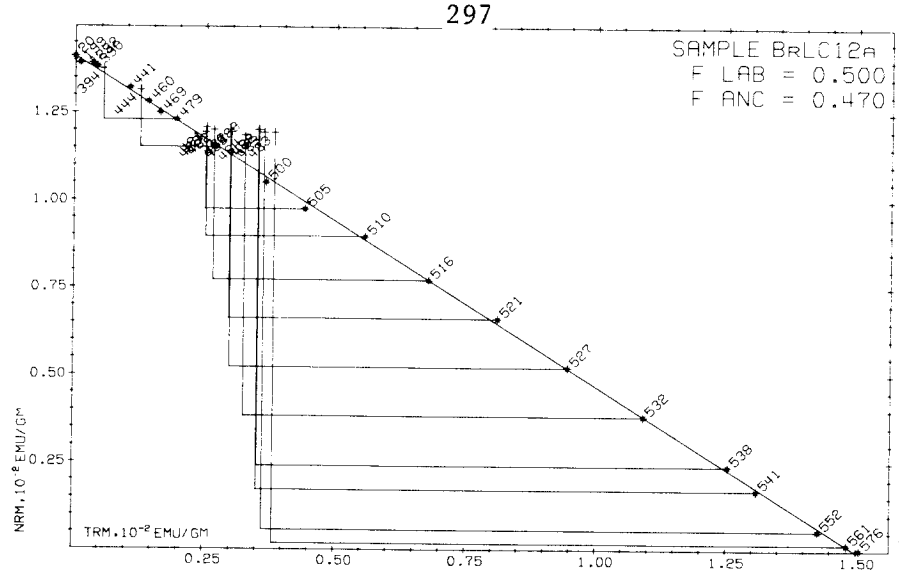
SAMPLE BRLC12A
F LAB = 0.500
F ANC = 0.470
NRM, 10^{-2} EMU/GM
TRM, 10^{-2} EMU/GM
0.25
0.50
0.75
1.00
1.25
1.50
441
460
469
479
505
510
516
521
527
532
538
541
552
561
576

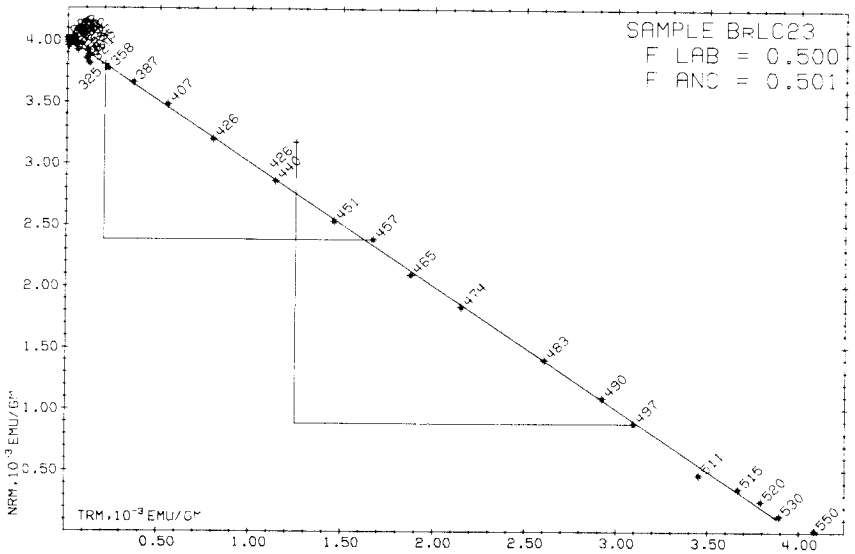
SAMPLE BRLC23
F LAB = 0.500
F ANC = 0.501
NRM, 10^{-3} EMU/GM
TRM, 10^{-3} EMU/GM
0.50
1.00
1.50
2.00
2.50
3.00
3.50
4.00
358
387
407
426
451
457
465
474
483
490
497
511
515
520
530
550

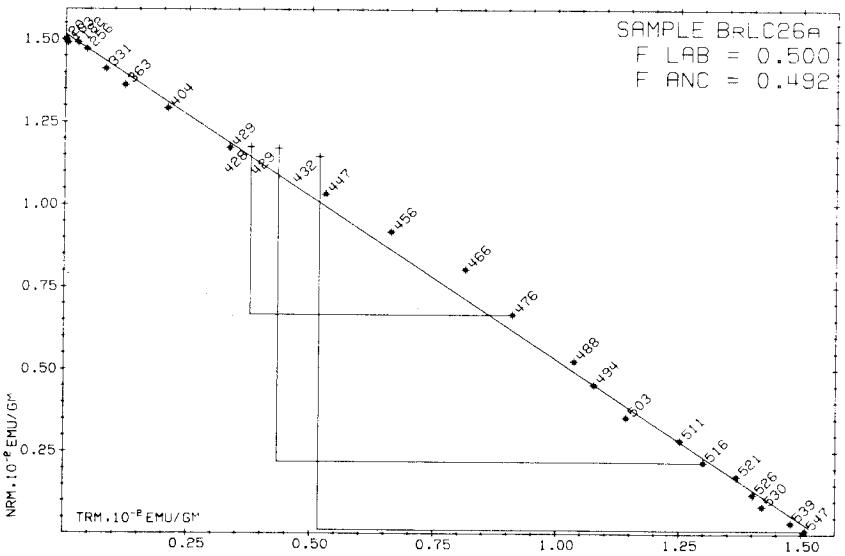
SAMPLE BRLC26A
F LAB = 0.500
F ANC = 0.492
NRM, 10^{-2} EMU/GM
TRM, 10^{-2} EMU/GM
0.25
0.50
0.75
1.00
1.25
1.50
331
363
404
429
432
447
456
466
476
488
494
503
511
516
521
526
530
539
547

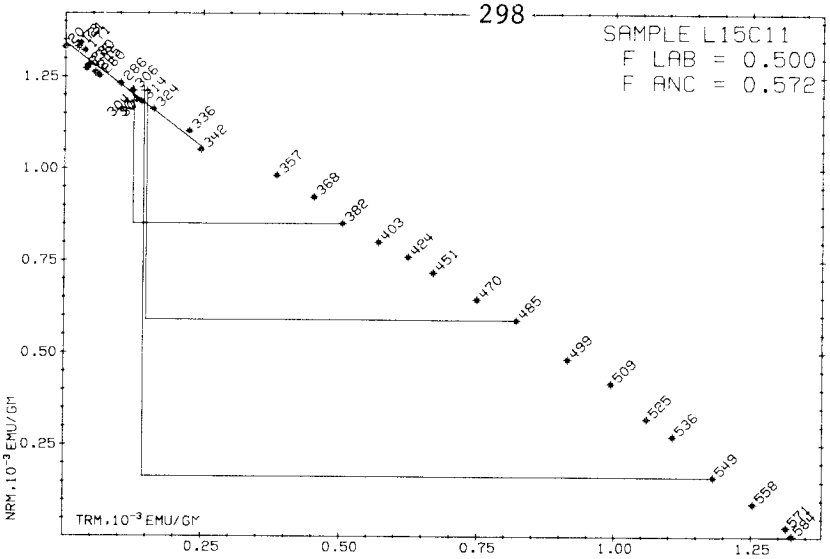
SAMPLE L15C11
F LAB = 0.500
F ANC = 0.572
NRM,10⁻³EMU/GM
TRM,10⁻³EMU/GM

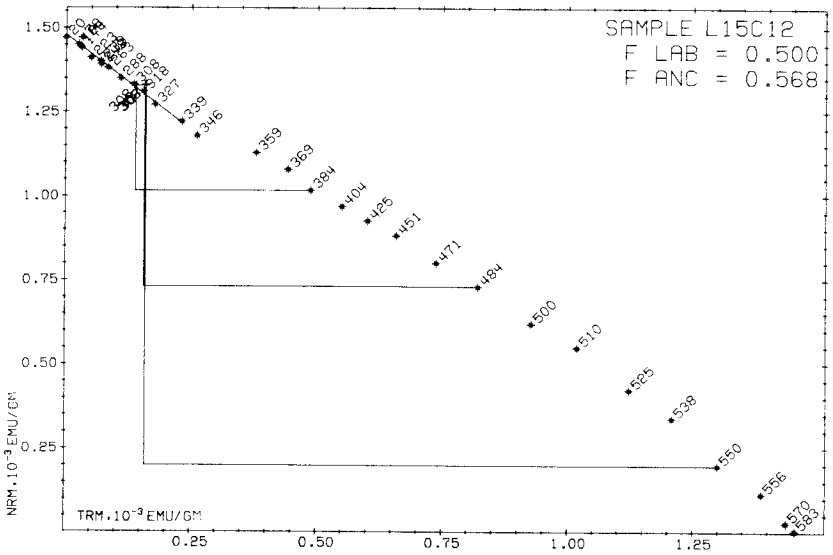
SAMPLE L15C12
F LAB = 0.500
F ANC = 0.568
NRM,10⁻³EMU/GM
TRM,10⁻³EMU/GM

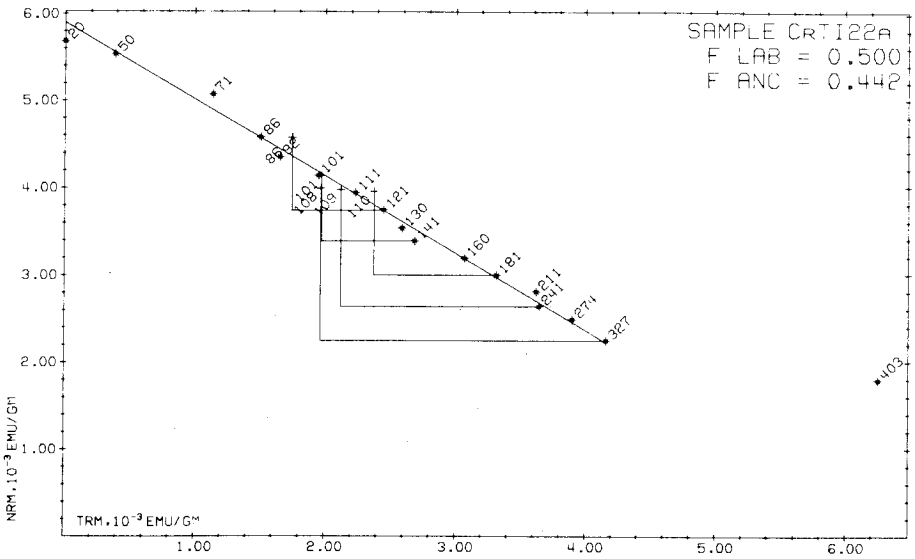
SAMPLE CRTI22A
F LAB = 0.500
F ANC = 0.442
NRM,10⁻³EMU/GM
TRM,10⁻³EMU/GM

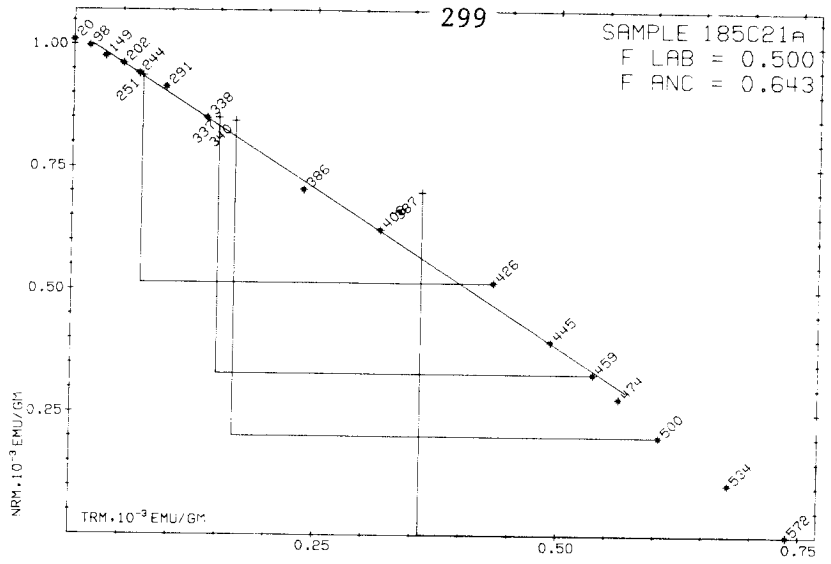
SAMPLE 185C21A
F LAB = 0.500
F ANC = 0.643
NRM,10⁻³ EMU/GM
TRM,10⁻³ EMU/GM
1.00
0.75
0.50
0.25
0.25
0.50
0.75
20
98
149
202
244
291
251
338
337
340
386
426
445
459
474
500
534
572

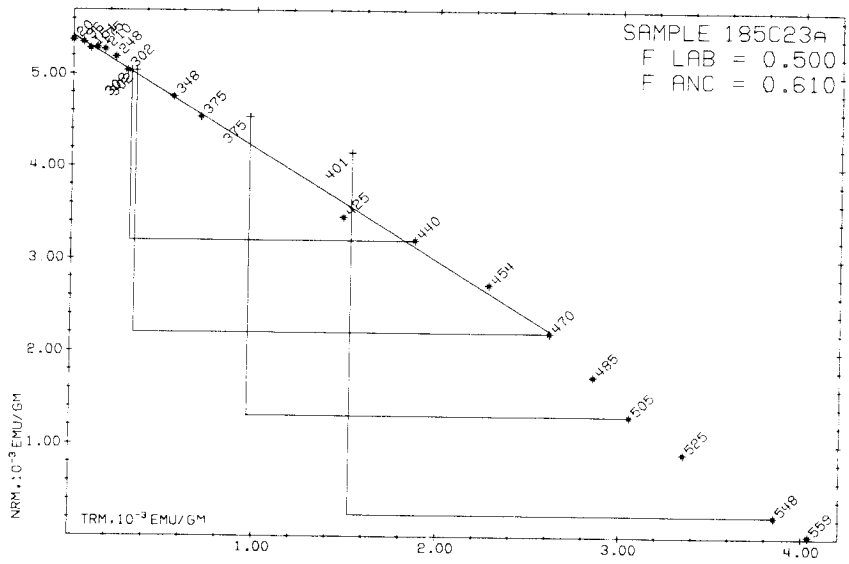
SAMPLE 185C23A
F LAB = 0.500
F ANC = 0.610
NRM,10⁻³ EMU/GM
TRM,10⁻³ EMU/GM
5.00
4.00
3.00
2.00
1.00
1.00
2.00
3.00
4.00
348
375
401
425
440
451
470
485
505
525
518
559

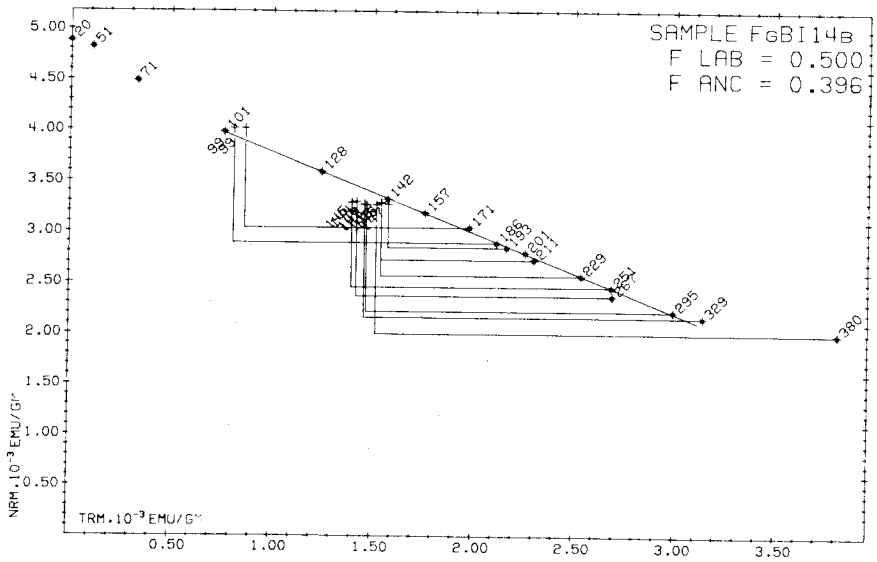
SAMPLE FGBI14B
F LAB = 0.500
F ANC = 0.396
NRM,10⁻³ EMU/GM
TRM,10⁻³ EMU/GM
5.00
4.50
4.00
3.50
3.00
2.50
2.00
1.50
1.00
0.50
0.50
1.00
1.50
2.00
2.50
3.00
3.50
20
51
71
101
128
142
157
171
186
193
201
211
229
251
261
295
329
380

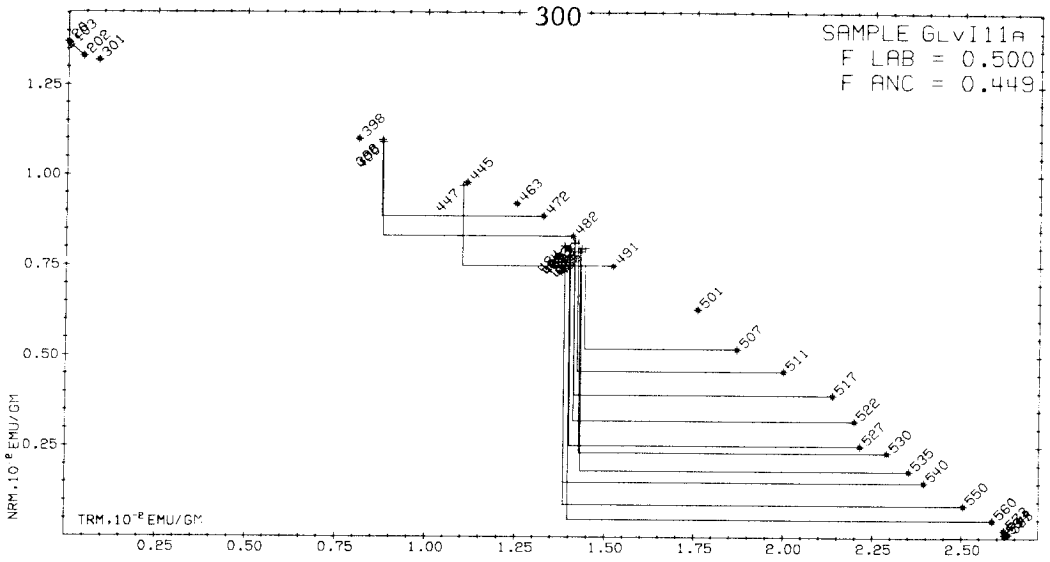
SAMPLE GLvI11A
F LAB = 0.500
F ANC = 0.449
NRM,10⁻³ EMU/GM
TRM,10⁻³ EMU/GM
0.25
0.50
0.75
1.00
1.25
1.50
1.75
2.00
2.25
2.50
398
445
447
463
472
482
491
501
507
511
517
522
527
530
535
540
550
560

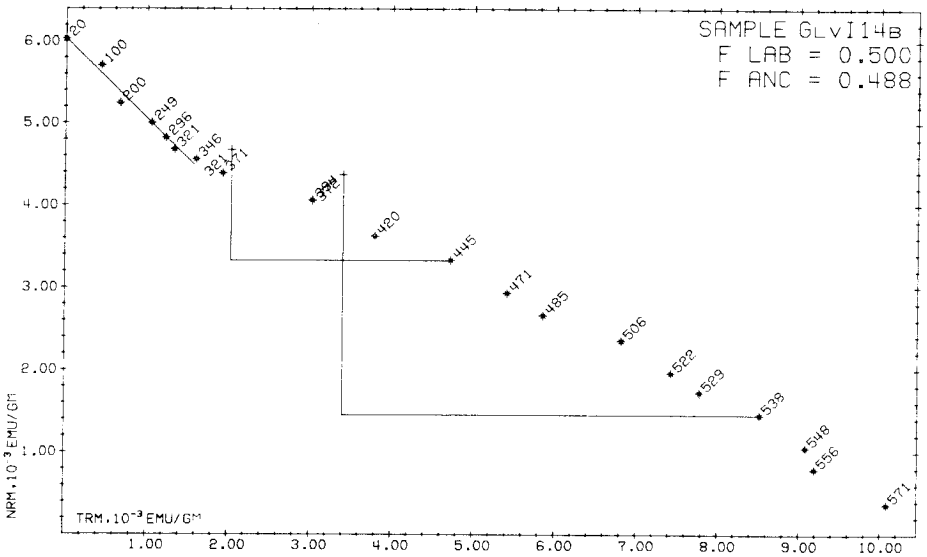
SAMPLE GLvI14B
F LAB = 0.500
F ANC = 0.488
NRM,10⁻³ EMU/GM
TRM,10⁻³ EMU/GM
1.00
2.00
3.00
4.00
5.00
6.00
7.00
8.00
9.00
10.00
20
100
200
249
296
321
346
371
420
445
471
485
506
522
529
538
548
556
571

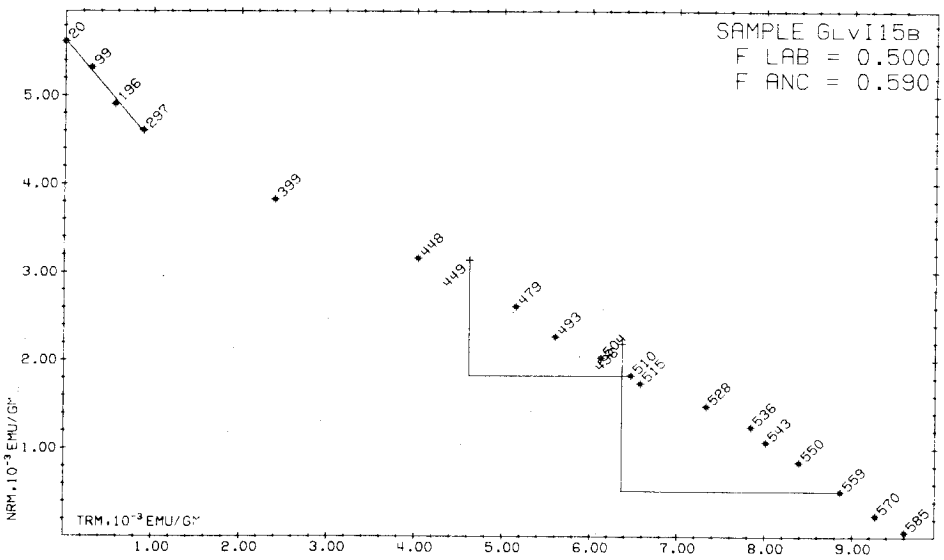
SAMPLE GLvI15B
F LAB = 0.500
F ANC = 0.590
NRM,10⁻³ EMU/GM
TRM,10⁻³ EMU/GM
1.00
2.00
3.00
4.00
5.00
6.00
7.00
8.00
9.00
20
99
196
297
399
448
449
479
493
510
515
528
536
543
550
559
570
585

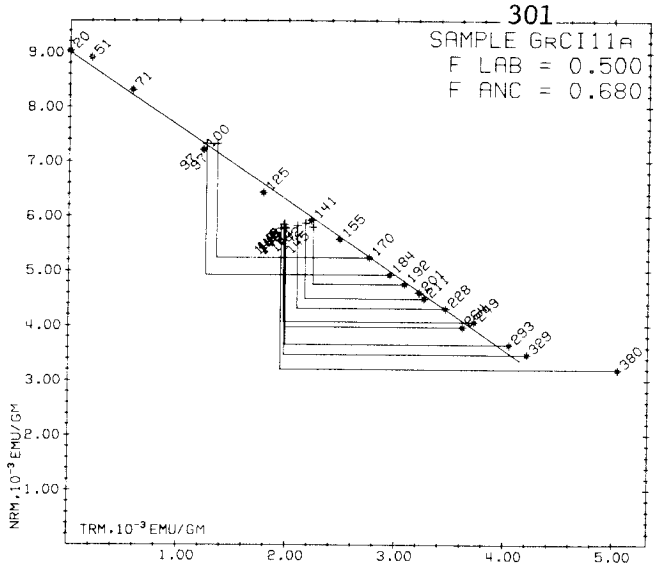
SAMPLE GRCI11A
F LAB = 0.500
F ANC = 0.680
NRM.10⁻³EMU/GM
TRM.10⁻³EMU/GM

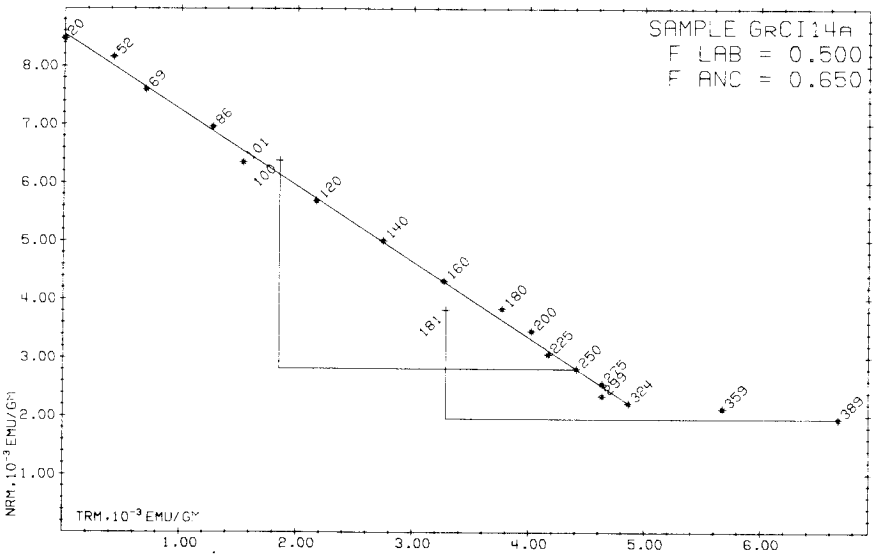
SAMPLE GRCI14A
F LAB = 0.500
F ANC = 0.650
NRM.10⁻³EMU/GM
TRM.10⁻³EMU/GM

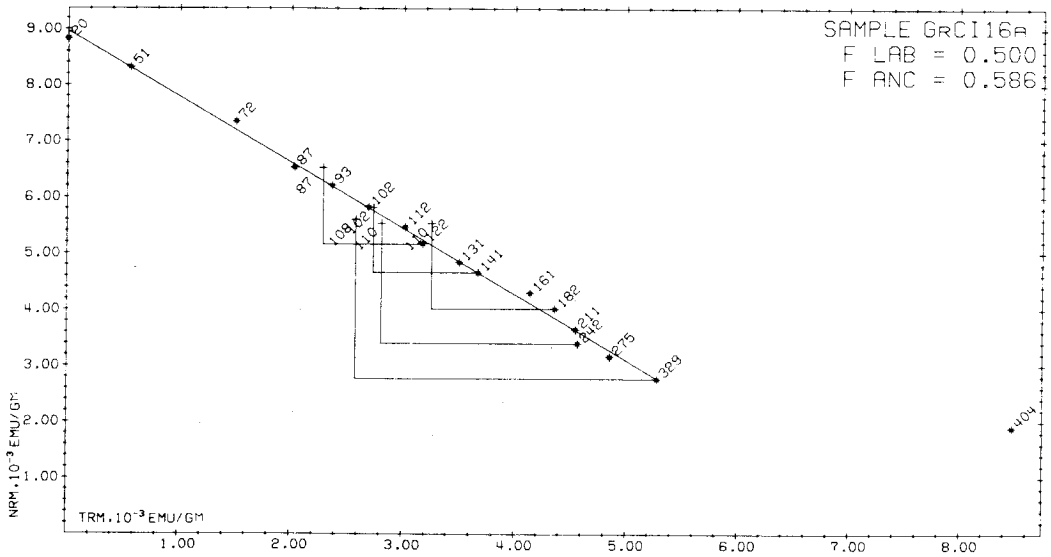
SAMPLE GRCI16A
F LAB = 0.500
F ANC = 0.586
NRM.10⁻³EMU/GM
TRM.10⁻³EMU/GM

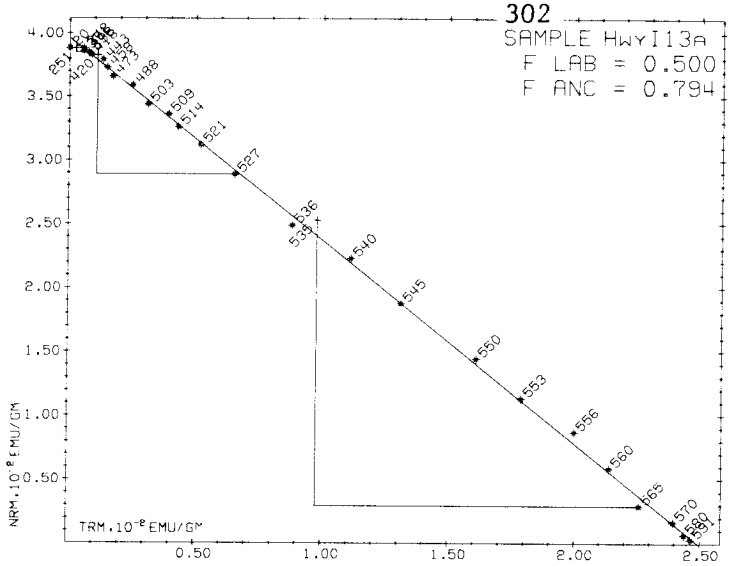
SAMPLE HWYI13A
F LAB = 0.500
F ANC = 0.794
NRM,10⁻³EMU/GM
TRM,10⁻³EMU/GM

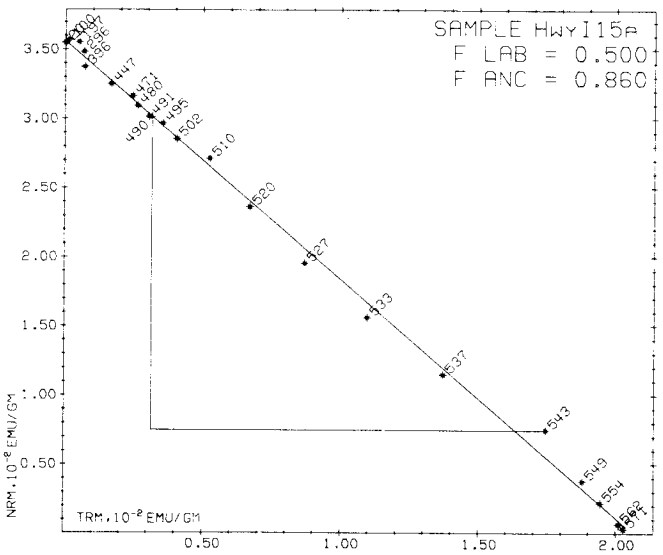
SAMPLE HWYI15A
F LAB = 0.500
F ANC = 0.860
NRM,10⁻³EMU/GM
TRM,10⁻³EMU/GM

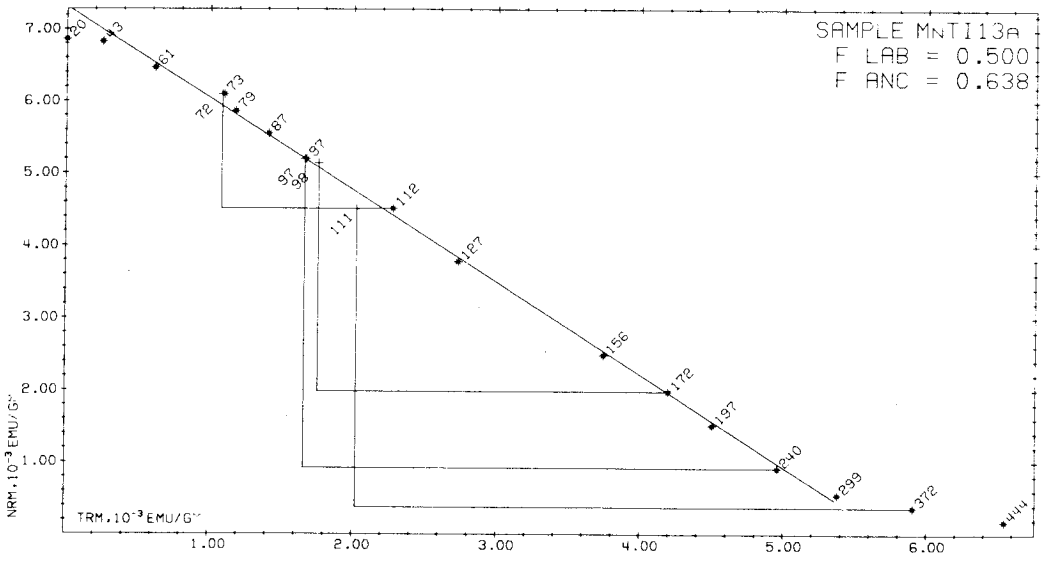
SAMPLE MNTI13A
F LAB = 0.500
F ANC = 0.638
NRM,10⁻³EMU/GM
TRM,10⁻³EMU/GM

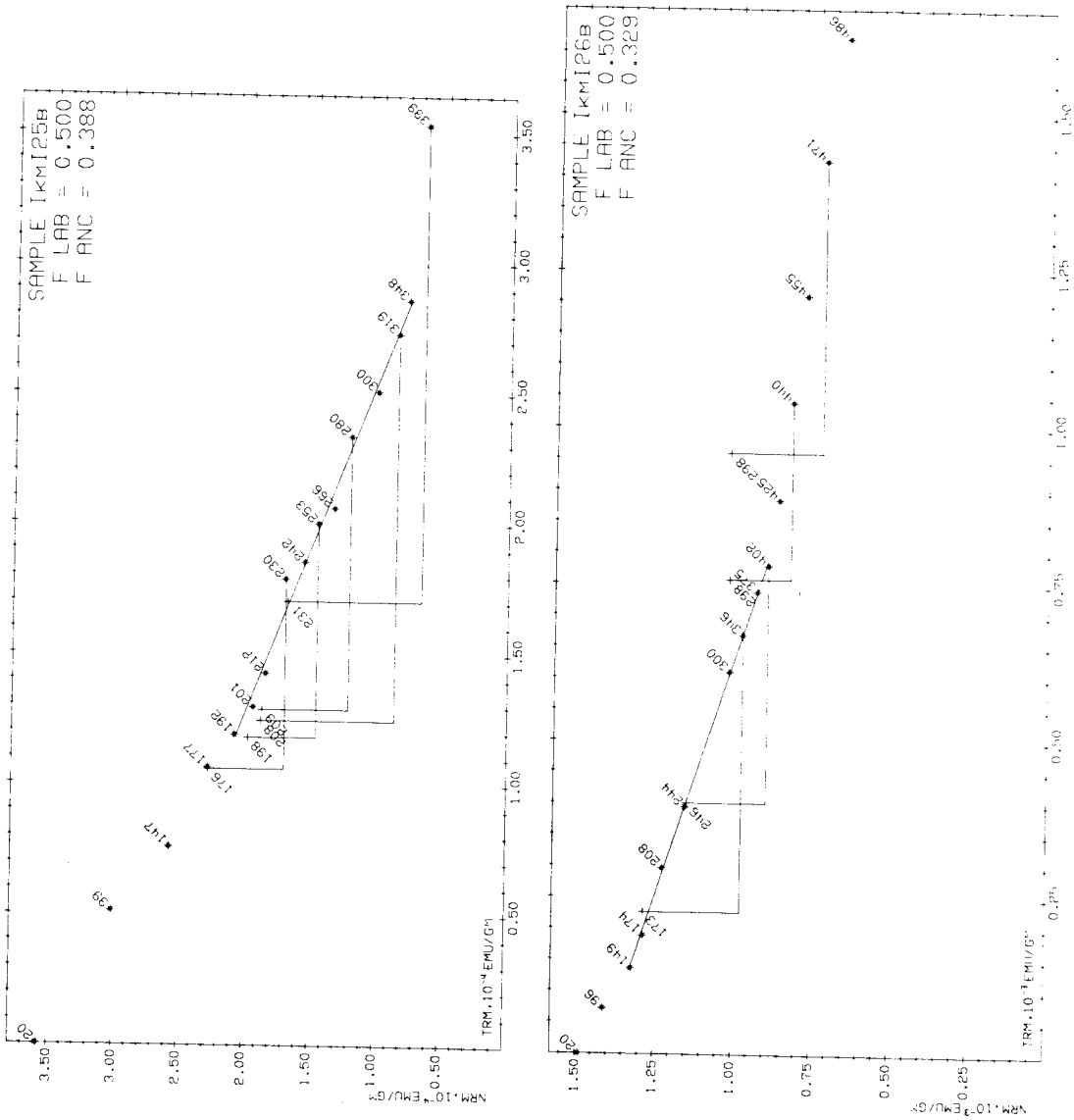
SAMPLE IkmI25B
F LAB = 0.500
F ANC = 0.388
NRM,10⁻⁴EMU/G³
TRM,10⁻⁴EMU/G³
SAMPLE IkmI26B
F LAB = 0.500
F ANC = 0.329
NRM,10⁻³EMU/G³
TRM,10⁻³EMU/G³

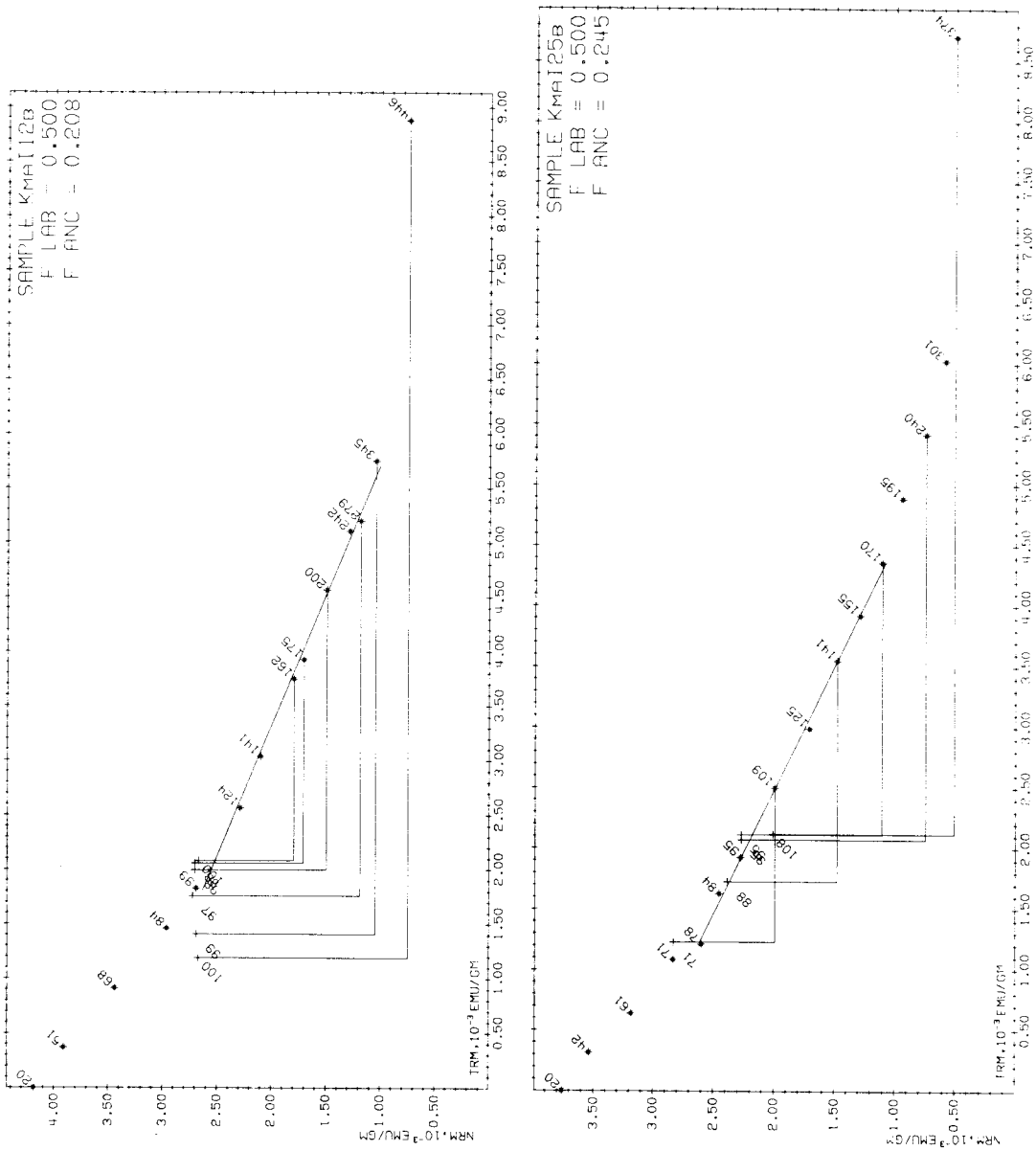
SAMPLE KMAI12B
F LAB = 0.500
F ANC = 0.208
SAMPLE KMAI25B
F LAB = 0.500
F ANC = 0.245
NRM,10⁻³EMU/GM
TRM,10⁻³EMU/GM

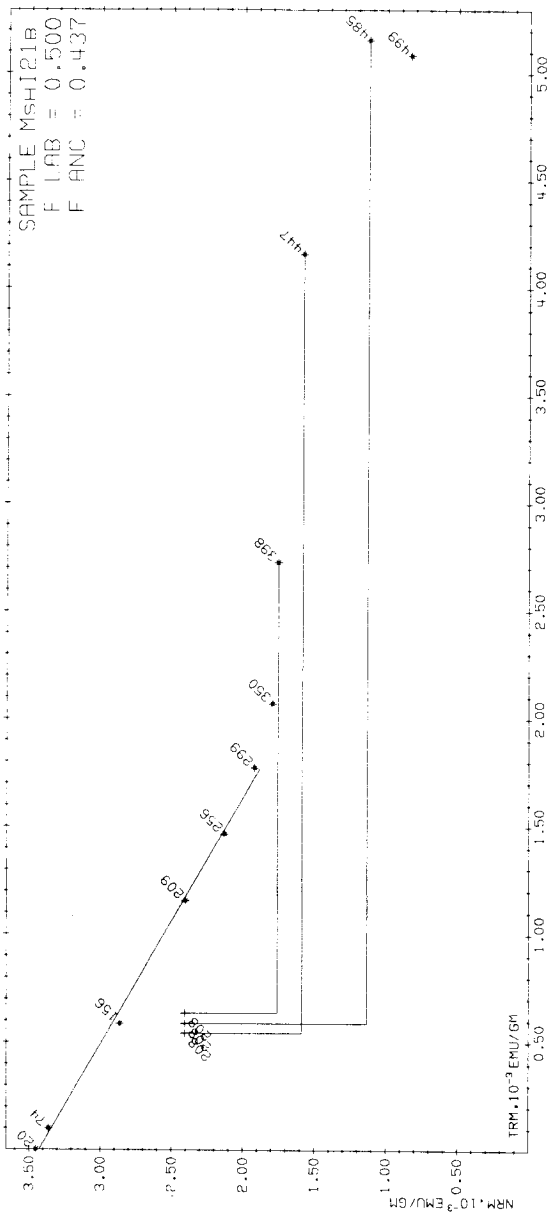
SAMPLE MSH121B
F LAB = 0.500
F ANC = 0.437
NRM,10⁻³EMU/GM
TRM,10⁻³EMU/GM

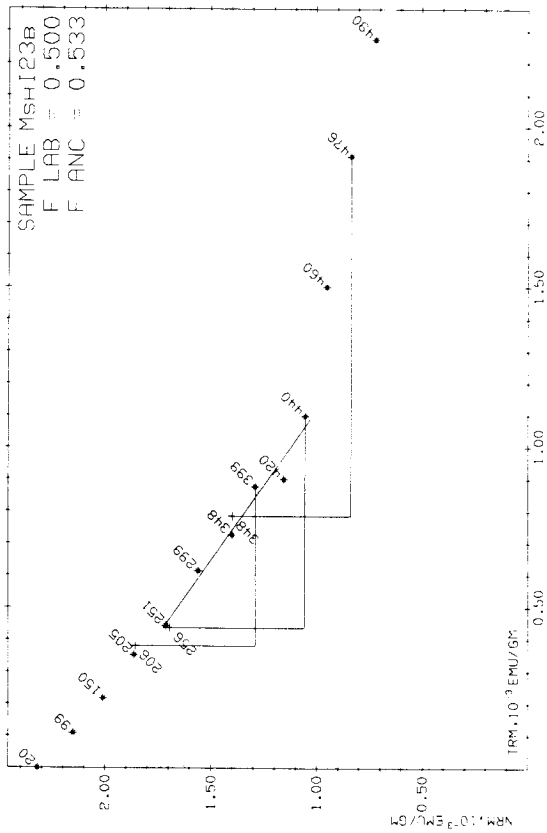
SAMPLE MSH123B
F LAB = 0.500
F ANC = 0.533
NRM,10⁻³EMU/GM
TRM,10⁻³EMU/GM

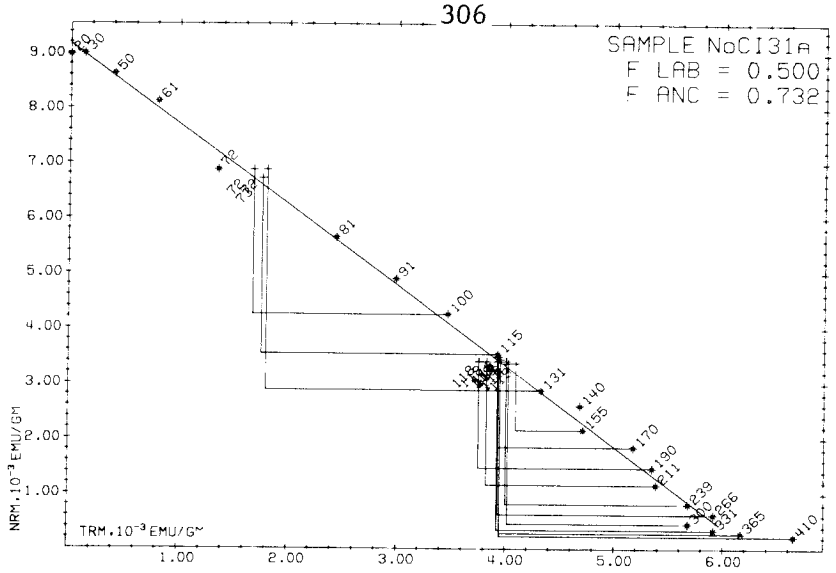
SAMPLE NoCI31A
F LAB = 0.500
F ANC = 0.732
NRM,10⁻³EMU/GM
TRM,10⁻³EMU/GM

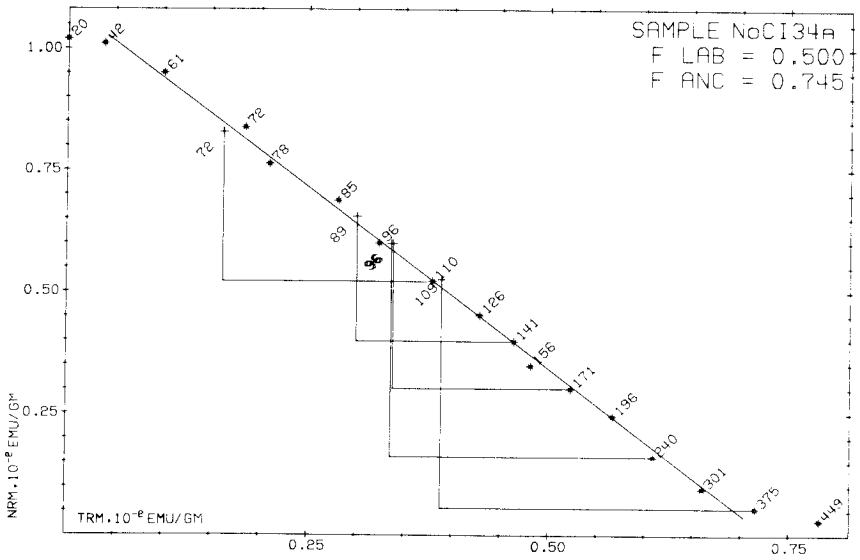
SAMPLE NoCI34A
F LAB = 0.500
F ANC = 0.745
NRM,10⁻³EMU/GM
TRM,10⁻³EMU/GM

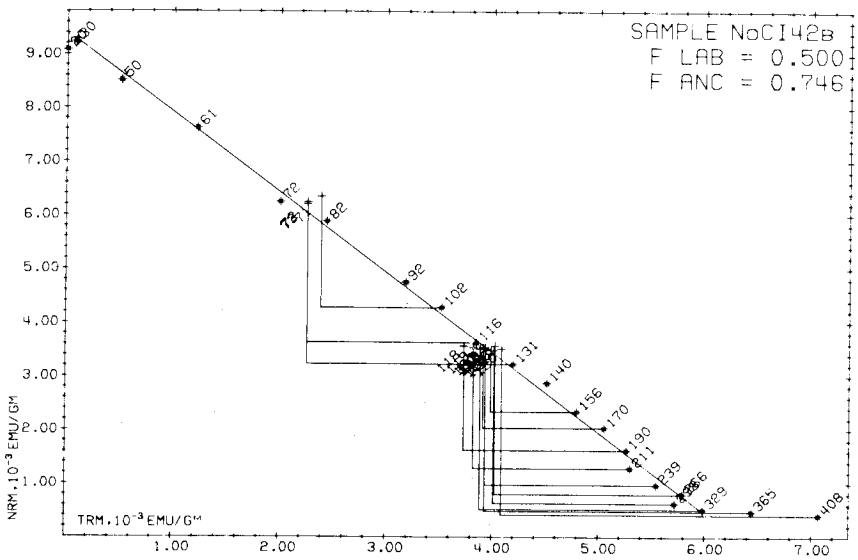
SAMPLE NoCI42B
F LAB = 0.500
F ANC = 0.746
NRM,10⁻³EMU/GM
TRM,10⁻³EMU/GM

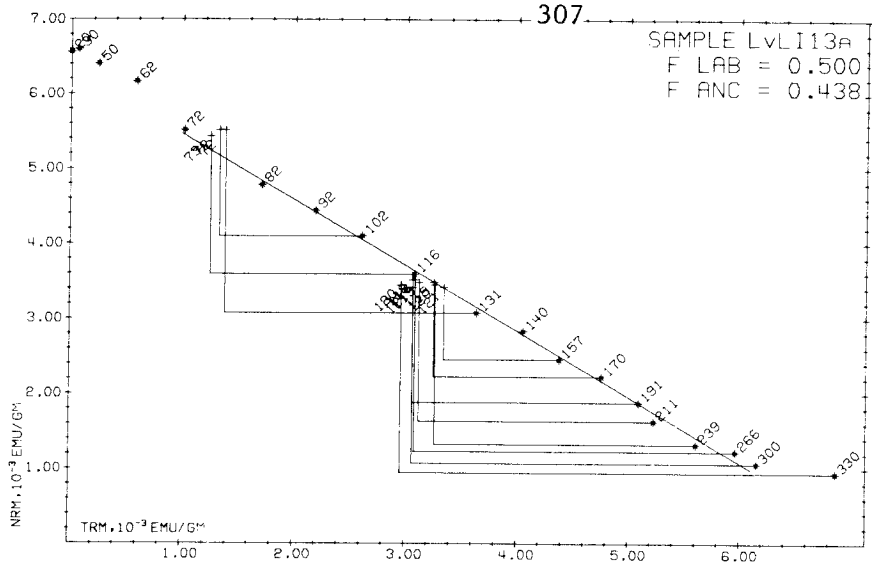
SAMPLE LvLI13A
F LAB = 0.500
F ANC = 0.438
NRM,10⁻³EMU/GM
TRM,10⁻³EMU/GM

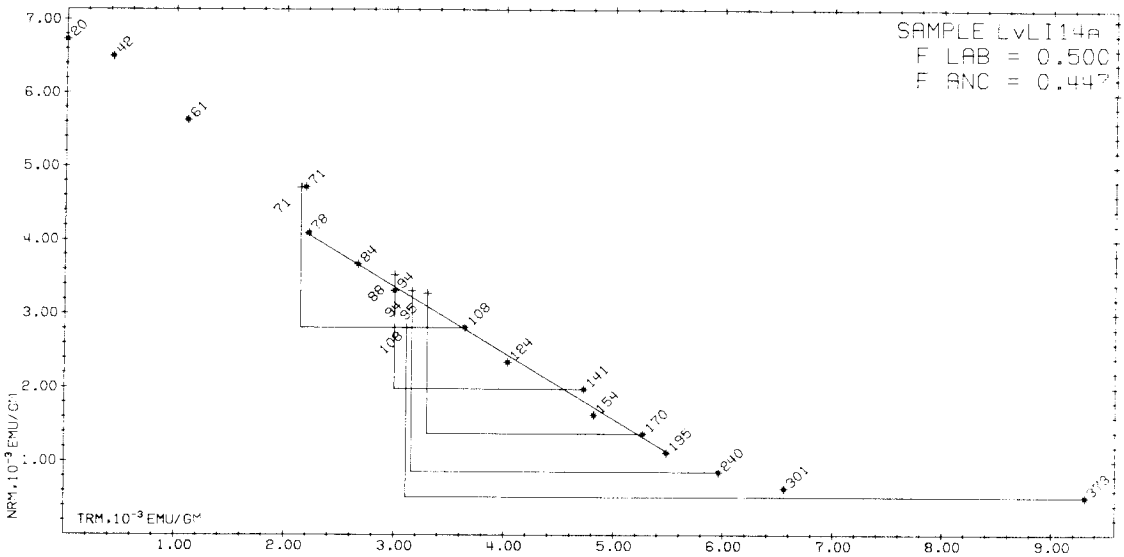
SAMPLE LvLI14A
F LAB = 0.500
F ANC = 0.447
NRM,10⁻³EMU/GM
TRM,10⁻³EMU/GM

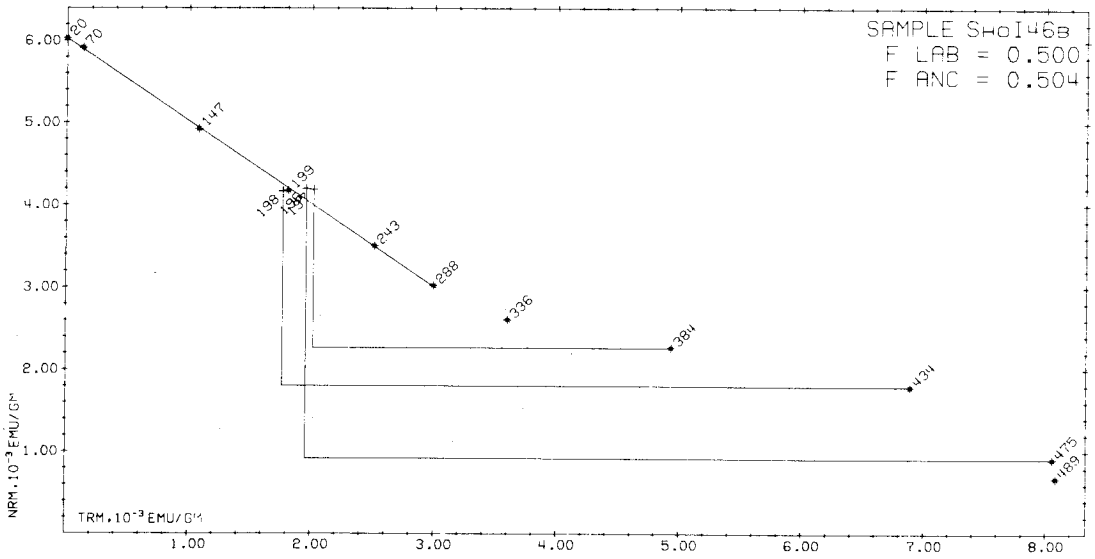
SAMPLE SHOI46B
F LAB = 0.500
F ANC = 0.504
NRM,10⁻³EMU/GM
TRM,10⁻³EMU/GM

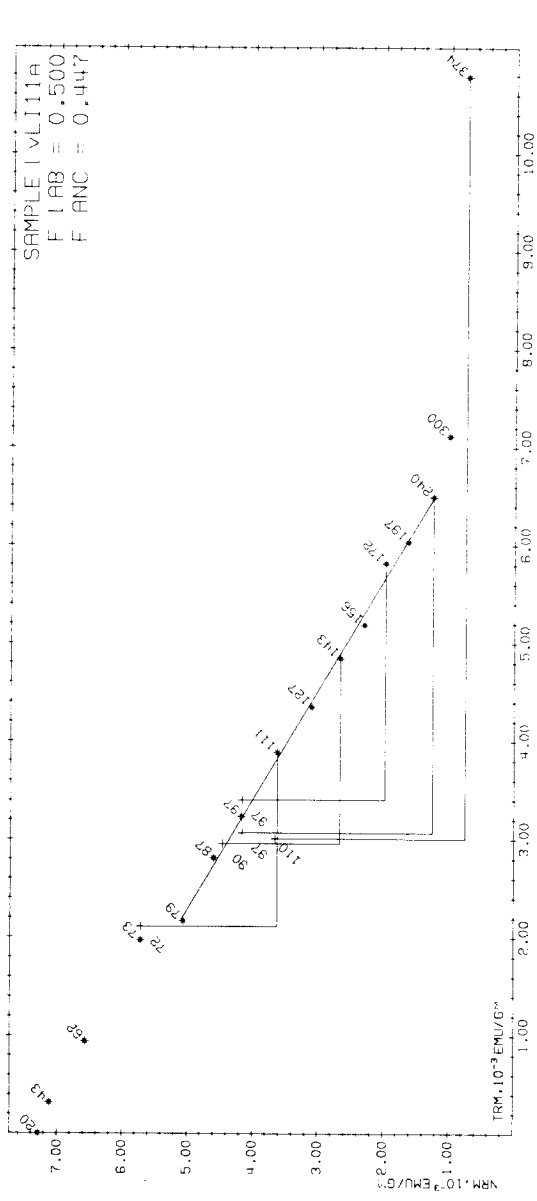
SAMPLE l vLJ11a
F LAB = 0.500
F ANC = 0.447
NRM,10⁻³EMU/G
TRM,10⁻³EMU/G

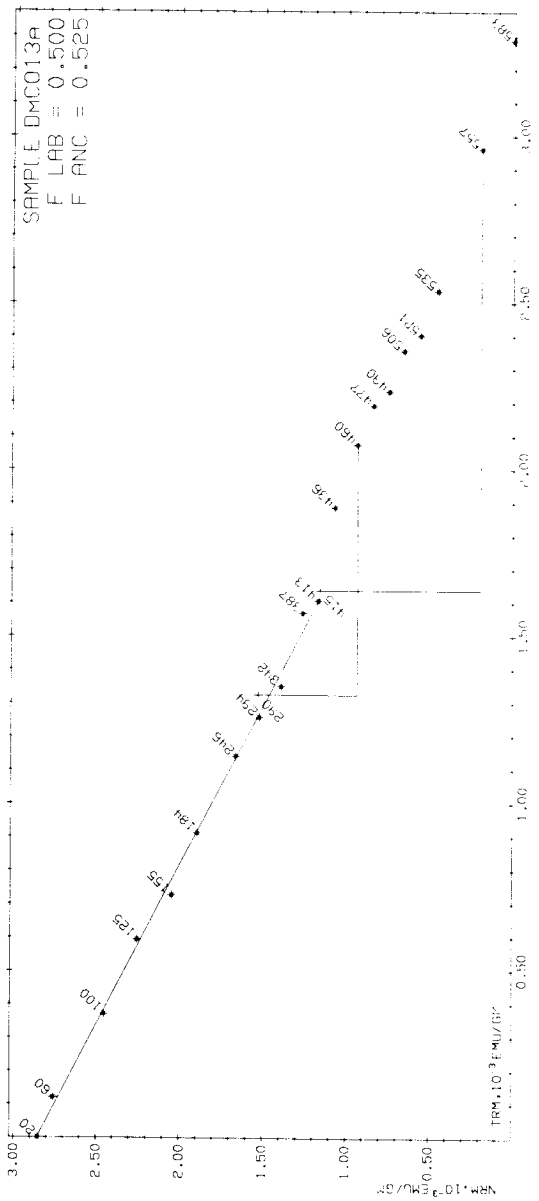
SAMPLE DmC013a
F LAB = 0.500
F ANC = 0.525
NRM,10⁻³EMU/G
TRM,10⁻³EMU/G

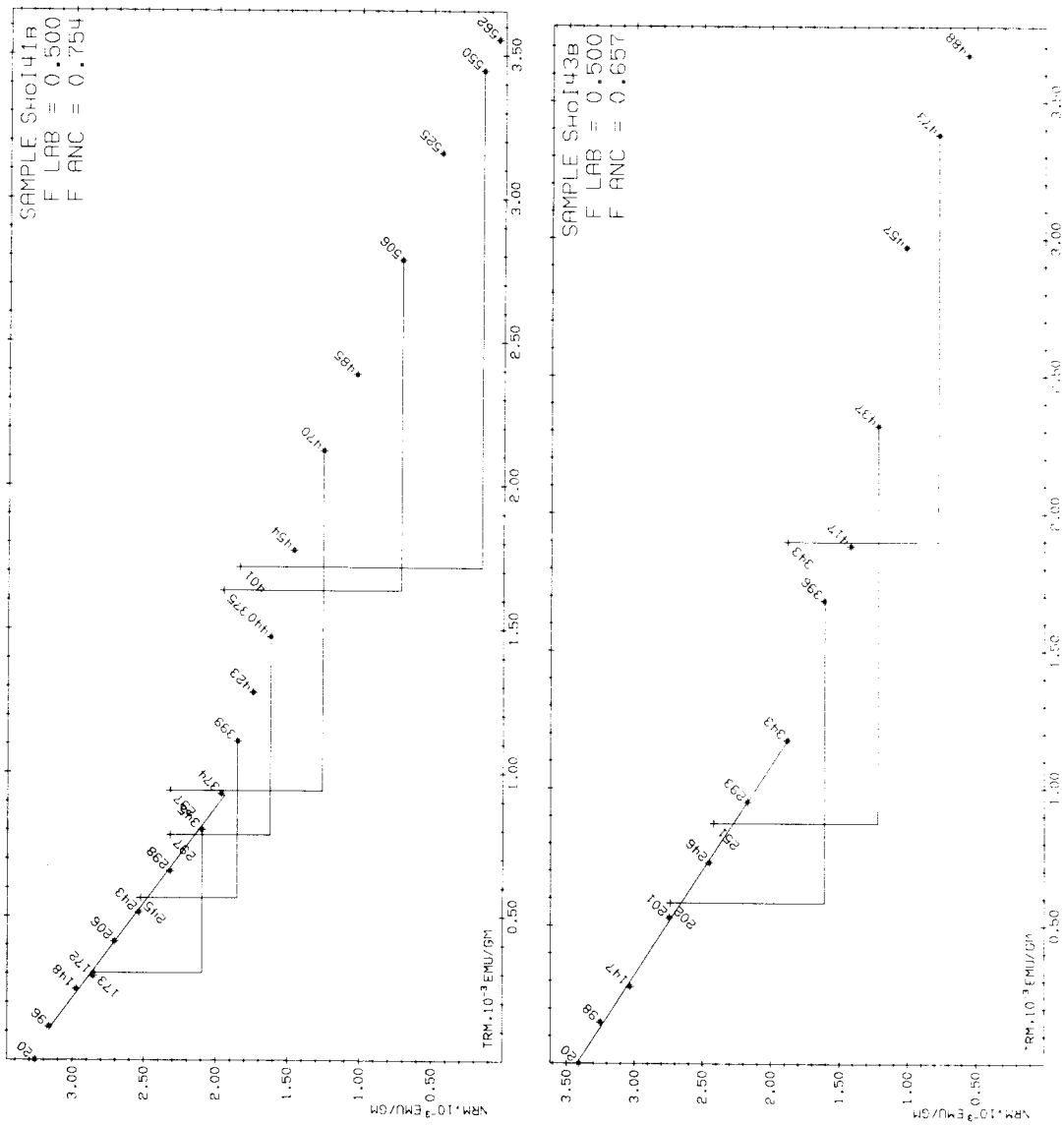
SAMPLE SH01418
F LAB = 0.500
F ANC = 0.754
NRM,10⁻³EMU/GM
TRM,10⁻³EMU/GM
SAMPLE SH01438
F LAB = 0.500
F ANC = 0.657
NRM,10⁻³EMU/GM
TRM,10⁻³EMU/GM

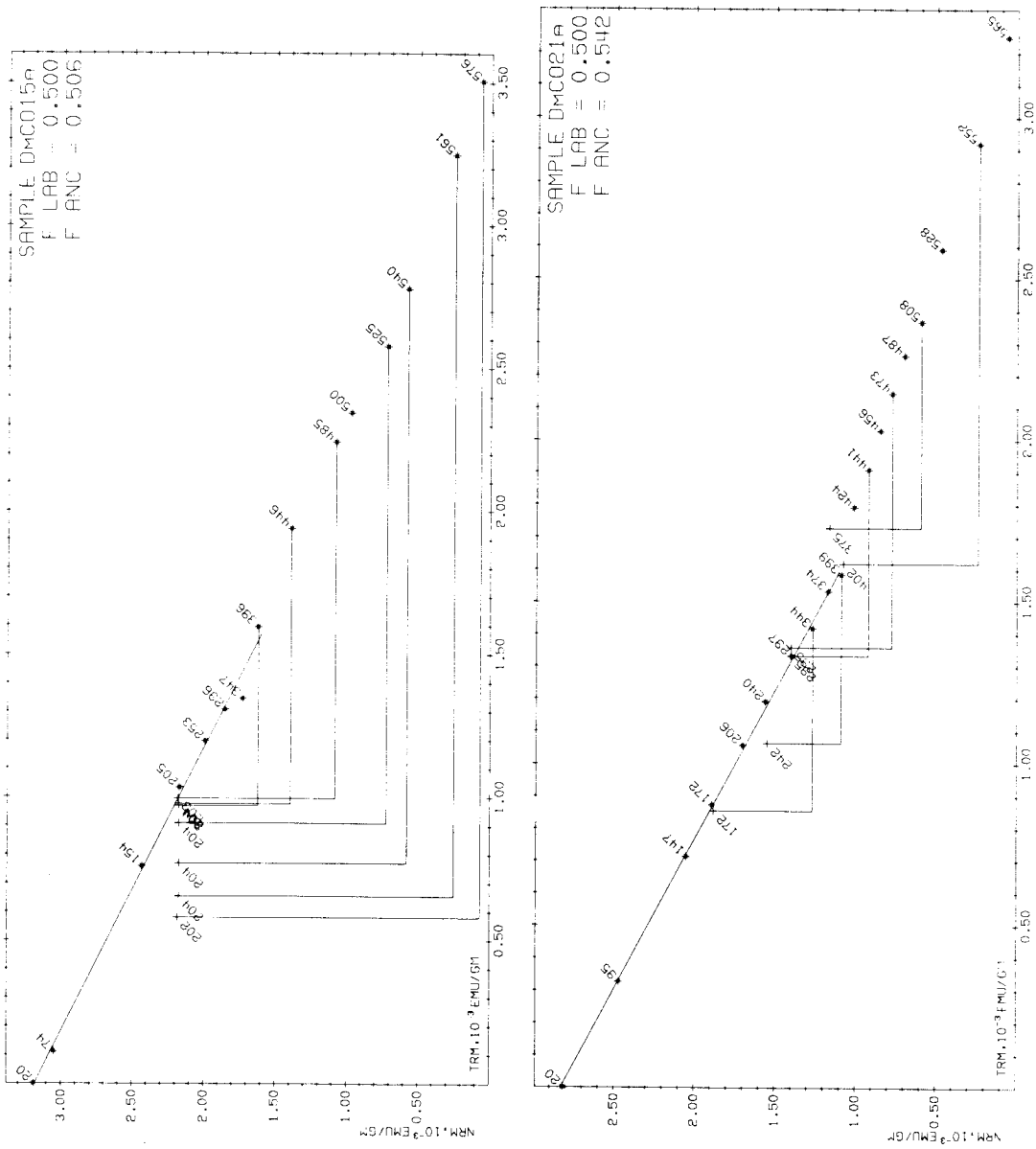
SAMPLE DMC015A
F LAB = 0.500
F ANC = 0.506
NRM,10⁻³EMU/GM
TRM,10⁻³EMU/GM
SAMPLE DMC021A
F LAB = 0.500
F ANC = 0.542
NRM,10⁻³EMU/GM
TRM,10⁻³EMU/GM

Appendix 5 - Paleodirectional data for Holocene Flows from the western United States

	LLA, deg	LLO, deg	H, mT	n	D, deg	I, deg	k	α95 deg	PLA, deg	PLO, deg
1. Bonito Flow, Sunset Crater, Arizona	35.4	248.5	--	29	346.4	58.1	499	1.2	78.6	180.0
2. Crater 84 Flow, San Francisco Volcanic Field, Arizona	35.4	248.6	40	8	4.5	56.4	163	4.4	86.1	313.7
3. Kana-a Flow, Sunset Crater, Arizona	35.4	248.6	--	19	353.7	65.1	406	1.7	77.4	228.5
4. Nixon Springs Flow, Grand Canyon N.P., Arizona	36.4	246.9	20+	20	23.2	61.2	175	2.5	71.2	311.3
5. Gyp Crater, San Francisco Volcanic Field, Arizona	35.3	248.5	--	21	345.0	61.4	407	1.6	76.3	194.8
6. S P Mountain Flow, San Francisco Volcanic Field, Arizona	35.6	248.4	40	8	6.9	55.1	259	3.5	84.4	335.6
7. Crater 130 Flow, San Francisco Volcanic Field, Arizona	35.3	248.7	20	12	9.4	29.3	150	3.6	68.6	43.2
8. Sunset Crater, San Francisco Volcanic Field, Arizona	35.4	248.5	40	22	350.1	58.7	398	1.5	81.1	188.8
9. Flow near Burnt Lava, Medicine Lake Highlands, California	41.5	238.5	--	14	0.1	49.3	360	2.1	78.6	58.1
10. Black Crater Flow, Modoc Plateau, California	41.8	238.5	--	12	359.2	55.9	2375	0.9	84.7	65.1
11. Black Flow, Modoc Plateau, California	41.7	238.4	--	12	4.5	51.2	240	2.8	79.6	37.0
12. Devil's Homestead Flow, Modoc Plateau, California	41.8	238.4	--	12	19.0	62.7	1077	1.3	75.9	312.4
13. Golden Creek Flow, Owens Valley, California	37.0	241.7	--	11	346.2	60.8	395	2.3	78.3	180.1
14. Hat Creek Flow, Mt. Lassen, California	40.7	238.6	20	12	4.0	65.1	956	1.4	83.0	261.5
15. Red Mountain Flow, Owens Valley, California	37.0	241.8	--	12	352.5	64.7	564	1.8	78.9	213.8
16. Schonchin Flow, Modoc Plateau, California	41.7	238.5	20	9	355.9	59.3	759	1.9	86.5	121.6
17. Dotsero Flow, Dotsero, Colorado	39.6	253.0	20	12	352.7	59.4	464	2.0	84.3	170.9
18. Flow near Bottleneck Lake, Craters of the Moon, Idaho	43.1	246.4	10	11	341.9	64.3	1159	1.3	76.8	175.6
19. North Robbers Flow, Snake River Plain, Idaho	43.4	247.0	30	17	339.4	47.1	237	2.3	67.6	121.5
20. Cerro Grande Field, Snake River Plain, Idaho	43.3	247.2	40+	22	355.9	57.0	663	1.2	83.4	97.2
21. Pahoehoe flow near Carey, Idaho from Craters of the Moon	43.3	246.2	--	12	16.7	60.2	1311	1.2	77.5	340.7

Appendix 5 - Continued

	LLA, deg	LLO, deg	H, mT	n	D, deg	I, deg	k	α95 deg	PLA, deg	PLO, deg
22. Pahoehoe flow near Fingers Butte from Craters of the Moon	43.4	246.7	30+	12	355.9	56.9	775	1.6	83.4	95.8
23. South Robbers Flow, Snake River Plain, Idaho	43.4	247.0	10	10	332.7	52.9	467	2.2	66.6	141.3
24. Grassy Cone Flow, Craters of the Moon, Idaho	43.4	246.4	30+	23	353.5	59.7	817	1.1	84.4	127.6
25. Highway Flow, Craters of the Moon, Idaho	43.5	246.4	10	12	358.1	65.9	194	3.1	85.1	231.2
26. Hells Half Acre Field, Snake River Plain, Idaho	43.4	247.5	--	24	2.1	65.2	579	1.2	85.9	268.1
27. Little Laidlaw Park Aa Flow, Craters of the Moon, Idaho	43.3	246.3	10	12	14.2	51.5	249	2.8	74.3	16.5
28. Lava Creek Flow, Craters of the Moon, Idaho	43.6	246.6	20	11	0.7	44.9	524	2.0	73.0	64.5
29. Flow nearest Minidoka, Idaho from Craters of the Moon	43.1	246.5	--	13	357.8	58.9	640	1.7	86.2	92.5
30. Flow near Pronghorn Reservoir from Craters of the Moon	43.1	246.4	10	10	14.5	58.3	1409	1.3	78.4	352.1
31. Shoshone Ice Cave Field, Snake River Plain, Idaho	43.0	245.6	--	18	359.1	56.8	814	1.2	84.4	73.0
32. Northeast Sunset Flow, Craters of the Moon, Idaho	43.5	246.5	20+	18	21.1	59.7	1012	1.1	74.1	340.1
33. Trenchmortar Flat Flow, Craters of the Moon, Idaho	43.4	246.5	--	12	357.1	64.9	352	2.3	86.0	217.3
34. Watchman Flow, Craters of the Moon, Idaho	43.4	246.5	--	13	350.9	64.4	489	1.9	83.0	183.4
35. Wapi Field, Snake River Plain, Idaho	42.8	246.8	--	25	13.2	62.8	991	0.9	80.4	324.4
36. Indian Wells Aa Flow, Craters of the Moon, Idaho	43.4	246.4	5	12	359.4	70.1	329	2.4	79.3	244.5
37. Larkspur Park Flow, Craters of the Moon, Idaho	43.0	246.4	--	11	0.3	63.1	407	2.3	88.4	254.7
38. Dead Horse Reservoir Flow, Craters of the Moon, Idaho	43.3	246.7	--	12	352.5	57.0	1089	1.3	82.0	114.1
39. Purdy Reservoir Aa Flow, Craters of the Moon, Idaho	43.2	246.5	5	12	7.4	56.0	623	1.8	81.2	24.0
40. Sawtooth Flow, Craters of the Moon, Idaho	43.3	246.5	--	11	355.1	64.7	466	2.1	85.2	201.3
41. Rangefire Aa Flow, Craters of the Moon, Idaho	43.1	246.6	10	6	2.1	53.3	3054	1.2	80.6	56.1
42. Blowout Reservoir Aa Flow, Craters of the Moon, Idaho	43.3	246.5	10	12	11.6	55.9	686	1.7	78.8	10.2

Appendix 5 - Continued

	LLA, deg	LLO, deg	H, mT	n	D, deg	I, deg	k	α95 deg	PLA, deg	PLO, deg
43. Questionable Flow, Craters of the Moon, Idaho	43.2	246.7	20	11	359.0	57.8	479	2.1	85.2	76.4
44. Serrate Aa Flow, Craters of the Moon, Idaho	43.5	246.5	--	10	352.7	60.0	724	1.8	84.0	133.9
45. Aspen Flow, Spencer-High Point Rift, Idaho	44.3	248.2	30	10	350.0	53.6	1328	1.3	77.3	109.1
46. Big Green Flow, Spencer-High Point Rift, Idaho	44.2	248.2	20	12	3.3	39.4	1497	1.1	67.9	60.2
47. Blue Lake Crater, Santiam Pass, Oregon	44.4	238.2	--	15	220.3	68.1	461	1.8	82.8	220.3
48. Charlies Cone, Northwest Rift, Newberry Crater, Oregon	43.9	238.8	--	11	350.3	59.7	420	2.2	82.1	126.9
49. Clear Lake Flow, Sand Mountain, Oregon	44.4	238.0	10+	24	6.3	49.5	194	2.1	75.1	36.5
50. Crescent Creek Flow, Crescent, Oregon	43.5	238.2	--	12	7.8	67.4	132	3.8	81.4	273.8
51. Crater Lake Ash Flow Deposit, Crater Lake, Oregon	42.9	237.9	--	41	354.7	73.0	575	0.9	74.0	227.9
52. Diamond Craters Field, Diamond, Oregon	43.1	241.3	--	12	4.0	71.2	743	1.6	77.1	251.4
53. Devils Garden Field, Fort Rock, Oregon	43.5	239.1	--	12	348.9	66.1	304	2.5	80.8	185.8
54. Forest Road Flow, Northwest Rift, Newberry Crater, Oregon	43.8	238.7	--	20	353.9	51.8	574	1.4	77.7	83.4
55. Gasline Flow, Northwest Rift, Newberry Crater, Oregon	43.9	238.6	--	12	343.1	57.6	367	2.3	76.1	130.5
56. Hackleman Creek Flow, Sand Mountain, Oregon	44.4	238.0	--	12	2.6	50.3	1323	1.2	76.5	48.6
57. Inter-Lake Obsidian Flow, Newberry Crater, Oregon	43.7	238.8	--	6	22.6	57.2	57	9.0	71.9	340.3
58. Jordan Crater, Jordan Valley, Oregon	43.1	242.6	--	12	2.7	51.0	1872	1.0	78.4	51.3
59. LeConte Flow, Three Sisters, Oregon	44.0	238.2	30	10	342.1	66.2	530	2.1	76.9	174.9
60. Little Belknap Flow, McKenzie Pass, Oregon	44.3	238.2	--	24	7.1	44.2	422	1.4	70.8	38.6
61. Mokst Butte Flow, Northwest Rift, Newberry Crater, Oregon	43.8	238.7	30	10	343.0	65.3	193	3.5	77.6	171.2
62. Parkdale Flow, Mt. Hood, Oregon	45.5	238.4	10+	23	23.5	61.2	269	1.8	72.9	330.6
63. Red Slide Flow, Newberry Crater, Oregon	43.7	238.8	20	9	359.2	56.9	432	2.5	83.7	64.4

Appendix 5 - Continued

	LLA, deg	LLO, deg	H, mT	n	D, deg	I, deg	k	α95 deg	PLA, deg	PLO, deg
64. South Belknap Cone Flow, McKenzie Pass, Oregon	44.2	238.1	--	19	0.2	44.7	392	1.7	72.1	57.5
65. The Dome Crater, Newberry Crater, Oregon	43.7	238.8	--	15	355.0	56.7	279	2.3	82.5	91.3
66. The Fissure, Newberry Crater, Oregon	43.7	238.8	--	12	358.6	57.0	356	2.3	83.8	68.9
67. West Belknap Flow, McKenzie Pass, Oregon	44.3	238.0	--	20	359.8	52.1	349	1.8	78.4	59.0
68. Wizard Island Small Block Flow, Crater Lake, Oregon	42.9	237.9	--	12	11.2	65.5	210	3.0	80.8	293.0
69. Yapoah Flow, McKenzie Pass, Oregon	44.3	238.2	--	19	14.0	61.4	506	1.5	79.7	333.0
70. Four in One Flow, McKenzie Pass, Oregon	44.2	238.2	--	11	10.4	72.5	118	4.2	75.0	260.0
71. Dry Valley Flow, Markagunt Plateau, Utah	37.5	247.3	20	9	15.8	49.8	209	3.6	75.3	0.5
72. Ice Spring Field, Black Rock Desert, Utah	39.0	247.5	30	17	352.1	63.7	390	1.8	81.4	207.6
73. Tabernacle Hill Field, Black Rock Desert, Utah	38.9	247.5	40	10	4.3	30.0	724	1.8	66.9	56.8
74. Crescent Creek Flow, Mt. St. Helens, Washington	46.3	237.7	--	12	12.4	50.3	581	1.8	72.1	21.2
75. Cave Basalt Flow, Mt. St. Helens, Washington	46.1	237.8	--	12	344.4	60.6	462	2.0	77.9	131.4
76. South Puyallup Block and Bomb Flow, Mt. Rainier, Washington	46.8	238.1	--	12	22.4	51.3	223	2.9	67.3	1.0
77. Waterfall Canyon, Flow, Mt. St. Helens, Washington	46.2	237.8	--	12	358.3	60.0	347	2.3	84.6	71.2

LLA and LLO are north latitude and east longitude of sampling sites. H is peak alternating demagnetizing field. n is number of oriented samples. D and I are declination eastward and inclination downward of mean remanent magnetization. Parameters k and α95 are precision parameter and radius of 95% confidence cone. PLA and PLO are north latitude and east longitude of virtual geomagnetic pole.